Heft 69
Jahr 2005

Die Küste, 69 PROMORPH (2005), 1-420

Die Küste

Die Küste

ARCHIV FÜR FORSCHUNG UND TECHNIK
AN DER NORD- UND OSTSEE

ARCHIVE FOR RESEARCH AND TECHNOLOGY
ON THE NORTH SEA AND BALTIC COAST

HERAUSGEBER: KURATORIUM FÜR FORSCHUNG IM KÜSTENINGENIEURWESEN

69
2005

Die Küste, 69 PROMORPH (2005), 1-420

Die Küste

ARCHIV FÜR FORSCHUNG UND TECHNIK
AN DER NORD- UND OSTSEE

ARCHIVE FOR RESEARCH AND TECHNOLOGY
ON THE NORTH SEA AND BALTIC COAST

Heft 69 · Jahr 2005

Herausgeber: Kuratorium für Forschung im Küsteningenieurwesen

Kommissionsverlag:
Boyens Medien GmbH & Co. KG, Heide i. Holstein
Druck: Boyens Offset

ISSN 0452-7739
ISBN 3-8042-1061-9

Anschriften der Verfasser dieses Heftes:

ABEGG, FRIEDRICH, Department of Geosciences, Bremen University, Klagenfurter Straße, D-28359 Bremen, Germany, abegg@uni-bremen.de; ASP NETO, NILS EDVIN, Universidade Federal do Pará, Alameda Leandro Ribeiro, s/n. – Bairro Aldeia, UFPA/Campus universitário de Bragança, 68600-000 BRAGANÇA, PA – Brasil, nilsasp@ufpa.br; BENKEL, ANDREAS, GKSS-Research Centre, Institute for Coastal Research/System Analysis and Modelling, Max-Planck-Straße 1, D-21502 Geesthacht, Germany, andreas.benkel@gkss.de; EDEN, HENDRIK, General Acoustics GmbH, Dorfstr. 57, D-24107 Kiel-Ottendorf, Germany, heden@generalacoustics.com; EGOZCUE RUBI, JUAN JOSÉ, Universitat Politècnica de Catalunya, DESPATX 307, Planta 3, Campus NORD – Edif. C2, C. Jordi Girona, 1–3, 08034 Barcelona, SPAIN, Juan.jose.egozcue@upc.edu; ESCOBAR SIERRA, CARLOS ALEJANDRO, Research and Technology Centre West Coast University of Kiel, Hafentörn 1, 25761 Büsum, Germany, cescobar@corelab.uni-kiel.de; GROSS, GÜNTER, Institute for Meteorology und Climatology Hannover University, Herrenhäuser Straße 2a, D-30419 Hannover, Germany, gross@muk.uni-hannover.de; HENSSE, JENS, General Acoustics GmbH, Dorfstr. 57, D-24107 Kiel-Ottendorf, Germany, jhensse@generalacoustics.com; HOYME, HELGE, Fluid Mechanics Institute, Hannover University, Applestraße 9a, D-30167 Hannover, Germany, hoyme@hydromech.uni-hannover.de; Jiménez Echeverri, Nestor Jaime, Research and Technology Centre West Coast University of Kiel, Hafentörn 1, 25761 Büsum, Germany, njimenez@corelab.uni-kiel.de; JIMÉNEZ GONZALEZ, SUSANA, Research and Technology Centre West Coast University of Kiel, Hafentörn 1, 25761 Büsum, Germany; JUNGE, INGO, Fluid Mechanics Institute, Hannover University, Applestraße 9a, D-30167 Hannover, Germany, junge@hydromech.uni-hannover.de; LEHNER, SUSANNE, German Aerospace Centre, Remote Sensing Technology Institute, Institute Oberpfaffenhofen, Münchner Str., 82234 Wessling, Germany, susanne.lehner@dlr.de; MÜLLER, VOLKER, General Acoustics GmbH, Dorfstr. 57, D-24107 Kiel-Ottendorf, Germany, vmueller@generalacoustics.com; MAYERLE, ROBERTO, Research and Technology Centre West Coast University of Kiel, Hafentörn 1, 25761 Büsum, Germany, rmayerle@corelab.uni-kiel.de; PALACIO TOBÓN, CARLOS ALBERTO, Grupo de Ingeniería y Gestión Ambiental – GIGA, Universidad de Antioquia, Calle 67 #53-108 Of. 20-413, Medellín-Colombia, cpalacio@udea.edu.co; POERBANDONO, Hydrographic Science and Engineering Working Group, Faculty of Civil and Environmental Engineering, Institute of Technology, Bandung Jl. Ganesha 10 – Bandung 40132 Indonesia, poerbandono@gd.itb.ac.id; PRAMONO, GATOT HARYO, National Coordinating Agency for Surveys and Mapping, Jl. Raya Jakarta – Bogor Km.46, CIBINONG 16911, Indonesia, gatothp@bakosurtanal.go.id; RAUSCH, JAN, Weinbergweg 32, 70569 Stuttgart, Germany; RICKLEFS, KLAUS, Research and Technology Centre West Coast University of Kiel, Hafentörn 1, 25761 Büsum, Germany, ricklefs@ftz-west.uni-kiel.de; SCHROTTKE, KERSTIN, Department of Geosciences, Bremen University, Leobener Straße, D-28359 Bremen, Germany, schrottke@rcom-bremen.de; SCHUBERT, BJÖRN, Fluid Mechanics Institute, Hannover University, Applestraße 9a, D-30167 Hannover, Germany, schubert@projektionisten.de; TORO, FERNANDO, International Marine and Dredging Consultants, Wilrijkstraat 37–45, box 4, 2140 Antwerp – Belgium, fernando.toro@imdc.be; TORO BOTERO, FRANCISCO MAURICIO, Universidad Nacional de Colombia, Facultad de Minas, Cra 80 No. 65–223, BI M2, Of 322, Colombia, fmtoro@unal.edu.co; WILKENS, JORT, HR Wallingford Ltd, Howbery Park, Wallingford, Oxon, OX10 8BA, United Kingdom, j.wilkens@hrwallingford.co.uk; WINDUPRANATA, WIWIN, Research and Technology Centre West Coast University of Kiel, Hafentörn 1, 25761 Büsum, Germany, windu@corelab.uni-kiel.de; WINTER, CHRISTIAN, MARUM Bremen University, Leobener Straße, D-28359 Bremen, Germany, acwinter@uni-bremen.de; ZIELKE, WERNER, Fluid Mechanics Institute, Hannover University, Applestraße 9a, D-30167 Hannover, Germany, zielke@hydromech.uni-hannover.de.

Vorsitzender des Kuratoriums: Dr.-Ing. Eiko Lübbe, BMVEL, PF 14 02 70, 53107 Bonn
Geschäftsführer: Dr.-Ing. Rainer Lehfeldt, Wedeler Landstraße 157, 22559 Hamburg
Schriftleitung „DIE KÜSTE“: Dr.-Ing. V. Barthel, Birkenweg 6a, 27607 Langen

Inhaltsverzeichnis

Die Küste, 69 PROMORPH (2005), 1-420

PROMORPH –
Predictions of Medium-Scale Morphodynamics: Project Overview and Executive Summary

By ROBERTO MAYERLE and WERNER ZIELKE

Summary

This paper presents an overview of the aims, strategies, main findings and deliverables of the research work carried out within the framework of the project PROMORPH – Predictions of Medium-Scale Morphodynamics. The project was funded by the German Ministry of Education and Research over the period 2000 to 2002. Detailed descriptions of the individual investigations and results obtained are presented in the remaining papers of this volume. The overall aim of the project was to develop, calibrate, validate and apply process-based models for the simulation of medium-scale morphodynamics in coastal areas on the basis of existing modelling systems. The study area is the central Dithmarschen Bight located between the Elbe and Eider estuaries on the North Sea coast. The project relied extensively on close cooperation between several research institutes in Germany, with a pooling of expertise, efforts and resources. These specifically include the Institute of Fluid Mechanics and Meteorology of the University of Hannover and the Research and Technology Centre "Westcoast" of the University of Kiel. The papers give a detailed account of the acquisition and analysis of the field data necessary to evaluate patterns of hydrodynamics, sediment dynamics and morphodynamics. The application of existing modelling systems for developing a coupled model for the simulation of flow, waves, sediment transport and bed evolution is also described. Special attention was given to the integration of field measurements and numerical model simulations with a view to improving our understanding of the physics of the system and the predictive capabilities of the models. The set-up and application of a medium-scale morphodynamic model based on a refined procedure for selecting representative conditions are presented. The main deliverables of the project regarding morphological developments in the short and medium-term are briefly described. An overview of typical results of simulations of the morphological impacts of land reclamation and natural developments over a period of several decades is presented. Comparisons between measured and modelled bathymetric developments confirm the suitability of the model for assisting coastal managers in decision-making processes. Recommendations are also made for further studies in areas where data gaps need to be filled and our knowledge of physical processes needs to be improved.

Zusammenfassung

Dieser Beitrag gibt einen Überblick zu Zielen, Strategien, und zu den wichtigsten Ergebnissen des rahmengebenden Forschungsprojekts „Vorhersage mittelskaliger Morphodynamik PROMORPH". Das Projekt ist in den Jahren 2000 bis 2002 vom Bundesminister für Bildung und Forschung finanziert worden. Beschreibungen der durchgeführten Arbeiten werden auf den folgenden Seiten dieses Bandes noch genauer vorgestellt. Das übergeordnete Ziel des Projekts lag darin, auf der Basis vorhandener Module prozessorientierte Modellsysteme zur Simulation der mittelskaligen Morphodynamik in Küstengebieten zu entwickeln, kalibrieren, validieren und anzuwenden. Arbeitsgebiet war die zentrale Dithmarscher Bucht zwischen Elbe- und Eider-Ästuar/Nordsee. Das Projekt fand in enger Zusammenarbeit und in besonderer Zusammenführung von Expertise, Kompetenz und Ressourcen aus mehreren deutschen Institutionen statt, namentlich den Instituten für Strömungsmechanik und Meteorologie der Universität Hannover und dem Forschungs- und Technologiezentrum Westküste der Universität Kiel in Büsum. Messdatenerhebung und Datenanalyse, aus denen sich Verbreitungsmuster der Hydrodynamik, Sedi-

mentdynamik und Morphodynamik ableiten lassen, werden beschrieben. Anwendungen vorhandener Modellsysteme im Zuge der Entwicklung eines gekoppelten Modells zur Simulation von Strömung, Seegang, Sediment Transport und Seebodenentwicklung werden vorgestellt und erläutert. Ein besonderes Augenmerk wird auf die Integration von Naturmessungen und numerischen Modellsimulationen gelegt, die zu einem verbesserten Verständnis der physikalischen Abläufe und der Vorhersagefähigkeit des Modells führen. Aufbau und Anwendung des mittelskaligen Morphodynamik-Modells, das eine fortentwickelte Prozedur zur Auswahl repräsentativer Bedingungen verwendet, werden vorgestellt. Zusammenfassend beschrieben werden Zentralergebnisse des Projekts mit Darlegung von Messabläufen einschließlich Entwicklung und Test neuer Messgeräte, Messdaten, sowie von prozessorientierten Modellen zur Simulation von Strömung, Seegang, Sediment Transport und Morphologienentwicklung in kurzen und mittleren Zeitskalen. Eine Übersicht über die Ergebnisse typischer Simulationen von Landgewinnungsmaßnahmen und natürlichen Morphologieentwicklungen für die Zeiträume von mehreren Dekaden wird gegeben. Vergleiche der gemessenen und simulierten Bathymetrie-Entwicklungen bestätigen das Potential des Modells, Küstenfachleute bei Entscheidungsabläufen zu unterstützen. Darüber hinaus werden Empfehlungen für weitere Untersuchungen in den Gebieten gegeben, in denen noch Daten- und Wissenslücken existieren.

Keywords

Promorph, Dithmarschen Bight, Short-Term and Medium-Scale Morphodynamics, Model Predictions, Research Needs, North Sea

Contents

1. Introduction

This paper gives an overview of the development of process-based models of flow, waves, sediment transport and bed evolution within the framework of the research project "PROMORPH – Predictions of Medium Scale Coastal Morphodynamics" funded by the German government. The research project was instigated by the need to develop coastal models for predicting morphological changes with time scales of years and decades. Such modelling efforts require accurate and computer-intensive simulations of flow, waves, sediment transport and morphological changes. Because the simulations of medium-scale morphodynamics are performed on the basis of input and process filtering techniques, high predictive capability of the process-based models is essential for the full range of conditions typical of the study area. Emphasis is placed on an evaluation of the performance of the models on the scales of relevance using field measurements with dense spatial and temporal coverage.

The project was initially funded by the German Ministry of Education and Research over a period of three years from 2000 to 2002 and has been continued up to the present. The research work carried out within the framework of the PROMORPH project was undertaken by a consortium comprised of the Institute of Fluid Mechanics and Meteorology of the University of Hannover and the Research and Technology Centre "Westcoast" of the University of Kiel (FTZ Büsum). The project relied extensively on close cooperation between several research institutes in Germany, with a pooling of expertise, efforts and resources. The project participants included experts in the fields of engineering, geology, meteorology and ecology as well as experimentalists and modellers. In conjunction with the main project a two-year investigation was also carried out by the FTZ Büsum and General Acoustics GmbH aimed at developing special devices for measuring near-bed suspended material concentrations.

The investigation area, covering about 600 km^2, is the central Dithmarschen Bight located on the German North Sea coast between the Elbe and Eider estuaries (Fig. 1). The study area may be easily accessed from the FTZ Büsum, thus making measuring campaigns less arduous. This particular area was also chosen owing to the availability of long-term monitoring data provided by government agencies as well as data collected during our own previous investigations. The morphology is dominated by tidal flats, sandbanks and a tidal channel system comprised of three tidal channels: the Norderpiep in the north west, the Suederpiep in the south west, and the Piep tidal channel, which originates at the confluence of the Norderpiep and Suederpiep. Under normal conditions the maximum mean water depth in the tidal channels is about 18 m, and approximately 50 % of the domain falls dry at low tide. The tidal flats and sandbanks are exposed at low water. The area is characterized by a meso-tidal regime with a mean tidal range of 3.2 m. Maximum wave heights in the study area are about 3-4 m along the edge of the tidal flats.

This paper summarises the aims, strategies, main findings and deliverables of the project. More detailed descriptions of the various investigations are presented in the following papers of this volume. They also describe the planning, execution and analysis of the field experiments required to determine the patterns of hydrodynamics, sediment dynamics and morphodynamics in the study area as well as the data necessary for adequately developing and testing the performance of the process-based models. The present paper also includes an overview of field measurements with a dense spatial and temporal coverage. The experiences gained in the continuing development and testing of existing measuring devices, especially for sediment concentration, are also outlined. The paper also describes the development of the process-based models and their application for predicting short-term and medium-scale morphological developments in the study area. The main deliverables of the project are listed,

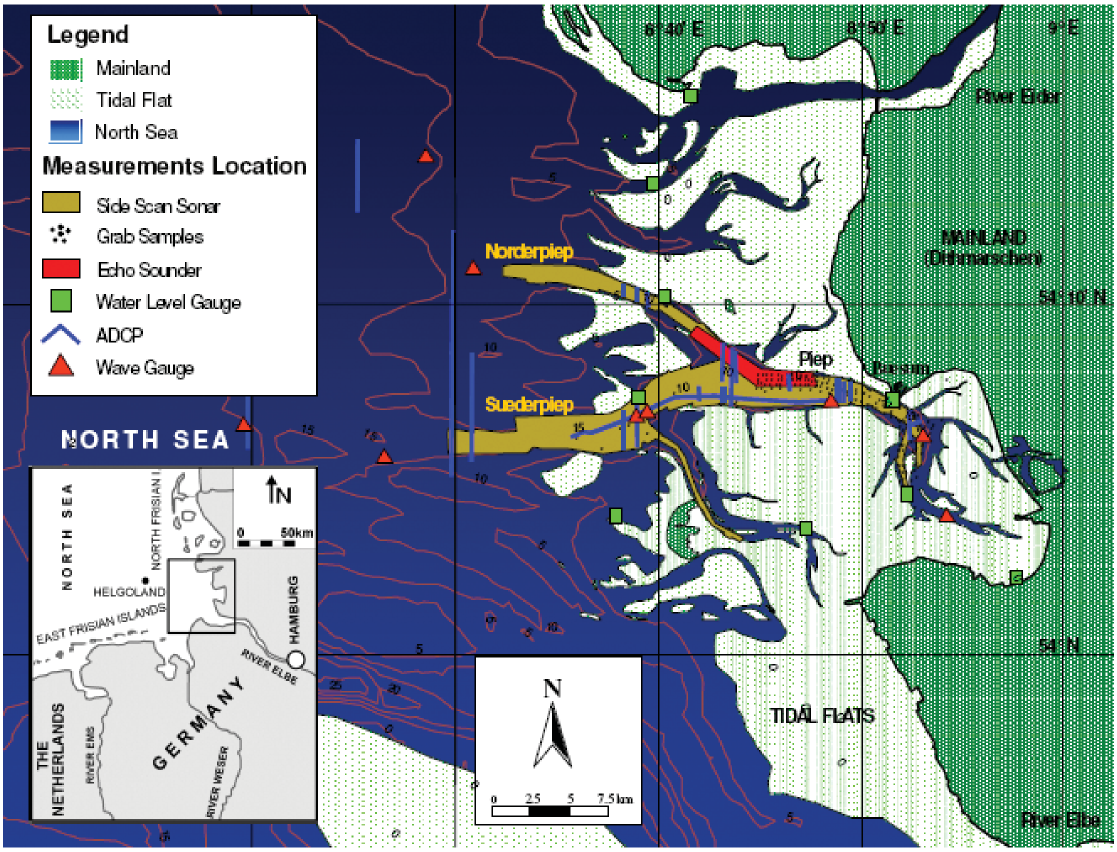

Fig. 1: Investigation area and measurement locations

and the research needs based on the investigations carried out within the framework of the project are identified. Recommendations are also made for further studies required to fill data gaps and improve our understanding of the physical processes involved.

It is hoped that the studies presented in this paper will serve as a platform for future research in the field of coastal engineering. This platform should also be helpful to practising engineers concerned with the evaluation of complex coastal behaviour as well as to coastal managers in the decision-making process relating to the planning and management of coastal areas, in particular the Dithmarschen Bight including the Elbe and Eider estuaries.

2. Objectives and Strategies

The main objective of the project described in the present paper was to develop and apply process-based numerical models for the simulation of morphological changes covering time scales of several years in a study area located on the German North Sea coast. In order to realise the project goals the following task areas were identified: 1) collection of suitable data to develop a model for simulating short-term and medium-scale morphodynamics, 2) planning of measurement strategies and testing of new devices specially designed to obtain the required data, 3) improvement of our understanding of the hydrodynamics, sediment dynamics and morphodynamics of the coastal system on the relevant time scales, 4) development and performance testing of process-based models of flow, waves, sediment transport and bed evolution for short periods covering the full range of conditions typical of the inves-

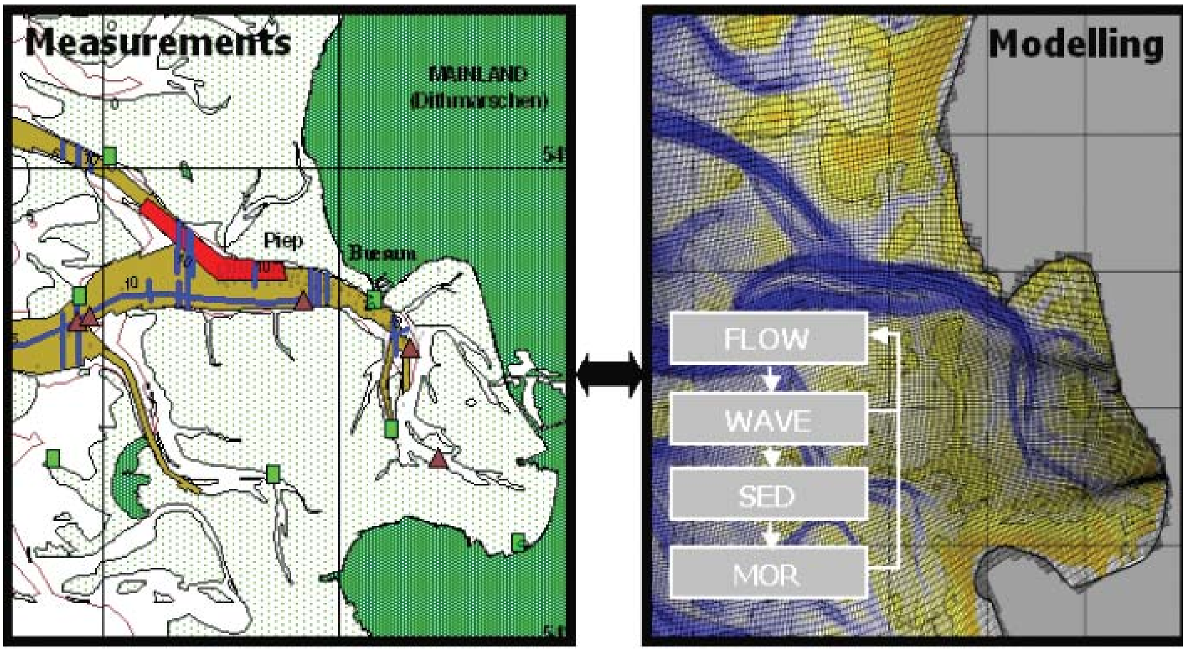

Fig. 2: Integration of process-based measurements and models

tigation area, 5) development and performance testing of a medium-scale morphodynamic model against field data covering several years, and 6) application of the validated model for predicting medium-scale morphodynamic behaviour.

In order to realise the project objectives special attention was focused on the integration of field measurements and numerical model simulations (Fig. 2). Process-based research consisting of field experiments, the compilation of existing data, the identification of information gaps, the planning and execution of measuring campaigns, field data analysis as well as the development of databases forms the basis of the investigations. The acquired data was used in the development and subsequent application of the process-based models. Two existing modelling systems were applied in the investigation area. The performance of these models for reproducing observed conditions was assessed. By adopting input and process filtering techniques the model for simulating morphological changes was further developed to yield a medium-scale morphodynamic model. In the development process special attention was given to the proper selection of representative conditions for the main driving forces, taking into account the morphological developments observed in the medium term. The model was subsequently applied for simulating the effect of individual storm events as well as for predicting morphological changes over periods of about ten years.

3. Field Experiments

In the planning and execution of the field surveys, special care was taken to ensure a dense spatial and temporal coverage of the study area for subsequent model development. The main purpose of the field data was to identify the most dominant physical processes governing medium-scale morphodynamics in the study area as well as to provide the data necessary for developing and evaluating the performance of process-based models for simulating hydrodynamics, sediment dynamics and morphodynamics. Testing of state-of-the-art measuring techniques and devices was also carried out.

Although numerical models find increasing application in coastal area management, such models are seldom tested thoroughly. The reason for this is that most of the measurements made in the past were only intended to clarify underlying physical processes and not for model development purposes. The evaluation of models, especially for coastal areas, imposes special requirements on field data, such as detailed measurements along the open sea boundaries and dense spatial and temporal coverage within the modelled area. As the predictive capability of models can be improved significantly with the aid of field measurements, emphasis was placed on the collection of complete sets of data for setting up and verifying the performance of the various process-based models.

Wind climate data, tidal levels, wave data and bathymetric data resulting from the monitoring programmes carried out by the relevant governmental agencies were supplemented by specially-designed field surveys providing dense spatial and temporal coverage of seabed and sediment characteristics, current velocities, suspended sediment concentrations, bed profiles etc. An overview of the spatial coverage of the field measurements is shown in Fig. 1. The field data were collected using a wide variety of devices and methods such as e.g. tide gauges, current meters, ship-mounted and stationary acoustic profilers, boomers, single beam, multiple beam and multiple frequency echo sounders, side-scan sonar, a selection of sediment and water samplers, and advanced remote sensing techniques.

Measurement campaigns were undertaken at regular time intervals (every few months) as well as for specific events. In order to obtain the data necessary to adequately validate the numerical models, a number of fully-equipped research vessels were deployed simultaneously so as to cover a larger area. Comprehensive data sets with dense spatial and temporal coverage were compiled for the purpose of model calibration and validation. An overview of the main investigations and the results obtained from an analysis of the measured data regarding patterns of hydrodynamics, sediment dynamics and morphodynamics is presented in the following.

3.1 Hydrodynamics

The patterns of hydrodynamics in the coastal system were investigated by TORO et al. (in this volume) based on measurements of water levels, current velocities and waves. The locations of these measurements are shown in Fig. 1. Water levels monitored by the Regional Office for Rural Areas in Husum (ALR Husum) were made available at several locations for tidal analysis and calibration of the flow models. The main tidal constituents that best represent the observed water levels at the tide gauge locations were derived from these data. Selective field measurements of current velocity at several cross-sections and locations were carried out in order to gain a better understanding of the spatial and temporal variations of flow in the main tidal channels. Due to low seabed roughness in the study area the vertical velocity distribution is fairly uniform. Owing to high tidal dominance, vertical profiles of temperature and salinity were found to be fairly uniform. This finding is consistent with the observed absence of vertical velocity stratification. Under normal conditions, flood dominance was identified in the cross-sections close to the seaward boundary of the investigation area. The maximum depth-averaged current velocity approximately doubles from neap to spring tide.

The analysis of field measurements has also helped to improve our understanding of wave characteristics in the study area. Information on waves was gathered from several sources. Wave data obtained from simultaneous measurements at five locations during a one-month period by the Coastal Research Station of the Lower Saxony Board of Ecology (CRS) on Norderney (NIEMEYER, 1997) were used for calibrating and validating the wave models. Measurements provided by the ALR Husum and the German Federal Maritime and Hydrographic Agency in Hamburg (BSH Hamburg) covering two longer periods of about 12 and 6 months yielded essential information regarding the range and probability of occurrence of wave characteristics. Maximum wave heights some 10 km westward of the outer tidal flats were found to be about 3.5 m. Wave heights of less than 2.0 m were measured along the edge of these tidal flats during the observation period. Based on the analysis of wave periods it was concluded that swell extends to the central part of the outer tidal flats, whereas locally-generated waves constitute the main source of energy further eastwards.

3.2 Sediment and Bed-Form Characteristics

The spatial distribution of seabed sediment characteristics in the upper layer over the tidal flats and in the tidal channels was investigated by RICKLEFS and ASP (in this volume) using side-scan sonar imagery as well as grab and water samples. The measurements covered the main tidal flats, sandbanks and tidal channels. It was found that the tidal flats are mainly comprised of fine sand and silt marked by a typical gradation from coarser sand in more exposed areas to finer deposits in sheltered regions. The maximum layer thickness of the young sediment deposits is about 20 m. The early Holocene consolidated clay exhibits a pronounced resistance to erosion, hence affecting bed roughness, sediment transport rates and morphological development. In the tidal channels the seabed is essentially comprised of sandy sediments and mud as well as consolidated deposits. In contrast to observations over the tidal flats, no clear trends could be identified regarding the spatial distribution of sediment sizes in the tidal channels. The very fine to medium-grain silt transported in suspension was found to be several times finer than bottom material (see POERBANDONO and MAYERLE, in this volume (a)). As the effect of bed roughness on sediment transport can be quite significant, investigations were carried out to determine the spatial and temporal variations of bed-form dimensions and associated roughness sizes (MAYERLE et al., in this volume (a)). Measurements of bed-form dimensions were performed at several locations using echo sounders and side-scan sonar devices. The spatial variation of bed-form dimensions was found to be quite significant and highly dependent on the layer thickness of potentially mobile sediments, the characteristics of surficial seabed sediments, and local flow conditions. Mega-ripples and dunes with lengths of up to about 20 m were mainly observed.

3.3 Sediment Dynamics

POERBANDONO and MAYERLE (in this volume (b)) studied the spatial distributions of suspended material concentration and transport on the basis of field measurements. Simultaneous measurements of current velocity were performed over several cross-sections using Acoustic Doppler Current Profilers (ADCPs) and optical beam transmissometers suspended from moving vessels. This investigation was focused on three cross-sections of the main tidal channels. Due to the small grain sizes of material transported in suspension and the high levels of turbulence induced by tides and waves, the vertical distribution of concentration was found to be fairly uniform. Depth-averaged suspended material concentrations of up to about 0.55 kg/m^3 were observed in the tidal channels. It was found that about 80 % of all material entering and leaving the system is via the Suederpiep tidal channel located in the south west. Estimates obtained with the aid of the numerical model indicate that most of this material is transported in suspension (WINTER et al., in this volume). Moreover, the sediment distribution over the vertical is clearly affected by the early Holocene layer, with limited sediment concentrations in the lower layers. In the deeper parts of the channels where the Holocene layer lies open no sediment is available for entrainment. This fact is clearly reflected in the sediment concentration profiles.

As the measurement of material concentrations in the near-bed region remains problematic, a special investigation programme was undertaken by the FTZ Büsum and General Acoustics GmbH to further the development of special devices for measuring near-bed sediment transport in the tidal channels. Two devices were tested for this purpose, namely a remote acoustic measurement device equipped with a special three-frequency echo sounder combined with a sophisticated digital signal processor system for cross-sectional measurements (EDEN et al., in this volume), and a moored near-bed sampling device designed for measuring and sampling sediment suspensions at a fixed location down to about 10 cm above the seabed (SCHROTTKE and ABBEG, in this volume). These systems were deployed simultaneously at a cross-section in the Piep tidal channel. It was found that both measuring systems are capable of resolving near-bed sediment concentrations reasonably well.

In conjunction with the main investigations, POERBANDONO and MAYERLE (in this volume (b)) tested the effectiveness of several methods for converting acoustic backscatter strength in the water column into suspended material concentrations at several locations in the main tidal channels. This investigation was based on simultaneous measurements performed using an ADCP, an optical beam transmissometer and a Niskin bottle sampler. The results confirm the acceptability of the investigated empirical approaches for converting acoustic backscatter strength into suspended material concentrations. This conversion offers the possibility of simultaneously measuring current velocities and suspended material concentrations, thus permitting direct estimates of sediment transport rates. By conducting measurements with ADCPs from moving vessels, a good spatial coverage can be achieved.

3.4 Morphodynamics

RICKLEFS and ASP (in this volume b) and WILKENS and MAYERLE (in this volume) studied the most significant morphological developments on different morphological time scales. Bathymetric data covering the central parts of the Dithmarschen Bight were made available by the BSH in Hamburg. The various digital data sets cover a time span of almost three decades (1974 to 2001) on a mainly annual basis. In order to evaluate medium and short-term morphological developments in the Piep channel system, several bed profiles at selected cross-sections were repeatedly surveyed by the FTZ Büsum from June 2000 to August 2003 (ASP, 2004 and RICKLEFS and ASP, this volume).

A clear landward migration of the most seaward located sandbanks has been observed during the past three to five decades. This was also confirmed by bathymetric survey and remote sensing data derived from optical sensor measurements and radar images (RICKLEFS et al., in this volume). In the deeper parts of the tidal channels the pronounced resistance to erosion of the early Holocene layer restricts morphological development to lateral migrations. Adaptation to land reclamation in the inner Meldorf Bight constitutes an additional ongoing process. Scouring of the channel beds in winter and infilling during the subsequent calm season is an active process on a seasonal scale, resulting in a trend towards narrowing and deepening of the tidal channels. Despite the scarcity of bathymetric measurements on the tidal flats, a tendency towards accretion is clearly evident.

The results of the analysis were applied to the definition of model strategies and representative conditions for the simulation of medium-scale morphodynamics. The data also served for calibrating and validating the numerical models.

4. Process-Based Models

Models of flow, waves, sediment transport and bed evolution have been used for the investigation area following the procedures of set-up, sensitivity studies, calibration and validation. Two modelling systems were employed within the scope of this study: the DELFT3D package, developed by Delft Hydraulics in the Netherlands (ROELWINK and VAN BANNING, 1994) and the TELEMAC modelling system, developed by the Laboratoire National d'Hydraulique of the Electricité de France (HERVOUET, 2000; GALAND et al., 1991). In both cases, two-dimensional depth-averaged (2DH) model approximations are implemented.

Fig. 3 shows the areas covered by the models in the present investigation. The DELFT3D model is based on a curvilinear grid covering the entire Dithmarschen Bight, including the Elbe and Eider estuaries, with a grid resolution ranging from 60 to 180 m. The TELEMAC model covers the central region of the bight, with a higher grid resolution ranging from about 30 to 80 m. In both cases the process-based models are coupled to yield a model for simulating morphological evolution. Fig. 3 illustrates the schemes adopted for the simulation of short and medium-term morphodynamics based on continuous model runs and the application of input filtering techniques, respectively.

The strategy adopted in the development of the coupled models for simulating bed evolution was as follows: initially, the flow and wave models were developed (PALACIO et al., in this volume and WILKENS et al., in this volume). At the same time the effectiveness of meteorological forcing for driving the process-based models was investigated (GROß and BENCKEL, in this volume). The calibrated and validated flow and wave models were then used to set up the sediment transport model (WINTER et al., in this volume). Finally, the various process-based models for simulating bed evolution changes were coupled (JUNGE et al., in this volume and WILKENS and MAYERLE, in this volume).

In order to achieve high model predictive capability for the full range of conditions typical of the study area special attention was given to the development and performance evaluation of the models with the aid of field data. Selective measurements of sediment characteristics, bed forms, water levels, current velocities, suspended sediment concentrations and transport rates with a dense spatial and temporal coverage were used for this purpose. In order to go beyond a purely descriptive and qualitative evaluation of model performance several statistical parameters were applied to obtain an objective assessment of model quality (PALACIO et al., in this volume). Moreover, existing quality standards for checking the performance of the models were adopted (WALSTRA et al., 2001 and VAN RIJN et al., 2002). As some of the statistical parameters require information on the accuracy of the measuring devices under field conditions, a method was proposed for this purpose (JIMÉNEZ GONZALEZ et al., in this volume).

The models applied in the investigation area were nested within a larger scale model covering the North Sea. The nesting sequence is based on the Continental Shelf Model

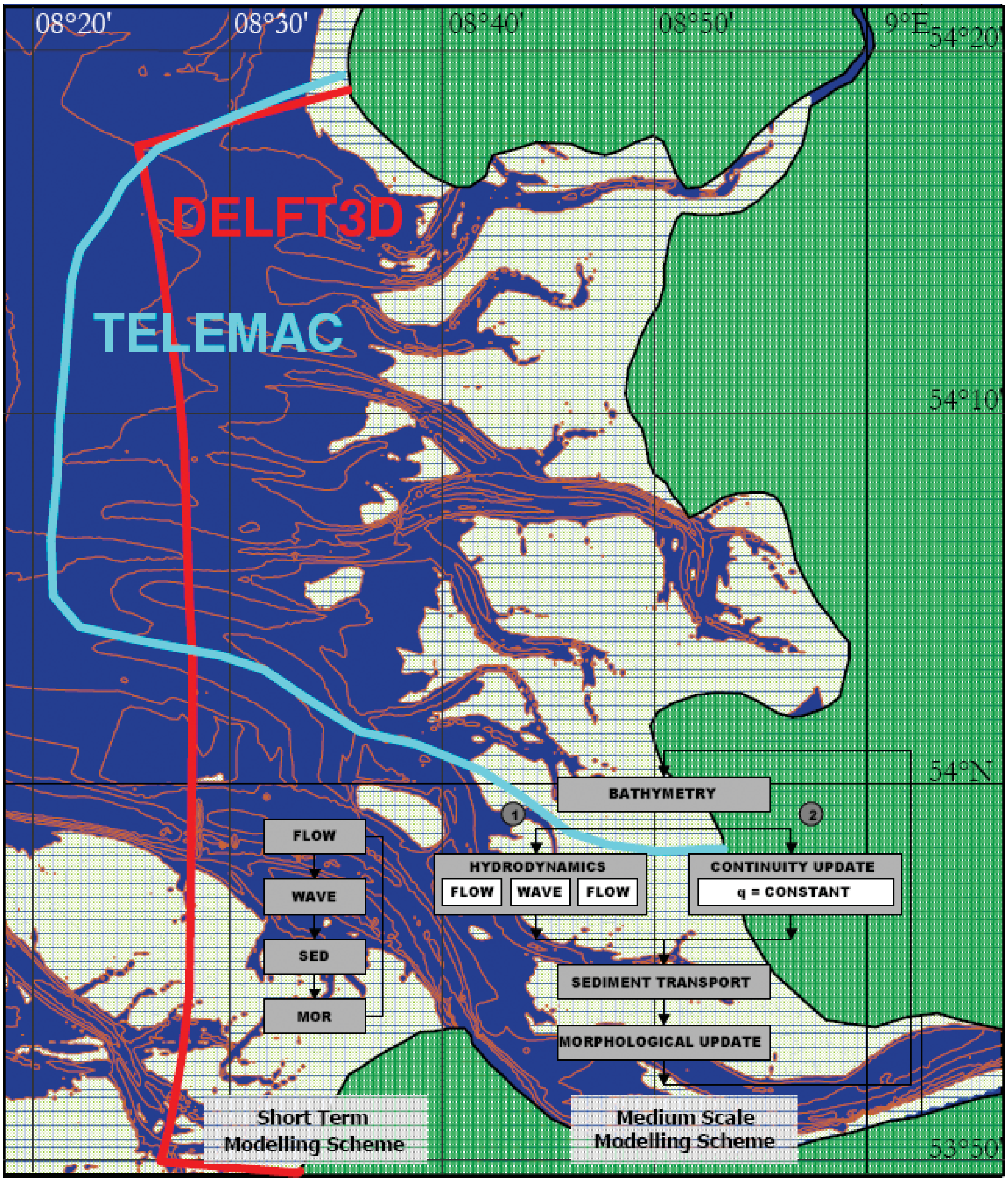

Fig. 3: Model domains and simulation schemes

(CSM) developed by Delft Hydraulics (VERBOOM et al., 1992). The flow model is driven by water levels resulting from the ten main astronomical tidal constituents along the open sea boundaries and by wind fields covering the entire North Sea. This nesting sequence was further extended for the simulation of waves and sediment transport (MAYERLE et al., in this volume (b)). This approach also permits the generation of open sea boundary conditions along other stretches of the German North Sea coast. On the basis of the available meteorological data it is possible to compute medium-scale morphodynamics over a time span of several decades.

4.1 Meteorological Forcing

The effectiveness of the meteorological models driving the process-based models was investigated by Benkel and Groß (in this volume). In this investigation comparisons were made between the results of the meteorological model of the German National Meteorological Service and the data from the PRISMA interpolation model developed by the Max Planck Institute of Meteorology in Hamburg (Luthardt, 1987). The PRISMA model generates synoptic meteorological forcing data for the entire North Sea by applying interpolation techniques to observations along the coastline and at other locations such as oil platforms. This data is available for the period 1989 to 2000. The results showed that although the PRISMA model tends to underestimate long-term mean wind speeds while overestimating the frequency and number of high wind speed events in Heligoland, the generated wind fields provide adequate forcing data for driving the flow and wave models applied in the study area (see also Mayerle et al., in this volume(b), Palacio et al., in this volume).

4.2 Flow Model

The results of model set-up, sensitivity studies, and model calibration and validation are summarised in Palacio et al. (in this volume). As the observed profiles of salinity, temperature and suspended material concentration are fairly uniform due to high levels of turbulence of the tidal flow (see Toro et al., in this volume and Poerbandono and Mayerle, in this volume), the 2DH approximation was considered to be sufficiently accurate. The flow model is driven by water levels along the open sea boundaries and flow discharges through the open boundaries across the mouths of the Elbe and Eider estuaries. Wind forcing is provided by the PRISMA interpolation model. It was found that hydrodynamic forcing along the open sea boundaries is the most significant factor governing the predictive capability of the model (Mayerle et al., in this volume(b)). The effect of spatially variable bed roughness on the flow field was found to be less significant (Mayerle et al., in this volume(a)). Sensitivity studies indicated that the effect of the seasonal variations in bathymetry observed by Ricklefs and Asp (in this volume) can have a significant effect on current velocities and may be partly responsible for the discrepancies observed between measured and computed values. The validation results showed that the model is capable of reproducing water levels and current velocities in the study area in fair agreement with observations. The mean absolute errors between computed and observed water levels at a number of locations covering periods of several months were found to be less than 10 cm and 20 cm at high and low water levels, respectively. The mean absolute errors between computed and observed depth-averaged current velocities at various cross-sections in the tidal channels were generally found to be less than 0.2 m/s. On the basis of the indicators of generally accepted quality standards (Walstra et al., 2001 and Van Rijn et al., 2002), computed current velocities can be considered to be between good and excellent.

4.3 Wave Model

Wilkens et al. (in this volume (a)) summarised the results of calibration, validation and subsequent application of four phase-averaged wave models in the central Dithmarschen Bight. These include the models HISWA (Holthuijsen et al., 1998) and SWAN (Booij et al., 1999 and RIS et al., 1999) that were set-up within the DELFT3D modelling system, and COWADIS and TOMAWAC (BENOIT et al., 1996), which are modules of the TELEMAC modelling system. The models are driven along the open sea boundaries by measured values or the results of the nesting sequence covering the German Bight (MAYERLE et al., in this volume (b)). Data recorded by five waverider buoys over a period of one month were used for calibration and validation purposes. On the basis of the quality standards usually adopted, the performance of the wave model regarding wave heights was found to vary between reasonable to good. Bearing in mind the complex hydrodynamic patterns and bathymetry of the study area, this result was considered satisfactory. The validated models were applied to analyse the wave height distribution over the study area during moderate conditions and storm scenarios. It was shown that during moderate conditions only locally-generated waves with limited heights occur in the sheltered eastern part of the domain. During storm conditions, however, wave heights may reach 2 m in the eastern part and 5 m near the outer edge of the tidal flats. The effects of waves on the flow field and vice versa were also investigated. The effect of current velocities on the wave field was found to be significant and was therefore taken into account in the computations (see Fig. 3). It could also be shown that waves have a limited effect on tidal currents in shallow areas and that wave-induced currents are negligible in the tidal channels. Boundary conditions for those periods with no wave measurements at the model's open sea boundaries were produced with a nesting sequence. For this purpose, the German Bight Model was implemented for wave computations and forced with PRISMA wind fields (MAYERLE et al., in this volume (b)).

4.4 Sediment Transport Model

WINTER et al. (in this volume) deployed the calibrated and validated flow and wave models for the set-up of the sediment transport model of the Central Dithmarschen Bight. The 2DH model computes the total load by the summation of bed and suspended loads. The suspended sediment concentrations are computed by solving the advection-diffusion equation whereas the bed load is determined on the basis of commonly accepted algebraic formulations. It was found that the predictive ability of the model can be improved significantly using measured profiles of suspended material concentration. Sensitivity studies to determine the effects of bed roughness on sediment transport clearly indicated the relevance of the spatial variation of bed roughness in sediment transport computations. Small variations in the bed roughness can have a significant effect on the resulting sediment transport rates. This was also confirmed by the investigations carried out by MAYERLE et al. (in this volume (a)). A quantitative assessment of model quality was carried out on the basis of parameters such as the discrepancy ratio and the adjusted relative mean absolute error. The results showed that the model is capable of predicting sediment concentrations in fair agreement with observations, with a less than two-fold discrepancy between all computed and measured values.

4.5 Bed Evolution Model

The model used for predicting short and medium-term morphological evolution was built by coupling the flow, wave and sediment transport modules on the basis of a bed evolution algorithm. The ability of the model to simulate short-term morphological developments was investigated on the basis of a 'real time' hindcast of a well-documented severe storm in the south-eastern part of the German Bight (WILKENS and MAYERLE, in this volume). The simulations were performed over a period of about 12 days with high temporal resolution of the imposed conditions and computed morphological changes. The results obtained were found to be in reasonable agreement with observations.

5. Medium-Scale Morphodynamic Model

The coupled process-based model for the simulation of flow, waves, sediment transport and bed level evolution was upgraded to a model for simulating medium-scale morphodynamics (JUNGE et al., in this volume and WILKENS, 2004). In order to limit computational requirements input and process reduction techniques were applied for tidal action and swell along the open sea boundaries as well as for the local wind field.

An enhanced procedure was adopted for selecting representative morphodynamic forcing based on an analysis of medium-term morphological evolution (Fig. 4). This procedure includes the definition of a representative tide, identification of the most relevant morphological developments on the medium scale, selection of sub-domains for volumetric analysis and adjustment of representative wave and wind climates. A morphological tide, which is a representative tide yielding a residual transport similar to that of a full spring-neap tidal cycle defined according to the approaches by STEIJN (1992) and LATTEUX (1995), was initially selected (JUNGE et al., in this volume and WILKENS and MAYERLE, in this volume). The representative wave and wind climates were adjusted by comparing modelled and measured bathymetric maps over a period of about 10 years from 1977 to 1987. For this purpose the study area was split into several sub-domains, taking into account the most predominant morphological developments and driving forces. Fine-tuning of the representative wind and wave climates was carried out separately for each sub-domain. By comparing computed morphological changes during storm events to averaged yearly morphological changes (WILKENS, 2004 and WILKENS and MAYERLE, in this volume) it was concluded that the inclusion of a few storms in a one-year morphodynamic simulation has a very limited effect on the resulting morphodynamics on the medium scale. Storm conditions were thus considered to be represented by the imposed swell and wind climate.

The representative conditions were validated on the basis of sedimentation and erosion patterns as well as volumetric analyses in several sub-domains of the central Dithmarschen Bight over a ten-year period from 1990 to 2000. Despite the different trends in morphological developments in different sub-domains of the investigation area, good agreement was obtained in overall terms regarding both morphological trends and quantitative changes in bed levels. On the basis of the latter it was concluded that the model is adequately capable of predicting medium-term morphological developments.

The results of applying the modelling system to forecast natural morphological developments over the period 1999 to 2009 and the significance of natural and anthropogenic influences due to land reclamation carried out in 1972 and 1978 are presented by JUNGE et al., (in this volume), WILKENS, 2004 and WILKENS and MAYERLE, (in this volume). The fact that the model developed for the investigation area was set up within a nested sequence as part of the entire north-west European Continental Shelf Model means that it may be applied to other coastal areas of the North Sea.

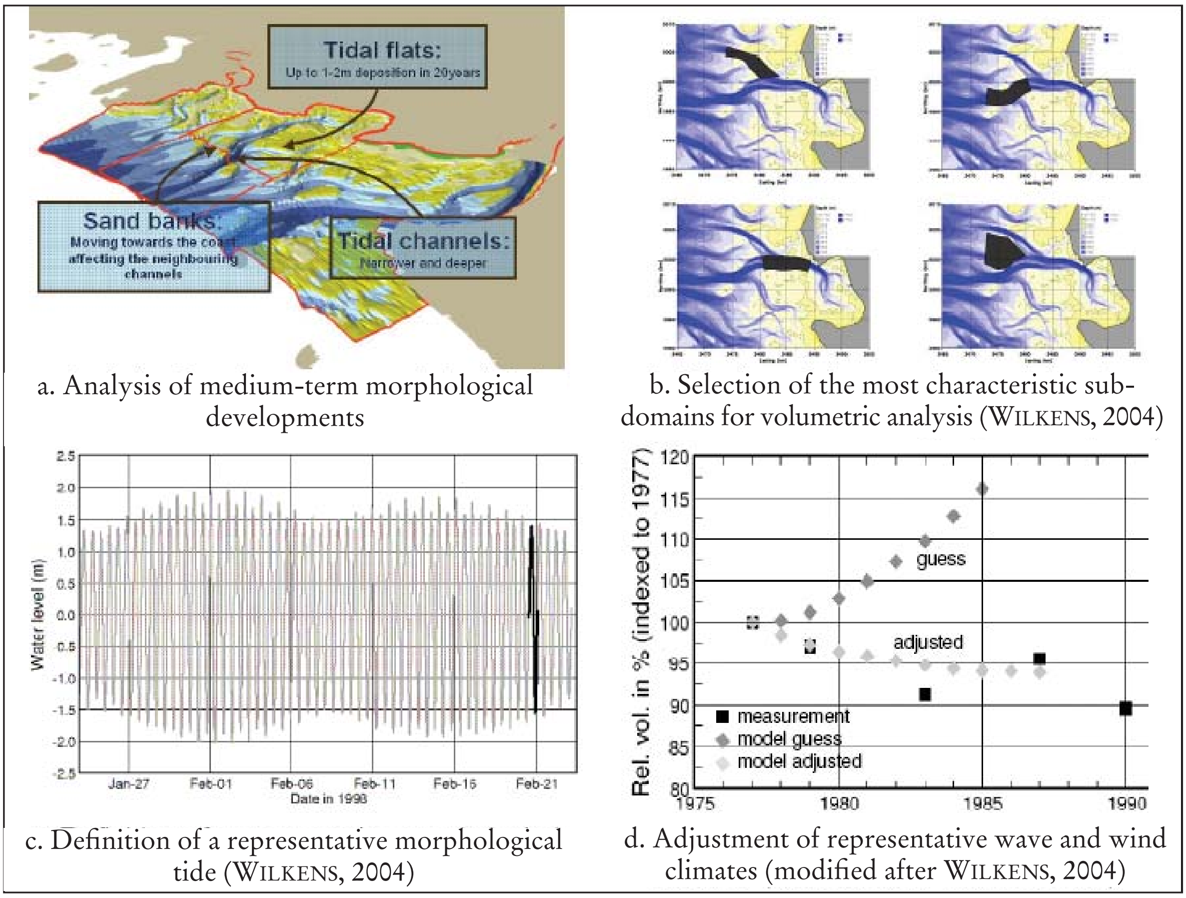

a. Analysis of medium-term morphological developments

b. Selection of the most characteristic sub-domains for volumetric analysis (WILKENS, 2004)

c. Definition of a representative morphological tide (WILKENS, 2004)

d. Adjustment of representative wave and wind climates (modified after WILKENS, 2004)

Fig. 4: Procedure proposed for the selection of representative forcing conditions

6. Main Deliverables

Having improved various aspects of coastal research, such as a denser spatial and temporal coverage of field data, the development of special measuring procedures and devices and the advancement of process-based models the latter may now be applied in future research or to perform numerical computations with more confidence. Further information is presented in the following sections.

6.1 Field Data

Field data on wind climate, tidal levels, waves and bathymetry were available from the ongoing monitoring programmes of governmental agencies. Information based on field measurements carried out within the framework of the PROMORPH research project with a dense spatial and temporal coverage of the seabed and sediment characteristics, bed forms and bed roughness, current velocities, suspended sediment concentrations and bed profiles were also available. These extensive field measurements provide an ideal database for improving our understanding of the physical system.

Besides clarifying various aspects of the modelling strategy, these data also served for testing the performance of the numerical models and assisted in the selection of a 2DH model approximation.

A database containing the data used in the investigation has now been established (JUNGE, in this volume). The stored information relates to the various aspects of the study presented and analysed in several papers of this volume and includes data sets describing the hydrodynamics, sediment characteristics, sediment dynamics and morphodynamics in the study area (POERBANDONO and MAYERLE, in this volume (a), RICKLEFS and ASP, in this volume, RICKELFS et al., in this volume and TORO et al., in this volume).

6.2 Measuring Procedures and Devices

Various techniques of field measurements have been investigated in order to provide optimum input data for the numerical models. Suggestions were made regarding the acquisition of the required data, such as current velocities in the tidal channels (TORO et al., in this volume) bed forms, and sediment concentrations (MAYERLE et al., in this volume (a)) and the suggested techniques were applied in the field studies. A new approach for estimating the accuracy of measuring devices under field conditions has also been proposed (JIMÉNEZ GONZALEZ et al., in this volume). In addition to a demonstration of the effectiveness of remote sensing strategies for collecting information on medium-term bathymetric developments (RICKLEFS et al., in this volume), advancements have also been made in the development of measuring devices for suspended material concentration (EDEN et al., in this volume, SCHROTTKE and ABEGG, in this volume, POERBANDONO and MAYERLE, in this volume).

6.3 Short-Term Morphodynamic Model

As already mentioned in Section 4.5, the model for simulating short-term morphological evolution was created by coupling the process-based models for flow, waves and sediment transport via the bed evolution model (Fig. 5). Fig. 6 shows the grid system employed in the simulations. The set-up procedure, results of sensitivity studies relative to the main numerical and physical parameters, and the calibration and validation of these models against field data were fully documented by e.g. PALACIO et al. (in this volume), MAYERLE et al. (in this volume (b)), WILKENS et al. (in this volume), WINTER et al. (in this volume) and WILKENS and MAYERLE (in this volume). The simulations of water levels, current velocities, waves, sediment transport and nutrient dynamics using these models have been shown to be in good agreement with observations. Short-term morphodynamic simulations are carried out continuously. The model may serve to assist coastal managers in questions relating to waste water management or in studies of morphological changes resulting from natural causes such as storm events or due to anthropogenic interventions such as land reclamation. Recommendations for improving the performance of the numerical models for coastal areas through the integration of field measurements and models have been derived and successfully applied within the framework of the project.

6.4 Medium-Scale Morphodynamic Model

A model with a temporal scale of up to about a decade combined with a spatial scale in the order of several kilometres was constructed using input and process reduction techniques. This model was to perform medium-scale morphodynamic simulations with a focus on the description of morphological features such as sand banks, tidal flats and tidal channels in the central Dithmarschen Bight. The calibration and validation of this model was carried out on the basis of over 20 years of bathymetric measurements. Comparisons between computed and observed morphological changes in the central Dithmarschen Bight (JUNGE et al., in this volume, WILKENS (2004) and WILKENS and MAYERLE, in this volume) show good agreement in both qualitative and quantitative terms. An improved selection process for representative conditions has been proposed and successfully applied, and is now available for use elsewhere. The morphological evolution from 1977 till 1987 was used to evaluate and improve model performance. The quality of the model in predicting the medium scale morphodynamics was verified from 1990 till 1999.

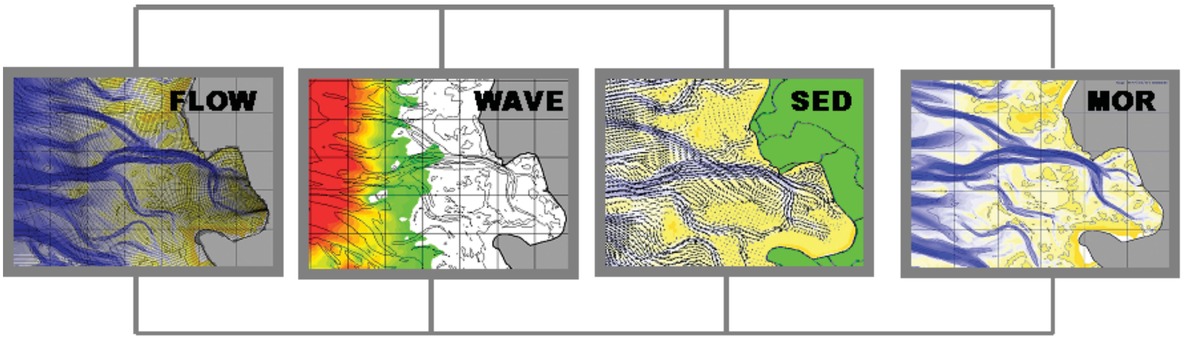

Fig. 5: Model family for the simulation of hydrodynamics, sediment dynamics and morphodynamics

6.5 Model Predictions

With regard to medium-scale morphodynamics our model will be helpful to coastal engineers for predicting morphological changes resulting from natural causes or anthropogenic interventions. Various applications of the developed models for supporting coastal managers in decision-making processes are summarised in JUNGE et al. (in this volume), WILKENS (2004) and WILKENS and MAYERLE (2004). We recommend that such models be used for scientific research, engineering analysis and design, and decision-making in the planning and management of coastal waters including issues on climatological changes and sea level rise. The existing model may be used among other things to investigate the effect due to land reclamations similar to those at the Meldorf Bight; due to the construction of coastal structures such as the Eider Storm Surge Barrier and due to the dredging activities in the Elbe Estuary that may impact on the adjacent coastal areas. The set-up of the model within a nesting sequence supports its application in other coastal areas of the North Sea. Fig. 7 shows typical results of the application of the model for predicting medium-term morphological developments. Fig. 7a shows the morphological developments along the eastern boundary of the Meldorf Bight following the construction of two dikes in 1972 and 1978, respectively. As a result of land reclamation the area of the Meldorf Bight was reduced by approximately 40 %, thereby decreasing the drainage area of the Piep tidal channel. Changes in the relative wet volume of the Meldof Bight over a thirty-year simulation period are presented. Both measurements and model results indicate a clear tendency towards a reduction in the relative wet volume at a diminishing rate with respect to time. Predictions of medium-scale morphodynamics have also been made in the central parts of the Dithmarschen Bight. Typical results for the Tertiussand tidal flat are shown in Fig. 7b. The predicted change in the trend of morphological developments from 1999 onwards is due to the formation of a new channel connecting the Suederpiep tidal channel with the open sea.

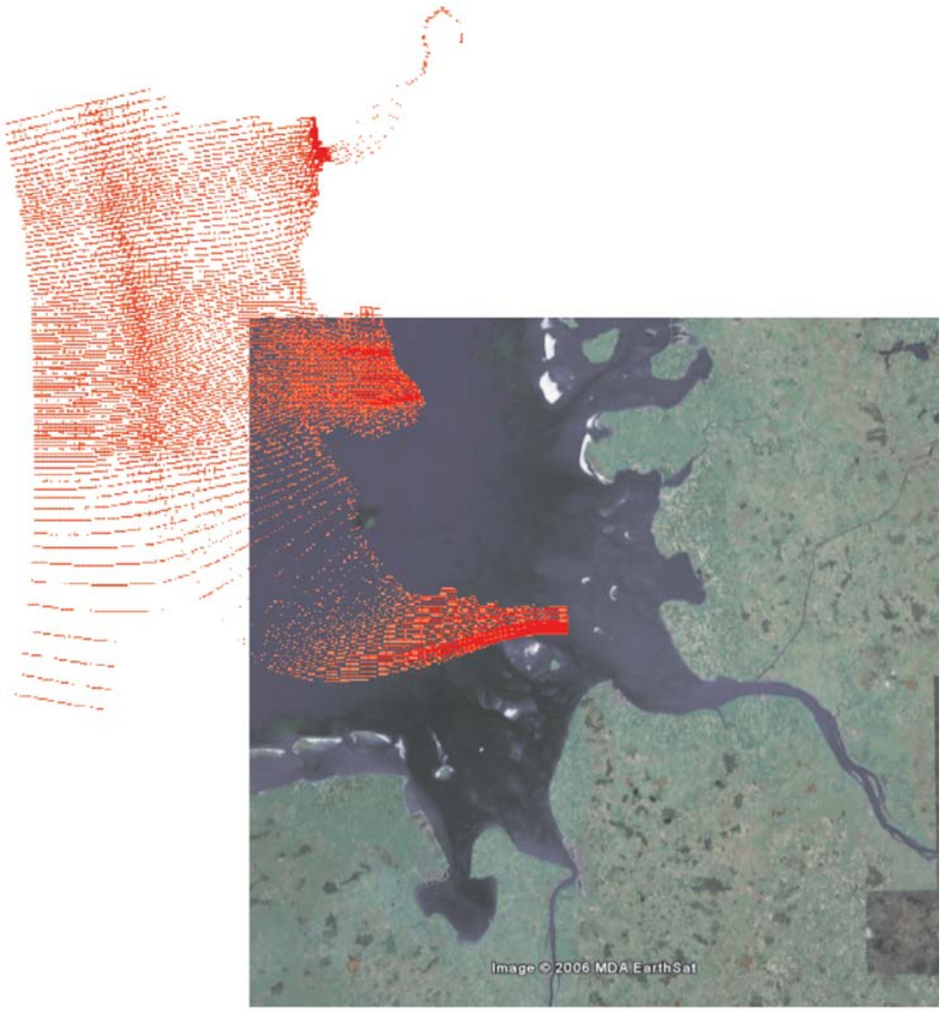

Fig. 6: Model domain and grid

7. Developments to Date and Future Research Needs

Significant advancements have been made in recent years regarding near-shore measuring techniques and the numerical modelling of coastal areas. With the exception of sediment concentration and transport the measurement of most of the remaining physical quantities has become standard practice. Instead of point measurements, there is an increasing shift towards measurements over wider areas with a dense spatial and temporal coverage using non-intrusive measuring devices. Moreover, the accuracy of measuring instruments under field conditions is steadily improving. In conjunction with the new developments in measuring devices and techniques there was also a rapid development of numerical models for coastal areas. Models for flow and waves have advanced significantly and have been applied successfully to many coastal areas worldwide. Owing to the difficulty of collecting field data on suspended sediment concentrations and the inherent complexity of sediment transport processes, morphodynamic modelling is still in its infancy. As most of the equations used in morphodynamic models are based on the results of laboratory experiments, uncertainties still remain regarding their applicability under field conditions.

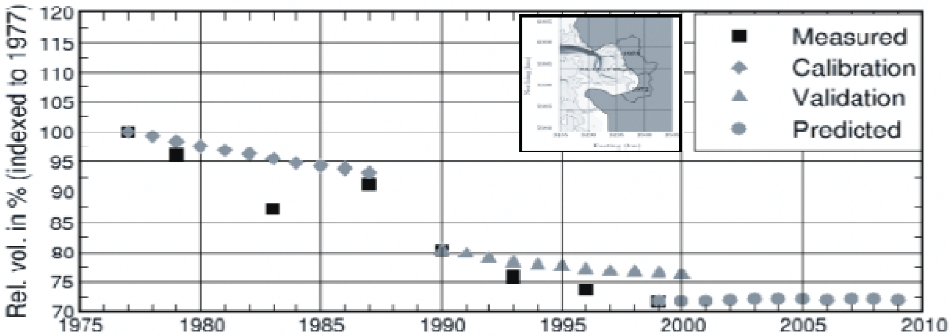

(a) Relative wet volume of the Meldorf Bight resulting from land reclamation (WILKENS and MAYERLE, 2004)

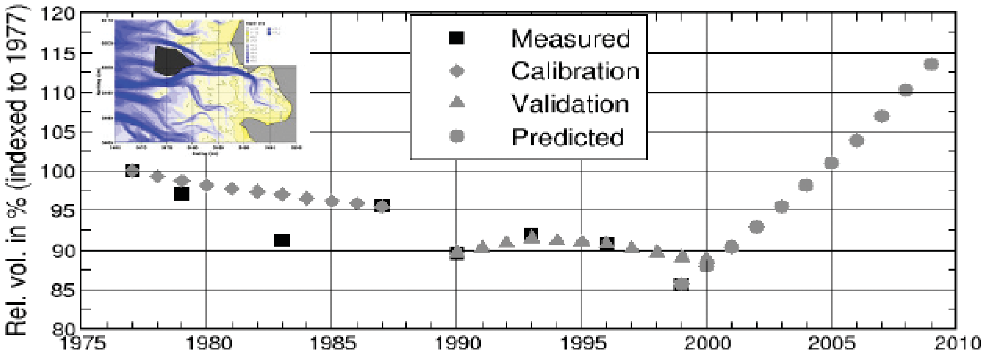

(b) Relative wet volume of the Tertiussand tidal flat (JUNGE et al., this volume)

Fig. 7: Predictions of medium-scale morphodynamics (s.a.)

Modelling of the governing processes of morphological developments for predicting coastal evolution has also advanced significantly. Anthropogenic interventions often have a significant impact on flow and sediment transport patterns and, therefore, their effect on coastal morphodynamics can be reasonably well predicted. Morphological developments due to natural causes, however, are more difficult to trace and to simulate. The modelling of short-term morphodynamics is usually performed continuously with coupling of the component process-based models. As already mentioned, the predictive capability of these models is dependent to a large extent on the performance of the models. Due to a scarcity of data and inaccuracies in measuring bed level changes in the short term, such models are seldom calibrated or validated. Medium-scale morphodynamic models incorporate input and process filtering techniques. The predictive capability of these models thus depends on the proper selection of representative conditions. The availability of bathymetric measurements covering the area of interest on a yearly basis is also essential for improving the predictive capability and reliability of such models.

The findings from the PROMORPH research project also enabled recommendations to be made regarding further studies and research necessary to fill data gaps and improve our knowledge of the physical system. Specific areas are identified in which basic and applied research is still required. The recommendations focus in particular on requirements concerning the development and application of coastal area models using existing modelling systems.

7.1 Measurement Requirements

As already mentioned, a lack of understanding of sediment dynamics due to the difficulties in performing accurate measurements under field conditions still remains one of the main limitations in coastal research. In order to fill data gaps and improve our knowledge of the underlying physical processes measuring devices need to be further developed. This is important, in particular, for measuring sediment transport near the seabed. In this context, the necessary adjustment of existing transport formulae to more adequately describe field conditions suffers from a lack of suitable field data. The majority of empirical equations for describing sediment transport rely on experiments carried out in the laboratory. It is therefore recommended to perform simultaneous measurements of bed forms, bed roughness, seabed characteristics, and sediment concentration and transport at several locations for a wide range of conditions. This would permit the testing and improvement of existing equations and/or the development of new sediment transport formulae, and, consequently, advance developments in morphodynamic modelling.

7.2 Modelling Requirements

An overview of modelling research needs for the simulation of short and medium-scale morphodynamics is presented in the following. Emphasis should be placed on the definition of quality standards and the selection of statistical parameters to be considered for verifying the performance of the various process-based models at different spatial and temporal scales. In order to advance developments in sediment transport modelling, the spatial and temporal variations of bed forms and bed roughness as well as their effects on sediment transport should be investigated in more detail.

Studies are also required to improve our knowledge of near-bed boundary conditions for solving the advection-diffusion equation for suspended sediment transport, taking into account the variation of seabed characteristics. It is also recommended to carry out further research on the coupling of flow, wave and sediment transport models. Although such coupling has been implemented successfully in several existing models, this approach has seldom been tested using field data. The use of field data for this purpose will provide better descriptions of bed shear stresses and permit more accurate estimates of sediment transport, particularly in the near-bed region.

As far as the modelling of medium-scale morphodynamics is concerned, we have also identified several areas on which future research should be focused. In order to improve the predictive capability of the numerical models these should include more detailed descriptions of the physical system. An example of this is the presence of the early Holocene layer in the investigation area. Unless this layer is properly identified with the help of field measurements and accounted for, both in the sediment transport and bed evolution models, it will not be possible to correctly reproduce sediment transport patterns and lateral migration of the tidal channels. Moreover, the representative conditions for tides, which are usually restricted to lunar cycles, should be extended to take additional account of seasonal effects. The chronology of waves and storm events in relation to medium-term morphodynamics is another aspect that should be investigated. In order to extend the temporal scale of the predictions, attention should also be given to descriptions of sediment concentrations in deeper areas. Equilibrium transport formulations, which are usually adopted to estimate the amount of sediment entering and leaving the coastal area, assume an instantaneous response of the sediment load to local equilibrium hydrodynamic conditions. Under certain conditions, however, the vertical sediment distribution and time lag effects along the open sea boundaries can have a significant influence on the results. In view of the latter, sediment transport models incorporating non-equilibrium equations covering the adjacent sea area should be applied to obtain a better representation of sediment concentrations along the open sea boundaries.

7.3 Model Applications

The modelling systems and strategies developed within the framework of the PROMORPH project should be extended for application in other coastal areas. In particular, further application of the modelling system is recommended for predicting short-term and medium-scale morphological developments due to natural causes and anthropogenic interventions. The monitoring of selected areas and the continuous development of numerical models in close cooperation with governmental agencies would greatly advance developments in this field.

It is also important to develop criteria for defining optimum locations and frequencies of measurements in order to provide the minimum data required for adequately verifying model performance and checking the need to implement three-dimensional model approximations. As complete sets of data covering periods of several decades are seldom available, the results of model simulations may be used to fill data gaps. With this aim in mind, the 40-year time series of HIPOCAS data sets (Weiße et al., 2003) for wind, water levels and waves are currently being validated within the framework of the project “Modelling of Medium-Term Wave Climate in Selected Coastal Areas of the German North Sea – MOSES” (KFKI 80) funded by the German Ministry of Education and Research from 2004 to 2007.

The set-up of models for nowcasting will also promote developments in measuring and modelling strategies. The possibility of measuring and modelling conditions in quasi-real time will provide a much better understanding of the processes involved and assist in defining measuring campaigns specially tailored to provide the required data for further model development. Investigations relating to the above are presently underway within the framework of the research project “Nordsee Monitoring System” funded by the Ministry of Science, Economics and Transport of the State of Schleswig-Holstein from 2005 to 2008. In addition to extensive field measurements using a wide range of modern devices, the model family developed within the framework of the PROMORPH project has been improved and already implemented in a nowcasting system at the FTZ Büsum.

8. Concluding Remarks

Process-based models for simulating medium-scale morphodynamics have been developed within the framework of the research project entitled “PROMORPH – Predictions of

Medium – Scale Coastal Morphodynamics". Based on the purpose of the study investigations were concluded satisfactorily and have added significantly to measuring and modelling strategies and techniques.

Special attention was placed on the integration of field measurements in numerical model simulations, leading to an improvement in our understanding of the physics of the system and the predictive capability of the developed models. Several new strategies for field measurements as well as for the development of process-based numerical models in the hydrodynamic and morphodynamic field have been proposed and implemented. In addition to comprehensive data sets specially tailored to match the needs of model development, advancements have been made in the development of measuring strategies and devices for sediment transport investigations.

On the basis of the two modelling systems, i.e. the DELFT3D and TELEMAC packages, simulation models were developed for the Dithmarschen Bight. These process-based models for the simulation of water levels, current velocities, waves and wave-induced currents, sediment transport and bed evolution in the short and medium term were calibrated and verified against extensive field data. Applications of the model system to reproduce a wide range of conditions have confirmed its suitability for use in scientific research, engineering analysis and design, and decision making in the planning and management of coastal waters.

Recommendations for further research have been identified. It has been shown that advancements in the measuring and modelling field can be enhanced by more stringently integrating field measurements. In order to fill information gaps future research should concentrate on field measurements of sediment dynamics in the near-bed boundary layer. An evaluation of the performance of the process-based models in a more quantitative way and the development of suitable quality standards is recommended. Emphasis should also be placed on the continuing development of input filtering techniques to provide a better description of the forcing conditions for tides, waves and sediment transport for medium-scale morphodynamic simulations. In order to advance developments in field applications it is also recommended to extend the approaches and strategies adopted in the present investigation to other coastal areas of the North and Baltic seas.

9. Acknowledgements

The authors wish to thank the German Ministry of Education and Research (BMBF) for funding the PROMORPH project (Funding number 03 F 0262A/ 03F0262B) from 2000 to 2002. Funds provided by the German Academic Exchange Service (DAAD) in Germany, COLCIENCIAS in Colombia and CAPES in Brazil for financing the doctorate studies of Dr. Poerbandono, Dr. Pramono, Dr. Asp and Dr. Palacio are also highly appreciated. We would like to thank Mr. Peter Petersen (KFKI Head of Coastal Research from 1988 to 2002) for his valuable support throughout the research project. Within the framework of the project we also appreciate the cooperation with our colleagues from the Institutes of Fluid Mechanics and Meteorology of the University of Hanover, the Research and Technology Centre "Westcoast" of the University of Kiel, and the GKSS Institute for Coastal Research. We are also grateful to the staff of the Research and Technology Centre "Westcoast" of the University of Kiel for their support during the measurement campaigns and in the analysis of field data. The support and cooperation of the following German governmental agencies is highly appreciated: the Regional Office for Rural Areas (ALR) in Husum, the Coastal Research Station of the Lower Saxony Central State Board for Ecology (CRS Norderney), the Federal Maritime and Hydrographic Agency (BSH Hamburg) and the German National Meteorological Service (DWD). The authors also express their thanks to the Max Planck Institute of Meteorology in Hamburg for providing the PRISMA model data. We are also indebted to Dr. Ian Westwood for his meticulous corrections and final proofreading of the English manuscripts. We also wish to thank Dr.-Ing. V. Barthel as well as the anonymous reviewers for their constructive remarks on the papers of this volume.

10. References

ASP NETO, N. E.: Long- to Short-term Morphodynamic Evolution of the Tidal Channels and Flats of the Dithmarschen Bight, German North Sea, Ph.D. thesis, University of Kiel, Germany, 2004.

BENKEL, A. and GROß, G.: Meteorological Data and Wind Field Modelling in the Dithmarschen Bight, Die Küste, Heft 69, 2005.

EDEN, H.; HENSSE, J. and MÜLLER, V.: Investigations on Transient Sediment Dynamics by DSLP-Method, Die Küste, Heft 69, 2005.

GALLAND, J.-C.; GOUTAL, N. and Hervouet, J.-M.: TELEMAC A New Numerical Model for Solving Shallow Water Equations, Adv. Water Resources, 14 (3), 1991.

HARTSUIKER, G.: Deutsche Bucht and Dithmarschen Bucht, Set-up and calibration of tidal flow models. Delft, Delft Hydraulics, Report H1821, 1997.

Hervouet, J.-M.: TELEMAC Modelling System: an overview. In: Hervouet, J.-M. and P. Bates. Special Issue: The TELEMAC Modelling System. Hydrological Processes, 14 (13), 2209–2210, 2000.

JIMÉNEZ GONZALEZ, S.; MAYERLE, R. and EGOZCUE, J. J.: A Proposed Approach for the Determination of the Accuracy of Acoustic Profilers for Field Conditions, Die Küste, Heft 69, 2005.

JUNGE, I. and SCHUBERT B.: Exchange and Archiving of Measurement Data Within the Research Project PROMORPH, Die Küste, Heft 69, 2005.

JUNGE, I.; WILKENS, J.; HOYME, H. and MAYERLE, R.: Modelling of Medium-Scale Morphodynamics in a Tidal Flat Area in the South-Eastern German Bight, Die Küste, Heft 69, 2005.

LATTEUX, B.: Techniques for Long-Term Morphological Simulation under Tidal Action, Marine Geology, Vol. 126, 1995.

MAYERLE, R.; PRAMONO, G. and ESCOBAR, C.: Dimension and Roughness Distribution of Bed Forms in Tidal Channels in the German Bight, Die Küste, Heft 69, 2005 (a).

MAYERLE, R.; WILKENS, J.; ESCOBAR, C. and WINDUPRANATA, W.: Hydrodynamic Forcing along the Open Sea Boundaries of Small-Scale Coastal Models, Die Küste, Heft 69, 2005 (b).

PALACIO, C.; MAYERLE, R.; Toro, M. and JIMÉNEZ, N.: Modelling of Flow in a Tidal Flat Area in the South-Eastern German Bight, Die Küste, Heft 69, 2005.

POERBANDONO and MAYERLE, R.: Composition and Dynamics of Sediments in Tidal Channels of the German North Sea Coast, Die Küste, Heft 69, 2005 (a).

POERBANDONO and MAYERLE, R.: Effectiveness of Acoustic Profiling for Estimating the Concentration of Suspended Material, Die Küste, Heft 69, 2005 (b).

RICKLEFS, K. and ASP NETO, N. E.: Geology and Morphodynamics of a Tidal Flat Area Along the German North Sea Coast, Die Küste, Heft 69, 2005.

RICKLEFS, K.; LEHNER, S. and RAUSCH, J.: Morphological Changes in a Tidal Flat Area: A Comparison of Radar, Optical and In-Situ Data, Die Küste, Heft 69, 2005.

ROELVINK, J. A. and VAN BANNING, G. K. F. M.: Design and Development of DELFT3D and Application to Coastal Morphodynamics, Hydroinformatics ’94, Verwey, Minns, Babovic & Maksimovic [eds], Balkema, Rotterdam, pp. 451–455, 1994.

SCHROTTKE, K. and ABEGG, F.: Near Bed Suspended Sediment Dynamics in a Tidal Channel of the German Wadden Sea, Die Küste, Heft 69, 2005.

STEIJN, R. C.: Input Filtering Techniques for Complex Morphological Models, Delft Hydraulics Report, H 824.53, 1992.

TORO, F.; MAYERLE, R.; POERBANDONO and WILKENS, J.: Patterns of Hydrodynamics in a Tide-Dominated Coastal Area in the South-Eastern German Bight, Die Küste, Heft 69, 2005.

VAN RIJN, L. C.; WALSTRA, D. J. R.; GRASMEIJER, B.; SUTHERLAND, J.; PAN, S. and SIERRA, J. P.: Simulation of Nearshore Hydrodynamics and Morphodynamics on the Time Scale of Storms and Seasons Using Process-Based Profile Models. In Van Rijn, L. C., B. G. Ruessink and J. P. M. Mulder (ed.), The Behaviour of a Straight Sandy Coast on the Time Scale of Storms and Seasons: Process Knowledge and Guidelines for Coastal Management: End Document March 2002. EC MAST Project, MAS3- CT97-0086 COAST3D – EGMOND, 2002.

VERBOOM, G. K.; DE RONDE, J. G. and VAN DIJK, R. P.: A Fine Grid Tidal Flow and Storm Surge Model of the North Sea, Continental Shelf Research, Vol. 12, No. 2/3, pp. 213–233, 1992.

WALSTRA, D. J. R.; VAN RIJN, L.; BLOGG, H. and VAN ORMONDT, M.: Evaluation of a Hydro-Dynamic Area Model Based on the COAST3D Data at Teignmouth 1999. Paper D4 of: COAST3D Final Volume of Summary Papers. Report TR121, HR Wallingford, UK, pp D4.1-D4.4, 2001.

WEIßE, W.; FESER, R. and GÜNTHER, H.: A Wind and Wave Climatology for the Southern North Sea Based on Numerical Simulations for the Period 1958 – 2001, GKSS 2003/10, 2003.

WILKENS, J.; JUNGE, I. and HOYME, H.: Modelling of Waves in a Tidal Flat Area in the South-Eastern German Bight, Die Küste, Heft 69, 2005 (a).

WILKENS, J. and MAYERLE, R.: Morphodynamic Response to Natural and Anthropogenic Influences in the Dithmarschen Bight, Die Küste, Heft 69, 2005 (b).

WINTER, C.; POERBANDONO; HOYME, H. and MAYERLE, R.: Modelling of Suspended Sediment Dynamics in Tidal Channels of the German Bight, Die Küste, Heft 69, 2005.

Die Küste, 69 PROMORPH (2005), 1-420

Patterns of Hydrodynamics in a Tide-Dominated Coastal Area in the South-Eastern German Bight

By FERNANDO TORO, ROBERTO MAYERLE, POERBANDONO and JORT WILKENS

Summary

The results of an analysis of field measurements leading to an identification of the basic patterns of hydrodynamics in a tidally-dominated area on the German North Sea coast are presented in this paper. The analysis was carried out within the framework of the research project "Predictions of medium-scale morphodynamics-PROMORPH" funded by the German Ministry of Education and Research from 2000 to 2002. The investigation area is the central Dithmarschen Bight between the Elbe and Eider estuaries. Recommendations for the set-up of the process-based models for flow and waves taking into account the available data and the dynamics of the study area were proposed. Continuous monitoring of water levels and waves by the relevant authorities was supplemented by field measurements at key locations. The planning and execution of field surveys specially intended to obtain a dense spatial and temporal coverage of current velocities is described. The tidal analysis, based on records from a number of tide gauge stations, yielded the 39 harmonic constituents that best represent the measured water level time series at several locations. An analysis of the seasonal variation of tidal asymmetries on the basis of water level measurements at several locations enabled flood or ebb dominance to be identified in the cross-sections of the tidal system. The current velocity measurements provided a good description of the spatial and temporal variation of current velocities. The measured wave data provided a better understanding of wave characteristics and wave transformation throughout the study area. The field measurements not only form a basis for identifying the most dominant physical processes governing the hydrodynamics of the study area but also provide a valuable data set for clarifying several aspects for developing and evaluating process-based models for the simulation of flow and waves.

Zusammenfassung

In diesem Artikel werden die Analysenergebnisse von Naturuntersuchungen vorgestellt, welche die grundlegende Verteilung der Hydrodynamik in einem tidedominierten Seegebiet der Deutschen Nordseeküste identifizieren. Diese Analyse wurde durchgeführt im Rahmen des Forschungsprojekts „Vorhersage mittelskaliger Morphodynamik – PROMORPH“, das vom Bundesministerium für Bildung und Forschung von 2000 bis 2002 finanziert wurde. Auf der Grundlage von mehreren Tidepegelstationen lieferte die Tideanalyse etwa 39 harmonische Komponenten, welche die gemessenen Wasserstand-Zeitreihen am besten repräsentieren. Um die räumlichen und zeitlichen Variationen der Strömung in den Hauptgezeitenrinnen besser zu verstehen, wurden über mehrere Querschnitte und Lokalitäten selektive Messungen der Strömungsgeschwindigkeit durchgeführt. Die maximalen Punktgeschwindigkeiten und tiefengemittelten Geschwindigkeiten lagen in den Gezeitenrinnen bei 2,8 m/s bzw. 1,7 m/s. Aufgrund der geringen Rauigkeit der Bodenformen ist die Geschwindigkeitsverteilung über die Vertikale nahezu gleichförmig. Es war möglich, in den Querschnitten nahe der seewärtigen Grenzen des Untersuchungsgebiets unter normalen Bedingungen eine Flutdominanz zu erkennen und einen signifikanten Anstieg der Strömungsgeschwindigkeit mit steigendem Tidehub. Etwa 10 km weiter seewärts der äußeren Wattflächen wurden Wellenhöhen bis 3,5 m aufgezeichnet. Landwärts wurde ein grader Abfall der Wellenhöhe gemessen, der mit dem immer stärker werdenden Effekt abnehmender Wassertiefe (führt zur Wellenenergie-Dissipation durch Wellenbrechen und Bodenreibung) wie auch mit der Hubwirkung der Wattflächen in Zusammenhang steht. Die maximalen Wellenhöhen entlang der äußeren Wattenkanten und in der zentralen Gezeitenrinne lagen bei jeweils 2,0 m und 1,5 m. Näher zur Küste weiter östlich lagen die Wellenhöhen generell unter 0,7 m. Aus der Analyse der Wellenperioden war zu schließen, dass die Dünung bis zum zentralen Bereich der äußeren Wattflächen reichte, während weiter östlich lokal erzeugte Wellen die Hauptenergiequelle bilden.

Keywords

Gauge Stations, Waverider Buoy, Tides, Tidal Analysis, Swell, Wind Waves, Tidal Channels, Tidal Flats, Measurements, Dithmarschen Bight, North Sea, PROMORPH

Contents

1. Introduction

Hydrodynamic phenomena constitute the underlying mechanisms governing sediment transport and reaction processes such as morphodynamics in coastal areas. Process-based numerical models for simulating morphological changes over time scales of several years have been developed, evaluated and applied within the framework of the research project "Predictions of Medium-Scale Coastal Morphodynamics – PROMORPH" funded by the German Ministry of Education and Research (PALACIO et al., in this volume; WILKENS et al., in this volume; WINTER et al., in this volume; JUNGE et al., in this volume; WILKENS and MAYERLE, in this volume). The investigation area considered in this project is the central Dithmarschen Bight located between the Elbe and the Eider estuaries.

This paper gives an overview of the data used to assist in identifying the basic features of hydrodynamics and to provide sets of data for the development of process-based models for simulating flow and waves in the investigation area. Gaps in information were identified, focusing on the requirements for the proper development of the coastal model. The planning and execution of field surveys specially designed to obtain a dense spatial and temporal coverage of current velocities is also described. Results of an analysis of field measurements of tidal flows, storm surge levels, current velocities and waves are presented. The main tidal constituents and asymmetries based on water level records at several locations as well as the results of an analysis of the spatial and temporal distribution of current velocities in the tidal channels are presented. Wave data provided by several authorities from waverider buoy recordings were analysed to investigate the distribution of wave characteristics and wave transformation throughout the study area. Vertical profiles of salinity and temperature were additionally measured at various locations along the current velocity measurement transects.

Although extensive measurements covering a wide area and a wide range of conditions were made during the investigations, only typical results are presented here for the sake of compactness.

2. Investigation Area

The investigation area consists of a tidal region on the German North Sea coast (Fig. 1). It is part of the Wadden Sea extending along the North Sea shore from the Netherlands to Denmark and covers an area of about 600 km² between the Elbe and Eider estuaries. The morphology of the area is dominated by tidal flats, intertidal channels and sandbanks in the outer parts of the domain. Water depths in the channels attain about 23 m, and approximately 50 % of the domain is intertidal. Water depths in the tidal flat region at high water are typically of the order of 0.5–2 m. Bed levels over the tidal flats range from about 0 to 1 m above NN (German Reference Datum, roughly equivalent to MSL). The system consists of three tidal channels; the Norderpiep in the northwest and the Suederpiep in the southwest, which intersect within the study area to form the Piep tidal channel. The surficial seabed sediment is mainly comprised of very fine to fine sand with varying proportions of silt and clay, whereas the sediment transported in suspension is mainly silt. Due to the high tidal range and small particle sizes the distribution of sediment concentration over the vertical is quite uniform and most of the sediment is transported in suspension. Similarly, the distribution of salinity over the vertical is fairly uniform and only very small spatial gradients are observed (POERBANDONO and MAYERLE, in this volume; RICKLEFS and ASP, in this volume).

The hydrodynamics of the investigation area are mainly driven by the combined effects of tides, waves, winds and storm surges. Under normal conditions, tidal action constitutes the main driving force. The area is characterised by a semi-diurnal tide with a mean tidal range of 3.2 m. Westerly winds prevail (SW–W). Although wave heights of up to 3–4 m are observed in the outer region, the influence of wave action on the resulting flow field is moderate over the tidal flats and negligible in the tidal channels. Wave-breaking usually occurs along the edge of the tidal flats.

The patterns of hydrodynamics in the outer and inner regions of the study area are quite distinctive. In the outer regions, with water depths of about 20 m, the hydrodynamics are mainly driven by tides and swell. The effect of waves on the sandbanks can be quite significant. In the inner regions of the domain there is a clear distinction between the physical processes over the tidal flats and in the channels. The hydrodynamics in the tidal channels are mainly driven by tides. Due to the large water depths in the channels (up to 20 m) the effect of waves on currents is relatively small. Under normal conditions wave heights are generally below about 0.5 m. On the tidal flats the flow is driven by the combined effect of tides, waves and winds. Due to the small water depths over the tidal flats the effects of waves and winds on currents and sediment transport can be significant. Storm surges may produce water level set-ups of up to 3.6 m, thus favouring wave propagation in shallow areas. Even under such conditions, however, wave effects are more pronounced on the outer sandbanks.

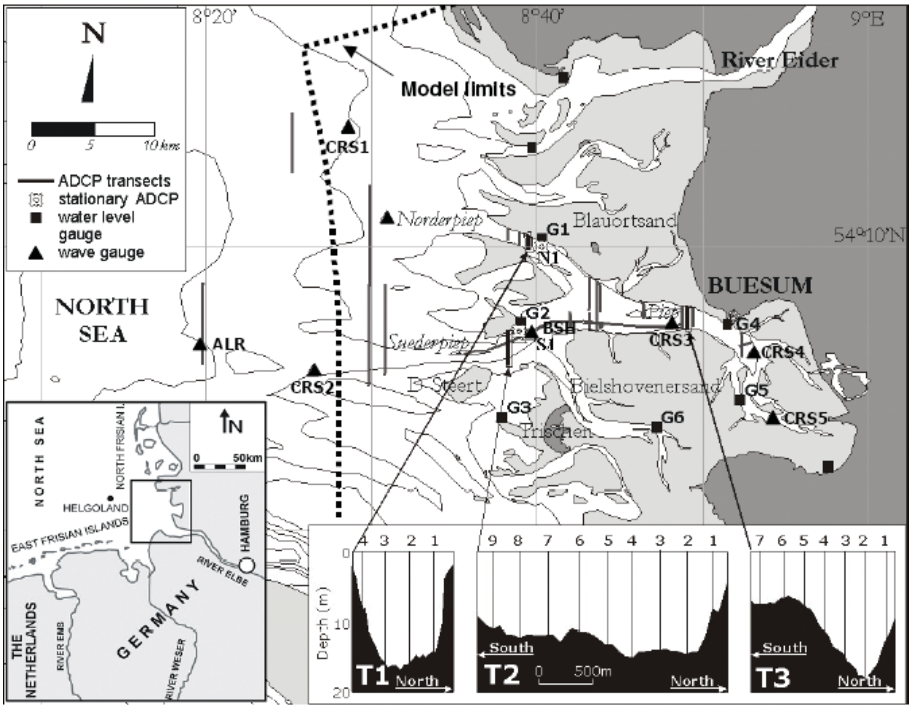

Fig. 1: Investigation area and measurement locations

3. Data Requirements

The data required to identify the most relevant physical processes governing hydrodynamics as well as the data necessary for developing and evaluating the process-based models for simulating flow and waves in the study area were made available during the early stages of the research project through close cooperation between experimentalists and numerical modellers. Initial simulations with ad-hoc models, i.e. non-calibrated models, were performed to analyse the general hydrodynamic behaviour in the study area. Field data requirements were subsequently determined on the basis of these model results and the data available from previous measurements.

3.1 General Knowledge from Ad-hoc Modelling

The results of initial simulations using a flow model of the German Bight developed by Delft Hydraulics (see HARTSUIKER, 1997), and made available by the CRS (Norderney), as shown in Fig. 2, clearly illustrate the propagation of a tidal wave in the German Bight during a tidal cycle. It is interesting to note that although the tidal wave propagates in the anti-clockwise direction in the German Bight, it approaches the Dithmarschen Bight almost parallel to the coastline. The tidal currents are directed onshore and offshore during the flood and ebb phases, respectively. From sensitivity tests with an initial ad-hoc flow model

Die Küste, 69 PROMORPH (2005), 1-420

of the Dithmarschen Bight it could be shown that the flow exchange in the area takes place mainly through the Norderpiep, Suederpiep and Piep tidal channels. Furthermore, it was shown that the dynamics of the study area are not influenced by the discharges of the Elbe and Eider rivers, as extensive tidal flats separate these systems from the study area. Similarly, the application of an ad-hoc wave model showed that these shallow tidal flats also prevent the intrusion of a significant amount of wave energy at these locations. Even under storm conditions, there is no evidence that interaction takes place over the shallow areas. Pronounced wave attenuation was also found to occur on moving from east to west through the Dithmarschen Bight.

3.2 Data Needs for Model Development

Although numerical models now find increasing application in the management of coastal areas, these models are rarely validated with adequate measurements. The reason for this is that the purpose of most of the field data collected in the past was to clarify physical processes rather than for developing numerical models. The evaluation of numerical models, particularly for coastal areas, places special requirements on the data such as detailed measurements along the open-sea boundaries and a dense spatial and temporal coverage within the modelled domain for calibration and validation purposes. Complete and simultaneous data sets are thus essential for driving and checking the performance of numerical models.

3.3 Available Data and Information Gaps

Table 1 gives an overview of the existing data on water levels, waves and winds available in the study area. The locations of existing gauge stations for water level measurements as well as the positions of waverider buoys are shown in Fig. 1. Water levels are monitored by the Regional State Office for Rural Areas in Husum (ALR). In this study, water level data recorded at the following gauge stations were used: G1: Blauort in the Norderpiep tidal channel; G2: Tertius in the Suederpiep tidal channel; G3: Trischen; G4: Buesum; G5: Steertloch West and G6: Flackstrom. Gauge stations G1 to G3 are situated along the western boundary of the investigation area whereas stations G4 to G6 are located in the inner part of the domain. The high spatial and temporal coverage of these gauge stations provides an ideal basis for calibration and validation of the flow model with respect to water levels.

Information on waves in the study area was gathered from several sources. An essential set of data was made available by the Coastal Research Station of the Lower Saxony Board of Ecology (CRS) on Norderney, who conducted a one-month measuring campaign with five waverider buoys within the framework of the German Coastal Engineering Research Council (GCERC-KFKI) Project "Bemessung auf Seegang" (grant number KFKI 45) funded by the German Ministry of Education and Research (grant number MTK 0561 – NIEMEYER, 1997). The positions of the waverider buoys in the study area were carefully defined in order to provide the data necessary for developing the wave model. Two directional waverider buoys (CRS1 and CRS2) were positioned some distance offshore of the study area at water depths of about 10 m to provide information for driving the model. The remaining waverider buoys were positioned in the inner parts of the study area to provide the data required for calibrating and validating the model (CRS3 to CRS5). Further wave data were collected with

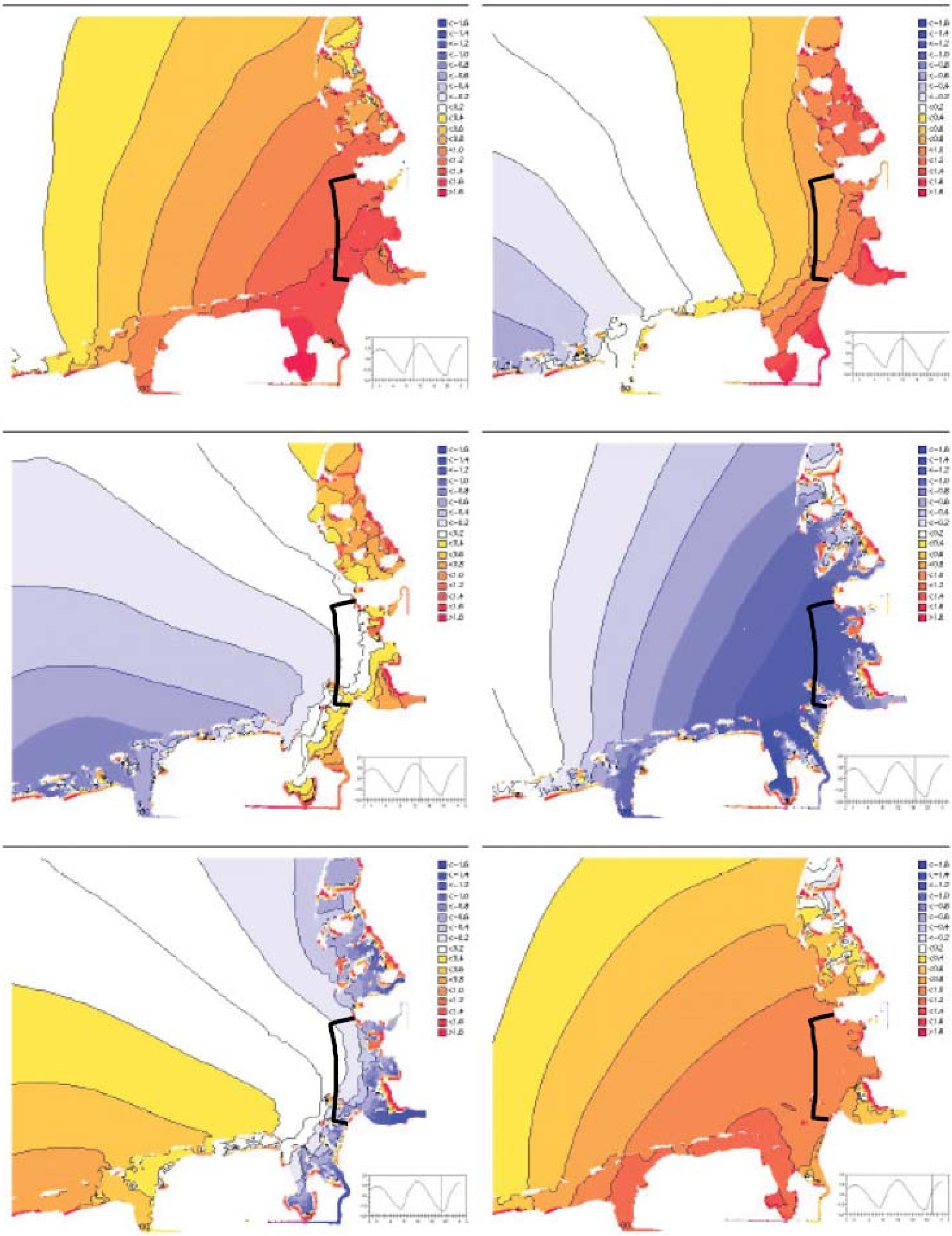

Fig. 2: Tidal wave propagation in the central part of the German Bight

Die Küste, 69 PROMORPH (2005), 1-420

Table 1: Overview of Available Data Recordings

Data	Device & Location (Fig. 1)	Period	Source
Water level	Gauge stations: G1 to G6	January 1989 till December 1990	Regional State Office for Rural Areas in Husum (ALR)
Waves	Waverider buoys: Directional: CRS1 & CRS2 Non-directional: CRS3 to CRS5	September–October 1996	Coastal Research Station of Lower Saxony Board of Ecology at Norderney
	Waverider buoy: Directional: ALR	June 2000–May 2001	Regional State Office for Rural Areas in Husum (ALR)
	Waverider buoy Directional: BSH	November 2000–April 2001	German Federal Maritime and Hydrographic Agency in Hamburg (BSH)
Wind	PRISMA interpolation model	1989–2000	Max Planck Institute of Meteorology in Hamburg (LUTHARDT, 1987).

aid of waverider buoys by the Regional State Office for Rural Areas in Husum (ALR) and the German Federal Maritime and Hydrographic Agency in Hamburg (BSH). The measuring locations at the approach to the Dithmarschen Bight and at the entrance to the Suederpiep tidal channel are shown Fig. 1.

The wind data used in the project were obtained with the aid of the PRISMA interpolation model developed by the Max Planck Institute of Meteorology in Hamburg (LUTHARDT, 1987). This model generates synoptic wind fields from a large set of measurements at locations along the coastline as well as from offshore stations covering the entire North Sea. The PRISMA model generates wind data every three hours at the nodes of a grid with a mesh spacing of 42 km.

Based on the available data and taking into consideration the hydrodynamics of the study area and the additional data required for developing the flow and wave models, gaps in information were identified and several aspects concerning the development and evaluation of process-based models for simulating flow and waves were clarified. As the hydrodynamics of the study area are very much governed by conditions along the western open-sea boundary, it was necessary to obtain simultaneous sets of data for driving the flow and wave models as well as data within the model domain for the purpose of model calibration and validation. Moreover, as the main exchange of flow in the study is through the tidal channels, for which little information on current velocities is available, it was planned to undertake several measuring campaigns to obtain essential information on the temporal and spatial variations of current velocities and directions at a number of key locations. The planning and execution of the field surveys as well as an analysis of the results are presented in the following sections.

3.4 Clarification of Various Aspects of Model Settings

With regard to the definition of the model limits it was decided to position the western open-sea boundary at right angles to the direction of propagation of the tidal wave and swell into the coastal area. In view of the intensive morphological changes that occur on the sand banks and outer tidal flats it was proposed to shift the model limits further westwards to a location where the bathymetry is reasonably stable. By setting up the western open-sea boundary in the near vicinity of the waverider buoys CRS1 and CRS2 it was possible to directly use the data from these buoys to drive the wave model and subsequently employ the simultaneous data from the waveriders CRS3 to CRS5 for calibration and validation purposes. Fig. 1 shows the proposed limit of the model covering the entire Dithmarschen Bight. With regard to the development of the flow model it was proposed to follow a two-step approach. In the first step a smaller model covering only the central parts of the study area was set-up. The western open-sea boundary of this model was positioned in the vicinity of the gauge stations G1 to G3, whereas the northern and southern boundaries were located on tidal flats. The eastern boundary of the model consists of the shoreline together with the open boundaries formed by the mouths of the Eider and Elbe estuaries. Hydrodynamic forcing along the western open-sea boundary of the flow model could thus be realised by specifying the water levels measured at one or more gauge stations in the proximity of this boundary (G1, G2 or G3 in Fig. 1), provided that the momentum balance could be maintained. The water level measurements at the remaining gauge stations (G4 to G6) could then be used for the purpose of model calibration and validation. In a second step it was proposed to extend the flow model to cover the same domain and utilise the same grid as the wave model. In order to permit flow and wave simulations for a wider range of conditions than those of the measuring periods it was additionally proposed to set-up nested and coupled flow and wave models covering the adjoining area of the North Sea (see MAYERLE et al., in this volume). Detailed descriptions of model set-up, sensitivity studies, and calibration and validation of the flow and wave models are given in PALACIO et al. (in this volume) and WILKENS et al. (in this volume), respectively.

4. Measurements of Current Velocity

4.1 Measuring Devices and Experimental Set-up

Measurements of current velocity and direction were performed over several cross-sections and at various locations in the tidal channels, as indicated in Fig. 1. The data were gathered with the aim of obtaining detailed information on the temporal and spatial variations of current velocity and direction at key locations in the study area. The field surveys were planned and executed in such a way as to provide the data necessary to gain a better understanding of the underlying physical processes, define the strategy for model development, and check the performance of the flow models. The temporal resolution of the measurements was dictated by the physical conditions prevailing in the investigation area. As the hydrodynamics of the study area are driven by tides, winds and waves, it was planned to perform the measurements over at least one tidal period in each case for the main range of tidal conditions.

Current velocity data were obtained using 1200 kHz Acoustic Doppler Current Profilers (ADCPs) manufactured by RD Instruments. These instruments were set to record a 0.5 m bin size over a 12 seconds averaging ensemble. An investigation of the accuracy of the ADCPs for measurements in the tidal channels of the central Dithmarschen Bight showed that the standard deviations for point measurements are approximately constant, with values of about 0.06 m/s and 0.14 m/s for distances above and below 1m from the seabed, respectively. The accuracy of the devices for measuring depth-averaged velocities was found to be about 0.015 m/s (JIMÉNEZ-GONZÁLEZ et al., in this volume).

The measurements from moving vessels were intended to provide detailed spatial coverage of the velocity distribution over a tidal period. These measurements covered several cross-sections of the main tidal channels, as indicated in Fig. 1. A number of vessels equipped with similar acoustic profilers were deployed simultaneously to cover a larger area. Fig. 3 shows the vessels used within the framework of the research project PROMORPH. The research vessel Suedfall and the research boat Seston are operated by the Research and Technology Centre "Westcoast" of the University of Kiel. The RV Suedfall, which is 19 m long, 5 m wide and has a draught of 1.6 m, is equipped for operations in coastal waters of the North and Baltic Sea. The research boat Seston, which is 6.3 m long, 2.5 m wide and has a draught of 0.6 m, is mainly deployed for measurements in the German Wadden Sea, particularly in shallow areas. In order to permit measurements in deeper areas and perform simultaneous measurements over several cross-sections the RV Ludwig Prandtl operated by the GKSS

(a) RV Suedfall operated by the FTZ Westcoast, Kiel University

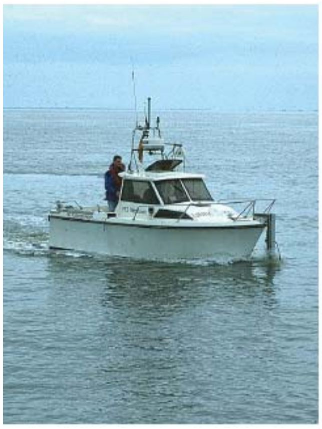

(b) RB Seston operated by the FTZ Westcoast, Kiel University

(c) RV Ludwig Prandtl operated by the GKSS Institute for Coastal Research

Fig. 3: Research vessels deployed for measuring current velocities

Institute for Coastal Research was also deployed in a number of measuring campaigns. The RV Ludwig Prandtl is 32.5 m long, 7.5 m wide and has a draught of about 1 m. During measurements from moving vessels the acoustic profiler was directed downwards from the bow of the vessel and deployed for the continuous measurement of current velocity profiles along cross-sectional transects.

Fig. 4 illustrates the approach adopted for profiling from moving vessels. In addition to current velocity measurements, profiling of suspended sediment concentration, salinity and temperature was also carried out at defined stations within the cross-sectional transects. Details of these measurements are given in Poerbandono and Mayerle (in this volume). During a full measuring campaign, which usually covers a complete tidal period, the survey vessel moves back and forth along a cross-sectional transect. Measurements of current velocity profiles covering the entire cross-section were carried out along each transect following approximately the same track. The number of cross-sectional transects surveyed during a tidal period depends primarily on the cross-sectional width and measuring conditions.

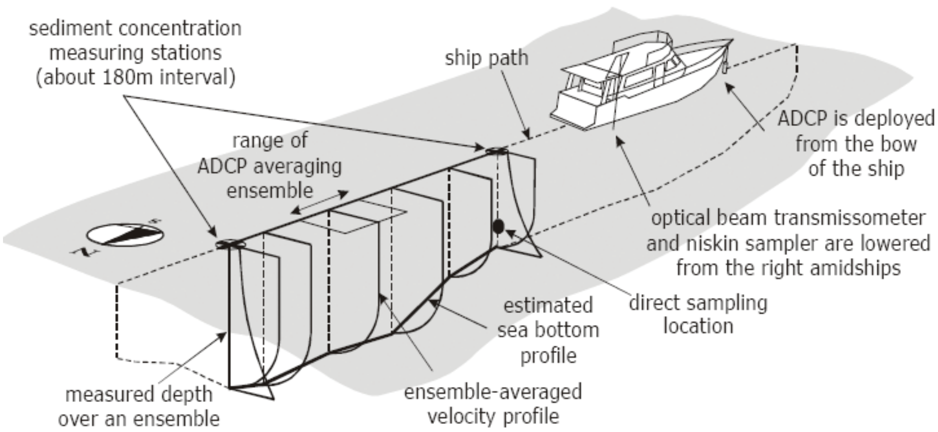

Fig. 4: Measurement procedure for profiling current velocities from moving vessels

Measurements over the water column were made from about 1.5 to 2.0 m below the free surface (to avoid the effects of transducer draught and blanking distance) down to about 6 % of the depth above the seabed (to avoid side lobe effects). As the measurements did not cover the entire water column, extrapolations were necessary in the surface and near-bed layers to obtain a complete velocity profile over the full depth. For this purpose a constant velocity value from the uppermost point measurement to the free surface and a linear variation from the lowest measured value towards zero at the seabed were adopted in this study.

Bearing in mind that measurements from a moving vessel are limited to calm weather conditions, moored devices were also deployed in order to gather information during more adverse weather conditions. The aim of this was to obtain information on the velocity distribution over the depth covering longer periods and more adverse weather conditions. Two locations along the main tidal channels at the entrance to the central Dithmarschen Bight (see N1 and S1 in Fig. 1) were chosen for the moored devices, which were anchored on the bed and directed towards the free surface. Profiles of current velocities were obtained during the entire period of measurements. A definition sketch illustrating the installation of the moored devices is shown in Fig. 5. Measurements from the moored devices covered the water column from the free surface to about 2 m above the seabed. The depth-averaged velocity was determined by assuming a linear variation from the lowest cell measurement towards zero at the seabed. It is noted that this approximation may lead to discrepancies compared with observed values, especially at low water levels.

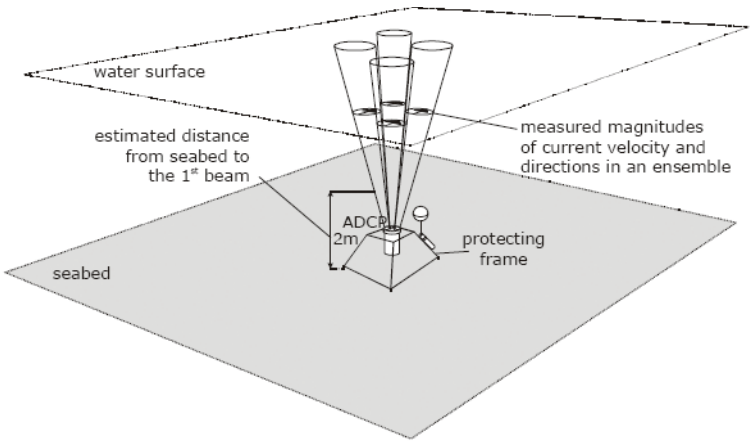

Fig. 5: Measurement procedure for profiling current velocities using acoustic devices moored on the seabed

4.2 Environmental Conditions

The measurements from moving vessels were performed over several cross-sections covering a wide area extending from the deeper regions of the central Dithmarschen Bight to the inner parts of the main tidal channels. Fig. 1 shows the locations of the surveyed cross-sections. The measurements were carried out at regular time intervals from March 2000 to September 2001 in order to account for seasonal variations. Each measuring campaign was conducted twice within about seven days to cover neap and spring tidal variations. Measurements were also carried out for a wide range of tidal conditions in order to investigate spatial (vertical and horizontal) and temporal (tidal phase, lunar cycles, seasonal) variations.

The sets of field data based on measurements from moving vessels are listed in Table 2. In this paper attention is focused on measurements carried out over two cross-sections T1 and T2 in the main tidal inlets, and an additional cross-section T3 near the coast (see Fig. 1). T1 in the Norderpiep tidal channel is about 770 m wide with water depths varying from 2.8 m to 16.1 m; T2 in the Suederpiep tidal channel is about 2040 m wide with water depths varying from 7.3 m to 15.6 m, and T3 in the Piep tidal channel is about 1200 m wide with water depths varying from 6.2 m to 17.9 m. The bed profiles of cross-sections T1, T2 and T3 are also shown in Fig. 1. In order to obtain full coverage over a complete tidal period, measurements were made over several cross-sectional transects per measuring campaign. The astronomical tidal range during the field surveys varied between 2.3 m and 4.2 m for neap and spring tides, respectively. The measuring campaigns were undertaken under relatively calm wind conditions not exceeding Beaufort 4-5. The maximum point, depth-averaged, and cross-sectionally averaged velocities derived from these measurements are listed in Table 2.

Table 2: Current velocity data sets based on measurements from moving vessels

Cross-section [width]	Date	Tidal range (m)	Number of transects – Measuring duration (h)	Max. point velocity (m/s)		Max. depth-avg. velocity (m/s)		Max. cross-sect.-avg. vel. (m/s)	
				Flood	Ebb	Flood	Ebb	Flood	Ebb
T 1 [775 m]	Mar. 16, 2000	3.2	31 – 11.7	1.4	–2.0	1.3	–1.2	1.0	–1.0
	Mar. 22, 2000	4.0	31 – 11.6	1.5	–1.6	1.5	–1.4	1.1	–1.2
	Jun. 5, 2000	3.7	10 – 6.1	1.8	–1.6	1.7	–1.4	1.5	–1.2
	Sep. 5, 2000	3.0	26 – 10.4	1.4	–1.4	1.2	–1.3	1.0	–1.0
	Sep. 12, 2000	3.4	33 – 11.6	1.3	–1.2	1.3	–1.2	1.1	–1.0
	Dec. 5, 2000	2.3	11 – 5.5	0.7	–1.0	0.6	–0.9	0.5	–0.7
	Mar. 21, 2000	4.1	15 – 11.9	2.1	–1.7	1.6	–1.4	1.2	–1.0
T2 [2040 m]	Jun. 5, 2000	3.7	10 – 8.4	NA	–1.5	NA	–1.5	NA	–1.1
	Sep. 5, 2000	3.1	8 – 9.8	1.8	–1.4	1.3	–1.1	1.0	–0.9
	Sep. 12, 2000	3.3	10 – 10.8	1.6	–1.4	1.6	–1.2	1.1	–0.9
	Dec. 5, 2000	2.3	9 – 10.8	1.0	–1.1	0.8	–1.1	0.7	–0.7
	Mar. 14, 2000	3.6	14 – 8.8	1.5	–1.7	1.2	–1.3	1.0	–1.0
	Mar. 23, 2000	4.2	24 – 13.0	1.6	–1.7	1.2	–1.4	1.1	–1.0
	Jun. 6, 2000	3.9	15 – 8.2	1.4	NA	1.4	NA	1.1	NA
	Jun. 14, 2000	3.6	19 – 11.8	1.4	–1.4	1.3	–1.4	0.9	–1.1
T3 [1200 m]	Sep. 6, 2000	2.9	14 – 10.7	1.1	–1.1	0.9	–1.1	0.8	–0.8
	Sep. 13, 2000	3.5	8 – 4.6	1.6	NA	1.3	NA	1.1	NA
	Dec. 6, 2000	2.5	22 – 12.0	1.2	–1.1	0.9	–0.9	0.7	–0.8
	Jun. 22, 2001	3.9	9 – 5.9	1.5	NA	1.4	NA	1.1	NA
	Jun. 28, 2001	3.6	13 – 11.4	1.4	–1.3	1.2	–1.1	1.0	–0.8
	Sep. 11, 2001	3.1	14 – 11.1	1.2	–1.4	1.1	–1.3	0.9	–0.9

Notes: 1) negative current velocities are directed offshore
2) NA means not available

The sets of field data based on measurements over longer periods from the moored devices are listed in Table 3. These devices were deployed along the two main tidal inlets at the entrance to the Dithmarschen Bight, i.e. in the Norderpiep and Suederpiep tidal channels at locations N1 and S1 shown in Fig. 1. The devices were moored close to the gauge stations G1 and G2 located in the vicinity of cross-sections T1 and T2 (see Fig. 1). The mean water depths at the measuring stations N1 and S1 are about 9 m and 13 m, respectively. The measurements were carried out during the year 2000 over two periods lasting about 15 days and one period lasting about 3 months. The astronomical tidal range during measurements varied between 1.6 m and 3.9 m. Wind velocities of up to 15 m/s were observed during the measuring periods.

Based on the cross-sectional measurements carried out from moving vessels, the maximum point current velocities in cross-sections T1, T2 and T3 were found to be 2.0 m/s, 2.1 m/s and 1.7 m/s, respectively. A similar order of magnitude was obtained for the maximum depth-averaged and cross-sectionally averaged values of current velocity observed in the two cross-sections at the entrance to the study area. Smaller values were observed in the cross-section nearer to the coast (cross-section T3). An analysis of longer-term measurements from moored acoustic profilers showed that maximum current velocities (depth-averaged values) in the Norderpiep and Suederpiep tidal channels (Stations N1 and S1) are about 2.8 m/s (1.3 m/s) and 2.1 m/s (1.5 m/s), respectively.

Table 3: Current velocity data sets based on measurements from moored devices

Location	Measurement period	Water depth (m) Range and (mean)	Tidal range (m)	Max. & (mean) wind speed (m/s)	Max. velocity values (m/s)					
					Point				Depth-averaged	
					top layer		bottom layer			
					Flood	Ebb	Flood	Ebb	Flood	Ebb
N1 Norderpiep tidal inlet	Aug. 10 to Sep. 27, 2000	6.5–11.0 (9.0)	1.8 to 3.9	15.0 (4.5)	1.86	1.55	1.00	0.93	1.27	1.07
	Nov. 15 to Dec. 7, 2000	6.9–10.8 (9.1)	1.6 to 3.6	15.2 (6.0)	2.79	2.18	0.99	0.85	1.19	0.93
S1 Suederpiep tidal inlet	May 31 to June 15, 2000	10.3–14.8 (12.8)	2.6 to 3.9	12.2 (4.6)	2.10	1.80	1.00	1.00	1.54	1.47

5. Data Analysis

5.1 Tides

Tidal oscillations in the North Sea are determined by its dimensions and the progressive semi-diurnal tides entering from the Atlantic Ocean. The tidal flow is deflected by the Coriolis force, resulting in three amphidromic systems. Tidal conditions in the central Dithmarschen Bight depend primarily on the rotation of the semi-diurnal tidal wave around the amphidromic point in the south eastern part of the North Sea. As previously mentioned, the tidal wave propagates counter-clockwise along the German Wadden Sea coast (see Fig. 2). According to Asp (2004), the area is characterised by a semi-diurnal tide with a tidal period of about 12 hrs and 24 min. The mean tidal range varies from about 3.1 m to 3.4 m between the mouth of the Elbe estuary in the south and the Eiderstedt peninsula in the north. Referred to NN, the mean high and low water levels at the gauge station Buesum (G4 in Fig. 1) are +1.6 m and –1.6 m, respectively. An analysis of a long time series of water level measurements reveals that the mean tidal range in the study area is about 3.2 m, with neap and spring tidal ranges of about 2.8 m and 3.5 m, respectively.

A tidal analysis was carried out for gauge stations G1 to G6 over a 65-day period characterised by relatively calm weather conditions from April 27 to June 30, 1990. The water level data was available at 30 min. intervals. During this period only a few storms of short duration were observed with wind velocities not exceeding 10 m/s. Fig. 6 shows the variations in water level and wind velocity during part of the period in question at the stations Tertius (G2) at the entrance to the domain, and Steertloch (G5) near the coastline. It is seen from the figure that the amplitudes of water levels nearer the coast are slightly higher than at the entrance to the domain. Although a time lag exists between the measured tidal curves at the two stations, this is hardly discernable in the plots.

The main astronomical constituents were identified on the basis of previous studies carried out in the area (HARTSUIKER, 1997). Based on sensitivity studies using different groups of constituents, 36 independent and 3 coupled harmonic constituents that best represent the measured water level time series were selected. The computed amplitudes and phases of the constituents considered in the tidal analysis are shown in Tables 5 and 6, respectively. Fig. 7 shows a comparison of the ten main constituents obtained at the five locations. It is interesting to note that the tidal constituents at the gauge stations located on the western boundary of the study area (G1 to G3) exhibit similar phases and amplitudes. This is due to the fact that the crest of the tidal wave approaches the study area almost aligned with the edges of the tidal flat areas (see Fig. 1 and 2). An examination of the maximum amplitudes of the main tidal constituents observed at all stations reveals the pronounced semi-diurnal nature of the tides in the region. The main tidal constituent is M2. The next constituent of importance is S2 followed by N2. The maximum amplitude is found at the station Steertloch (G6). ASP (2004) analysed the variation of water level measurements at the gauge stations Blauort and Tertius (G1 and G2 in Fig. 1) at the entrance to the domain and at Buesum (G4) near the coast. As a result of this analysis it was found that high water occurs at station G4 about 10 to 12 min. later than at stations G1 and G2 whereas low water occurs at about the same time at the gauge stations Buesum (G4) and Tertius (G2), and 4 min. later at Blauort (G1).

In order to verify the quality of the constituents, comparisons were made between hindcasted and observed water levels. Hindcasts for the three periods listed in Table 4 were computed using the derived constituents. A comparison between measured and predicted tidal elevations for the three periods is shown in Fig. 8 for the gauge station Tertius. Fig. 9 shows the standard deviations of the discrepancies between measurements and hindcasts in cm and as a percentage of the tidal range. The discrepancies presented in Fig. 9 are given in terms of the mean error (ME) and the corresponding standard deviation (STD) and the mean absolute error (MAE). The results indicate fair agreement between measurements and hindcasts, with a mean absolute error at all locations and for all periods of generally less than 20 cm, i.e. less than about 6 % of the mean tidal range.

Table 4: Periods selected for checking the accuracy of hindcasted water levels

Period	Beginning & end dates	Duration (days)	Wind characteristics and storms
1	May 31 to June 26, 1989	27	Wind velocities less than 8 m/s
2	May 31 to July 12, 1989	43	Incorporates 2 small storms with wind velocities of 9 m/s and 11 m/s, respectively
3	July 07 to August 18, 1990	43	Incorporates 4 storms with durations longer than 1 day but with wind velocities ≤ 10 m/s

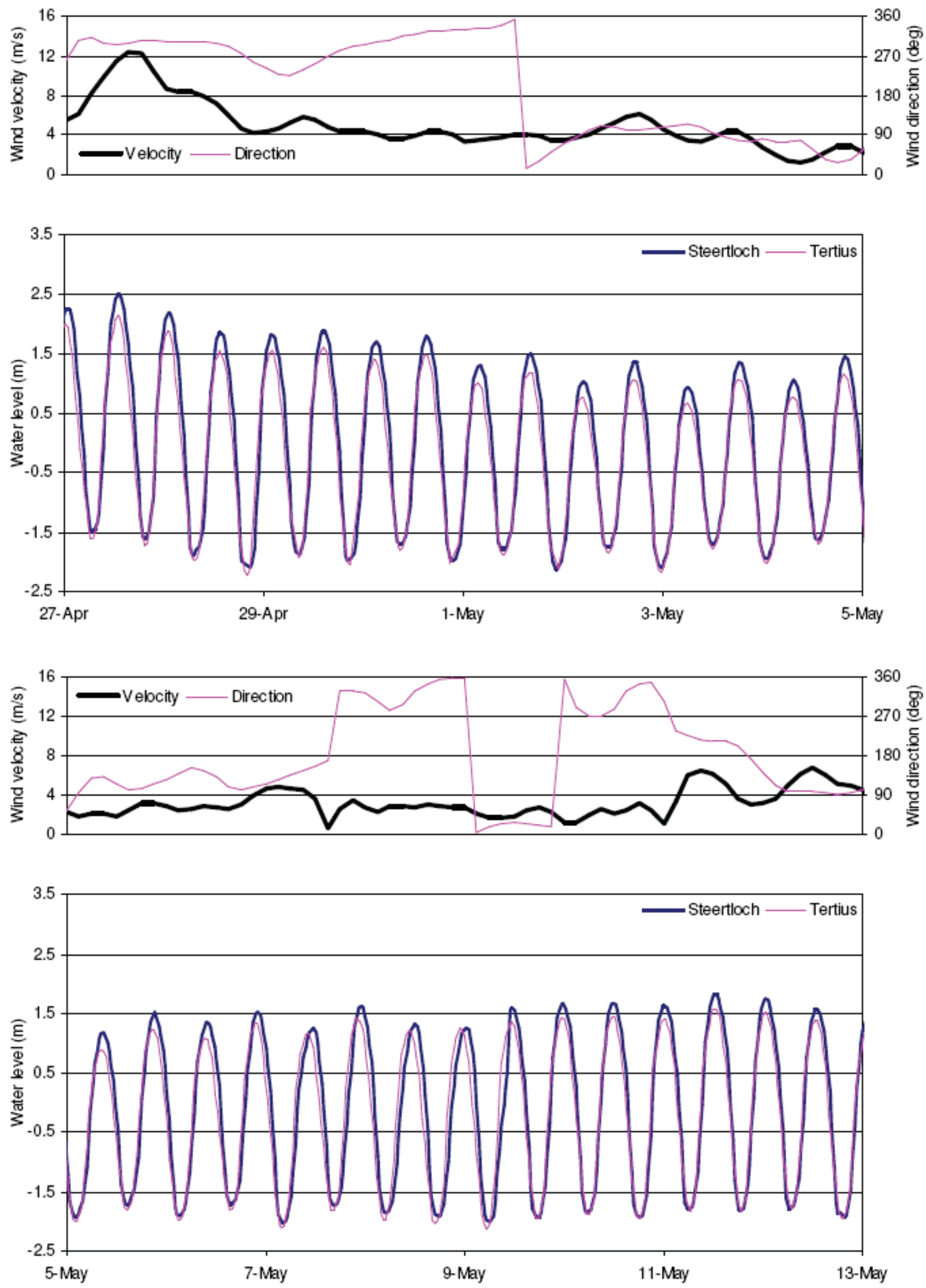

Fig. 6: Tidal records at the gauge stations Tertius (G2) and Steertloch (G5) for the period considered in the tidal analysis

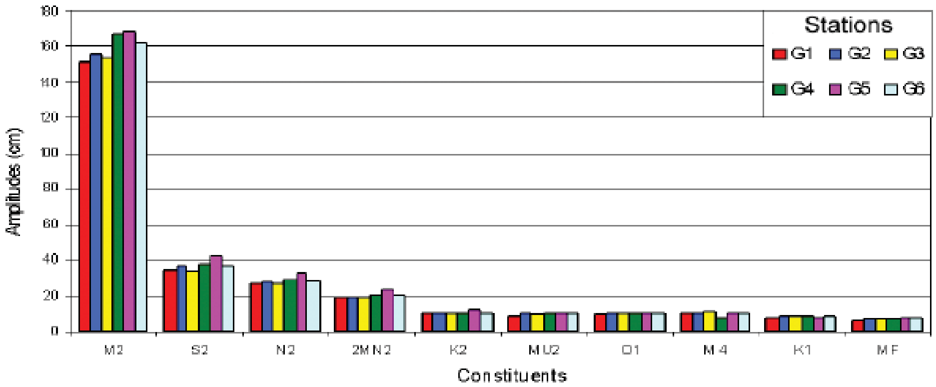

(a) Amplitude

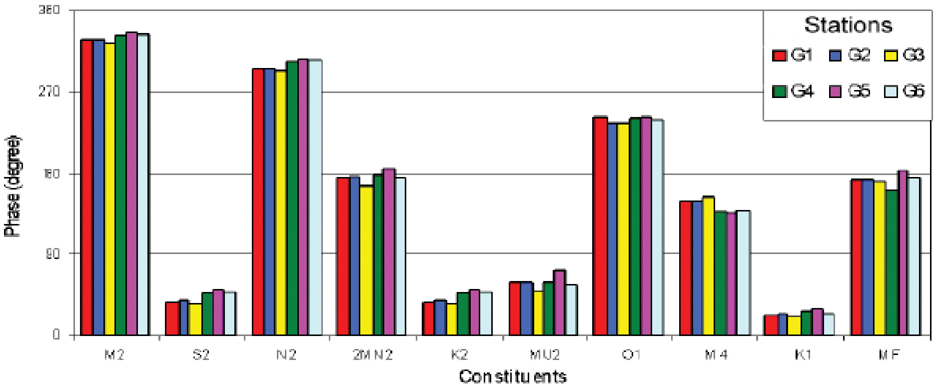

(b) Phase

Fig. 7: Comparison of the main tidal constituents at gauge stations G1 to G6 in the Dithmarschen Bight

The seasonal variation of tidal asymmetry was investigated at several locations in the tidal channels by ASP (2004). This investigation was carried out owing to the relevance of tidal asymmetry regarding sediment transport and accumulation. The water levels measured at several locations in the tidal channels were used to determine flood or ebb dominance, i.e. dominant phases corresponding to phases of shorter duration and hence with higher velocities, as defined by FRIEDRICHS and AUBREY (1988). The water levels used in the investigation were measured at three gauge stations; stations Blauort (G1) and Tertius (G2) at the entrance to the study area and station Buesum (G4) in the Piep tidal channel near the coast, representing the cross-sections T1, T2 and T3, respectively (see Fig. 1). The analysis covered the months of June, September and December 2000, corresponding to summer, autumn and winter periods, respectively. Fig. 10 shows the duration of ebb and flood phases separately for neap and spring tides. Differences of up to about 45 min. between ebb and flood phases were identified. According to the results, the cross-sections located at the entrance to the central

Die Küste, 69 PROMORPH (2005), 1-420

Dithmarschen Bight (T1 and T2) are flood-dominated during most of the year, particularly during the winter months and for spring tides. The cross-section nearer the coast (T3), on the other hand, is generally ebb-dominated during the summer. During the autumn and winter months, however, the ebb and flood phases are more or less balanced, i.e. almost no tidal asymmetry exists during these periods.

Fig. 11 shows the variation of monthly mean ebb and flood durations, water level set-ups and wind velocities from July 1999 to August 2002 at the gauge station Buesum (G4). It is seen that under relatively calm and moderate wind conditions, corresponding to almost undisturbed water levels, there is a clear tendency towards shorter ebb phases and hence ebb dominance. During the winter months, on the other hand, there is a tendency towards similar durations of ebb and flood phases due to more frequent and stronger westerly winds and hence higher water level set-ups. A sharp reduction in tidal asymmetry at this gauge station was observed for a threshold value of water level set-up of about 0.2 to 0.3 m.

Table 5: Amplitudes of the harmonic constituents (in cm) at gauge stations G1 to G6 in the Dithmarschen Bight

Harmonic Constituents	G1 Blauort	G2 Tertius	G3 Trischen	G4 Buesum	G5 Steertloch	G6 Flackstrom
M2	151.619	156.018	153.496	167.277	168.296	162.592
S2	34.998	36.928	34.282	38.129	42.518	36.736
N2	26.147	26.949	26.691	28.957	33.600	28.021
2MN2	18.559	18.612	19.048	20.385	23.363	20.264
K2	9.940	10.488	9.736	10.829	12.075	10.433
MU2	8.550	10.121	8.858	10.034	9.675	10.030
O1	9.415	9.898	10.190	10.447	10.668	9.872
M4	10.834	10.741	11.113	7.783	9.528	9.624
K1	7.722	8.259	8.363	8.648	7.480	8.692
MF	6.407	6.585	6.728	6.576	7.797	7.374
NU2*	5.073	5.228	5.178	5.618	6.518	5.436
MS4	4.773	4.779	4.684	4.271	5.299	5.085
MSN2	2.953	2.550	3.321	3.521	5.300	4.130
MN4	4.351	4.161	4.296	2.855	3.578	3.910
MNS2	3.984	4.401	4.113	4.337	7.795	3.812
2SM2	2.843	2.530	3.041	3.124	2.372	3.480
3MN4	3.458	2.986	3.071	3.053	3.843	3.457
M6	3.337	4.160	5.680	5.571	6.816	3.336
P1	2.533	2.709	2.743	2.836	2.453	2.851
2MN6	2.120	2.806	3.820	3.961	5.487	2.437
MM	3.288	3.048	1.653	0.98	2.916	2.402
3MS2	2.303	1.237	1.818	1.425	3.167	2.344
3MS4	1.320	1.607	1.474	1.625	2.268	2.153
M8	2.065	1.993	1.747	3.012	3.532	1.910
2MSN4	1.775	1.727	2.092	1.436	1.349	1.826
Q1	2.111	1.783	1.994	2.221	1.914	1.658
2MS6	2.161	2.311	3.612	3.035	4.260	1.452
3MS8	1.723	1.531	1.156	2.834	3.561	1.452
3MNS6	0.362	0.724	0.513	1.59	2.480	1.253
MK3	1.625	0.512	1.154	1.153	1.335	1.058
MSN6	0.202	0.307	0.828	1.183	1.678	1.034
2MNS4	1.013	0.895	0.881	1.024	1.417	0.989
M3	0.922	0.593	0.734	0.821	0.818	0.805
2MSN8	0.312	0.194	0.377	0.729	1.224	0.565
4MS6	0.438	0.152	0.388	0.564	0.687	0.548
S4	0.392	0.227	0.399	0.115	0.528	0.413
2SM6	0.098	0.296	0.251	0.172	0.266	0.396
4MS10	0.996	1.044	0.702	0.931	0.979	0.324
2(MS)8	0.310	0.181	0.198	0.446	0.628	0.028

* coupled constituent

Table 6: Phases of the harmonic constituents (in degrees) at gauge stations G1 to G6 in the Dithmarschen Bight

Harmonic Constituents	G1 Blauort	G2 Tertius	G3 Trischen	G4 Buesum	G5 Steertloch	G6 Flackstrom
M2	326.9	327.6	323.1	332.9	335.7	333.5
S2	37.1	38.2	35.0	46.3	50.7	47.7
N2	295.7	295.2	294.7	303.7	306.2	304.6
2MN2	173.9	176.7	165.3	177.5	185.1	175.3
K2	37.1	38.2	35.0	46.3	50.7	47.7
MU2	59.7	57.7	49.3	60.2	72.4	54.7
O1	241.3	234.3	234.3	240.5	241.7	238.6
M4	149.1	149.1	153.7	138.3	136.6	139.7
K1	22.5	24.6	21.9	27.3	30.2	24.9
MF	171.8	171.0	170.6	160.5	182.2	174.6
NU2*	295.7	295.2	294.7	303.7	306.2	304.6
MS4	211.2	205.3	209.0	198	203.3	201.1
MSN2	234.4	230.4	203.9	210.3	220.1	221.0
MN4	107.3	108.9	120.7	100.4	105.2	106.2
MNS2	47.4	41.4	25.8	31	24.1	30.0
2SM2	248.1	218.2	226.3	232	258.2	243.4
3MN4	335.0	333.8	335.2	320.1	311.3	323.6
M6	22.5	43.9	19.4	120	134.1	127.0
P1	22.5	24.6	21.9	27.3	30.2	24.9
2MN6	344.4	7.2	343.9	86.2	103.8	94.1
MM	265.3	277.1	264.6	221.4	304.3	282.0
3MS2	177.7	227.2	207.6	222.4	204.0	213.8
3MS4	216.9	217.1	205.6	185.1	166.8	182.5
M8	280.3	283.1	265.7	293.3	299.4	298.8
2MSN4	38.8	34.7	28.6	32.7	21.6	15.8
Q1	169.0	171.6	178.0	172.4	165.4	186.6
2MS6	60.6	85.1	65.0	188.9	208.1	211.7
3MS8	342.7	344.5	314.0	350.7	355.8	355.0
3MNS6	185.8	172.5	111.1	218.6	225.8	236.5
MK3	136.9	183.5	152.5	163.2	114.4	139.8
MSN6	154.9	238.5	165.6	315.6	318.4	344.2
2MNS4	213.1	201.8	203.2	147.6	141.1	165.1
M3	147.7	106.7	125.7	174	169.4	172.6
2MSN8	64.1	60.9	18.9	52.5	44.7	60.2
4MS6	283.2	284.7	358.5	270.9	337.6	300.4
S4	52.6	10.5	61.5	34.2	348.6	352.1
2SM6	143.5	64.3	96.8	43.5	307.6	80.9
4MS10	162.2	203.2	185.3	150.5	127.5	269.2
2(MS)8	336.4	326.5	340.7	51.3	57.7	270.3

* coupled constituent.

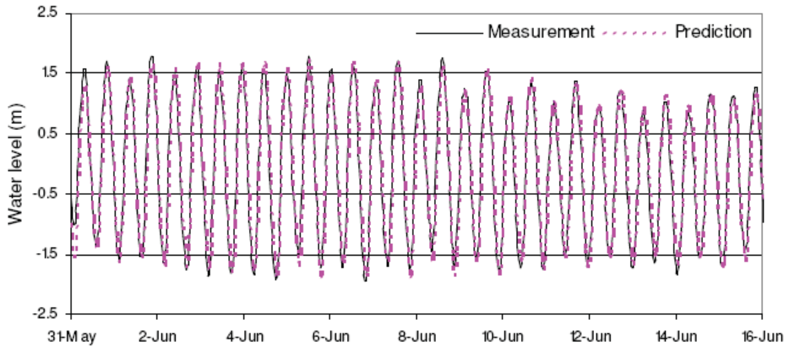

a) Period 1

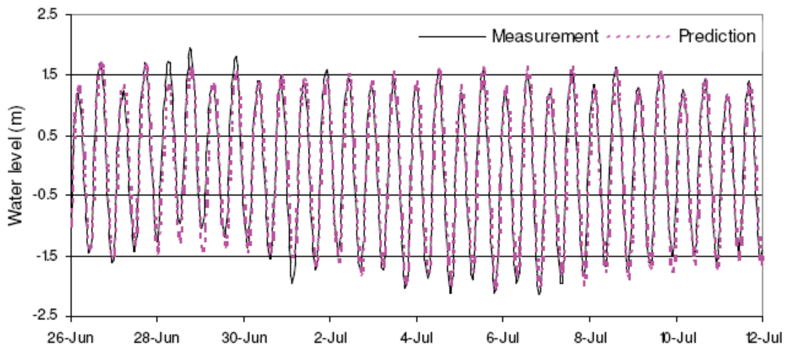

b) Period 2

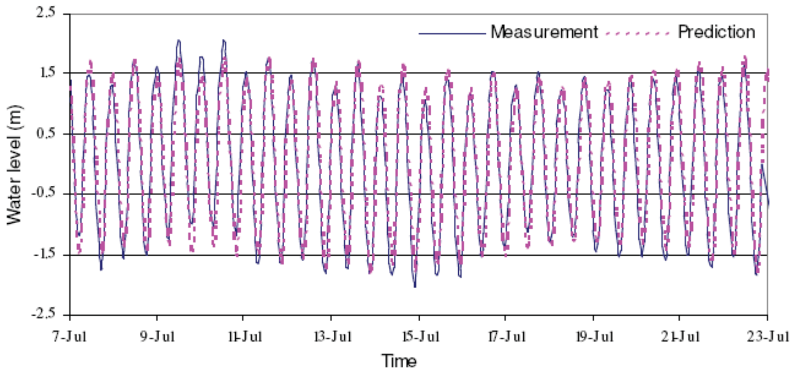

c) Period 3

Fig. 8: Comparison of tidal records and astronomical predictions at the gauge station Tertius (G2)

Die Küste, 69 PROMORPH (2005), 1-420

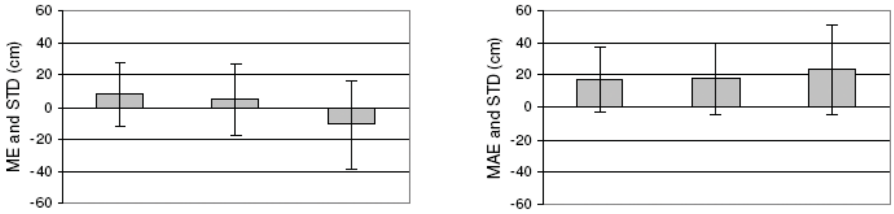

(a) Station G1 – Blauort

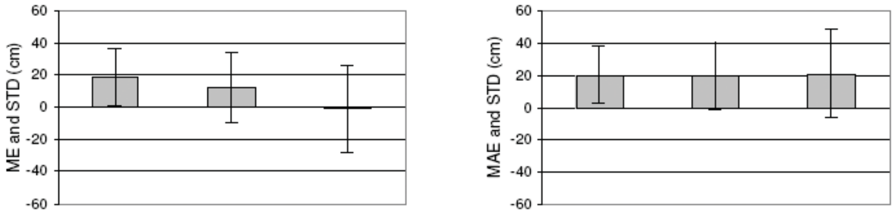

(b) Station G2 – Tertius

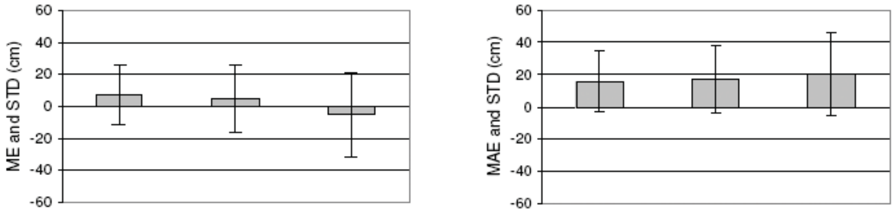

(c) Station G3 – Trischen

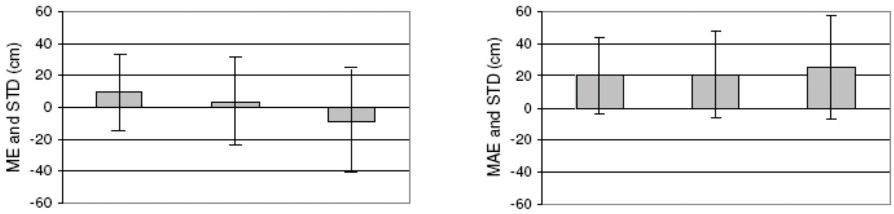

(d) Station G5 – Steertloch

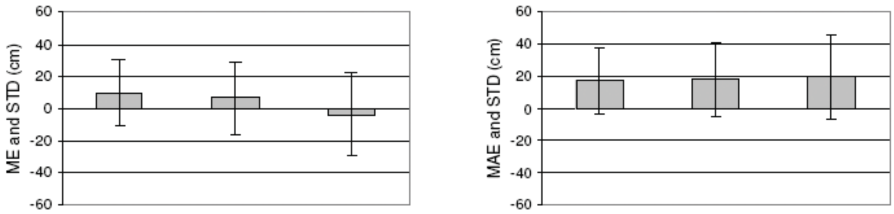

(e) Station G6 – Flackstrom

Fig. 9: Mean Error (ME), Mean Absolute Error (MAE), and corresponding standard deviations of water level at gauge stations G1, G2, G3, G5 and G6 in the Dithmarschen Bight

Die Küste, 69 PROMORPH (2005), 1-420

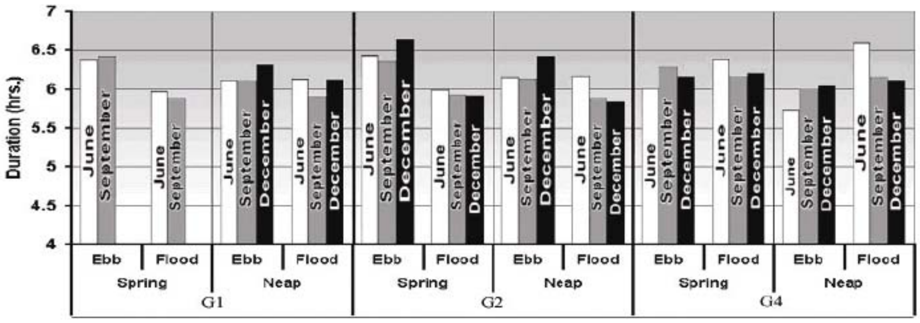

Fig. 10: Mean duration of ebb and flood phases at gauge stations G1, G2 and G4 (ASP, 2004)

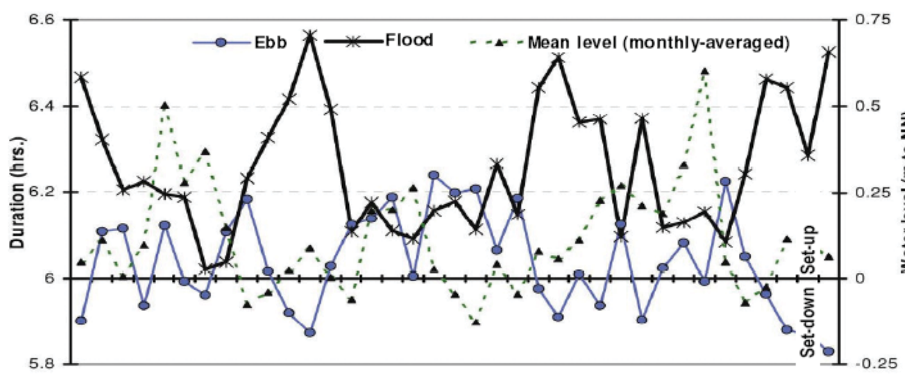

a) Duration of flood and ebb phases

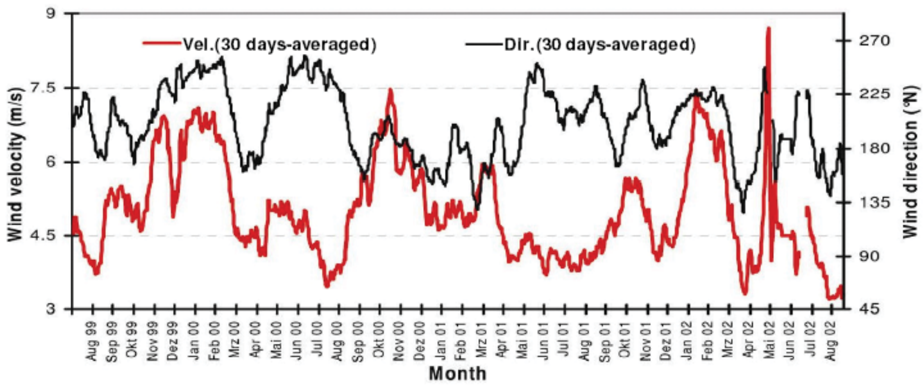

b) Wind velocity

Fig. 11: Variation of the duration of ebb and flood phases at gauge station G4 (ASP, 2004)

5.2 Storm Surges

Storm surges, which result from extreme meteorological events, lead to a temporary increase in water levels in the near-coast region. The magnitude of a surge depends primarily on the size, intensity and movement of the storm responsible, and may be further influenced by the shape of the coastline, local bathymetry and state of the astronomical tide. The actual height of a storm surge is determined by subtracting the instantaneous astronomical tidal water level from the observed water level. A surge is mainly generated by the shear stresses exerted by the wind on the water surface and may be enhanced by the reduced atmospheric pressure associated with a storm depression. Since the wind-induced water level set-up is inversely proportional to the local water depth, the tidal flat areas of the Dithmarschen Bight are strongly affected by storm surges.

ROHDE (1992) found that the probability of storm surges exceeding 1.5 m at the mouth of the Elbe (Cuxhaven) annually is centred around December, with over 60 % occurring from November to January and over 80 % from October to February. MERTSCH (2004) presented a list of severe storm surges at Sankt Peter-Ording between 1990 and 2002 based on water level measurements supplied by the Regional State Office for Rural Areas (ALR) in Husum. This list contains 15 records of high water levels exceeding 3.5 m. Subtracting a mean high water level of an estimated 1.5 m above NN from the recorded high water levels results in storm surges of 2.0 m and above. It should be noted that these results are based on the mean high water level, as the instantaneous astronomical tidal water levels were not available for the periods in question. Similarly, the height of the maximum storm surge based on this list was found to be 2.85 m. The largest well-documented storm surge at Buesum occurred in 1967, when a maximum water level of 5.16 m above NN was observed (EAK, 2002). Subtracting a mean high water level of approximately 1.6 m above NN from the latter results in a storm surge of approximately 3.6 m. Again, the mean high water level was assumed due to lack of information on instantaneous astronomical tidal water levels during the storm surge.

5.3 Currents

The spatial and temporal variations of current velocity were investigated by analysing measured current velocities in the main tidal channels. This analysis focused on the sets of field data obtained from moving vessels and moored devices, as summarised in Table 2 and 3. Plots showing the variation of current velocity over the vertical and across the surveyed cross-sections as well as the variations of depth-averaged current velocity during a spring tide (21 to 23 March 2000) are shown in Fig. 13. Profiles of current velocity obtained from moored devices at two locations in the main tidal channels (stations N1 and S1 in the Norderpiep and Suederpiep tidal channels, respectively) are presented for selected conditions in Fig. 14. The variations of current velocity in the bottom and surface layers as well as depth-averaged values are also shown for neap and spring tides under relatively calm wind conditions as well as for periods with stronger winds.

Typical current velocity profiles during a spring tide are shown in Fig. 12. The results are shown for two measuring stations (marked in red and solid black) in cross-sections T1, T2 and T3. The variation of current velocities over the vertical is typical for tidal areas, with almost zero current velocity during low and high water slack and maximum values during the ebb and flood phases. In cross-section T2, through which most of the flow is conveyed into and out of the central Dithmarschen Bight, however, a different behaviour is observed in this respect during neap and spring tides. Whereas the maximum current velocity is along the south bank during the flood phase and the north bank during the ebb phase during spring tides, the opposite behaviour is observed during neap tides.

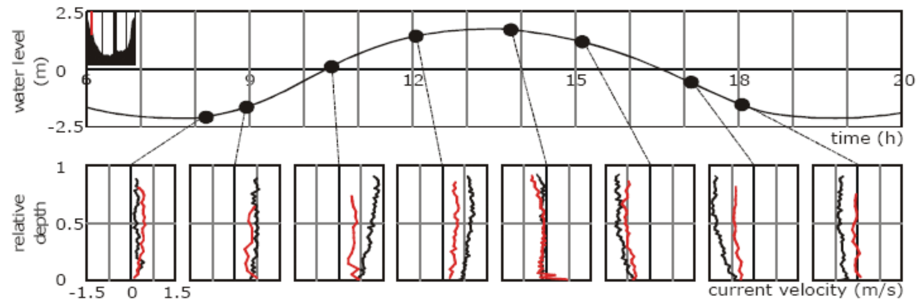

a) Cross-section T1 on 22 March 2000

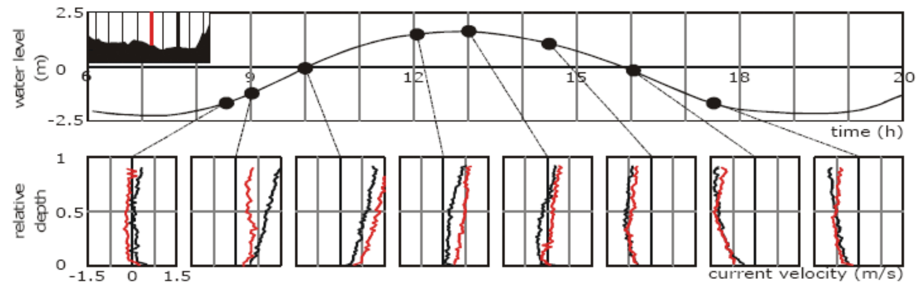

b) Cross-section T2 on 21 March 2000

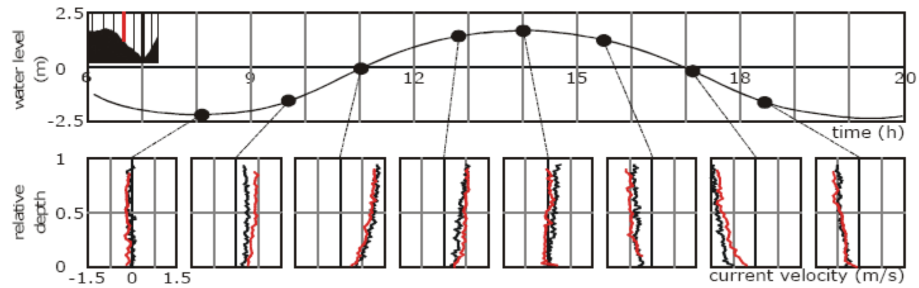

c) Cross-section T3 on 23 March 2000

Fig. 12: Variation of current velocity profiles for a spring tide during relatively calm weather conditions

The cross-sectional variation of current velocity in the tidal channels was investigated by analysing the distributions of measured velocities over the surveyed cross-sections. Typical distributions of current velocity in cross-sections T1, T2 and T3 for a spring tide are shown in Fig. 13. The results shown are for high and low water slack conditions and at times of maximum ebb and flood currents. These results reveal that in cross-sections T1 and T3 the cross-sectional variations during the flood and ebb phases attain a maximum at approximately the same location and that the gradient over the width is less pronounced than in cross-section

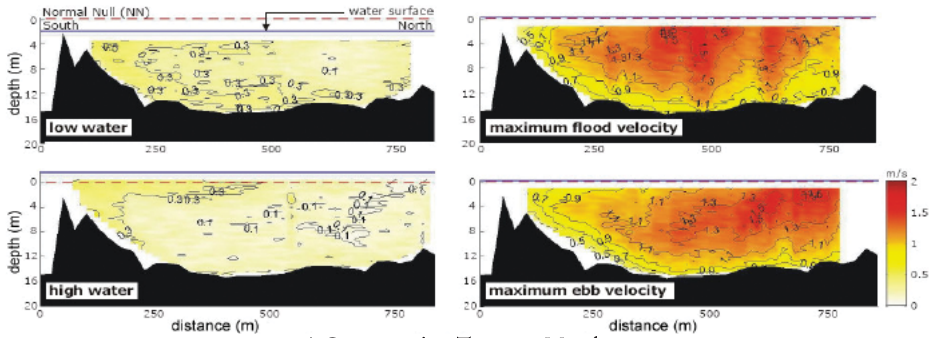

a) Cross-section T1 on 22 March 2000

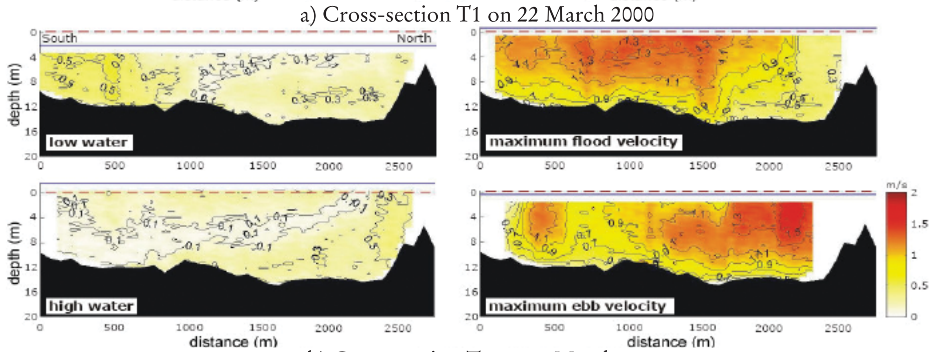

b) Cross-section T2 on 21 March 2000

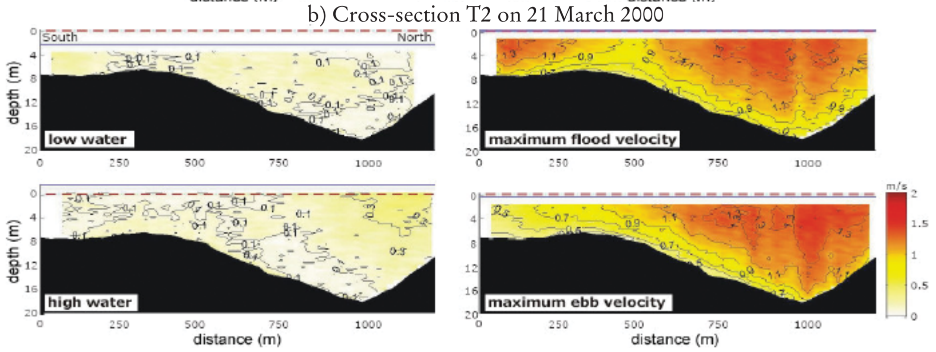

c) Cross-section T3 on 23 March 2000

Fig. 13: Current velocity variations over the surveyed cross-sections during a spring tide

T2. In cross-section T2 it is also evident that the flood flow enters the study area predominantly through the northern part of the cross-section, whereas the ebb flow leaves the study area essentially through the southern part.

The cross-sectional variations of depth-averaged current velocity in cross-sections T1, T2 and T3 during a full spring tidal period are shown in Fig. 14. The spatial plots were obtained by interpolating the current velocities measured along the cross-sectional transects with respect to time. It is interesting to note that the maximum current velocities during the flood and ebb phases of neap and spring tides are at approximately the same location in cross-sections T1 (Norderpiep channel) and T3 (Piep channel), namely in the deepest parts of the channels. In cross-section T2, through which most of the flow is conveyed into and out

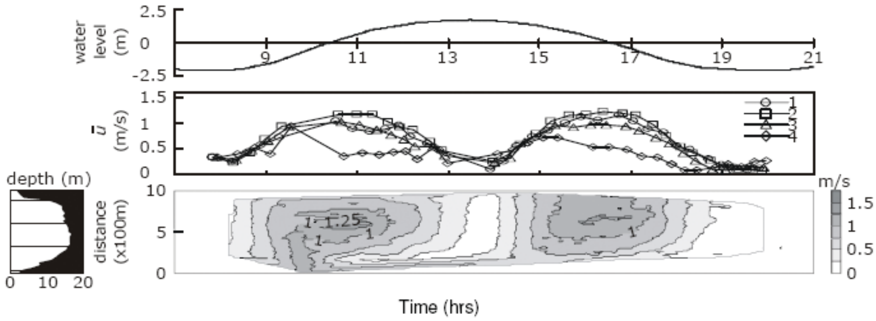

a) Cross-section T1 on 22 March 2000

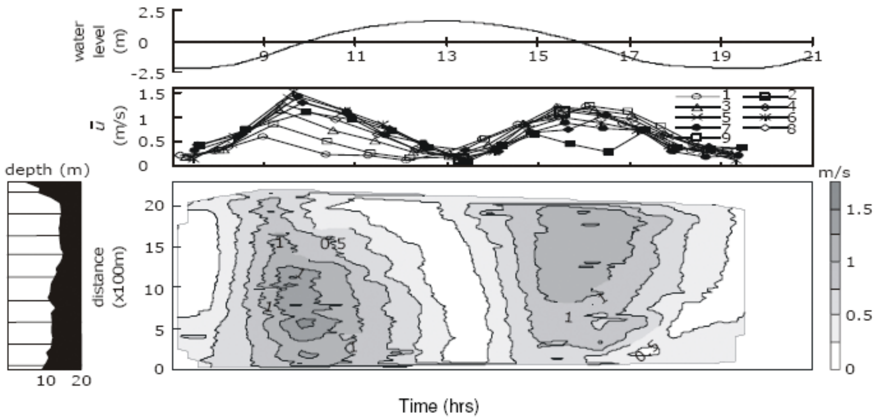

b) Cross-section T2 on 21 March 2000

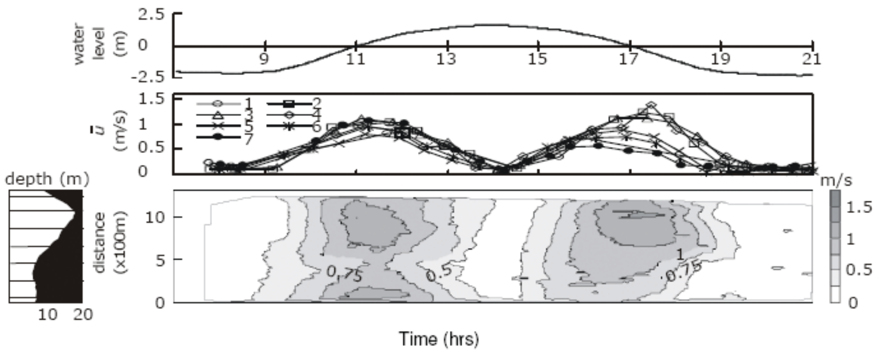

c) Cross-section T3 on 23 March 2000

Fig. 14: Variations of depth-averaged current velocity over the cross-sections during a spring tide

of the central Dithmarschen Bight, however, a different behaviour is observed in this respect during neap and spring tides.

In order to investigate the variations of current velocity during spring and neap tides under different weather conditions the measurements obtained from the moored devices were analysed. Typical results are shown for periods with stronger winds. Current velocities measured near the free surface and the seabed as well as depth-averaged values are shown together with water level variations and observed wind speed and direction in Fig. 15. Maximum values of current velocity of about 1.8 m/s were observed in the Suederpiep tidal channel during the flood phase of a spring tide. Flood dominance is clearly evident in the Norderpiep channel, and to a lesser extent also in the Suederpiep. The current velocities in the upper layers are seen to be influenced by wind velocity, particularly at the measuring station N1 in the Norderpiep tidal channel. This measuring station is more exposed than station S1 and is not protected by sand banks.

The temporal variations of flow discharge through cross-sections T1, T2 and T3 for a spring (March 21 to 23, 2000) and neap (December 5 to 6, 2000) tide are shown in Figs. 16 and 17, respectively. These estimates were obtained by assuming constant cross-sectional widths. The discharges through cross-section T2 were found to be significantly higher than through the other two cross-sections (T1 and T3). On the basis of calculations it was found

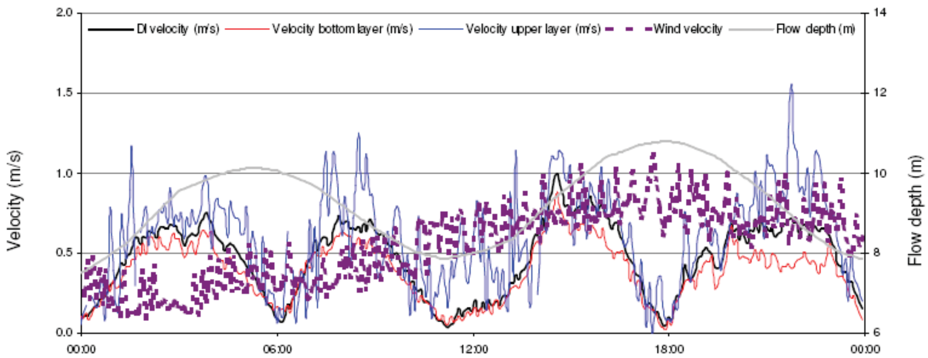

Station N1 in the Norderpiep tidal channel on 24 August 2000 – tidal range of 3.25 m and wind velocities of up to 10 m/s

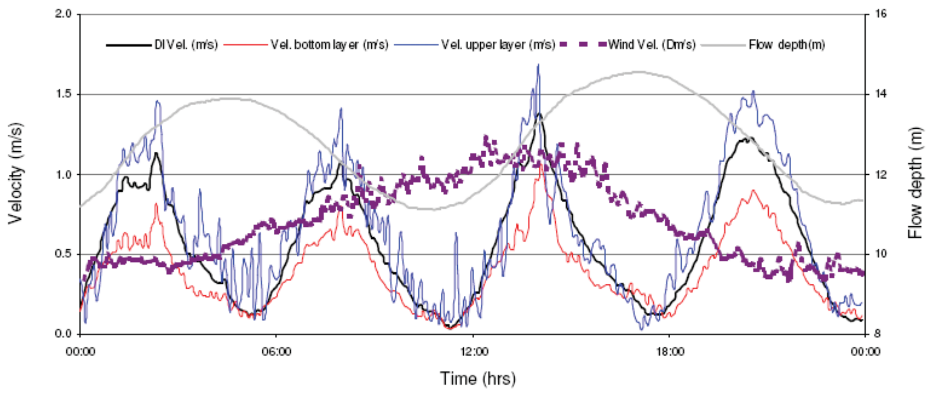

Station S1 in the Suederpiep tidal channel on 9 June 2000 – tidal range of 3.5 m and wind velocities of up to 13 m/s

Fig. 15: Variation of current velocities in the Norderpiep and Suederpiep tidal channels recorded by moored devices during periods with strong winds

that the flow discharge through cross-section T2 almost doubles from about 15,000 m^3/s during neap tides to about 30,000 m^3/s during springs. In the case of cross-sections T1 and T3 the increase in flow discharge with tidal range was found to be less pronounced. An investigation of current velocity variations over lunar cycles was carried out by analysing measured values of current velocity for different tidal ranges. This analysis was performed on the basis of the measurements listed in Table 2. The variations of maximum depth-averaged and cross-sectionally averaged current velocities with tidal range are shown in Fig 18. As would be expected, the results clearly indicate an increase in measured current velocities with tidal range, with maximum values during spring tides. The maximum depth-averaged and cross-sectionally averaged current velocities for a given tidal range were found to be similar in each of the surveyed cross-sections.

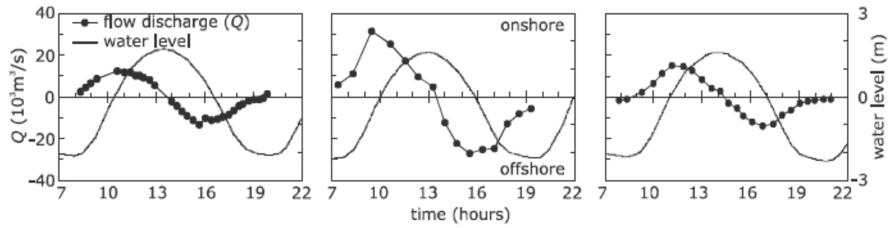

a) Cross-section T1 b) Cross-section T2 c) Cross-section T3

Fig. 16: Total flow discharges through cross-sections T1–T3 during a spring tide on March 21–23, 2000

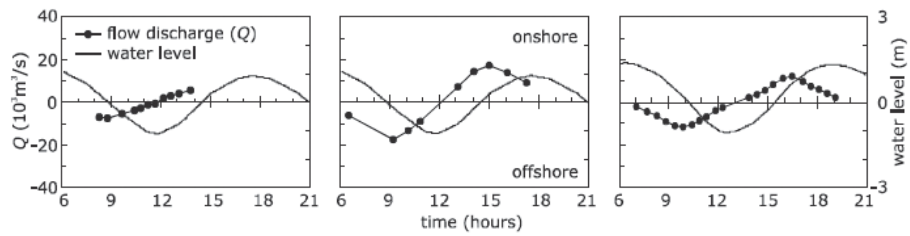

a) Cross-section T1 b) Cross-section T2 c) Cross-section T3

Fig. 17: Total flow discharges through cross-sections T1–T3 during a neap tide on December 5–6, 2000

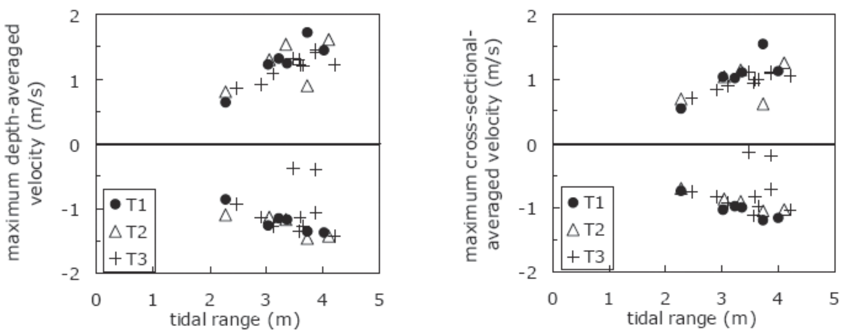

Fig. 18: Variation of depth-averaged and cross-sectionally averaged current velocities with tidal range in cross-sections T1–T3

5.4 Waves

Data from several waverider buoys provided by the Coastal Research Station of the Lower Saxony Board of Ecology (CRS) on Norderney, the Regional State Office for Rural Areas in Husum (ALR) and the German Federal Maritime and Hydrographic Agency in Hamburg (BSH) were analysed to investigate wave characteristics in the study area. The available data were analysed to gain a better understanding of wave characteristics and wave transformation throughout the study area and also to identify the data required for developing the wave model. The locations of the waverider buoys listed in Table 1 are shown in Fig. 1. Typical results of this analysis as well as an interpretation of the results are presented in the following sections.

5.4.1 Data from the CRS

During the one-month measuring campaign undertaken in September and October 1996 by the CRS, Norderney (NIEMEYER, 1997), wave measurements were obtained from five waverider buoys developed by Datawell in the Netherlands. Waverider buoys are equipped with an installed accelerometer that measures the vertical movements (heave) of the buoy. The buoys were strategically located in the Dithmarschen Bight in order to provide the data necessary for developing the wave model. The two buoys located further offshore were directional waveriders equipped with two additional accelerometers to measure north-south and east-west displacements.

The waverider buoys record hourly displacements based on wave sampling at 20-minute intervals. 20-minute intervals are considered long enough to measure a sufficient number of waves for analysis and at the same time short enough to avoid significant changes in wave conditions during a single interval. Recording takes place at a frequency of 2.56 Hz and 1.28 Hz for non-directional and directional waveriders, respectively. The significant wave height, peak period and wave direction are determined from the relative fluctuations over the 20-minute sampling intervals.

The time series of significant wave heights recorded by the five waverider buoys during September and October 1996 are shown in Fig. 19. The occurrence of at least two storms

Die Küste, 69 PROMORPH (2005), 1-420

during the measurement period with significant wave heights of up to 2 m makes this data set ideal for calibration and validation of the wave model. Generally speaking, it was found that waves are much higher at positions CRS1 and CRS2 than at the other measurement locations. Most of the wave energy apparently dissipates between the two exposed buoys to the west and the three landward buoys to the east. This energy dissipation is due to depth-induced wave-breaking and bottom friction once the waves enter shallower water. Owing to refraction and diffraction wave energy is partly re-directed into shallower water, thus enhancing the afore-mentioned dissipation.

Relatively high significant wave heights were observed around 13 September and at the end of September 1996, with values attaining up to 2 m at positions CRS1 and CRS2. Wave heights during the remainder of the recording period are significantly lower. Although these trends are reflected in the wave heights recorded by the buoys at positions CRS3, CRS4 and CRS5, wave heights at these locations were found to remain below 0.7 m during the entire measurement period. This is due to the sheltering effect of the tidal flats combined with refraction and diffraction of the wave energy that penetrates beyond them.

Fig. 20 shows the mean wave direction recorded by the waverider buoy at location CRS1. After an initial period of fluctuations during stormy conditions the wave direction remains relatively constant in the onshore direction at about 280° N. About 6 days later the wave direction reverses over north to the offshore direction at about 90° N. The wave heights during this period are in the range of only 0.3 to 0.7 m, which may be explained by the short fetch between the coastline and the CRS1 buoy. Following this calm period with very low wave heights the wave direction turns over south back towards west-northwest after about 25 September. At the same time the waves again increase in height, attaining up to 2.0 m at the CRS1 buoy. This increase in wave height is explained by the fact that westerly (onshore) winds have much larger fetches. From an analysis of the wave spectra (not shown here for the sake of compactness) it was found that double-peaked spectra may occur during periods of westerly winds, indicating a mixture of swell and locally-generated wave energy. During the identified periods of easterly winds, on the other hand, only single-peaked spectra were observed. This is explained by the fact that no swell enters the investigation area during these periods. Fig. 21 shows the wind speed and direction in the study area during the measurement period. These data were generated by the synoptic PRISMA interpolation model (LUTHARDT, 1987), which processes meteorological observations from various coastline and offshore stations. Although the wind and wave directions are fairly dissimilar up to 18 September, a clear correlation between the two is observed subsequently. During the second stormy period, i.e. around 30 September, a dissimilar trend is again apparent. As waves from the west consist to a large extent of swell energy, their direction does not necessarily correspond to the instantaneous local wind direction. In the case of easterly winds, however, the wave energy is almost entirely associated with locally wind-generated waves and thus a much higher correlation is obtained between wind and wave directions.

.

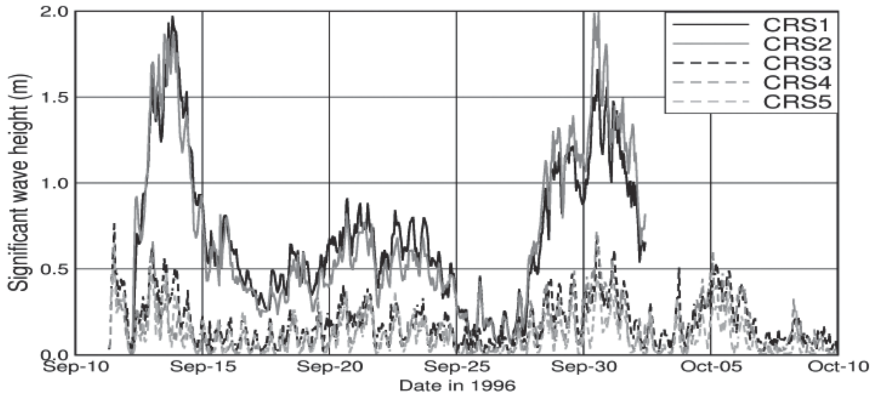

Fig. 19: Observed significant wave heights at the five CRS waverider buoy locations

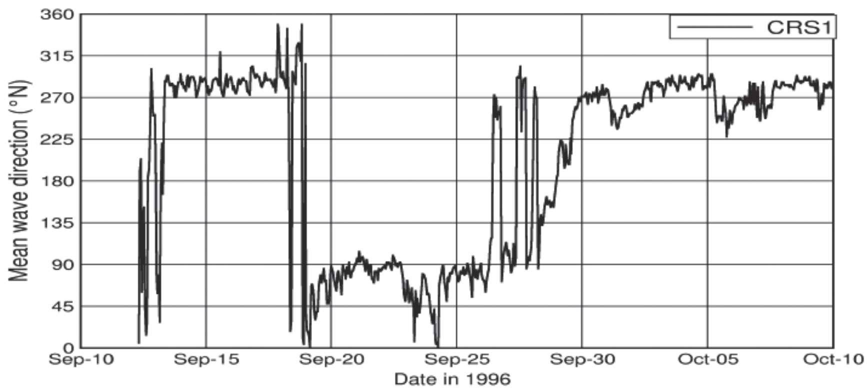

Fig. 20: Observed wave direction at waverider buoy location CRS1

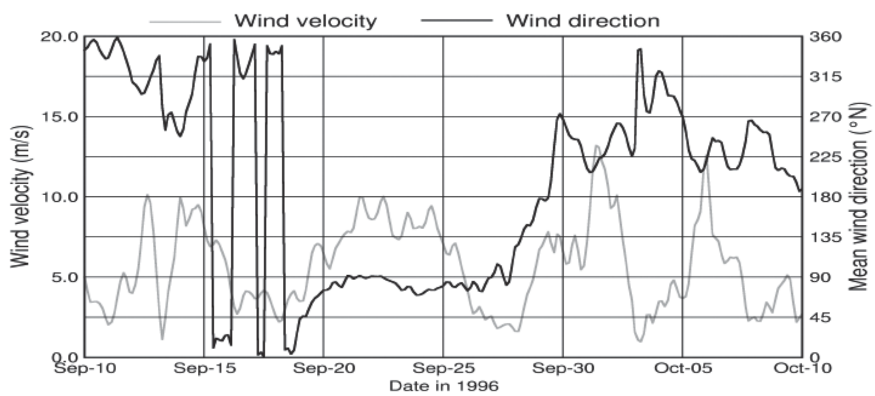

Fig. 21: Wind speed and direction in the Meldorf Bight. Data generated by the PRISMA model (LUTHARDT, 1987)

Die Küste, 69 PROMORPH (2005), 1-420

5.4.2 Data from the ALR and BSH

Simultaneous measurements of significant wave heights and mean wave direction were made available from November 2000 to May 2001 by the ALR in Husum and BSH in Hamburg. Fig. 22 shows significant wave attenuation between the ALR buoy at the entrance to the Suederpiep tidal channel and the BSH buoy in the near vicinity of Tertius. It is evident that the wave heights recorded by the BSH buoy are as much as 50 % lower than those recorded by the ALR buoy. Wave measurements from the ALR waverider buoy show significant wave heights of up to 3.4 m. Average wave heights were generally found to lie within the range of 0.5 to 1.5 m. These wave heights reflect the relatively exposed location of this buoy at the entrance to the Suederpiep tidal channel. The measured wave heights recorded by the BSH waverider buoy generally lie within the range of 0.0 to 1.0 m. During a number of brief periods, however, wave heights of up to 1.5 m were attained. Considering the fact that the predominant wave direction is from southwest to northwest, wave heights tend to reduce towards the east. This reduction may be due to several processes, e.g. wave-breaking, energy dissipation due to bottom friction, diffraction behind shallow or dried-up flats and shoals, and refraction towards channel banks and shoals. Although not deducible from the presented measurements, wave-breaking and shoaling are suspected to play an important role along the western edge of the outer tidal flats. Waves approaching from the east are locally-generated wind waves with a limited fetch, which is longer at the ALR buoy than at the BSH buoy. The increase in depth, and fewer morphological obstacles such as shoals and tidal flats, also account for a reduction in the magnitude of wave energy dissipation on moving eastwards.

As may be seen in Fig. 23, the mean wave directions recorded by the two buoys are nonetheless very similar. These are either governed by the local wind direction in the case of locally-generated waves, or by the mean swell direction. Differences in the mean wave direction are thus only expected for waves from the southwest to northwest. With regard to waves entering the investigation area from this sector, they may be swell-dominated at the ALR buoy and wind-dominated at the BSH buoy. This may well account for differences in the mean wave direction at the two measurement locations. A second possibility is that residual swell energy arriving at the BSH buoy from the western sector has already been diffracted or refracted, thus altering the mean wave direction at this location.

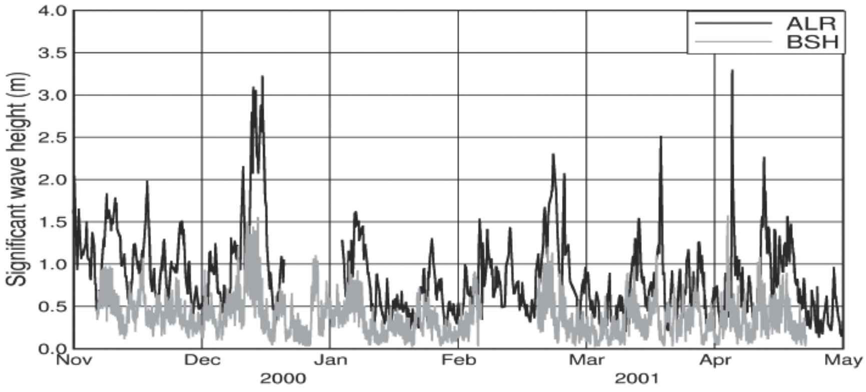

Fig. 22: Wave heights measured simultaneously by the ALR and BSH waverider buoys

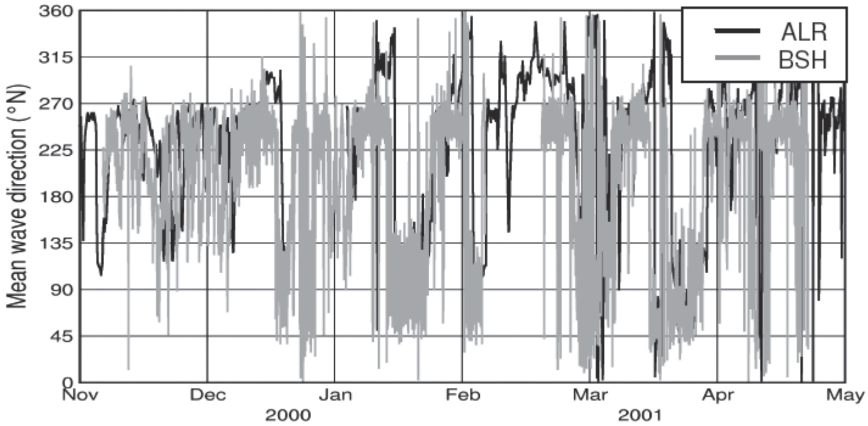

Fig. 23: Wave directions measured simultaneously by the ALR and BSH waverider buoys

5.5 Salinity and Temperature

The seasonal variations of salinity and temperature in the study area were also analysed within the framework of the present investigation. Vertical profiles of salinity and temperature were measured at 3-monthly intervals during the year 2000 from vessels at cross-section T2 at the entrance to the investigation area and at cross-section T3 closer to the coast (see Fig. 1). Fig 24 shows measured vertical salinity profiles over complete tidal periods at cross-sections T2 and T3 on 21–23 March 2000 (tidal range of about 3.9 to 4.1 m), 5–6 June 2000 (tidal range of about 3.7 m), 5–6 September 2000 (tidal range of about 2.9 to 3.1 m) and 5–6 December 2000 (2.3 to 2.5 m). It is seen that the vertical salinity distributions in both cross-sections are fairly uniform throughout the year. This is not surprising, considering the fact that the water column in this fairly shallow area is always well-mixed due to strong tidal currents. The salinity values range from about 20 to 28 psu, indicating the influence of coastal freshwater run-off derived mainly from the discharge of the Elbe estuary in the south. It is interesting to note that not only salinity values but also their tidal variations are slightly higher further away from the coast. A certain seasonal variation in salinity is also evident, with lower values prevailing during the month of March. The maximum variation in salinity throughout the year is found to be about 7–8 psu. This is most probably due to seasonal variations in the freshwater discharges of the Elbe and Eider estuaries in combination with prevailing meteorological conditions. Extensive measurements carried out in the area within the framework of the research project TRANSWATT (SÜNDERMANN et al., 1999) have clearly shown that the salinity distribution in the Dithmarschen Bight is highly dependent on the magnitude of riverine discharges and local wind conditions.

Variations in the vertical temperature profile were analysed in a similar manner to salinity. Fig. 25 shows vertical profiles of temperature at cross-sections T2 and T3 measured in conjunction with the above-mentioned salinity measurements. Similar to salinity, the variation in temperature over the water column was found to be fairly uniform. The seasonal variation in water temperature was found to range from about 6–7 °C in March to about 16–17 °C in September. Spatial variations, on the other hand, were found to be negligible. The uniform vertical profiles of salinity and temperature in the study area is indicative of well-mixed conditions without flow stratification due to density effects.

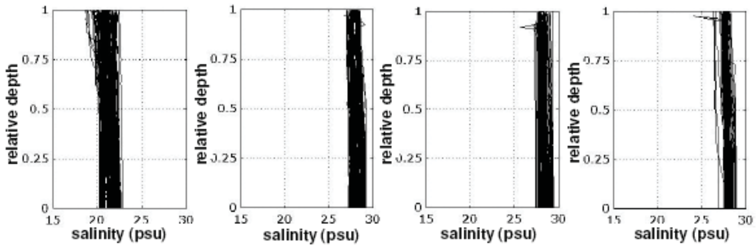

March 21, 2000 June 5, 2000 September 5, 2000 December 5, 2000

a) Cross-section T2

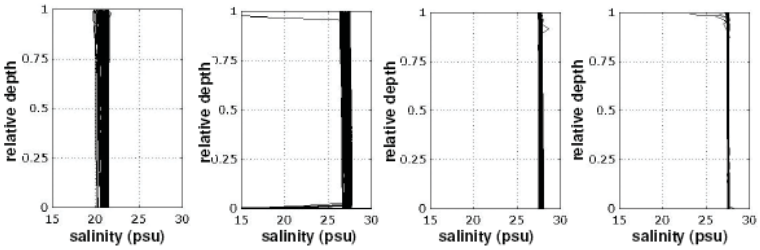

March 23, 2000 June 6, 2000 September 6, 2000 December 6, 2000

b) Cross-section T3

Fig. 24: Seasonal variation of vertical salinity profiles in cross-sections T2 and T3

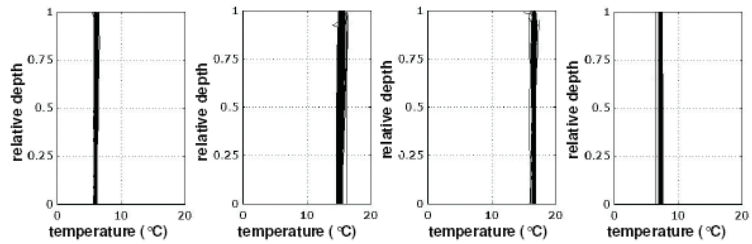

March 21, 2000 June 5, 2000 September 5, 2000 December 5, 2000

a) Cross-section T2

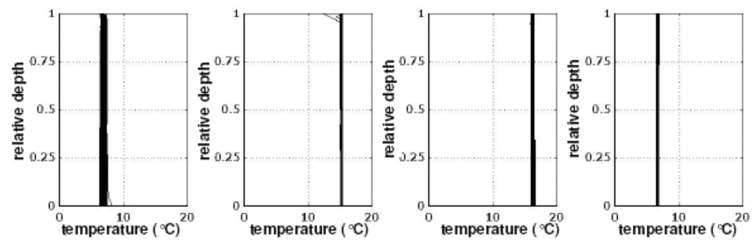

March 23, 2000 June 6, 2000 September 6, 2000 December 6, 2000

b) Cross-section T3

Fig. 25: Seasonal variation of vertical temperature profiles in cross-sections T2 and T3

6. Conclusions

This paper presents the results of an analysis of field measurements of water levels, current velocities, waves, salinity, and temperature for a wide range of conditions in a tidally-dominated area of the German North Sea. The area investigated is the central Dithmarschen Bight located between the Elbe and Eider estuaries. Continuous monitoring of wind speed, water levels and waves by the relevant authorities was supplemented by field measurements specially intended to provide a dense spatial and temporal coverage of current velocities. The field measurements not only serve as a means of identifying the most dominant physical processes governing the hydrodynamics of the study area but also provide a valuable data set for defining the modelling strategy as well as for developing and evaluating process-based models for the simulation of flow and waves.

Water levels at six locations were implemented for the purpose of tidal analysis and calibration of the flow model. The mean tidal range in the study area was found to vary from about 3.1 m to 3.4 m between the mouth of the Elbe estuary in the south and the Eider peninsula in the north. The neap and spring tidal ranges in the study area are 2.8 m and 3.5 m, respectively. As a result of the tidal analysis it was possible to identify the 39 tidal constituents that best represent the observed water levels at the six monitoring stations. The quality of the tidal constituents was verified for three periods of up to 43 days under relatively calm wind conditions. On the basis of this analysis, satisfactory agreement was obtained between observed and predicted tidal elevations. A mean absolute error of less than 20 cm was obtained at all locations, representing about 6 % of the mean tidal range.

The seasonal variation of tidal asymmetries was analysed on the basis of water level measurements at the entrance to the main tidal channels, i.e. the Norderpiep channel to the northwest, the Suederpiep channel to the southwest, and the Piep channel nearer the coast. This analysis revealed differences of up to 45 min in the duration of the tide at the latter three locations. The results of this analysis indicate that cross-sections located at the entrance to the study area are flood-dominated during most of the year, whereas the cross-section nearer the coast is generally ebb-dominated during the summer and exhibits virtually no asymmetries during the autumn and winter months. Flood dominance in the cross-sections at the entrance to the main tidal channels, in particular the Norderpiep tidal channel, was also confirmed by current velocity measurements.

The highest storm surge in the study area, measuring approximately 3.6 m (EAK, 2002), was recorded in 1967. About 60 % of all storm surges occur between November and January; a further 20 % between October and February. At the nearby gauge station of Sankt Peter-Ording, storm surges exceeding approximately 2.0 m occurred on average once a year during the period 1990 to 2002 (MERSCH, 2004).

Selective measurements of current velocities over several cross-sections were performed using acoustic profilers from moving vessels. Additional current velocity measurements over the water column were provided by moored devices. These measurements covered a wide range of conditions typical of the study area. The measurements from ship-based devices provided a good description of the spatial variation of current velocities. Measurements were carried out for a variety of tidal conditions, with tidal ranges varying from about 2.3 m to 4.1 m under relatively calm weather conditions. The resulting data sets provided a good description of spatial and temporal variations of current velocities in the study area.

The maximum values of point and depth-averaged current velocity in the main tidal channels were found to be about 2.8 m/s and 1.7 m/s, respectively. The vertical distribution of current velocity was also found to be fairly uniform at all surveyed locations due to low bed roughness. Owing to high tidal dominance in the study area, vertical profiles of temperature and salinity were found to be fairly uniform. This is concomitant with the observed absence of vertical velocity stratification. An increase in current velocity with increasing tidal range was clearly evident. The maximum depth-averaged current velocity approximately doubles from neap to spring tide.

Wave data obtained from simultaneous measurements at five locations during a one-month period (NIEMEYER, 1997) provided a valuable insight into wave transformation throughout the study area. Measurements covering two longer periods of about 12 and 6 months at locations about 10 km seawards of the outer tidal flats as well as in the Suederpiep tidal channel yielded essential information regarding the range and probability of wave characteristics. On the basis of these wave data it was found that the major part of swell energy is dissipated along the edge of the outer tidal flats. The limited depths to the east of this location are responsible for energy dissipation due to wave-breaking, bottom friction, refraction, and diffraction. Together with the sheltering effect of the tidal flats and shoals, the wave energy in the eastern part of the study area is essentially locally-generated. Maximum wave heights some 10 km westward of the outer tidal flats were found to be about 3.5 m. Wave heights of less than 2.0 m were measured along the edge of these tidal flats during the observation period, with maximum values of approximately 1.5 m in the Suederpiep tidal channel. Further eastwards, no waves exceeding 0.7 m were recorded.

Besides providing the basis for a better understanding of the governing physical processes in the study area, the data acquired in the present investigation were also of considerable value for the further development of the flow and wave models. From an analysis of the data it was possible to clarify various aspects of model development. Suggestions regarding the dimensions and limits of the model have also been proposed. As the hydrodynamics of the study area are very much dependent on conditions along the western boundary, it was proposed to locate the open-sea boundary of the model eastwards of the approach to the main tidal channels in regions where morphological activity is less intense. In view of the available wave data it was recommended to develop a model covering the entire Dithmarschen Bight. Owing to the fairly uniform vertical distributions of velocity, salinity, and temperature, the application of a 2DH model approximation should be considered initially in preference to a 3D approach.

The derived data have been used among others for the assessment of open-sea boundary condition approaches (MAYERLE et al., in this volume), the development of set-up flow and wave models (PALACIO et al., in this volume; WILKENS et al., in this volume), and the definition of representative conditions for the simulation of medium-scale morphodynamics (JUNGE et al., in this volume; WILKENS and MAYERLE, in this volume).

7. Acknowledgements

The authors wish to thank the German Ministry of Education and Research for funding the research project PROMORPH (fonding number 03 F 0262 A) over a three-year period (2000 to 2002). We also appreciate the cooperation throughout the project with our colleagues from the Research and Technology Centre "Westcoast" (University of Kiel), the Institute of Fluid Mechanics and the Institute of Meteorology (University of Hanover), and the GKSS Institute for Coastal Research (Geesthacht). Our thanks are also due to the following German authorities for providing field data: the Coastal Research Station of the Lower Saxony Central State Board for Ecology (CRS Norderney), the Federal Maritime and Hydrographic

Agency (BSH Hamburg), the Regional State Office for Rural Areas (ALR Husum) and the German National Meteorological Service (DWD). The CRS Norderney is also gratefully acknowledged for making available the German Bight Model, which was developed by Delft Hydraulics (the Netherlands) within the German-Dutch project WADE (Wadden Sea Morphodynamic Development) and funded by the German Ministry of Education and Research. We are also indebted to Dr. Ian Westwood for his meticulous corrections and final proofreading of the English manuscript. Finally, we wish to thank the anonymous reviewers for their constructive remarks.

8. References

ASCE TASK COMMITEE: Sediment Transportations Mechanics: Suspension of Sediment. Proc. Am. Soc. Civil Engrs., Vol. 89, No. HY5 (September 1963) p. 45, 1963.

ASP NETO, N. E.: Long- to Short-term Morphodynamic Evolution of the Tidal Channels and Flats of the Dithmarschen Bight, German North Sea, Ph.D. thesis, University of Kiel, Germany, 2004.

EAK: Empfehlungen für Küstenschutzwerke, Die Küste, Heft 65, in German, 2002.

HARTSUIKER, G.: Deutsche Bucht and Dithmarschen Bucht, Set-up and calibration of tidal flow models. Delft, Delft Hydraulics, Report H1821, 1997.

JIMÉNEZ GONZALEZ, S.; MAYERLE, R. and EGOZCUE, J. J.: On the accuracy of Acoustic Doppler Current Profilers for in-situ measurements. A proposed approach and estimations for measurements in tidal channels. 7th IEEE Conference on Current Measurement Technology, March 13–15, San Diego, USA, 2003.

JIMÉNEZ GONZALEZ, S.; MAYERLE, R. and EGOZCUE, J. J.: A Proposed Approach for the Determination of the Accuracy of Acoustic Profilers for Field conditions, Die Küste, Heft 69, 2005.

JUNGE, I.; WILKENS, J.; HOYME, H. and MAYERLE, R.: Modelling of Medium-Scale Morphodynamics in a Tidal Flat Area in the South-Eastern German Bight, Die Küste, Heft 69, 2005.

LUTHARDT, H.: Analyse der Wassernahen Druck- und Windfelder über der Nordsee aus Routinebeobachtungen, Hamburger Geophysikalische Einzelzeitschriften, A 83, in German, 1987.

MAYERLE, R. and PALACIO, C.: Assessment of Open Sea Boundary Condition Approaches for Coastal Models, in 13th Congress of the Asia and Pacific Division of the International Association for Hydraulic Engineering and Research, Asia and Pacific Division of IAHR, Singapore, August, 2002.

MAYERLE, R.; RAZAKAFONIAINA, T.; PALACIO, C. and PRAMONO, G.: Bed forms and equivalent roughness sizes in tidal channels. Proceedings of the International Conference on Fluvial Hydraulics (River Flow 2002), IAHR, Louvain-la-Neuve. Belgium, 2002.

MAYERLE, R.; WILKENS, J.; ESCOBAR, C. and WINDUPRANATA, W.: Hydrodynamic Forcing along the Open Sea Boundaries of Small-Scale Coastal Models, Die Küste, Heft 69, 2005.

NIEMEYER, H. D.: Bemessung auf Seegang. Entwicklung abgesicherter Verfahren zur Ermittlung der Bemessung des Wellenauflaufs. KFKI-project No. 45, in German, 1997.

PALACIO, C.; MAYERLE, R. and TORO, F.: Tidal Analysis in the Meldorf Bight, North Sea Coast, Germany (in Spanish), XV National Seminar of Hydraulic and Hydrology, Colombia, 2002.

PALACIO, C.; MAYERLE, R.; TORO, M. and JIMÉNEZ, N.: Modelling of Flow in a Tidal Flat Area in the South-Eastern German Bight, Die Küste, Heft 69, 2005.

POERBANDONO and MAYERLE, R.: Composition and Dynamics of Sediments in Tidal Channels of the German North Sea Coast, Die Küste, Heft 69, 2005.

RICKLEFS, K. and ASP NETO, N. E.: Geology and Morphodynamics of a Tidal Flat Area along the German North Sea Coast, Die Küste, Heft 69, 2005.

ROHDE, H.: Entwicklung der hydrologischen Verhältnisse im deutschen Küstengebiet. In: Kramer, J. and H. Rohde: Historischer Küstenschutz, Verlag K. Wittwer, Stuttgart, in German, 1992.

SÜNDERMANN, J.; HESSE, K.-J.; BEDDIG, S. and WILKENS, J.: Coastal mass and energy fluxes in the southeastern North Sea. German Journal of Hydrography Vol. 51, No. 2/3, 113–132, 1999.

VAN RIJN, L. C.: Principles of Sediment Transport in Rivers, Estuaries and Coastal Seas. Aqua Publications, Amsterdam, The Netherlands, 1993.

WILKENS, J.: Medium Scale Morphodynamics of the Central Dithmarschen Bight, Ph.D. thesis, University of Kiel, Germany (available under http://e-diss.uni-kiel.de/diss_1369/d1369.pdf), 2004.

WILKENS, J.; ASP NETO, N. E.; RICKLEFS, K. and MAYERLE, R.: Medium-scale Morphodynamic Modelling in the Meldorf Bight. Proceedings of the EWRI/ASCE World Water and Environmental Resources Congress 2001, Orlando, USA, 2001.

WILKENS, J.; JUNGE, I. and HOYME, H.: Modelling of Waves in a Tidal Flat Area in the South-Eastern German Bight, Die Küste, Heft 69, 2005 (a).

WILKENS, J. and MAYERLE, R.: Calibration of Coupled Flow-Wave Models and Generation of Boundary Conditions for the Central Dithmarschen Bight, Germany. Poster at the 11th International Biennial Conference on Physics of Estuaries and Open Seas (PECS) 2002, Hamburg, Germany, 2002.

WILKENS, J. and MAYERLE, R.: Modelling of Medium Scale Morphodynamics of a Tidal Flat Area in the German Wadden Sea, Proceedings of the 29th ASCE International Conference on Coastal Engineering (ICCE), Lisbon, Portugal, 2004.

WILKENS, J. and MAYERLE, R.: Morphodynamic Response to Natural and Anthropogenic Influences in the Dithmarschen Bight, Die Küste, Heft 69, 2005 (b).

WINTER, C.; POERBANDONO, HOYME, H. and MAYERLE, R.: Modelling of Suspended Sediment Dynamics in Tidal Channels of the German Bight, Die Küste, Heft 69, 2005.

ZIELKE, W.; GROSS, G.; HOYME, H.; MAYERLE, R.; RICKLEFS, K.; WINTER, C.; EPPEL, D. and WITTE, G.: Predictions of medium-scale morphodynamics (PROMORPH). Proceedings of the 27th ASCE International Conference on Coastal Engineering (ICCE) 2000, Sydney, Australia, 2000.

Die Küste, 69 PROMORPH (2005), 1-420

Composition and Dynamics of Sediments in Tidal Channels of the German North Sea Coast

By POERBANDONO and ROBERTO MAYERLE

Summary

This paper presents the results of the analysis of field measurements used for identifying the basic patterns of sediment composition and sediment dynamics in the main tidal channels of the central Dithmarschen Bight on the German North Sea coast. The study was carried out within the framework of the research project "Predictions of Medium Scale Morphodynamics – PROMORPH" funded by the German Ministry of Education and Research. The spatial distribution of the characteristics of the upper layer of seabed sediments and the composition of the material transported in suspension were determined on the basis of measurements using side-scan sonar imagery, grab and water samples. It was found that the seabed in the tidal channels is essentially comprised of sandy sediments and mud as well as consolidated deposits. Contrary to the tidal flats, no clear trends could be identified regarding spatial distribution. The material transported in suspension is much finer than that on the bottom and consists of very fine to medium-grain silt. The spatial and temporal distributions of suspended material concentration and transport were investigated. Current velocities and suspended material concentrations were measured simultaneously from moving vessels at several cross-sections by means of Acoustic Doppler Current Profilers and optical beam transmissometers, respectively. The measurements were performed for tidal ranges of 2.3 m to 4.2 m under essentially calm weather conditions. Due to the small grain sizes of material transported in suspension its vertical distribution was found to be fairly uniform with maximum depth-averaged values of 0.55kg/m^3. It is estimated that approximately 35,000 and 105,000 metric tons of suspended material are transported through the two main tidal channels during neap and spring tidal cycles, respectively. The adopted measuring strategy proved to be quite satisfactory for the purpose of the present investigation, and the results were found to be very helpful for clarifying various strategic aspects of numerically modelling these processes.

Zusammenfassung

Dieser Beitrag stellt Ergebnisse der Analyse von Feldmessungen vor, die zur Identifikation von grundlegenden Mustern der Sedimentzusammensetzung und -dynamik in den Haupttiderinnen der zentralen Dithmarscher Bucht an der deutschen Nordseeküste führen. Die Studie wurde im Rahmen des Forschungsprojekts „Prognose mittelfristiger Küstenmorphologieänderungen – PROMORPH" vom deutschen Bundesministerium für Bildung und Forschung gefördert. Die räumliche Verteilung der Merkmale der Oberflächensedimente des Meeresbodens wird mit Hilfe von Side-Scan Sonar-Messungen, Greifer- und Wasserproben ermittelt. Es wurde herausgefunden, dass sich die oberste Schicht des Meeresbodens in den Tiderinnen im Wesentlichen aus sandigen Sedimenten, Schlamm und konsolidierten Ablagerungen zusammensetzt. Im Gegensatz zu den Sandbänken konnte kein klarer Trend hinsichtlich der räumlichen Verteilung gefunden werden. Das in Suspension transportierte Material, das feinem bis mittlerem Schluff entspricht, ist viel feiner als das oberflächliche Meeresbodensediment. Die räumliche und zeitliche Verteilung der Konzentration und des Transports des suspendierten Materials wurde untersucht. Strömungsgeschwindigkeiten mittels ADCP und Konzentrationen des suspendierten Materials mittels optical beam transmissometer wurden gleichzeitig von fahrenden Schiffen an verschiedenen Querschnitten gemessen. Die Messungen wurden bei einem Tidehub von 2,3 bis 4,2 m während ruhiger Wetterbedingungen durchgeführt. Aufgrund der geringen Korngröße des in Suspension transportierten Materials ergaben sich ziemlich gleichförmige vertikale Verteilungen der Konzentration. Mit maximalen tiefengemittelten Werten von 0,55 kg/m^3. Es wird geschätzt, dass etwa 35.000 bzw. 105.000 t suspendierten Materials durch die beiden Haupttiderinnen während eines

Nipp- bzw. Springtidezyklus befördert werden. Die benutzte Messstrategie stellte sich als sehr geeignet heraus, und die Ergebnisse halfen, verschiedene Aspekte bezüglich der Strategie bei der numerischen Modellierung der Vorgänge zu klären.

Keywords

Seabed Sediment, Suspended Material Concentration, Sediment Transport, Field Measurements, Tidal Channel, Numerical Modelling, Dithmarschen Bight, North Sea.

Contents

1. Introduction

An understanding of the hydrodynamics, sediment dynamics and morphodynamics in coastal regions requires detailed knowledge of the various processes involved. Field measurements are of vital importance for improving this knowledge in view of the relatively poor understanding of the physical system and hence the corresponding uncertainties associated with mathematical models. Within the framework of the research project "Predictions of Medium-Scale Coastal Morphodynamics – PROMORPH" funded by the German Ministry of Education and Research, process-based numerical models for simulating flow, waves and sediment transport have been developed and evaluated for simulating morphological changes over time scales of several years in a tidally-dominated area of the German Wadden Sea (Overview in MAYERLE et al., 2005; WILKENS et al., 2005; WINTER et al., 2005; WILKENS and MAYERLE, 2005). The investigation area is a tidally-dominated region of the central Dithmarschen Bight between the Elbe and Eider estuaries. For the purpose of model development, continuous monitoring of wind speed, water levels and bathymetry by the relevant authorities were supplemented by specially-designed field surveys for high-resolution measurements of the spatial and temporal variations of waves, current velocities and suspended material concentrations. The purpose of collecting field data was to identify the dominant acting physical processes, thereby assisting in the definition of the modeling strategy as well as providing data for developing and evaluating the models. Considering the fact that sediment motion is very difficult to estimate using state-of-the-art numerical and analytical techniques, the present research project marks a first step towards a better understanding of sediment transport processes in the study area.

In this paper particular attention is given to the analysis of field measurements in order to provide a better understanding of sediment composition and sediment dynamics in the investigation area. The investigation focuses on the main tidal channels of the central Dithmarschen Bight. The results of an analysis of seabed sediment characteristics and material transported in suspension as well as suspended material concentration and transport along the main tidal channels are presented. The characteristics of seabed sediments were obtained by means of side-scan sonar surveys validated with seabed sediment samples. A large number of water samples were also collected at various locations in the tidal channels to provide information on the characteristics of material transported in suspension. Current velocity and suspended material concentration were measured simultaneously from moving vessels along several tracks at different tidal cycles by means of Acoustic Doppler Current Profilers and optical beam transmissometers, respectively. The ranges of suspended material concentration and transport variations were identified and the main patterns of sediment dynamics responsible for spatial and temporal variations were investigated. The suspended load transport through the main tidal channels over the ebb and flood period was also estimated in order to assess the morphological evolution in the study area. From the multitude of field measurements only typical results could be included in this paper.

2. Description of the Study Area

The investigation focuses on the main tidal channels of the central Dithmarschen Bight on the German North Sea coast (Fig. 1). The study area is located about 100 km north of Hamburg between the Eider and Elbe estuaries.

The morphology of the study area is dominated by tidal flats and a tidal channel system comprised of three channels: Norderpiep in the northwest, Suederpiep in the southwest, and the Piep tidal channel, which originates at the junction of the Norderpiep and Suederpiep. For average conditions the maximum water depth in the tidal channels is 18 m. The tidal flats and sandbanks are exposed at low water. The area is characterized by a meso-tide regime with a mean tidal range of 3.2 m and neap and spring tidal ranges of about 2.8 m and 3.5 m, respectively. According to the classification by EHLERS (1988) this leads to an open tidal flat without barrier island. Westerly winds (SW-W) prevail and the area is classified as a storm wave environment. Wave heights in the outer region can reach 3 to 4 m but break along the edge of the tidal flats on intertidal and supratidal sandbanks. Locally generated waves of up to 0.5 m in height are observed in the study area. The influence of local waves on currents is moderate on the tidal flats and negligible in the tidal channels. Storm surges can result in water level setups of up to 5 m, favoring the propagation of waves into shallow regions. Even under such conditions, however, wave effects are mostly confined to the outer sandbanks. The seabed sediments in the tidal channels and flats consist mainly of sands with varying proportions of silt and clay. The grain sizes of sediment transported in suspension are much finer.

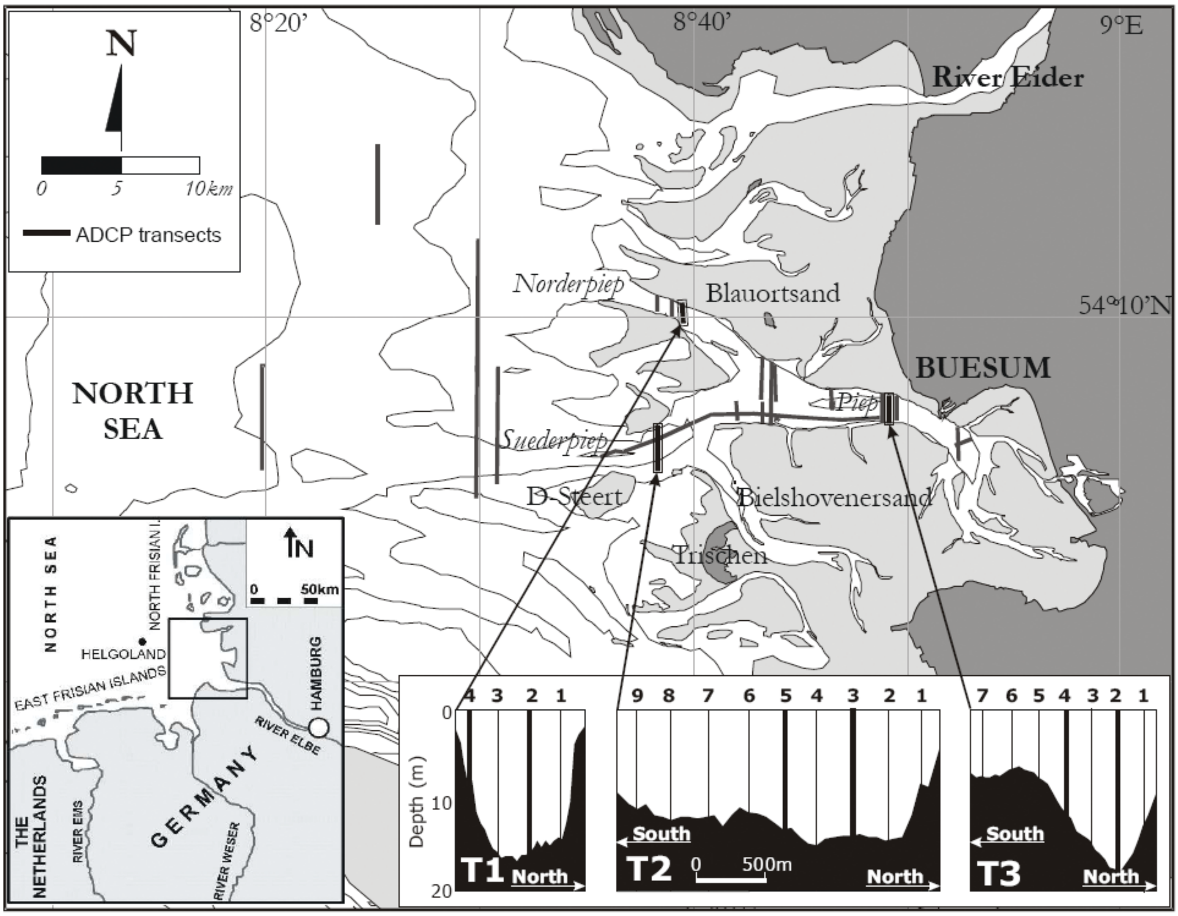

Fig. 1: Investigation area and selected cross-sections

3. Sediment Deposits and Characteristics

An investigation of recent sediment deposits, their layer thickness and the characteristics of mobile sediments was carried out by ASP NETO (2004) and RICKLEFS and ASP NETO (in this volume), while seabed sediments in the tidal channels were mapped by VELA-DIEZ (2001). The characteristics of the seabed sediments and material transported in suspension were studied by POERBANDONO (2003).

3.1 Recent Sediment Deposits

Fig. 2 shows the distribution of the layer thickness of sediment deposits in the study area. The composition of the sediment deposits corresponds extensively with recent tidal flat sediments. The layer thickness of the intertidal deposits is up to about 20 m on the tidal flats. The layer thickness of potentially mobile sediments increases towards the northern and the southern banks of the main tidal channels. The results of field observations have shown that the thickness of sediment deposits above the Early Holocene layer (EHL) may be as much as 16m along the channel banks, reducing to zero towards the deeper parts of the channels.

The early Holocene consolidated cohesive sediments form a natural base that delays or even prevents erosion in the tidal channels, thereby restricting morphological changes to lateral displacements. In the central and deeper parts of the tidal channels where shear stresses are generally larger sediment deposits have been entirely eroded and the EHL shows (ASP, 2004).

Fig. 3 shows the evolution of three cross-sections in the main tidal channels over the past two decades, indicating layer thickness of mobile sediments. In the deeper parts of the cross-sections the EHL, resulting in a lateral displacement of the bed profiles towards the North.

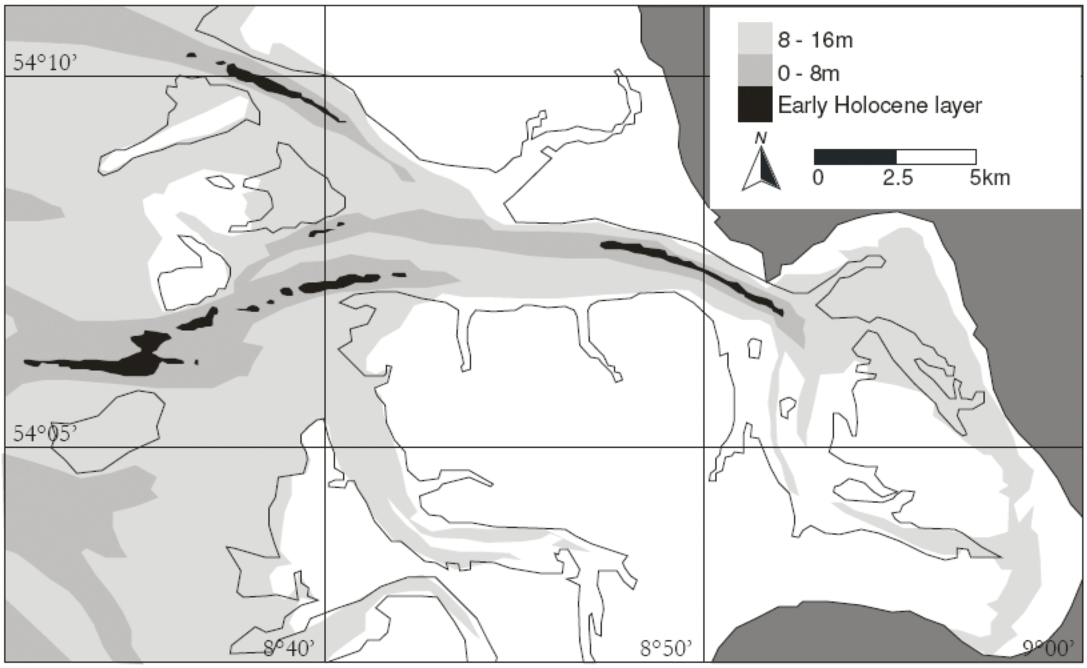

Fig. 2: Thickness of the potentially mobile sediment layer above the EHL (modified after ASP, 2004)

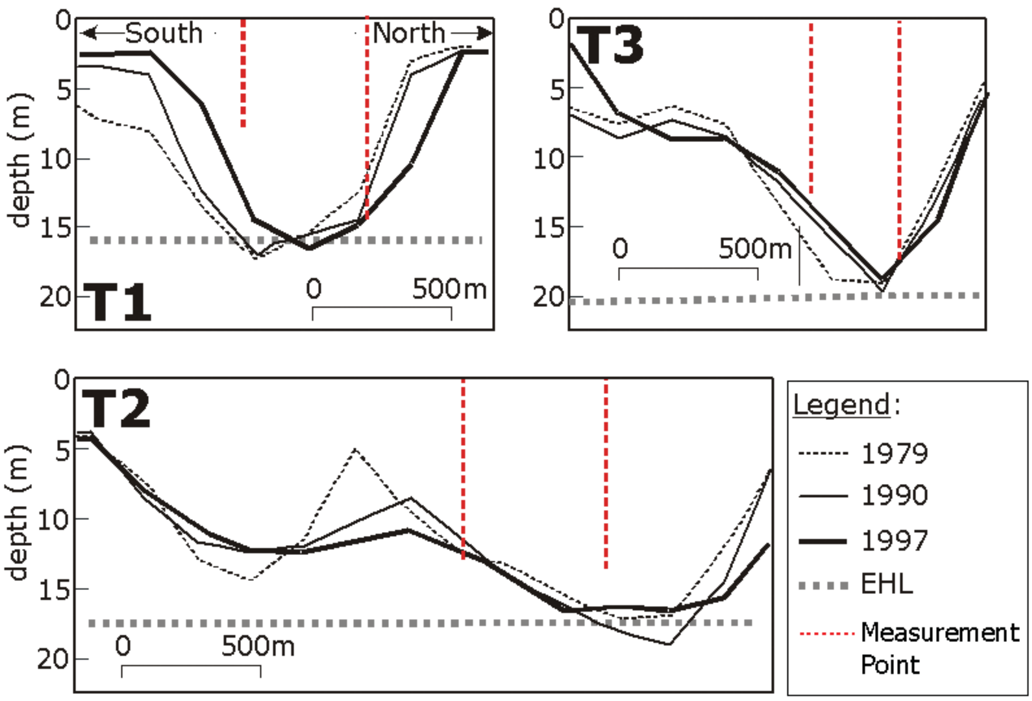

Fig. 3: Thickness of the potentially mobile sediment layer at selected cross-sections (modified after ASP, 2004)

3.2 Seabed Surface Sediments

On the basis of side-scan sonar (SSS) images and grab samples (GS) VELA-DIEZ (2001) mapped the distribution of seabed surface sediments in the tidal channels. The SSS surveys were carried out using a *Klein* system operating at a frequency of 500 kHz. The horizontal distribution of sediment patterns on the seabed was determined by towing the measuring device alongside a survey vessel. The SSS surveys over an area of approximately 30 km^2 were carried out in May and June, 1999 and September and November, 2000. Fig. 4 shows the area covered and the locations where samples were taken.

The SSS images were interpreted through correlation of their texture with characteristic grain-size parameters obtained from 15 GS, which were collected from the survey vessel using a van Veen sampler. Sampling is restricted to some parts of the domain. GS were taken mainly along the regions of transition between fine and medium sands to distinguish them on the grey scale of SSS images. Fig. 5 shows the distribution of seabed sediments in the tidal channels. The distribution appears variable. Areas with sandy sediments and mud as well as zones of consolidated deposits were identified. Consolidated fine-grained sediments were found to show at a number of deeper locations in the channels. The sands are mainly very fine to fine with isolated patches of medium sands. Although the measurements achieved full spatial coverage, the hydroacoustic detection was not sufficiently clear to distinguish between very fine and fine sands.

Sediment size analyses were carried out by dry sieving. The resulting sieve curves are shown in Fig. 6. Table 1 summarizes the results. The d_{50} varied between 80 µm and 230 µm, corresponding to very fine (63 µm < d_{50} < 125 µm) to fine (125 µm < d_{50} < 250 µm) sand,

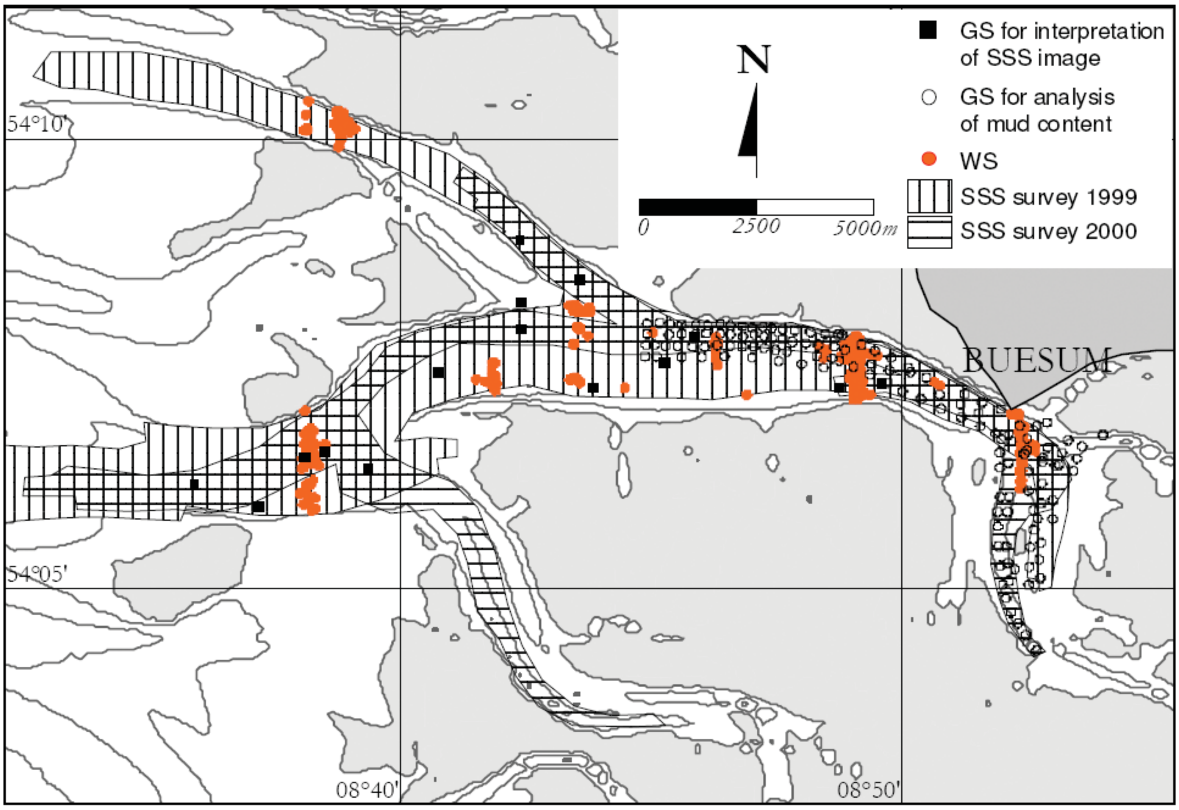

Fig. 4: Locations of side-scan sonar (SSS) surveys, grab samples (GS) and water samples (WS)

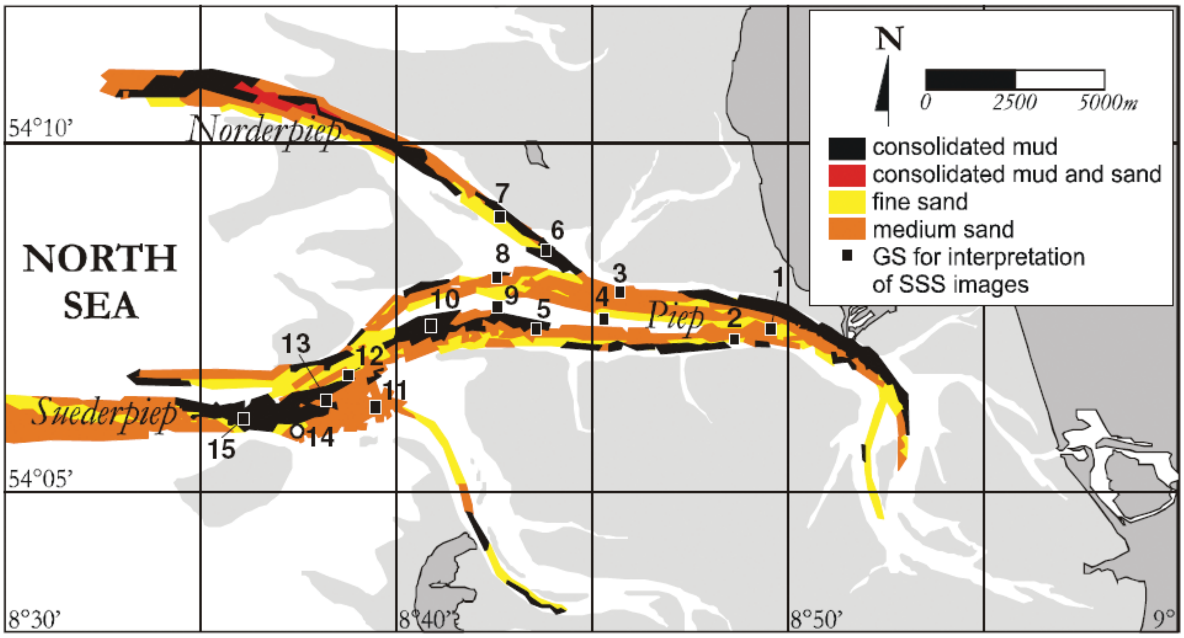

Fig. 5: Seabed surface sediment distribution in the main tidal channels
(modified after VELA-DIEZ, 2001)

respectively. Moreover, the median sediment sizes of most of the samples were found to be equal to or less than 100 µm. The majority of the samples were well-sorted, as also confirmed by the small values of the geometric standard deviation (σ_g) and the d_{90} to d_{50} ratio.

An analysis of the mud content (% of fines; $d < 63$ µm) of 145 seabed sediment samples collected with a van Veen sampler in the less exposed tidal channels at the locations shown in Fig. 4 was also carried out. The mud content was determined by separating the fines from the samples with water using a 63 µm sieve. Mud was found in all samples. The measurements indicate that the percentage of fines in the sediments of the sampling area is generally greater than 5 %, attaining maximum values of 75 %–80 %. Moreover, the percentage of fines was found to exceed 10 % in about 50 % of the samples. Although no clear trend could be identified regarding the spatial distribution of mud content, a tendency of increasing values with increasing depth was observed at the sampling locations. This is illustrated in Fig. 7, which shows the variation of mud content with water depth for all sediment samples collected in the study area. It can be seen that sediments with higher silt and clay fractions are found in the deeper areas of the main channels.

The characteristics of seabed surface sediments in the intertidal areas have been studied by REIMERS (2003). He found that the characteristic median sediment size ranges from fine sand ($d_{50} \approx 230$ µm) to coarse silt ($d_{50} \approx 70$ µm). Fine sands are found mainly at the supratidal sites and on the exposed sandbanks of Blauort, Bielshovenersand and Blauortsand (Fig. 1). RICKLEFS and ASP NETO (in this volume) identified a clear gradual decrease in the grain size of the seabed sediments from the outer regions to the inner tidal flat region, changing from coarse sand (grain size of about 355 µm) to coarse silt (grain size of about 38 µm). In the more exposed outer regions in the proximity of the main tidal channels the content of fines ($d < 63$ µm) is generally less than 5 %. Towards the inner parts of the study area the content of fines increases to between 50 % and 100 %.

Table 1: Characteristics of seabed sediments

Station	Position N	Position E	Depth (m)	d_{50} (µm)	d_{90} (µm)	d_{90}/d_{50}	σ_g	Sorting
1	54° 7‘ 15.6“	8° 49‘ 36.6“	10.0	103	124	1.2	1.3	Well-sorted
2	54° 7‘ 13.8“	8° 48‘ 46.2“	6.3	104	130	1.3	1.0	Well-sorted
3	54° 7‘ 48.6“	8° 45‘ 56.4“	14.4	137	203	1.5	1.5	Intermediate
4	54° 7‘ 29.4“	8° 45‘ 20.4“	1.0	86	115	1.3	1.2	Well-sorted
5	54° 7‘ 12.6“	8° 43‘ 56.4“	5.0	124	189	1.5	1.4	Well-sorted
6	54° 8‘ 26.9“	8° 43‘ 40.2“	7.0	107	222	2.1	1.7	Intermediate
7	54° 8‘ 54.8“	8° 42‘ 29.4“	12.4	103	132	1.3	1.3	Well-sorted
8	54° 8‘ 11.4“	8° 42‘ 31.6“	10.0	109	134	1.2	1.3	Well-sorted
9	54° 7‘ 52.8“	8° 42‘ 30.6“	12.5	100	131	1.3	1.3	Well-sorted
10	54° 7‘ 22.8“	8° 40‘ 54.4“	3.0	125	207	1.7	1.5	Intermediate
11	54° 6‘ 15.7“	8° 39‘ 32.3“	7.5	230	295	1.3	1.6	Intermediate
12	54° 6‘ 28.0“	8° 38‘ 40.8“	11.0	84	117	1.4	1.3	Well-sorted
13	54° 6‘ 24.0“	8° 38‘ 17.5“	10.5	90	136	1.5	1.4	Well-sorted
14	54° 5‘ 49.8“	8° 37‘ 23.4“	5.0	159	210	1.3	1.4	Well-sorted
15	54° 6‘ 5.4“	8° 36‘ 8.0“	15.4	80	123	1.5	1.3	Well-sorted
		Minimum	1.0	80	120	1.2	1.0	
		Maximum	15.4	230	300	2.1	1.7	

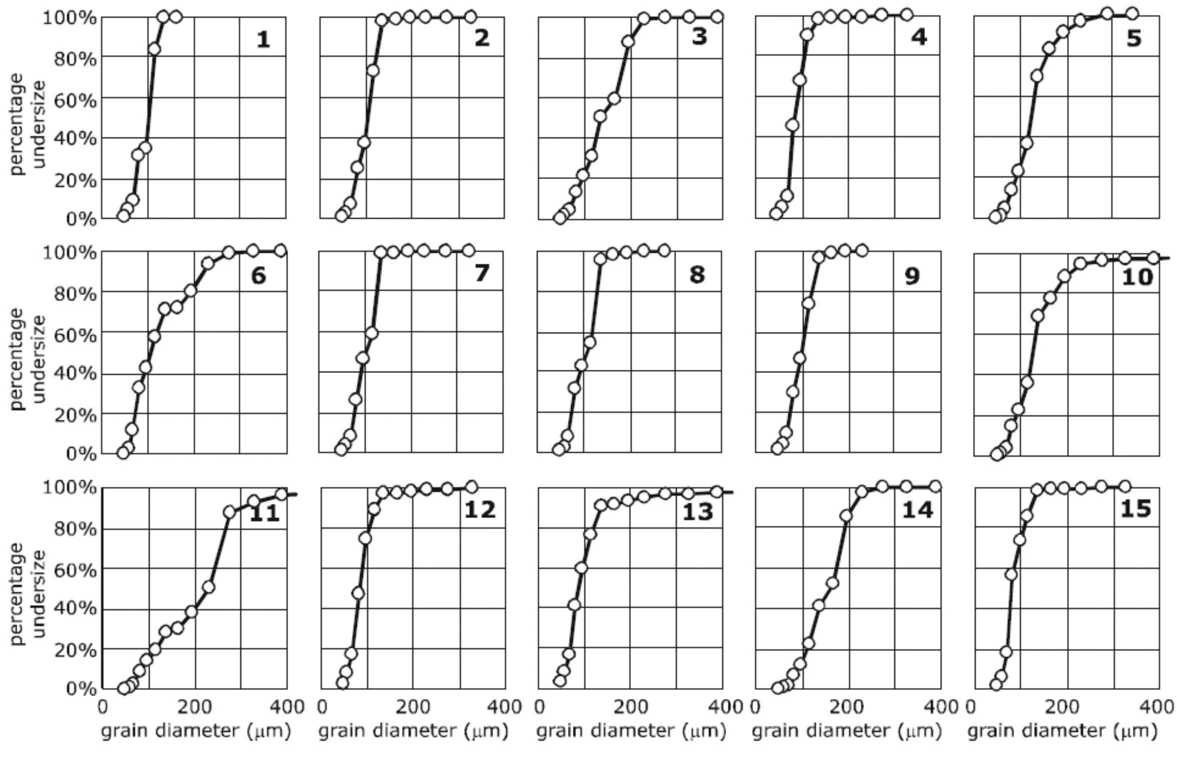

Fig. 6: Sieve curves of seabed sediment samples used for interpreting SSS images

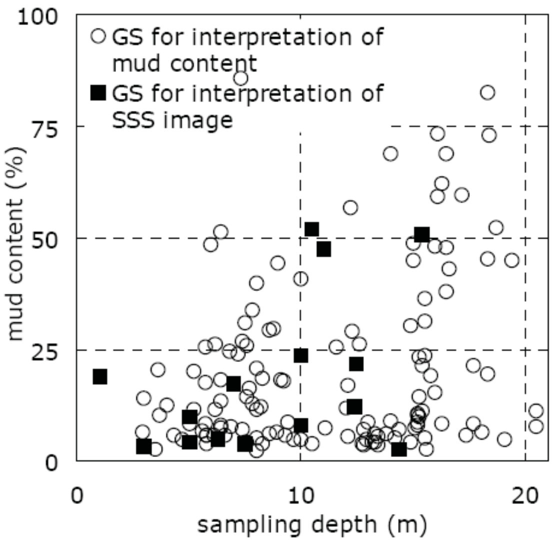

Fig. 7: Variation of mud content with water depth

3.3 Material Transported in Suspension

The characteristics of the material transported in suspension were investigated by POERBANDONO (2003). 233 water samples (WS) were collected at three cross-sections in the main tidal channels as shown in Fig. 4. The WS were taken at 1 m above the seabed using a Niskin bottle sampler in water depths ranging from 5 m to 26 m. Depth-averaged current velocities of up to 1.6 m/s and point sediment concentrations ranging from 0.04 kg/m^3 to 1.1 kg/m^3 were measured at the sampling stations. The sample grain sizes were determined using a Galai CIS-1 laser granulometer. Since the fine particle fraction of the samples tends to flocculate soon after collection, a pre-analysis treatment was undertaken. This involved exposing the water samples to ultrasonic waves for a period of about 10 minutes before carrying out the grain-size analysis.

It was found that the material transported in suspension is much finer than the seabed sediments in the tidal channels and on the tidal flats. Besides, the sandy material on the seabed is seldom found in suspension. In general, the mean grain-sizes of suspended material are about 1 to 5 times smaller than those of seabed sediment. Fig. 8 shows histograms of median sediment sizes for the samples with pre-treatment (186 samples out of 233) and without pre-treatment (233 samples). Although the samples without pre-treatment exhibit a wide band of median sediment sizes ranging from about 5 µm to 90 µm, the median grain size of about 60 % of the samples was found to be between 10 µm and 25 µm, corresponding to very fine to medium silt. The median sediment sizes of samples with pre-treatment were found to be between 4 µm and 19 µm. No clear pattern could be identified regarding the spatial and temporal variation of the sizes of suspended material.

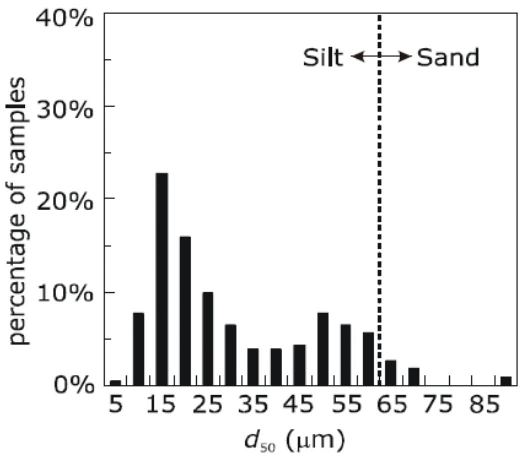

(a) Without pre-treatment (233 samples)

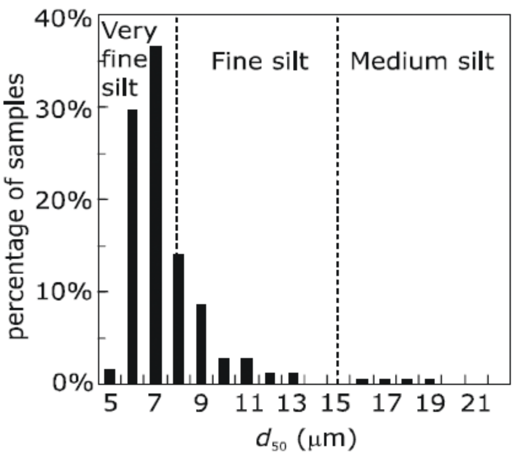

(b) With pre-treatment (186 samples)

Fig. 8: Frequency histogram of the median sizes of suspended material

4. Suspended Material Concentration and Transport

The aim of the present investigation is to identify patterns of sediment dynamics in the tidal channels of the central Dithmarschen Bight based on the spatial and temporal variations of suspended material concentration and transport derived from field measurements. The results of investigations of near-bed sediment transport in the same tidal channels are summarized in SCHROTTKE and ABEGG (2005).

4.1 Measuring Devices and Experimental Set-up

The data that required for investigating the patterns of suspended material concentration and transport were derived from simultaneous measurements of current velocity and suspended material concentration at several cross-sections in the main tidal channels. These measurements were mainly made from moving vessels provided by the University of Kiel.

Current velocity data was obtained using 1200 kHz Acoustic Doppler Current Profilers (ADCPs), as shown in Fig. 9a. The instrument was set to record a 0.5 m bin size over a 12 seconds averaging ensemble. Details of the device and its accuracy for point measurements under laboratory conditions and for cross-sectional measurements of current velocities in the investigated tidal channels are summarized in JIMÉNEZ-GONZÁLEZ et al. (in this volume). The accuracy of ADCPs for point measurements in the field is found to be fairly constant, with standard deviations of 0.14 m/s and 0.06 m/s for vertical distances below and above 1m from the seabed, respectively. The ADCP was directed downward from the bow of the vessel and deployed for the continuous measurement of current velocity profiles. Measurements over the water column were made from 1.6 m below the free surface (due to the effects of transducer draught and blanking distance) down to 6 % of the depth above the seabed (due to side lobe effects). Since the measurements of current velocity did not cover the entire water column, extrapolations were carried out in order to provide an adequate description of the velocity distribution over the full depth. For this purpose a constant velocity was assumed between the uppermost point measurement to the free surface and a linear variation from the lowest measured value to zero at the seabed.

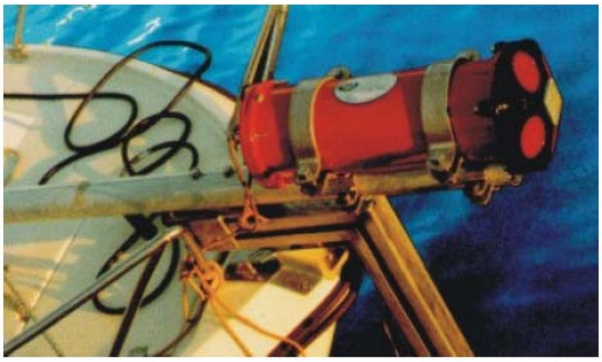

(a) Acoustic Doppler Current Profiler

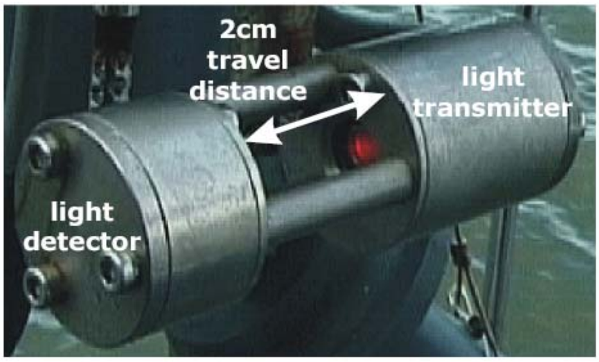

(b) Optical beam transmissometer

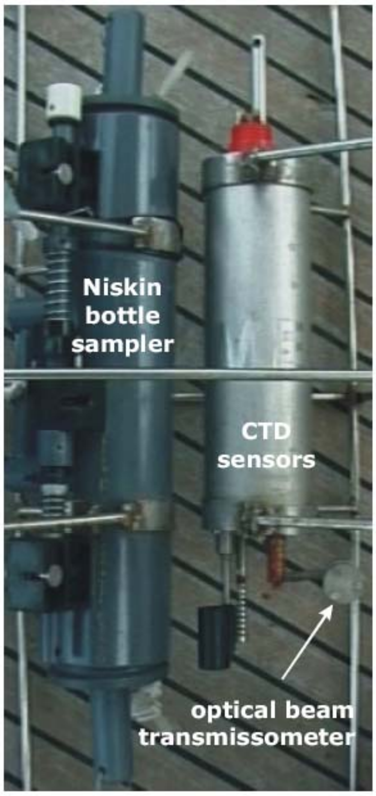

(c) Niskin bottle and CTD

Fig. 9: Measuring devices used in the study

Suspended material concentrations were measured by means of optical beam transmissometers mounted in CTD sensors and equipped with a Niskin bottle sampler (Fig. 9c). The device, which employs visible light with a wavelength of 660 ± 12 nm and a 2 cm travel distance, provides a relative measure of suspended material concentration in terms of the percentage of optical transmission. In order to convert the optical transmission data into suspended material concentrations the device was calibrated against the concentrations determined from direct samples. The accuracy of the optical measurements and details of the device and calibration procedure are summarized in POERBANDONO and MAYERLE (2005). It was found that the representative relative agreement between optical and direct sampling measurements is about 30 %. The devices were lowered midships at the vessels starboard side, and optical measurements in the water column were performed from close to the free surface to approximately 0.25 m above the seabed. This restriction is due to the separation distance between the optical transmissometer and the protective frame mounted below the device (Fig. 9b). In order to describe the suspended sediment concentration over the entire water column an extrapolation based on the last three lowest point measurements was undertaken.

In order to investigate the variation of suspended sediment concentration and transport during a tidal period measurements of current velocity and optical transmission profiles from moving vessels were carried out in various cross-sections, as illustrated in Fig. 10. The vessel moves back and forth in a cross-section during the entire measuring period. The number of measurement verticals and the separation distance between them depend on shape and dimensions of the cross-section. The vertical resolution of the optical beam transmissometer was set to 0.2 m. The number of runs during a tidal cycle depends primarily on the width of the cross-section and measuring conditions. In order to obtain simultaneous measurements at different cross-sections, which is ideal for the calibration and validation of numerical models, two vessels equipped with similar devices were deployed during several of the measurement campaigns.

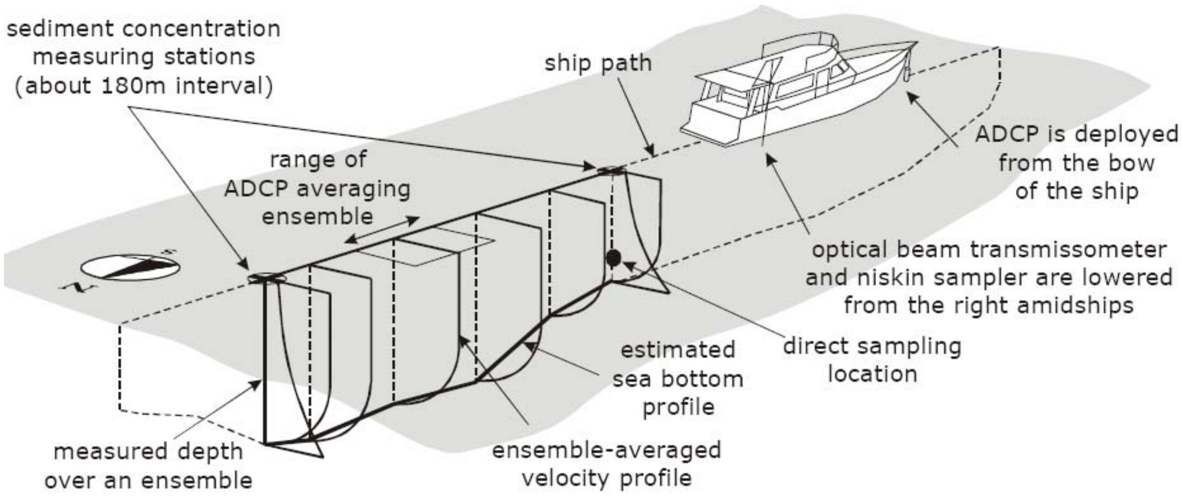

Fig. 10: Measuring technique along a transect

In order to study the variation of suspended material concentration and transport during a lunar cycle measurements were performed for a variety of tidal conditions. Measurement campaigns were undertaken at three months intervals in order to account for seasonal variations, with repetitions at approximately seven day intervals to account for neap and spring tide variations. A wide range of tidal conditions was also covered in order to investigate spatial (vertical and horizontal) and temporal (tidal and lunar cycles) variations. Details of the vessels operated by the Research and Technology Centre Westcoast simultaneously are given in TORO et al. (in this volume).

4.2 Field Measurements

Within the framework of the research project PROMORPH field measurements were performed in the tidal channels of the central Dithmarschen Bight. These measurements were made during the period May 1999 to June 2002 and covered a wide range of tidal conditions. Most of the field data used in this study were collected from moving vessels under calm weather conditions over the investigated cross-sections in different tidal channels. Although extensive measurements were undertaken over a wide area, only typical results are considered in this paper. The analysis is focused on conditions in the cross-sections of the main tidal channels, i.e. T1 and T2 at the entrance to the tidal area, representing the channels Norderpiep to the northeast and Suederpiep to the southeast, respectively, and T3 in the Piep tidal channel located in the coastal region of the study area. The locations and bed profiles of these three cross-sections are shown in Fig. 1. T1 is about 775 m wide with water depths varying from 2.8 m to 16.1 m, T2 is about 2040 m wide with water depths varying from 7.3 m to 15.6 m, and T3 is about 1200 m wide with water depths varying from 6.2 m to 17.9 m. In order to obtain good coverage over one tide 20 to 75 transects were surveyed during each measurement campaign. The measuring technique adopted has already been described in Section 4.1 (Fig. 10).

The measuring stations were positioned at approximately 180 m intervals along each transect. Simultaneous measurements of current velocity and suspended material concentration were made at each measuring station. The number of measuring stations in cross-sections T1, T2 and T3 were 4, 9 to 12, and 6 to 7, respectively.

Table 2 summarizes the results of the measurement campaigns undertaken between March 2000 and September 2001. The measurements covered entire tidal cycles under relatively calm wind conditions. The tidal range during the survey period varied from 2.3 m at neap tides to 4.2 m at spring tides. The maximum point values, depth-averaged values and cross-sectional average values of suspended material concentration and transport are given in the table. Negative values refer to offshore conditions. Intermediate values of suspended material concentration in each cross-section were obtained by linearly interpolating values between the measuring stations. The ranges of variation of these quantities during slack water are also entered in Table 2 to provide an indication of background values. The maximum rates of suspended material transport in each cross-section as well as the values integrated over a tidal phase (ebb and flood) are also shown. Depth-averaged values were obtained by integration from the reference level up to the free surface and subsequent division by the corresponding vertical distance.

Cross-sectional average values were obtained by integration over the entire cross-section and subsequent division by the corresponding cross-sectional area. The cross-sectional distribution of suspended material concentration was obtained by linear integration between the measuring stations. The material transported through each cross-section during a tidal phase (ebb or flood) was calculated by linear integration of the cross-sectional averages over the duration of measurements for each phase.

4.3 Ranges of Measured Values

The variation of the distribution of suspended material concentration and transport was investigated by comparing the measured values of suspended material concentration and transport in cross-sections T1, T2 and T3, as summarized in Table 2. The maximum depth-averaged sediment concentrations at cross-sections T1, T2 and T3 were computed to be 0.27 kg/m^3, 0.55 kg/m^3 and 0.40 kg/m^3, respectively. The maximum computed value is at cross-section T2 in the main tidal channel whereas the maximum value at cross-section T1 is generally much smaller than the values computed at the other two cross-sections.

The differences in magnitude are more significant at higher tidal ranges. During neap tidal cycles there is a definite tendency towards convergence of the observed values at the three cross-sections. Minimum values were measured during slack water (= 60–90 min) at high and low tidal ranges. Depth-averaged suspended material concentrations at cross-sections T1, T2 and T3 varied from 0.04 to 0.10, 0.06 to 0.14 and 0.06 to 0.14 kg/m^3, respectively.

The range of approximate ebb to flood ratios of tidally-integrated transport at cross- sections T1, T2 and T2 were found to be 0.61 to 0.95, 0.82 to 1.09 and 0.79 to 1.30, respectively. A tendency towards flood domination was observed at cross-section T1. Bearing in mind the inaccuracies of measurements and interpolations in space and time, it was not possible to identify any clear pattern of ebb or flood domination at cross-sections T2 and T3. It is estimated that approximately 35,000 and 105,000 metric tons of suspended material are transported through the two main tidal channels (T2 and T3) during one tide in a neap and spring cycle, respectively. Based on these figures, for the two main channels (T1 and T2) one can assume that more than 80 % is conveyed through cross-section T2 located in the southwest.

Table 2: Resume of current and sediment dynamics measurements

Cross section [width]	Date	Tidal range (m)	Number of transects – Measuring duration (h)	Maximum current velocity (m/s)				Maximum suspended matter concentration (kg/m³)				Maximum sediment transport rate (kg/m²s)				Slack water concentration (kg/m³)		Slack water transport (kg/m²s)		Tide-intgrd. sediment transport in cross-section (10³tons)	
				Depth-avg.		Cross-sect.-avg.		Depth-avg.		Cross-sect.-avg.		Depth-avg.		Cross-sect.-avg.		Depth-avg.	Cross-sect.-avg.	Depth-avg.	Cross-sect.-avg.		
				F	E	F	E	F	E	F	E	F	E	F	E					F	E
T1 [775m]	Mar. 16, 2000	3.2	31 – 11.7	1.3	-1.2	1.0	-1.0	0.27	0.23	0.19	0.18	0.23	-0.24	0.19	-0.17	0.10	0.10	0.10	0.03	20.2	-18.7
	Mar. 22, 2000	4.0	31 – 11.6	1.5	-1.4	1.1	-1.2	0.14	0.20	0.13	0.14	0.20	-0.17	0.14	-0.15	0.09	0.09	0.09	0.01	18.4	-17.5
	Jun. 5, 2000	3.7	10 – 6.1	1.7	-1.4	1.5	-1.2	0.19	0.15	0.15	0.10	0.25	-0.18	0.20	-0.11	0.05	0.06	0.06	0.02	19.0[u]	- 4.7[u]
	Sep. 5, 2000	3.0	26 – 10.4	1.2	-1.3	1.0	-1.0	0.10	0.08	0.07	0.07	0.09	-0.08	0.06	-0.06	0.04	0.04	0.04	0.01	7.8	- 4.8
	Sep. 12, 2000	3.4	33 – 11.6	1.3	-1.2	1.1	-1.0	0.13	0.19	0.09	0.09	0.13	-0.13	0.09	-0.08	0.05	0.06	0.06	0.01	10.1	- 9.0
	Dec. 5, 2000	2.3	11 – 5.5	0.6	-0.9	0.5	-0.7	0.12	0.11	0.09	0.09	0.06	-0.07	0.05	-0.06	0.07	0.07	0.07	0.01	1.7[u]	- 4.7[u]
T2 [2040m]	Mar. 21, 2000	4.1	15 – 11.9	1.6	-1.4	1.2	-1.0	0.55	0.53	0.29	0.33	0.64	-0.54	0.29	-0.33	0.11	0.14	0.14	0.03	84.2	-89.5
	Jun. 5, 2000	3.7	10 – 8.4	n/a	-1.5	n/a	-1.1	n/a	0.26	n/a	0.16	n/a	-0.24	n/a	-0.17	0.06	0.07	0.07	0.02	n/a	-40.6
	Sep. 5, 2000	3.1	8 – 9.8	1.3	-1.1	1.0	-0.9	0.40	0.29	0.18	0.17	0.39	-0.22	0.19	-0.14	0.06	0.07	0.07	0.01	32.2	-32.1
	Sep. 12, 2000	3.3	10 – 10.8	1.6	-1.2	1.1	-0.9	0.42	0.33	0.18	0.20	0.41	-0.32	0.20	-0.17	0.06	0.07	0.07	0.02	40.6	-33.3
	Dec. 5, 2000	2.3	9 – 10.8	0.8	-1.1	0.7	-0.7	0.23	0.28	0.16	0.17	0.13	-0.24	0.10	-0.12	0.06	0.09	0.09	0.02	29.3	-32.0
T3 [1200m]	Mar. 14, 2000	3.6	14 – 8.8	1.2	-1.3	1.0	-1.0	0.39	0.39	0.29	0.29	0.46	-0.39	0.28	-0.25	0.12	0.14	0.14	0.03	30.5[u]	-32.1[u]
	Mar. 23, 2000	4.2	24 – 13.0	1.2	-1.4	1.1	-1.0	0.40	0.35	0.22	0.22	0.44	-0.39	0.22	-0.20	0.10	0.11	0.11	0.01	31.4	-31.0
	Jun. 6, 2000	3.9	15 – 8.2	1.4	n/a	1.1	n/a	0.34	n/a	0.19	n/a	0.26	n/a	0.19	n/a	0.06	0.07	0.07	0.01	27.1	n/a
	Jun. 14, 2000	3.6	19 – 11.8	1.3	-1.4	0.9	-1.1	0.31	0.32	0.14	0.21	0.31	-0.24	0.13	-0.14	0.06	0.08	0.08	0.01	19.5	-21.8
	Sep. 6, 2000	2.9	14 – 10.7	0.9	-1.1	0.8	-0.8	0.26	0.33	0.15	0.17	0.19	-0.24	0.13	-0.13	0.07	0.08	0.08	0.01	16.0[u]	-19.2
	Sep. 13, 2000	3.5	8 – 4.6	1.3	n/a	1.1	n/a	0.30	n/a	0.13	n/a	0.38	n/a	0.14	n/a	0.07	0.09	0.09	0.01	17.8	n/a
	Dec. 6, 2000	2.5	22 – 12.0	0.9	-0.9	0.7	-0.8	0.20	0.20	0.11	0.12	0.12	-0.13	0.08	-0.08	0.07	0.09	0.09	0.01	14.2	-15.6
	Jun. 22, 2001	3.9	9 – 5.9	1.4	n/a	1.1	n/a	0.24	n/a	0.17	n/a	0.28	n/a	0.17	n/a	0.08	0.10	0.10	0.02	24.5	n/a
	Jun. 28, 2001	3.6	13 – 11.4	1.2	-1.1	1.0	-0.8	0.22	0.28	0.15	0.13	0.23	-0.23	0.15	-0.11	0.07	0.08	0.08	0.01	18.5	-14.6
	Sep. 11, 2001	3.1	14 – 11.1	1.1	-1.3	0.9	-0.9	0.27	0.35	0.18	0.20	0.20	-0.32	0.13	-0.18	0.07	0.10	0.10	0.02	21.7	-28.2

Notes:

- \- negative current velocities and sediment transport rates refer to offshore directions
- n/a not available
- F Flood phase
- E Ebb phase
- u underestimation due to incomplete tidal cycle coverage

4.4 Vertical Variations

The variation of suspended material concentration and transport over the water column was studied by analyzing the measured profiles. Typical profiles of measured current velocity and suspended material concentration and transport at two measuring stations in cross-sections T1, T2 and T3 are shown in Fig. 11. The results presented here are based on a data set obtained on March 21, 22 and 23, 2000, during a sequence of spring tides with an average tidal range of approximately 4m. Due to the small grain sizes of sediment material transported in suspension and the strong levels of turbulence maintained by the tidal currents the vertical distributions of suspended material concentration and transport were generally found to be fairly uniform.

In cross-section T1 the variation in the magnitude of suspended material concentration remains approximately constant throughout the entire tidal cycle. In cross-sections T2 and T3 increases in the suspended material concentration of less than one order of magnitude are observed in the lower layers of parts of the cross-sections during periods of high current velocities. The outcropping EHL in the deeper parts of the tidal channels is responsible for it (see also Fig. 3). As there is no loose sediment to be entrained the sediment concentration remains approximately uniform over the depth and unchanged throughout the entire tide. This can be noticed at both measuring stations in cross-section T1 (see Figs. 11a and 12b), and even more clearly in cross-section T2 in which one of the measuring stations is located on top of EHL and the other in places with potentially mobile sediment layer. Figs. 11b and 13b show that sediment is entrained from the bed during highest current velocities only in places in which loose material is available.

At low current velocities below the threshold of motion background concentration values raging between 0.04 to 0.14 kg/m^3 are observed. The high levels of turbulence sustained by the tidal currents in combination with small falling velocities of the material transported in suspension prevent the material from settling.

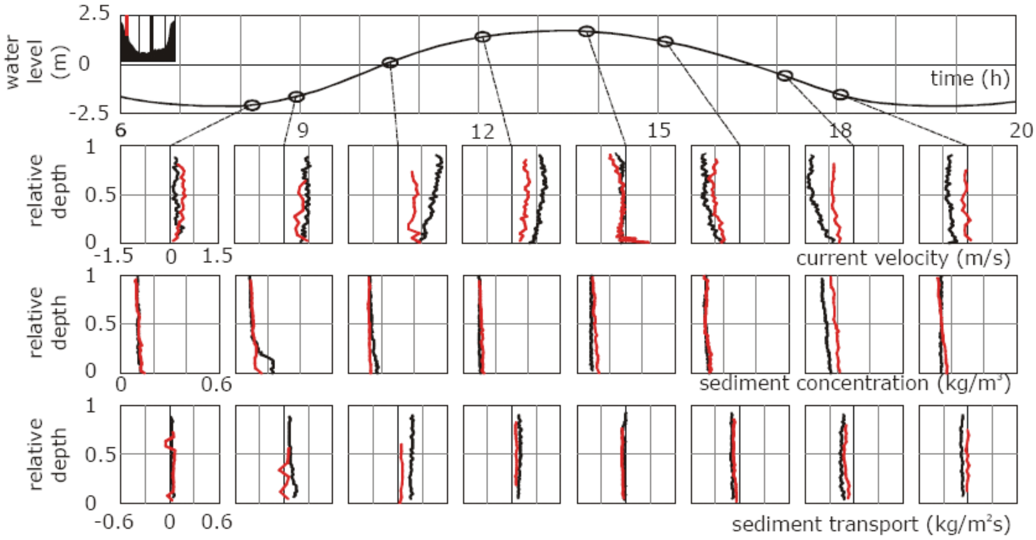

a) Cross-section T1

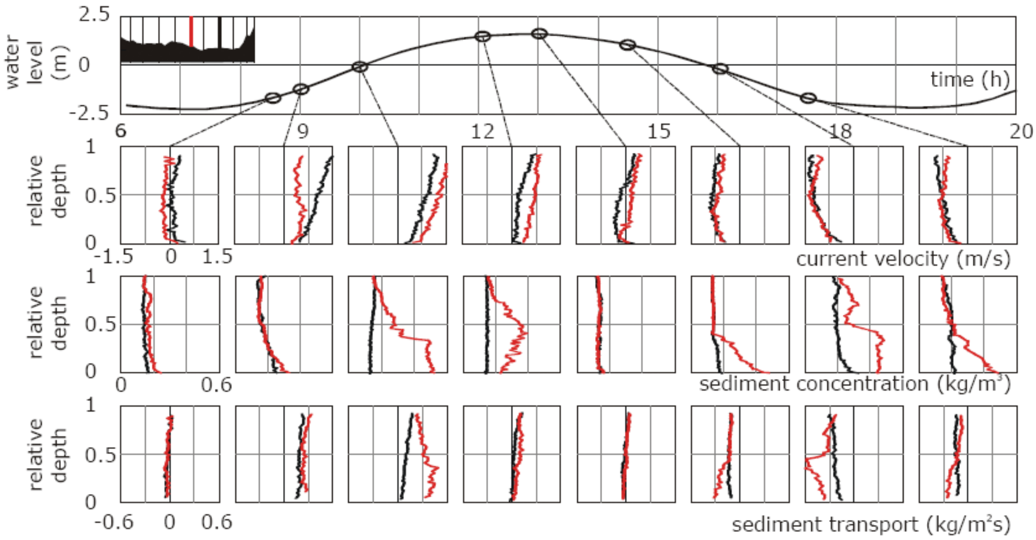

b) Cross-section T2

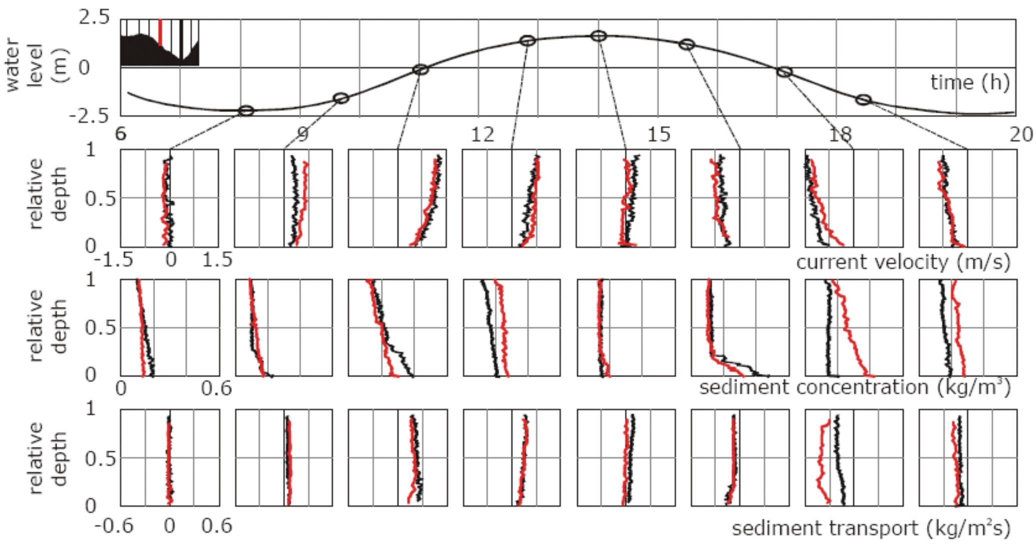

c) Cross-section T3

Fig. 11: Profiles of current velocity and suspended material concentration and transport at measuring stations in cross-sections T1, T2 and T3 on March 21 to 23, 2000

4.5 Cross-Sectional Variations

Cross-sectional variations of suspended material concentration and transport were studied by analyzing the distributions of these quantities over the investigated cross-sections. Figs. 12 to 14 show typical examples of the cross-sectional distributions of current velocity and suspended material concentration and transport. Values are shown for cross-sections T1, T2 and T3 surveyed on March 21 to 23, 2000 during a succession of spring tides with an average tidal range of about 4m. Intermediate values of suspended material concentration were determined by interpolating between the observed values at the measuring stations indicated in the figures.

The results reveal that the distributions of suspended material concentration and transport are in general fairly uniform, particularly over cross-section T1. Minimum current velocities as well as suspended material concentrations and transport values are also found to be fairly uniform over the cross-section at slack water. Resuspension of the seabed material is clearly evident during maximum flood and ebb currents, leading to non-uniform variations of these quantities over some parts of cross-sections T2 and T3. Isolated zones of higher suspended material concentrations and transport can be clearly seen in the close proximity of the seabed at maximum current velocities. These increases are more pronounced at cross-section T2 and to some extent also at cross-section T3. Intensive morphological activity is observed in parts of the cross-sections where resuspension takes place (see RICKLEFS and ASP NETO, in this volume). On the other hand, no increase in near-bed sediment concentration is observed where the EHL shows due to the lack of sediment available for entrainment at these locations (see Figs. 2 and 3).

Fig. 15 shows the variation of the estimated distributions of tidally-integrated transport over the width of the cross-sections T1, T2 and T3 (flood and ebb phases). The results were obtained by integrating the cross-sectional suspended material concentrations over time during the flood (onshore) and ebb (offshore) phases of the tide. These computations were based on the data collected during 31, 15 and 24 transects at cross-sections T1, T2 and T3, respectively. Although the distribution at cross-section T1 remains fairly uniform over the entire tidal cycle, regions of higher transport rates can be identified in the other two cross-sections. Under the investigated spring tide conditions the total amount of tidally-integrated suspended material transported during the flood and ebb phases was computed to be about 18,400 and 17,500 metric tons, 84,200 and 89,500 metric tons, and 31,400 and 31,000 metric tons through cross-sections T1, T2 and T3, respectively. Bearing in mind the inaccuracies of measurements as well as interpolation and integration errors, it would appear that the total amount of suspended material transported onshore and offshore during flood and ebb phases, respectively, is fairly well balanced at each of the investigated cross-sections.

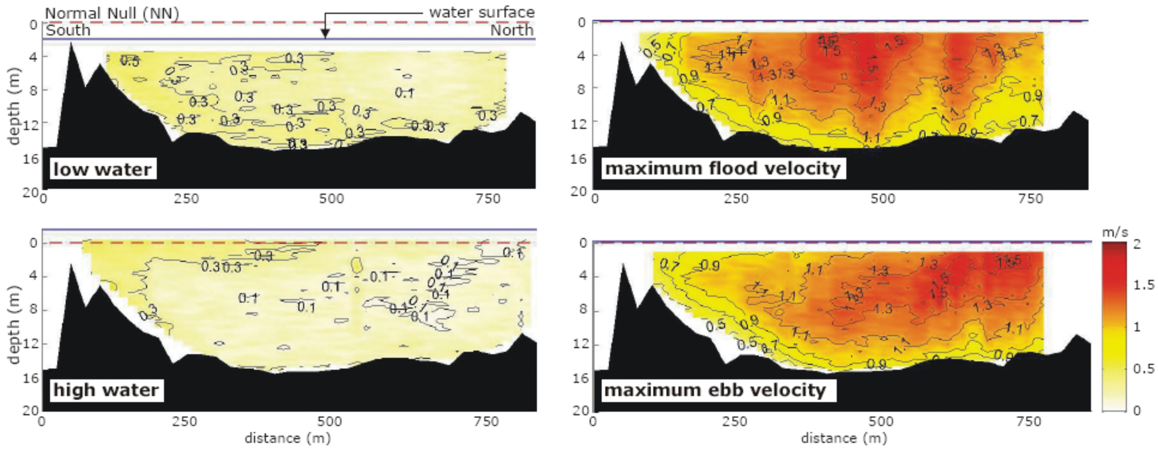

a) Current velocity

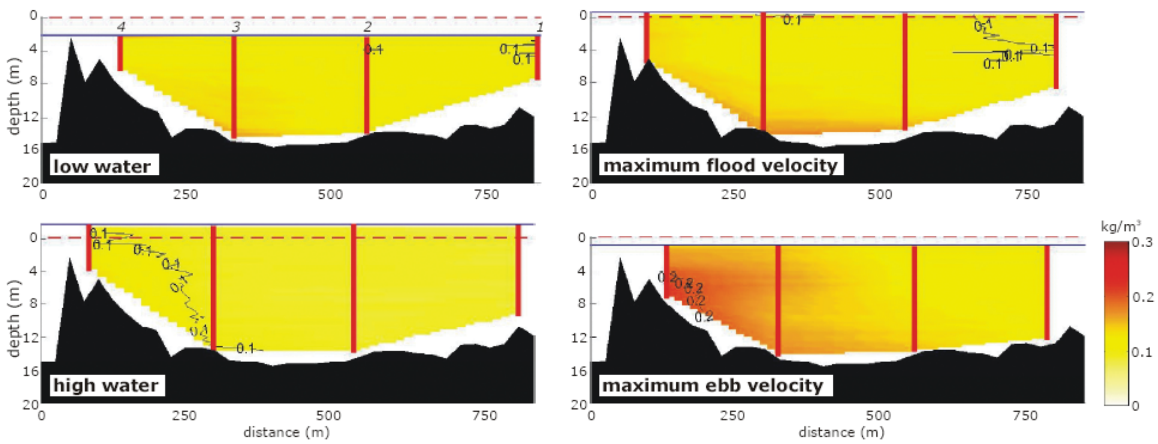

b) Suspended material concentration

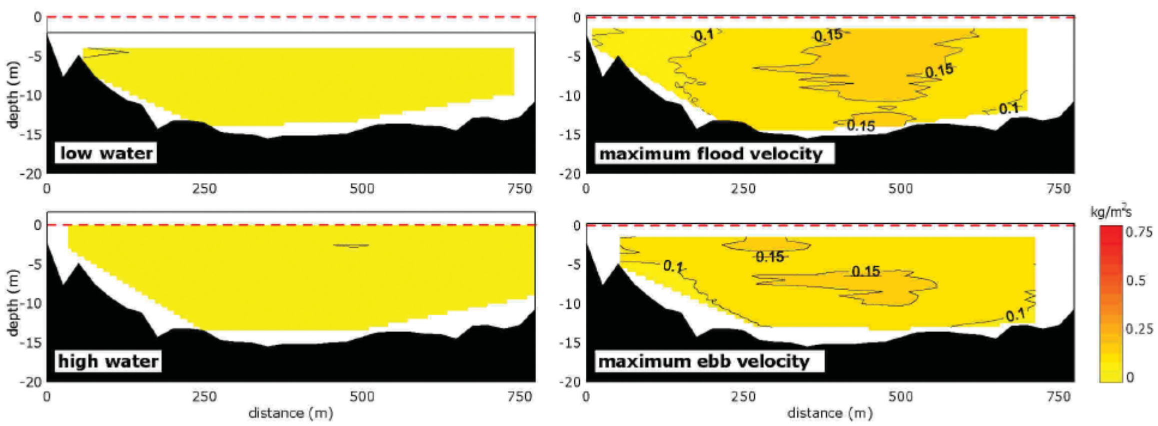

c) Transport of suspended material concentration

Fig. 12: Variations of current velocity, suspended material concentration and transport in cross-section T1 during a spring tide on March 22, 2000

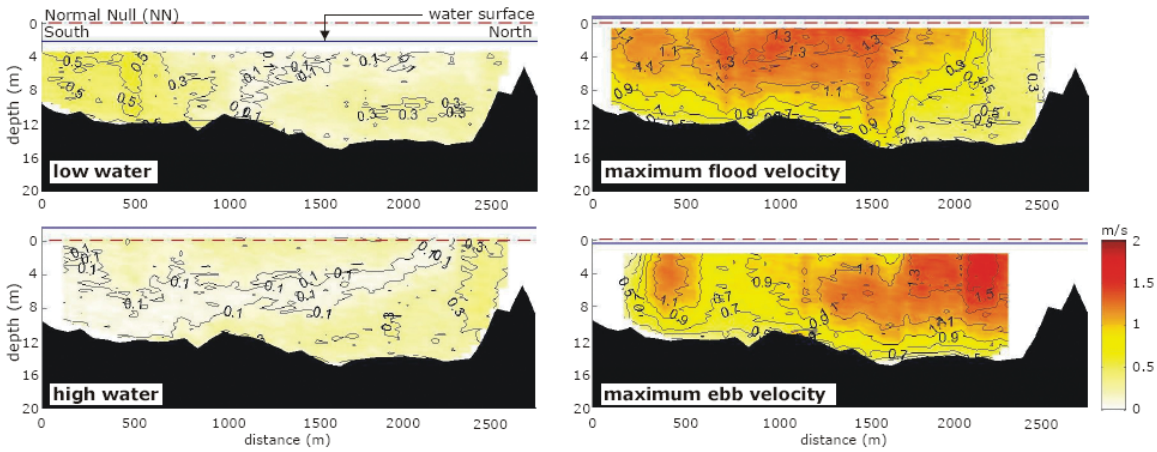

a) Current velocity

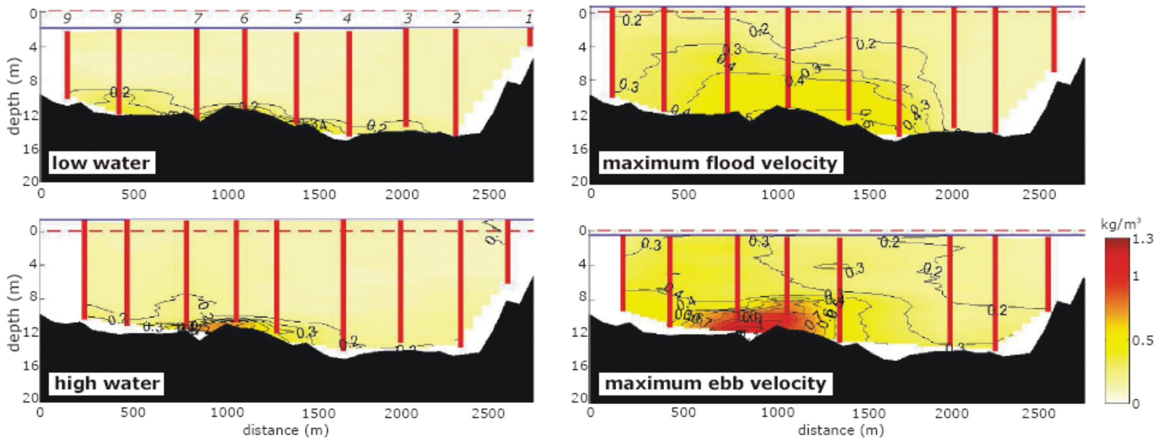

b) Suspended material concentration

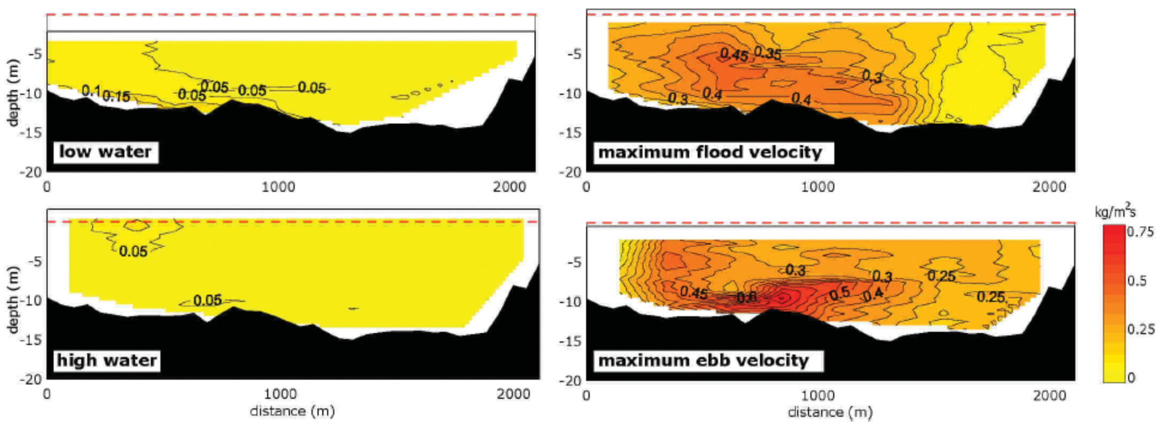

c) Transport of suspended material concentration

Fig. 13: Cross-sectional variations of current velocity, suspended material concentration and transport in cross-section T2 during a spring tide on March 21, 2000

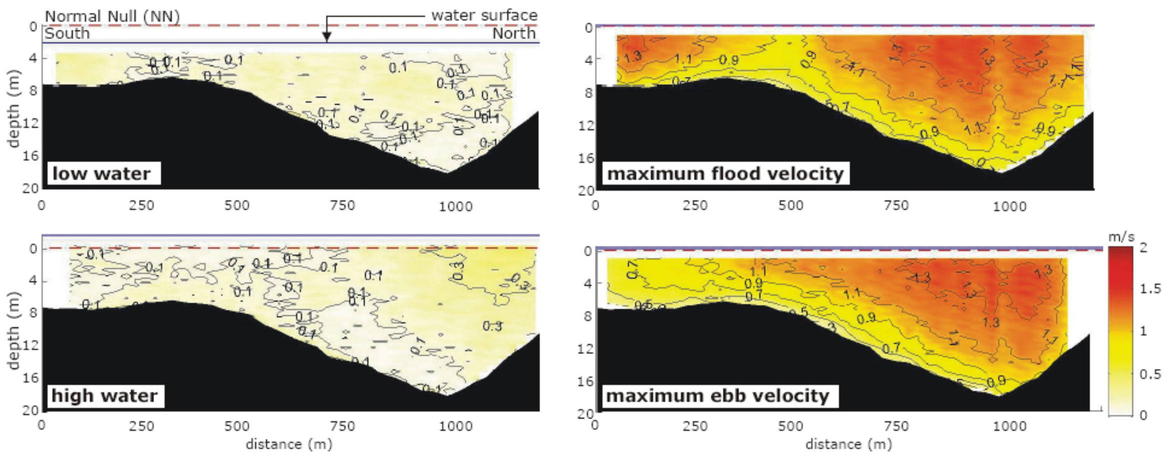

a) Current velocity

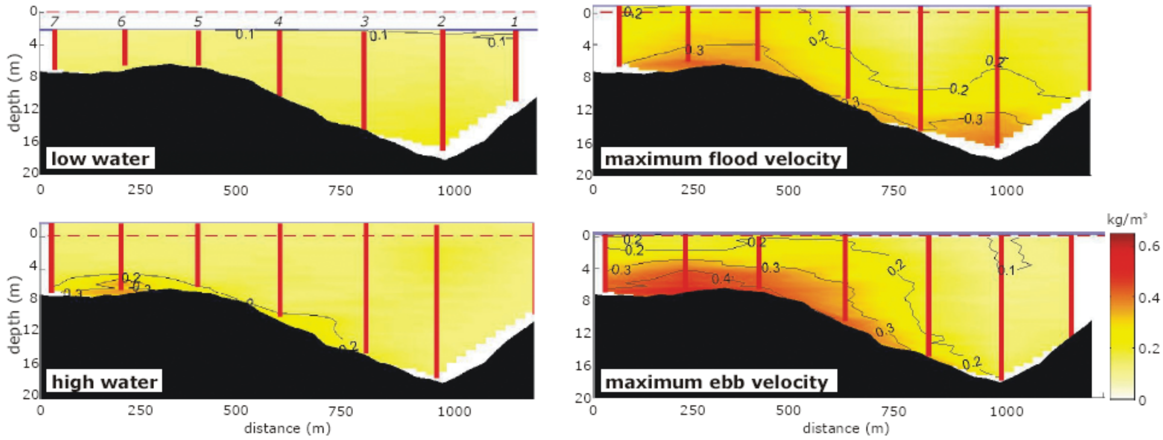

b) Suspended material concentration

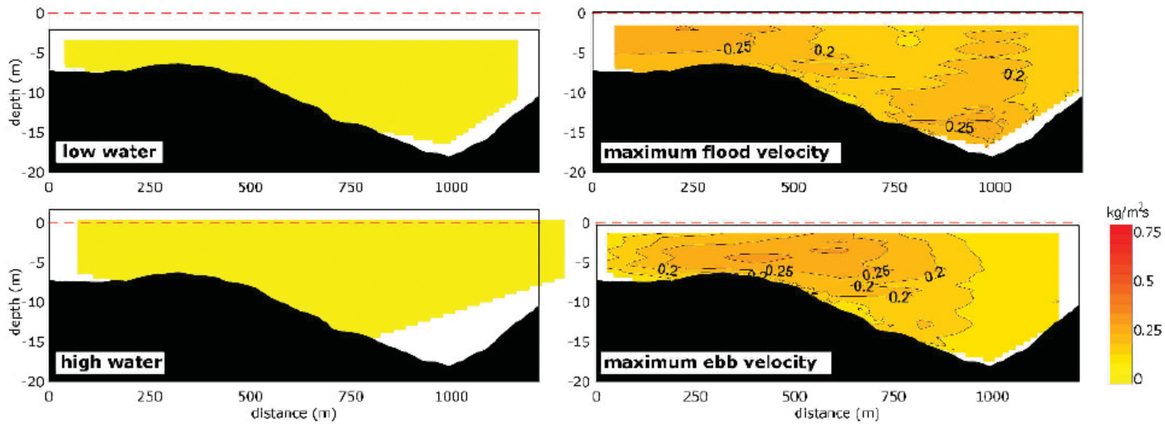

c) Transport of suspended material concentration

Fig. 14: Cross-sectional variations of current velocity, suspended material concentration and transport in cross-section T3 during a spring tide on March 23, 2000

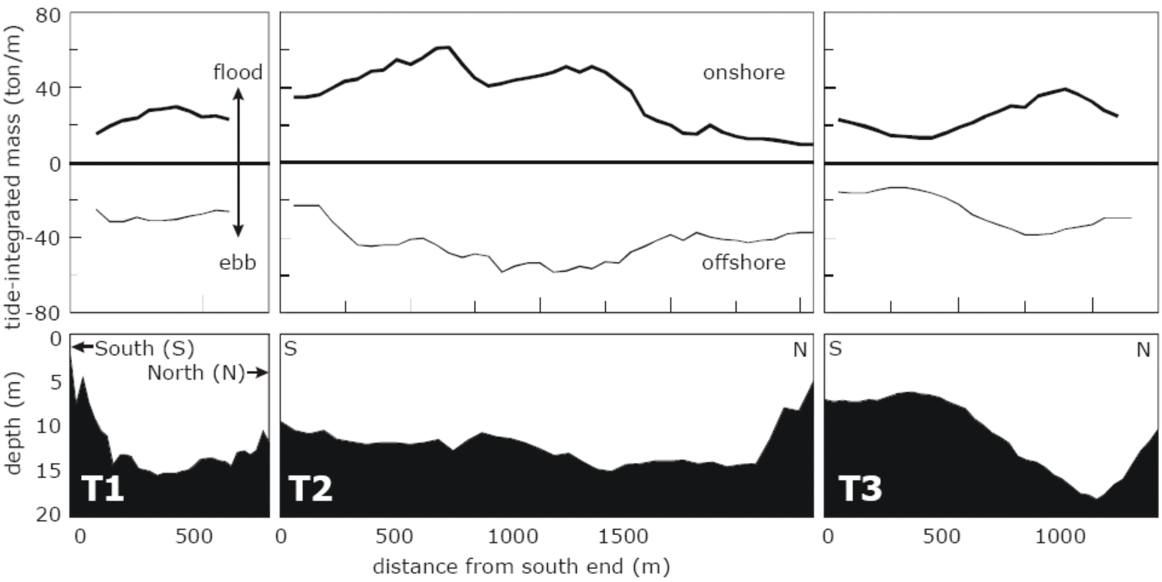

Fig. 15: Accumulation of suspended material transported during one tide based on data collected during a spring tide sequence from March 21 to March 23, 2000

4.6 Variations During a Tide

Figs. 16, 17 and 18 show the variations of depth-averaged current velocity and suspended sediment concentration and transport during a tide at cross-sections T1, T2 and T3, respectively. The values observed at the measuring stations as well as the values determined from interpolations in space and time are shown in the figures. The dots in the figures indicate the positions of the measuring stations between which the interpolations were carried out. Values are shown for a succession of spring tides (tidal range of about 4m) from March 21 to 23, 2000. The results show that for the period in question the suspended material concentrations and transport values increase from a minimum during slack water (at both high and low water) to a maximum during phases of maximum current velocities. A more detailed analysis of local variations at the three cross-sections reveals that suspended material concentrations are generally out of phase with tidal velocities, with maxima occurring towards the end of the flood phase. This fact would indicate that the observed variations are generally governed by advective transport rather than current-induced local resuspension. As already pointed out, resuspension is restricted to just a few locations over short periods in cross-sections T2 and T3.

The variations of flow discharge and suspended material transport through cross-sections T1, T2 and T3 are shown over the entire period from March 21 to 23, 2000, in Fig. 19. It may be seen that the flow discharges and sediment transport rates at cross-section T2 are much higher than at the other two cross-sections (T1 and T3). Compared to the values determined for cross-section T1, the maximum sediment transport through cross-sections T3 and T2 may be as much as 2 and 5 times greater, respectively. Bearing in mind the inaccuracies of the measurements and the errors associated with spatial and temporal interpolations, the flow discharges and suspended material transport values during the ebb and flood phases were found to be fairly similar at each cross-section.

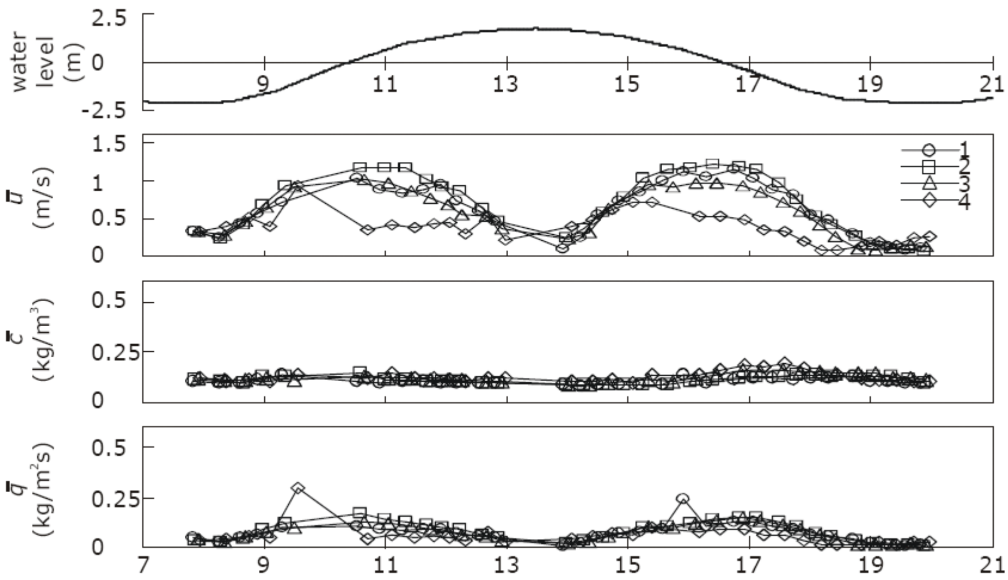

a) Observed values at the measuring stations

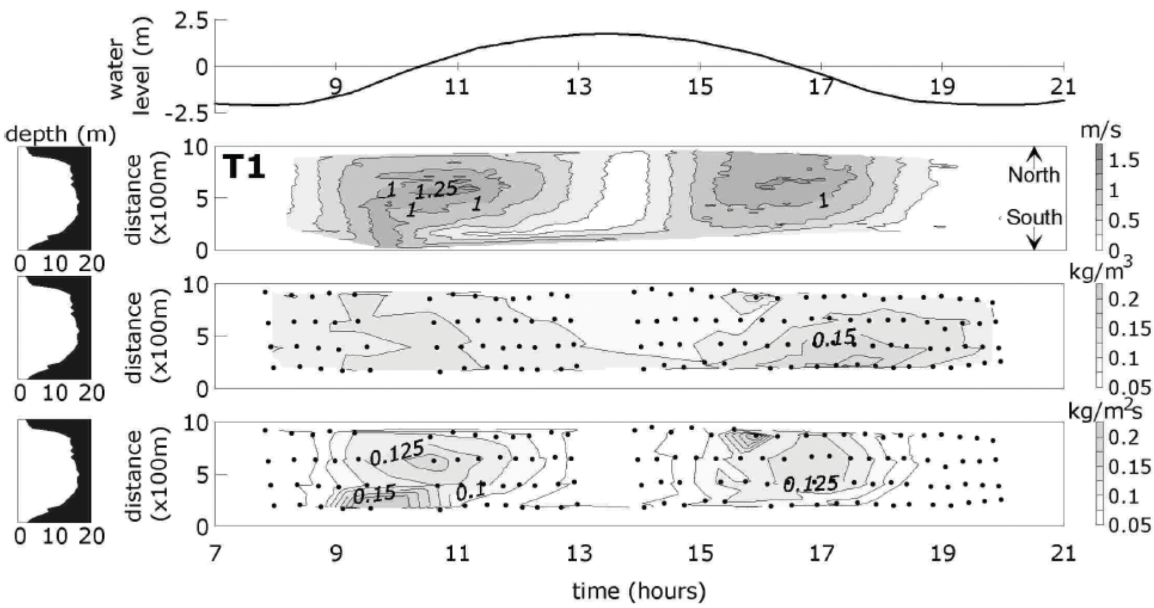

b) Spatial and temporal interpolation

Fig. 16: Variation of depth-averaged current velocity (top), suspended sediment concentration (middle) and transport (bottom) at cross-section T1 during a spring tide on March 22, 2000

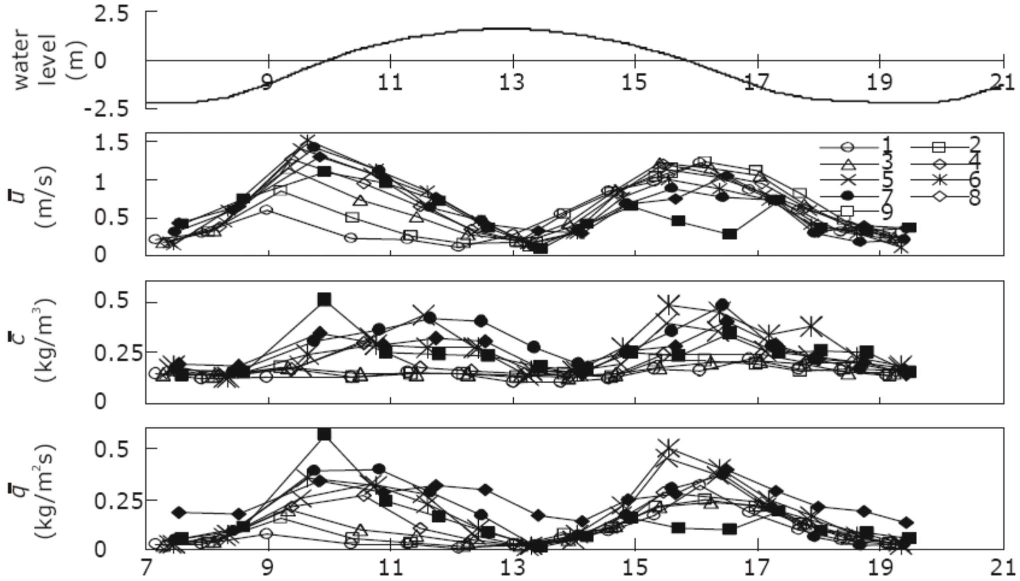

a) Observed values at the measuring stations

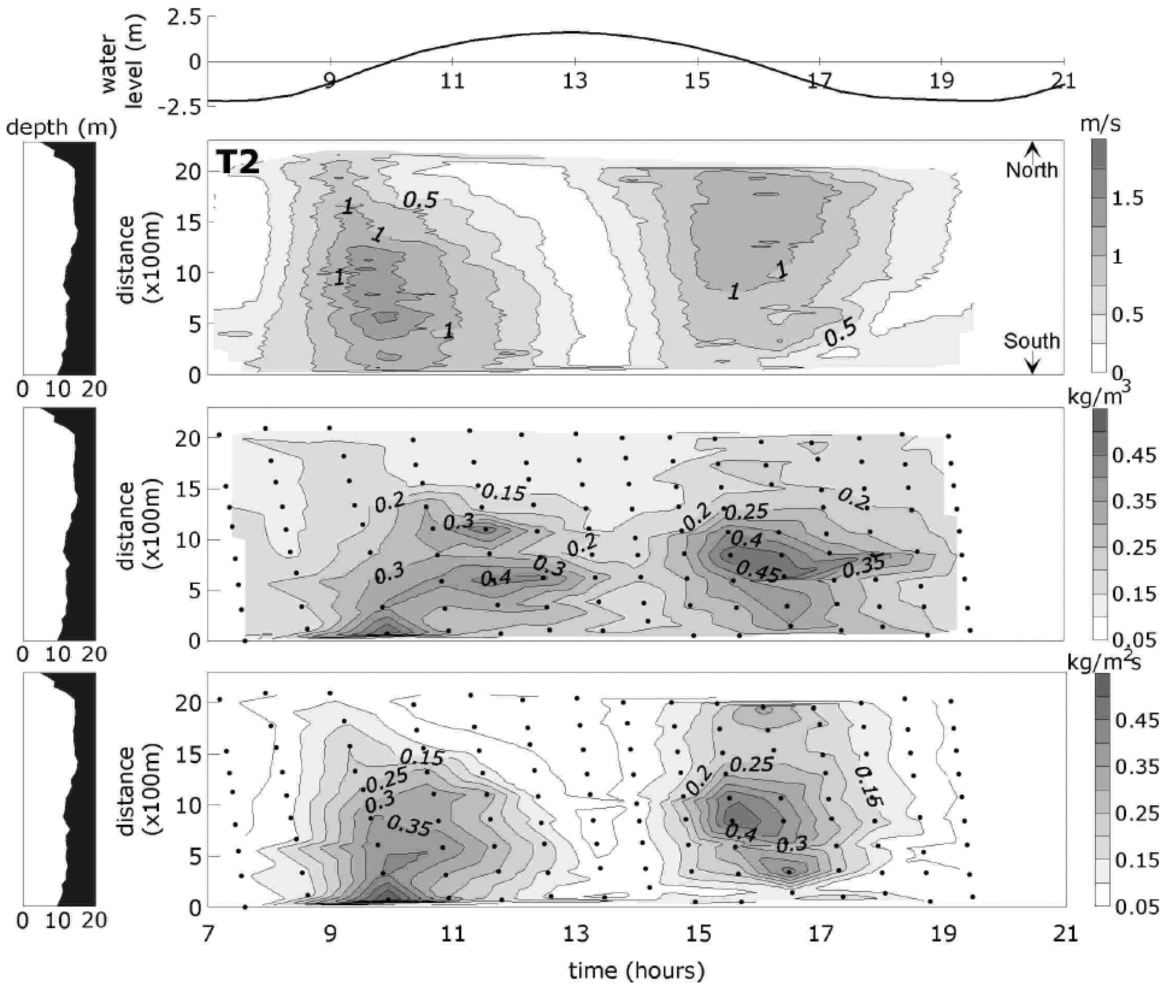

b) Spatial and temporal interpolation

Fig. 17: Variation of depth-averaged current velocity (top), suspended sediment concentration (middle) and transport (bottom) at cross-section T2 over a spring tide on March 21, 2000

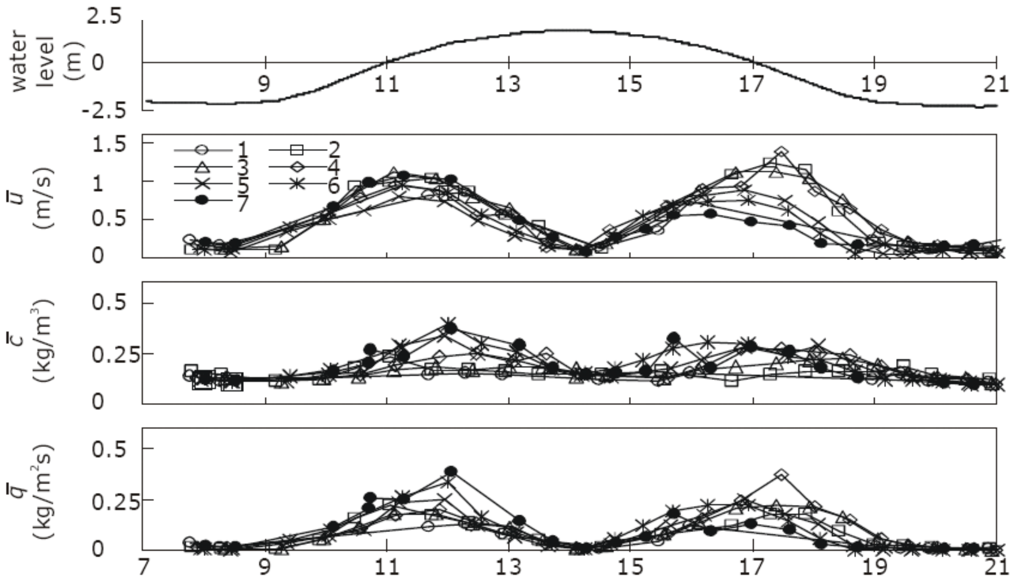

a) Observed values at the measuring stations

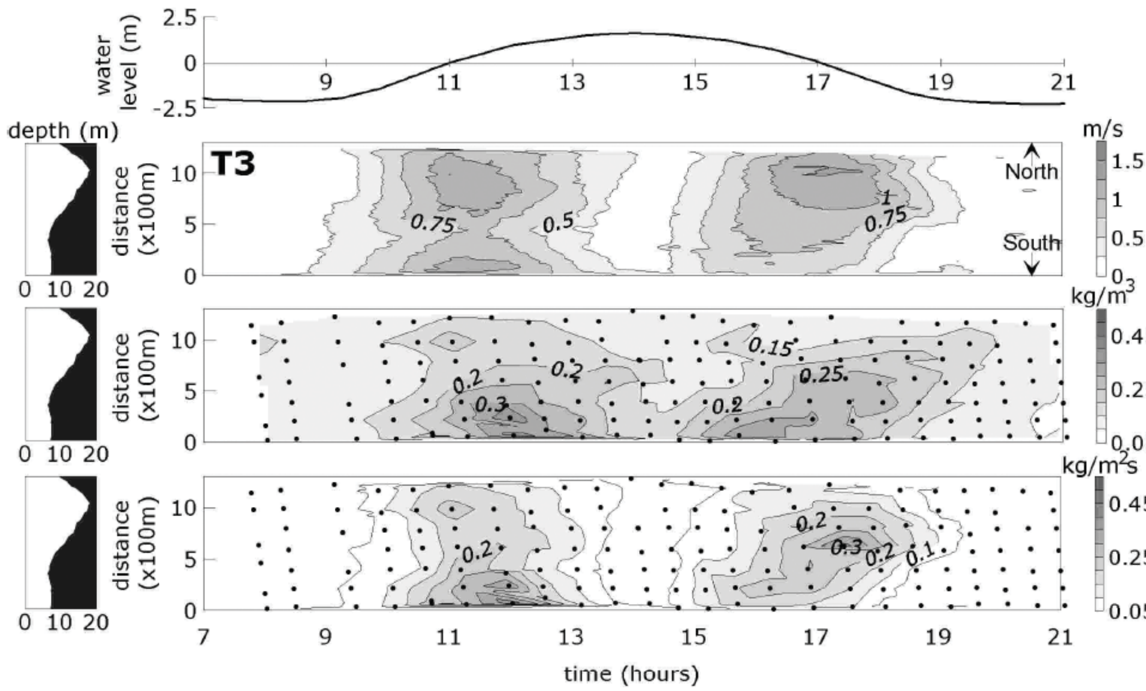

b) Spatial and temporal interpolation

Fig. 18: Variation of depth-averaged current velocity (top), suspended sediment concentration (middle) and transport (bottom) at cross-section T3 over a spring tide on March 23, 2000

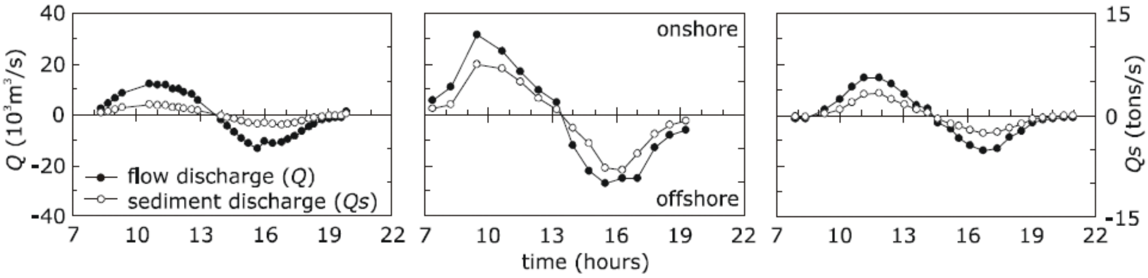

a) Cross-section T1 b) Cross-section T2 c) Cross-section T3

Fig. 19: Total flow discharges and transport during spring tide from March 21 to 23, 2000

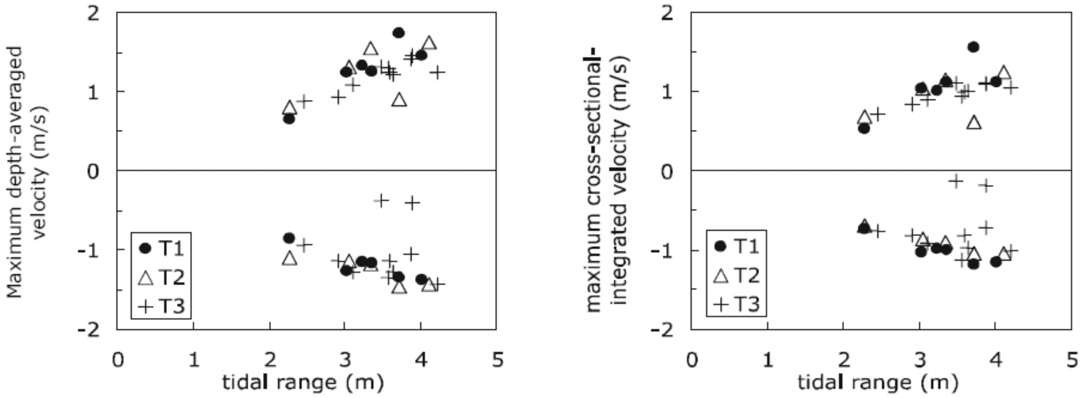

a) Current velocities

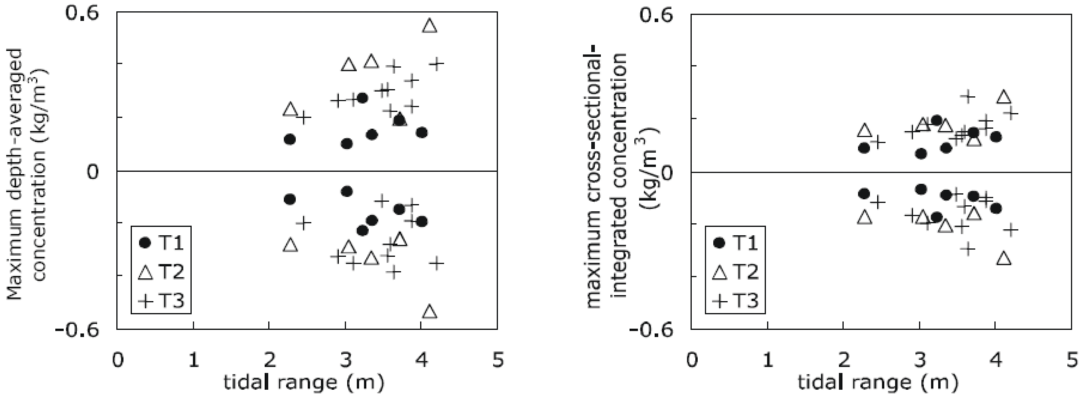

a) Suspended material concentration

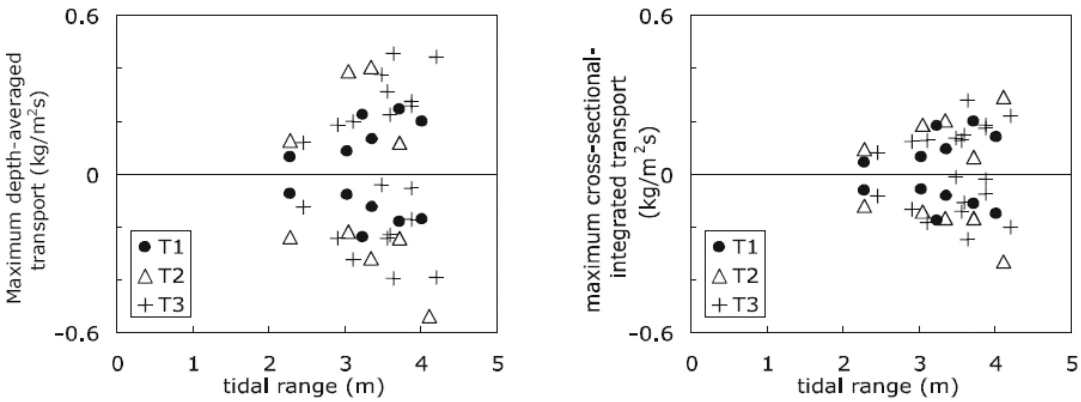

a) Suspended material transport

Fig. 20: Dependency of current velocity (top), suspended material concentration (middle) and transport (bottom) on tidal range at cross-sections T1, T2 and T3

4.7 Variations over a Lunar Cycle

An investigation of the variation of suspended material concentration and transport over the lunar cycle was undertaken by comparing the measured values obtained for different tidal ranges. The measurements covered the full range of tidal conditions typical of the study area (Table 2). Fig. 20 shows the dependency of maximum depth and cross-sectionally averaged current velocities, suspended material concentrations and transport on tidal range. The results indicate that the measured current velocities and quantities of transported sediment increase with tidal range. Maximum depth-averaged and cross-sectionally averaged current velocities were found to be similar at each cross-section for a given tidal range. With regard to suspended sediment concentration and transport, an increase with increasing tidal range was more far more pronounced at cross-sections T2 and T3 than at cross-section T1. In contrast to cross-sections T2 and T3, the maximum values of suspended material concentration at cross-section T1 were found to remain approximately constant over the full range of tidal conditions.

4.8 Bed Load versus Suspended Load

The magnitude of the bed load relative to the suspended load was investigated with the aid of numerical model simulations. Details of the sediment transport model are given in WINTER et al. (in this volume). Based on the model results, it is found that the contribution of the bed load to the total amount of transported material is far less significant. This confirms the importance of suspended sediment concentration as the primary mode of material transport in the investigation area. The average contribution of bed load transport to the total load transport amounts to only about 2 %. In the main tidal channels it is found that the suspended load transport contribution is equal to or greater than 99 %, compared to about 96 to 98 % on the tidal flats (POERBANDONO, 2003).

5. Conclusions

The results of extensive field measurements at several cross-sections of a tidally dominated coastal area have provided a valuable insight into the patterns of sediment composition and sediment dynamics. The measuring strategy, involving a combination of side scan sonar, grab sampling, Acoustic Doppler Current Profilers and optical transmissometers deployed from moving vessels, proved to be highly satisfactory for gathering information on the distribution of seabed surface sediments and the spatial and temporal variation of suspended material concentration and transport over a wide area. The investigations focused on the main tidal channels of the central Dithmarschen Bight on the German North Sea coast.

The results show that the spatial distribution of seabed sediments in the tidal channels is quite variable. Areas with essentially sandy sediments and mud as well as areas with consolidated deposits were identified. The sands are mainly very fine to fine with the occasional occurrence of medium sands. Consolidated fine-grained sediments are found at a number of deeper locations in the channels. Most of bed sediment samples were found to be well-sorted. The percentage of fines in the seabed sediment samples is generally higher than 5 %. It was also found that the material transported in suspension is essentially silt. The grain sizes of material in suspension are up to 5 times smaller than those of mobile sediments on the bottom. The transport of sandy material is thus restricted to the near-bed layers.

The distribution of sediment concentration and transport was found to be fairly uniform over the depth as well as over the investigated cross-sections. As a result, most of the sediment is transported in suspension. On the basis of numerical model simulations it was found that the average percentage contribution of bed load transport to the total transport is only about 2 %. Results of the analysis of field measurements showed that a background concentration of suspended material ranging from 0.04 to 0.14 kg/m^3 persist even during slack water. Deposition is prevented by the high levels of turbulence sustained by tidal currents in combination with the small settling velocities of the fine material transported in suspension. As a result, large amounts of fine material are always in motion, thus restricting the entrainment of seabed sediments to short periods of high current velocities during the ebb and flood phases. The characteristics of seabed sediments in the main channels also seem to play a significant role in governing entrainment activity and thus morphological changes. At locations where the EHL is not covered there is no sediment available for entrainment. Moreover, the high percentage of mud found in the seabed sediment delays or prevents the transport of seabed material. An increase in the suspended material concentration in the lower flow layers as a result of resuspension during maximum ebb and flood currents was identified in the southern part of cross-sections T3 and T2 where potentially mobile sediment is present. Intensive morphological activity is observed at such locations.

The maximum depth-averaged suspended material concentration along the main tidal channels was found to be about 0.55 kg/m^3. It was also found that about 80 % of all material entering and leaving the system are via the main tidal channel located in the southwest. Bearing in mind the inaccuracies in the measurements, it was not possible to identify any clear patterns regarding ebb or flood domination in the channels. At each of the investigated cross-sections a balance could be identified between the total amount of suspended material transported onshore and offshore during the flood and ebb phases, respectively. With regard to the magnitude of sediment concentrations and transport, a clear dependency on the tidal range was evident; sediment concentrations and transport were found to increase with increasing tidal range. It is estimated that approximately 35,000 and 105,000 metric tons of suspended material are transported through the two main tidal channels at the entrance to the study area during neap and spring tide, respectively.

The extensive field measurements provide an ideal data set for clarifying various aspects of the modelling strategy as well as for testing the performance of the numerical model. The measurements also provide reliable input data regarding particle sizes and sorting of the material transported near the bed and in suspension. Moreover, the composition of the seabed can have a significant effect on the dimensions of bed forms and hence bed-form roughness. Differences in the grain sizes of material transported in suspension and near the seabed should also be taken into consideration. The fairly uniform sediment concentration profile observed during most of the tidal period favours the use of two-dimensional depth-averaged formulations. The existence of the EHL has consequences for the modeling of medium-scale morphodynamics since it constrains morphological developments to lateral displacements. To provide adequate descriptions of the suspended sediment concentration the boundary condition near the seabed required for solving the convection-diffusion equation should account for the rigid and loose characteristics of the seabed. Similarly the EHL should also be accounted for in the solution of the depth-integrated mass-balance equation for the bed level changes constraining the morphological development to lateral displacements. Moreover, the spatial and temporal variations derived from the measurements serve as valuable criteria for testing the performance of the numerical model. The measurements along the two main inlets are particularly helpful for testing and improving the treatment of the open-sea boundary conditions in transport simulations. An advantage offered by the large amount of collected information is the ability to split the data into separate sets for the purpose of model calibration and validation. The cross-sectional measurements performed in deeper water (see Fig. 1) also provide valuable supplementary information regarding conditions along the open sea boundaries.

6. Acknowledgements

The authors wish to thank the German Ministry of Education and Research for funding the research project PROMORPH (fonding number 03 F 0262 A) over a three-year period (2000 to 2002). We also appreciate the cooperation throughout the project with our colleagues from the Research and Technology Centre Westcoast (University of Kiel), the Institute of Fluid Mechanics and the Institute of Meteorology (University of Hanover), and the GKSS Research Centre (Geesthacht). The research would not have been possible without the financial support of Poerbandono by the German Academic Exchange Service (DAAD).

7. References

ASP NETO, N. E.: Long-to Short-term Morphodynamic Evolution of the Tidal Channels and Flats of the Dithmarschen Bight, German North Sea. Berichte, Forschungs- und Technolgiezentrum Westküste der Universität Kiel, Nr. 34, 166 p., 81 Abb., 3 Tab., Büsum, 2004.

EHLERS, J.: The Morphodynamics of the Wadden Sea. Balkema. Rotterdam, The Netherlands, 1988.

JIMÉNEZ-GONZÁLEZ, S., MAYERLE, R. and EGOZCUE, J. J.: On the Accuracy of Acoustic Doppler Current Profilers for In-situ Measurements. A Proposed Approach and Estimations for Measurements in Tidal Channels. In: Rizoli, J. A. (Ed.), Proc. IEEE 7th Working Conference on Current Measurement Technology, San Diego, USA, 2003.

JIMÉNEZ-GONZALEZ, S.; MAYERLE, R. and EGOZCUE, J. J.: A Proposed Approach for the Determination of the Accuracy of Acoustic Profilers for Field conditions, Die Küste, Heft 69, 2005.

MAYERLE, R.; PRAMONO, G. and ESCOBAR, C.: Dimension and Roughness Distribution of Bed Forms in Tidal Channels in the German Bight, Die Küste, Heft 69, 2005.

MAYERLE, R.; RAZAKAFONIAINA, N.; PALACIO, C. and PRAMONO, G. H.: Bedforms and Equivalent Roughness Sizes in Tidal Channels. River Flow 2002, IAHR, Louvain-la-Neuve, Belgium, 2002.

POERBANDONO and MAYERLE, R.: Field Measurements of Sediment Dynamics in Tidal Channels: Preliminary Results. In: Proc. 5th Int'l Symp. on Coastal Engineering and Science of Coastal Sediment Process. Florida, USA, 2003.

POERBANDONO; WINTER, C. and MAYERLE, R.: Field Measurements of Sediment Dynamics in Tidal Channels: Preliminary Results. In: Proc. 5th Int'l Symp. on Coastal Engineering and Science of Coastal Sediment Process. Florida, USA, 2003.

POERBANDONO: Sediment Transport Measurement and Modeling in the Meldorf Bight Tidal Channels, German North Sea Coast. Dissertation. Christian Albrechts Universität, Kiel, Germany, 2003.

POERBANDONO and MAYERLE, R.: Effectiveness of Acoustic Profiling for Estimating the Concentration of Suspended Material, Die Küste, Heft 69, 2005.

REIMERS, H.-C.: Sedimentverteilung und Benthosverbreitung in den Watten der Dithmarscher Bucht als Indikator für morphodynamische Veränderungen. Abschlußbericht zum Forschungsvorhaben "Sedimorph" im GKSS Hochschulprogramm. Berichte der GKSS 2003/18, 49 p., 2003.

RICKLEFS, K. and ASP NETO, N. E.: Geology and Morphodynamics of a Tidal Flat Area along the German North Sea Coast, Die Küste, Heft 69, 2005.

SCHROTTKE, K. and ABEGG, F.: Near Bed Suspended Sediment Dynamics in a Tidal Channel of the German Wadden Sea, Die Küste, Heft 69, 2005.

TORO, F.; MAYERLE, R.; POERBANDONO and WILKENS, J.: Patterns of Hydrodynamics in a Tide-Dominated Coastal Area in the South-Eastern German Bight, Die Küste, Heft 69, 2005.

VELA-DIEZ, S.: Sediment Mapping of the Tidal Flat Channels off Büsum. MSc thesis, Christian Albrechts Universität, Kiel, Germany, 2001.

WILKENS, J.; JUNGE, I. and HOYME, H.: Modelling of Waves in a Tidal Flat Area in the South-Eastern German Bight, Die Küste, Heft 69, 2005 (a).

WINTER, C. and MAYERLE, R.: Calibration and Validation of a Sediment Transport Model with Extensive Data-sets for a Tidal Channel System in the German Wadden Sea. In: Proc. 5th Int'l. Symp. on Coastal Engineering and Science of Coastal Sediment Process, Florida, USA, 2003.

WINTER, C.; POERBANDONO; HOYME, H. and MAYERLE, R.: Modelling of Suspended Sediment Dynamics in Tidal Channels of the German Bight, Die Küste, Heft 69, 2005.

WILKENS, J. and MAYERLE, R.: Morphodynamic Response to Natural and Anthropogenic Influences in the Dithmarschen Bight, Die Küste, Heft 69, 2005 (b).

Die Küste, 69 PROMORPH (2005), 1-420

Geology and Morphodynamics of a Tidal Flat Area along the German North Sea Coast

By KLAUS RICKLEFS and NILS EDVIN ASP NETO

Summary

It is the aim of the study is to give an overview about the geology and the morphodynamics of the Dithmarschen Wadden Sea area, a low macrotidal section of the German North Sea coast. The environment is composed of mainly fine-sandy and silty sediments, which show a typical gradation from hydrodynamically exposed areas with coarser sands to sheltered regions with finer deposits. This sequence is not only true for the surface sediments but also for the deposits of the upper few metres. The overall thickness of the young tidal flat sediments is up to 20 m. Also of Holocene age are consolidated, clay rich silt layers, which exhibit a pronounced resistance against erosion and scouring. They widely form a kind of erosion basis above which most of the morphodynamic processes occur.

The most obvious morphological evolution recognised in the area is the landward migration of the most seaward located sandbanks. Probably active since longer periods this process is clearly visible and always orientated in the same direction since the last three to five decades. Another still ongoing process is the morphological adaptation to the land reclamation of the inner Meldorf Bay in the 70th of the last century. However, there are indications that this evolution, mainly visible as an infilling of channels, at least in some compartments approaches stages of a dynamic equilibrium. Beside these long and medium term evolutions there are pronounced morphological processes being active on a seasonal scale. One of these cycles is the scouring of the channel beds in winter and the infilling in the subsequent calm season.

In spite of the fairly good data basis and the variety of discussed aspects no comprehensive conceptional model of the morphodynamics of the domain could be developed. To realize such tasks, new methods, which go beyond classic morphological research approaches, are needed.

Zusammenfassung

Ziel dieser Studie ist es, einen Überblick über den geologischen Aufbau und die morphologischen Abläufe im Dithmarscher Wattenmeer, einem niedrig makrotidalen Abschnitt der deutschen Nordseeküste, zu geben. Das Gebiet wird von feinsandig, schluffigen Sedimenten aufgebaut, die eine typische Abfolge von gröberen Sanden in den hydrodynamisch exponierten Gebieten hin zu feinkörnigen Ablagerungen in geschützten Bereichen zeigen. Diese Sequenz umfasst nicht nur die eigentlichen Oberflächensedimente, sondern auch die obersten Meter der Wattablagerungen. Die rezenten Wattsedimente erreichen eine Mächtigkeit von bis zu 20 m. Ebenfalls holozänen Alters sind tonreiche Schluffschichten, die aufgrund ihres Konsolidierungsgrades einen erheblichen Widerstand gegenüber Erosions- und Auswaschungsprozessen zeigen. Diese Schichten bilden weithin eine Art Erosionsbasis, oberhalb derer die meisten der morphologischen Umgestaltungsvorgänge ablaufen.

Die offensichtlichste der im Gebiet erkannten morphologischen Entwicklungen ist die landwärtige Verlagerung der seewärtigsten Sandbänke. Vermutlich schon sehr viel länger aktiv, ist dieser Prozess innerhalb der letzten drei bis fünf Jahrzehnte deutlich sichtbar und immer gleich gerichtet gewesen. Eine ebenfalls noch andauernde Entwicklung ist die morphologische Anpassung an die Eindeichung der inneren Meldorfer Bucht in den 70er-Jahren des letzten Jahrhunderts. Es gibt allerdings Hinweise darauf, dass diese Anpassung, die hauptsächlich als Auffüllung von Gezeitenrinnen sichtbar wird, zumindest in einigen Teilbereichen eine Art dynamisches Gleichgewicht erreicht hat.

Neben lang- und mittelfristigen Entwicklungen kommen auch ausgeprägte morphologische Prozesse auf jahreszeitlichen Skalen vor. Eine dieser zyklischen Erscheinungen ist die festgestellte

Ausräumung der Prielbetten im Winter, die von Wiederauffüllung in der nachfolgenden ruhigeren Jahreszeit abgelöst wird.

Trotz der recht guten Datenlage und ungeachtet der Vielzahl von diskutierten Aspekten konnte kein umfassendes konzeptionelles Modell der morphologischen Evolution des Arbeitsgebietes entwickelt werden. Um eine derartige Aufgabe zu realisieren, bedarf es neuerer Methoden, die über die klassischen Ansätze morphologischer Forschung hinausgehen.

Keywords

German North Sea Coast, Tidal Flat, Low Macrotidal, Geological Setting, Holocene Evolution, Short-Term and Long-Term Morphodynamics.

Contents

1. Introduction

The coastal deposits of the German North Sea coast consist of geologically young soft sediments. Especially the wide tidal flats between the mainland and the open sea are characterised by intensive sediment turnover which results in pronounced morphological changes. The aim of this paper is to give an overview of the geological architecture, the distribution of recent sediments, and the type, scale and magnitude of morphodynamic processes of an exposed and very dynamic part of the German Wadden Sea. The individual studies were carried out within the framework of the joint research project PROMORPH (Prognosis of Medium Scale Morphological Changes), which was funded by the German Federal Ministry of Education and Research.

1.1 Investigation Area

The study area is located in the south-eastern part of the German Bight. Stretching from the mouth of the Elbe estuary in the south to the Eiderstedt peninsula in the north it approximately covers the entire Dithmarschen Wadden Sea (Fig. 1), which forms the southern compartment of the Wadden Sea of the federal state of Schleswig-Holstein. The domain is bordered by the mainland coast in the east and the 008° 25' E meridian in the west, which approximates the 10 m isobath of the open North Sea. This paper focuses on an area comprising the tidal channel system of the "Piep" with its adjacent intertidal flats (Fig. 1). Most results presented in this study are thus confined to this region.

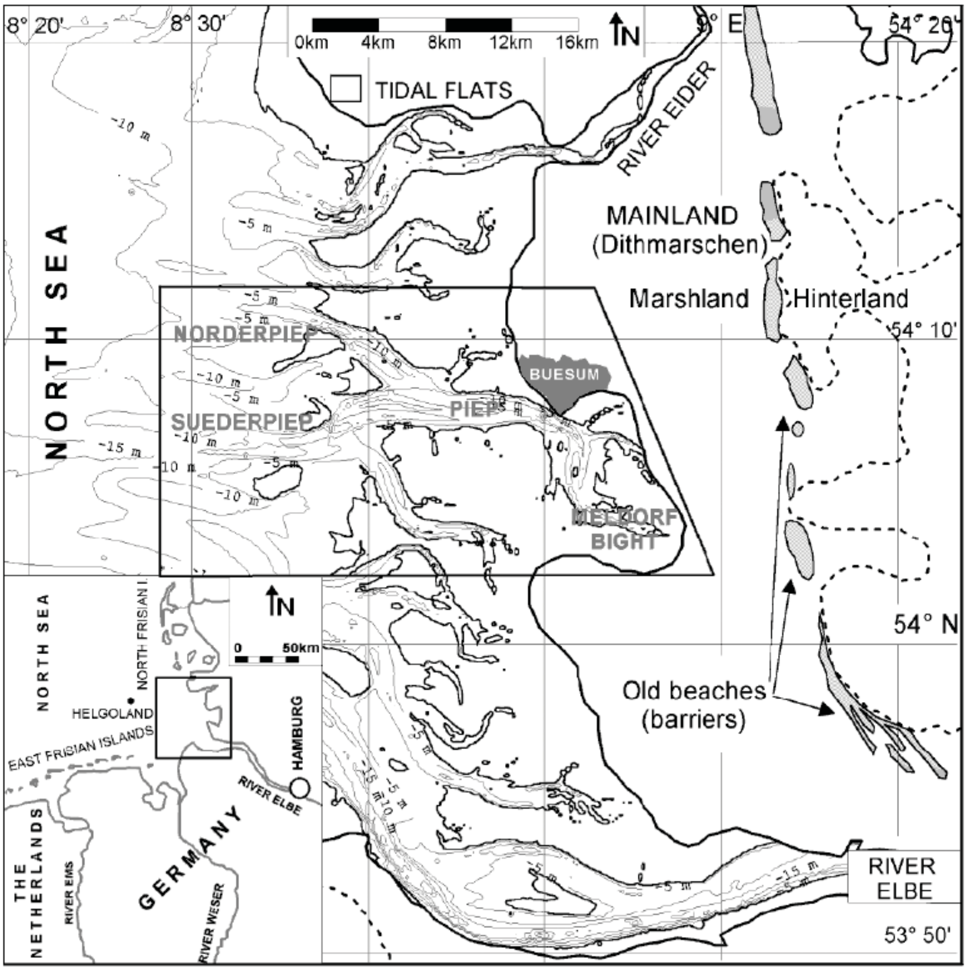

Fig. 1: Map of the investigation area

1.2 Holocene Geological Evolution

The Holocene evolution of the south-east coast of the North Sea has been controlled by the post-glacial sea-level rise. The deposits of the study area are almost exclusively characterised by silty and sandy siliciclastic sediments. Although a number of investigations on the geological structure have been carried out in the past, the level of knowledge about the temporal evolution of the area is considerably lower than that of adjacent areas to the west north. This is due to the lithological composition, intensive redeposition processes, and the lack of datable organic material.

The earliest and most comprehensive investigations were carried out by DITTMER (1938, 1952). Based on numerous core samples, the Holocene deposits were described and the principal (litho)-stratigraphic structure was identified. According to him as well as to RUCK (1969), MENKE (1976), LINKE (1979) and TIETZE (1983), the pre-Holocene landscape was bordered by the melt-water valleys of the river Elbe in the south and river Eider in the north. In addition DITTMER (1938, 1952) was able to show that the surface of the Pleistocene sediments dips down from east to west (more rapidly in the south) to a depth of approximately 30 m below present sea-level. The higher parts of the Pleistocene surface are often composed of till whereas, the deeper parts consist of glacio-fluvial sands. On these sandy plains generated by glacier run-off the history of the post-Pleistocene deposition commences with a thin peat layer. Due to a rapid sea-level rise at the beginning of the Holocene transgression, the peat was partly eroded and is almost completely missing on the more elevated till areas. In the lower parts of the area, the initial brackish and marine deposits are composed of a succession of clayey and sandy silt layers reaching an overall thickness of up to 10 m. The infauna of this widely distributed consolidated mud deposit (Fig. 2), the "Dithmarscher Klei", indicates that the sedimentation of the upper clay-rich beds occurred under permanent submarine conditions.

In a later phase, this early Holocene clayey silt was overlain by partly discordant and partly concordant sandy sediment sequences with some interlayered cohesive, muddy deposits. The facies-change from clay deposition to more and more sandy accretion indicates a change from deep water to intertidal shallow water conditions (DITTMER, 1952; STREIF and KÖSTER, 1978). At the beginning of this period (approx. 7000 BP) the sea level rise has reached a level where intensive erosional and depositional processes started to alter the ancient coastline. Around 5000 BP these processes lead to the formation of narrow coast parallel forms similar to beach ridges or barrier islands (Fig. 1, HUMMEL and CORDES, 1969; SCHMIDT, 1976). Today these accumulations of coarse sand and gravel can be found some 10 km inland and are still visible as elongated, higher elevated areas partly covered with dunes. The first organic rich deposits formed in the shelter of these barrier-like structures are dated from the period from 4000 to 3500 BP (HUMMEL and CORDES, 1969). At this time, the process of shore line grading became less important and was replaced by a final and still ongoing phase of deposition of mainly fine sandy, partly silty material which builds up the marshes and tidal flats of today (HOFFMAN, 1998). These deposits, which account for the bulk of the

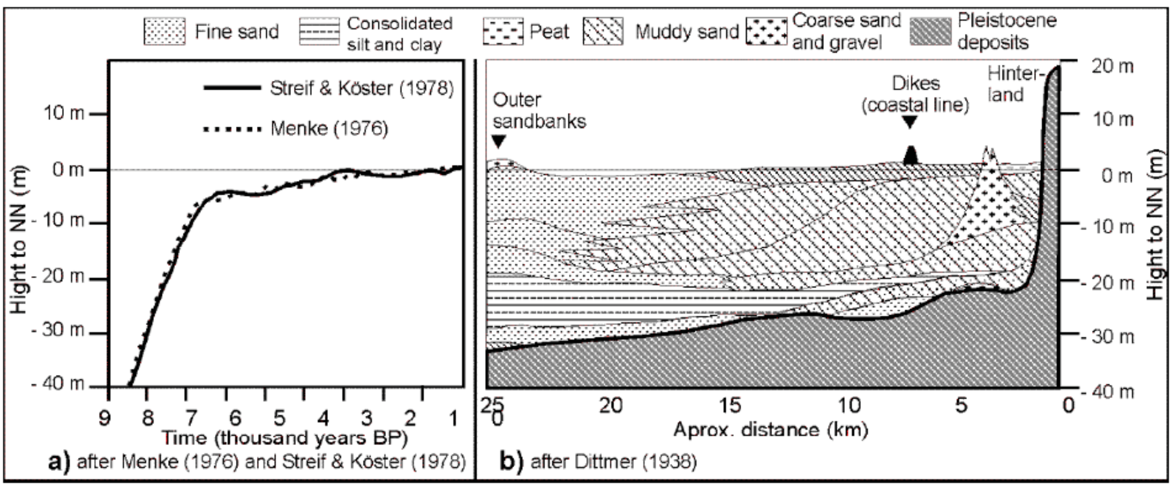

Fig. 2: Mean sea level evolution and a schematic profile of the Holocene sedimentary sequence (after DITTMER, 1952). From east (right) to west (left), the surface profile displays Pleistocene deposits of Saalian age, supratidal marshes, and tidal flats

Holocene sequence, can reach a thickness of around 20 m (Fig. 2). A possible reconstruction of the morphological evolution of the marshes and the coastline over the last 7000 years is given by WIELAND (1990), who compiled information from several authors.

1.3 History of Settlement and Land Reclamation

The first relicts of human settlement in the coastal area of Dithmarschen can be found on the elevated barrier-like sand accumulations close to the Pleistocene hinterland (Fig. 1). The artefacts have been dated as pre-Roman (2500–2000 BP). From there, the people migrated into the adjacent marshes which at that time were still rather narrow. This first wave of colonisation occurred in the Roman period of the first four centuries AD. During the following "migration period" there is no evidence of human occupation in the marshlands. A new phase of colonisation commenced in early mediaeval times (7^{th} century) (MEIER, 2000). People now settled on the younger and more elevated marshes which were formed to the west of the old settlement belt of the Roman period. Since the $11–12^{th}$ century, the marsh colonists started to change the coastline by protecting their land against the forces of the sea through the construction of dikes (KÜHN, 1992). In the following centuries, more and more land was diked (PRANGE, 1986) to ensure freshwater drainage of the marshes, and for general coastal protection. The last two considerations lead to the embankment of the inner part of the Meldorf Bay (Meldorfer Bucht) between 1972 and 1978 what marks the last phase of the land reclamation history in Dithmarschen. Detailed maps of the reclaimed coastal areas are presented in WIELAND (1984) and KÜHN (1992).

1.4 Morphological Evolution

Detailed information about the morphological evolution of the tidal flats and tidal channels over past centuries is quite sparse and inaccurate. According to LANG (1975), the first reference to the "Piep", which is the main tidal channel in the area dates back to a sailing instruction from 1558. The supratidal sandbanks of Trischen and Blauort were also first mentioned in the 16^{th} and 17^{th} century. A sailing instruction from 1701 described the northern inlet "Norderpiep" as a straight, narrow and deep approach to the harbour of Büsum, whereas the southern inlet "Süderpiep" was depicted as a more braided channel system.

The coastal zone of Dithmarschen was completely surveyed for the first time in 1838 using standard hydrographic techniques. This resulted in the publication of the first "scientifically measured chart" of the area in 1846. A comparison of this chart with topographic information dating from the 16^{th} and 17^{th} century reveals an intensive morphodynamic activity. In this context, WIELAND (1984) mentions a general tendency of the channel to shift from a south-north to a more east-west orientation. Beside this change, the comparison of the 1846 chart with more recent ones and those of today reveals further tendencies in the morphological evolution. Thus, the Piep system with its two inlets has migrated northwards, whereas the sandbank Tertiussand, which separates the two channel branches, as well as the supratidal banks of Blauort and Trischen, have been displaced landwards by several kilometres. Under the influence of a continuing sea-level rise this landward migration of morphological features is still an ongoing process in the German tidal flats (WIELAND, 1972, 1984, 2000; EHLERS, 1988; SPIEGEL, 1997; HOFSTEDE 1999a, b; RICKLEFS et al., this volume). For the supratidal bank of Blauortsand in the centre of the area, WIELAND (1972) calculated a mean migration rate of 32 m/year for the period from 1932 to 1969, whereas KESPER (1992) observed that the rates increased from 40 to 80 m/year between 1970 and 1988.

With the diking of the Meldorf Bay in 1972 and 1978 approximately 480 km^2 of former intertidal flats were reclaimed. This massive encroachment on the natural environment resulted in several morphological adjustments and adaptations in adjacent areas. A detailed analysis of the morphological impact of land reclamation is given by WITEZ (2002). This study, and that of HIRSCHHÄUSER and ZANKE (2001), revealed that the main morphological adaptation in the inner Meldorf Bay concerned channel migration and a reduction of the subtidal channel volume. For the outer parts of the Piep channel system WITEZ (2002) detected a trend towards slightly deeper channels with steeper embankments. This, however, was considered a reaction to the rising sea level (SPIEGEL, 1997; WITEZ, 2002).

In summary, the Dithmarschen Wadden Sea is a typical example of an open tidal flat system exposed to the forces of the open sea, resulting in strong sediment displacement associated with rapid channel and shoal migration. Taking into account the morphological processes and tendencies outlined above one can conclude that in this area, which is caught between coastal defences and rising sea levels, the natural features of the Wadden Sea could be lost or drowned, a process which is known as coastal squeeze.

1.5 Modern Topography

The topography of the inner or central investigation area is dominated by the Piep tidal channel and its adjacent tidal flats. The channel has the shape of a lying Y, in which the northern and southern inlet (Norderpiep and Süderpiep) form the transition zone to the open North Sea. From the point of intersection of the two sub channels the actual Piep stretches in a more or less straight line eastward towards the city of Büsum. The mean water depth along the channel axis is 10 m on an average with maximum values of 26 m. Southeast of Büsum, the Piep splits up into three second-order channels and finally into several tidal creeks which are scattered across the tidal flat area of the Meldorf Bay. The south-western border of the area is characterised by the Bielshövener Loch tidal channel. It separates from the Süderpiep, runs southwards as a bifurcated channel, bends to the east in the vicinity of Trischen island, and finally splits up into a number of gullies (Fig. 3).

The ratio of intertidal to subtidal areas is approximately 60 by 40. The intertidal flats comprise a 15 km wide belt of sandbanks and shoals along the coast. The most seaward banks are relatively complex sand bodies with finger-shaped inter- and supratidal extensions stretching some kilometres westwards. At the transition from these sands to more sheltered areas, a number of isolated horseshoe-shaped supratidal banks such as “Blauortsand” and the incomplete barrier island of “Trischen” can be found. Compared to the seaward banks, the tidal flats in the inner parts consist of relatively large, successional units. Although their outer margins are clearly defined by the main channels, they are often subdivided into smaller units by gullies and tidal creeks.

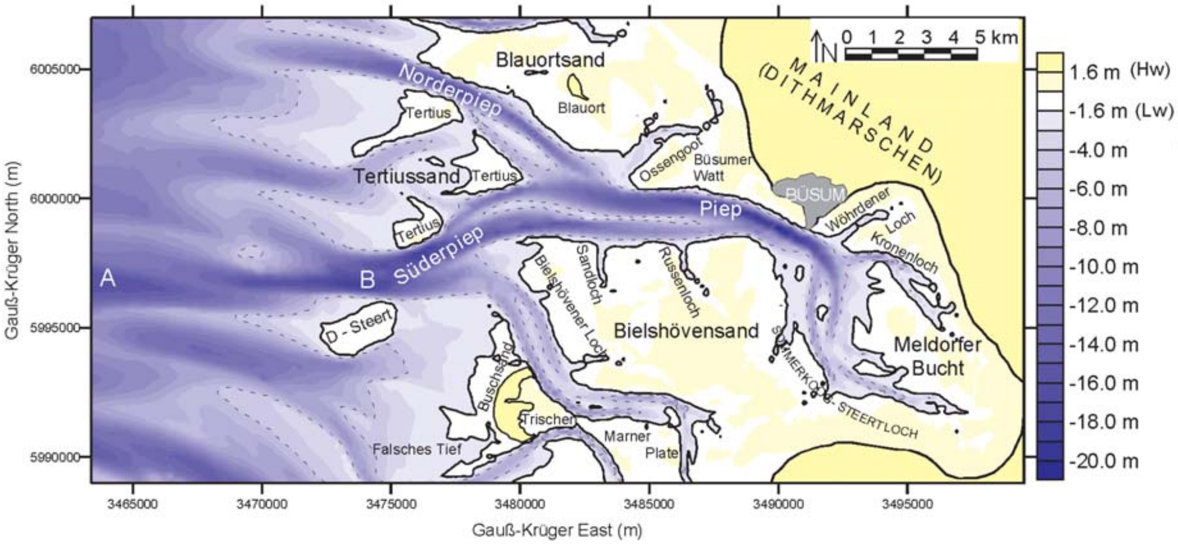

Fig. 3: Topography of the study area. A and B mark own wave gauge stations

1.6 Hydrodynamics

From the mouth of the Elbe Estuary to the Eiderstedt peninsula the mean tidal range varies from 3.1 to 3.4 m. Relative to the German topographic chart datum (NN), the mean high water at Büsum is +1.6 m NN and the mean low water is around –1.7 m NN. The difference between the neap and spring tidal ranges amounts to approximately 0.9 m. Storm surges can result in water level setups of more than +5 m NN (EHLERS, 1988). According to WITEZ (2002), the tidal prism of the embayment east of a line connecting the supratidal sands of Blauortsand and Trischen and the mainland of is of the order of 577×10^6 m^3.

The hydrodynamic conditions in the study area are dominated by strong currents associated with the semidiurnal tides. Current measurements carried out with acoustic Doppler current profilers revealed peak current velocities of up to 1.8 m/s in the main channels, whereas maximum ebb and flood currents typically range between 1 to 1.2 m/s. On the tidal flats currents are much weaker, within a typical range from 20 to 30 cm/s. However, velocities exceeding 80 cm/s were measured, near exposed channel margins. Additional information about tides and currents is given in SIEFERT et al. (1980, 1983), and WIELAND et al. (1984).

Whereas in the German Bight storm wave heights of several meters are common, wave heights strongly diminish when entering the shallow Wadden Sea waters. A good example of this attenuation is illustrated in Fig. 4. It shows that from the approach to the Süderpiep shipping lane to the still relatively exposed D-Steert sandbank, the significant wave height is already reduced by at least 50 %.

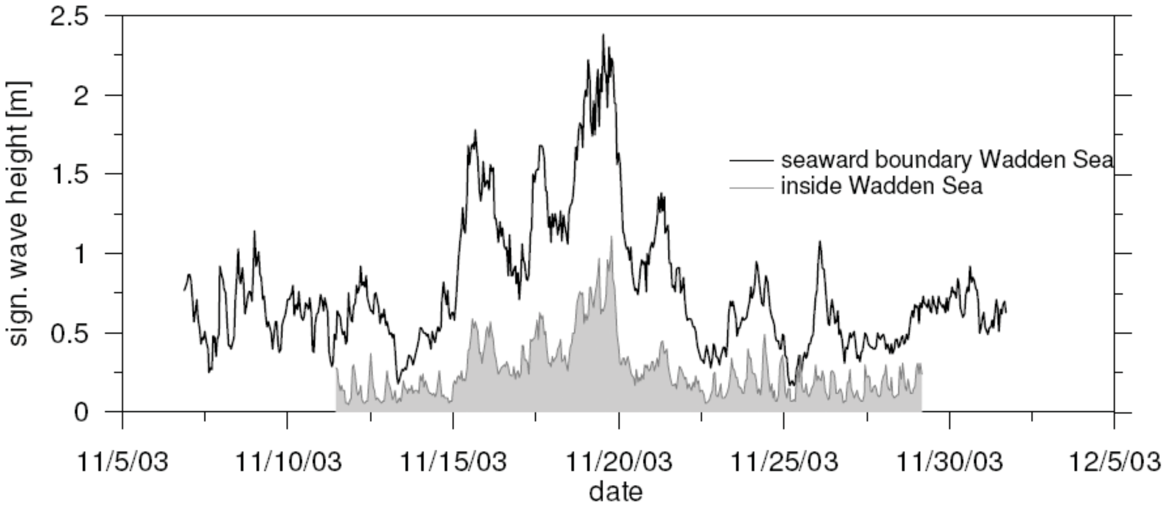

Fig. 4: Time series of significant wave heights recorded at the approach to the Süderpiep shipping lane and north of the D-Steert sandbank (see position A and B in Fig. 3). Measurements were made with an RDI 1200 kHz acoustic Doppler current profiler

Within the tidal flat areas, mainly locally generated waves are observed which are strongly dependent on factors such as water depth (NIEMEYER et al., 1996), wind direction and tidal currents (visible in the lower curve of Fig. 4).

2. Materials and Methods

2.1 Data Base

Bathymetric data of the central study area covering about 600 km² were made available by the German Federal Agency for Navigation and Hydrography (BSH). The different digital data sets cover a time span of 27 years (1974 to 2001) on a mainly annual but sometimes also monthly basis.

For the reconstruction of the Pleistocene surface and the interpretation of seismic records, all accessible data of previous studies were evaluated. Due to the generous support of the Landesamt für Natur und Umwelt, Schleswig-Holstein, the logs of more than 30 core samples collected in the area between 1936 and 1987 and reaching down to the Pleistocene, were made available for this study. The positions of some selected cores are shown in Fig. 5.

For the setup of a pre-Holocene surface elevation model, geological information on the Dithmarschen area available in DITTMER (1938, 1952), FISCHER (1955), HUMMEL and CORDES (1969), SCHMIDT (1976), MENKE (1976), HOFFMANN (1998) and MEIER (2000) was used. For the river Eider mouth region, data were taken from RUCK (1969), TIETZE (1983) and RUPRECHT (1999) and for the outer Elbe estuary from LINKE (1979). In the region of the East Friesian Islands and the river Weser, the investigations of GWINNER (1954), LANG (1959), and especially of STREIF (1990) were used to reconstruct the paleo-topography. To obtain information about the most probable former land surface in the open German Bight, data published in FIGGE et al. (1980) and ZEILER et al. (2000) were consulted. Beside these records, useful information was also gleaned from the sedimentological chart of the German Bight (FIGGE, 1981) and modern bathymetric charts.

Die Küste, 69 PROMORPH (2005), 1-420

2.2 Field Measurements

To evaluate the middle- to short-term morphological changes in the Piep channel system, several additional measurements were carried out. These mainly included bathymetric (morphological) and geological surveys.

For a more detailed investigation of the morphological variability of the Piep channel system, several bathymetric cross-sections were repeatedly surveyed (Fig. 5). For this, we used our own research boats equipped with 200 kHz echo sounders and Differential GPS positioning systems. All data were corrected for sound velocity variations in the water column (measured by CTD during the survey) and referenced to the German topographic chart datum (NN) using water level data from the Büsum gauge station. Table 1 gives an overview of the spatial-temporal resolution of the measurement program.

Assessing the quality of the echo-sounder measurements and data processing, four main error sources were identified: a) the precision of the survey equipment (echo-sounder and positioning system); b) water level corrections (tides); c) variations of the speed of sound in the water due to changes in salinity and temperature; and d) data interpolation when generating digital elevation models. The maximum cumulative error was estimated to be of the order of 0.3 m. For the purpose of this paper, variations under 0.5 m were thus not considered in the analysis of morphological changes.

Table 1: Repeated measurements of different cross-sections (see Fig. 6 for location)

	2000			2001			2002							2003			
Fieldwork areas	6	9	12	5	7	12	3	6	8	9	10	11	12	3	4	5	8
Norderpiep (A)	X	X	X		X	X								X			X
Süderpiep (B)		X	X	X	X				X			X		X			
Piep (C)	X	X	X	X	X	X						X		X			
Büsum						X	X	X		X		X					
Sommerkoog-Steertloch						X		X	X		X		X		X	X	

Since the stratigraphic architecture of the Holocene sediments has a substantial influence on the morphological evolution of the study area, and the history of the morphological evolution in turn can, to some extent, be extracted from stratigraphic records, the three-dimensional distribution of the sediments was investigated using hydro-acoustic methods such as side-scan sonar and reflection seismic profiling (Boomer; LURTON, 2002) in addition to conventional coring.

Repeated sonographic surveys of seabed features were performed using a KLEIN-595, 100/500 kHz dual frequency side-scan sonar. Measuring campaigns were carried out in July 2000, September 2000, July 2001 and March 2002. The sub-bottom profiling was mainly carried out with a "Boomer" system. This device sends out pulses at energy levels ranging from 100 to 300 joules and frequencies of 0.5 to 15 kHz. During the measuring campaigns in July and September 2000, shallow seismic profiling was also done with a 3.5 kHz sub-bottom profiler. The operation principles of sub-bottom profilers are described in D'OLIER (1979).

To complement the study of short- to medium-term morphological changes, several sediment cores were taken in the Dithmarschen tidal flats in September and November 2001. These cores were 1.8 to 5.5 m long and were taken in intertidal or shallow subtidal areas using a specially designed coring boat. The principles of vibrocoring techniques are described in LANESKY et al. (1979). The sampling locations were chosen on the basis of the results of previous morphological analyses. Of particular interest were those areas in the inner, central and outer part of the study area, where substantial deposition over many years had taken place. Figure 6 shows the coring locations.

Surface sediment samples in the channels were taken with a medium sized van Veen grab and on the intertidal areas by small coring tubes 10 cm in length and 4 cm in diameter. A schematic overview of the locations and coverage of the field measurements mentioned above can be seen in Fig. 5.

2.3 Digital Elevation Models (DEM)

The available bathymetric data were used to generate digital elevation models (DEM). These DEMs permit a numerical comparison between different morphological model stages and thereby, a quantification of erosional or accretional tendencies. On the basis of the data density and coverage, grid spacing between 50 and 200 m was used for the interpolation of the BSH data sets. For the more detailed bathymetric measurements carried out in this investigation a grid resolution of 10 to 15 m was chosen. In both cases, the applied interpolation method was based on triangulation. Interpolation, visualisation and volume computations were carried out with the software package SURFER TM (Golden Software).

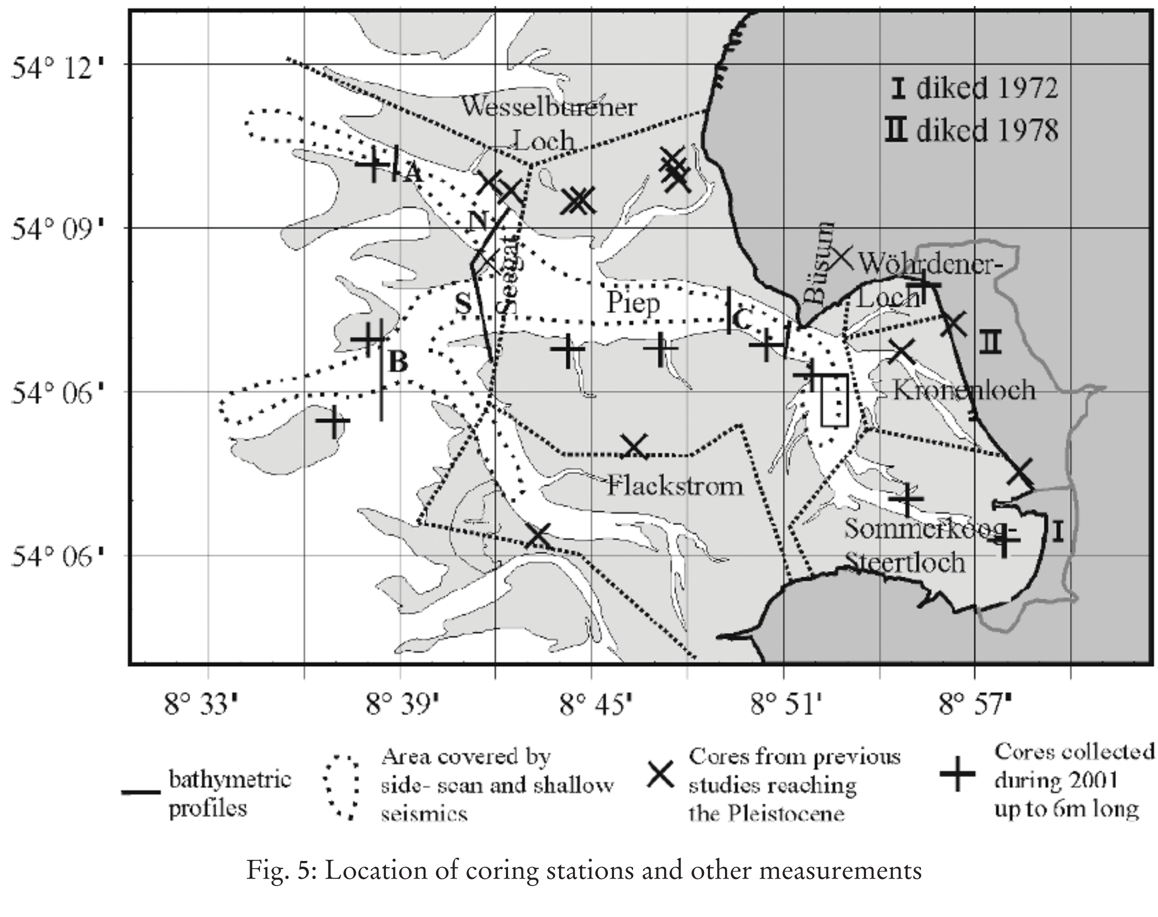

Fig. 5: Location of coring stations and other measurements

3. Results

3.1 Geology

Data from the literature, archived core logs, own core drillings, and shallow seismic records were compiled to set up a digital elevation model of the pre-Holocene surface of the innermost German Bight (Fig. 6) with special focus on the Dithmarschen area (ASP et al., 2003). The simulated Holocene-Pleistocene boundary is based on a 600 by 600 m grid.

The most prominent element in this DEM is the wide NW-SE striking melt water valley of the river Elbe. Other distinct features are the Pleistocene valleys of the river Weser in the SW and the Eider in the NE (Fig. 6). Along the Dithmarschen coast the mainland shore is evidently shaped by relatively wide and shallow embayments. To the west of these bays, the area can be divided in two parts. In a zone extending roughly from the latitude of Büsum southward to the Elbe melt water valley, the Pleistocene surface rapidly dips down to the west and southwest to depths of more than 30 m below the present surface. North of Büsum the westerly dip slope is gentler. However, this surface is dissected by the melt water valley of the Eider. Although the depth of the Holocene base in the region of the modern estuary (RUCK, 1969) and further offshore (FIGGE, 1980) is relatively well known, the course of the former valley along or below the Eiderstedt peninsula has still not been completely reconstructed.

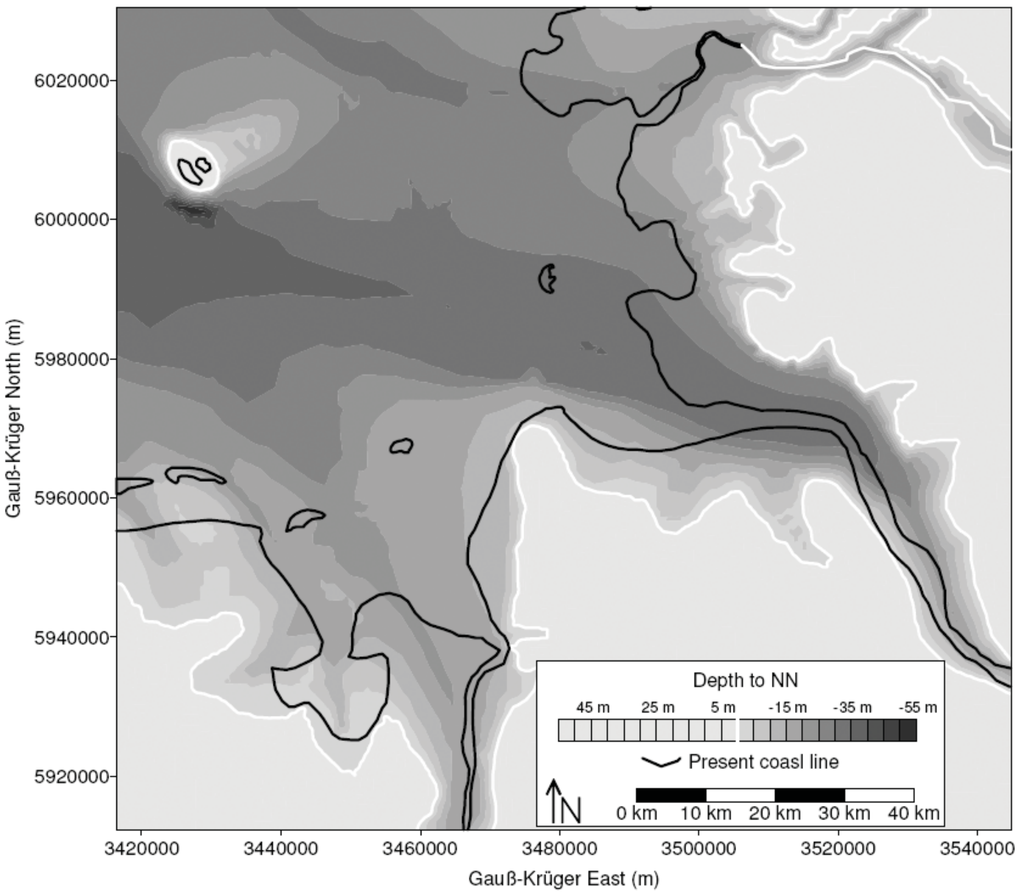

Fig. 6: Reconstructed Pleistocene surface (DEM)

In the central study area, a second major stratigraphic unit has been identified. It is the clayey and sandy silt bed called "Dithmarscher Klei". This consolidated mud deposit directly overlies mostly thin layers of different composition which mark the beginning of the Holocene transgression (Fig. 7). The very cohesive sediment was deposited between 5000 and 7000 years BP (DITTMER, 1938) and has a thickness of up to 10 m (average: 5 m). On the basis of side-scan sonar records it was possible to identify several outcrops in the deeper channels. The depth of contact to the water varies between –15 and –24 m NN. In addition to this unit, a second cohesive mud deposit was detected in the vicinity of the Tertius sandbank. Here, this "Upper Klei" typically reaches depths of up to –12 m NN (Fig. 9). Its thickness is of the order of 1–2 m.

Since both mud beds are very resistant to erosion and scouring, they form a certain discontinuity layer for morphodynamic processes affecting the overlying recent, mainly fine sandy tidal sediments. Under the assumption that the consolidated layers prevent or delay scouring and are therefore important for the "draught" of morhodynamic processes, we developed an elevation model of the surface defining the top of the "Lower Klei" and the top of the "Upper Klei" on the basis of core samples and hydro-acoustic data (Fig. 8). Since this horizon forms the basis of the modern tidal deposits, the DEM also quantifies the thickness and volume of the potentially more erodible sediments.

Based on these results Fig. 8a shows a certain dichotomy. While the eastern part is characterised by the top of the "Lower Klei" sloping down in westerly direction, the western part shows the extent of the overlying "Upper Klei". The top elevation of this layer is highest in the north and lowest in the south. Consequently the thickness of modern sediments

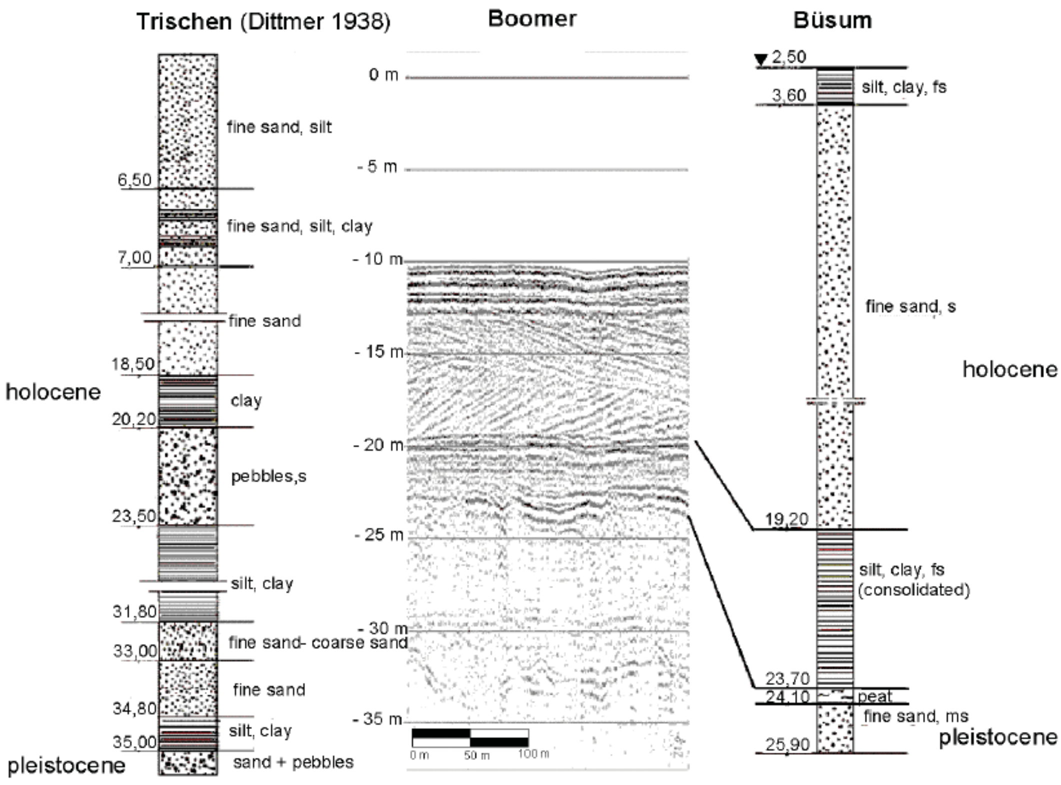

Fig. 7: Shallow seismic record from a location close to Büsum.
Note the good correlation with core data

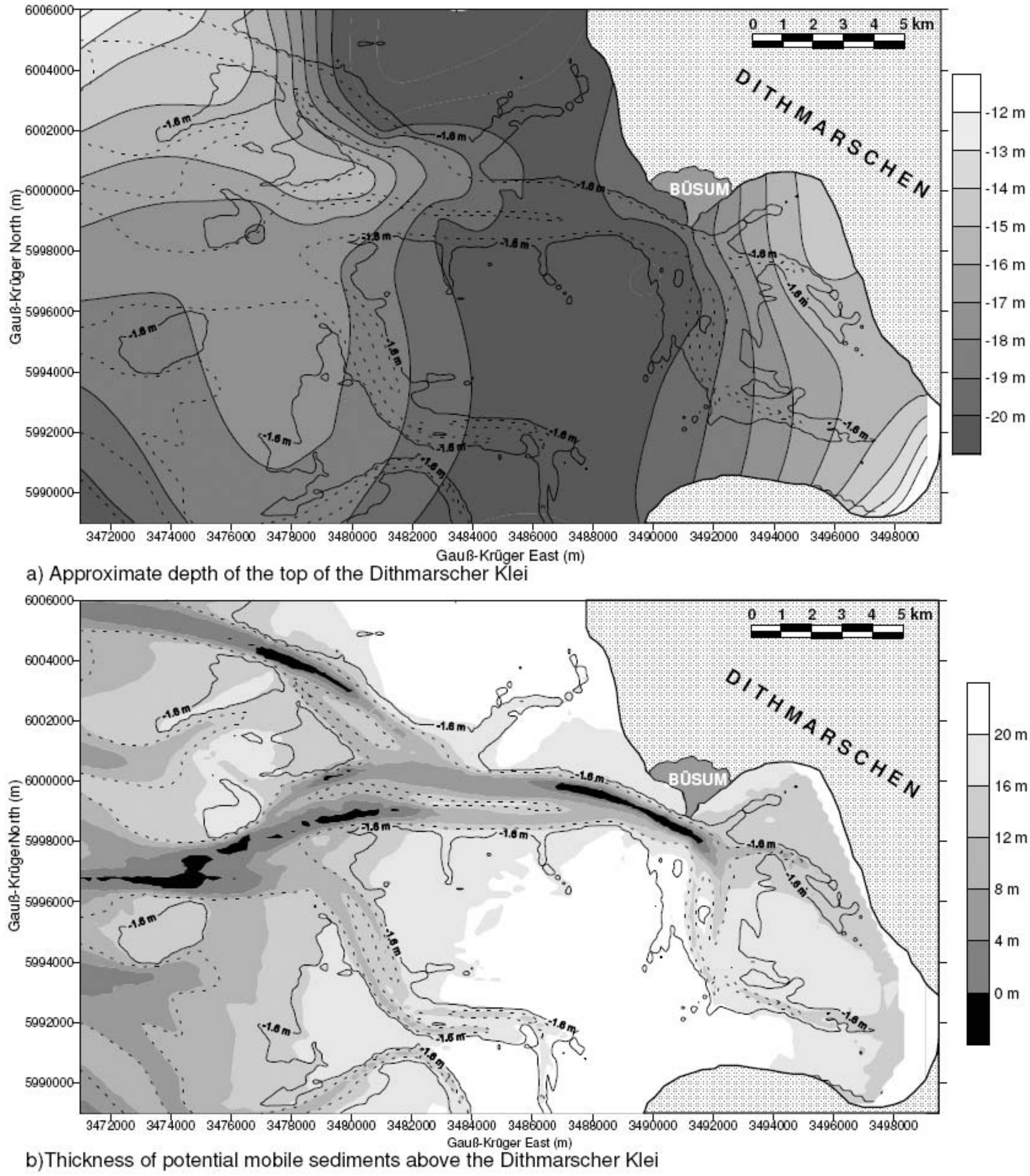

Fig. 8: Depth of the "Dithmarscher Klei" and thickness of modern tidal flat sediments.

is highest in those areas where no "Upper Klei" could be found and the top of the "Lower Klei" is low lying.

As pointed out earlier, the modern tidal flat and channel sediments were mapped using side-scan sonar, seismics, sediment samples and cores. The survey of the channel deposits reveals that these sediments consist mainly of fine-to medium-grained sands, interrupted by outcrops of the consolidated, fine-grained "Dithmarscher Klei" (Fig. 9). This pattern reflects the high-energy hydrodynamic regime in the main channels. Local occurrences of sandy mud either represent a mixture of partially eroded consolidated silty-clays and mobile sands or they may be associated with rapid local sediment deposition. In contrast to the channel deposits, whose distribution is strongly influenced by the local hydrodynamics, the intertidal sediments show a clear gradual decrease in mean grain size from the outer to the inner parts of the study area. This tendency is particularly well displayed by the distribution pattern of mud contents (Fig. 10). As in the case of the channels, the mud distribution pattern reflects the hydrodynamic regime from exposed and more dynamic depositional environments close

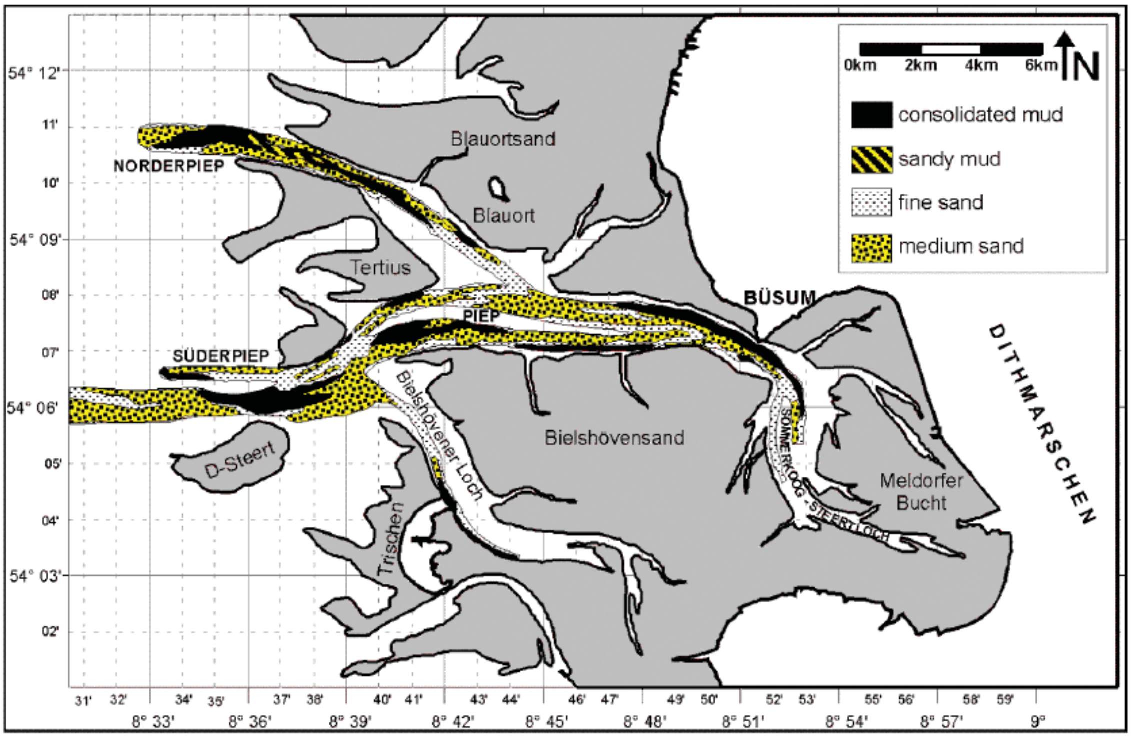

Fig. 9: Sediment distribution in the tidal channels

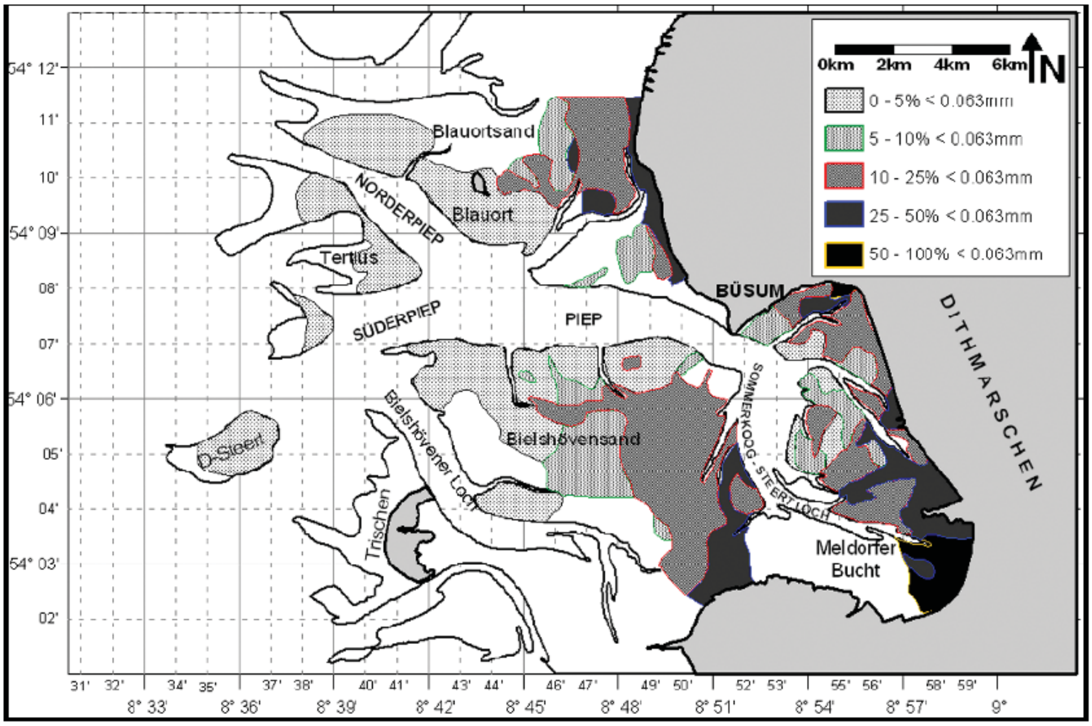

Fig. 10: Sediment distribution on the tidal flats. (after REIMERS, 2003)

to the open sea to more sheltered and generally more elevated accretional areas close to the coastline. In Fig. 11 a number of grain-size distribution curves are presented which characterize the sediments in depositional areas. Thus, the medium-sized type "A" sands can only be found on very high intertidal or partly supratidal sites of energetically exposed sandbanks close to the open sea (mainly Tertiussand, D-Steert and Blauortsand, Fig. 3). Type "B" sediments basically characterize the widespread sand flat facies (REINECK and SINGH, 1980). Here the mud content is less than 10 %. In the mixed flats with 10–50 % fines, bimodal sediments similar to type "C" are often observed. They are typical of depositional environments where frequent mixing of coarser and finer sediment fractions takes place. Type "D" distribution curves represent samples from areas with soft, fine-grained sediments (mud). The shapes of the grain-size distribution curves also indicate that some sediments are composed of differently sorted grain-size populations. However, it is evident that the study area is dominated by very fine sands and silts.

Besides sampling surface sediments, a series of cores was taken to study the structure of the upper metres of the deposits in more detail. The drilling sites are located along a transect from the inner Meldorf Bay to the outermost sandbanks in the west (Fig. 12).

Without going into a detailed discussion, it is obvious that the western sandbanks are almost completely composed of compact sand layers (Ke 1 to Ke 3 in Fig.12). The different bedding types show that the sands are transported by currents as well as by wave action. The upper metres of the sediment body in the central part of the study area, i. e. along the Bielshöfensand, are again primarily composed of sandy layers. However, here thin strata of silt and clay (mud) are now intercalated. Further towards the mainland and the inner parts of the Meldorf Bay muddy layers become more and more frequent. Here the sediments are typically composed of tidal rhytmites with alternately bedded thin strata of fine sand and mud. The only exception in this sequence from sandy to more and more muddy deposits shows core KE 6, which is located in a very dynamic channel meander belt south of Büsum (Fig. 12). Here, sediment transport is dominated by the migration of large bedforms generated by strong tidal currents. As a result, the composition of the sediments more closely resembles that of the outer regions.

In summary, it can be concluded that both the upper meters of the recent intertidal deposits as well as the surface sediments basically show the same well known gradual decrease in grain-size from exposed to sheltered tidal flat areas.

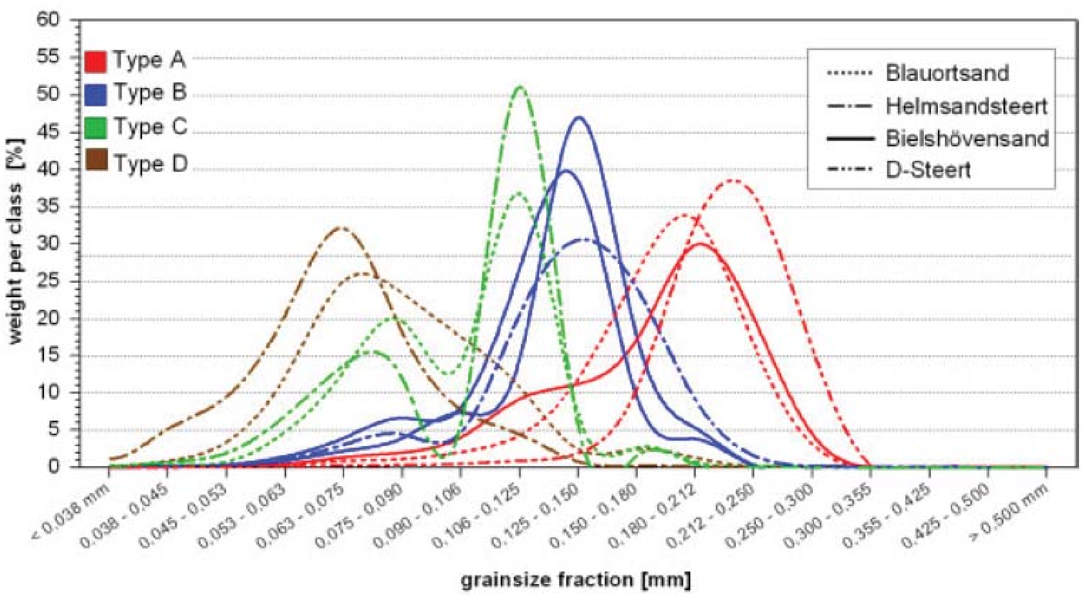

Fig. 11: Grain-size distribution curves of typical intertidal sediments (after REIMERS, 2003)

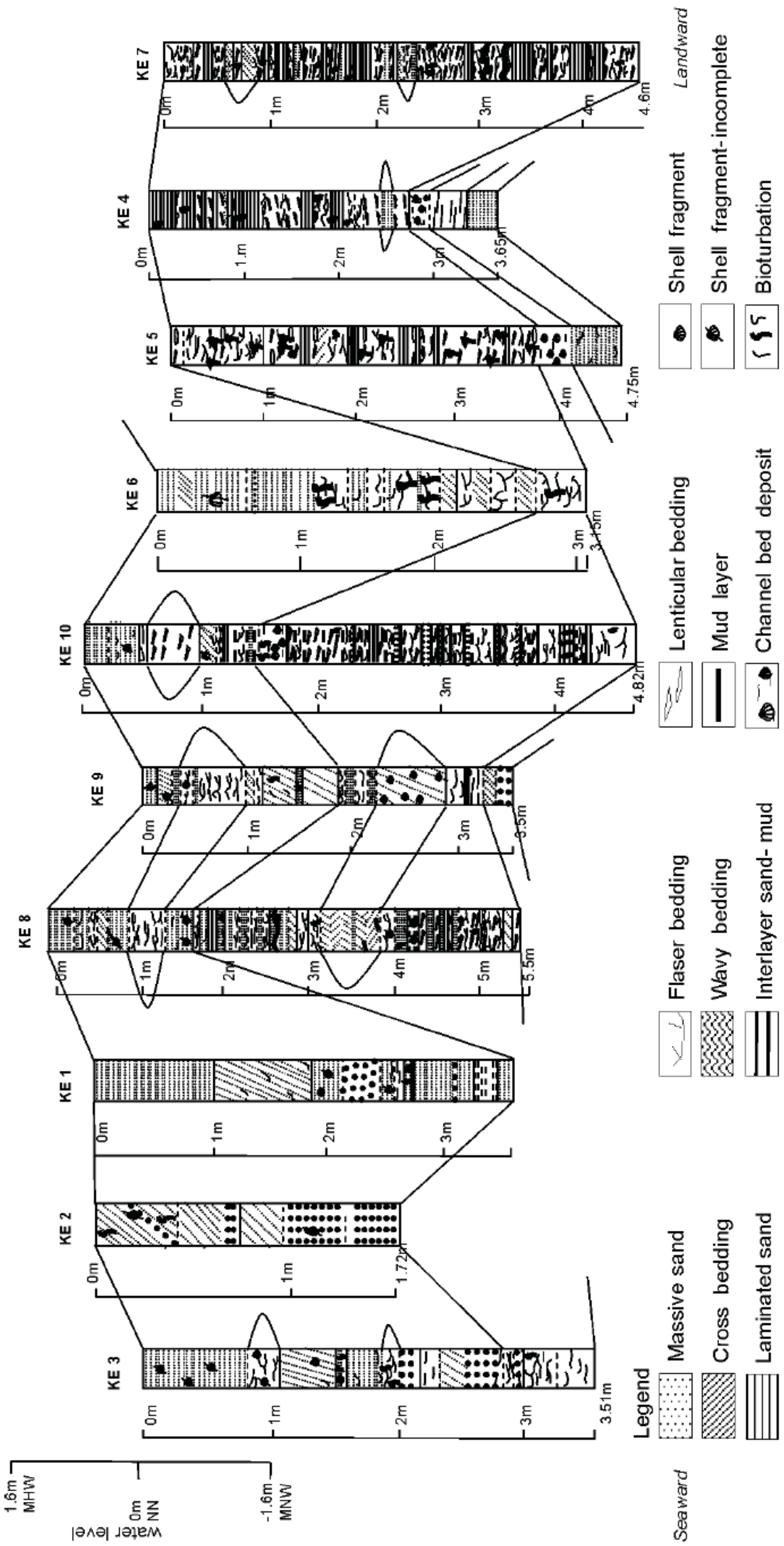

Fig. 12: Stratigraphic cross-section through the study area as revealed in cores. See locations in Fig. 5 marked by "+"

3.2 Long-Term Morphological Changes on Temporal Scales of Years and Decades

The morphological analysis is mainly based on bathymetric data collected by the German Federal Agency for Navigation and Hydrography in the course of annual surveys over a period of almost 30 years. For morphological comparisons and particularly for trend analyses, digital elevation models were run for almost all the available data sets. The visual and numerical analysis of the various simulated topographies reveals both minor short term and major long-term trends. The latter trends cover periods of several years to decades. To give an integrative overview and a rudimentary quantification of the longer-period morphodynamic evolution, the numerical elevation difference between the 1977 and 1996 bathymetries is illustrated graphically in Fig 13.

For the Meldorf Bay the figure shows that in the time span from 1977 to 1996 some smaller tidal channels silted up. This can be understood as a response to the reclamation of the inner Meldorf Bay, which took place in the 1970s. This artificial reduction of the tidal prism also resulted in adaptations of the Sommerkoog Steertloch tidal drainage system. Together with intensified meandering and lateral channel migration in an easterly direction, a decrease of the subtidal volume can be observed. This trend to stronger meandering is most pronounced in the main channel opposite the harbour entrance of Büsum (Fig. 14) where relatively strong accretion can be observed along the southern flank and erosion along the channel slope in front of the Büsum waterfront. A more detailed analysis of the progressive channel displacement suggests that the breakwaters of Büsum port and other coastal defence structures counteract erosion along the channel's stoss-side. Whereas the shrinkage of the subtidal volume in the inner bay caused by siltation is directly related to the reduced water masses passing through the channels, migration and meandering seem to be controlled by other factors, considering that an increasing meandering tendency was already detectable prior to the diking (WIELAND, 1984).

Following the Piep channel further towards the west, a significant departure in the depositional trends on either side of the mid channel shoal can be observed. While erosion prevails south of the shoal, a tendency towards accretion is observed along the northern slope and on the shoal itself. However, despite this internal reshaping, the reach and position of the central Piep channel remain relatively stable. An even stronger growth of the mid-channel shoal can be found in the southern channel of the Bielshövener Loch. Again, the general position of the tidal stream seems to be relatively stable. In contrast to the Piep, however, the stronger vertical accretion of the central shoal confines the channels an either side, causing these to deepen and producing some erosion along the northern and southern banks. In the field this is revealed by steep slopes and some shell accumulations. East of the island of Trischen the erosion of the southern channel bank becomes more pronounced. This is due to continued southward migration of the meander belt in this area.

On the other hand, the extensive intertidal flat of the Bielshövensand, located between the Piep and the Bielshövener Loch tidal streams, has remained relatively stable, at least within the limits of the vertical resolution of the DEM. Only very local sedimentation or erosion can be recognized together with a more pronounced change being restricted to the western tip of the sandbank which has expanded towards the north-west.

In contrast to the relatively stable situation on the Bielshövensand, the Blauortsand, a tidal flat north of the Piep channel shows more substantial changes. Here, data analysis reveals a deepening of gullies and a slight decrease in tidal flat elevation between 1977 and 1996.

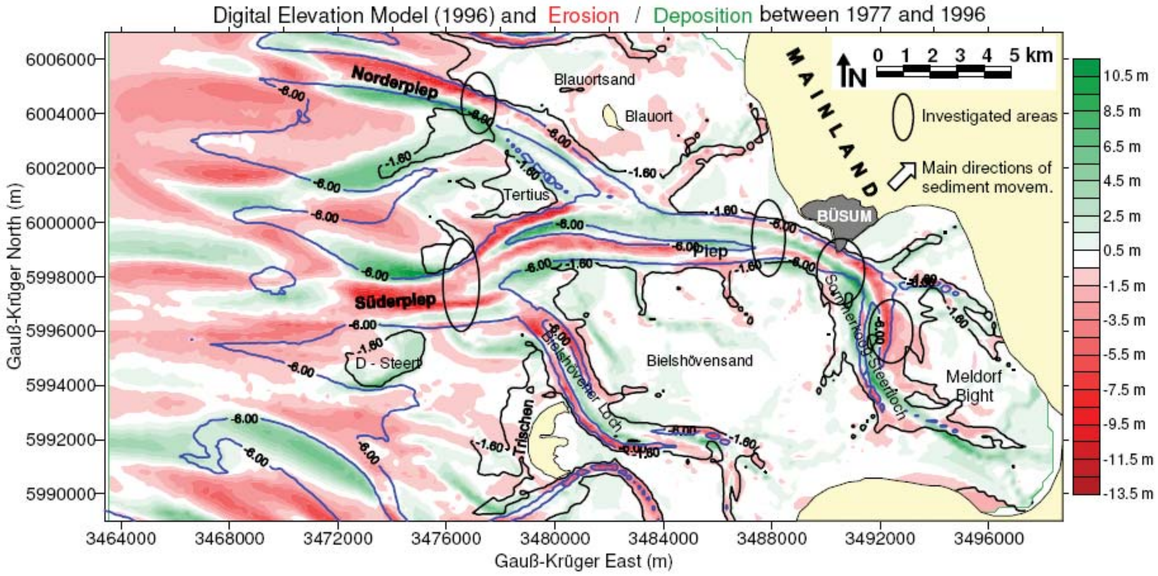

Fig. 13: Overview of long-term morphological changes in the study area

Compared to the relatively stable central part of the study area, the more westerly and most exposed regions are characterised by intense erosion and re-deposition processes. Hydrodynamic forces have driven the outer sandbanks such as Tertiussand and the D-Steert landwards. In the case of the Tertiussand, the migration has produced a compressed morphology. The reason for this is that the sandbank is trapped like a wedge between the two bordering inlets of the Süder- and Norderpiep. The morphological response is revealed by erosion in the seaward parts and accretion in the more easterly regions, especially along the channel banks. This wedge-like advance also forces the inlet of the Norderpiep to the north, as clearly recorded by erosion along the northern and accretion along the southern bank (Figs. 13 and 14).

In contrast to the evolution of the northern channel, the situation in the Süderpiep is more complex. Here, the channel is bifurcated (cross-section B-Süderpiep and Seegatt–S in Fig. 14) over wide stretches. At the section Seegatt-S the stronger morphodynamic response of the southern, flood-dominated channel is associated with increased meandering. In both cases a northward migration of the mid-channel shoal and the northern channel section is observed. This northward migration in combination with the ebb-domination of the northern channel, results in erosion along the flanks of the Tertius sandbank (stoss-side for the ebb current). Comparable but weaker bank erosion can be observed at the more westerly B- Süderpiep profile (Fig. 14). However, here the most affected area is the mid-channel shoal. During the observation period from 1977 to 1996, the shoal initially accretes up to the end of 1979 the trend reversing from the early 1980s onwards until it almost disappears by 1996. Still further west, a strong downward erosion of the channel is evident (Fig. 14). This deepening might again reflect the evolution from a bifurcated to a single channel as seen in the previous profile. However, it may also be related to the landward migration of the Tertius and D-Steert sandbanks. As a consequence, the channel would get more and more compressed, resulting in stronger incision by the tidal stream. Since this latter process could also explain the disappearance of the mid-channel shoal, a reliable interpretation of the erosion pattern in this area can not be given at the present stage of the investigation. However, we think that

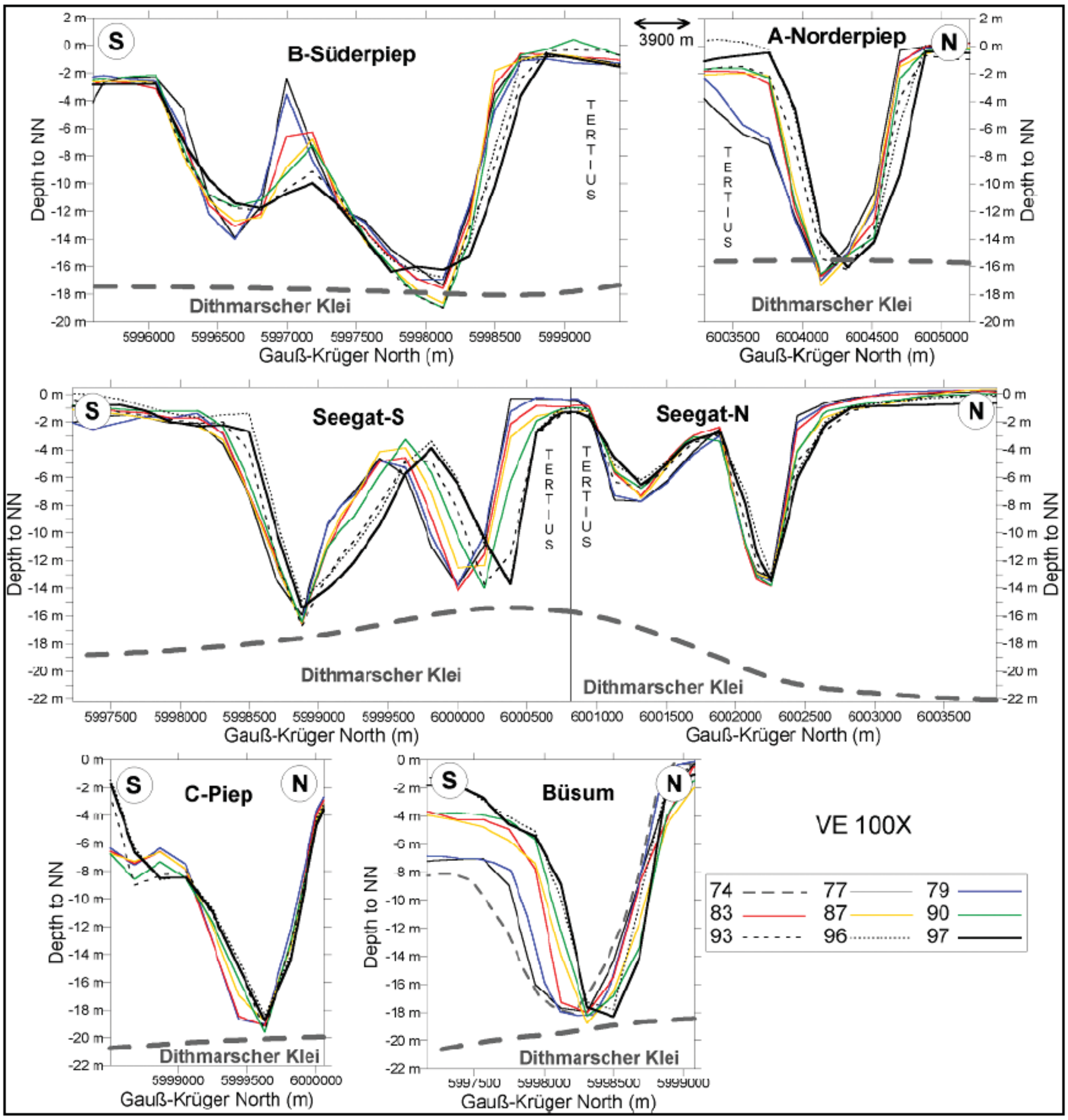

Fig. 14: Annual to decadal morphological evolution along several channel cross-sections relative to the depth of the Dithmarscher Klei. Locations of cross-sections see Fig. 5

the downward erosion will be limited due to the consolidated layer of "Dithmarscher Klei". From Fig. 14 and other fieldwork it is evident that the maximum channel depth often matches the elevation of the "Dithmarscher Klei".

In summary, the study area can be divided into three regions. In the innermost part represented by the Meldorf Bay, the change in hydrodynamic conditions caused by land reclamation in the 1970s has controlled the morphodynamic evolution. The central part of the study area has remained relatively stable and is characterized by minor internal reshaping processes. The outer region, west of the bifurcation of the Piep channel into the Norder- and Süderpiep, is exposed to intense erosion processes. Landward migration of sandbanks, vertical accretion, especially of those parts of the sandbanks which border the channels and erosion tendencies in the channels are typical for this area. Finally, there is the transition to the open sea where widespread erosion seems to prevail. The question, to what extent this overall loss in sediment volume is real or an artefact of data quality can not be answered reliably at the present stage of the study.

3.3 Short-Term Morphological Changes on Temporal Scales of Weeks to Months

Beside the analysis of long-term (years to decades) morphological changes, the investigation also included an analysis of short-term morphological changes at temporal scales of months or weeks. The aim was to identify seasonal effects and effects of singular events. The data for this purpose were collected in the course of repeated bathymetric surveys. These soundings mainly concentrated on the same cross-sections discussed in the previous chapter (Fig. 14).

Cross-section “A”-Norderpiep:
Old nautical charts of the 19th and beginning of the 20th century show a much wider northern inlet of the bifurcated Piep channel system and the presence of a well developed mid-channel shoal. (LANG, 1975). Since that time the Norderpiep shows a progressive decrease in width and a gradual reduction of the mid-channel-shoal. Today the central reach is relatively narrow and shows a simple U-shaped profile (Fig. 14). The results of bathymetric measurements (Fig. 15), carried out between summer 2000 and summer 2003, confirm the tendency for a general northward migration of the channel. Although depth variations of up to 4 m can be recognised in the process of this relocation, the cross-sectional area of the tidal stream stays relatively stable. However, Fig. 15 also reveals localized accretional and erosional phases. A temporal analysis of these variations shows that deposition prevails from winter to summer, and erosion from summer to winter. This is most obvious in the centre of the channel but also holds true for the flanks. Along the northern channel bank, by contrast, erosion mainly occurs in autumn and winter. This increase in cross-sectional area is compensated by the deposition of a comparable sediment volume along the southern bank in the subsequent calmer late spring and summer period. It is noteworthy that, especially in the region of the surveyed profile, lateral deposition as well as lateral erosion produces remarkably steep channel slopes. As a result, the occurrence of submarine slides due to either erosional or depositional processes is quite common.

In summary, the channel in this region can be considered to be in dynamic stability with seasonal variations and the superposition of a tendency towards northward migration in the longer-term.

Cross-section “B” – Süderpiep:
The bathymetric profile at cross-section “B-Süderpiep” (Fig. 16) is much more complex than cross-section “A-Norderpiep”. Here the passage to the Bielshövener Loch channel branches out from the Süderpiep tidal stream to produce two channels separated by an elongated sill which increases in height from west to east (Fig. 16). A short distance landward of the bathymetric profile, the Süderpiep splits up again into a flood dominated southern and an ebb dominated northern branch. The cross-sectional area of this profile is about three times larger than that of the Norderpiep. As a consequence, the discharge should be correspondingly higher. This has in fact been confirmed by current measurements, which suggest a 2 to 2.5 times larger water volume passing through the Süderpiep.

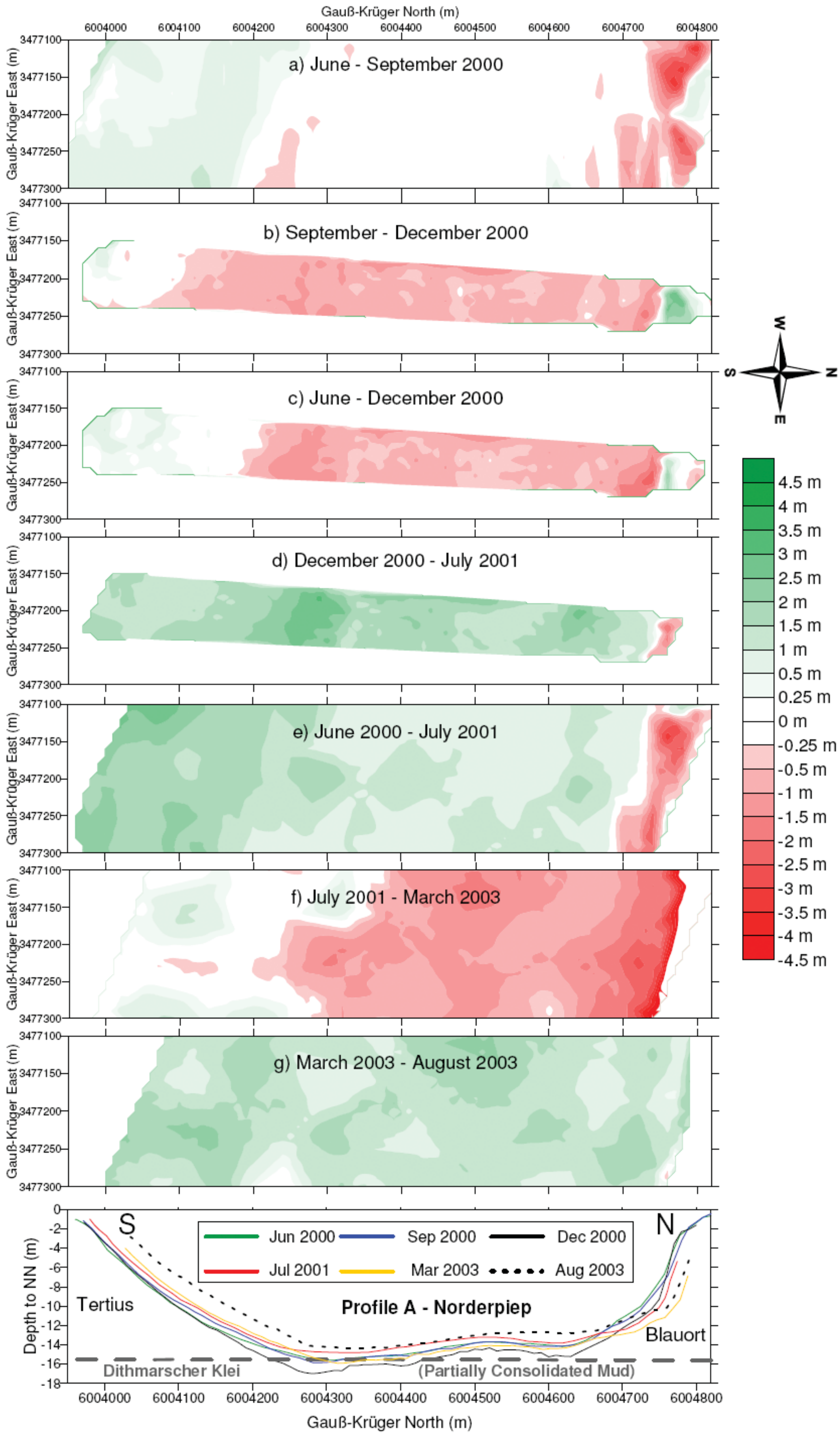

Fig. 15: Comparison of bathymetric data and quantification of elevation changes (red: erosion /green: deposition) at cross-section A – Norderpiep

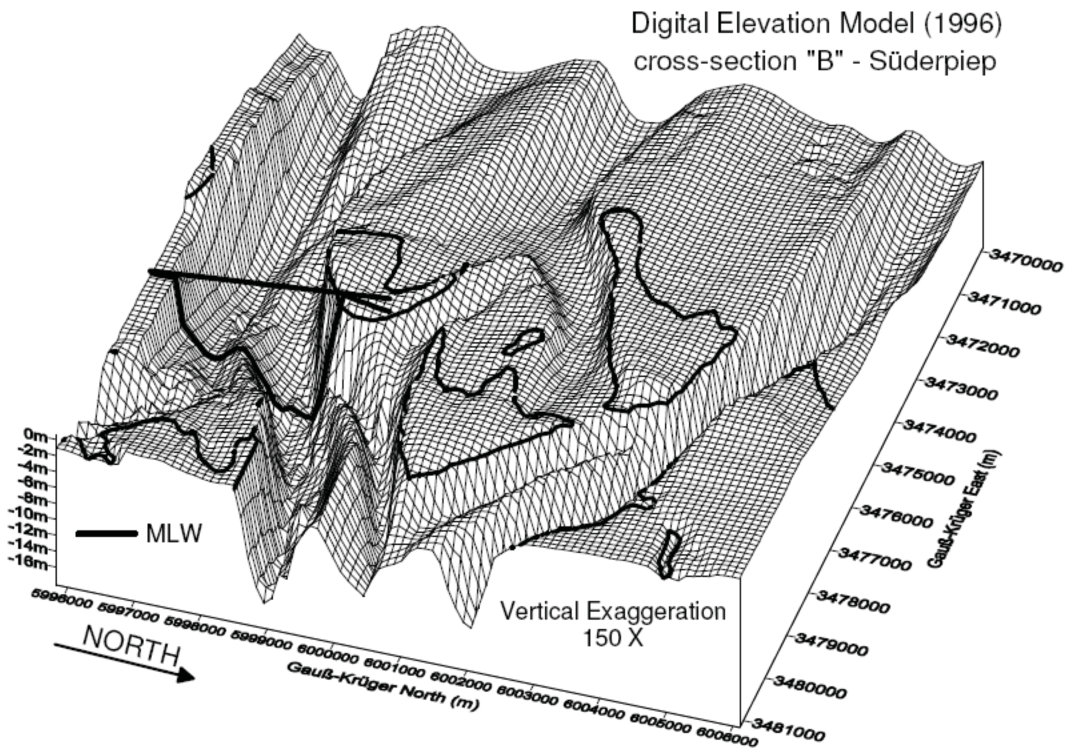

Fig. 16: 3-D view of the Tertius Sand with marked position of the cross-section B – Süderpiep

In the course of six surveys between late summer 2000 and spring 2003, depth variations of one to two meters were observed along the deeper parts of profile (Fig. 17).

Higher values were measured only on the northern side where erosion seems to prevail. Here the ongoing attack of especially the ebb current has sculptured a very steep slope along the Tertius sandbank. In this context, the existence of an underwater ledge in the lower slope of the bank is noteworthy. Results of different hydro-acoustic measurements show that this ledge is associated with a cuesta-like outcrop of cohesive sediment beds (Upper Klei). In our opinion the formation of this inconsistency in the slope indicates that the consolidated layers prevent an even stronger displacement of the slope. The obvious question, whether this bank erosion results from a widening or from a northward migration of the channel, can not be answered on the basis of the available data. Thus, the interpretation of Fig. 17 does not permit any statement concerning a net deposition on the southern side of the cross-section which would be an argument in favour of channel migration. However, the morphological setting in that area is so complex that nearby deposition balancing the erosion due to channel migration can not be excluded. Unfortunately the quality of the digital elevation models to some extent suffers from the presence of megaripples (dunes) in this area. Due to the high natural variability of these bedforms, the uncertainty imparted by the bedforms on successive DEMs can add up to produce a purely numerical patchiness in erosional and depositional trends. This could mask any real bathymetric trends. Despite these uncertainties and considering the complexity of the morphological evolution of this cross-section, we are nevertheless confident that we can recognize a pattern suggesting erosion in autumn / winter and deposition in spring / summer. However, in some cases, e. g. between August and November 2002, the observed morphological changes do not match this seasonal cycle.

In summary, the cross-section B-Süderpiep can be considered to be relatively stable in the period from summer 2000 to spring 2003. Depth variations of 1-2 m were monitored

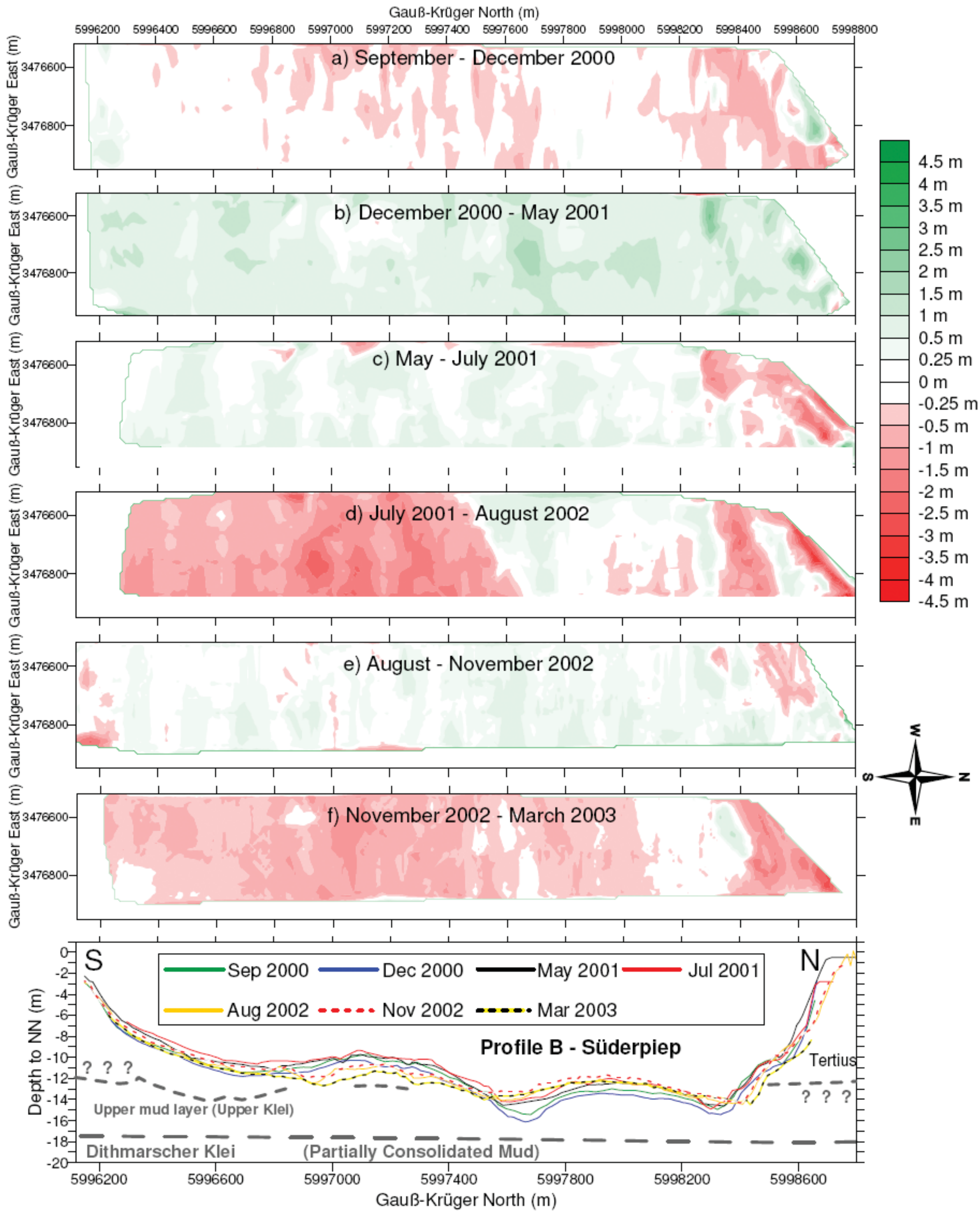

Fig. 17: Comparison of the various bathymetric measurements along cross-section B – Süderpiep

without showing any clear evolutionary trend. Persistent erosion was only observed along the northern embankment of the Tertius sandbank.

Cross-section "C" – Piep:

The cross-section C – Piep is located approximately three nautical miles west of the town of Büsum (Fig. 5, 14). It covers the eastern junction of the main Piep tidal channel and its southern flood dominated branch called Dwarsloch. The data show this profile to be morphologically very stable. Although maximum depth changes of up to three meters were measured, they more commonly remain below 0.5 m (Fig. 18) on short time scales (months). Since the morphological changes along this cross-section are not very large, there is no clear evidence for a directional displacement or a seasonal cyclic behaviour comparable to that discussed earlier. On the contrary, a comparison of data from June, September and December 2000 suggests deposition from summer to winter. This trend, however, reverses in the period from December 2000 to May 2001 when erosion occurred from winter to summer instead.

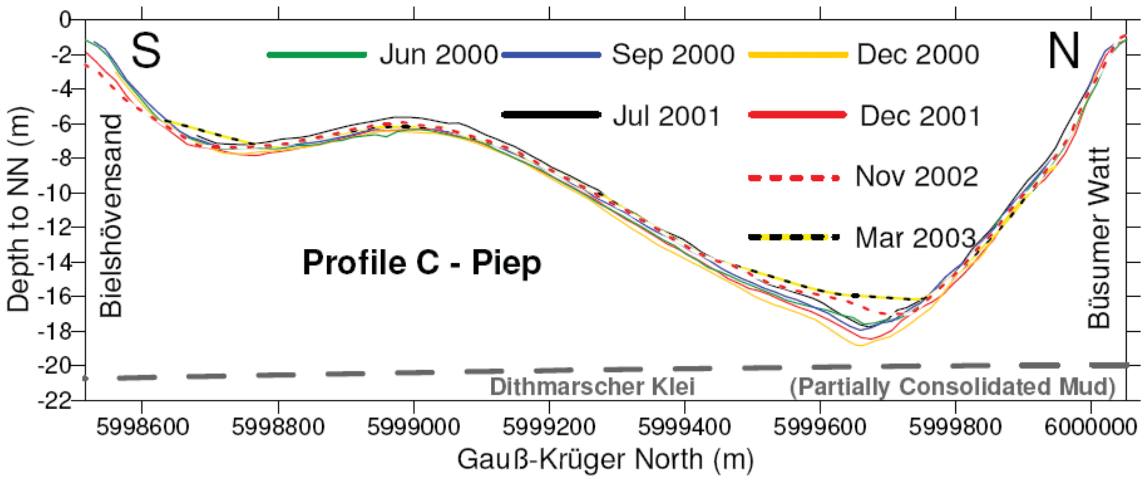

Fig. 18: Bathymetric profiles measured between summer 2000 and spring 2003 at location "C"

Cross-section Sommerkoog Steertloch:

This profile covers the eastern branch of the Piep tidal stream after entering the inner Meldorf Bay (Fig. 15). The large gully is part of the so-called Sommerkoog Steertloch and has a South – North orientation. It reaches depths of about 8 meters, and the cross-section has an intermediary shape between a "V" and a "U". In contrast to the other cross-sections, a 1400 m long channel section was monitored in this case (Fig. 19).

The most obvious morphological change in this area is the pronounced easterly migration of the channel. This progressive displacement was already pointed out in the previous chapter when discussing changes on larger temporal scales since the late 1970s. On the basis of the short-term bathymetric monitoring carried out between December 2001 and September 2003, migration rates of 50 to 75 m/a were calculated (Fig. 19). These data also show that a seasonal depositional cycle is superimposed on the net eastward migration of the gully. The erosion clearly dominates the cold season and affects almost the entire channel. However, the scouring is to a certain extent counter-balanced by accretion in the summer months. Furthermore, erosion during autumn/winter is more intense on the eastern flank of the channel, whereas deposition is more pronounced on the western flank during spring/summer and occurs more seldom in the cold season. Similarly, deposition along erosional eastern bank is reduced to very small quantities even during the net accretional phase in spring/summer. This distribution of net depositional and net erosional areas is responsible for the net easterly migration of the channel.

According to Fig. 19 the channel geometry has not changed significantly in the course of migration, although the pattern of deposition and erosion would suggest that a split-up of the

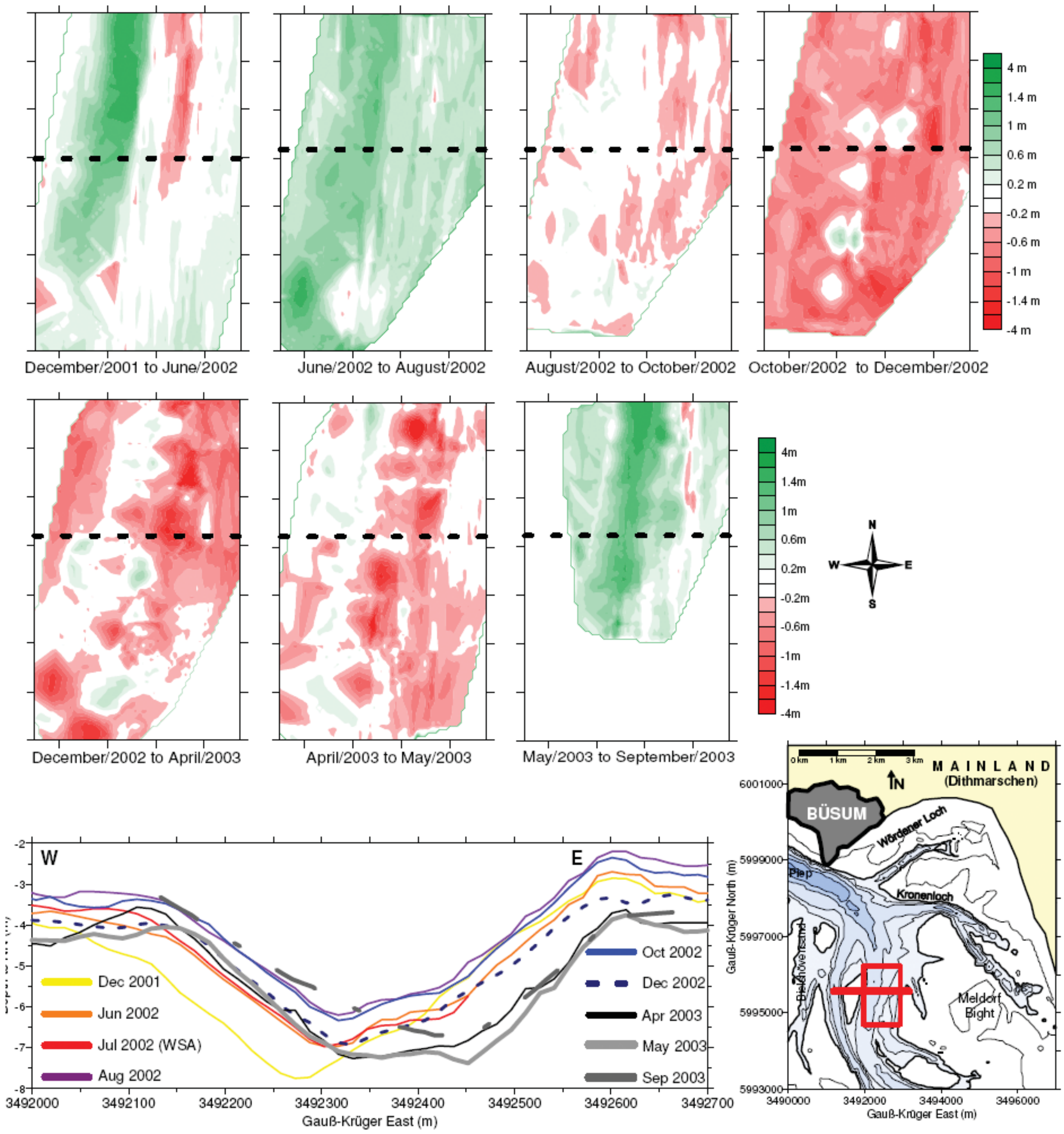

Fig. 19: Morphological changes along the surveyed cross-section in the Sommerkoog-Steertloch

gully into two branches separated by a new elongated mid-channel shoal is imminent. More recent surveys actually demonstrate that this development has become more pronounced since the last measurement carried out in this study.

When integrating all the results, some general aspects of the morphodynamic evolution of the study area can be recognised. Most of the phenomena are visible on both long-term (years and decades) and short-term (weeks to months) time scales. In addition, in most parts of the area directional trends seem to be superimposed by a seasonal cycle, dominated by channel scouring in the cold season and deposition in the warm season.

Substantial morphological changes, especially in the outer regions, result from a landward migration of highly mobile sandbanks such as the Tertius Sand of the D-Steert. In the case of the Tertius sandbank, the migration towards the mainland seems to be combined with a slight displacement of the entire morphological complex to the north. This is particularly well documented by the migration of the northern inlet and, to a lesser extent, the southern inlet.

Significant morphological changes in the channels themselves can be mainly attributed to either lateral migration or to the formation and/or re-formation of mid-channel shoals in areas where a channel splits into flood- and ebb-dominated branches. Especially the latter process leads to pronounced changes in the cross-sectional channel profiles which are often associated with the erosion and redeposition of huge amounts of sediment. However, the present data do not give any reliable indication to what extent the morphodynamic changes cause net increases or decreases in the subtidal volume. This is mainly due to the insufficient quantity and quality of the data but also to the limited resolution of the DEMs applied for this study. This is especially true for the outer and central part of the study area. However, a satisfactory assessment can be given with regard to the changes observed along the cross-sectional profiles. For the period from 1977 to 1996, a decrease in cross-sectional area has been demonstrated for all three of the investigated sites. For profile A – Norderpiep the loss in area is of the order of 28 %, for cross-section B – Süderpiep around 24 %, and for cross-section C – Piep it is approximately 12 %.

Over the time period under consideration, the inner part of the Meldorf Bay proper shows a tendency to a net sediment import. This trend is mainly documented by channel infilling and vertical accretion of shore-connected tidal flats.

Finally, the results show that the recent morphodynamic evolution is to some extent limited by the existence of older consolidated cohesive sediment deposits. In regions where only one deep horizon exists, the channel depth can be 20 m or more, whereas in the north-western part, where a second upper layer is present, the channels are significantly shallower.

4. Discussion

While discussing the results of the geological analysis one has to keep in mind that the quality of the digital elevation model defining the base of the Holocene (Fig. 8) partly suffers from a limited quantity and/or quality of data. This is inevitable because the coverage of stratigraphic control points is rather sparse in many compartments of the study area. The map presented in this study therefore does not claim to reproduce the actual natural situation in every aspect. In fact, it was only compiled to have a model bathymetry as a basis for numerical simulations of tidal action at the beginning of the Holocene transgression (ASP NETO et al., 2003). In the central study area, however, the quality of the DEM is regarded to be relatively good. A variety of different information sources has been used for its compilation. Due to the general limitations and because of the wide grid size of the elevation model, not all natural features can be depicted even in the central area. Thus, small channel structures known to exist in the Pleistocene surface (SCHMIDT, 1976) are not resolved in the map.

Furthermore, the DEM of the top of the early Holocene consolidated cohesive sediment sequence (Lower und Upper Dithmarscher Klei) is based on the same data set as the DEM map of the Holocene base. However, since in this case known outcrop locations have been included, this map is considered more reliable. The importance of these cohesive layers for the morphodynamics of the channels in the area has been demonstrated in Fig. 14 by the fact that in many cases their depth is controlled by outcrops of the erosion-resistant strata. The lower and upper "Klei" deposits thus form a physical barrier which effectively limits depth erosion. This would suggest that in locations where these deposits prevent deeper excavation, the channels must become wider in order to satisfy the rule of hydraulic continuity.

Two cases are known which vividly accentuate the protective function of the "Dithmarscher Klei" against erosion. In both situations the layers were penetrated by depth erosion, as a result of which the seabed was scoured down to depths of more than 30 m. One case was reported by LÜNEBURG (1969). Not far from Büsum he found an oval scour pit in the channel bed of a size of about 500 by 200 m and quite steep flanks. Here the water depth was around 30 m and coarse Pleistocene melt water sands outcropped on the bed. According to LÜNEBURG, the structure discovered in autumn of 1966 was unknown to the local authorities and the fishing community. He concluded that the scour pit must have formed over a rather short period of time. Today this hole in the cohesive beds is silted up, but it is still visible on shallow seismic records as an area of stratigraphic discontinuity.

The second report concerns a location at the Eider estuary storm surge barrier. In this area, an upper and a lower layer of "Dithmarscher Klei" are present (RUCK, 1969). Due to the constriction of the channel cross-section within the flood gates, deep scours formed on either side of the dam. These scours remained relatively stable for several years. Their depth was effectively controlled by the cohesive sediments present in the subsurface. Due to maintenance works in the early 1990s, one of the gate sections had to be closed for several months. Consequently, the concentration and increase of the currents led to scouring of the clayey silt bed and, within a very short time, a huge and deep (40 m) scour pit formed on the seaward side of the construction. Since retrogressive erosion threatened the stability of the dam construction, extensive and expensive measures had to be taken to stabilise the scour. This case not only emphasizes the importance of the geological structure for natural morphological adaptation processes but also for the stability of man-made structures in the coastal zone.

Above the old consolidated beds, late Holocene and modern tidal flat sediments are present. These younger deposits can reach a thickness of more than 20 m (Fig. 9). The composition is dominated by fine sands with variable portions of either finer or coarser components. As pointed out earlier, the intertidal surface sediments show a distinctive sequence from coarser material in the westerly, exposed areas to smaller grain sizes in the sheltered, inner regions. This characteristic grain-size gradient reflects the progressive decrease in hydrodynamic energy from the open sea to the more elevated flats close to the shoreline (REINECK and SINGH, 1980). The close relationship between sediment distribution and hydrodynamics poses the question to what extent the sediments in the study area may have been affected by the diking of the inner Meldorf Bay in the 1970s.

Land reclamation in general has a serious impact on the environment. With the new 15 km dike almost 50 km^2 of tidal flats were reclaimed. This resulted in a decrease of the tidal prism of about 37 x 10^6 m^3 (TARNOW et al., 1978). Compared to that of the entire tidal basin of the Piep channel system (413 x 10^6 $m^{3)}$, as quantified by SPIEGEL (1997), this amounts to a loss of 8 %. The sedimentological response to this environmental impact was studied by REIMERS (2003). Comparing his results with maps of 1978 (GAST et al., 1984) and 1989 (VAN BERNEM, 1994) as well as with those of DIJKEMA (1989), he was able to show that a clear trend towards finer sediments occurred after the diking of the inner Meldorf Bay. Between 1978 and the year 2000 the areas covered with fine-grained (< 63 nm) sediments had increased significantly. However, this tendency was limited to the area of the Meldorf Bay while already the eastern part of the adjacent Bielshövensand sandbank was left almost unaffected by this development.

The main aspects of the morphological response of the Meldorf Bay to the artificial reduction in the tidal prism were already dealt with earlier in this paper. From 1977 to 1996 a decrease in the sub-tidal volume was registered. Moreover, intensified deposition especially of fine-grained sediments enhanced the vertical accretion of the intertidal areas. Quantifications of this evolution are given in WITEZ (2002) and HIRSCHHÄUSER and ZANKE (2001). The latter authors also show that the most intense morphological adaptation occurred in the period from 1979 to 1982, i. e. directly after the last reclamation in 1978. These findings support the widely accepted perception that the volume of the tidal prism or the basin size is directly proportional to the cross-sectional area of the inlet (O'BRIEN, 1931; RENGER, 1976; MISDORP et al. 1990). NIEMEYER et al. (1995) developed numerical formulations of the correlation of channel size at its mouth and the tidal volume (approx. twice the tidal prism) for different sub-basins of the Meldorf Bay. For the situation from 1942 to 1969, which is equivalent to the time before the first diking, their equation is loaded with a factor of 6.98. For the period from 1973 to 1990, i. e. mainly after the last diking, this factor is 7.72. This means that after the land reclamation and the related reduction of the tidal water masses, the channel cross-sectional areas increased. At first sight, this finding appears to disagree with the empirical knowledge that a decreased tidal prism should lead to smaller channel cross-sections. Instead, it shows that the process of morphological adaptation after the land reclamation was not completed until 1990. At that time the channel cross-sections were still a bit too wide relative to the tidal volume.

In her work, WITEZ (2002) used the parameter "characteristic elevation" to describe the morphological state of tidal basins. The "characteristic elevation" reflects the ratio of intertidal sediment volume to intertidal area and describes the specific height which a tidal flat area can attain under given boundary conditions (GÖHREN, 1968). WITEZ calculated this parameter for three sub-basins of the Meldorf Bay and for the tidal basin of the Piep channel. Thus, ten morphological states are characterized covering the time span from 1937 to 1991. On the basis of these values we graphically displayed the temporal morphological evolution of the four tidal basins (Fig. 20). The morphological trend before as well as after the diking can be approximated by a simple linear function. The good correlation permits an extrapolation of the best fit line. This reveals the extent to which the morphological adaptation after the final land reclamation of the inner Meldorf Bay in the 1970s has proceeded.

In the four decades before the diking the analysed basins show relatively stable trends. Whilst for the Kronenloch tidal basin the "characteristic elevation" increases over time, the situation in the other three areas is fairly balanced. In all tidal basins the dikings of 1972 (mainly influencing the southern part of the Sommerkoog-Steertloch basin) and of 1978 have caused a drop in the elevation values. The trend lines evaluated for the period following the closure of the basin indicate that the system tends to revert to the initial state. Following the idea of our conceptional model i.e. the trend lines, full morphological adaptation of the small shore-connected basins Wöhrdener Loch and Kronenloch should be completed within the next 40 to 50 years. The data for the more exposed Sommerkoog-Steertloch area, by contrast, suggest that this basin has already returned to the state of 1972. By the same token, the huge and open tidal basin of the Piep (Fig. 20) is not far away from the "characteristic elevation" values prior to 1978.

Besides man-made impacts such as land reclamation the morphodynamics of the area are also driven by natural processes. These processes act on different time scales. There are, for example, short periodical changes due to a single tide or the neap-spring cycle. Although their effects on individual small-scale morphological units like bedforms can clearly be recognised, the implications for complex units like a tidal basin are still obscure. The same is true for single storm events. The shortest time scale at which we were able to quantify morphological

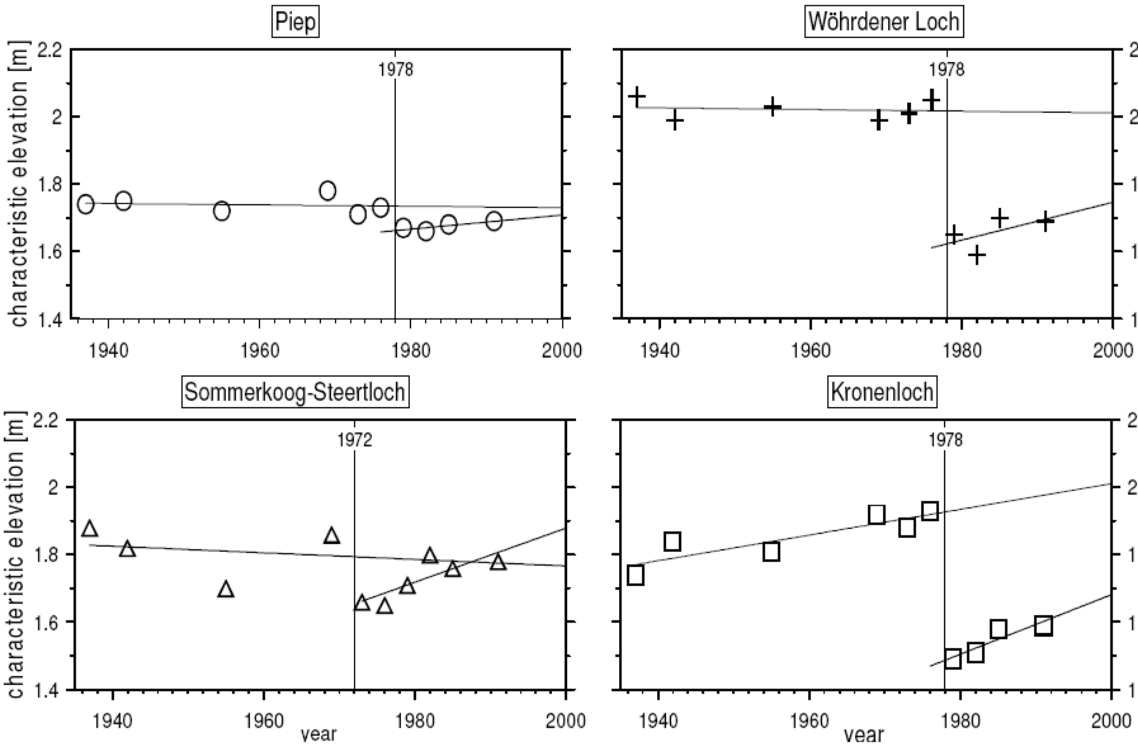

Fig. 20: Temporal evolution of the "characteristic elevation" for four tidal basins. For locations see Fig. 5

changes was the seasonal time scale. Although not all results point in the same direction, it became apparent that in the tidal channels erosion prevails in the cold and deposition in the warm season. Attempts to correlate this variability with seasonal fluctuations of the tides or seasonal meteorological characteristics were not satisfactory (ASP, 2004). FLEMMING and BARTHOLOMÄ (1997) attribute the winterly erosion of fine-grained sediments on the East Frisian tidal flats to a higher kinematic viscosity of the cold water. Higher kinematic viscosity aids the entrainment and favours the suspension of sediments (a decrease in water temperature from 20 to 5 °C results in a reduction of particle settling velocity of around 25 %). This could explain that in the cold season the channel beds are scoured. However, this hypothesis does not explain the whereabouts of the interim storage for the channel deposits, which are present in the warm season and absent in the cold season. In this context an observation of REIMERS (1999) is of importance. He observed that on accreting mudflats of the Meldorf Bay small runnels completely silted up in winter and were cleared again in summer. This means that there must be a transport of sediments towards the shore in winter and an export out of this region during the warm season. Massive shoreward transport and material imported from deeper levels are also visible in the migration of the supratidal Blauortsand sandbank. According to WIELAND (1972), migration rates of 30 m per year, tantamount to the cold season, are typical. Based on numerical model simulations HIRSCHHÄUSER and ZANKE (2001) also postulate an exchange between intertidal and subtidal regions. Based on their findings, they conclude that a transport of sediments from the tidal flats into the channels can be traced back to storm events. Since storms are more frequent in winter this would contradict the field observations made by REIMERS (1999) and our findings that channel scouring is more frequent in the period from late autumn to early spring. Moreover, redeposition of sediments is not only limited to a transport between intertidal and subtidal compartments. It also occurs between the tidal flat system including its channels and the bars and shoals (e.g. ebb-delta) located at the transition to the open sea (NIEMEYER and KAISER, 1994). In this case, seaward transport is often caused by an interaction between storm effects and ebb currents. During ebb-surges following storm-elevated water levels in tidal basins the ebb-current velocities in the deeper channels can be significantly higher (66 %; FLEMMING, 2004) than under average weather conditions. Under extreme conditions this can lead to an irreversible export of intertidal sands into the open sea, traceable as sand layers in the muddy deposits of the open shelf (GADOW and REINECK, 1969).

In the context of seasonal variability, the question arises whether the seasonal changes are a finely balanced back and forth movement or whether there is a net one-directional gain or loss of sediments. One of the most significant morphological trends visible on wider spatio-temporal scales is the lateral migration of the tidal channels. In many cases this is related to meandering which is not only a tidal phenomenon (TRUSHEIM, 1929; REINECK, 1958; AHNERT, 1960; REID and FROSTICK, 1994; GÖNNERT, 1995). In this context the formation of ebb and flood channel systems already described by VAN VEEN (1950) and AHNERT (1960), must be mentioned. A typical example for such a system is the central Piep. Between the flood branch in the south, i. e. on the right hand side of the inflowing flood current, and an ebb branch in the north, i. e. on the right hand side of the outflowing ebb current, intensive sediment reworking takes place (for details, see previous chapter).

Lateral migration of channels, however, is also forced by displacements of sandbanks induced by prevailing meteorological conditions. This is the case for the supratidal Blauortsand sandbank. Mainly due to heavy winter storms from the westerly sector, this sandbank migrates towards the east (WIELAND, 1972; KESPER, 1992). During the last 30 years, wind conditions at Büsum monitoring station have been fairly stable at a relatively high energy level (BENKEL and GROSS, this volume). Therefore, the simultaneous displacements of the Tertius Sand and the D-Steert sandbanks may, to a certain extent, be generated or amplified by storms or frequent strong winds from westerly directions. The study of old nautical charts, however, reveals that the landward progression of these banks is a process which has been active for several centuries (LANG, 1975; WIELAND, 2000). Landward displacement of morphological features is inevitably accompanied by displacements of tidal watersheds which, in turn, results in a progressive decrease in basin size. This development is also known from other compartments along the southern North Sea coast. In the case of the East Frisian barrier-island system, FLEMMING (2004) traces back the basin size reductions primarily to morphological adjustments triggered by land reclamation. He also notes that this influence is often underestimated in morphological analyses. Besides the reaction of tidal basins to land reclamation (DIECKMANN, 1985; EISMA and WOLFF, 1980; FLEMMING, 2002; WIELAND, 1984, 2000; WITEZ, 2002), the effects of a rising sea level are widely discussed (FERK, 1995; FLEMMING and BARTHOLOMÄ, 1997; HOFSTEDE, 1999b; MISDORP et al., 1990; REISE, 1998; SPIEGEL, 1997). Conceptual models (e. g. FLEMMING and DAVIES, 1994) suggest that the elevation of tidal flats and saltmarshes follows a rising sea level, provided that the rate of sediment supply can compensate the rate of sea-level rise (e. g. FLEMMING, 2002). The sediments needed for this accretion can either be derived from external sources or from internal redistribution. In the latter case, the material can stem from a reduction of tidal basin size. This may also be accompanied by stronger gouging of the tidal channels. The sediments eroded here may then bolster intertidal accretion. Modern examples for this kind of morphological response are given in DIECKMANN, (1985), EISMA and WOLFF (1980) or REISE (1998). Especially in the tidal flats north of our study area (North Frisian Wadden Sea), channel gouging is a widespread phenomenon (overview in SPIEGEL, 1997). Forecasts of the morphological adjustment under an increased sea-level rise scenario mainly focus on stronger channel excavation activity (e. g. MISDORP et al., 1990 and SPIEGEL, 1997).

In contrast to frequent examples for channel gouging, our analysis reveals a more stable situation for the Piep channel system or an even slightly reverse tendency. The widely observed correlation between maximum channel depth and the presence of cohesive, erosion-resistant sediment layers in the subsurface suggests that these layers effectively oppose scouring of the channels in this case. This means that the sediment demand for morphological adaptation in the Meldorf Bay after the land reclamation and for adjustments to a rising sea level has to be supplied from other sources. Since the landward dislocation of the outer sandbanks is undisputed, the most obvious sediment source would be the internal redistribution due to a decrease in basin size. However, in a sense, this contradicts the concept that the Dithmarschen Wadden Sea is characterised by a certain surplus of sediments (EHLERS, 1988). In this context DIEKMANN (1985) discusses possible longshore sediment transport pathways. According to him, sediment streams coming from the west and from the north end in this coastal compartment. However, this idea of generalized sediment flows is not based on direct observations but is inferred to be a consequence of large-scale land reclamation in the Dithmarschen area during the last 200 years (WIELAND, 1984, 2000), the strong and rapid siltation of the Eider estuary after construction of the barrier (WIELAND, 1999), or the quantification of the huge amounts of mobile fine-grained deposits present in adjacent offshore areas (ZEILER et al., 2000a, 2000b).

5. Conclusions

The present study has combined a variety of investigations in order to provide an integrated approach for a better understanding of the litho-stratigrafical, sedimentological and morphological setting of the Dithmarschen Wadden Sea. Beside typical characteristics of a low-macrotidal environment, the area exhibits some unique features. Thus, one of the most important outcomes of the study is the insight that morphodynamic erosional processes are depth-limited by the existence of cohesive deposits of early Holocene age in the subsurface (Dithmarscher Klei). The resistance to erosion of these layers is significantly higher than that of the modern tidal flat sediments. This, in turn, changes the way morphological adaptations in the region occur. Channel gouging, which is often observed in other tidal flat environments observed as a response to changed hydrodynamics, seems to play a minor role in the Dithmarschen Wadden Sea. Nevertheless, intensive morphological changes are active on various temporal and spatial scales. In this context, a new process has been identified, namely a seasonal erosion-sedimentation-pattern in the channels. Most of the processes acting on longer time scales can be correlated with the observations of other authors. Although this investigation is based on a variety of information sources, it has not been possible to even generate a simple qualitative conceptional model which would explain the different aspects of the complex morphological processes in the area. Particularly those processes occurring on large spatial scales still require reliable quantification. These present shortcomings signify a major challenge for future numerical simulations.

6. Acknowledgements

The study has been carried out as part of the "PROMORPH" project (Funding number 03 F 0262 A) funded by the German Federal Ministry of Education and Research (BMBF). The research would not have been possible without the financial support of Nils Asp Neto by the German Academic Exchange Service (DAAD).

The authors would like to thank the following authorities for their help: Federal Maritime and Hydrographic Agency of Germany (BSH), Amt für Ländliche Räume Husum and Landesamt für Natur und Umwelt Schleswig-Holstein. We also appreciate the good cooperation with Dr. K. Schwarzer (Institute of Geosciences of Kiel University).

Finally we gratefully want to acknowledge constructive comments from Dr.-Ing. V. Barthel and an anonymous reviewer.

7. References

AHNERT, F.: Estuarine Meanders in the Chesapeake Bay Area. Geographical Review, 50: 390–401, 1960.

ASP NETO, N. E.; RICKLEFS, K. and MAYERLE, R.: An Approach to Reconstruct the Early Holocene Tidal Conditions in the Inner German Bight, North Sea. – In: Proceedings of the 5th International Symposium on Coastal Engineering and Science Sediment Processes (Clearwater Beach), Florida, USA, 2003.

ASP NETO, N. E.: Long- to Short-term Morphodynamic Evolution of the Tidal Channels and Flats of the Dithmarschen Bight, German North Sea. Berichte Forschungs- und Technolgiezentrum Westküste der Universität Kiel, 34, 2004.

BENKEL, A. and GROSS, G.: Meteorological Data and Wind Field Modelling in the Dithmarschen Bight, Die Küste, Heft 69, 2005.

BERNEM, K.-H. VAN; GROTJAHN, M.; KNÜPLING, J.; KRASEMANN, H. L.; MÜLLER, A.; NEUGEBORN, L.; PATZIG, S.; RAMM, G.; RIETHMÜLLER, R.; SACH, G. and SUCHROW, S.: Thematische Kartierung und Sensitivitätsraster im deutschen Wattenmeer Juni 1987–Juni 1993. GKSS-Bericht, 94/E/10, 1994.

D'OLIER, B.: Side-Scan Sonar and Reflection Seismic Profiling. In Dyer, K. R. (ed.): Estuarine Hydrography and Sedimentation, Cambridge University Press, 1979.

DIECKMANN, R.: Geomorphologie, Stabilitäts-und Langzeitverhalten von Watteneinzugsgebieten der Deutschen Bucht. Mitt. Franzius-Instituts für Wasserbau und Küsteningenieurwesen, 60, 1985.

DIJKEMA, K. S.: Habitats of the Netherland, German and Danish Waddensea. Research Institute for Nature Management, Texel, 1989.

DITTMER, E.: Schichtenaufbau und Entwicklungsgeschichte des Dithmarscher Alluviums, Westküste, 1, 1938.

DITTMER, E.: Die nacheiszeitliche Entwicklung der Schleswig-Holsteinischen Westküste. Meyniana, 1, 1952.

EHLERS, J.: The Morphodynamics of the Wadden Sea. Balkema, 1988.

EISMA, D. and WOLFF, W. J.: The Development of the Wersternmost Part of the Wadden Sea in Historical Time. In Dijkema, K. S.; Reineck, H.-E and Wolff, W. J. (eds.): Geomorphology of the Wadden Sea Area. Final Report of the Section Geomorphology of the Wadden Sea Working Group, Report 1. Leiden, 1980.

FERK, U.: Folgen eines beschleunigten Meeresspiegelanstiegs für die Wattgebiete der Niedersächsischen Nordseeküste. Die Küste, Heft 57, 1995.

FIGGE, K.: Das Elbe-Urstromtal im Bereich der Deutschen Bucht (Nordsee). Eiszeitalter u. Gegenwart, 30, 1980.

FIGGE, K.: Begleitheft zur Karte der Sedimentverteilung in der Deutschen Bucht 1:250000 (Nr. 2900), Deutsches Hydrographische Institut, 1981.

FIGGE, K.; KÖSTER, R..; TIEHL, H. and WIELAND, P.: Schlickuntersuchungen im Wattenmeer der Deutschen Bucht – Zwischenbericht über ein Forschungsprojekt des KFKI. Die Küste, Heft 35, 1980.

FISCHER, O.: Sonderprobleme und Einzelfragen des Küstenraumes, Reimer, 1955.

FLEMMING, B. W.: Effects of Climate and Human Interventions on the Evolution of the Wadden Sea depositional system (southern North Sea). In Wefer, G.; Berger, W.; Behre; K.-E. and Jansen, E. (eds.), Climate development and history of the North Atlantic realm. Springer, Berlin, 2002.

FLEMMING, B. W.: The Upper Mesotidal East Frisian Barrier Island System (Southern North Sea): A Comparison with other Modern Analogues. – Abstract volume 6th International Conference on Tidal Sedimentology, Copenhagen, 2004.

FLEMMING, B. W. and DAVIS, R. A.: Holocene Evolution, Morphodynamics and Sedimentology of the Spiekerkoog Barrier Island System (Southern North Sea). Senckenbergiana marit., 24, 1994.

FLEMMING, B. W. and BARTHOLOMÄ, A.: Response of the Wadden Sea to a Rising Sea Level: A Predictive Empirical Model. German Journal of Hydrography, 49 (2/3), 1997.

GADOW, S. and REINECK, H. E.: Ablandiger Sandtransport bei Sturmfluten. – Seckenbergiana marit., 1, 1969.

GAST, R., KÖSTER, R. and RUNTE, K.-H.: Die Wattsedimente in der nördlichen und mittleren Meldorfer Bucht. Die Küste, Heft 40, 1984.

GÖHREN, H.: Triftströmung im Wattenmeer. Mitt. Franzius-Institut, 30, 1968.

GÖNNERT, G.: Mäandrierung und Morphodynamik im Eider Ästuar. Berliner geograph. Studien, 41, 1995.

GWINNER, M. P.: Zum Aufbau des Küstenalluviums in Bremerhaven. Abh. naturw. Verein Bremen, 33, 1954.

HIRSCHHÄUSER, T. and ZANKE, U. C. E.: Morphologische Langfristprognose für das System Tidebecken – Außensände am Beispiel Sylts und der Dithmarscher Bucht. Die Küste, Heft 64, 2001.

HOFFMANN, D.: Das junge Küstenholozän an der Nordseeküste Schleswig-Holsteins. Meyniana, 50, 1998.

HOFSTEDE, J. L. A.: Reginal Differences in the Morphological Behaviour of four German Wadden Sea Barriers. Quarternery International, 60, 1999a.

HOFSTEDE, J. L. A.: Mögliche Auswirkungen des Klimawandels im Wattenmeer. Petermanns Geograph. Mitt., 134 (4), 1999b.

HUMMEL, P. and CORDES, E.: Holozäne Sedimentation und Faziesdifferenzierung beim Aufbau der Lundener Nehrung (Norderdithmarschen). Meyniana, 19, 1969.

KESPER, J.: Sedimentdynamik ausgewählter Außensände vor der Schleswig-Holsteinischen Westküste. Dissertation, Univ. Kiel, 1992.

KÜHN, H.-J.: Anfänge des Deichbaus. Boyens, 1992.

LANESKY, D. E.; LOGAN, B. W.; BROWN, R. G. and HINE, A. C.: A New Approach to Portable Vibracoring Underwater an on Land. Journal of Sedimentary Petrology, 49, 1979.

LANG, A. W.: Untersuchungen zur morphologischen Entwicklung des Dithmarscher Watts von der Mitte des 16. Jahrhunderts bis zur Gegenwart. Hamb. Küstenf., 31, 1975.

LANG, H. D.: Über den Aufbau der Butjadinger Marsch. Geol. Jb., 76, 1959.

LINKE, G.: Ergebnisse geologischer Untersuchungen im Küstenbereich südlich Cuxhaven – Ein Beitrag zur Diskussion holozäner Fragen. Probleme der Küstenforschung in südlichen Nordseegebiet, 13, 1979.

LÜNEBURG, H.: Sedimenthabitus und Sedimentdynamik in den Pieprinnen vor Büsum und im Hörnum-Tief vor Sylt (Deutsche Bucht). Veröffentl. Inst. Meeresforsch. Bremerhaven, 11, 1969.

LURTON, X.: An Introduction to Underwater Acoustics. Principles and Application. Springer, 2002.

MEIER, D.: Landschaftsgeschichte, Siedlungs- und Wirtschaftsweise der Marsch. In Verein für Dithmarscher Landeskunde (ed.), Geschichte Dithmarschens, Boyens, 2000.

MENKE, B.: Befunde und Überlegungen zum nacheiszeitlichen Meerespiegelanstieg (Dithmarschen und Eiderstedt). Probleme der Küstenforschung in südlichen Nordseegebiet, 11, 1976.

MISDORP, R.; STEYAERT, F.; HALLIE, F. and DE RONDE, J.: Climate Change, Sea Level Rise and Morphological Developments in the Dutch Wadden Sea, a Marine Wetland. In Beukema, J. J. et al. (eds.), Expected Effects of Climatic Change on Marine Coastal Ecosystem. Kluwer Academic Publ., 1990.

NIEMEYER, H. D.; GOLDBOGEN, R.; SCHROEDER, E. and KUNZ, H.: Untersuchungen zur Morphodynamik des Wattenmeeres im Forschungsvorhaben WADE. Die Küste, Heft 57, 1995.

NIEMEYER, H. D. and KAISER, R. (1994): Hydrodynamik im Ökosystem Wattenmeer. Texte des Umweltbundesamtes, 1994.

NIEMEYER, H. D.; BRANDT, G.; GÄRTNER, J.; GLASER, D.; GRÜNE, J.; JENSEN, F. and KAISER, R.: Naturmessungen von Wattseegang an der deutschen Nordseeküste. Ber. Forsch.-Stelle Küste, Bd. 40, 1996.

O'BRIEN, M. P.: Estuary Tidal Prisms Related to Entrance Areas. ASCE, Civil Eng., 1 (8), 1931.

PRANGE, W.: Die Bedeichungsgeschichte der Marschen in Schleswig-Holstein. Probleme der Küstenforschung in südlichen Nordseegebiet, 16, 1986.

REID, I. and FROSTICK, L. E.: Fluvial Sediment Tansport. In K. Pye (ed.), Sediment Transport and Depositional Processes, Blackwell Scientific Publications, 1994.

REIMERS, H.-C.: Wirkungsweise von Buschlahnungen auf den Sedimenthaushalt von aufgewachsenen Deichvorländern an der schleswig-holsteinischen Westküste. – Berichte, Forschungs- und Technologiezentrum Westküste der Univ. Kiel, 1999.

REIMERS, H.-C.: Sedimentverteilung und Benthosverbreitung in den Watten der Dithmarscher Bucht als Indikator für morphodynamische Veränderungen. Abschlußbericht zum Forschungsvorhaben „Sedimorph" im GKSS Hochschulprogramm. – Berichte der GKSS 2003/18, 2003.

REINECK, H.-E.: Longitudinale Schrägschicht im Watt. Geol. Rdsch., 47, 1958.

REINECK, H.-E. and SINGH, I. B.: Depositional Sedimentary Environments. Springer, 1980.

REISE, K.: Coastal Change in a Tidal Backbarrier Basin of the Northern Wadden Sea: Are Tidal Flats Fading Away? Senckenbergiana Marit., 29, 1998.

RENGER, E.: Grundzüge der Analyse und Berechnung von morphologischen Veränderugen in Wattengebieten. Mitt. Franzius-Institut, 4, 1976.

RICKLEFS, K.; LEHNER, S. and RAUSCH, J.: Morphological Changes in a Tidal Flat Area: A Comparison of Radar, Optical and In-Situ Data. Die Küste, Heft 69, 2005.

RUCK, K.-W.: Ein Geologisches Profil durch die Eidermündung. Meyniana, 19, 1969.

RUPRECHT, L.: Der geologische Aufbau des Küstenvorfeldes von Dithmarschen / Nordfriesland erarbeitet auf der Basis von seismischen Profilen und Sedimentkernen. Diploma Thesis, Univ. Kiel, 1999, unp.

SCHMIDT, R..: Das Küstenholozän der östlichen Meldorfer Bucht und angrenzender Marschen in Dithmarschen, Schleswig-Holstein. Meyniana, 28, 1976.

SIEFERT, W.; FAHSE, H.; MIESSNER, F.; RICHTER, H.-H.; TAUBERT, A. and WIELAND, P.: Die Strömungsverhältnisse vor der Westküste Schleswig-Holsteins. Die Küste, Heft 35, 1980.

SIEFERT, W.; MIESSNER, F.; RICHTER, H.-H. and WIELAND, P.: Triftströme vor der Küste zwischen Eider und Elbe. Die Küste, Heft 38, 1983.

SPIEGEL, F.: Die Tidebecken des schleswig-holsteinischen Wattenmeeres: Morphologische Strukturen und Anpassungsbedarf bei weiter steigendem Meeresspiegel. Berichte, Forsch.- u. Technologiezentrum Westküste d. Univ. Kiel, 1997.

STREIF, H.: Das Ostfriesische Küstengebiet. Nordsee Inseln, Watten und Marschen. Sammlung geologischer Führer 57, Borntraeger, 1990.

STREIF, H. and KÖSTER, R.: Zur Geologie der deutschen Nordseeküste. Die Küste, Heft 32, 1978.

TARNOW, R.; PETERSEN, P. and PETERSEN, K.: Speicherkoog Dithmarschen: Ein neuer Deich verändert die Landschaft. Evers, 1978.

TIETZE, G.: Das Jungpleistozän und marine Holozän nach seismischen Messungen nordwestlich Eiderstedts/Schleswig-Holstein. Dissertation, Univ. Kiel, 1983.

TRUSHEIM, F.: Zur Bildungsgeschwindigkeit geschichteter Sedimente im Wattenmeer, besonders solcher mit schräger Parallelschichtung. Senckenbergiana, 11, 1929.

VEEN, J. VAN: Ebb and Flood Channel Systems in the Netherlands Tidal Waters. – Translated reprint of; J. Royal Dutch Geogr. Soc., 67, Delft Univ. Press, 1950.

WIELAND, P.: Untersuchungen zur geomorphologischen Entwicklungstendenz des Außensandes Blauort. Die Küste, Heft 23, 1972.

WIELAND, P.: Untersuchungen über geomorphologische Veränderungen in der Dithmarscher Bucht. Die Küste, Heft 40, 1984.

WIELAND, P.: Küstenfibel. Boyens, 1990.

WIELAND, P.: Entwicklungen in der Eider nach ihrer mündungsnahen Abdämmung. – HTG-Jahrbuch, 1999.

WIELAND, P.: Trischen – die Geschichte einer alluvialen Insel im Dithmarscher Watt. – Die Küste, Heft 62, 2000.

WIELAND, P., FLADUNG, B. and BERGHEIM, V.: Tidedynamische und meteorologische Randbedingungen im Bereich des Schlick-Testfeldes Dithmarscher Bucht. Die Küste, Heft 40, 1984.

WITEZ, P.: GIS-gestützte Analysen und dynamische 3D-Visualisierungen der morphologischen Entwicklung schleswig-holsteinischer Tidebecken, Dissertation, Univ. Kiel, 2002.

ZEILER, M.; SCHULZ-OHLBERG, J. and FIGGE, K.: Mobile Sand Deposits and Shoreface Dynamics in the Inner German Bight (North Sea). Marine Geology, 170, 2002a.

ZEILER, M.; SCHULZ-OHLBERG, J. and FIGGE, K.: Materialinventur an der deutschen Nordseeküste. – Die Küste, Heft 62, 2000b.

Die Küste, 69 PROMORPH (2005), 1-420

Meteorological Data and Wind Field Modelling in the Dithmarschen Bight

By ANDREAS BENKEL and GÜNTER GROß

Summary

The topic of this study was to identify meteorological data suitable for forcing numerical simulations of morphodynamic processes in the Dithmarschen Bight.

A comparison between Numerical Weather Prediction (NWP) output data from the Local Model (LM) of the German Weather Service (Deutscher Wetterdienst – DWD) and PRISMA (PRozesse Im Schadstoffkreislauf Meer-Atmosphäre) data demonstrates the applicability of both data sets for forcing hydrodynamic models. PRISMA data are available on a regular grid and are based on field measurements. Compared with station data from Heligoland (German Bight of the North Sea), PRISMA data tend to underestimate long-term mean wind speeds while overestimating the frequency and number of high wind speed events.

Furthermore, time series of wind measurements were statistically analyzed and checked for quality. By evaluating the statistics of the wind field over the German Bight it was possible to classify meteorological conditions for the purpose of morphodynamic modelling. The results of simulations with a high-resolution version of the LM were used to identify areas where the station data may be confidently used to represent the wind field.

Zusammenfassung

Ziel der Studie war es, geeignete meteorologische Antriebsdaten für die numerische Simulation morphodynamischer Prozesse in der Dithmarscher Bucht zu identifizieren und bereit zu stellen.

Ein Vergleich zwischen den Ausgabedaten numerischer Wettervorhersagemodelle (hier dem Lokalmodell (LM) vom Deutschen Wetterdienst) und den PRISMA-Daten (PRozesse Im Schadstoffkreislauf Meer-Atmosphäre) zeigt die Eignung beider Datensätze zum Antrieb hydrodynamischer Modelle mit meteorologischen Randbedingungen. PRISMA-Daten stehen auf einem äquidistanten Gitter zur Verfügung und werden auf der Basis von Stationsbeobachtungen berechnet. Im Vergleich zu Stationsmesswerten von Helgoland zeigen die PRISMA-Daten im langjährigen Mittel eine zu geringe mittlere Windgeschwindigkeit, während sie gleichzeitig die Häufigkeit des Auftretens von Starkwindereignissen sowie die dabei auftretenden Windgeschwindigkeiten überschätzen.

Weiterhin werden lange Zeitreihen von Windmessungen statistisch analysiert und auf Fehler geprüft. Durch die Auswertung der Windstatistik in der Deutschen Bucht kann die meteorologische Situation für den Zeitraum der morphodynamischen Modellierung klassifiziert und eingeordnet werden. Dazu wurden Simulationsrechnungen mit einer hochaufgelösten Version der LM durchgeführt, um Flächen über dem Meer zu bestimmen, für die die Stationsmessungen als repräsentativ angesehen werden können.

Keywords

Dithmarschen Bight, LM, PRISMA, Wind Measurements

Contents

1. Introduction

The aim of the investigation described in this paper was to supply hydrodynamic models in the project PROMORPH (PROgnose mittelfristiger küstenMORPHologieaänderungen: PROgnosis of medium-term coastal MORPHology) (cf. ZIELKE et al., 2003) with the most realistic atmospheric data possible for simulating forcing effects on the sea surface. The morphodynamic models implemented in PROMORPH to study bathymetry changes in the Dithmarschen Bight are nested within the hydrodynamic model CSM (Continental Shelf Model). The CSM, which covers the entire area of the North Sea, uses shear stress data based on wind measurements at a height of 10 m above the sea surface according to the scheme of SMITH and BANKE (1975) (ZIELKE et al., 1996). The discussion about useful meteorological data hence focuses on these 10 m-wind data distributed over all water grid points of the hydrodynamic model. One method of obtaining these data is to make use of station measurements of wind speed and barometric pressure. These data are interpolated to obtain values at the grid points of a mesh covering a certain area as described by e.g. LUTHARDT (1987). An alternative method is to use the output data of Numerical Weather Prediction (NWP) models. Both NWP model output data and station data were examined in the present study to check their suitability for forcing hydrodynamic models.

During the period chosen for the PROMORPH simulations a variety of weather conditions were experienced over the North Sea as well as the coastal region of the German Bight. Periods of calm winds alternate with periods of storm surge conditions. These different weather conditions have a significant influence on the evaluation of bathymetric changes. Moreover, it is necessary to compare the statistical behaviour of the wind situation during the simulation period with long-term wind behaviour in order to assess the impact of single events on long-term bathymetric changes.

In order to generate wind-forcing data for medium-term and long-term hydrodynamic computations it is necessary to extrapolate point measurements so as to cover the entire investigation area. This was carried out using both the time series of wind speed and direction at 6 stations in the German Bight and the results of numerical simulations performed with the high-resolution version of the LM. The LM is an operational NWP model run by the German Weather Service (Deutscher Wetterdienst – DWD). The simulation results of the NWP model, which covers an entire area in a physically consistent manner, may be used for comparisons with point measurements and PRISMA data.

In order to simulate morphological changes in the Dithmarschen Bight wave modelling is also necessary. In wave modelling, both local and regional wind fields play an important role. For storm conditions, however, a wind field on the continental shelf scale is more relevant than local wind behaviour. Whether the wind characteristics of the German Bight (e.g. characterised by Heligoland measurements) may be applied to smaller bights within the German Bight area such as the Dithmarschen Bight is examined in the present study with the aid of the high-resolution version of the LM.

2. Meteorological Data for Forcing Hydrodynamic Models

2.1 PRISMA Data

Meteorological forcing of the hydrodynamic models implemented in PROMORPH may be realised using the surficial distributions of wind and surface pressure from the PRISMA dataset. PRISMA data consist of observed wind fields, sophistically modulated and interpolated over a grid with a regular mesh spacing of 42 km and a time resolution of 3 hours. In addition to measured winds, the observed surface pressure data are used to generate a synoptic scale wind field by means of the geostrophic wind equation. A detailed account of the generation of PRISMA datasets from measurements is given by LUTHARDT (1987). Although the use of PRISMA datasets offers some advantages – e.g. the fact that they are generated from measurements means that they are free of forecast errors and that they also have a relatively sharply defined land-sea mask in the speed of the wind (NIELINGER, 1998) – the use of these datasets also has a number of serious shortcomings. Because there are no regular meteorological stations in the open sea the only means of generating these datasets is from measurements made from ships, platforms and coastal synoptic stations. The fact that wind measurements from platforms are performed at a height exceeding the standard height of 10 m and not reduced to the standard height means that wind speeds over the sea are likely to be overestimated. Moreover, the quantity of in situ wind and barometric pressure measurements over sea within the entire North Sea area is small. At e.g. 21 UTC (Universal Time Coordinates) the number of wind and barometric sea level pressure reports is below an average of 30. Additionally, the locations of reporting platforms and ships are irregularly distributed, leaving large areas of the North Sea domain without reported wind and pressure measurements. Therefore, for these large areas it is highly unlikely to detect regional deviations from the synoptic scale wind and sea level pressure field that are for example created by frontal systems, thunderstorms or squall lines. As a result, in general the processed PRISMA data cannot show that small-scale deviations in the wind field over sea. For further information on the latter refer to ZIELKE et al. (1997) or LUTHARDT (1987). It is a serious shortcoming for the practical use of PRISMA data in current studies that these data only become available in March of the calendar year following the year of measurements.

2.2 NWP Data

Due to a lack of near-surface wind measurements over the open sea it is only possible to obtain a realistic representation of the offshore wind field with sufficient temporal and spatial resolution by means of numerical simulations. In order to generate a physically consistent wind field in this study the Local Model (LM) of the German Weather Service was used.

The LM is an operational NWP model with a grid resolution of 0.0625 degrees (approx. 7 km). The LM is a state-of-the-art non-hydrostatic NWP model based on the compressible Navier-Stokes equations and is suitable for application with high-resolution grids. The application as an operational NWP model guarantees maintenance of the model. The version used in PROMORPH is LM version 2.17., which is described by DOMS et al. (2001).

The LM is operationally forced by GME (MAJEWSKI et al., 2002) forecasts. The DWD uses the global general circulation model GME operationally to run numerical weather forecasts. The GME has a grid size of approx. 60 km. These forecasts were also used in PROMORPH to initialise the LM. Access to the GME data as well as the operationally produced LM output data at the DWD is provided via the oracle database of the DWD. This permits numerical simulations of specific synoptic weather situations for the present as well as the past.

Numerical simulations have been performed on a Cray T3E massive parallel supercomputer at the NIC (John von Neumann Institute for Computing), Jülich.

In order to resolve the pronounced land-sea contrast of the wind field close to the ground a small grid size is necessary. Such high-resolution data will become available once the grid size of the LM has been reduced to 0.025 degree (approx. 2.8 km). The 2.8 km grid version of the LM requires initial and boundary values, which are obtained by operational running of the LM and interpolation over the 0.025 degree grid.

The output data, with a time resolution of 2 hours and a spatial resolution of 7 km and approx. 60 km in the LM and GME model, respectively, have been checked for quality and processed specifically for use in the PROMORPH hydrodynamic models. These data were interpolated barycentrically from the original NWP model grid to the grid implemented in the hydrodynamic models. The inclusion of GME data is necessary because the operational LM does not completely cover the entire domain of the hydrodynamic model. It was only found necessary, however, to force 3 of the 3743 CMS model grid points by GME model output wind data.

The results of the numerical simulations performed using the high-resolution version of the LM show a very detailed and structured wind field in areas characterised by pronounced changes in orography or roughness length such as, e.g. along the transition region between the shoreline and the sea or over the ascent from the German lowlands to the highlands. The simulations also demonstrate that the observed wind speed at Heligoland may be assumed to be representative of wind conditions throughout the German Bight at a distance of approx. 10–15 km from the shoreline. With the 7 km version of the LM this result would not have been so pronounced because the land-sea mask is much coarser (approx. 3 times). With 3 grid points necessary to resolve the land-sea contrast the 7 km LM would have smeared the wind-field transition zone between the land and sea over a length of 21 km due to numerical effects, thus yielding an incorrect representation of the natural characteristics of the wind field.

3. February 2000 – A Case Study

The output data from the NWP models LM and GME were compared to synoptic station data measurements and PRISMA data with regard to wind speed and direction. The simulated water levels generated from different input data (LM, GME or PRISMA) were also compared to each other as well as to measured water levels in order to analyse the effects of uncertainties in meteorological forcing on the results of the hydrodynamic simulation.

The period chosen for the case study was from 01 December 1999 to 31 December 2000. During this period a situation with strong north westerly winds lasting several days only occurred in February 2000. As this wind situation has the potential to cause high water levels along the coastline of the German Bight, the month of February 2000 was chosen for the comparison study.

For the whole of February 2000 the wind speed and direction given by the numerical weather prediction models as well as the PRISMA data were interpolated barycentrically relative to the synoptic station on Heligoland. Heligoland was chosen because it is located far enough away from the coastline to represent the wind field over the open sea. A distortion of the wind field nevertheless exists due to a change in the surface roughness between the island and the sea surface as well as the air flow around the island. As Heligoland is neither resolved in the NWP model nor in PRISMA, NWP data may be compared with PRISMA data at this location.

In Table 1 the wind data measurements at the Heligoland station are compared with the data generated by PRISMA and the NWP models LM and GME. The model data are interpolated to obtain a value at the grid point representing the Heligoland station. The wind speeds are compared as monthly mean values for February 2000. It is seen that the LM yields the smallest vector difference between the measured and simulated wind speed.

Table 1: Monthly mean wind speed at the Heligoland station/grid point

	Observed (synoptic)	PRISMA	GME	LM
wind speed in m/s	10.15	9.73	9.94	10.03
vector difference between observed and modelled wind speed in m/s	–	2.81	2.68	2.62

The time series of predicted and observed wind speed is shown in Fig. 1. The differences between simulated and measured wind speeds are found to be smaller for LM results than for PRISMA results, especially during periods of maximum wind speed. With regard to wind direction, all datasets (PRISMA, GME and LM) show a deviation to the right compared to the synoptic station report. This is in good agreement with the fact that the direction of

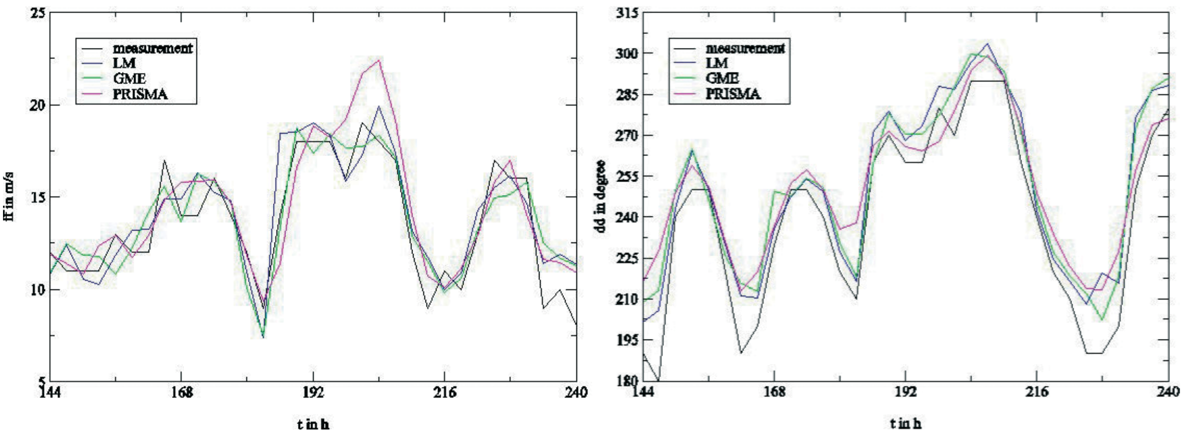

Fig. 1: Wind speed in m/s (left) and direction in degrees (right) at the Heligoland station/grid point. A time series of observed data, PRISMA, GME and LM data from 07 February 2000, 00 UTC to 11 February 2000, 00 UTC

onshore winds tends to deviate 15 degrees to the left (northern hemisphere) at near-coastal land stations (VESELOV, 1988).

Operational NWP output data from the LM and the GME model may be used for the meteorological forcing of hydrodynamic models for simulating sea level changes. The results of such a coupled model system are shown in Fig. 2. This 4-day time segment of the February 2000 simulation includes periods of high wind speeds with a significant increase in shear stress acting on the sea surface whereas in periods of low wind speed the astronomical tide dominates. Although forcing of the hydrodynamic models with PRISMA, GME or LM data yields different results, these differences are small compared to the differences between modelled and observed water levels. It should be noted that the hydrodynamic model CSM used here is appropriately adapted to make use of PRISMA data (ZIELKE et al., 1997). The simulated maximum water levels (PRISMA: 2.19 m, GME: 2.23, LM: 2.26) are also found to be in close agreement with observations (observed: 2.27 m).

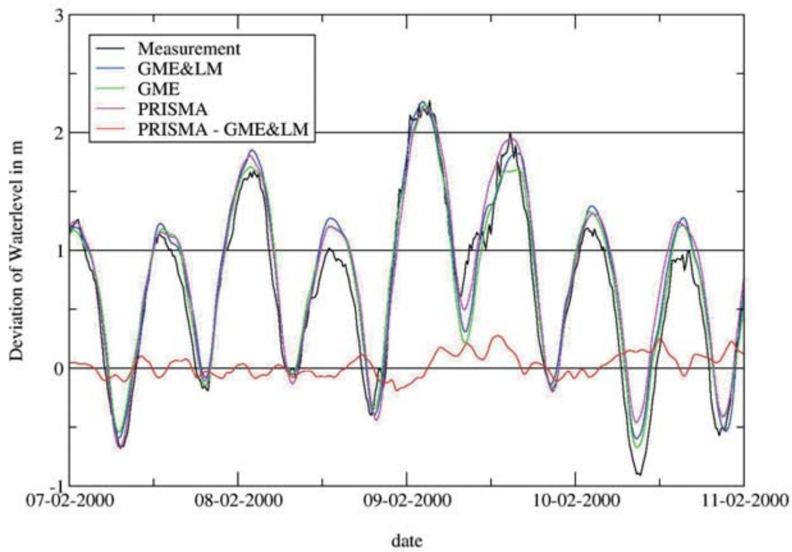

Fig. 2: Modelled and observed water level changes during the strong wind period from 07 February 2000, 00 UTC to 11 February 2000, 00 UTC at Westerland (HOYME, pers. comm., 2001)

4. Wind Statistics

4.1 Station Data

Hydrodynamic models are able to simulate morphodynamic changes in the area of the Dithmarschen Bight for specific meteorological conditions. In order to classify such conditions on a long-term basis a statistical analysis of meteorological observations is necessary. For this analysis the surface wind observations at different weather stations around the Ditmarschen Bight were selected which fulfil the following conditions:

- The time series must be as complete and as long as possible.
- Station measurements should represent the statistical behaviour of the wind in the study area as far as possible. The stations should be located either on an island, at an inland site removed from the coastline but sufficiently close to detect the influence of sea breezes, or directly on the shoreline of the German Bight.

Considering these requirements, the following stations were chosen:

- Heligoland (an island in the open sea),
- Norderney (an island approx. 10 km north of the shoreline),
- Cuxhaven (shoreline),
- Büsum (shoreline),
- Jever (land station),
- Hamburg-Fuhlsbüttel (land station).

The observed data at these synoptic stations ("SYNOPTIC data") are available in the form of time series consisting of mean values over one-hour intervals at a resolution of 0.1 m/s and 10 degrees. The SYNOPTIC data records date back to 01-01-1959 at the Heligoland station, and back to 01-01-1969 at the other stations. Only the data recorded between 01-01-1969 and 31-12-2001 were used in the comparative study.

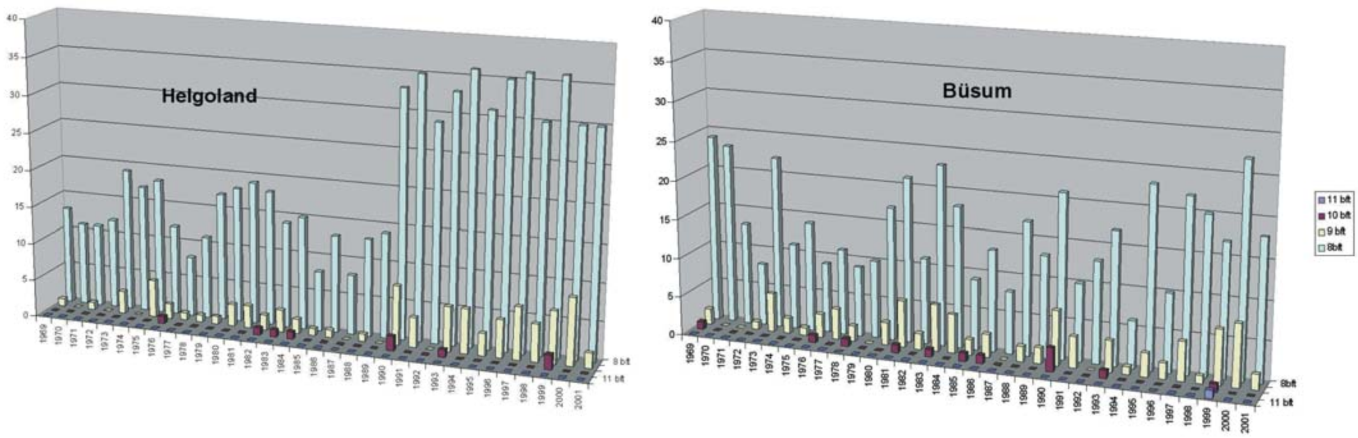

Fig. 3: Yearly number of days during which the wind force exceeds defined thresholds

Unfortunately the station anemometers were relocated several times during the observation period, thus making the time series inconsistent. On Heligoland the anemometer was removed from its original position close to the rocky headland and relocated on the harbour mole in 1989. At the new location it was found that the recorded wind speed was reduced for wind directions between 340 and 10 degrees due to various orographic disturbances. In 1993 the anemometer was again shifted a further 550 m in the seaward direction to the end of the mole. The apparent increase in storm activity at Heligoland during the period from 1989 to 1993 (Fig. 3) is unrealistic as it is directly related to the relocation of the anemometer. Also in Büsum the anemometer was relocated twice during the observation period. In Büsum, however, wind measurements were not so much affected by relocation of the instrument (Fig. 3). The changes in wind behaviour due to anemometer relocation make it difficult to draw a comparison with published results (e.g. SCHMITT, 1988; CHRISTOFFER and ULBRICHT-EISSING, 1989; TROEN and PETERSEN, 1989).

The most frequent wind direction at all six stations is south to west (Fig. 4 shows this for Heligoland and Büsum), whereby the most frequent combination of wind speed and direction at the Heligoland station occurs in the interval 170 to 210 degrees and 8 m/s to 10 m/s. The mean wind speeds at the 6 selected stations during the entire observation period are shown in Table 2.

Table 2: Mean wind speed during the period 01-01-1969 to 31-12-2001, calculated from one-hour means

Norderney	Heligoland	Büsum	Cuxhaven	Jever	Fuhlsbüttel
6.47 m/s	7.62 m/s	7.04 m/s	5.59 m/s	4.30 m/s	3.97 m/s

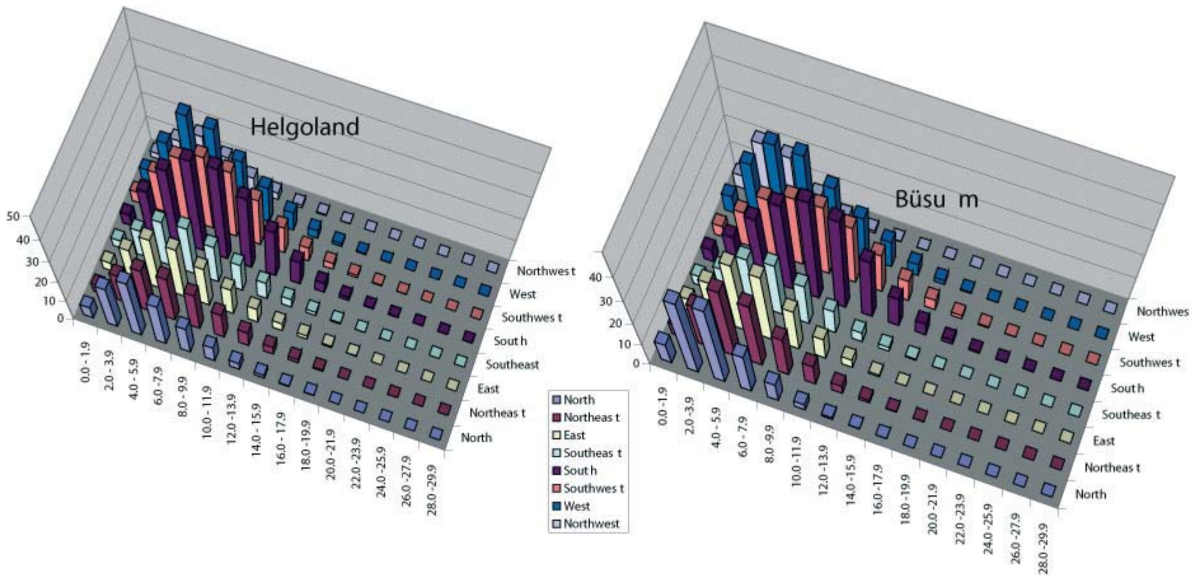

Fig. 4: Frequency distribution of wind speed (in m/s) and wind direction

4.2 PRISMA Data: A Comparison with Station Measurements

Although the applicability of both PRISMA and LM/GME data for forcing hydrodynamic models has been confirmed (ZIELKE et al., 2002), deviations naturally exist between NWP/PRISMA data and "real" (measured) data. Especially for long-term simulations and reference measurements it is necessary to obtain a realistic estimation of systematic differences between simulated data and observations.

In this investigation the PRISMA data time series was analysed at the Heligoland grid point because the Heligoland station is located further away from the coastline than Büsum or Norderney. The PRISMA data were interpolated barycentrically from the 42 km x 42 km grid to the Heligoland grid point. PRISMA grid points around Heligoland are located over the sea whereas those around Norderney or Büsum are just partially located over the sea. Therefore an interpolation of PRISMA grid points to Büsum or Norderney would also include wind information from grid points over land leading to large errors in the interpolated wind speed and direction for Büsum or Norderney.

A comparison was carried out between the time series of the PRISMA data and station measurements over the period 01-01-1989 to 31-12-2000. Mention should be made, however, of a discrepancy in this comparison: the PRISMA data, based on ten-minute means, are stored at 3-hour intervals whereas the station data are available at 1-hour intervals as hourly means. Due to the gustiness of the wind the mean of the shorter time-averaging period is greater than that of the longer time-averaging period. According to SCHROERS and LÖSSLEIN (1983) the 90%-value of the 10-minute mean serves as a good approximation of the hourly mean.

Although the synoptic station data (Table 3) yield the highest mean wind speed during the period 01-01-1989 to 31-12-2000 (with wind speeds above 8 m/s occurring more frequently in the station time serie and wind speeds below 8 m/s occurring more frequently in the PRISMA time series) (Fig. 5), wind speeds above 20 m/s are found to occur more frequently in the PRISMA data record (not shown).

Table 3: Overall mean wind speed (in m/s) from 01-01-1989 to 31-12-2000 at Heligoland

Station data (hourly mean)	PRISMA (10-minute mean)	PRISMA (hourly mean)
8.31	7.37	6.64

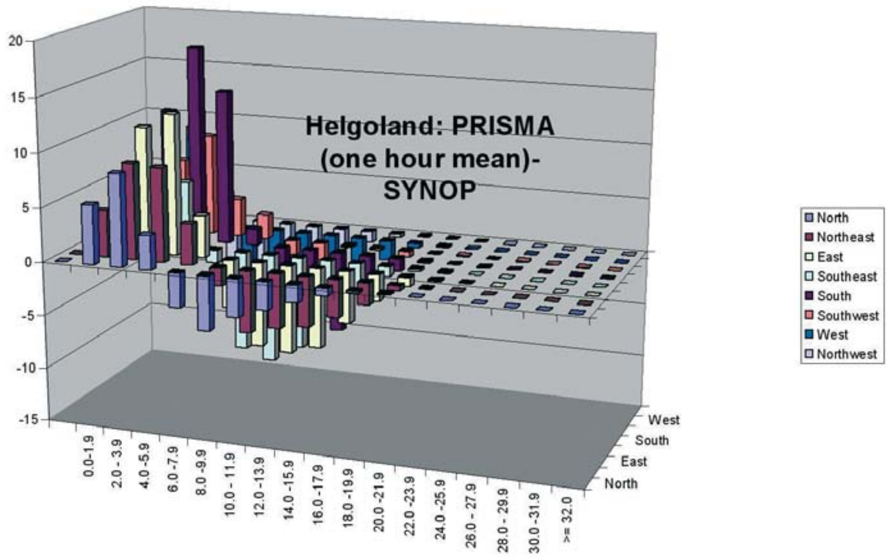

Fig. 5: Frequency distribution of wind speed difference (observations Heligoland – PRISMA) for different wind directions

4.3 Characteristic Forcing for a One-Year Period

The morphodynamic changes in the Dithmarschen Bight were studied for the period 01-05-1998 to 30-04-1999. These 12 months are characterized by a period of high wind speeds in the autumn, as it is typical for this season. Particularly extreme high wind speeds did not occur, however.

In order to simulate a first guess result for a longer period the hydrodynamic models were driven by a characteristic wind speed and direction representative of conditions throughout the German Bight. In accordance with the foregoing, the time series at Heligoland was chosen to generate these representative values.

As the PRISMA data show some deviations from the observed station data during a period when the measurements of wind speed and direction at Heligoland were as accurate as possible, the observed data at Heligoland were used as input forcing for hydrodynamic modelling during this period (May 1998 to April 1999). Measurements at the Heligoland station were considered to be representative for the German Bight area, as demonstrated by the results of numerical (NWP) simulations for this specific area.

By subdividing a distribution into classes the maximum number of classes may be expressed a function of the sample size, e.g.:

$K = 5 \log(n)$,

with K: number of classes,
log: logarithm to base 10,
n: sample size (PANOFSKY and BRIER, 1958).

By definition, the modal centre of the wind distribution is assumed to describe the characteristic wind for the whole period. With 0.5 m/s wind speed classes and 20 degree wind direction classes the location of the modal centre is calculated to be 8.75 m/s and 225 degrees. This wind was assumed to be representative for the 12-month period considered in the present study and was thus used as input to the hydrodynamic models. However, this classification is too fine to fulfil the condition formulated by PANOFSKY and BRIER (1958). In fact, 1080 classes are obtained if all wind speed measurements up to 30 m/s are considered. As the sample size is 8760, the condition formulated by PANOFSKY and BRIER (1958) would permit a maximum of 20 classes. If, however, only the classes from 180 to 260 degree and from 7.5 to 9.4 m/s are considered, a sample size of 564 falls into these 16 classes as these classes occur much more frequently than other classes (see also Fig. 4, which shows a similar distribution for a longer time scale). Instead of selecting a subset of the sample it would also have been possible to increase the class width. Although a class width of e.g. 90 degrees and 7.5 m/s would have fulfilled the classifying condition mentioned above, it would have been worthless due to its coarse and inadequate resolution as well as a misleading location of the modal centre. With 0.5 m/s wind speed classes and 20 degree wind direction classes the modal centre of both the full sample and the subset may be clearly identified. The dependence of the location of the modal centre on the chosen classification is shown in Table 4.

Table 4: Dependence of modal centre location on chosen classification

Class width	0.5 m/s and 10 degrees	0.5 m/s and 20 degrees	2.0 m/s and 45 degrees
Location of modal centre	8.75 m/s, 230 deg. 7.75 m/s, 200 deg.	8.75 m/s, 225 deg.	9.00 m/s, 180 deg.
Percentage of modal centre occurrence	0.32	0.64	4.6

The wind considered here to be representative (8.75 m/s and 225 degrees) is also in agreement with other statistical results: the median of the wind speed is found to be 8.7 m/s while the mean wind speed is computed to be 8.82 m/s for a mean wind direction of 210 degrees.

5. Conclusions

Hydrodynamic simulations using PRISMA and NWP data for external forcing were carried out in the present study for conditions of high winds over the German Bight in order to demonstrate the influence of meteorological data on simulated water levels. Even for the case of maximum water levels during storm surge conditions in February 2000 the differences between the simulated results using different forcing data (LM, GME, PRISMA) were less than the differences between each of the simulated results and measured water levels. Moreover, the differences between measurements and the results of the LM-forced simulation were found to be less than the corresponding differences with PRISMA forcing. In general, the results demonstrate that both the PRISMA and NWP data (in particular, the LM data) are suitable for forcing hydrodynamic models in a realistic way.

A comparison between PRISMA data and SYNOPTIC measurements at the Heligoland station from 01-01-1989 to 31-12-2000 indicates that the PRISMA results tend to underestimate the mean wind speed, even though PRISMA data usually overestimate wind speed. On the other hand, the frequency of occurrence of particularly high wind speeds based on PRISMA data is higher than that given by SYNOPTIC station measurements.

The results of numerical simulations using a cascade of NWP models (GME, LM) demonstrate the applicability of these models for meteorological forcing in morphodynamic computations. The finer the horizontal grid resolution of the meteorological models, the better are the results. Especially near the coast with a well-defined change in surface characteristics, it is found that the high-resolution LM with a 2.8 km grid is necessary to resolve the distinct modification of the wind field. Over the open sea, however, even the results of the coarse-resolution version of the GME are usually in closer agreement with observations than PRISMA data.

On the basis of numerical simulations it has been shown that observations at the Heligoland station may be adopted as representative wind information for the whole of the German Bight (with the exception of near-coastal areas).

6. Acknowledgements

The authors are very grateful to the German Federal Ministry of Education and Research (BMBF) for funding this study within the scope of the BMBF project PROMORPH (03F0262A). The investigation would also not have been possible without the support of the DWD, who made available the NWP model LM, permitted access to its database to obtain the data necessary for initialising the LM, and provided time series of wind speed and direction from synoptic stations. We wish to thank the Federal Maritime and Hydrographic Agency in Hamburg (BSH) for supplying NWP output data and interpolation routines as well as the DWD for permission to use the NWP output data archived at the BSH. We are also grateful to the University of Bonn for releasing an experimental version of the lm2lm (a necessary interpolation tool for generating initialisation and boundary values to force the 2.8 km version of the LM), which made it possible to perform simulation runs with the 2.8 km version of the LM. We also express our thanks to the NIC (John von Neumann Institute for Computing) at Jülich, Germany for allowing us to perform all simulations with the 7 km and 2.8 km version of the LM (version 2.17) on their Cray T3E massive parallel supercomputer. Finally we would like to thank Dr. Volker Barthel, Dr. Ian Westwood and an anonymous reviewer for helpful comments and revisions which led to an improvement of the manuscript.

7. References

CHRISTOFFER, J. and ULBRICHT-EISSINIG, M.: Die bodennahen Windverhältnisse in der Bundesrepublik Deutschland. Berichte des Deutschen Wetterdienstes 147. 1989.

DOMS, G.; SCHÄTTLER, U. and SCHULZ, J.-P.: Kurze Beschreibung des Lokal-Modells LM und seiner Datenbanken auf dem Datenserver (DAS) des DWD. Deutscher Wetterdienst, Offenbach, 2001.

LUTHARDT, H.: Analyse der wassernahen Druck- und Windfelder über der Nordsee aus Routinebeobachtungen. Hamburger Geophysikalische Einzelschriften, Reihe A 83. Fachbereich Geowissenschaften, Universität Hamburg, 109 pp, 1987.

MAJEWSKI, D.; LIERMANN, D.; PROHL, P.; RITTER, B.; BUCHHOLD, M.; HANISCH, T.; PAUL, G.; WERGEN, W. and BAUMGARDNER, J.: Icosahedral-hexagonal gridpoint model GME: description and high-resolution tests. Mon. Weather Rev., 130, 319–338, 2002.

NIELINGER, J.: Kopplung numerischer Simulationsmodelle zur Regionalisierung von Ergebnissen globaler Klimaszenarien. Berichte des Instituts für Meteorologie und Klimatologie der Universität Hannover, Nr. 57, 131 pp, 1998.

PANOFSKY, H. A. and BRIER, G. W.: Some Applications of Statistics to Meteorology. Pennsylvania State Univ., University Park (USA), 1958.

SCHMIDT, H.: Extremwindverhältnisse im norddeutschen Küstenbereich. PROMET Heft 2/3, 1984.

SCHROERS, H. and LÖSSLEIN, H.: Extremwertextrapolation und Windprofile bei Starkwind und Sturm. Meteorol. Rdsch. 36: 205–213, 1983.

SMITH, S. D. and BANKE, E. G.: Variations of the sea surface drag coefficient with wind speed. Quart. J. R. Met. Soc., 101, 665–673, 1975.

TROEN, I. and PETERSEN, E. L.: European Wind Atlas. Ed.: Commission of the European Communities, 1989.

VESELOV, E. P.: Marine Meteorology and Related Oceanographic Activities. In: Coastal Wind. Report No. 21. WMO / TD – No. 275, 1988.

ZIELKE, W.; MAYERLE, R.; KÜCK, F.; HOYME, H.; GROSS, G.; ROTH, R.; NIELINGER J., and BUSCH, U.: Auswirkungen von Klimaänderungen auf die Wasserstände und Windverhältnisse an der Deutschen Nordseeküste. BMBF-Projekt Nr. 03F0141A, 2. Zwischenbericht, Institut für Strömungsmechanik und ERiB, Universität Hannover, 1996.

ZIELKE, W.; MAYERLE, R.; KÜCK, F.; HOYME, H.; GROSS, G.; ROTH, R.; NIELINGER J., and BUSCH, U.: Auswirkungen von Klimaänderungen auf die Wasserstände und Windverhältnisse an der Deutschen Nordseeküste. BMBF-Projekt Nr. 03F0141A, 3. Zwischenbericht, Institut für Strömungsmechanik und ERiB, Universität Hannover, 1997.

ZIELKE, W. et al.: Prognose mittelfristiger Küstenmorphologieänderungen (PROMORPH). BMBF-Projekt Nr. 03F0262A, 2. Zwischenbericht. Institut für Strömungsmechanik und ERiB, Universität Hannover, 2002.

ZIELKE, W. et al.: PROMORPH – Prognose mittelfristiger Küstenmorphologieänderungen (Prognosis of Medium-Term Coastal Morphology). BMBF-Projekt Nr. 03F0262A / 03F0262B, Schlussbericht. Institut für Strömungsmechanik und ERiB, Universität Hannover, 2003.

Die Küste, 69 PROMORPH (2005), 1-420

Modelling of Flow in a Tidal Flat Area in the South-Eastern German Bight

By CARLOS PALACIO, ROBERTO MAYERLE, MAURICIO TORO and NESTOR JIMÉNEZ

Summary

This paper sums up the development phases of a flow model for a tidally-dominated area of the German North Sea. The study area is the Dithmarschen Bight located between the Elbe and Eider estuaries. The model presented is a two-dimensional depth-integrated flow model based on the DELFT3D Modelling System developed by Delft Hydraulics in the Netherlands. A description of model set-up as well as the results of sensitivity studies and model calibration and validation procedures are outlined in this contribution. Measurements of water levels and current velocities with a dense spatial and temporal coverage were used for this purpose. It was found that hydrodynamic forcing along the open sea boundaries is by far the most important factor governing the predictive capability of the model. Sensitivity studies indicated that the effect of seasonal bathymetric changes on current velocities may be quite significant. The effect of spatially variable bed roughness on the flow field was found to be less significant. The validation results showed that the model is capable of reproducing water levels and current velocities in the study area in fair agreement with observations. The mean absolute errors between computed and observed water levels at a number of locations covering periods of several months were found to be less than 10 cm (3 % of the mean tidal range) and 20 cm (6 % of the mean tidal range) at high and low water levels, respectively. The mean absolute errors between computed and observed depth-averaged velocities at various cross-sections in the tidal channels were generally found to be less than 0.2 m/s, which represents less than 20 % of the tidally-averaged value. The model simulation results indicated a certain tendency towards underestimation of current velocities in the tidal channels. On the basis of the quality standards usually adopted (WALSTRA et al., 2001 and VAN RIJN et al., 2002), the performance of the model with regard to current velocity predictions was found to range between good and excellent.

Zusammenfassung

Dieser Beitrag fasst die Entwicklungsphasen eines Strömungsmodells für ein tidedominiertes Gebiet, Deutsche Nordsee, zusammen. Untersuchungsgebiet ist die Dithmarscher Bucht zwischen Elbe- und Eiderästuar. Auf Grundlage des DELFT3D Modellsystems von Delft Hydraulics (Niederlande) wurde ein 2-dimensionales tiefenintegriertes Strömungsmodell entwickelt. Beschrieben werden Modellaufbau, Ergebnisse der Sensitivitätsstudien sowie Modellkalibrierung und Validierung. Hierzu wurden Messungen von Wasserständen und Strömungsgeschwindigkeiten mit dichter zeitlicher und räumlicher Deckung verwendet. Es stellte sich heraus, dass der hydrodynamische Antrieb auf Grundlage der Wasserstände entlang der Offene-See-Grenzen den bei weitem signifikantesten Faktor für die Vorhersagefähigkeit des Modells darstellte. Signifikanztests ergaben, dass Effekte saisonaler bathymetrischer Veränderungen für die Strömungsgeschwindigkeit durchaus signifikant sein können. Es zeigte sich, dass räumlich variable Bodenrauheiten für die Ausprägung des Strömungsfelds weniger signifikant waren. Die Ergebnisse der Validierung zeigten, dass das Modell in der Lage ist, Wasserstände und Strömungsgeschwindigkeiten im Untersuchungsgebiet in recht guter Übereinstimmung mit den Beobachtungen zu reproduzieren. Die mittleren absoluten Fehler zwischen den simulierten und den an mehreren Orten über mehrere Monate gemessenen Wasserständen lagen bei Hochwasser unter 10 cm (entsprechend 3 % des mittleren Tidehubs) und bei Niedrigwasser unter 20 cm (entsprechend 6 % des mittleren Tidehubs). Die mittleren absoluten Fehler zwischen simulierten und den in verschiedenen Querschnitten der Gezeitenrinnen gemessenen tiefenintegrierten Geschwindigkeiten lagen unter 0,2 m/s, entsprechend weniger als 20 % des tidegemittelten Wertes. Die Simulationsergebnisse zeigen eine *gewisse Tendenz, die Strömungsgeschwindigkeiten in den Gezeitenrinnen zu unterschätzen. Legt man den Ergebnissen die normalerweise angewandten Qualitätsstandards (*WALSTRA *et al., 2001;* VAN RIJN *et al., 2002) zugrunde, so lag die Leistung des Modells für Vorhersagen der Strömungsgeschwindigkeit zwischen gut und sehr gut.*

Keywords

Coastal Flow Models, Sensitivity Analysis, Model Calibration, Model Validation, Open Sea Boundaries, Field Measurements, PROMORPH, North Sea, Dithmarschen Bight.

Contents

1. Introduction

Process-based models for simulating flow, waves, sediment transport and morphological evolution have been developed within the framework of the research project "Predictions of Medium-Scale Morphodynamics – PROMORPH" funded by the German Ministry of Education and Research (BMBF) over the period 2000 to 2002. The research project was motivated by the need to predict morphological changes in a tidally-dominated area on the German North Sea coast over periods of several years.

This paper sums up the development phases of a flow model for the central Dithmarschen Bight (see Fig. 1). The model implements a two-dimensional depth-integrated (2DH) flow model solver developed by Delft Hydraulics in the Netherlands. The results of model set-up, sensitivity studies, calibration and validation are presented. The variability of the computed water levels and current velocities relative to the main physical and numerical parameters was investigated at several monitoring stations. The model was calibrated and validated using water level recordings at a number of gauge stations over a period of several months and current velocities measured over several cross-sections in the main tidal channels in order to cover the full range of tidal and meteorological conditions typical of the study area. The performance of the model was determined quantitatively on the basis of a set of statistical parameters. The results of an evaluation of the predictive capability of the model with regard to water levels and current velocities are also presented.

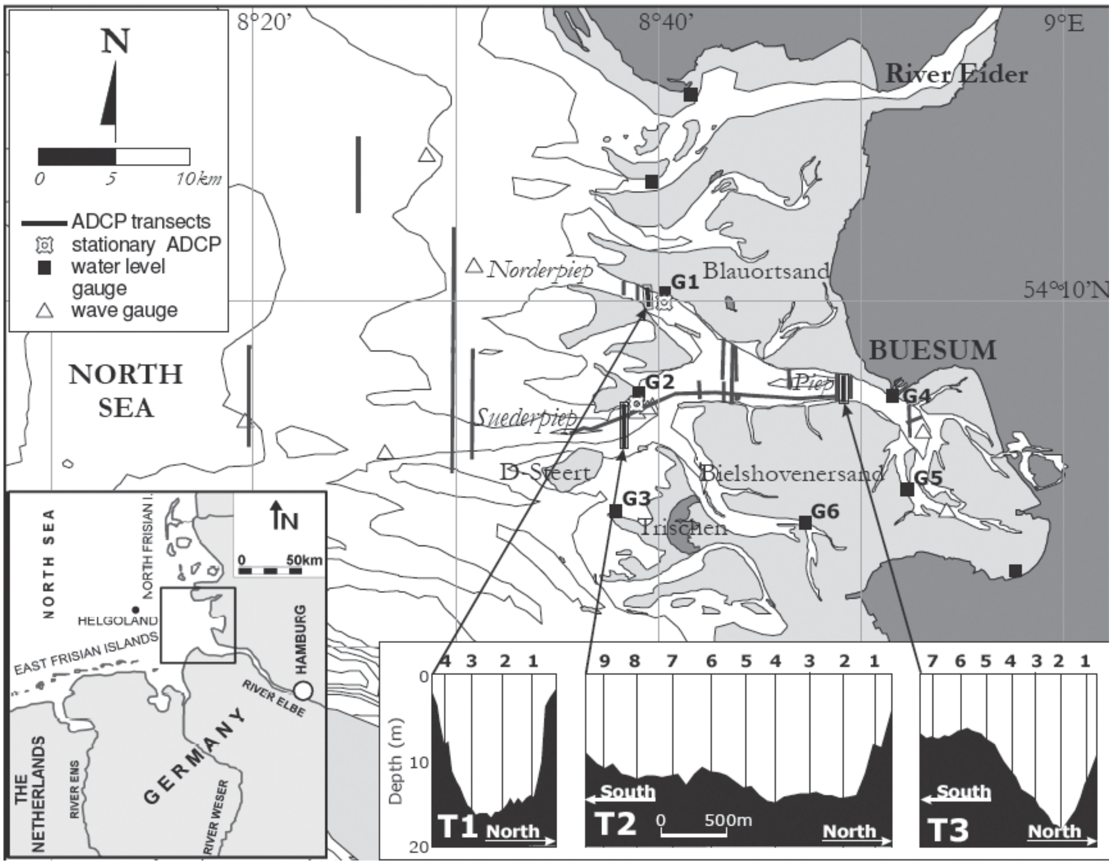

Fig. 1: Investigation area showing surveyed cross-sections and gauge stations

2. Description of the Study Area

The study area is located about 100 km north of Hamburg between the Eider and Elbe estuaries. The morphodynamics of the study area are dominated by tidal flats and a tidal channel system comprised of three channels: the Norderpiep in the northwest, the Suederpiep in the southwest, and the Piep tidal channel, which is formed at the confluence of the Norderpiep and Suederpiep. Under normal conditions the maximum mean water depth in the tidal channels is about 18 m. The tidal flats and sandbanks are exposed at low water. The area is characterized by a meso-tidal regime with a mean tidal range of 3.2 m and neap and spring tidal ranges of about 2.8 m and 3.5 m, respectively. The current velocities in the tidal channels attain maximum values of about 2.8 m/s (Toro et al., in this volume). The small bed forms and correspondingly low bed roughness coefficients are responsible for the generally fairly uniform distribution of velocities over the vertical (Mayerle et al., in this volume(a)).

With regard to the wave and wind climate, the study area is classified as a storm wave environment with prevailing westerly winds (SW-W). Although wave heights in the outer region may attain 3 to 4 m, these break along the edge of the tidal flats (margins) of the investigation area. Despite the absence of barrier islands, intertidal and supratidal sandbanks in the outer regions prevent the penetration of waves into the tidal flat area. Small wind-generated waves of up to about 0.5 m in height are observed in the study area (Toro et al., in this volume). The influence of local waves on currents is moderate over the tidal flats and negligible in the tidal channels. Storm surges may produce water level set-ups of up to 5 m, favouring the propagation of waves into shallow regions. Even under such conditions, however, wave effects are mostly confined to the outer sandbanks. The seabed sediment in the tidal channels and on the tidal flats consists mainly of sands with varying proportions of silt and clay (RICKLEFS and ASP, in this volume). The grain sizes of sediment transported in suspension are much finer than those of seabed sediment (POERBANDONO and MAYERLE, in this volume).

3. Flow Model

Several models for simulating flow, sediment transport and morphological evolution have been developed in the past for the Dithmarschen Bight (HARTSUIKER, 1997; HIRSCHHÄUSER and ZANKE, 2001). Due to a lack of field data, however, very little is known about the performance of the models, particularly regarding the quality of simulated current velocities.

The simulations carried out in the present study were performed using the two-dimensional depth-integrated (2DH) DELFT3D flow model developed by Delft Hydraulics in the Netherlands. This model solves the non-steady depth-integrated momentum and continuity equations for depth-integrated velocities and water levels. The implicit scheme adopted for the time integration enables simulations to be performed for Courant numbers as high as 10. An algebraic approach for turbulence closure using a constant value of eddy viscosity was adopted (ROELVINK and VAN BANNING, 1994).

The set-up procedure for the flow model includes in the definition of the model limits, the construction of a grid system, and preliminary runs to detect spurious oscillations was done initially. Fig. 2 shows the bathymetry and limits of the flow models implemented in the present investigation. Details of the models developed in this study are given in Table 1. Preliminary investigations to check the global behaviour of the model system as well as sensitivity studies were only carried out for the model covering the central Dithmarschen Bight (CDBM). As the sandbanks and entrances to the main tidal channels are subject to intensive morphological changes, the western open sea boundary of the CDBM was extended a further 15 km seawards to yield the Extended Central Dithmarschen Bight Model (ECDBM). Finally, a model covering the entire bight with the inclusion of the Elbe and Eider estuaries was set-up. This larger model is referred to as the Dithmarschen Bight Model (DBM). The open sea boundaries are located in deeper water at a fair distance from the region of interest (see also Fig. 3).

The bathymetry used to set up the models was based on measurements made in 1998 by the Federal Maritime and Hydrographic Agency (BSH) in Hamburg. The bathymetry of the tidal flat regions was obtained from bathymetric maps drawn up in 1990 by the Office for Rural Development in Husum. The effect of bathymetry on computed water levels and current velocities was investigated for the reference grid (as defined in Section 4) based on bathymetric measurements made in 1990, 1996 and 1998 covering the Central Dithmarschen Bight. The curvilinear grids adopted for model computations were appropriately matched to the bathymetry of the various model domains. Due to the fact that the numerical errors in the cross-advection term of the DELFT3D flow model are proportional to the orthogonality value, the orthogonality of the grids was kept as low as possible.

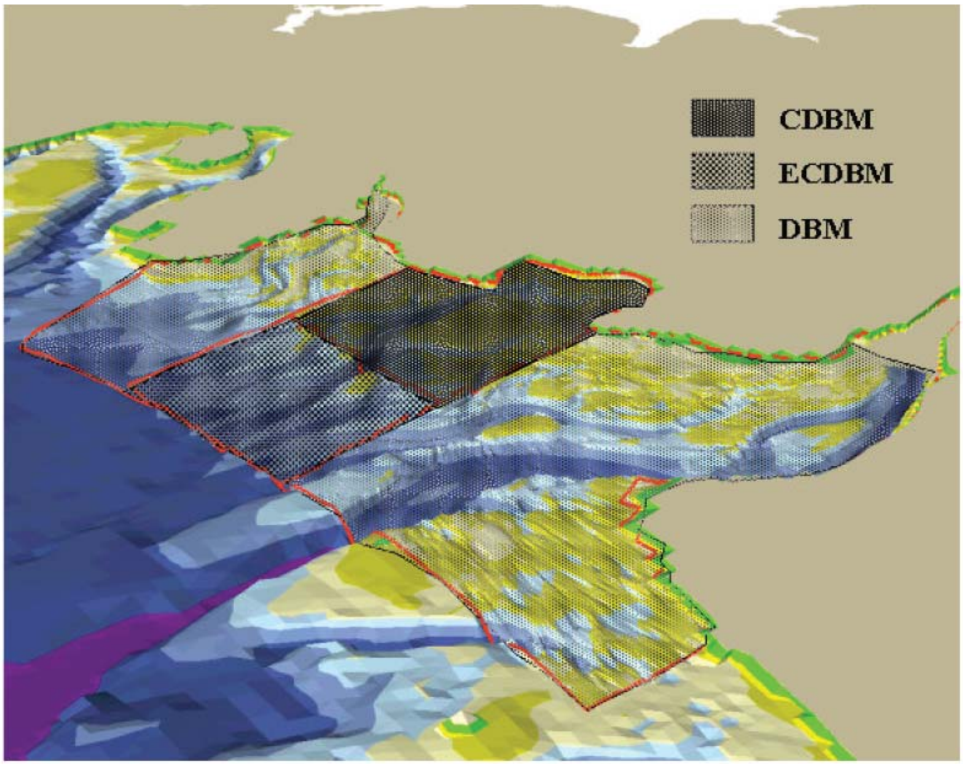

Fig. 2: Perspective view of the study area showing bathymetry and the limits of the flow models

Table 1: Details of the flow models

	Central Dithmarschen Bight Model (CDBM)	Extended Central Dithmarschen Bight Model (ECDBM)	Dithmarschen Bight Model (DBM) – Fig. 3
Dimensions (km)	20 by 17	35 by 17	37 by 54
Area (km^2)	300	520	1640
Seaward boundary	14 km west of Buesum	29 km west of Buesum	29 km west of Buesum
Grid spacing	60 × 180 m	90 × 150 m	80 × 200 m
No. of Grid Cells	30,000	36,000	43,250

The flow model is driven by the combined effects of hydrodynamic forcing along the open sea boundaries and winds. Each of the models has three open sea boundaries, i.e. a western, northern and southern boundary (see Fig. 2). The flow field in the central Dithmarschen Bight is mainly governed by the tidal wave propagating through the western seaward boundary. The northern and southern open sea boundaries of the CDBM are located on the tidal flats, which fall dry during low tide. As the latter boundaries are far removed from the region of interest, their effect on flow conditions in the central Dithmarschen Bight is negligible. For the purpose of hydrodynamic forcing in the present study, water levels were specified along the western open sea boundaries. Along the open boundaries of the Elbe and Eider estuaries, flow discharges were specified.

Wind fields were obtained with the aid of the PRISMA interpolation model developed by the Max Planck Institute of Meteorology in Hamburg (LUTHARDT, 1987). This model

Die Küste, 69 PROMORPH (2005), 1-420

generates synoptic wind fields from a large set of measurements at locations along the coastline and at offshore stations covering the entire North Sea. The data is generated every three hours with a spatial resolution of 42 km. A comparison of the PRISMA model results with wind measurements made by the Research and Technology Centre Westcoast of the University of Kiel over a period of 8 years confirmed the high quality of the PRISMA model results (WILKENS, 2004). Wind data generated by the PRISMA model were interpolated in time and space to provide the required information for driving the flow model of the investigation area.

After completing the flow model set-up procedure, flow simulations were carried out using "standard" physical and numerical parameters in order to detect spurious velocity fields and anomalous water level contours due to incorrect settings. The model simulations were found to yield smooth water levels, smooth and realistic velocity fields, and no spurious circulation patterns.

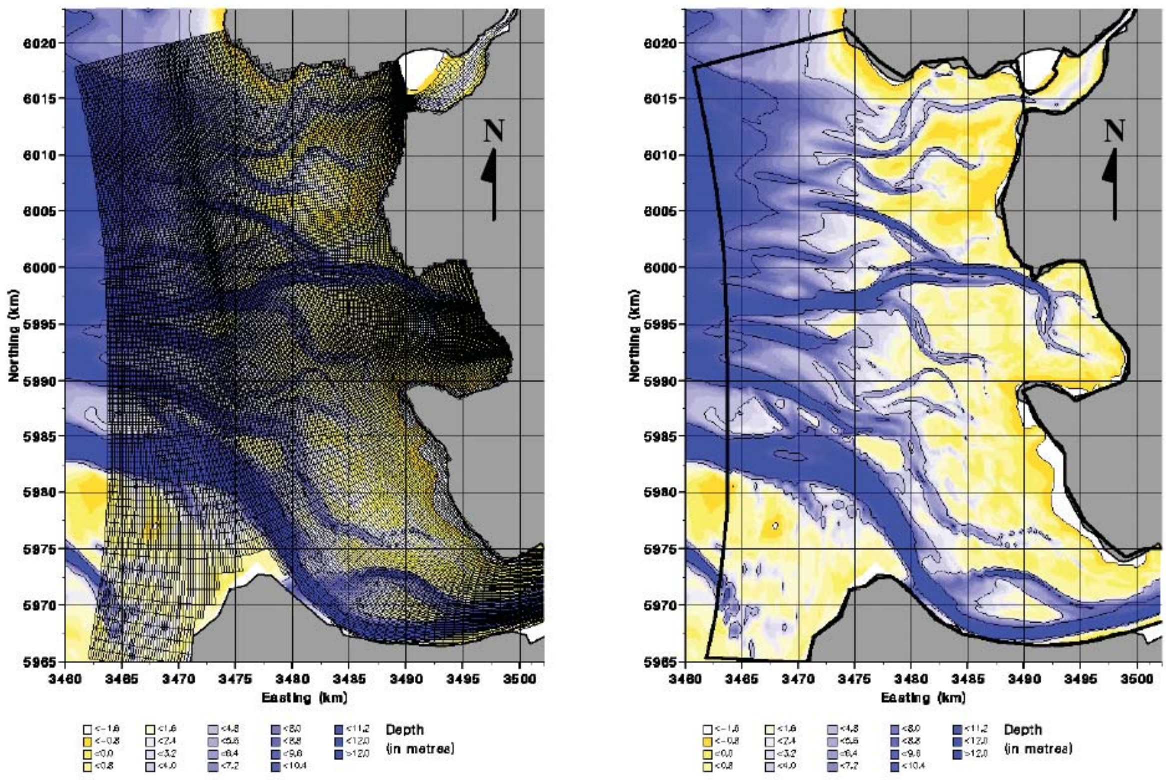

Fig. 3: Bathymetry and curvilinear grid of the DBM

4. General Model Behaviour and Sensitivity Studies

The purpose of sensitivity studies is to gain an understanding of the overall behaviour of a model and its response to changes in the physical and numerical parameters adopted. On the basis of a sensitivity analysis it is also possible to identify the particular physical parameters that have a predominant effect on computed water levels and current velocities.

The sensitivity analysis was carried out at several locations throughout the study area for a variety of situations representative of the main flow conditions, i.e. for different tidal phases and tidal periods as well as for different meteorological conditions. A plan view of the CDBM indicating the defined cross-sections and monitoring stations selected for the sensitivity analysis is shown in Fig. 4. The variability of computed water levels and velocities at the selected monitoring stations was investigated in relation to the computational time step, grid resolution, various approaches for defining hydrodynamic forcing along the open sea boundaries, wind speed and direction, bottom roughness, eddy viscosity and bathymetry. Moreover, the influence of waves on currents and the relevance of a three-dimensional model approximation were also investigated. The analysis was carried out on the basis of comparisons of computed water levels and velocities obtained at the monitoring stations over a three-day simulation period (May 18 to May 21, 1999) for different model settings and parameters. The results of sensitivity tests for grid spacing, bed roughness, influence of waves and relevance of 3D model approximations and morphology are presented. The results of sensitivity tests with respect to the remaining parameters are summarized in PALACIO et al. (2003).

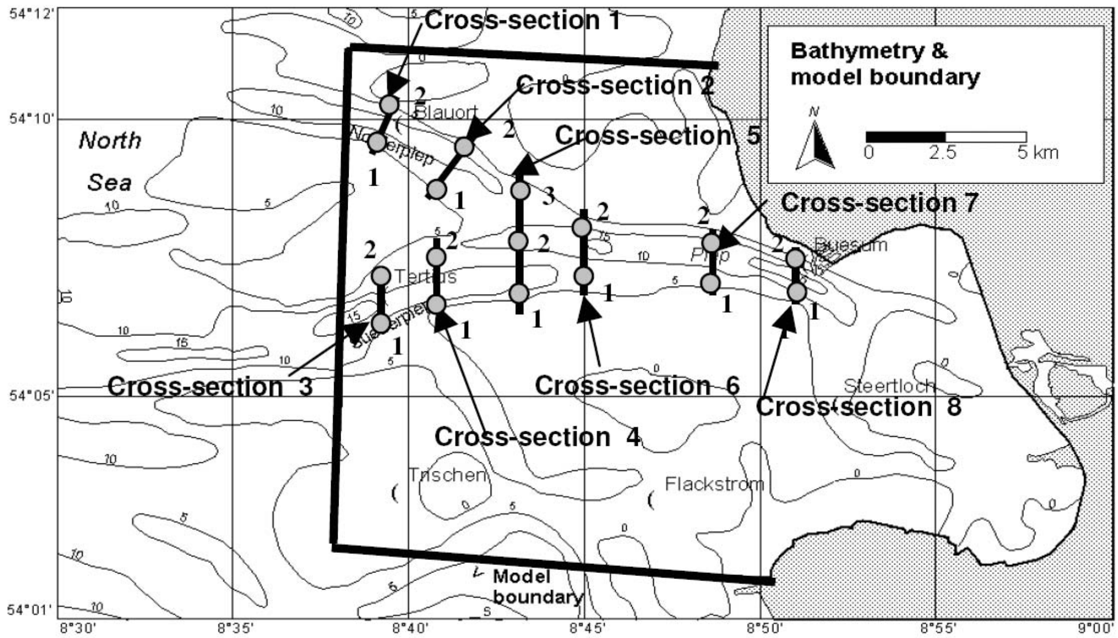

Fig. 4: Selected cross-sections and monitoring stations for the sensitivity analysis

With regard to the computational grid, the mesh size should be sufficiently small to correctly reproduce hydrodynamic conditions in the study area and at the same time permit simulations of coupled flow, wave and sediment transport processes for the purpose of modelling morphological evolution. Investigations of the effect of grid spacing on flow conditions were carried out considering three grid systems: a) a reference grid with a mesh size ranging from 60 m to 180 m; b) a fine grid with a mesh size ranging from 30 m to 90 m and c) a coarse with a mesh size ranging from 120 m to 360 m. Fig. 5 shows the grid resolution of the three grids. The reference grid with about 30,000 cells was initially generated and the fine and coarse grids were subsequently obtained by refining and coarsening the reference grid once in each case. The DBM incorporating these different grid resolutions is also shown in Fig. 5 together with a comparison between the modelled bed profile given by the three different grids and the measured bed profile over cross-section A-A at the intersection of the Norderpiep, Suederpiep and Piep tidal channels. As is evident in the figure, the coarse grid is unable to adequately describe the measured bathymetry. The volumetric consistency of the model for the different grids was checked by comparing the volumes calculated below a defined reference level for the three grid systems with the volume computed from bathymetric measurements. This check resulted in only minor volumetric differences. In the case of the coarse grid, however, discrepancies were observed between computed and measured water levels and current velocities throughout the domain. The largest velocity discrepancies given by the coarse grid were found in cross-section 7 (see Fig. 6). Based on the results of this analysis it was concluded that the reference grid is quite adequate for realistically reproducing hydrodynamic conditions in the modelled domain.

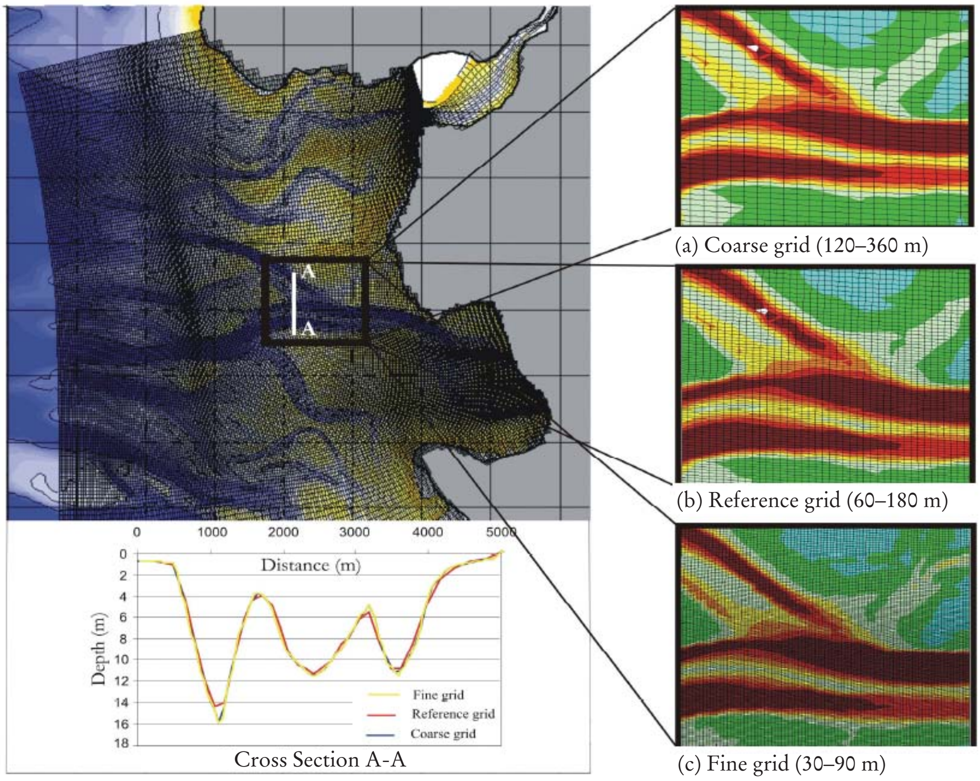

Fig. 5: Grid resolutions showing a comparison between the modelled and measured depth profile over cross-section A-A

The response of the flow model to changes in the bed roughness was investigated by varying the Chézy coefficient throughout the modelled domain. Constant temporal and spatial values of 40 $m^{1/2}/s$, 50 $m^{1/2}/s$ and 60 $m^{1/2}/s$ were considered for this purpose. As indicated in Fig. 7, the bottom roughness has a clear influence on the computed depth-averaged velocities. This effect is more pronounced in the case of the highest roughness value. Small phase shifts also resulted in the computed water levels, which were found to be most pronounced in cross-sections near the coastline. As the highest roughness value of 60 $m^{1/2}/s$ yielded the best results in overall terms, this value was adopted for model calibration. A detailed investigation of the spatial and temporal variations of the dimensions of bed-form features and associated bed roughness values based on field measurements is given in MAYERLE et al. (in this volume(a)), which also includes roughness maps accounting for the layer thickness of potentially mobile sediments, the characteristics of superficial seabed sediments and local flow conditions.

In view of the intense morphological activity observed at various locations in the study area, the influence of bathymetry on computed water levels and velocities was also investigated throughout the domain. In order to permit a better evaluation of bathymetric variations over shorter periods a monitoring programme was set up. Within the scope of this programme the bed profiles of cross-sections T1, T2 and T3 were surveyed between June 2000 and August 2003 (see ASP, 2004 and RICKLEFS and ASP, in this volume). As a result, it was found that changes in the bed profiles can be quite significant, especially in the most exposed areas such as, e.g. over cross-sections T1 and T2 in the Norderpiep and Suederpiep tidal channels, respectively (see Fig. 1). Bathymetric changes of up to 4–5 m were observed in these cross-sections during the period of measurements. Although cross-section T3 in the Piep tidal channel proved to be fairly stable, bathymetric changes of up to 2–3 m were observed in this cross-section. For the purpose of investigating the effect of bathymetry on computed flow values the reference grid was adjusted to match three different bathymetries based on measurements made in 1990, 1996 and 1998. The computed volumetric *percentage differences* between the model bathymetries of 1990 and 1996 and the model bathymetry based on 1998 measurements revealed only minor differences (0.73 % and 0.03 % respectively). Similarly, the results of model simulations using the three bathymetries mentioned above yielded only slight differences in computed water levels. With regard to depth-averaged current velocities, on the other hand, differences of up to 0.2 m/s were obtained at a number of monitoring stations (see Fig. 8). The fact that seasonal variations in the bathymetry of the tidal channels can be quite significant stresses the importance of updating the model bathymetry regularly.

Investigations of the effects of wind and waves on currents were also carried out. With regard to wind conditions it was found that wind speeds below 8 m/s have little influence on the model results. In order to assess the influence of waves on currents, simulations were carried out using a coupled flow and wave model. Details of the wave model are presented in WILKENS et al. (in this volume). Wave simulations were performed using the DBM for wave heights ranging between 1 m and 3 m along the open sea boundary. Comparisons between computed current velocities with and without wave influence were made at a position located in a shallow channel on Tertiussand and at a location near Buesum. Under these conditions, wave heights of up to 3 m were computed on the western boundary, resulting in differences of about 0.10 m/s in depth-averaged flow velocities. At the monitoring station near Buesum, on the other hand, the differences in computed flow velocities were generally found to be negligible due to large local depths and smaller wave heights at this location. A noticeable difference was observed, however, during slack water. It may be concluded from these results that the effect of waves on depth-averaged currents is negligible in the tidal channels for the wave conditions considered.

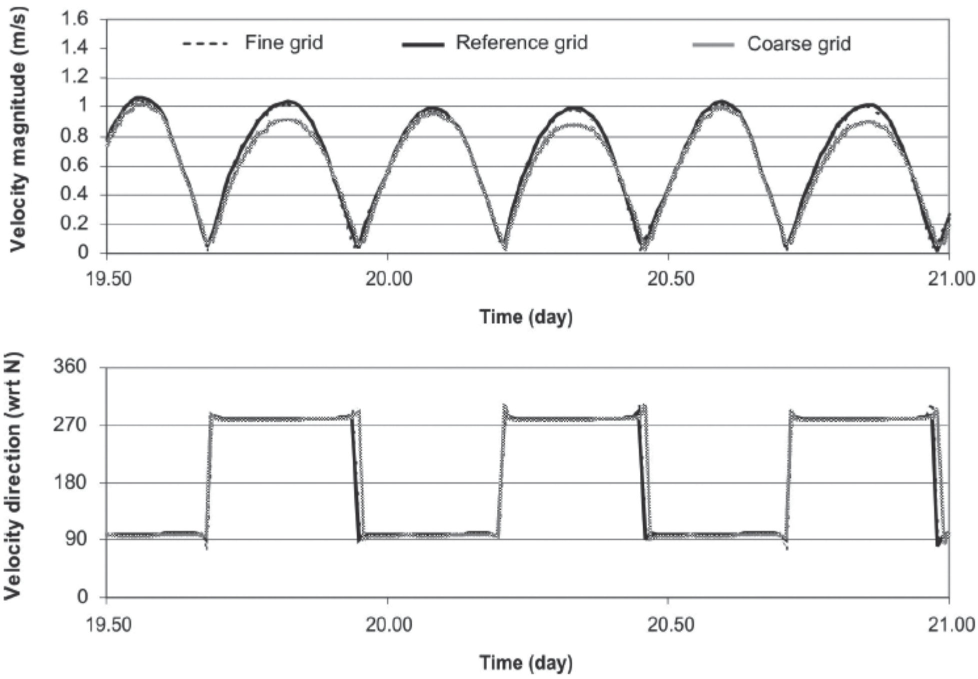

Fig. 6: Dependency of velocity variability on grid resolution in cross-section 7 – position 2 (Fig. 4)

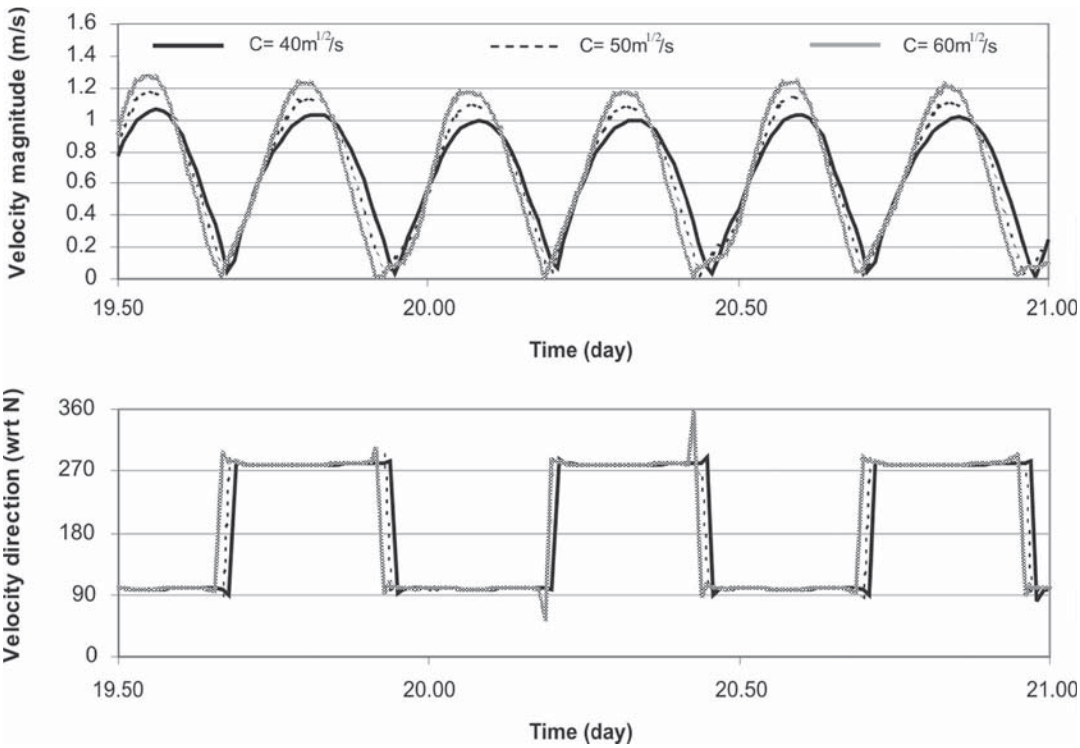

Fig. 7: Dependency of velocity variability on bottom roughness in cross-section 7 – position 2 (Fig. 4)

In order to compare the results obtained from a 2DH and a 3D flow model the reference grid of the 2DH model was extended to include 10 layers in the vertical direction. The vertical grid size distribution of the 3D model was chosen to follow a logarithmic distribution in order to accurately reproduce the vertical flow profile. Comparisons between the 2DH and 3D flow model computations were made for water levels at several locations and

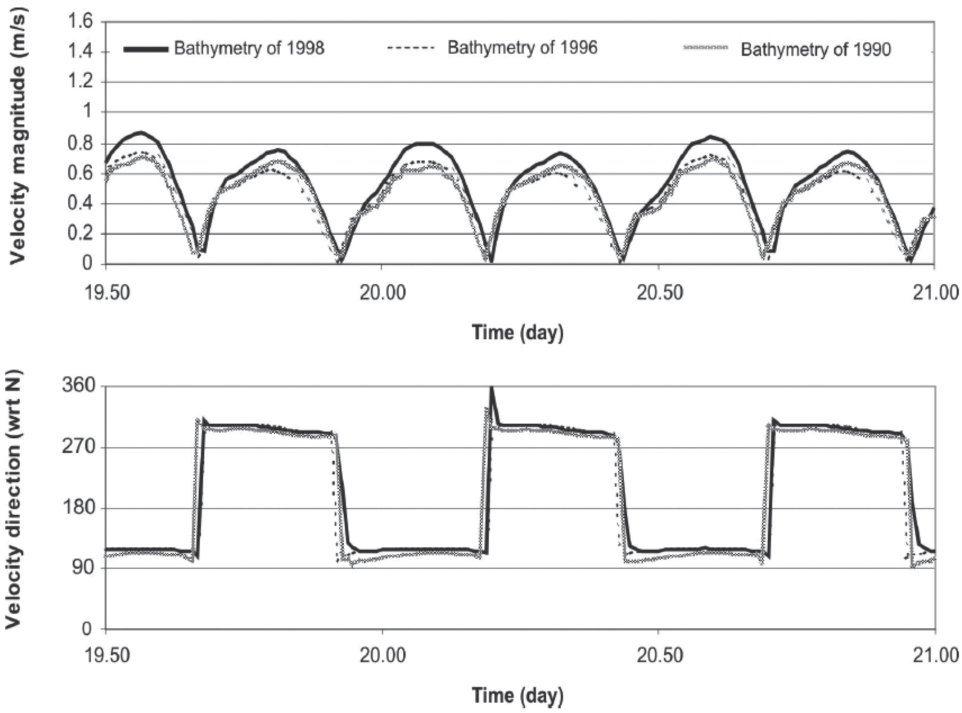

Fig. 8: Dependency of velocity variability on bathymetry in cross-section 8 – position 1 (Fig. 4)

current velocities in a number of cross-sections. A comparison between the depth-averaged current velocities computed by the 2DH model and those obtained by depth-averaging the results of the 3D model runs is shown by way of example during maximum ebb flow over the cross-section at the intersection of Suederpiep and Norderpiep tidal channels in Fig. 9. It was found that the results given by the two flow models are fairly similar during most of the tidal period, except during slack water, when current reversal occurs.

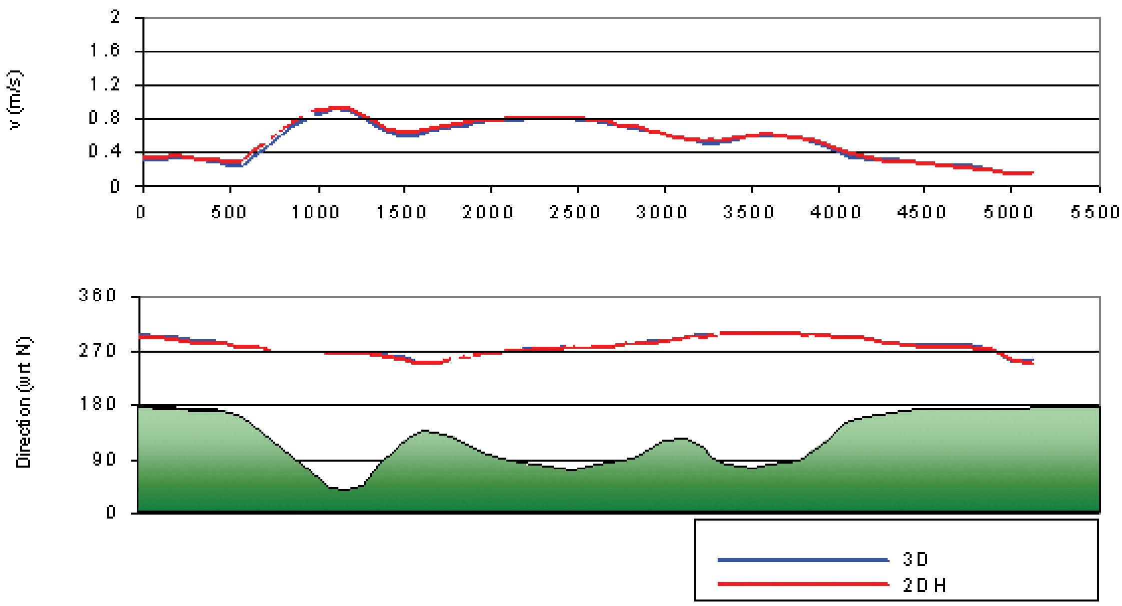

Fig. 9: Comparison between measured depth-averaged current velocities and the results obtained from 2DH and 3D model simulations during maximum ebb flow

Based on the results of the sensitivity tests presented in the foregoing, the following main model settings were chosen: a) a time step of 0.5 min; b) a constant spatial and temporal eddy viscosity value of 1 m²/s; c) a curvilinear grid with a grid spacing ranging between 60 and 180 m. Furthermore, the sensitivity tests indicated that the flow field in the study area is mainly governed by the forcing conditions imposed on the open sea boundary, and to a lesser extent by bathymetry and the selected value of bed roughness. These parameters were taken into consideration in the calibration process presented in the following section. In order to avoid the effects of initial conditions on the computational results a sufficiently long warming-up period (of about 48 hours) was included in all simulations.

Fig. 10 shows the resulting variation of depth-integrated current velocities over a tidal period computed using the above-mentioned models settings. The results indicate that the model is capable of realistically reproducing the main flow patterns, with current velocities directed onshore and offshore during the flood and ebb phases, respectively, and a tendency towards zero current velocities at high and low water slack. Based on visual observations, drying and flooding of the sandbanks are also reproduced well by the model.

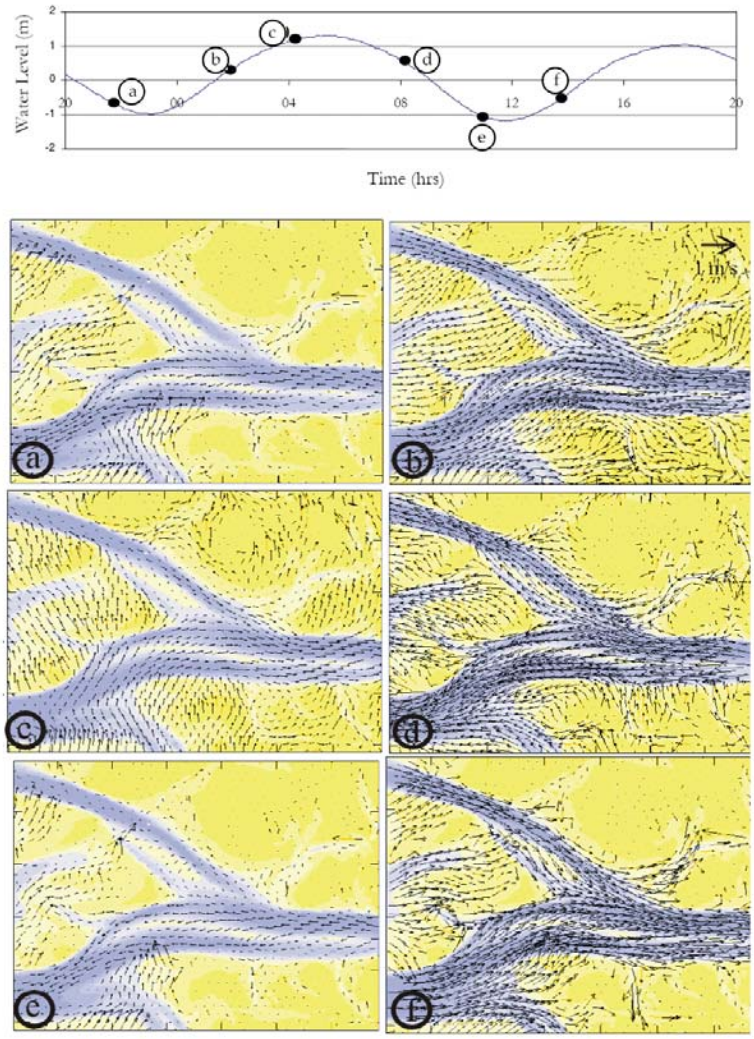

Fig. 10: Patterns of tidal currents in the Central Dithmarschen Bight

5. Calibration and Validation Data

Calibration and validation of the flow model were carried out using measured water levels and current velocities covering the full range of conditions typical of the study area. Complete sets of data were compiled for driving the model and evaluating its performance. These include wind velocity fields covering the modelled area and water levels near the open sea boundaries for driving the flow model as well as water levels measured at a number of locations and current velocities measured over several cross-sections for calibration and validation purposes. The selected sets of measured data are listed in Table 2.

Water levels measured over six periods (P_{N1} to P_{N6}) covering entire lunar cycles were used for calibrating and validating the model with respect to surface elevation. The astronomical tidal range varied from about 2.3 m to 4.2 m from neap to spring tides, respectively. The predictive capability of the model with regard to surface elevations during harsher meteorological conditions was also tested for three periods (P_{S1} to P_{S3}) incorporating storms with water level set-ups and wind velocities of up to about 4.5 m and 33 m/s, respectively.

The data measured at the following gauge stations were used for model calibration and validation: G1: Blauort; G2: Tertius; G3: Trischen; G4: Buesum, G5: Steertloch and G6: Flackstrom. The locations of these gauge stations are shown in Fig. 1. Stations G1 to G3 are located along the western boundary of the investigation area at the entrances to the Norderpiep and Suederpiep tidal channels, station G4 is located near Buesum harbour, and stations G5 and G6 are situated fairly close to the coastline.

Table 2: Observation periods considered for model calibration and validation

Periods			Duration	Characteristics	Gauges/ Transects
Calibration	Water levels	P_{N1}	May 31–Jun 26/1989	Relatively calm weather conditions	G1 to G6
		P_{N2}	May 31–Jul 12/1990		
		P_{N3}	Apr 27–Jun 30/1990		
	Current Velocities	P_{V4}	Jun 5–6/2000		T1 to T3
		P_{V3}	Sep 12–13/2000		
Validation	Water levels	P_{N4}	Jul 7–Aug 18/1990	Relatively calm weather conditions	G1 to G6
		P_{N5}	Aug 15–Sep 15/2000		
		P_{N6}	Sep 22–Oct 22/2000		
		P_{S1}	Jan 25–31/1990	Storm periods with wind speeds of up to 33 m/s and water level set-ups of up to 4.5 m	
		P_{S2}	Feb 25–Mar 1/1990		
		P_{S3}	Nov 26–Dec 5/1999		
	Current Velocities	P_{V5}	Mar 21–23/2000	Relatively calm weather conditions	T1 to T3
		P_{V2}	Sep 5–6/2000		
		P_{V1}	Dec 5–6/2000		

Flow measurements over several cross-sections in the tidal channels served as a basis for calibrating and validating the model with respect to current velocities. The cross-sections surveyed by moving vessels are shown in Fig. 1. These measurements were made under relatively calm weather conditions using a 1200 kHz Acoustic Doppler Current Profiler (ADCP) manufactured by RD Instruments. Details of the measurement procedure as well as the results of an analysis to determine the spatial and temporal variations of current velocity in the tidal channels are given in TORO et al. (in this volume).

Five relatively calm periods (P_{V1} to P_{V5}) covering tidal ranges varying from about 2 m to 4 m were selected for calibrating and validating the model with respect to current velocities. During the calibration and validation procedures, attention was focused on the ability of the model to reproduce current velocities in three cross-sections, i.e. T1 and T2 at the entrance to the central Dithmarschen Bight in the Norderpiep and Suederpiep tidal channels, respectively, and T3 in the Piep tidal channel nearer to the coast. The bed profiles of these cross-sections are shown in Fig. 1. Further details of the selected cross-sections and the procedure adopted for determining depth-averaged current velocities are given in TORO et al. (in this volume).

6. Assessment of Model Performance

The predictive capability of the flow model with regard to water levels and current velocities was verified by comparing measured and modelled values. A set of statistical parameters was used to assess the quality of the model results. In this study the Mean Error (ME), the Mean Absolute Error (MAE), the Relative Mean Absolute Error (RMAE) and the Adjusted Relative Mean Absolute Error (ARMAE) were used for assessment purposes. Definitions of these parameters are listed in Table 3. The ME serves to indicate a general tendency of predictions towards overestimation or underestimation. The standard deviation of the differences between predicted and observed values is a measure of the variability of the differences about the mean value of the differences. As a dimensional parameter, it indicates quite clearly the magnitude of the error and hence the accuracy of a simulation. Division of the MAE by the mean absolute value of the measurements yields the non-dimensional RMAE.

WALSTRA et al. (2001) and VAN RIJN et al. (2002) have proposed a set of standards for assessing model performance in connection with model studies of two coastal areas (see Table 4). The severity of these standards depends on the complexity of the environmental conditions at the location concerned. It should be noted that the measurements used to check model performance in the latter cases were made at fixed locations in both coastal areas. The viability of applying such standards to measurements from moving vessels with a much wider spatial and temporal coverage (as in the present investigation) should thus be borne in mind. As measurements always include errors, a suggested approach to account for the influence of observational errors is to subtract these from each absolute error, thereby yielding an Adjusted Relative Mean Absolute Error (ARMAE). In the present study the accuracy of water level measurements at the gauge stations was taken to be 1 cm. Based on an investigation by JIMENEZ-GONZÁLEZ et al. (in this volume) of the accuracy of acoustic profiling measurements from moving vessels, it was deduced that the accuracy of depth-averaged current profiles over the cross-sections of the tidal channels surveyed in the present study was about 0.015 m/s.

7. Model Calibration

The model calibration procedure involved the adjustment of physical parameters so as to obtain the best possible reproduction of hydrodynamic conditions in the study area. The periods selected for model calibration in the present investigation (see Table 2) were chosen to cover a wide range of conditions typical of the modelled domain. Calibration with respect to water levels was carried out for three periods characterized by relatively calm weather conditions. The predictive capability of the model with regard to current velocities (as defined in Section 6) was investigated for two relatively calm periods, i.e. June 5 to 6, 2000 and September 12 to 13, 2000 with tidal ranges of 3.9 m and 3.3 m, respectively.

Simulations were performed for the three model domains shown in Fig. 2. Comparable results were obtained in each case. Only the results obtained from the Extended Central Dithmarschen Bight Model (ECDBM) using measured water levels along the open sea boundaries are presented in the following. The wind field obtained from the PRISMA interpolation model was applied in all simulations (LUTHARDT, 1987).

Calibration of the flow model was carried out in two steps. In the first step, hydrodynamic forcing along the open sea boundary was adjusted to improve the predictive capability of the model with respect to water levels. For this purpose measured and computed water levels were compared at a number of locations. In the second step, the bed roughness in the tidal channels was adjusted so as to obtain the best possible agreement between measured and computed current velocities. Although the bathymetry of the study area was also found to influence current velocities, it was not possible to quantify this effect in detail due to a lack of adequate bathymetric measurements covering the entire domain for periods corresponding to the dates of the measuring campaigns.

Table 3: Statistical parameters used for model calibration and validation

Parameter	Equation
Mean Error	$ME = \sum_{j=1}^{n} (Mod_j - Mea_j) / n$ (1)
Mean Absolute Error	$MAE = \sum_{j=1}^{n} \mid (Mod_j - Mea_j) \mid / n$ (2)
Relative Mean Absolute Error	$RMAE = \sum_{j=1}^{n} \left(\mid Mod_j - Mea_j \mid \right) / \sum_{j=1}^{n} \mid Mea_j \mid$ (3)
Adjusted Relative Mean Absolute Error	$ARMAE = \sum_{j=1}^{n} \left(\mid Mod_j - Mea_j \mid Ac \right) / \sum_{j=1}^{n} \mid Mea_j \mid$ (4)

Note: Mod= Model results; Mea=Measured values;
n= Number of values; Ac= Accuracy of measurements

Table 4: Performance rating according to the RMAE of velocity values

Rating	RMAE VAN RIJN et al. (2002)	RMAE WALSTRA et al. (2001)
Excellent	< 0.1	< 0.2
Good	0.1–0.3	0.2–0.4
Reasonable / Fair	0.3–0.5	0.4–0.7
Poor	0.5–0.7	0.7–1.0
Bad	> 0.7	> 1.0

7.1 Hydrodynamic Forcing along the Open Sea Boundaries

As the computed water levels in the study area were found to depend primarily on the conditions specified along the western open sea boundary, the performance of several approaches for prescribing hydrodynamic forcing in terms of water levels was investigated. The results of a detailed investigation of the effects of hydrodynamic forcing along the open sea boundaries of coastal models are presented by MAYERLE et al. (in this volume(b)). The effectiveness of several approaches was tested for a wide range of conditions covering periods of up to two months. These include approaches based on measured water levels at gauge stations located close to the model open sea boundaries and the use of simulated water levels obtained from a larger-scale model covering the adjacent sea area. The results obtained by specifying water levels along the open sea boundaries of the ECDBM are presented in this study. Due to the fact that water levels specified along the western open sea boundary of the flow model were obtained from gauge stations located some 10 km further eastwards within the model domain (stations G1 to G3 in Fig. 1), appropriate corrections to the measured water levels were necessary. Satisfactory predictions were obtained by reducing the amplitudes and phases of the measured water levels by about 5 % and 15 min, respectively.

The statistical parameters obtained at the six gauge stations G1 to G6 are listed in Table 5. Fig. 12 and 13 show the resulting mean errors (ME) and mean absolute errors (MAE) with the corresponding standard deviations for high and low water amplitudes and phases, respectively. The results indicate that the MAE of amplitudes and phases are generally less than about 10 cm and 20 cm, and 15 min and 25 min at high and low water, respectively.

7.2 Bed Roughness

The effect of bed roughness on model predictions of current velocities was assessed according to the procedure outlined in Section 6. For this purpose a comparison was made between measured and modelled current velocities at cross-sections T1 in the Norderpiep, T2 in the Suederpiep and T3 in the Piep tidal channel based on simulations covering two two-day periods (June 5 to 6, 2000 and September 12 to 13, 2000).

The simulations were initially performed using Chézy coefficients ranging between 50 and 65 $m^{1/2}/s$. On the basis of these simulations it was found that a Chézy coefficient of about 60 $m^{1/2}/s$ yielded the best agreement between modelled and measured current velocities. Fig. 11a shows the corresponding equivalent roughness sizes. Further simulations were then performed with bed roughness under additional consideration of geological features and bed-form dimensions (see Fig. 11b). Comparisons between the results obtained using the two maps of bed roughness shown in Fig. 11 indicate that although there is a certain reduction in the magnitudes and changes in the patterns of depth-averaged current velocities due to a higher bed roughness at certain locations, only minor changes resulted in the statistical parameters obtained for the entire analysis period (see Table 6). The depth-averaged current velocities computed in the channels using the two roughness maps showed little difference owing to their large water depths. The most pronounced differences in the magnitudes and patterns of depth-averaged current velocities due to a higher bed roughness were observed at cross-sections T2 and T3. With regard to currents, the main effect of higher bed roughness values is to delay the time of occurrence of peak velocities. Investigations carried out by MAYERLE et al. (in this volume (a)) have shown that bed roughness has a much greater effect on sediment concentrations. This stresses the importance of describing bed roughness as accurately as possible in order to adequately reproduce the patterns of sediment dynamics and associated morphological developments.

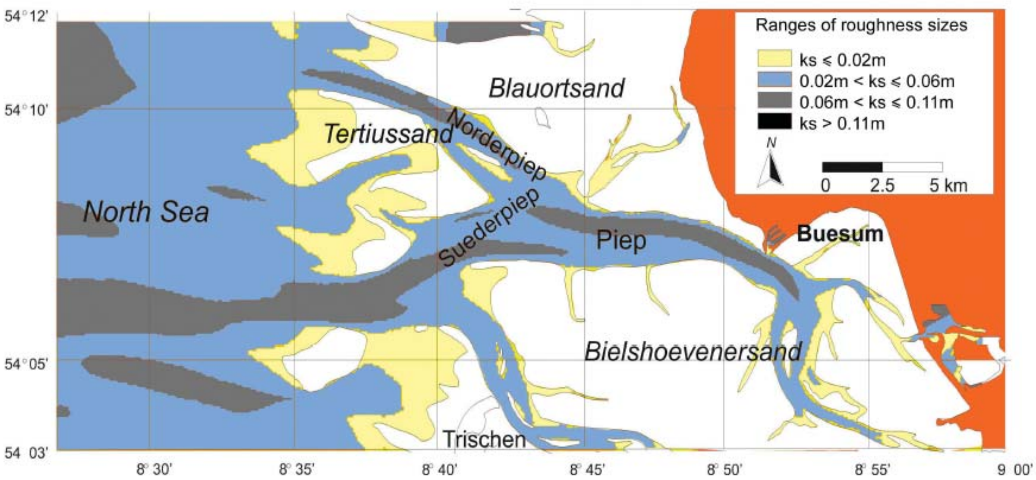

a) Based on a constant Chézy coefficient of 60 $m^{½}/s$

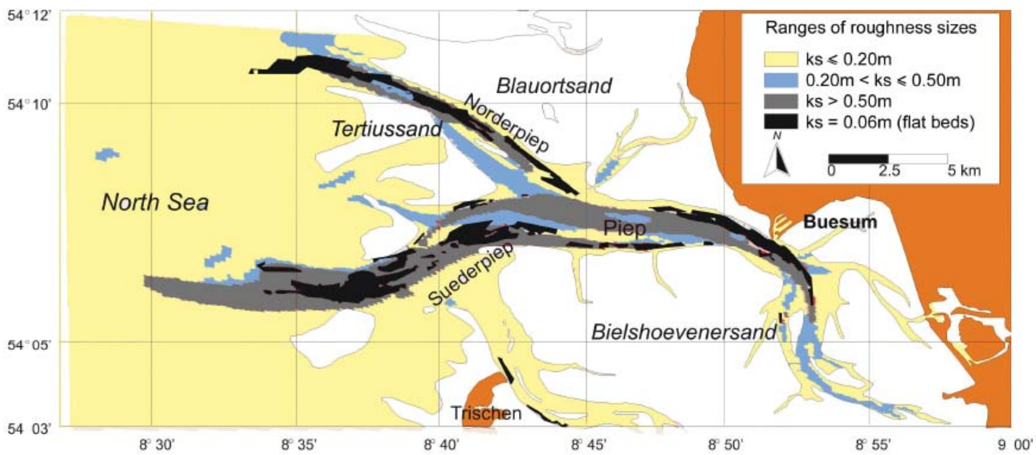

b) Accounting for geological features and bed-form dimensions

Fig. 11: Maps of equivalent roughness sizes (MAYERLE et al., this volume (a))

Table 6 lists the statistical parameters obtained from a comparison of measured and computed current velocities in the main tidal channels. The mean errors (ME), mean absolute errors (MAE), and corresponding standard deviations between measured and computed values of high and low water amplitudes, phases (gauge stations G1 and G5), and depth-averaged current velocities (cross-sections T1 to T3) are shown in Figs. 12, 13 and 18, respectively. On the basis of the ME values the model shows a certain tendency to underestimate the magnitude of current velocities, particularly at cross-section T1. The MAE of depth-averaged current velocities is found to vary between 0.10 m/s and 0.30 m/s, with ARMAE values ranging between 0.09 and 0.27. For the conditions investigated, slightly better agreement was obtained at cross-section T3 nearer the coast.

8. Model Validation

The ability of the model to correctly reproduce field conditions was assessed in the validation procedure by comparing the results of model simulations with measured data. The numerical and physical parameters defined for model set-up, sensitivity studies and calibration were held constant throughout the entire validation process. As in the calibration procedure, all model runs were performed using water levels along the open sea boundaries based on measurements at nearby gauge stations and wind fields generated by the PRISMA model. Although the data sets used for model validation differed from those used for model calibration (see Table 2), the same gauge stations (G1 to G6) and cross-sections (T1 to T3) were used for validating water levels and current velocities, respectively. Model validation with respect to water levels included three relatively calm periods (P_{N4} to P_{N6} in Table 2) and three periods with storms (P_{S1} to P_{S3} in Table 2). The predictive capability of the model with regard to current velocities (see Section 6) was verified for three relatively calm periods during the year 2000, i.e. March 21 to 23, September 5 to 6, and December 5 to 6. Similar to the approach adopted in the calibration procedure, the water levels measured at gauge station G2 were suitably adjusted to obtain representative values along the western open sea boundary.

The model validation results for water levels and current velocities are listed in Table 5 and 6, respectively. The mean errors (ME), mean absolute errors (MAE), and corresponding standard deviations between measured and computed values of high and low water amplitudes and phases (gauge stations G1 and G5) are shown in Fig. 12 and 13, respectively.

The ME values for water levels indicate a tendency towards overestimation of high water levels and underestimation of low water levels. The corresponding MAE values are found to generally lie below 10 cm and 20 cm for high and low water levels, respectively, representing about 3 % to 6 % of the mean tidal range. With regard to tidal phase, the computed times of high and low water were found to lag measurements. A time lag of between 10 and 20 min (1.5 % to 3 % of the tidal period) and 10–30 min (1.5 % to 4 % of the tidal period) were obtained at high and low water levels, respectively. As would be expected, better agreement is obtained at the gauge stations located closer to the western open sea boundary.

Fig. 14 and 15 show comparisons of measured and computed water levels at gauge stations G1 to G6 for the period August 4 to August 18, 2000 (period P_{N4}). The results presented in the figures cover about two weeks of the simulated periods. It is seen that fairly good agreement is obtained between observations and model predictions at all gauge stations, with only minor discrepancies confined mainly to low water conditions. The ability of the model to handle extreme events was also investigated. Comparisons of measured and computed water levels obtained from simulations covering several storms are shown in Fig. 16 and 17. As may be seen in the figures, the model is able to simulate extreme events fairly well, with discrepancies generally less than about 30 cm at high water.

Fig. 18 shows ME and MAE values with corresponding standard deviations between measured and computed values of depth-averaged current velocities at cross-sections T1 to T3 (see Fig. 1). The MAE for depth-averaged current velocities was found to range between 0.12 m/s and 0.22 m/s for the majority of cross-sections and observation periods, which represents about 10 % to 20 % of tidally-averaged values. Agreement between model results and observations was found to be much better for neap tides than for spring tides. Better agreement was obtained at cross-section T3 located nearer the coast and at cross-section T2, through which most of the tidal discharge is transported into and out of the domain. At cross-section T1 the model tends to underestimate depth-averaged current velocities. The ARMAE values were found to lie below 0.2 for the majority of measurement conditions and cross-sections. According to the standards proposed by WALSTRA et al. (2001) and VAN RIJN et al. (2002), the performance of the model is classified as being excellent, and between good and excellent, respectively. It should be noted that the discrepancies between model predictions and observations are partly attributable to a lack of bathymetric measurements close to the periods during which measurements were made over the surveyed cross-sections. The fact that measurements were performed from moving vessels as well as the application of an extrapolation procedure to describe velocity profiles over the entire depth are also potential sources of error.

Comparisons of measured and computed current velocities for a neap tide (December 5 to 6, 2000) are shown in Figs. 19 to 24. It is seen that the model is capable of reproducing current velocities over the selected cross-sections fairly well. In general, it was found that the model is unable to correctly reproduce the variation of current velocities during certain phases of the tidal cycle, particularly at slack water. This may be related to the 2DH model approximation, which appears to inadequately reproduce changes in flow direction.

Table 5: Model calibration and validation results for water levels (ECDBM)

		Gauge Station	Amplitude				Phase			
			High water level		Low water level		High water level		Low water level	
			ME (STD) in cm	MAE (STD) in cm	ME (STD) in cm	MAE (STD) in cm	ME (STD) in min	MAE (STD) in min	ME (STD) in min	MAE (STD) in min
CALIBRATION	P_{N1}	**G1**	5.4 (1.0)	5.4 (1.0)	–13.3 (2.5)	13.3 (2.5)	–8.1 (11.7)	11.5 (8.4)	–8.2 (13.4)	12.2 (9.8)
		G2	9.9 (1.7)	9.9 (1.7)	–8.4 (6.4)	8.4 (6.4)	–6.0 (12.3)	10.8 (8.2)	–0.7 (17.7)	12.6 (12.3)
		G3	4.4 (1.2)	4.4 (1.2)	–8.1 (2.8)	8.1 (2.8)	–7.5 (11.0)	10.4 (8.3)	–25.3 (9.7)	25.3 (9.7)
		G4	N.A.	N.A.	N.A.	N.A.	N.A.	N.A.	N.A.	N.A.
		G5	–9.6 (2.1)	9.6 (2.1)	–3.9 (3.5)	4.1 (3.3)	–5.3 (13.7)	11.7 (8.8)	13.1 (15.8)	17.4 (10.8)
		G6	7.7 (2.2)	7.7 (2.2)	–18.6 (4.5)	18.6 (4.5)	–9.1 (10.6)	11.3 (8.0)	1.0 (15.4)	11.5 (10.2)
	P_{N2}	**G1**	5.4 (1.0)	5.4 (1.0)	–12.8 (2.7)	12.8 (2.7)	–8.6 (12.8)	12.3 (9.2)	–7.6 (12.3)	11.3 (9.0)
		G2	9.0 (2.1)	9.0 (2.1)	–7.9 (5.1)	7.9 (5.1)	–3.8 (11.6)	9.7 (7.3)	–1.6 (15.1)	11.3 (10.0)
		G3	4.1 (1.4)	4.1 (1.4)	–8.4 (3.4)	8.4 (3.4)	–6.6 (10.3)	9.6 (7.5)	–23.2 (10.2)	23.2 (10.2)
		G4	N.A.	N.A.	N.A.	N.A.	N.A.	N.A.	N.A.	N.A.
		G5	–10.5 (2.8)	10.5 (2.8)	–3.2 (9.0)	5.1 (8.1)	–6.2 (14.2)	12.4 (9.1)	13.7 (19.7)	19.0 (14.6)
		G6	7.3 (2.2)	7.3 (2.2)	–17.9 (5.2)	18.0 (5.0)	–9.7 (10.0)	11.6 (7.8)	2.3 (14.5)	10.8 (9.8)
	P_{N3}	**G1**	5.2 (1.7)	5.2 (1.7)	–13.0 (2.8)	13.0 (2.8)	–8.4 (12.6)	12.0 (9.2)	–6.5 (11.6)	11.0 (7.5)
		G2	9.8 (2.8)	9.8 (2.8)	–5.2 (3.4)	5.5 (3.0)	–2.7 (16.1)	12.1 (11.0)	–7.1 (13.2)	11.5 (9.6)
		G3	6.0 (4.4)	6.7 (3.3)	–5.9 (5.0)	6.4 (4.3)	–1.3 (12.6)	9.4 (8.5)	–21.0 (14.0)	21.3 (13.5)
		G4	4.2 (6.1)	5.9 (4.4)	–27.6 (6.7)	27.6 (6.7)	5.2 (14.6)	11.7 (10.0)	9.7 (18.2)	16.0 (13.1)
		G5	4.7 (5.9)	5.8 (4.8)	–33.0 (7.3)	33.1 (7.3)	13.0 (19.4)	18.5 (14.2)	24.6 (25.2)	30.0 (18.4)
		G6	8.0 (4.8)	8.4 (4.1)	–16.7 (6.6)	16.7 (6.4)	–7.5 (13.7)	12.0 (10.0)	5.0 (10.4)	9.1 (7.1)
VALIDATION	P_{N4}	**G1**	0.2 (2.0)	1.5 (1.2)	–7.3 (3.4)	7.3 (3.4)	–16.5 (16.9)	19.6 (13.1)	–7.3 (3.4)	10.4 (9.7)
		G2	6.0 (2.7)	6.2 (2.3)	1.5 (3.5)	3.2 (2.0)	–11.6 (16.1)	15.6 (12.2)	2.7 (13.5)	11.3 (7.8)
		G3	3.1 (0.8)	3.1 (0.8)	–2.6 (1.5)	2.6 (1.5)	–12.4 (11.9)	13.7 (10.4)	–11.0 (14.4)	13.7 (11.8)
		G4	4.1 (3.7)	4.2 (3.5)	–6.1 (3.4)	6.2 (3.3)	–1.1 (14.2)	11.2 (8.8)	13.3 (13.4)	16.1 (9.8)
		G5	3.7 (7.3)	5.3 (6.2)	–10.4 (4.7)	10.5 (4.6)	5.0 (22.0)	16.0 (15.4)	21.8 (18.8)	24.2 (15.5)
		G6	5.5 (2.8)	5.6 (2.7)	–1.6 (3.8)	3.4 (2.3)	–14.0 (13.4)	15.8 (11.2)	10.6 (13.5)	14.4 (9.3)
	P_{N5}	**G1**	4.6 (1.2)	4.6 (1.2)	–8.8 (2.9)	8.8 (2.9)	–0.4 (14.5)	12.0 (7.9)	–3.0 (13.5)	10.8 (8.4)
		G2	0.0 (1.4)	1.0 (0.9)	–11.2 (2.9)	11.2 (2.9)	1.0 (9.6)	7.5 (5.9)	–5.4 (10.3)	8.2 (8.2)
		G3	5.1 (1.6)	5.1 (1.6)	–2.8 (3.7)	4.0 (2.3)	–4.9 (8.9)	7.7 (6.6)	–18.1 (10.6)	18.1 (10.6)
		G4	5.3 (3.0)	5.3 (3.0)	–18.5 (5.2)	18.5 (5.2)	10.4 (10.1)	11.4 (8.9)	9.9 (22.8)	21.1 (13.0)
		G5	1.9 (5.1)	4.3 (3.2)	–21.9 (6.9)	21.9 (6.9)	6.3 (11.9)	10.2 (8.7)	10.8 (33.6)	31.9 (14.5)
		G6	N.A.	N.A.	N.A.	N.A.	N.A.	N.A.	N.A.	N.A.
	P_{N6}	**G1**	4.6 (1.3)	4.6 (1.3)	–7.2 (3.4)	7.3 (3.2)	–2.3 (16.3)	13.6 (9.0)	–8.9 (11.9)	12.1 (8.6)
		G2	–0.1 (2.0)	1.6 (1.2)	–9.6 (3.8)	9.6 (3.8)	0.9 (13.1)	9.6 (8.9)	–7.4 (12.6)	11.6 (8.7)
		G3	5.5 (1.9)	5.5 (1.9)	–1.5 (3.1)	2.8 (2.0)	–3.3 (8.2)	6.7 (5.8)	–16.8 (13.2)	17.5 (12.3)
		G4	5.3 (2.3)	5.3 (2.3)	–12.0 (4.5)	12.0 (4.5)	12.3 (12.9)	13.7 (11.4)	–2.1 (35.9)	29.3 (19.3)
		G5	6.6 (3.9)	6.7 (3.7)	–17.6 (8.3)	17.8 (8.0)	9.8 (13.3)	12.2 (11.1)	0.3 (36.1)	31.3 (17.5)
		G6	N.A.	N.A.	N.A.	N.A.	N.A.	N.A.	N.A.	N.A.

where: NA: values not available

Table 6: Model calibration and validation results for current velocities (ECDBM)

Period		Range of WL and (V)	Cross-Sections (No. of transects)	Bed roughness based on a constant Chézy coefficient of 60 $m^{0.5}/s$			Bed roughness considering geological features and bed-form dimensions		
				ME (STD) in m/s	MAE (STD) in m/s	ARMAE	ME (STD) in m/s	MAE (STD) in m/s	ARMAE
CALIBRATION	P_{V4}	3.7 to 3.9 (1.4 to 1.7)	T1 (15)	–0.29 (0.17)	0.30 (0.16)	0.27	–0.27 (0.17)	0.28 (0.16)	0.25
			T2 (13)	–0.09 (0.21)	0.18 (0.14)	0.19	–0.09 (0.22)	0.19 (0.14)	0.2
			T3 (9)	0.04 (0.20)	0.17 (0.11)	0.18	–0.04 (0.21)	0.18 (0.11)	0.19
	P_{V3}	3.3 to 3.5 (1.3 to 1.6)	T1 (28)	–0.13 (0.16)	0.17 (0.13)	0.17	–0.15 (0.18)	0.18 (0.14)	0.19
			T2 (7)	–0.04 (0.24)	0.20 (0.15)	0.21	–0.05 (0.26)	0.21 (0.15)	0.24
			T3 (6)	–0.06 (0.11)	0.10 (0.08)	0.09	–0.11 (0.15)	0.16 (0.11)	0.17
VALIDATION	P_{V5}	4.0 to 4.2 (1.4 to 1.6)	T1 (18)	–0.04 (0.19)	0.16 (0.11)	0.15	–0.08 (0.2)	0.18 (0.12)	0.18
			T2 (6)	0.09 (0.25)	0.22 (0.15)	0.34	0.06 (0.24)	0.20 (0.14)	0.32
			T3 (16)	0.04 (0.16)	0.13 (0.09)	0.14	–0.01 (0.16)	0.13 (0.10)	0.13
	P_{V2}	2.9 to 3.2 (0.9 to 1.3)	T1 (20)	–0.15 (0.20)	0.20 (0.14)	0.22	–0.14 (0.21)	0.20 (0.16)	0.22
			T2 (10)	–0.05 (0.19)	0.15 (0.12)	0.18	–0.06 (0.19)	0.16 (0.12)	0.2
			T3 (7)	–0.07 (0.13)	0.12 (0.09)	0.11	–0.11 (0.11)	0.13 (0.08)	0.12
	P_{V1}	2.3 to 2.5 (0.6 to 1.1)	T1 (35)	–0.11 (0.12)	0.14 (0.09)	0.19	–0.12 (0.12)	0.14 (0.10)	0.19
			T2 (12)	–0.05 (0.14)	0.12 (0.09)	0.16	–0.06 (0.14)	0.13 (0.09)	0.17
			T3 (17)	–0.07 (0.15)	0.13 (0.10)	0.21	–0.07 (0.14)	0.12 (0.09)	0.18

where:
WL: Water level (m)
V: Current velocity (m/s)
STD: Standard deviation

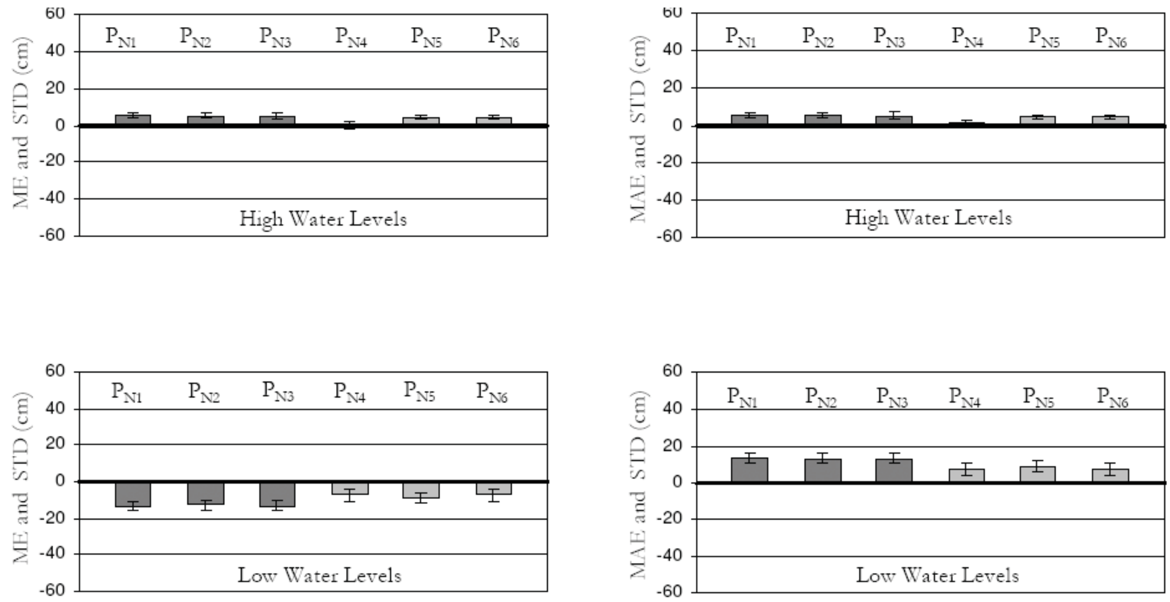

a) Gauge Station 1

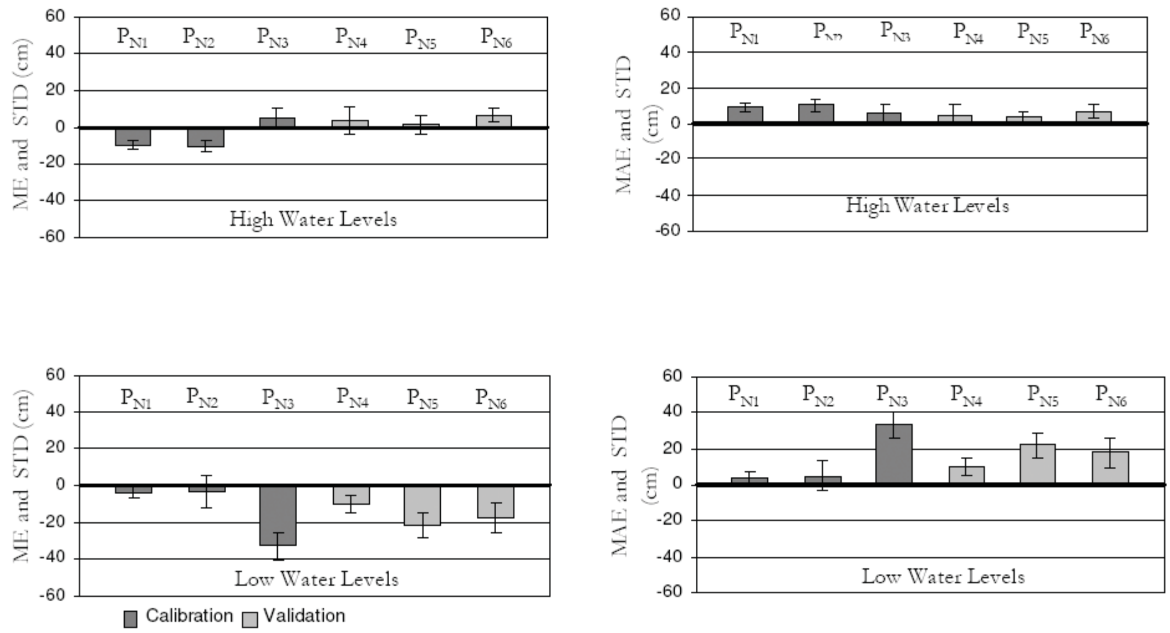

b) Gauge Station 5

Fig. 12: Mean Error (ME), Mean Absolute Error (MAE), and corresponding standard deviations of amplitudes at high and low water levels (gauge stations G1 and G5)

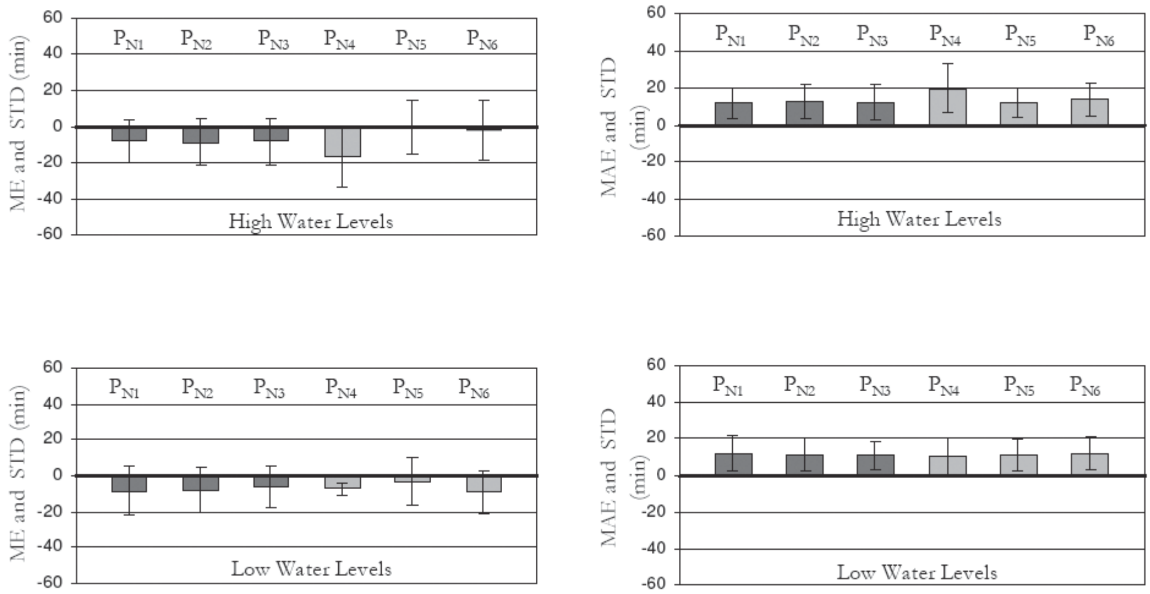

a) Gauge Station 1

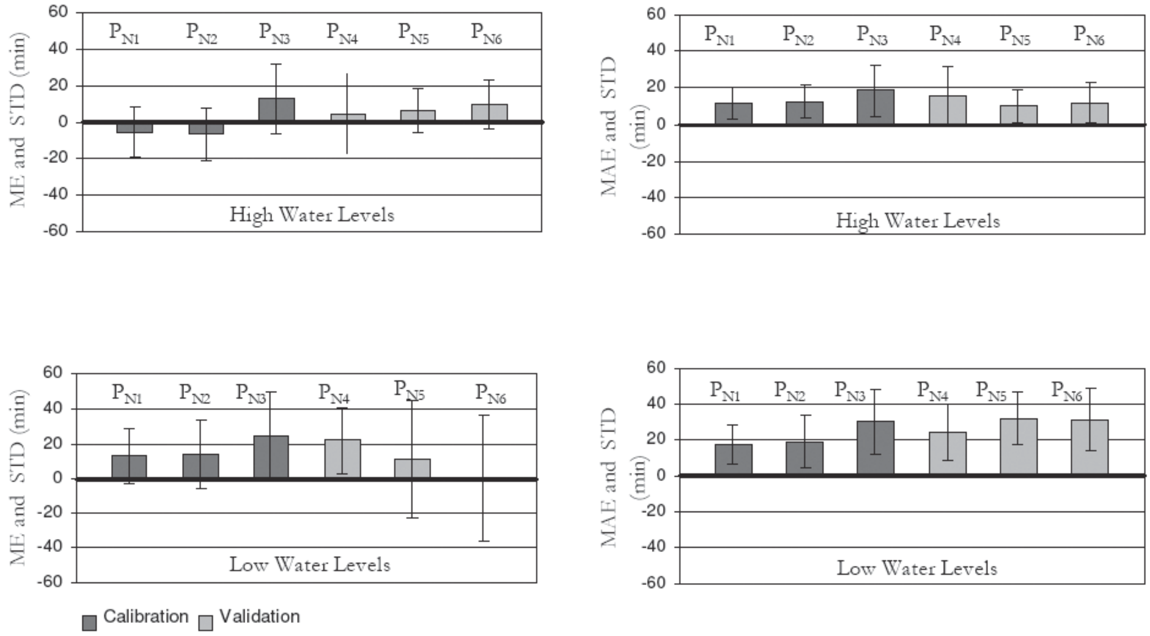

b) Gauge Station 5

Fig. 13: Mean Error (ME), Mean Absolute Error (MAE), and corresponding standard deviations of phases at high and low water levels (gauge stations G1 and G5)

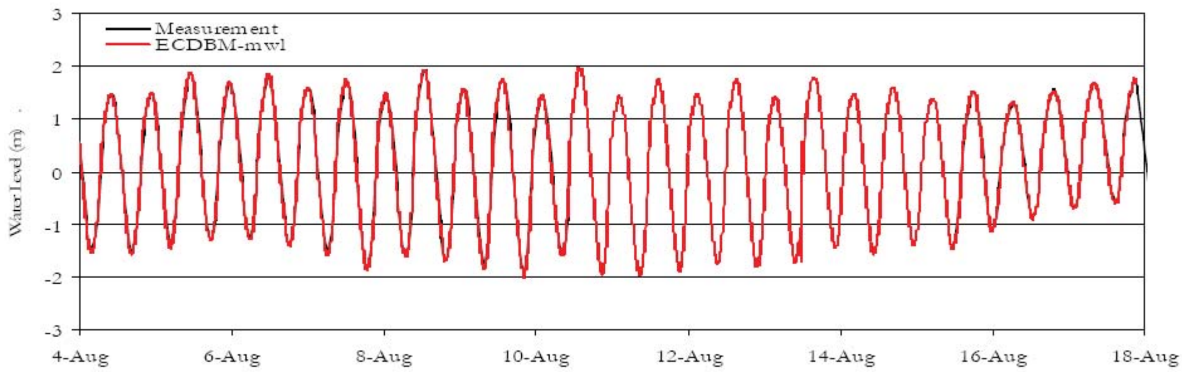

a) Gauge Station G1 (Blauort)

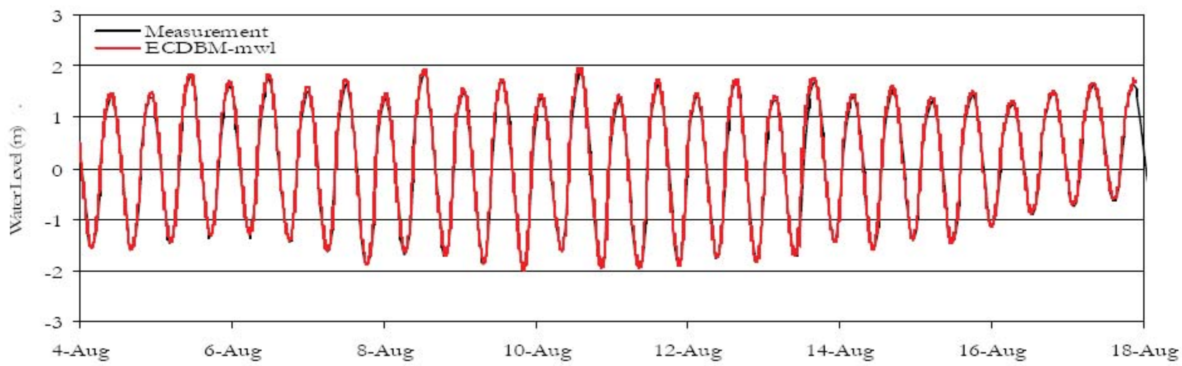

b) Gauge Station G2 (Tertius)

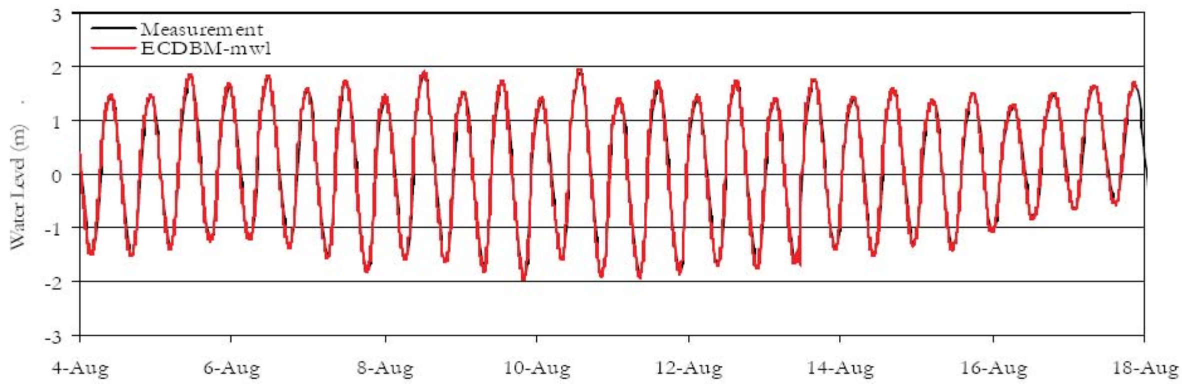

c) Gauge Station G3 (Trischen)

Fig. 14: Comparisons between measured and computed water levels at gauge stations G1 to G3 for observation period P_{N4}

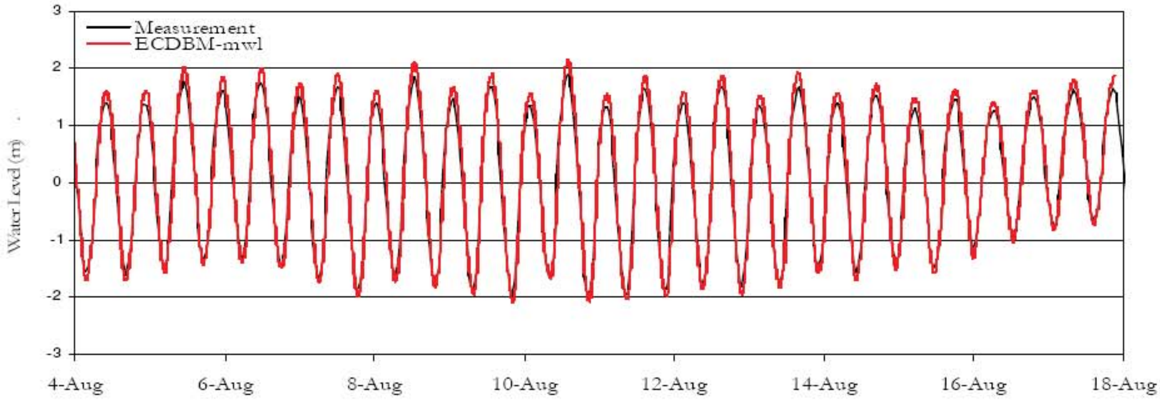

a) Gauge Station G4 (Buesum)

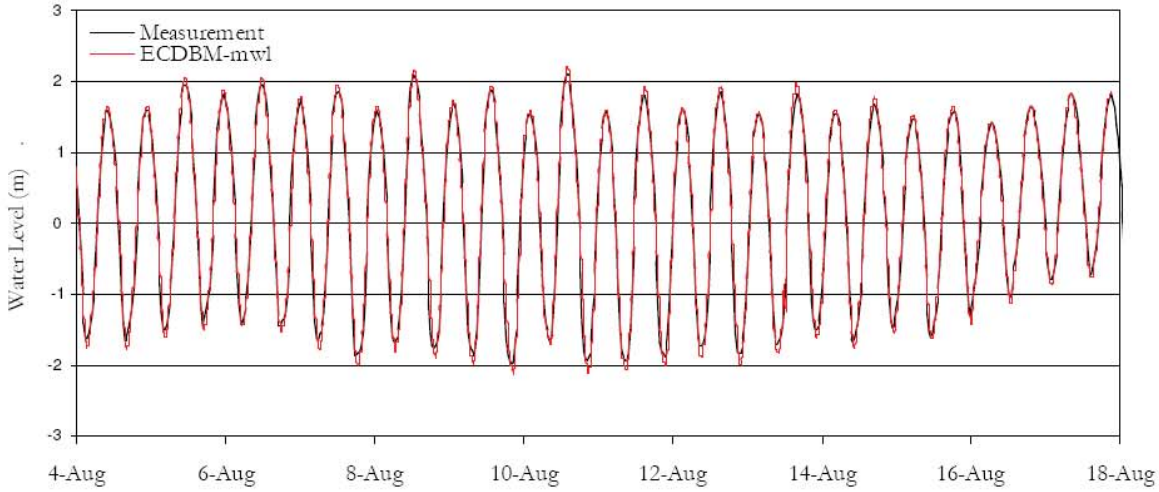

b) Gauge Station G5 (Steertloch)

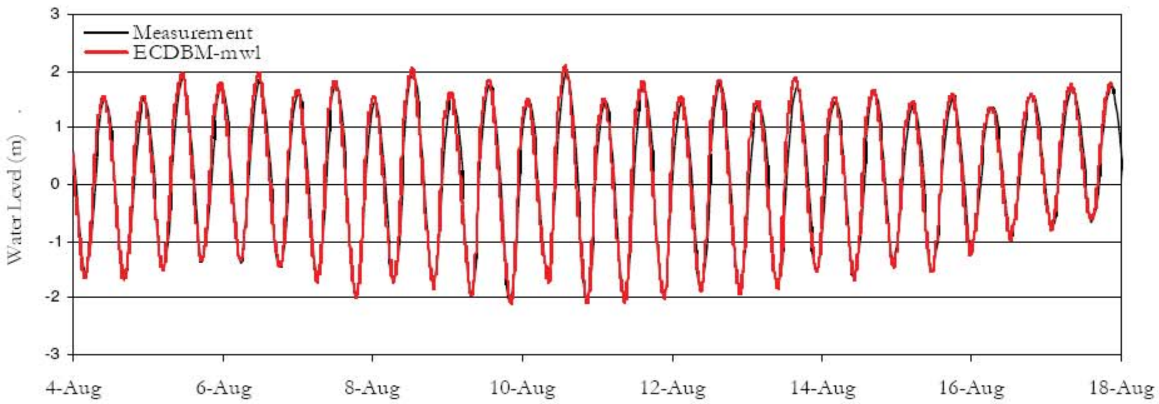

c) Gauge Station G6 (Flackstrom)

Fig. 15: Comparisons between measured and computed water levels at gauge stations G4 to G6 for observation period P_{N4}

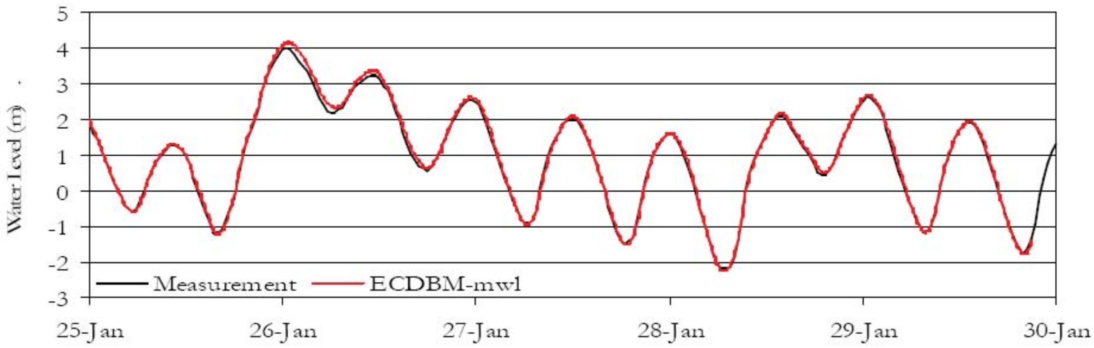

a) Period P_{S1}: Jan 25 to 31, 1990

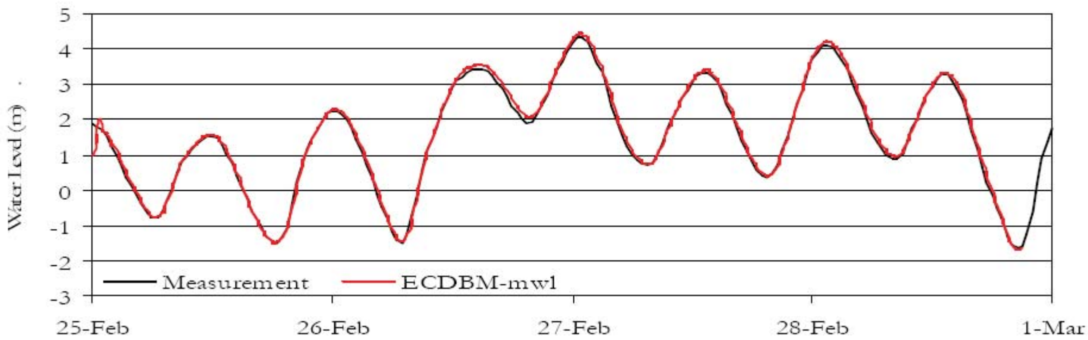

b) Period P_{S2}: February 25 to March 1, 1990

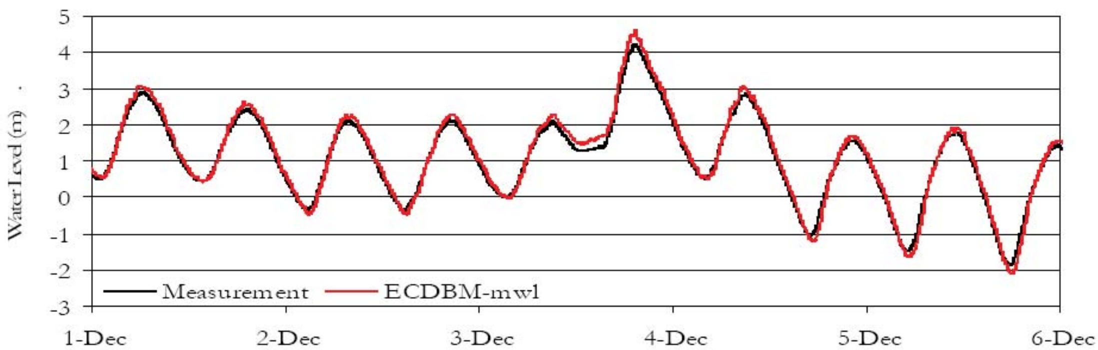

c) Period P_{S3}: December 1 to 6, 1999

Fig. 16: Comparisons between measured and computed water levels during storm periods at gauge station G1 (Blauort)

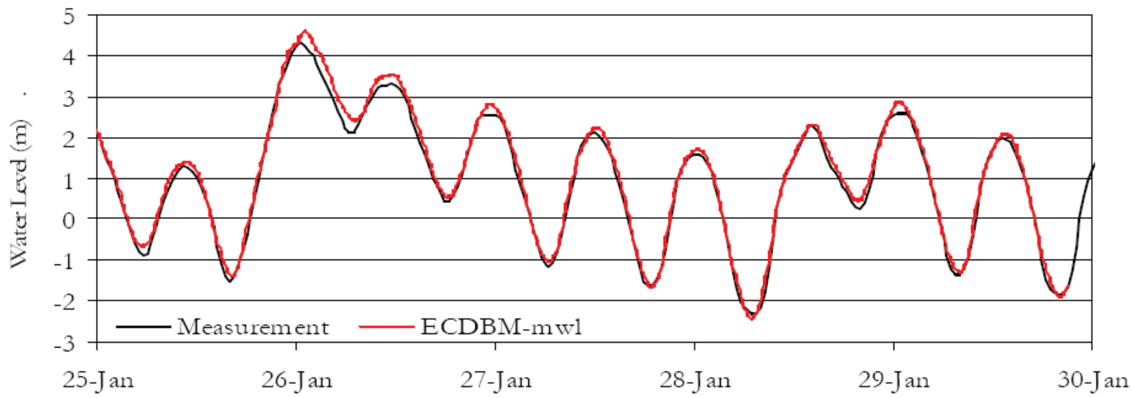

a) Period P_{S1}: Jan 25 to 31, 1990

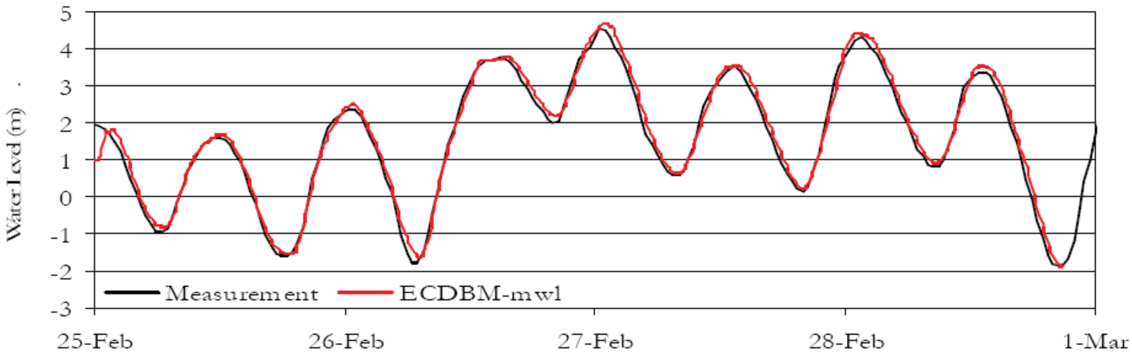

b) Period P_{S2}: February 25 to March 1, 1990

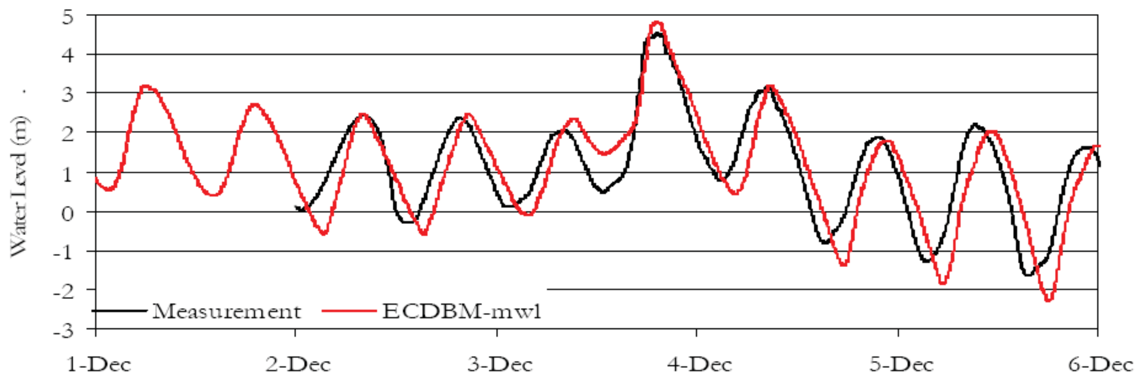

c) Period P_{S3}: Dec 1 to 6, 1999

Fig. 17: Comparisons between measured and computed water levels during storm periods at gauge station G4 (Buesum)

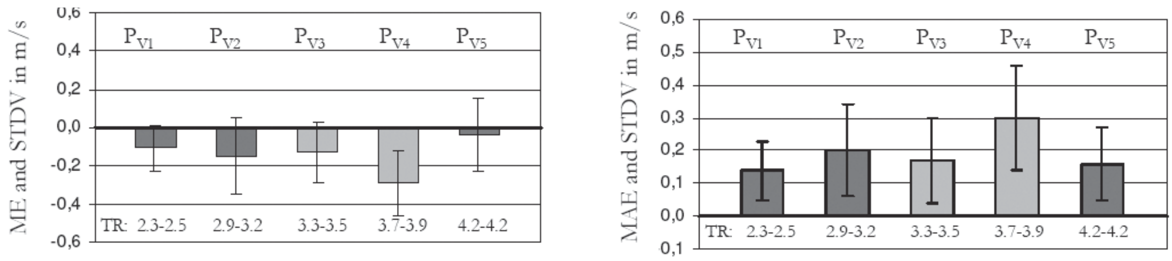

a) Cross-section T1

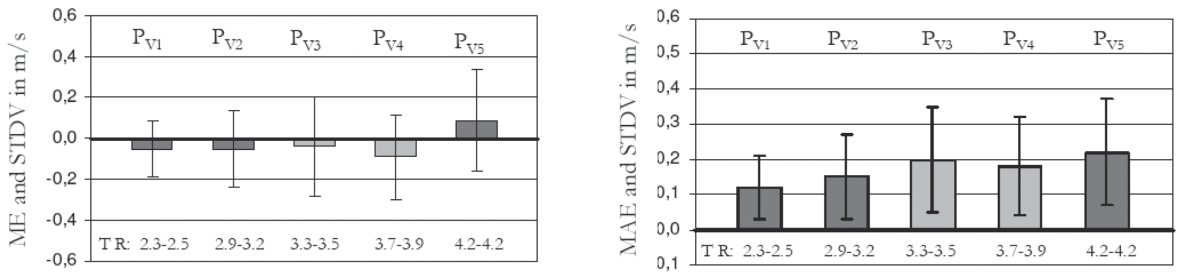

b) Cross-section T2

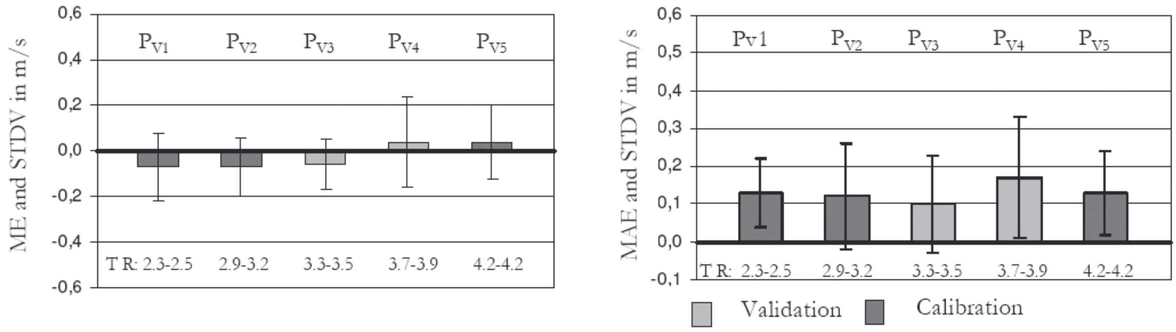

c) Cross-section T3

Fig. 18: Mean error (ME), Mean Absolute Error (MAE), and corresponding standard deviations of depth-averaged current velocities at cross-sections T1 to T3 for observation periods P_{V1} to P_{V5} shown in Table 2

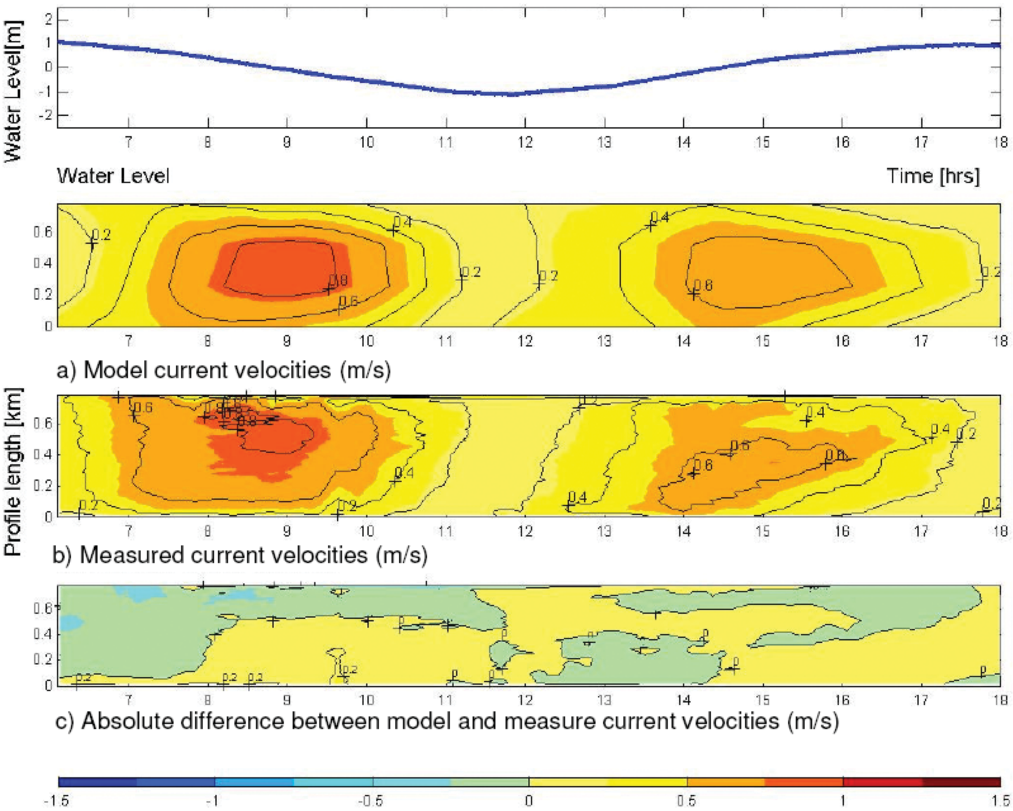

Fig. 19: Measured versus computed variation in depth-averaged current velocity at cross-section T1 on December 5, 2000

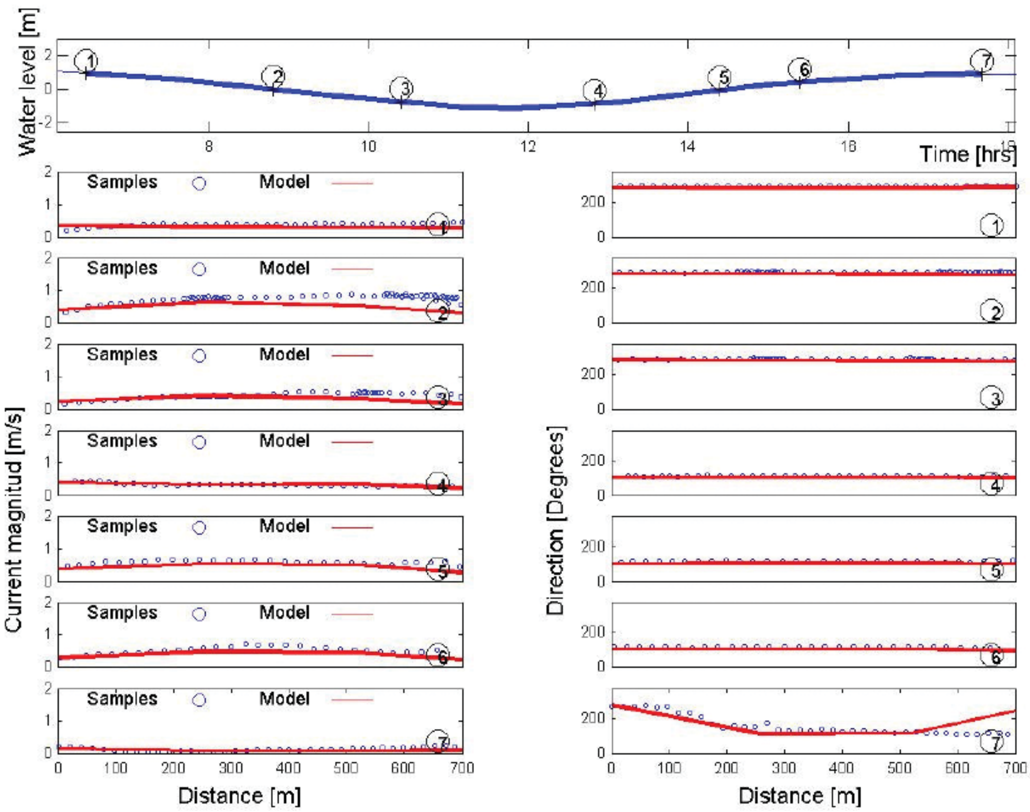

Fig. 20: Measured versus computed variation of cross-sectional distribution of current velocity at cross-section T1 on December 5, 2000

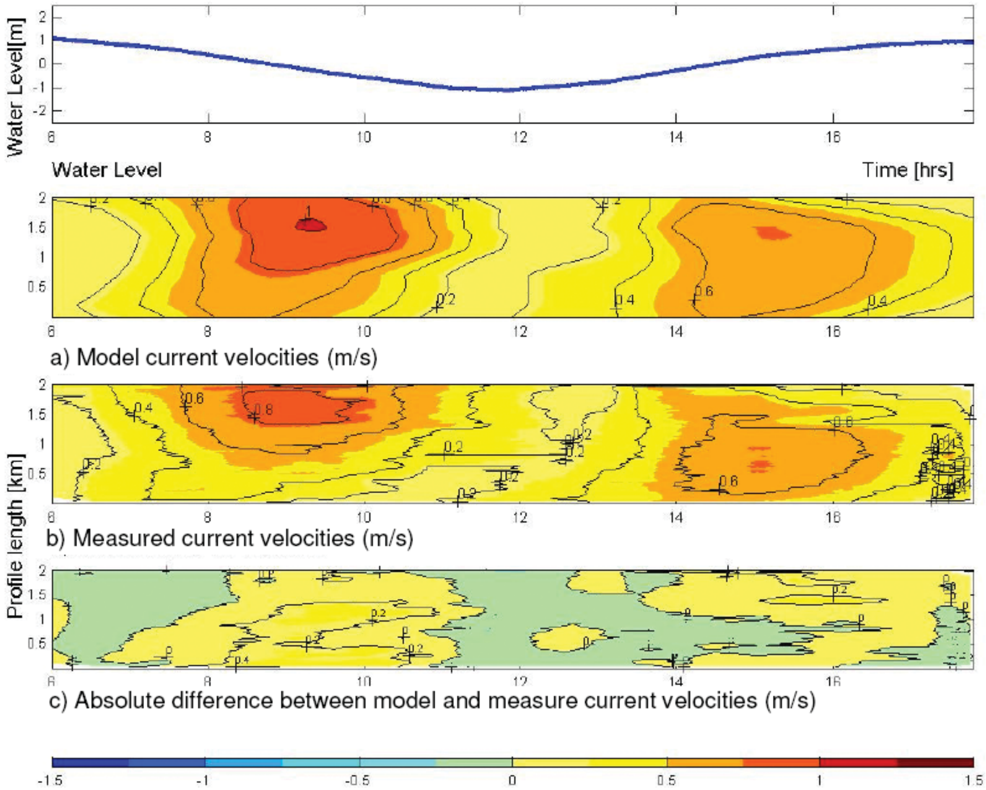

Fig. 21: Measured versus computed variation in depth-averaged current velocity at cross-section T2 on December 5, 2000

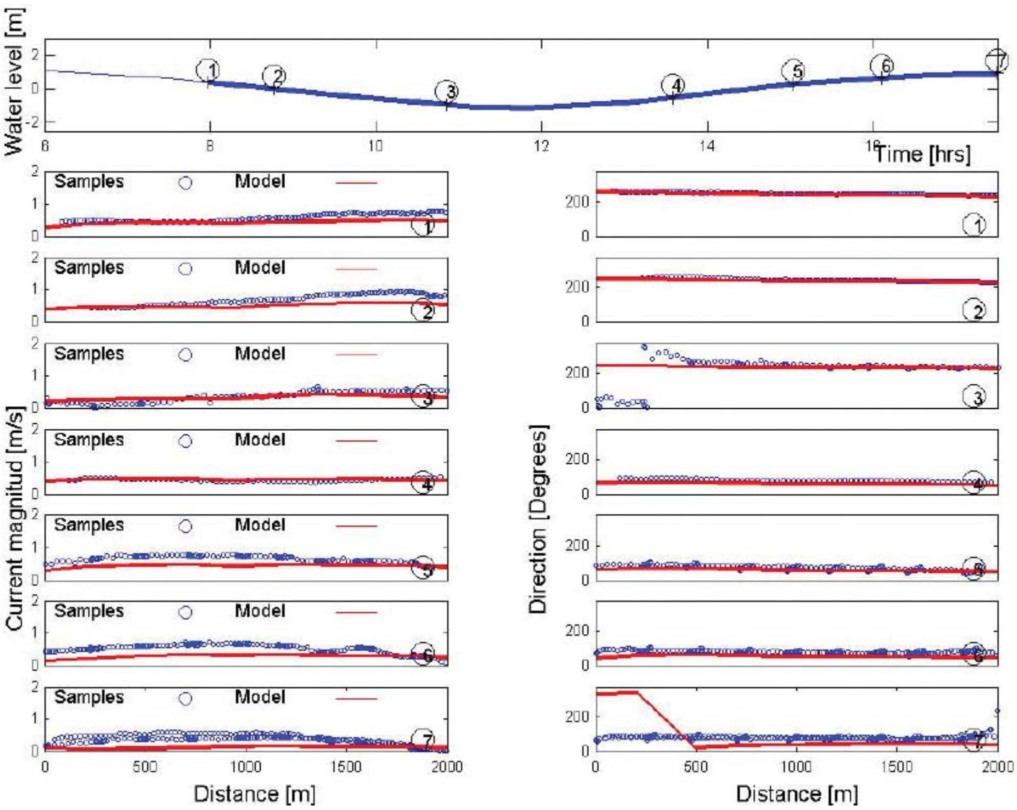

Fig. 22: Measured versus computed variation of cross-sectional distribution of current velocity at cross-section T2 on December 5, 2000

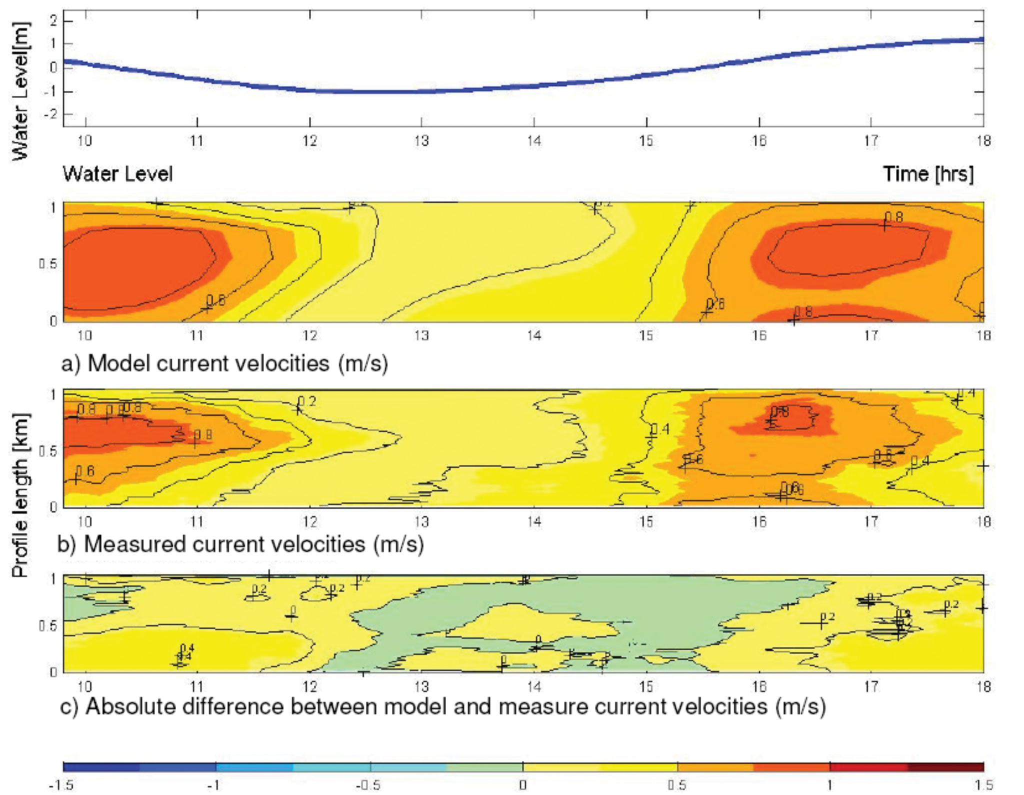

Fig. 23: Measured versus computed variation in depth-averaged current velocity at cross-section T3 on December 6, 2000

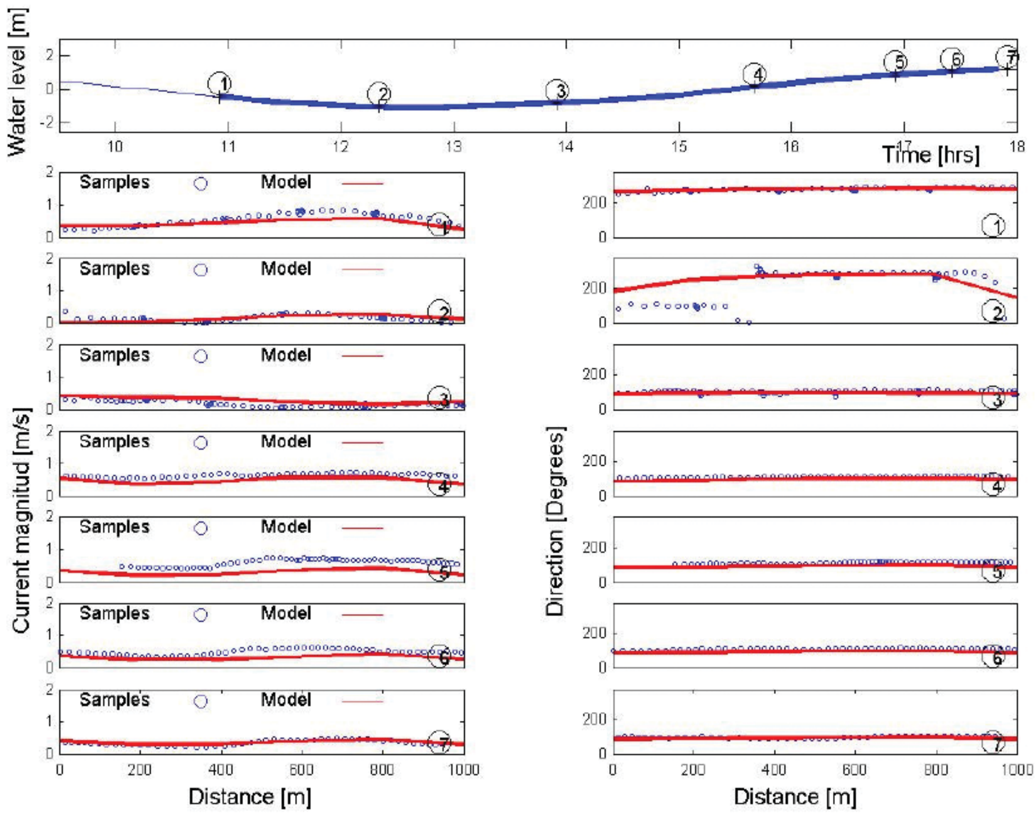

Fig. 24: Measured versus computed variation of cross-sectional distribution of current velocity at cross-section T3 on December 6, 2000

9. Conclusions

- This paper describes the development stages of a flow model for the central Dithmarschen Bight. The flow model was developed in several steps, including model set-up, sensitivity studies, and model calibration and validation. A two-dimensional depth-integrated flow approximation based on the DELFT3D Modelling System developed by Delft Hydraulics in the Netherlands was implemented in the study.
- Three flow models covering areas ranging from 300 km^2 to 1640 km^2 were set-up. The models implement curvilinear grid systems adjusted to the bathymetry derived from measurements made in 1998. Bathymetric maps prepared in 1990 were employed for modelling the tidal flat regions of the study area. In the model simulations water levels were imposed along the open sea boundaries and wind data were specified at the grid nodes using the PRISMA wind interpolation model developed at the Max Planck Institute of Meteorology in Hamburg (LUTHARDT, 1987). Flow discharges were specified along the open boundaries at the mouths of the Eider and Elbe estuaries.
- Sensitivity studies were carried out in order to assess the relative influence of the main physical and numerical model parameters on computed water levels and current velocities at various locations and cross-sections in the modelled domain. The optimum settings were determined. The sensitivity studies also revealed that wind speeds below 8 m/s have almost no effect on local water levels or depth-averaged current velocities. By comparing the results of simulations with and without the effect of waves it was found that although the effect of waves on currents is negligible in the tidal channels, this can be appreciable on the sandbanks. The relevance of three-dimensional flow model approximations was also investigated. A comparison between depth-averaged velocity distributions (2DH model) and averaged three-dimensional velocity profiles over the vertical (3D model) yielded similar results during the flood and ebb phases. The most pronounced differences between the simulation results occur at slack water, particularly during current reversal.
- A central aspect of the investigation concerns model calibration and validation based on extensive field measurements. In addition to water level recordings at several gauge stations covering several months, selective measurements of current velocities over a number of cross-sections in the main tidal channels covering the entire range of tidal conditions were employed for this purpose. Based on the quality standards normally adopted (WALSTRA et al., 2001; VAN RIJN et al., 2002), the performance of the model with regard to current velocity predictions was estimated to lie between excellent and good. In view of the fact that these assessments are still in their infancy, further work is necessary to arrive at generally acceptable standards.
- It was found that the predictive capability of the flow model mainly depends on the hydrodynamic forcing specified along the open sea boundaries. More detailed investigations of the effects of hydrodynamic forcing along the open sea boundaries of coastal models are presented in MAYERLE et al. (in this volume(b)). All of the approaches considered yield good predictions regarding water levels and current velocities. Slightly better agreement was obtained by specifying water levels measured at gauge stations along the open sea boundaries. In view of the latter, this approach was subsequently adopted throughout this study.
- The influence of bathymetry on water levels and particularly current velocities is also significant, bearing in mind that seasonal variations in seabed levels may be as much as 3 to 5 m. A certain percentage of the observed discrepancies is thus attributable to a dynamically changing bathymetry, which is not accounted for in the model.

- Investigations were also carried out to assess the effects of varying bed roughness on flow conditions in the modelled domain. It was found that relatively small equivalent roughness sizes corresponding to Chézy coefficients of about 60 $m^{1/2}/s$ yielded the best agreement between measured and computed current velocities. Although the effects of bed roughness were found to have a minor influence on the overall flow field, investigations by MAYERLE et al. (in this volume(a)) have shown that bed roughness may have a significant effect on sediment transport. It was found that the spatial variation of bed-form dimensions and associated roughness values are highly dependent on the layer thickness of potentially mobile sediments, the characteristics of superficial seabed sediments, and local flow conditions. In view of the fact that spatial variations in bed roughness may significantly affect bed shear stresses and hence sediment transport rates, it is important to take account of the latter in the flow model.
- Verification of the performance of the model for simulating water levels and current velocities was carried out for a wide range of conditions typical of the study area. The results showed that the flow model is capable of reproducing water levels and current velocities in the study area in fair agreement with observations. In general, the mean absolute error in terms of water levels at various locations over a period of several months was found to lie below 10 cm and 20 cm at high and low water levels, respectively. This corresponds to less than about 3 % to 6 % of the mean tidal range. The mean absolute error in terms of depth-averaged current velocities in several cross-sections of the tidal channels for a wide range of conditions generally ranged between 0.12–0.22 m/s, corresponding to about 10 % to 20 % of the tidally-averaged value. In this respect, better agreement was obtained for smaller tidal ranges. As bed-form dimensions are directly related to tidal range, improvements in the predictive capability of the model may be achieved by adjusting the bed roughness accordingly.

10. Acknowledgements

The results presented in this paper form a contribution to the research project "Predictions of Medium-Scale Morphodynamics – PROMORPH". We would like to thank the German Ministry of Education and Research (BMBF) for funding the project (Funding number 03 F 0262A). Funds provided by COLCIENCIAS in Colombia to finance the doctorate studies of Dr. Carlos Palacio are also highly appreciated. We are also grateful to the staff of the Research and Technology Centre "Westcoast" of the University of Kiel for carrying out the field measurements. The Regional Office for Rural Areas (ALR) in Husum is acknowledged for kindly providing the water level data and bathymetric data for the tidal flat areas. We also wish to thank the Federal Maritime and Hydrographic Agency (BSH) in Hamburg for providing the bathymetric data in the tidal channels as well as the Max Planck Institute of Meteorology in Hamburg for providing the PRISMA model data. We are also indebted to Dr. Ian Westwood for his meticulous corrections and final proofreading of the English manuscript. The constructive comments by Dr.-Ing. V. Barthel and an anonymous reviewer are also gratefully acknowledged.

11. References

ASP NETO, N. E.: Long- to Short-term Morphodynamic Evolution of the Tidal Channels and Flats of the Dithmarschen Bight, German North Sea, Ph.D. thesis, University of Kiel, Germany, 2004.

HARTSUIKER, G.: Deutsche Bucht and Dithmarschen Bucht, Set-up and Calibration of Tidal Flow Models. Delft, Delft Hydraulics, Report H1821, 1997.

HIRSCHHÄUSER, T. and ZANKE, U.: Morphologische Langfristprognose für das System Tidebecken-Außenände am Beispeil Sylts und der Dithmarscher Bucht, Die Küste, Heft 64, 2001, pp 127–160.

JIMÉNEZ-GONZÁLEZ, S.; MAYERLE, R. and EGOZCUE, J. J.: A Proposed Approach for Determination of the Accuracy of Acoustic Profilers for Field Conditions, Die Küste, Heft 69, 2005.

LUTHARDT, H.: Analysis of pressure and wind fields along the Nord Sea on the basis of routine observations (in German) Hamburger Geophysikalische Einzelschriften, Reihe A 83. Department of Geosciences, University of Hamburg, Germany, 109 pp., 1987.

MAYERLE, R.; PRAMONO, G. and ESCOBAR, C. A.: Dimension and Roughness Distribution of Bed Forms in Tidal Channels in the German Bight, Die Küste, Heft 69, 2005 (a).

MAYERLE, R.; WILKENS, J.; ESCOBAR, C. A. and WINDUPRANATA, W.: Hydrodynamic Forcing Along the Open Sea Boundaries of Small-Scale Coastal Models, Die Küste, Heft 69, 2005 (b).

PALACIO, C. A.; MAYERLE, R. and TORO, F. M.: Sensitivity analysis for the Meldorf Bight Hydrodynamic Model. XXX International Association of Hydraulic Engineering and Research Congress, Thessaloniki, Greece, August 2003.

POERBANDONO and MAYERLE, R.: Composition and Dynamics of Sediments in Tidal Channels of the German North Sea Coast, Die Küste, Heft 69, 2005 (a).

RICKLEFS, K. and ASP NETO, N. E.: Geology and Morphodynamics of a Tidal Flat Area Along the German North Sea Coast, Die Küste, Heft 69, 2005.

ROELVINK, J. A. and VAN BANNING, G. K. F. M.: Design and Development of DELFT3D and Application to Coastal Morphodynamics, Hydroinformatics '94, Verwey, Minns, Babovic & Maksimovic [eds], Balkema, Rotterdam, pp. 451–455, 1994.

TORO, F.; MAYERLE, R.; POERBANDONO and WILKENS, J.: Patterns of Hydrodynamics in a Tide-Dominated Coastal Area in the South-Eastern German Bight, Die Küste, Heft 69, 2005.

VAN RIJN, L. C.; WALSTRA, D. J. R.; GRASMEIJER, B.; SUTHERLAND, J.; PAN, S. and Sierra, J. P.: Simulation of Nearshore Hydrodynamics and Morphodynamics on the Time Scale of Storms and Seasons Using Process-Based Profile Models. In Van Rijn, L. C., B. G. Ruessink and J. P. M. Mulder (ed.), The Behaviour of a Straight Sandy Coast on the Time Scale of Storms and Seasons: Process Knowledge and Guidelines for Coastal Management: End Document March 2002. EC MAST Project, MAS3- CT97-0086 COAST3D – EGMOND, 2002.

WALSTRA, D. J. R.; VAN RIJN, L.; BLOGG, H. and VAN ORMONDT, M.: Evaluation of a hydrodynamic area model based on the COAST3D data at Teignmouth 1999. Paper D4 of: COAST3D Final Volume of Summary Papers. Report TR121, HR Wallingford, UK, pp D4.1-D4.4, 2001.

WILKENS, J.: Medium Scale Morphodynamics of the Central Dithmarschen Bight, Ph.D. thesis, University of Kiel, Germany, (available under http://e-diss.uni-kiel.de/diss_1369/d1369.pdf), 2004.

WILKENS, J.; JUNGE, I. and HOYME, H.: Modelling of Waves in a Tidal Flat Area in the South-Eastern German Bight, Die Küste, Heft 69, 2005.

Die Küste, 69 PROMORPH (2005), 1-420

Modelling of Waves in a Tidal Flat Area in the South-Eastern German Bight

By JORT WILKENS, INGO JUNGE and HELGE HOYME

Summary

As part of the project PROMORPH funded by the German Federal Ministry of Education and Research the calibration, validation and application of four wave models for the central Dithmarschen Bight are presented in this paper. The models have been coupled to flow models, which is necessary for correctly modelling the wave characteristics in this tidal environment. In the calibration and validation measurements taken by five wave buoys over a period of one month were considered. Using the root mean average error (RMAE) evaluation, the model results are qualified as reasonable to good. Considering the complex hydrodynamic patterns and bathymetry of the area this is satisfactory. The validated models have been applied to analyse the wave height distribution over the area during moderate and storm scenarios. It is shown that during moderate conditions in the sheltered eastern part of the domain only locally generated waves with limited heights occur. During storm conditions wave heights may reach 2 m in the eastern part and 5 m near the outer edge of the tidal flats. Furthermore, the significance of wave-induced currents was investigated. It could be shown that the waves have a limited effect on the tidal currents in shallow areas. In the tidal channels the wave-induced currents are negligible. Coupled to the flow models, the wave models form a good basis for the morphodynamic model simulations that have been carried out within the project PROMORPH.

Zusammenfassung

Die vorliegende Arbeit zeigt die Kalibrierung, Validierung und Anwendung von vier Wellenmodellen im Untersuchungsraum der Dithmarscher Bucht. Die Modelle wurden mit Strömungsmodellen gekoppelt, um die Wellencharakteristik in dem tidegeprägten Wattgebiet mit guter Genauigkeit wiederzugeben. Der Kalibrierungs- und Validierungsprozess erfolgte mittels einer einmonatigen Seegangsmessung, die Aufzeichnungen von fünf Messbojen umfasst. Die erzielten Ergebnisse können unter Berücksichtigung der komplexen Strömungscharakteristik und der anspruchsvollen Bathymetrie als gut bezeichnet werden, was durch Ermittlung des „root mean average error“ (RMAE) belegt wird. Die validierten Modelle wurden anschließend eingesetzt, um die Wellenverteilung im Untersuchungsgebiet bei mäßigen Wetterbedingungen und unter Berücksichtigung eines Sturmereignisses zu ermitteln. Die Analyse der Wellenhöhen zeigt, dass bei moderaten Wetterbedingungen das Wellenfeld im östlichen, geschützten Teil des Untersuchungsgebietes allein lokal generierte Wellen enthält. Bei Sturmverhältnissen können die Wellenhöhen in diesem Abschnitt bis zu zwei Meter anwachsen. Am westlichen Rand des Wattgebietes erreichen die Wellen Maximalwerte um fünf Meter. Im Weiteren wurde der Einfluss der welleninduzierten Strömungen näher untersucht. Im westlichen Modellgebiet bei geringen Wassertiefen ist der Einfluss begrenzt, in den tieferen Tiderinnen sogar vernachlässigbar gering. Es lässt sich festhalten, dass die im Folgenden vorgestellten Modelle in der Lage sind, die beobachtete Wellencharakteristik in angemessener Weise zu reproduzieren. Gekoppelt mit entsprechenden Strömungsmodellen bilden sie die Grundlage für die weiterführenden morphodynamischen Simulationen im Rahmen des Forschungsprojektes PROMORPH.

Keywords

Wave Modelling, Wadden Sea, Dithmarschen Bight, Promorph, Calibration, Validation, RMAE, COWADIS, HISWA, SWAN, TOMAWAC, DELFT3D, TELEMAC, PROMORPH

Contents

1. Introduction

The objective of this investigation was to set up and optimise several wave models to be used as modules of morphodynamic models for the central Dithmarschen Bight in the southeastern North Sea (for details refer to HOYME, 2002 and WILKENS, 2004). Therefore, a focus was placed on the distribution of wave energy between the exposed western edge of the domain and the sheltered eastern part. Due to the fact that the wave models were to be applied in medium scale morphodynamic simulations, the computational requirements formed a restricting factor for their spatial and spectral resolution. The models were optimised through calibration on the basis of the results of several one-day periods during a one-month field campaign using five Wave Rider buoys. The analysis of the field data is described in Section 2. Consequently, their performance was evaluated in the validation process considering the entire measurement period. Several scenarios were simulated after a successful validation in order to investigate the significance and characteristics of waves in the study area.

A total of four wave models were set up. These models and their characteristics are the topic of Section 3. In Section 4 the set-up of the coupled flow-wave models is presented. This is followed by a description of the calibration and validation in Section 5. The validated wave models were applied to investigate the wave characteristics during moderate and storm conditions. Furthermore, the effect of wave induced currents on the main current regime was examined. These investigations are discussed in Section 6. In Section 7 the conclusions are given.

2. Field Data

For evaluation of the coupled flow-wave models, field data of bathymetry, water levels, waves and wind were considered.

Bathymetric data from 1995 to 1997 with varying coverage of the study area that were made available by the Federal Maritime and Hydrographic Agency (BSH) in Hamburg were used to generate the model bathymetries. Gaps were filled with bathymetric data from 1986 through 1993, provided by the Office of Rural Development (ALR) in Husum.

The ALR also provided the water level data for various stations that were used for the evaluation of the flow model results.

Field measurements of waves considered in this study were made available by the Coastal Research Station at Norderney and the Office of Rural Development in Husum, Germany. These measurements had been obtained using 5 waverider buoys deployed in September and October 1996 (KFKI project 'Bemessung auf Seegang' (grant number KFKI 45), funded by the German Ministry of Education and Research (BMBF) under grant number MTK 0561, NIEMEYER, 1997). 20-Minute records have been taken at hourly intervals. The locations of the buoys are shown in Fig. 1.

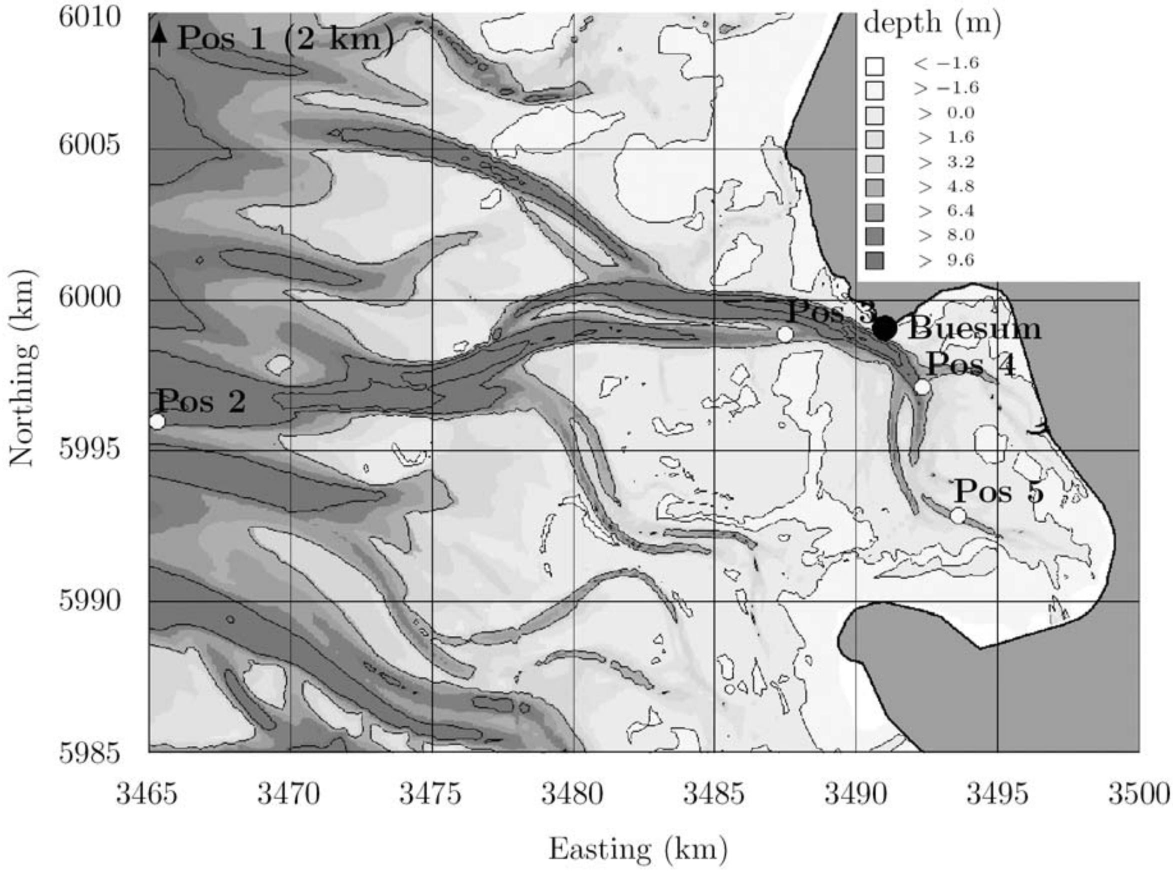

Fig. 1: Location of the wave measurements, taken during September and October 1996

The analysis of the wave data resulted in time series of significant wave height as shown in Fig. 2. Maximum values can be seen at the beginning and end of the observation period. They reach 2 m at Pos 1 and Pos 2, and up to 0.7 m at Pos 3, Pos 4 and Pos 5. During the intermediate period the waves are much lower. The wave heights at the western buoys are much higher than those of the three eastern buoys, due to the sheltering effect of the tidal flats.

Further wave data from two buoys near the study area taken during the storm event Anatol (see Section 6.3) were made available by the BSH.

Synoptic wind data sets were generated by using the PRISMA interpolation model developed by the Max Planck Institute of Meteorology (MPI-M) in Hamburg (LUTHARDT, 1987). This model creates temporally (every three hours) and spatially (approx. 42 km-spacing) varying wind fields from a large set of measurement locations along the coastline and offshore. Comparison of the synoptic model results to wind measurements at the Research and Technology Centre Westcoast (FTZ Büsum) for a period of 8 years confirmed the good quality of the PRISMA model, as shown in Fig. 3 (WILKENS, 2004). Due to the grid spacing of the PRISMA model, the selected output location was some 20 km westward (offshore) from Buesum. Together with the fact that the measurement station in Buesum is somewhat sheltered from westerly and northerly winds (pers. comm. Mr. Vanselow, FTZ Buesum) simulated values are slightly higher than measured ones (< 10 %).

Wind speed and direction in the study area as produced by the PRISMA model are shown in Fig. 4 for the wave observation period. It is apparent that calculated wind velocities are higher (up to 15 m/s) at the beginning and end of the period, corresponding to the peaks in the time series of significant wave heights of Fig. 2. The wind came from northwest during the beginning and from west during the end of the investigation period, causing sufficient fetch for waves to build up. The relatively strong wind in between, coming from the east, did not result in waves, as high as those by wind coming from the West. This is confirmed by the fact that the two western buoys do show some increase in wave height, related to the presence of a (limited) fetch, whereas the eastern buoys show no significant wave action.

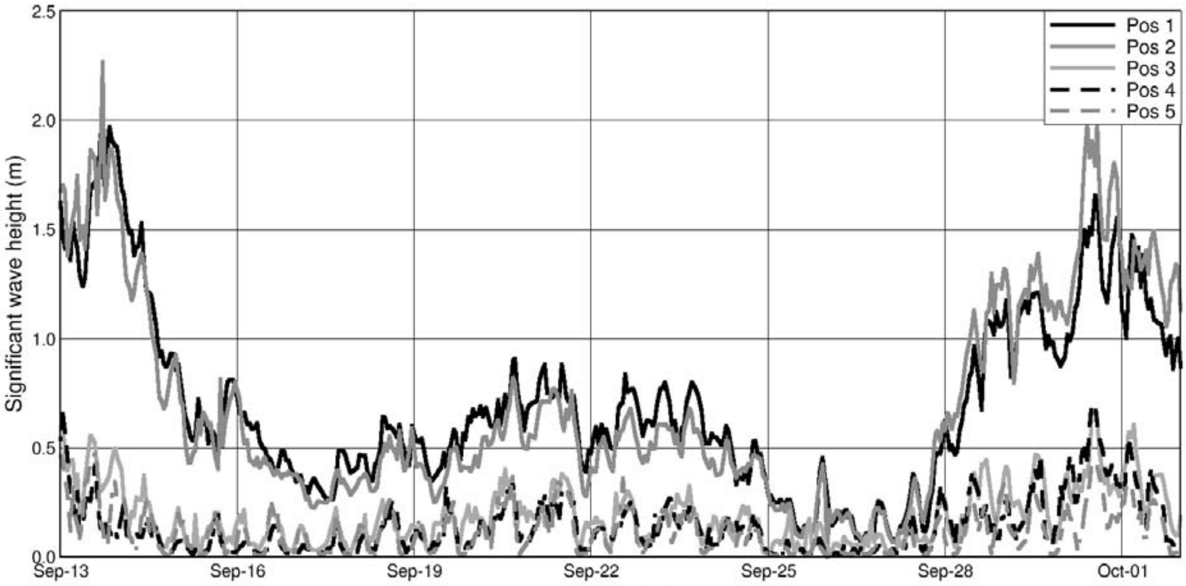

Fig. 2: Significant wave heights at the five wave buoys (data from NIEMEYER, 1997)

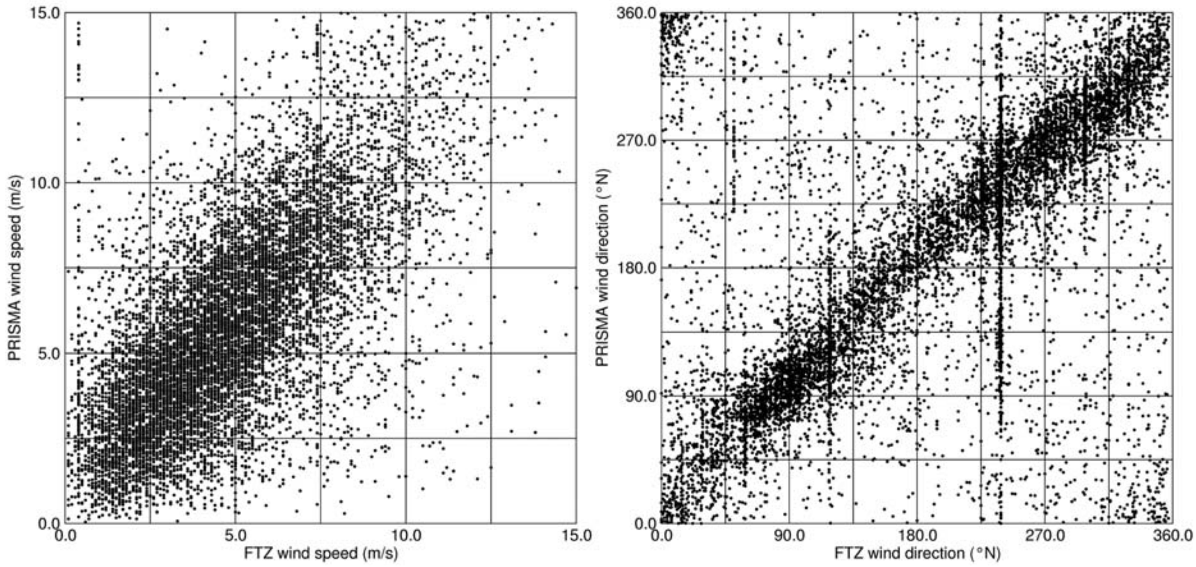

Fig. 3: Comparison between measured and PRISMA wind speed and direction at Büsum between March 1991 and December 1998 (WILKENS, 2004)

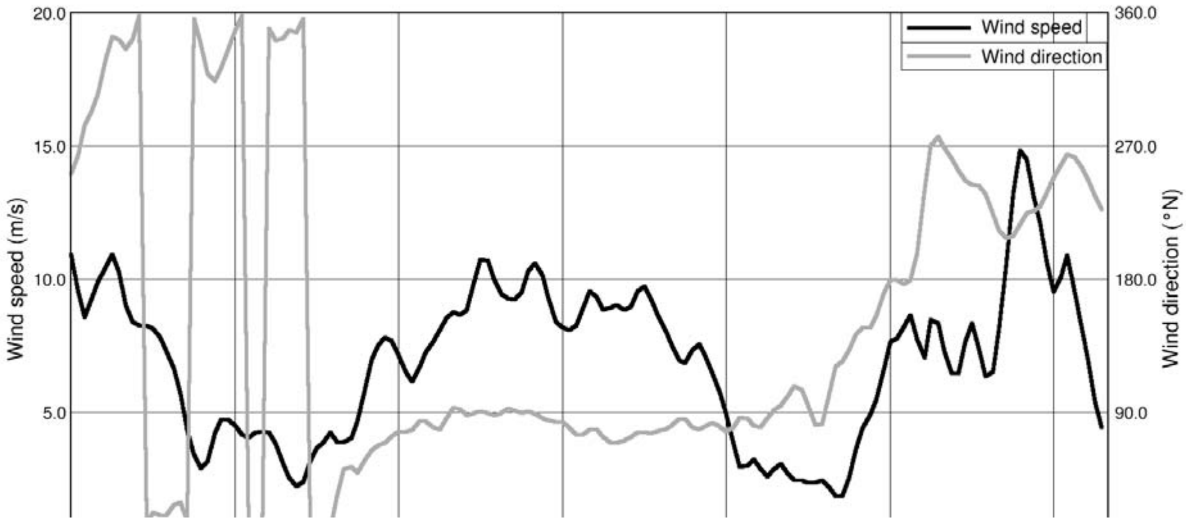

Fig. 4: Wind speed and direction during the wave measurement campaign. Based on the PRISMA interpolation model by LUTHARDT (1987)

3. Description of The Applied Wave Models

For a correct representation of the wave characteristics in the Meldorf Bight several phase-averaged wave models have been applied. Because of the influence of strong tidal currents in the channels as well as of varying water depths – particularly on and near tidal flats and shoals – all wave models were coupled to a flow model. Thus the ambient flow conditions are taken into account in the wave models.

The first two models used in the course of the investigation were set up within the DELFT3D modelling system, developed by Delft Hydraulics in the Netherlands (ROELVINK and VAN BANNING, 1994). The first was the wave model HISWA (HOLTHUIJSEN et al., 1998), the other one on the SWAN wave model (BOOIJ et al., 1999; RIS et al., 1999). These models have been developed at Delft Technical University in the Netherlands. The third and fourth wave model, COWADIS and TOMAWAC (BENOIT et al., 1996), are modules of the TELEMAC modelling system, developed by the Laboratoire National d'Hydraulique of the Electricité de France (refer to HERVOUET, 2000; GALAND et al., 1991). TELEMAC-2D provides the basis for currents and water levels and takes into account flow-wave interaction.

The HISWA wave model is a second generation stationary wave model that includes shoaling, refraction, wind-induced wave generation and energy dissipation due to wave breaking and bottom friction. The model is based on a parameterised formulation of the wave spectrum in the frequency domain and can only be applied on rectilinear grids.

The wave model SWAN is a third generation wave model, capable of simulating wave propagation, refraction, shoaling, wind-induced generation and dissipation due to white-capping, depth-induced wave breaking, bottom friction and wave-wave interactions. The model is fully spectral, meaning that it solves the spectral action balance for a specified number of directional sectors and frequency intervals. The model can be applied on both rectilinear and curvilinear grids.

The COWADIS wave model reproduces refraction due to the seabed and ambient currents, wave generation by wind, energy dissipation due to bottom friction, depth-induced wave breaking, white-capping and non-linear interactions, on a finite element grid.

The wave model TOMAWAC is a third generation wave model solving the balance equation of the action density directional spectrum, similar to the SWAN model. The main physical processes taken into account are wind shear stress, wave propagation, depth-induced refraction, shoaling, interaction with unsteady currents, non-linear wave-wave interactions and energy dissipation due to whitecapping, bottom friction, depth-induced wave breaking and wave blocking. Processes which are not included by the model are diffraction, reflection and wave blocking due to wind. It is noteworthy that in the present TOMAWAC release the COWADIS model is completely integrated. The user can activate the stationary model by choosing the steady parameterized mode. Otherwise the wave simulation is processed in the instationary third generation mode. In both cases the model runs on an unstructured triangular mesh.

The main characteristics of the four applied wave models are summarised in Table 1.

Table 1: Summary of the characteristics of the applied wave models

Model	**SWAN**	**HISWA**	**COWADIS**	**TOMAWAC**
Structure	Finite difference	Finite difference	Finite elements	Finite elements
Time dependency	Stat./instat.	Stationary	Stationary	Instationary
Frequency domain	Differentiated	Parametrical	Parametrical	Differentiated
Spectral shape	–	JONSWAP	JONSWAP	–
Direction domain	Differentiated	Differentiated	Differentiated	Differentiated
Refraction	Yes	Yes	Yes	Yes
Diffraction	No	No	No	No
Wind generation	Yes	Yes	Yes	Yes
Bottom friction	Yes	Yes	Yes	Yes
Depth-ind. breaking	Yes	Yes	Yes	Yes
Wave blocking	Yes	No	No	Yes
White-capping	Yes	No	Yes	Yes
Non-lin. interaction	Yes	No	Yes	Yes

4. Set-Up and Sensitivity Analysis

Only the HISWA model requires a grid orientation approximately parallel to the incident wave direction. Therefore, several grids have to be generated to cover the entire directional sector needed to represent these wave directions. The number of grids was varied in a sensitivity analysis. The sensitivity analysis for all applied models led to a basic configuration and a shortlist of calibration parameters.

For moderate conditions within the range of the field data (up to 2.5 m significant wave heights at the western edge of the domain, near Pos 1 and 2) the effect of waves on water levels and currents is limited, especially when considering that in a significant part of the investigation area strong tidal currents occur (see also Section 6.2). Therefore, a single forward coupling of the flow model to the wave model (solid lines in Fig. 5) was considered sufficient. For extreme conditions a second loop (dotted lines in Fig. 5) may be necessary when the wave-induced effects on the flow cannot be ignored. The coupling is schematically shown in Fig. 5.

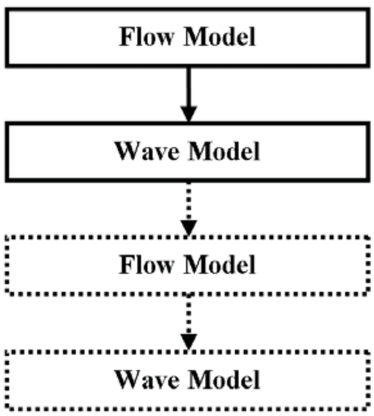

Fig. 5: Schematics of interaction between the coupled flow and wave models

Because of the different grid structures (see Table 1) and requirements, the horizontal extent and resolution vary. In Fig. 6 and Fig. 7 the grids for the COWADIS, TOMAWAC and the SWAN model are shown. The COWADIS and TOMAWAC grid is identical to the TELEMAC flow model grid whereas the SWAN model grid operates on the same grid as the DELFT3D flow model. Thus, interpolations during the information transfer between the flow and wave models are avoided. The rectilinear grid used for HISWA (not shown) consists of a large and a small grid for each direction. While the large grid covers the entire curvilinear flow grid, and provides the boundary conditions for a smaller high-resolution grid, the latter only covers the domain of interest. Due to geometrical differences between the HISWA wave grids and the flow grid, interpolations take place for the information transfer, constituting a source of inaccuracy. The grid resolutions of the four models are listed in Table 2. The COWADIS and TOMAWAC grids have the highest resolution concentrated on the eastern-most part of the domain (in Fig. 6). The SWAN and HISWA models cover a larger area, with the resolution increasing towards the area of interest with its tidal channels and flats (Fig. 7).

Within the DELFT3D modelling system, wave modelling can be carried out in stationary mode only, even though SWAN also contains an instationary. In combination with the TELEMAC system COWADIS can only be applied in stationary mode, too. A stationary model can produce satisfactory results when the time of wave propagation through the model domain is short in comparison with the time scale of the variation of the driving forces wind and swell. For the West-East domain length of approximately 30 km and typical wave speeds of 5 to 10 m/s, the wave conditions should remain relatively stable for a minimum period of 1 to 1.5 hours. This assumption holds for the available field data, considering the temporal resolution of the wind data and associated level of detail of the model evaluation, i.e. changes of wave characteristics on a time scale smaller than the temporal variability of the imposed wind data should not be evaluated. The variations in the tidal conditions, that are significant on a shorter time scale, are taken into account through the computational interval of one hour for the stationary models.

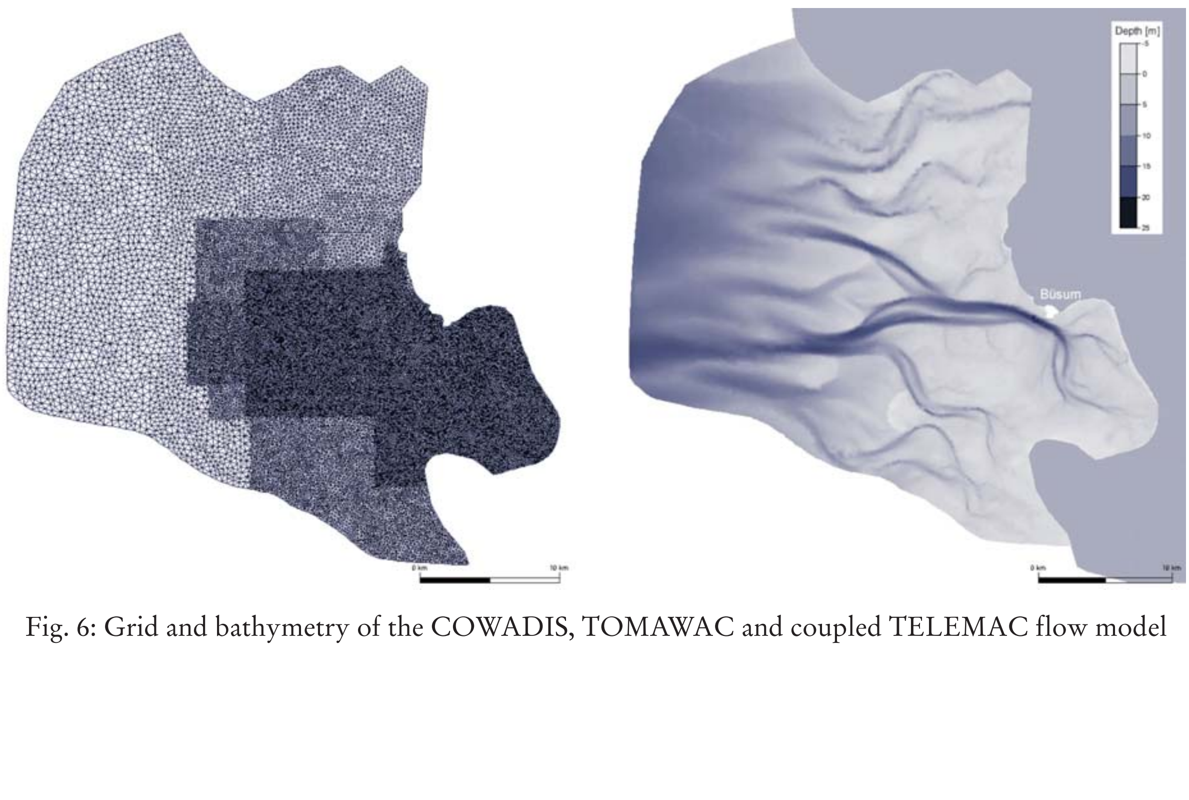

Fig. 6: Grid and bathymetry of the COWADIS, TOMAWAC and coupled TELEMAC flow model

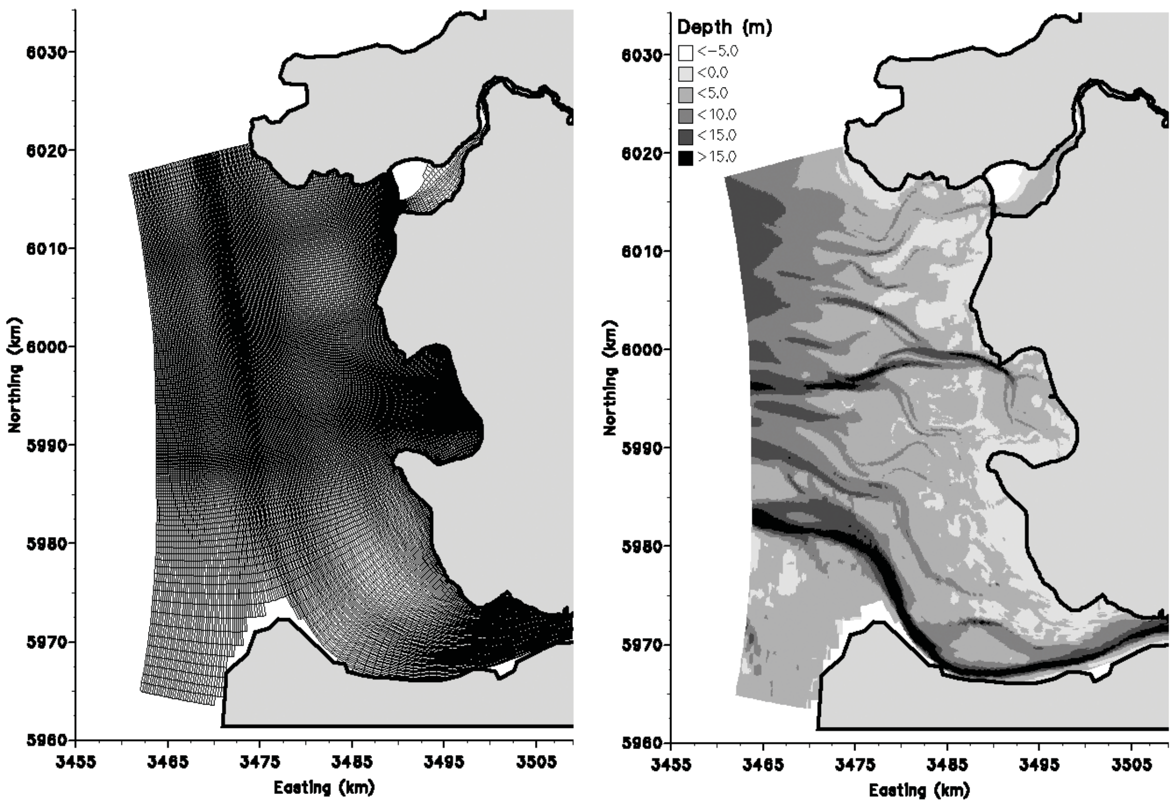

Fig. 7: Grid and bathymetry of the SWAN and coupled DELFT3D flow model

The spatial as well as the spectral resolution varies between the applied models. COWADIS and HISWA are parameterised in the frequency domain, i.e. a frequency-integrated energy and a mean frequency are computed rather than resolving the wave energy variation in the frequency domain, as the SWAN model does. All three models, however, solve the energy distribution over the directional space. The spectral resolution of the models was also defined on the basis of sensitivity analyses and is listed in Table 2.

Table 2: General settings of the applied wave models

Model	SWAN	COWADIS	HISWA	TOMAWAC
Cell size (m)	80–600	Triangles, 30–80	100–500	Triangles, 30–80
Time dependency	Stationary	Stationary	Stationary	Instationary
Frequency interval	~ 0.1 Hz (log.dist.)	–	–	~ .01 Hz (log.distr.)
Direction interval	15 degrees	30 degrees	10 degrees	30 degrees
Calculation interval	1 hour	1 hour	1 hour	–

5. Calibration and Validation of the Wave Models

5.1 HISWA and SWAN

In the calibration of the HISWA model only wave heights and directions were considered, for the SWAN model the peak periods have been analysed as well. Wave data from the outer buoys (Pos 1 and 2) were used as boundary values for the HISWA model, whereas the

SWAN model has been nested in a SWAN model for the German Bight. These German Bight model results were verified with the field data from the outer buoys. Fig. 8 and Fig. 9 show the measured and computed wave heights and periods at Pos 2. The main advantage of model nesting rather than imposing the field data directly is that periods outside the measurement period can be simulated as well. For the evaluation of the model performance the buoys in the inner part of the investigation area (Pos 3, 4 and 5 in Fig. 1) were considered.

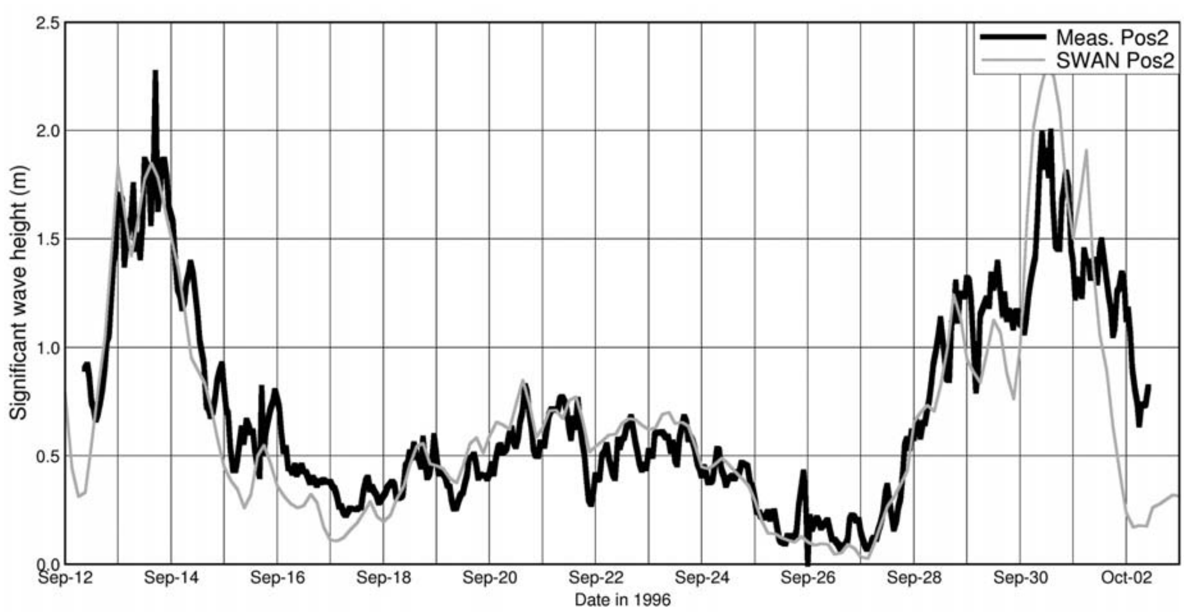

Fig. 8: Measured and computed significant wave heights at Pos 2, using model nesting

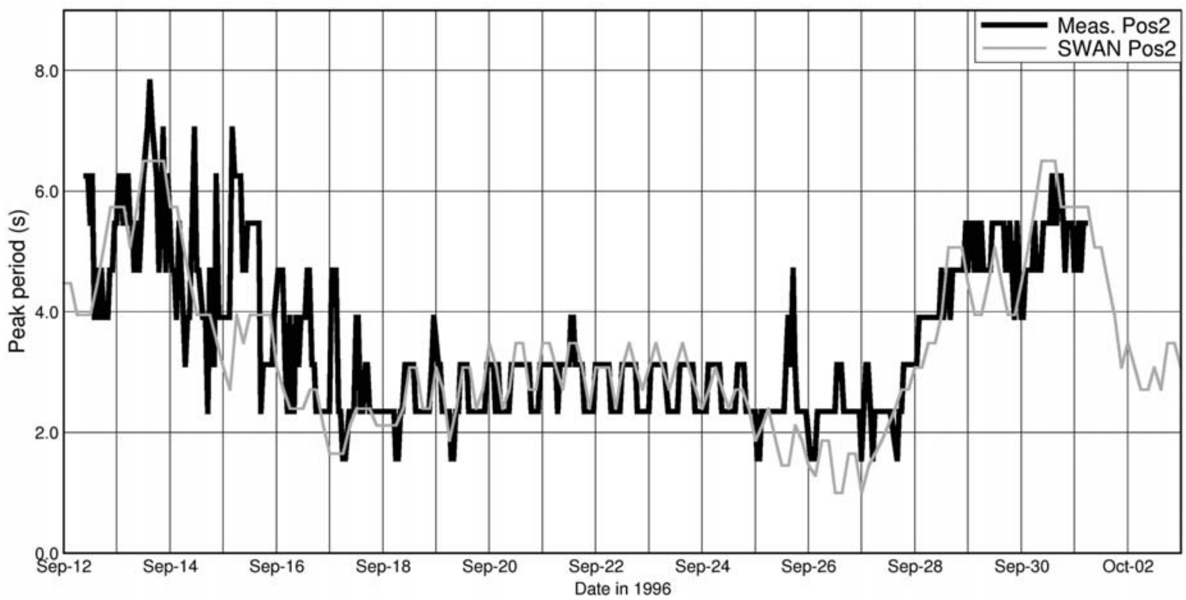

Fig. 9: Measured and computed peak periods at Pos 2, using model nesting

For calibration, five one-day periods with varying conditions were selected. Since the main objective of this study was to create a reliable wave model for deployment within a morphodynamic model, the computational efforts had to be kept within limits. Therefore, an increase of the horizontal and spectral resolution was not considered, although this might have improved the results through a more detailed representation of the bathymetry and local current patterns near the wave buoy locations. Main improvements could be made by tuning the bottom friction. Varying other parameters such as wave breaking and directional diffusion led only to insignificant improvements. The calibration study also led to the conclusion that an interval of one hour between the wave calculations was acceptable for the considered period. The variations in the ambient currents and water levels as well as the encountered wind conditions did not permit a larger interval.

On the basis of optimised model settings, the models were validated for the entire length of the field campaign. In a strict sense, the one-day calibration periods should have been excluded for validation of the models. However, they were included in the one-month simulation in order to obtain an uninterrupted overview of model quality during the entire period. The results of the validation are discussed in Section 5.3.

5.2 COWADIS and TOMAWAC

The calibration process of COWADIS was similar to that of HISWA. The procedure for the instationary TOMAWAC model, however, is different. During the simulation, the boundary conditions have been generated by the model in form of a JONSWAP-spectrum under considering of wind input (PRISMA data) and a presetting of a 250 km fetch length. For this reason, the calibration of TOMAWAC is based predominantly on data collected at wave buoys Pos 1, 2 and 3 (refer to Fig. 1).

5.3 Validation Results

The comparison between observed and computed wave heights of all four models, divided into three sections for more clarity, is shown in Fig. 10 to Fig. 12 for Pos 3 to 5. Fig. 13 to Fig. 15 show the comparison of the measured and computed peak periods (SWAN only).

All models reproduce the trend in wave height development quite well. HISWA reproduces the lower wave heights rather well, whereas SWAN shows good results for the higher wave heights (with some overpredictions). COWADIS shows good results for moderate wave conditions but under-predicts relatively high waves. The peak periods are somewhat underestimated by the SWAN model, however, they generally follow the observed trends in a good manner. The underestimation of the peak periods is a well-known problem of the SWAN model (ROGERS et al., 2003). Although TOMAWAC tends to under-predict low wave heights it does reproduce the observed trends and peak values. This is particularly true under easterly winds. It has to be mentioned again that the wave boundary conditions for this model were obtained by using wind input generated by the PRISMA model with a spatial resolution of approximately 42 km.

Although some discrepancies between the modelled and observed wave heights were found, generally speaking all models produce acceptable results for the entire period. Considering the relatively low waves, the complex bathymetry together with the strong ambient currents, the results are rather good.

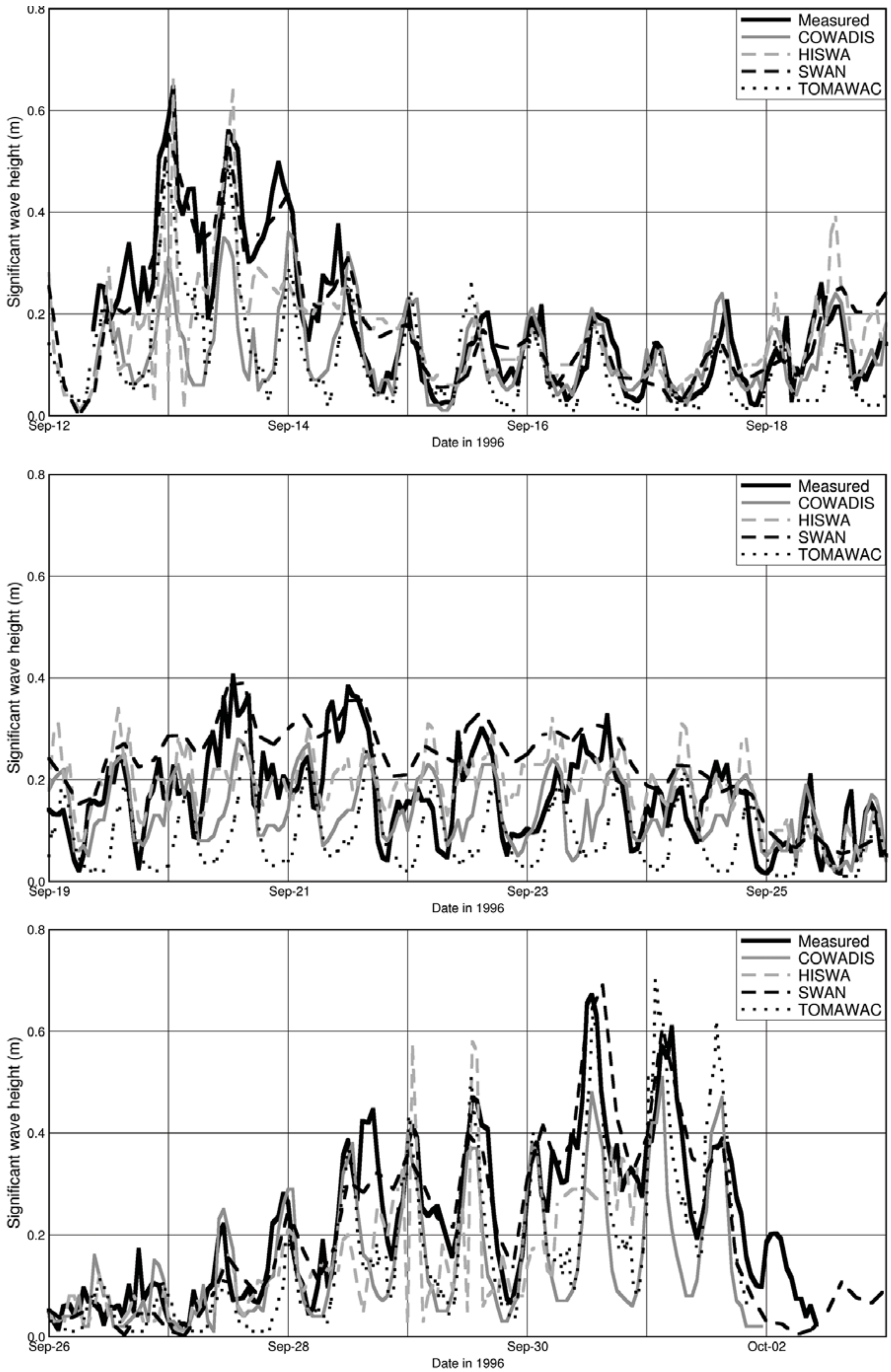

Fig. 10: Measured and computed significant wave heights at Pos 3 after model calibration

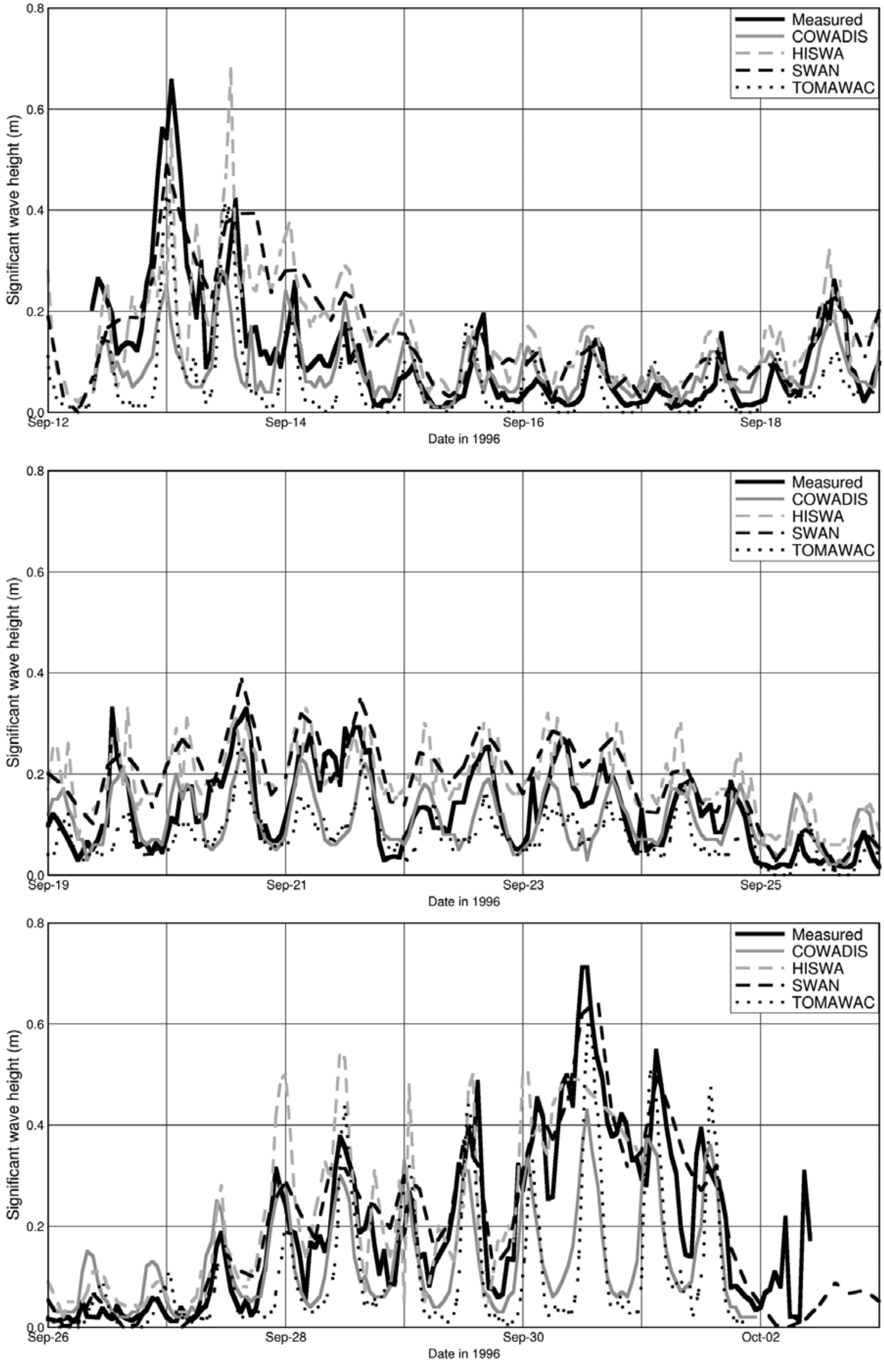

Fig. 11: Measured and computed significant wave heights at Pos 4 after model calibration

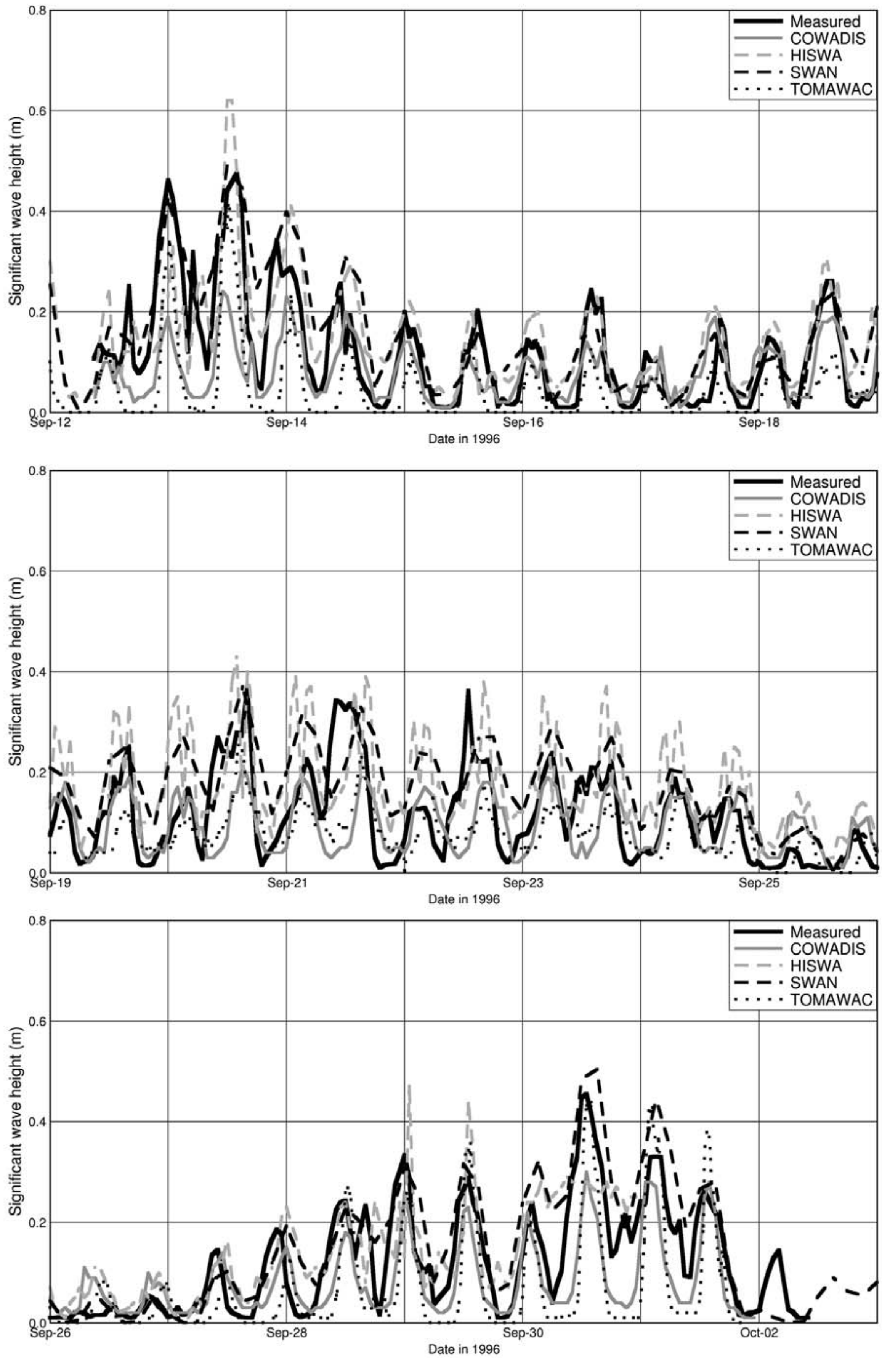

Fig. 12: Measured and computed significant wave heights at Pos 5 after model calibration

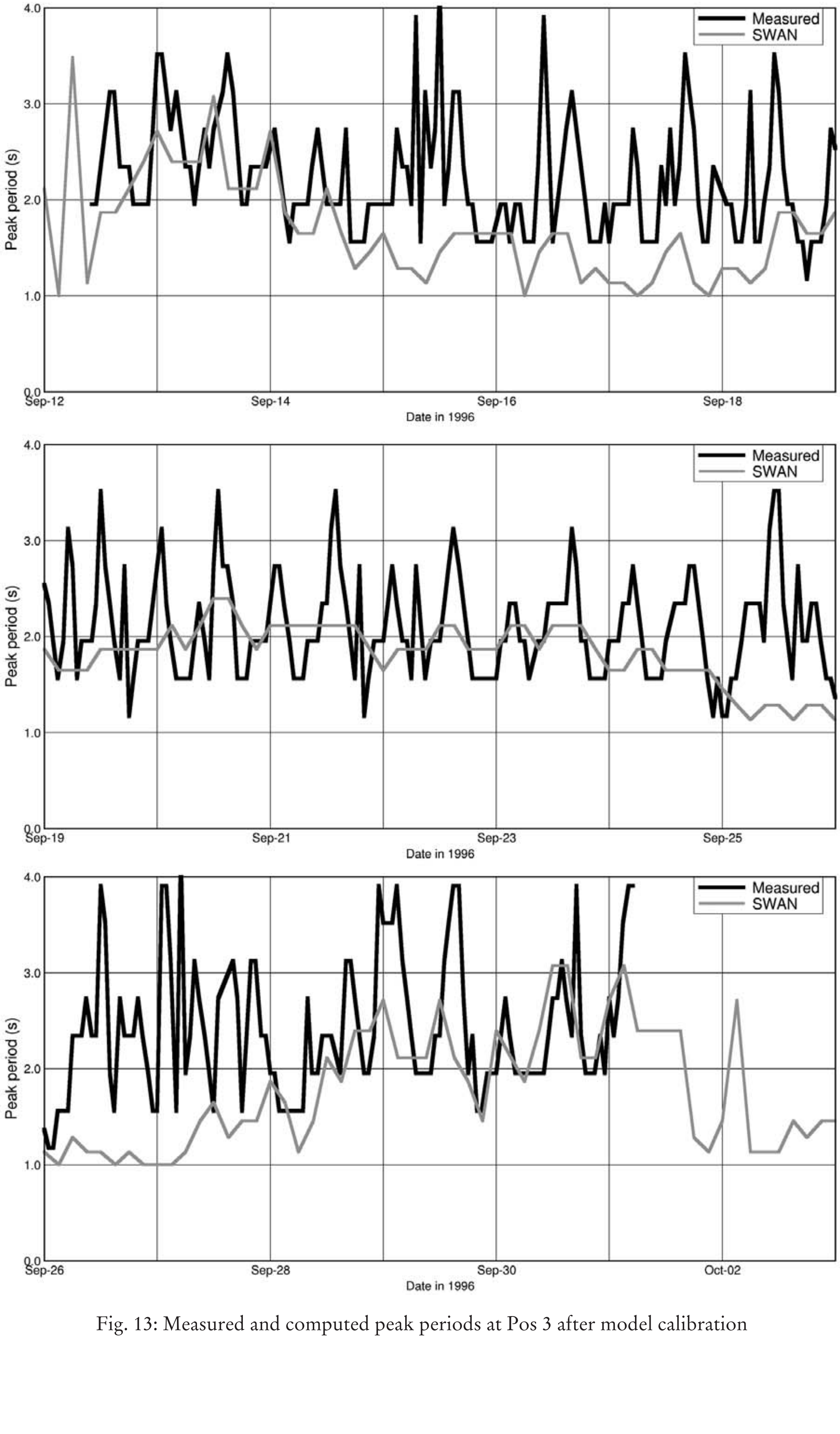

Fig. 13: Measured and computed peak periods at Pos 3 after model calibration

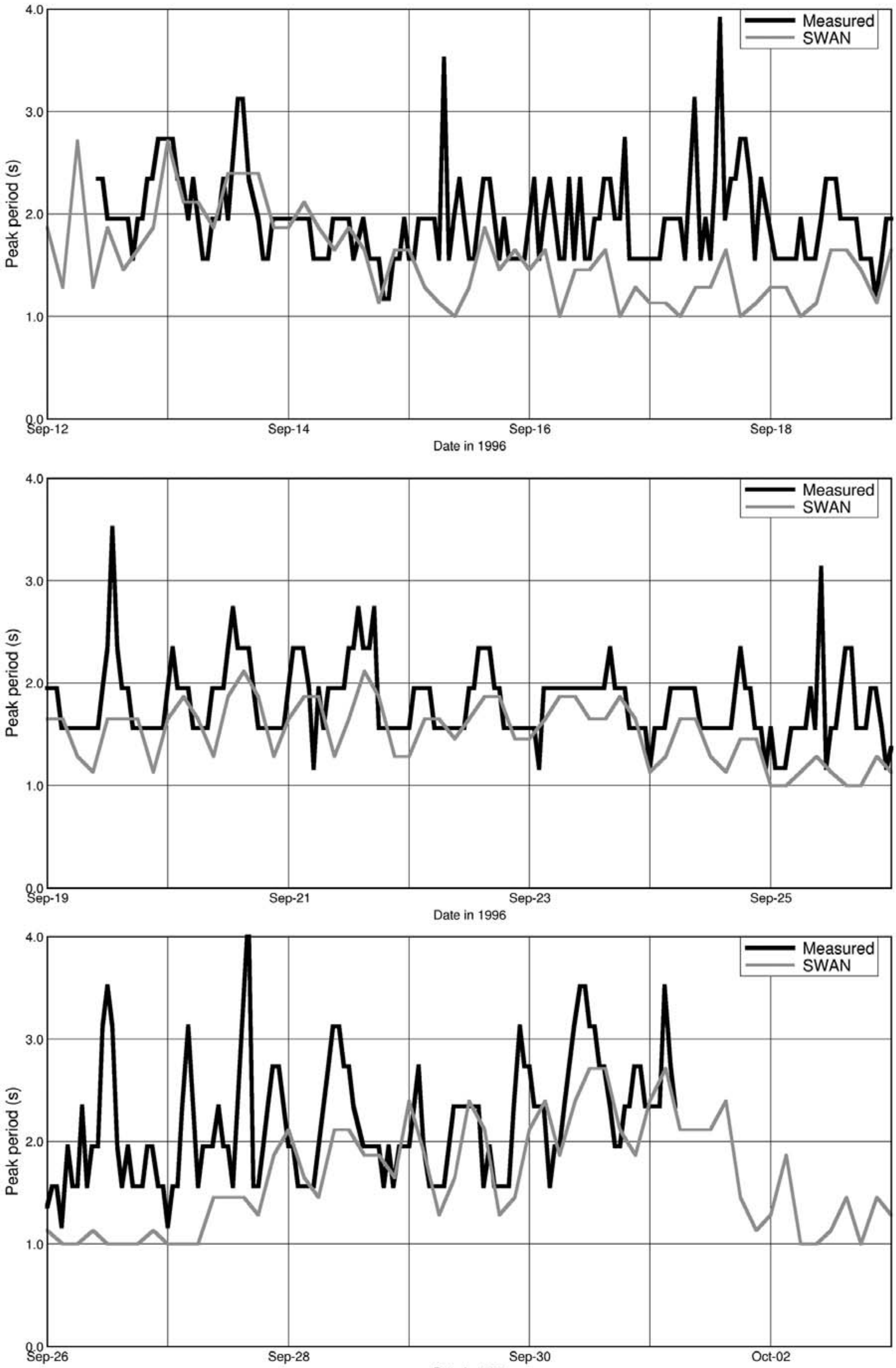

Fig. 14: Measured and computed peak periods at Pos 4 after model calibration

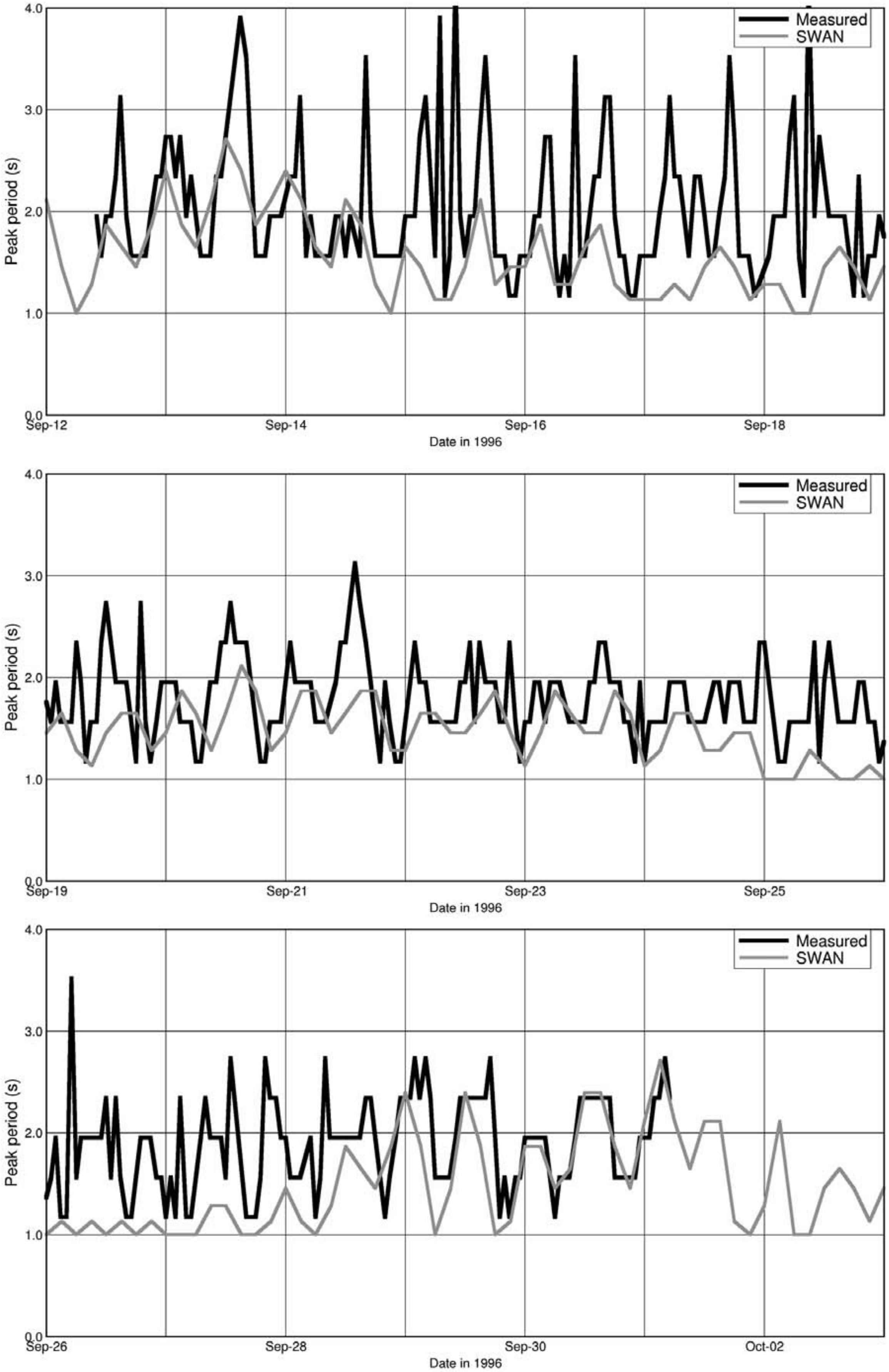

Fig. 15: Measured and computed peak periods at Pos 5 after model calibration

To evaluate the results more objectively than through visual comparison, the approach by VAN RIJN et al. (2002) was adopted in which the discrepancy between the computed and measured parameters is quantified through the relative mean absolute error (RMAE). The RMAE is defined as:

$$RMAE = \frac{\max\{|P_c - P_m| - \Delta P_m, 0\}}{\overline{P}_m}$$

with:

P_m = measured parameter (either wave height or period);
P_c = computed parameter; and
ΔP_m = inaccuracy of the measured parameter (value of 0.1 m respectively 0.3 s have been assumed).

The operator and denominator are averaged over the evaluation period. VAN RIJN et al. (2002) define the model quality based on the RMAE value for the significant wave heights as shown in Table 3. No such qualification is presently available for wave periods.

Table 3: Quality of simulated wave heights based on RMAE values (VAN RIJN et al., 2002)

Qualification	**RMAE value**
Excellent	< 0.05
Good	0.05 – 0.10
Reasonable / fair	0.10 – 0.20
Poor	0.20 – 0.30
Bad	> 0.30

Fig. 16 shows scatter plots of the modelled and measured significant wave heights at the three eastern wave buoys for the models COWADIS, HISWA and SWAN. The corresponding RMAE values are indicated in the top-left corner. In Fig. 17 the scatter plots of the peak periods are shown for the SWAN model, together with the RMAE values. Since the TOMAWAC model evaluation was carried out using data for Pos 1, Pos 2 and Pos 3, the corresponding scatter plots are shown in Fig. 18.

As can be seen, the quality index of the four wave models varies between "reasonable" and "good". The obtained RMAE values and the scatter plots confirm the findings based on the time series comparison. The SWAN model results show an over-prediction of the higher wave heights, especially for Pos 4 and Pos 5. The COWADIS and HISWA model show good results for the lower wave heights. The scatter plots of the peak periods show that the SWAN model underpredicts the wave periods, a general problem of SWAN for low-frequency energy (see for example ROGERS et al., 2003).

The TOMAWAC model shows good results for Pos 1 and Pos 2 and is less accurate for Pos 3. Once more considering the complex bathymetry and current patterns, the results are satisfactory.

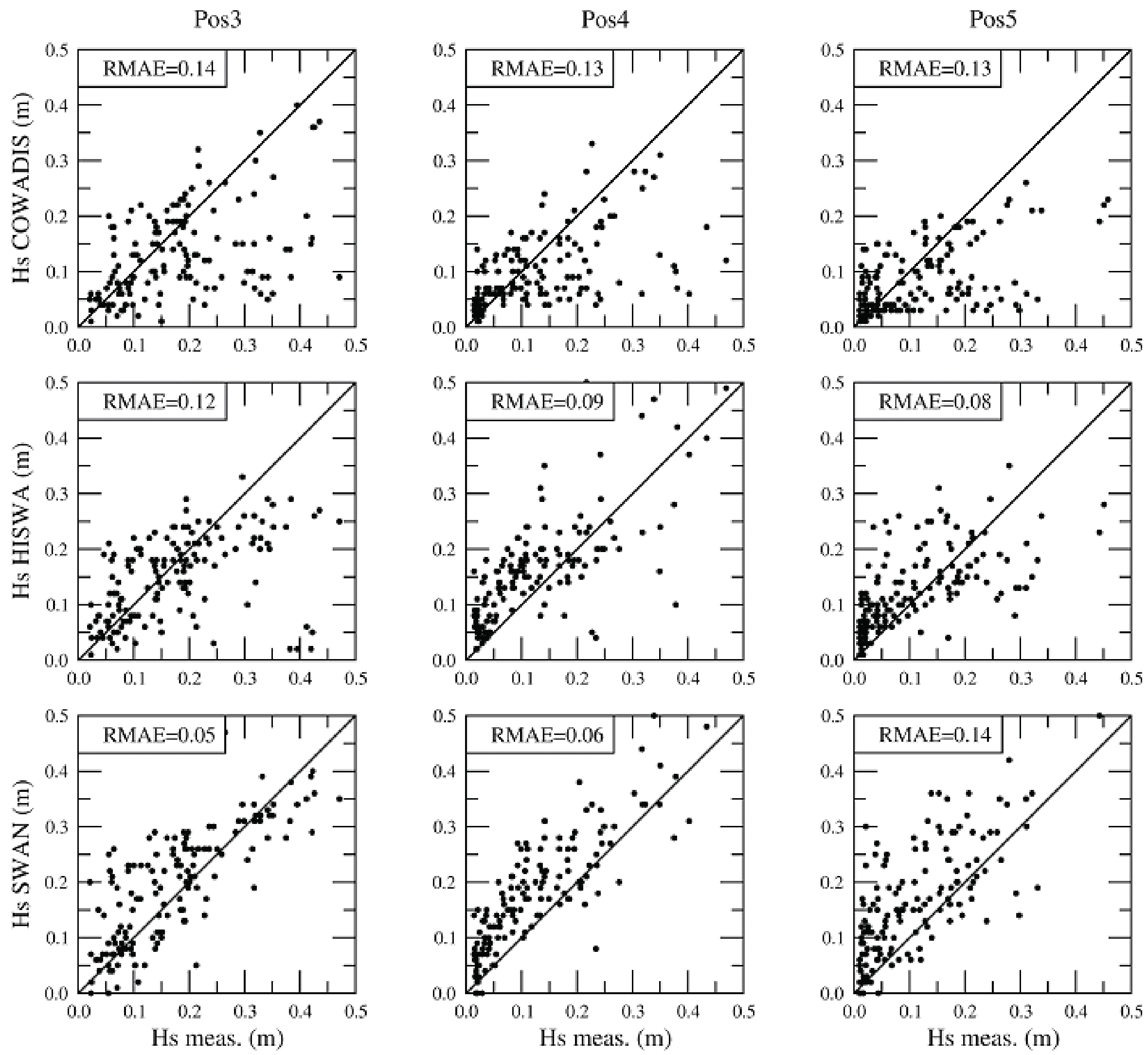

Fig. 16: Modelled vs. measured wave heights at Pos 3, 4 and 5 for COWADIS, HISWA and SWAN

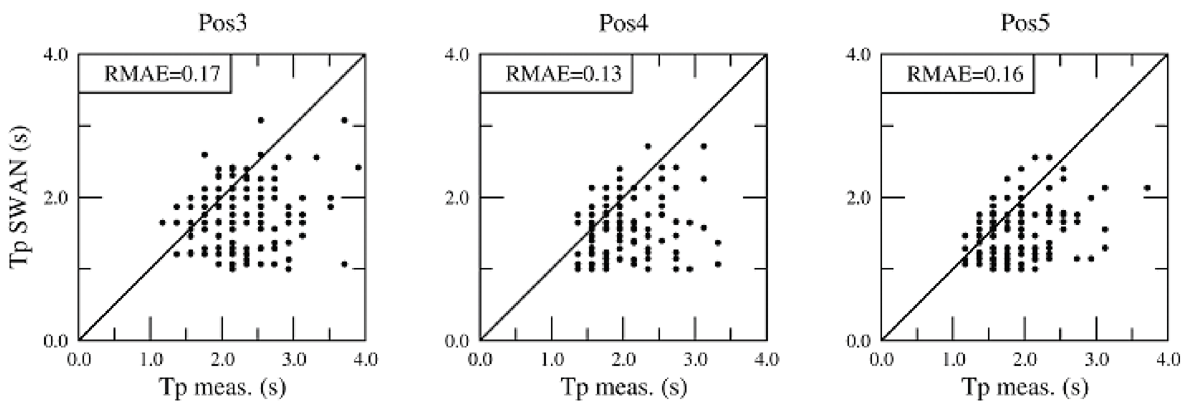

Fig. 17: Modelled vs. measured peak periods at Pos 3, 4 and 5 for SWAN

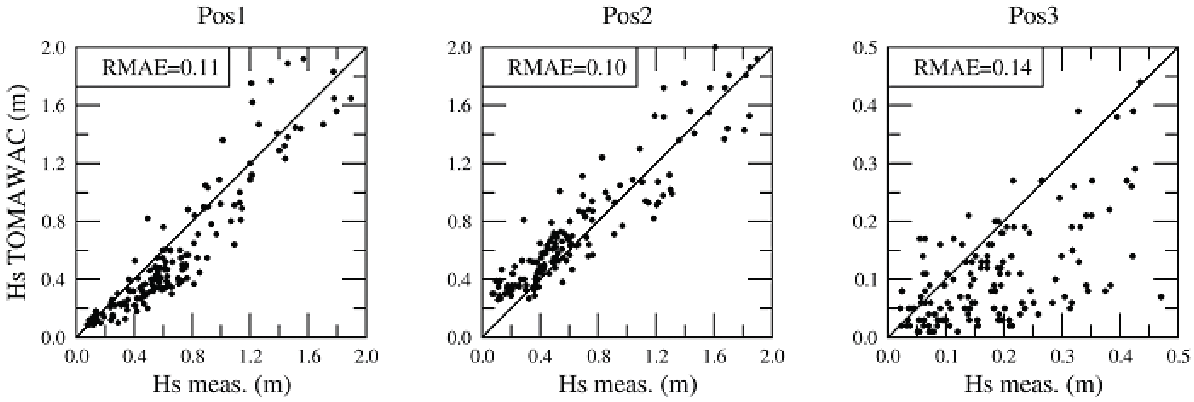

Fig. 18: Modelled vs. measured significant wave heights at Pos 1, 2 and 3 for TOMAWAC

6. Application of the Wave Models

The two third generation models SWAN and TOMAWAC were applied to analyse the behaviour of waves in the investigation area. Analysis results are discussed hereafter. Firstly, the wave fields at representative instants in the tidal cycle are presented and show the general distribution of the sea state over the area. The DELFT3D-SWAN model was applied for this purpose. Secondly, the impact of wave action on the current velocities was investigated. Results from the coupled TELEMAC-TOMAWAC model with and without waves were compared. Finally, a wave hindcast for the storm event "Anatol" in December 1999 was carried out with the DELFT3D-SWAN model. The wind conditions of this event were fed into the entire nesting sequence from the North Sea model, over the German Bight model to the Dithmarschen Bight model (see Fig. 22). This approach ensured an accurate simulation of the actual storm conditions for the boundary conditions of the Dithmarschen Bight model. The results display a realistic image of wave conditions during a major storm event.

6.1 General Wave Distribution in the Central Dithmarschen Bight

To find out whether the observed sheltering effect of the tidal flats with respect to the location of the eastern buoys is reproduced by the models, the computed spatial distribution of wave heights over the investigation area was analysed. The analysis was carried out for typical points in the tidal cycle, i.e. high water, low water, maximum ebb currents and maximum flood currents. In the following, the wave conditions computed with the SWAN model and covering the first day of the field campaign (September 13th) are discussed. The imposed conditions are listed in Table 4.

Table 4: Conditions considered at the western open boundary

Parameter	Value
H_s	1.5 m
Swell direction	285 °N
Wind speed	10 m/s
Wind direction	315 °N

With these boundary conditions, which have been kept constant during the simulation, and the ambient tidal conditions derived from the flow model the results shown as wave height distributions in Fig. 19 are as follows:

The main wave action is found in the western half of the area domain for all four instants of the tidal cycle. The sheltering effect of the western tidal flats is rather significant, limiting the wave energy in the eastern part of the domain. Wave action in the sheltered part is largely due to locally generated waves, whereas in the western part it is a combination of incoming swell and locally generated waves. These model results are consistent with the observed wave heights. From spectral analysis of the field data of the western buoys double-peaked spectra confirm the different sources of waves at these locations. For the inner buoys, single-peaked spectra indicate only local wave generation as energy source.

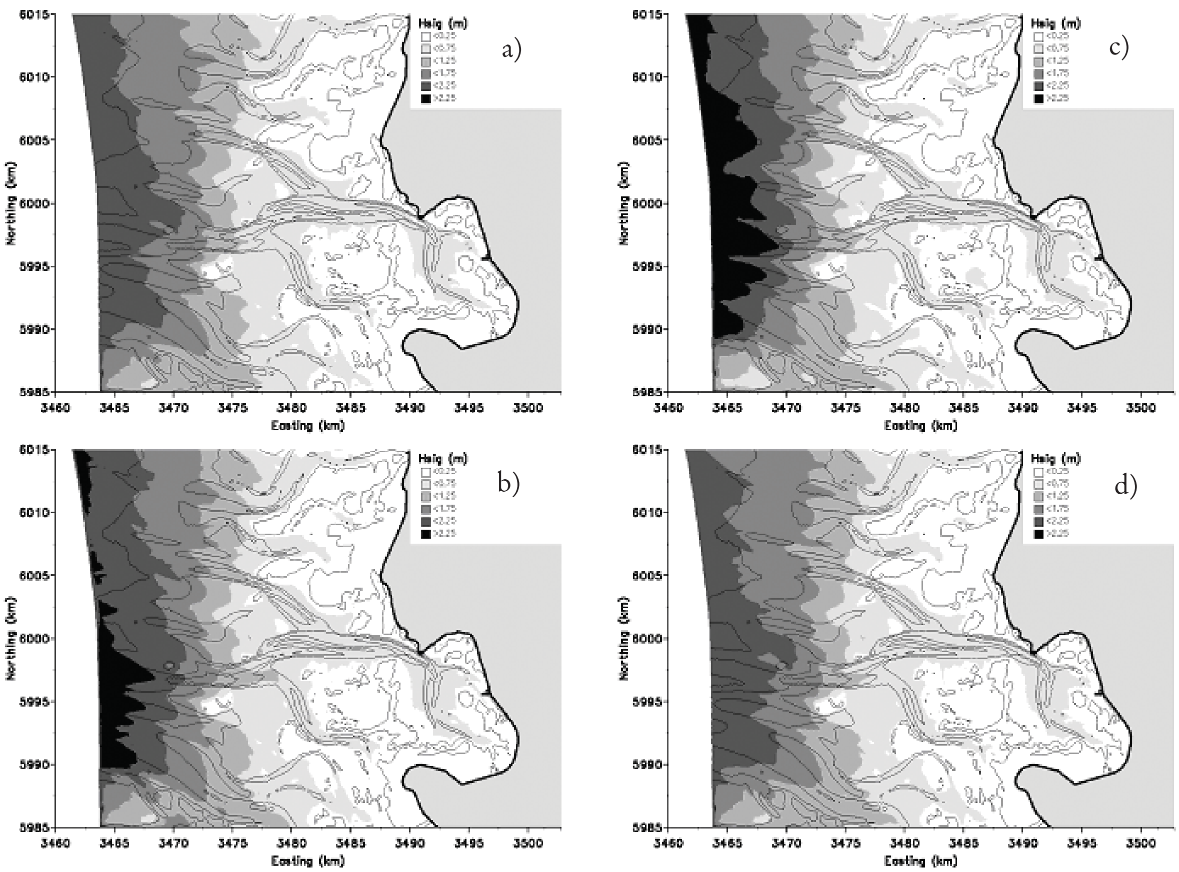

Fig. 19: Modelled significant wave heights during a) high water, b) ebb, c) low water and d) flood

6.2 Investigation of the Significance of Wave–Induced Currents

Waves in the coastal zone are generally an important driving force for sediment transport and, consequently, morphodynamic evolution. While orbital movement stirs up the sediment other wave-induced together with tidal currents will transport sediment over larger distances. To evaluate the importance of waves in this process the calibrated wave models SWAN and TOMAWAC were applied to calculate the wave driven forces for several monitoring points in the area of investigation, shown in Fig. 20. The imposed waves at the open boundary vary between 1 and 3 m.

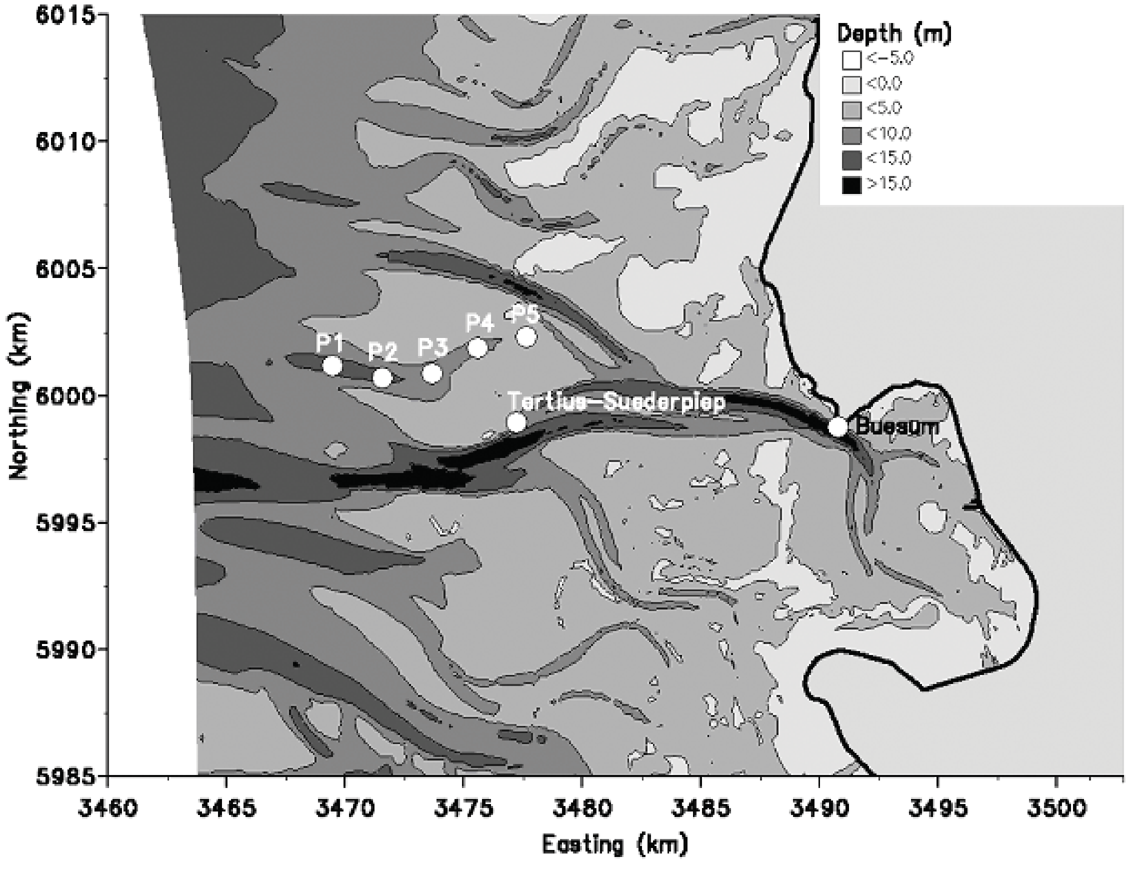

Fig. 20: Location of the monitoring points

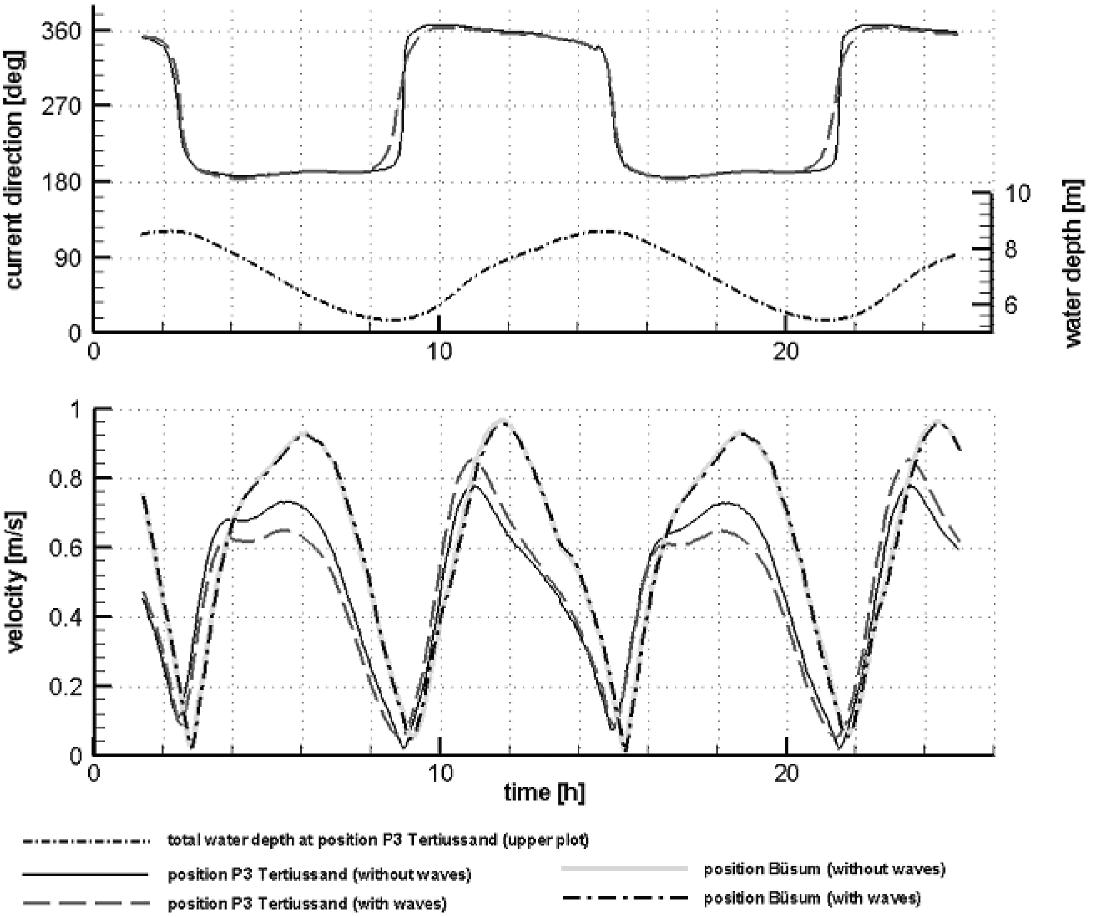

Fig. 21: Wave impact on currents at Tertiussand P 1 and near Büsum

Fig. 21 exemplarily illustrates the computed current velocities with and without wave influence for position P 3 located in a shallow channel on Tertiussand and for a location near Buesum. The results were generated by the wave model TOMAWAC with an imposed wind speed of 15 m/s from the Southwest and a fetch of 200 km. Under these conditions the computed wave heights at the western boundary measure up to 3 m and cause a deviation of the depth-integrated flow velocities up to 0.10 m/s (approximately 15 %) at location P 3. At the monitoring point near Buesum the deviations are negligible due to the large local depth and smaller wave heights. In Fig. 21 the effect on flow directions is also displayed (for point P 3 only). A significant deviation is only observable during slack water.

A similar consideration of the changes at all monitoring points led to the conclusion that the impact of waves on the depth-integrated currents is negligible in the tidal channels for the considered wave conditions. A distinct influence can be seen in both the SWAN and TOMAWAC model results for the considered observation points in shallow water. Simulation results for more moderate wave conditions, with wave heights of 1 and 2 m at the open boundary, have also been analysed (not shown). Wave heights of 1 m have a limited effect even on the tidal flat, whereas those of 2 m show effects similar to but smaller than those presented in Fig. 21, as computed with the TOMAWAC model.

6.3 Hindcast of the Storm Event "Anatol"

The storm "Anatol" occurred in December 1999. An extreme low pressure area moved from West to East over the central North Sea, inducing strong onshore winds. In order to correctly hindcast the hydrodynamic conditions during the storm with the coupled DELFT3D-SWAN model, wind conditions were initially imposed in all three models of the nesting sequence of Fig. 22. This approach resulted in a reasonable hindcast of the storm surge. By hourly updating the wind conditions a satisfactory representation of the storm was ensured. For the TOMAWAC model the flow boundary conditions were also generated by a nesting sequence similar to Fig. 22. During the instationary computation the boundary conditions are updated in a time interval of 15 minutes. The wave boundary conditions are determined with a fetch-based approach under consideration of PRISMA wind data.

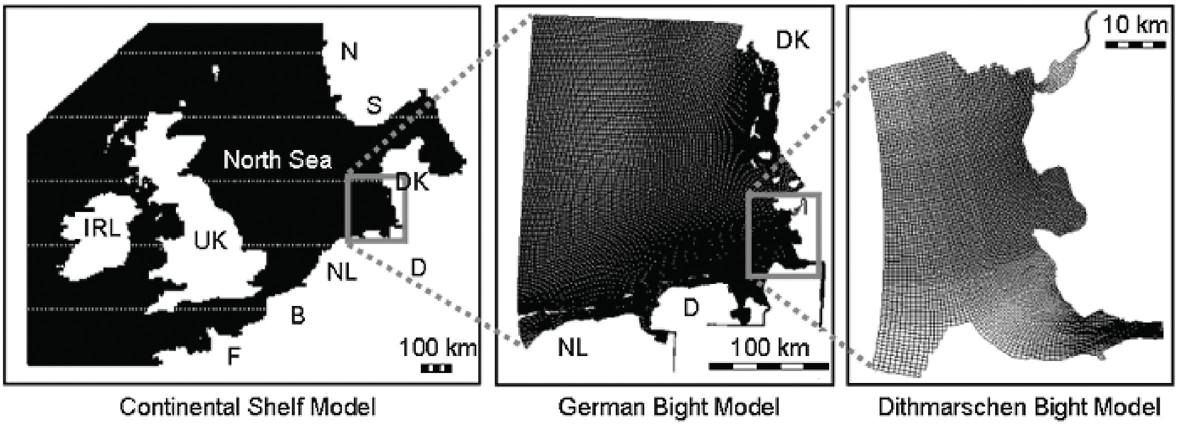

Fig. 22: Nesting sequence for the generation of open boundary conditions

Since the SWAN model within Delft3D can only be run in stationary mode resulting wave heights are based on the actual wind field, and previously generated waves are not considered. A sensitivity analysis on all three grids showed that the inclusion of the Continental Shelf Model, i.e. imposing wave boundary conditions in the German Bight model would not significantly influence the wave fields in the vicinity of the Dithmarschen Bight. Therefore wave modelling was carried out only with the German Bight model and the Dithmarschen Bight model. Currents and water levels have been computed throughout the entire nesting sequence, however.

For the German Bight field data for two locations, one near Heligoland, the other between Heligoland and the mouth of the Elbe were made available by the BSH. Observed and computed wave heights (German Bight model) are shown in Fig. 23. The comparison indicates an under-prediction of wave heights before the storm and too fast a decrease after peak values have been reached. The latter may well be related to the stationary approach. The maximum values as well as the main trends are simulated satisfactorily. Therefore, it can be expected that the German Bight model produces acceptable boundary conditions for the Dithmarschen Bight model.

Wave heights computed with SWAN and TOMAWAC for the locations of the wave buoys Pos 2 and Pos 3 (cf. Fig. 1) are illustrated in Fig. 24. One can see that both models yield similar results. The graph shows that at the western boundary (Pos 2) maximum wave heights reached 5 m whereas at the eastern buoy almost 2 m were computed. Because of the storm surge with elevated water levels the tidal flats did not provide the same sheltering as is typical during moderate conditions.

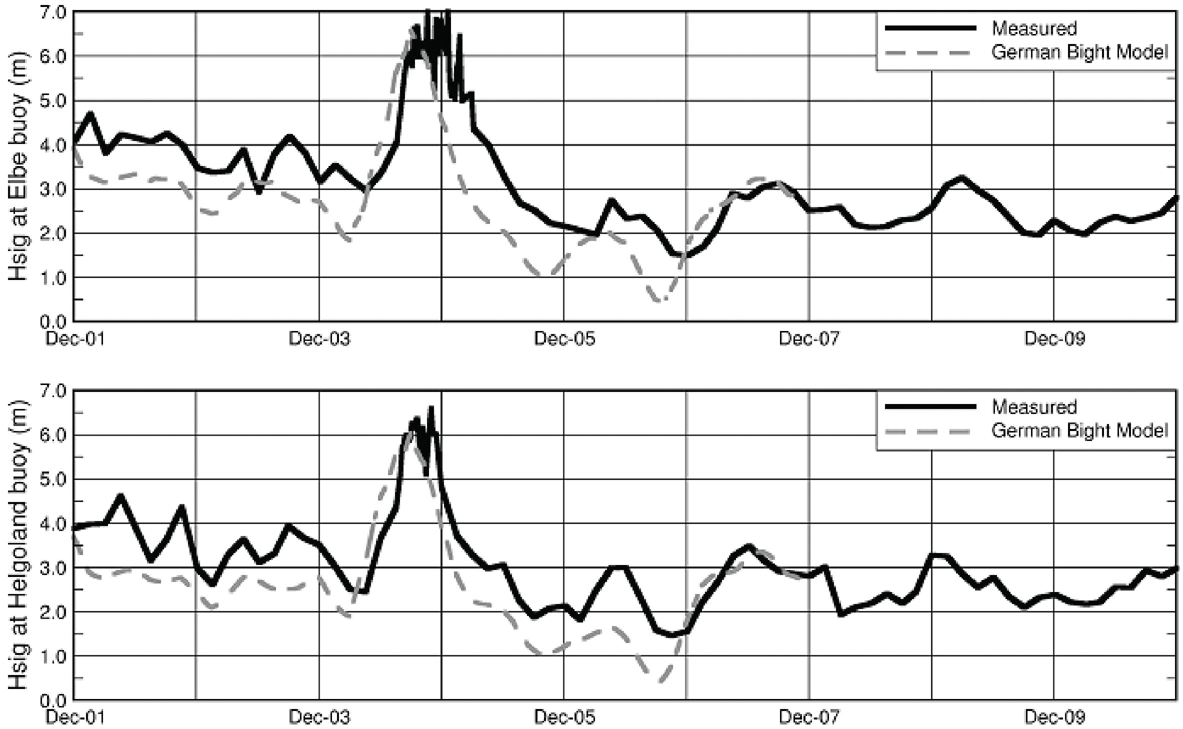

Fig. 23: Observed and computed (German Bight model) wave heights during the storm "Anatol"

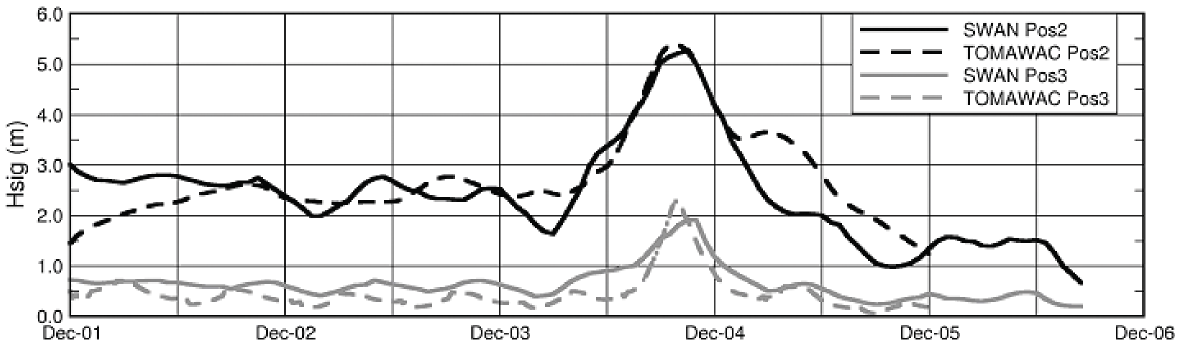

Fig. 24: Hindcast wave heights (storm "Anatol") computed with SWAN and TOMAWAC

7. Discussion and Conclusions

It was shown that the four wave models used in the investigation were able to reproduce the observed wave heights during the one-month measurement period satisfactorily. The quantitative evaluation based on the RMAE parameter showed that the results could be qualified as "reasonable" and "good" for all five locations of the field campaign. Differences between computed and observed data are partly due to the limited spatial and spectral resolution. This limitation was necessary to maintain reasonable computational costs when including the wave modules in medium scale morphodynamic models.

The first application, simulating wave height distribution during a tidal cycle at moderate wind conditions provided a good insight into the wave climate in the area of interest with higher waves near the exposed outer tidal flats and relatively low wind waves in the sheltered eastern part. Hardly any swell enters the sheltered part during moderate conditions.

In the second application, investigations of wave-induced currents showed that even higher waves have only a moderate impact on the depth-averaged currents in shallow-water areas.

Finally, the hindcast of the storm Anatol showed that wave heights up to 2 m may occur even in the sheltered parts of the area. The increase in water level diminishes the natural protection by the tidal flats. Both applied models show similar results.

8. Acknowledgements

This investigation was carried out within the framework of the project PROMORPH. We would like to thank the German Ministry of Education and Research (BMBF) for funding the project (Funding number 03 F 0262A). The Coastal Research Station of the Lower Saxon Board for Ecology at Norderney is thanked for making available the wave data, without which the model evaluation could not have been carried out so effectively. They are also acknowledged for providing the German Bight Model, which has been developed by Delft Hydraulics (the Netherlands) within the German-Dutch project WADE (Wadden Sea Morphodynamical Development of Wadden Sea Areas), funded by the German Ministry of Education and Research. The Office for Rural Areas (ALR) in Husum is acknowledged for kindly providing the water level data and bathymetric data of the tidal flat areas. Furthermore, the Federal Maritime and Hydrographic Agency (BSH) in Hamburg are thanked for provision of the bathymetric data in the tidal channels and wave data in the German Bight. The cooperation with the staff of the participating institutes is gratefully acknowledged. The authors furthermore thank the Max Planck Institute for Meteorology in Hamburg for providing the PRISMA model. Finally, we thank Dr.-Ing. V. BARTHEL as well as the anonymous reviewer for their constructive remarks.

9. References

BENOIT, M.; MARCOS, F. and BECQ, F.: Development of a Third Generation Shallow-Water Wave Model with Unstructured Spatial Meshing. Proc. 25th Int. Conf. on Coastal Eng., (Orlando, USA), 1996.

BOOIJ, N.; RIS, R. C. and HOLTHUIJSEN, L. H.: A Third-Generation Wave Model for Coastal Regions, Part I, Model Description and Validation. Journal of Geophysical Research, Vol. 104, C4, 1999.

GALLAND, J.-C.; GOUTAL, N. and HERVOUET, J.-M.: TELEMAC A New Numerical Model for Solving Shallow Water Equations, Adv. Water Resources, 14 (3), 1991.

HERVOUET, J.-M.: TELEMAC Modelling System: an Overview. In: Hervouet, J.-M. and P. Bates. Special Issue: The TELEMAC Modelling System. Hydrological Processes, 14 (13), 2209–2210, 2000.

HOYME, H. H.: Mesoskalige morphodynamische Modellierungen am Beispiel der Meldorfer Bucht, Institut für Strömungsmechanik und Elektron. Rechnen im Bauwesen der Universität Hannover, Bericht Nr. 67, in German, 2002.

HOLTHUIJSEN, L. H.; BOOIJ, N. and HERBERS, T. H. C.: A Prediction Model for Stationary, Short-Crested Waves in Shallow Water with Ambient Currents. Coastal Engineering, Vol. 13, 1989.

LUTHARDT, H.: Analyse der wassernahen Druck- und Windfelder über der Nordsee aus Routine-Beobachtungen. Hamburger Geophysikalische Einzelschriften, Fachbereich Geowissenschaften, Universität Hamburg, Germany, Reihe A83, in German, 1987.

NIEMEYER, H. D.: Bemessung auf Seegang. Entwicklung abgesicherter Verfahren zur Ermittlung der Bemessung des Wellenauflaufs. KFKI-project No. 45, in German, 1997.

RIS, R. C.; BOOIJ, N. and HOLTHUIJSEN, L. H.: A Third Generation Wave Model for Coastal Regions, Part II, Verification, Journal of Geophysical Research, Vol. 104, C4, 1999.

ROELVINK, J. A. and VAN BANNING, G. K. F. M.: Design and Development of DELFT3D and Application to Coastal Morphodynamics, Proc. Hydroinformatics 1994 (Delft, the Netherlands), H. H. Balkema Publishers, Rotterdam, the Netherlands, 1994.

ROGERS, W. E.; HWANG, P. A. and WANG, D. W.: Investigation of Wave Growth and Decay in the SWAN Model: Three Regional-Scale Applications, Journal of Physical Oceanography, Vol. 33 (2), 2003.

VAN RIJN, L. C.; WALSTRA, D. J. R.; GRASMEIJER, B.; SUTHERLAND, J.; PAN, S. and SIERRA, J. P.: Simulation of Nearshore Hydrodynamics and Morphodynamics on the Time Scale of Storms and Seasons Using Process-Based Profile Models. In Van Rijn, L. C., B. G. Ruessink and J. P. M. Mulder (ed.), The Behaviour of a Straight Sandy Coast on the Time Scale of Storms and Seasons: Process Knowledge and Guidelines for Coastal Management: End Document March 2002. EC MAST Project, MAS3- CT97-0086 COAST3D – EGMOND, 2002.

WILKENS, J.: Medium Scale Morphodynamics of the Central Dithmarschen Bight, Ph.D. thesis, University of Kiel, Germany, (available under http://e-diss.uni-kiel.de/diss_1369/d1369.pdf), 2004.

Die Küste, 69 PROMORPH (2005), 1-420

Hydrodynamic Forcing Along the Open Sea Boundaries of Small-Scale Coastal Models

By Roberto Mayerle, Jort Wilkens, Carlos Escobar and Wiwin Windupranata

Summary

This paper deals with hydrodynamic forcing along the open sea boundaries of process-based models for simulating flow and waves in the central Dithmarschen Bight, a tidally-dominated area on the German North Sea coast. The effectiveness of various approaches for determining water levels and waves as open sea boundary input to coastal area models was verified. Comparisons of measured and computed water levels and waves at several locations for a wide range of conditions typical of the study area were carried out in order to verify the performance of the approaches adopted. The results obtained were found to be in good agreement with observations and confirmed the suitability of the different approaches for describing the hydrodynamics in the study area. In the case of the flow model better agreement was obtained using the approach based on water levels measured directly along the open sea boundaries. The mean absolute error in amplitudes and phases at high and low water levels was found to be less than 3 % of the mean tidal range and about 5 % of the tidal period, respectively. Corrections to the results obtained from the north-west European Continental Shelf Model based on measured water levels proved to be quite effective for improving the water levels prescribed along the open sea boundaries of larger models. The open sea boundary conditions for the wave model, which represent incoming swell energy, were defined by directly imposing (parametric) values deduced from measurements at a location along the open boundary and by the application of a model nesting sequence. A comparison between the results of the latter approach and direct measurements showed good agreement. On the basis of the quality standards adopted, the results obtained by applying model nesting were rated as 'good' for significant wave heights and 'reasonable to fair' for peak periods.

Zusammenfassung

Der Beitrag beschäftigt sich mit dem hydrodynamischen Antrieb prozessgebundener Modelle zur Simulation von Strömung und Seegang in der Zentralen Dithmarscher Bucht, einem tidedominierten Seegebiet vor der Deutschen Nordseeküste. Verifiziert wurde die Effektivität verschiedener Näherungen zur Bestimmung von Wasserständen und Wellen als Eingabeparameter für Küstenmodelle an den Offene-Seegrenzen. Um die Leistungsfähigkeit der verwendeten Näherungen zu verifizieren, wurden Vergleiche gemessener und modellierter Wasserstände und Wellen an mehreren Stellen für weites Feld von Bedingungen durchgeführt, die für das Untersuchungsgebiet typisch waren. Die erzielten Ergebnisse wiesen eine gute Übereinstimmung mit den Beobachtungen auf und unterstrichen die Eignung der verschiedenen Näherungen zur Beschreibung der Hydrodynamik im Arbeitsgebiet. Beim Strömungsmodell wurde eine bessere Übereinstimmung erzielt, wenn für die Näherung die unmittelbar an den Offene-Seegrenzen gemessenen Wasserstände verwendet wurden. Der mittlere absolute Fehler bei Amplitude und Phase bei Hochwasser und Niedrigwasser lag unter 3 % des mittleren Tidehubs bzw. bei 5 % der Tideperiode. Die Korrekturen zu Ergebnissen, die aus dem Nordwesteuropäischen „Continental Shelf Model" gewonnen wurden, und auf gemessenen Wasserständen beruhten, erwiesen sich als recht effektiv, um die Wasserstände, die an den Offene-Seegrenzen größerer Modelle vorgegeben sind, zu verbessern. Die Offene-Seegrenze-Bedingungen für das Wellenmodell, die die einlaufende Seegangsenergie repräsentieren, wurden durch ein direktes Einsetzen parametrischer Werte definiert, die aus örtlichen Messungen entlang der Offene-Seegrenze und aus der Anwendung einer Modell-Nesting-Sequenz hergeleitet wurden. Ein Vergleich zwischen den Ergebnissen letzterer Näherung und direkten Messungen zeigte eine gute Übereinstimmung. Gemäß der verwendeten Qualitätsmaßstäbe wurden die Ergebnisse aus dem Modell-Nesting für signifikante Wellenhöhen als „gut" und für die Peakperioden als „befriedigend bis mäßig" eingestuft.

K e y w o r d s

Open Sea Boundary, Boundary Conditions, Hydrodynamics, Waves, Modelling, Dithmarschen Bight, Tidal Flats, Tidal Channels, DELFT3D, SWAN, PROMORPH

C o n t e n t s

1. Introduction

Numerical models of flow and waves are finding increasing application in the management of coastal areas. As these models usually cover only part of the coastal area under investigation, open sea boundaries with the enclosed sea are introduced to limit the size of the modelled domain and hence reduce computational effort. Open sea boundaries are virtual "water-water" boundaries representing the influence of the sea area surrounding the modelled domain. The predictive capability of process-based models of coastal areas depends very much on an adequate description of environmental forcing along the open sea boundaries. In order to avoid a predominant influence of environmental forcing on model results the open sea boundaries are usually specified at a sufficiently large distance away from the area of interest. The type of open sea environmental forcing applied in practice often depends on the available data. Measured values or the results of simulations performed with larger-scale models covering the adjacent sea area are usually used for this purpose.

This paper summarizes the results of investigations carried out to verify the effectiveness of the approaches usually adopted for determining water levels and waves as open sea boundary input to process-based flow and wave models is verified. Several approaches were tested for a coastal area on the German North Sea coast. Comparisons between measured and computed water levels and waves at several locations along the open boundaries and within the modelled domain were made for a wide range of conditions typical of the study area in order to verify the quality of the various approaches.

2. Study Area and Process-Based Models

The study area considered in the present investigation is the central Dithmarschen Bight on the German North Sea coast, located between the Elbe and Eider estuaries (Fig. 1).

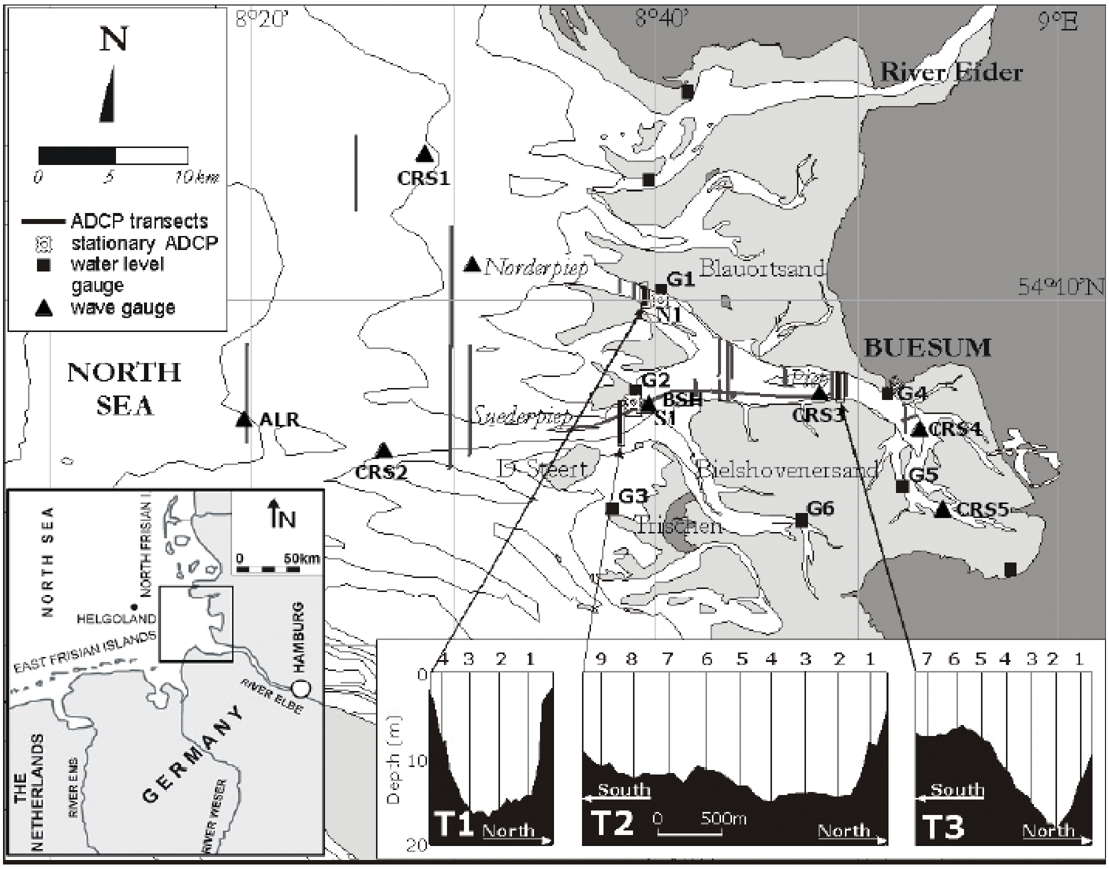

Fig. 1: Investigation area (Dithmarschen Bight) and location of gauge stations

The hydrodynamics of the central Dithmarschen Bight are not directly influenced by the discharges of these rivers, as extensive tidal flats separate these systems from the study area. Two major tidal channels, namely the Norderpiep and Suederpiep, connect the bight with the open sea. These channels intersect within the domain to form the Piep tidal channel. These channels attain a width of up to 4 km, with maximum depths of about 20 m. Approximately 50 % of the study area is inter-tidal and the entire area is submerged during high tide.

The hydrodynamics and sediment dynamics in the study area are driven by the combined effects of tides, waves and winds. The mean tidal range in the region is about 3.2 m. The propagation direction of the tidal wave is normal to the western boundary of the Dithmarschen Bight, with an easterly and westerly tidal flow during the flood and ebb phases, respectively. Wave heights of up to 4 m are observed in the outer region of the investigation area. Under normal conditions, however, the influence of waves on the flow field is moderate on the tidal flats and negligible in the tidal channels. Wave breaking generally occurs along the edge of the tidal flats. Wind effects may include the afore-mentioned wind-induced wave generation as well as the forcing of wind-driven currents. The enhanced wave action and currents may initiate additional sediment transport and alter the patterns of sediment dynamics.

Within the framework of the research project PROMORPH, process-based models for simulating flow, waves, sediment transport and bed level changes have been developed and subsequently calibrated and validated using field data. The aim of the project was to develop a modelling system for predicting medium-scale morphological changes in the central Dithmarschen Bight. Several curvilinear grids adjusted to the bathymetry of the study area were developed. Two-dimensional depth-averaged (2DH) flow and sediment transport models based on the DELFT3D modelling system developed by Delft Hydraulics in the Netherlands (ROELVINK and VAN BANNING, 1994) as well as the phase-averaged spectral wave model SWAN (BOOIJ et al., 1999; RIS et al., 1999) were implemented in the project. Confirmation of the good quality of the model results for flows is given in PALACIO et al. (in this volume); for waves in WILKENS (2004) and WILKENS et al. (in this volume); for sediment transport in WINTER et al. (in this volume) and for morphodynamics, in WILKENS (2004), WILKENS and MAYERLE (2004) and JUNGE et al. (in this volume).

Fig. 2 shows the computational grid and local bathymetry of the Dithmarschen Bight Model (DBM) indicating the limits of the two nested models, namely the Central Dithmarschen Bight Model (CDBM) and the Extended Central Dithmarschen Bight Model (ECDBM). Flow simulations were carried out for all three domains whereas wave simulations were only performed for the larger domain. The size of the CDBM is approximately 20 km by 17 km and covers an area of about 300 km². The offshore boundary of the CDBM lies about 14 km west of Buesum. The computational grid of the CDBM consists of about 30,000 cells with a grid spacing ranging from 60 m to 180 m. In view of the intense morphological changes that occur along the western open sea boundary of the CDBM, particularly on the sand banks and outer tidal flats (see WILKENS et al., 2001), the model was extended a further 14 km westwards. The resulting ECDBM measures 35 km by 17 km and covers an area of approximately 520 km². The computational grid of the ECDBM consists of almost 36,000 cells with a grid spacing ranging between 90 m and 180 m. The good performance of the flow models is documented in PALACIO et al. (2001) and PALACIO et al. (in this volume).

In order to simulate waves and medium-scale morphodynamics in the study area an even larger model domain was found to be necessary (WILKENS et al., 2001). By extending the ECDBM in the northward and southward directions it was possible to reduce the influences

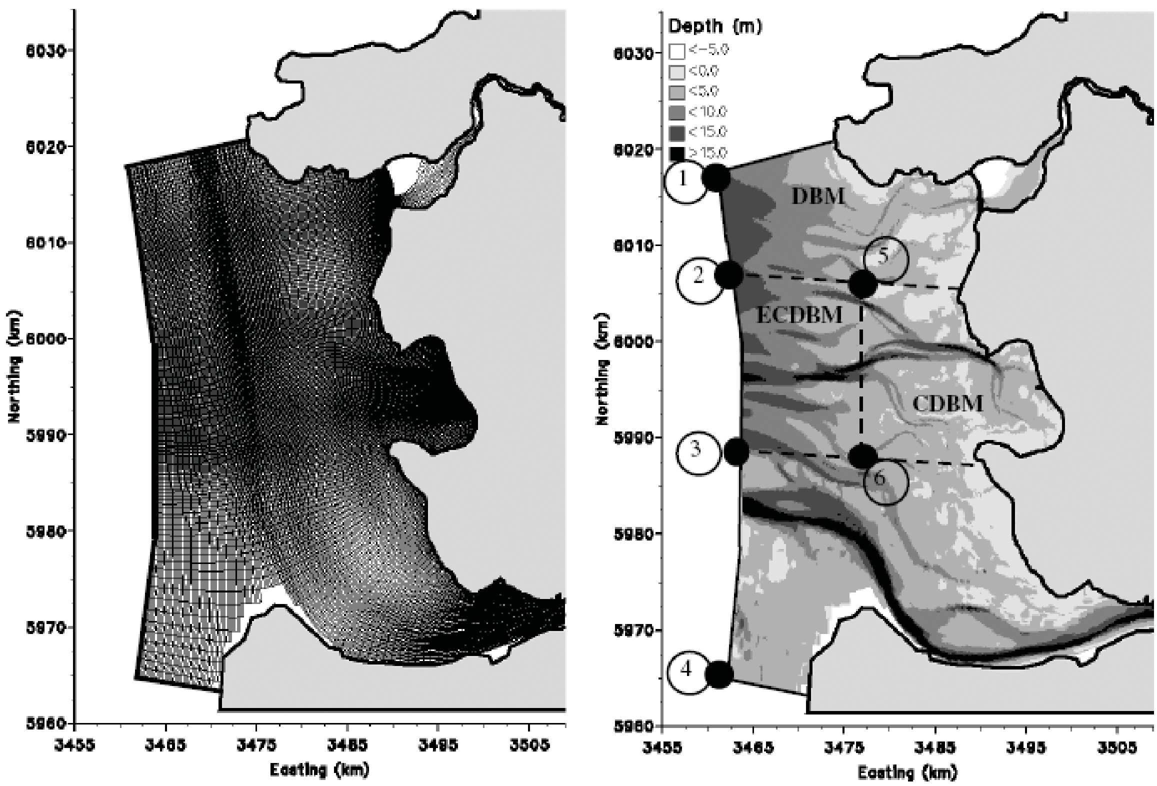

Fig. 2: Computational grid, bathymetry and model limits

of the respective open sea boundaries on the computed wave characteristics and medium-scale morphodynamics in the central Dithmarschen Bight. For the purpose of wave modelling it was also possible to dispense with boundary conditions on the northern and southern open sea boundaries, as these boundaries are located in very shallow tidal flat areas. The resulting Dithmarschen Bight Model (DBM) measures approximately 37 km by 54 km and covers an area of about 1,640 km^2. The model grid consists of approximately 43,250 cells with a grid spacing ranging from 80 m to 200 m. The offshore boundary is located about 29 km west of Buesum. The performance of the DBM for predicting water levels and current velocities was found to be similar to that of the CDBM and ECDBM (PALACIO et al., in this volume).

3. Flow Models

Flow models solve the non-steady flow field resulting from tidal and meteorological forcing. Along the open sea boundaries of models it is necessary to prescribe water levels, current velocities or a combination of both in order to ensure a well-posed mathematical initial boundary-value problem.

Water levels obtained from astronomical constituents are usually prescribed along the open sea boundaries of larger models. As the open sea boundaries are located far away from the coast in the present study, the effects of wind set-up may be accounted for by proper wind forcing. Typical examples of this set-up for the north-west European Continental Shelf area are implemented in the Continental Shelf Model (VERBOOM et al., 1992), the Promise Model (BRUMMELHUIS et al., 1997), and the BSHcmod Model (DICK et al., 2001). The latter model combines the tidal forcing of 14 harmonic constituents with water levels from an even larger model.

Small-scale coastal area models, on the other hand, are either driven by measured water levels from gauge stations or by computed water levels or current velocities. Water levels and current velocities may also be obtained from simulations using larger models covering the adjacent sea area, such as those mentioned above. Under calm weather conditions, where meteorological forcing is negligible, water levels obtained from astronomical constituents may also be applied directly along the open sea boundaries of coastal models. Examples of models driven by water levels specified along open sea boundaries have been reported among others by ELIAS et al. (2000) and ASPELIEN and WEISSE (2005). Models driven by velocities or a combination of water levels and velocities have also proved their effectiveness in several coastal regions (see, for example, MEWIS et al., 1998; ANNAN, 2001; SIEGLE et al., 2002; MILBRADT and PLÜSS, 2003).

The use of water levels based on measurements at gauge stations located in the proximity of the open sea boundaries is probably the most suitable and straightforward approach for specifying the hydrodynamic forcing of coastal flow models. In this approach, measured water levels that account for astronomical and meteorological effects are imposed directly along the open sea boundaries. For cases in which meteorological effects are negligible, water levels hindcasted from astronomical tidal constituents may also be used. If the open sea boundaries are long, interpolation between measurements from a limited number of gauge stations may be carried out to provide water level approximations at intermediate boundary grid points. Water levels along the open sea boundaries may also be obtained with the aid of models covering the adjacent sea area. This approach is recommended for larger models with long open sea boundaries, where interpolation between gauge measurements could introduce errors. In some cases a combination of the latter approach with measured water levels may be applied to correct water levels along the open sea boundaries.

3.1 Model Limits and Modelling Approaches

The effectiveness of the various approaches for prescribing water levels along the open sea boundaries was assessed for several flow models of the central Dithmarschen Bight, i.e. the CDBM, ECDBM and DBM. The limits of the models shown in Fig. 2 were selected on the basis of the results of preliminary model runs covering the German Bight (see Fig. 4). The flow models considered have open sea boundaries along their western, southern and northern extremities. It was found that the hydrodynamics of the study area are mainly determined by conditions along the western boundaries, through which the tidal wave and swell propagate into the coastal region. The northern and southern open sea boundaries of the models are either located on the tidal flats and fall dry during low water (CDBM and ECDBM in Fig. 2) or are fairly distant from the region of interest (DBM). Sensitivity tests were carried out to check the effects of the conditions specified along these boundaries on flow patterns. Generally speaking, it was found that the effects of hydrodynamic forcing specified along these boundaries are negligible.

Fig. 3 shows comparisons of the main tidal components at the northern and southern corners of the open sea boundaries of the three model domains. It is seen that the amplitudes and phases of the water levels at the corners of the CDBM (points 5 and 6 in Fig. 2) and ECDBM (points 2 and 3) are fairly similar. This is due to the fact that the crest of the tidal wave entering the domain of interest is almost aligned with the western open sea boundaries of the models as well as the edges of the tidal flat areas (TORO et al., in this volume). Hydrodynamic forcing along the western boundary of the flow models may thus be realised by specifying the water levels measured at one of the gauge stations located in the proximity of this boundary (G1, G2 or G3 in Fig. 1). The measured water levels (MWL) at the gauge stations G1 (Blauort) and G3 (Trischen) as well as the results of simulations using the larger-scale model covering the north-west European Continental Shelf were used in the present study (see Fig. 4). For periods during which meteorological effects are negligible, water levels along the western open sea boundary were hindcasted with the aid of tide tables (TT). Tide tables of the harmonic constituents obtained for the six tide gauges are summarized in TORO et al. (in this volume). Spatial and temporal linear interpolation was carried out between the measured water levels at one of the gauge stations in the vicinity of the boundary (G1, G2 or G3) and G5 (Steertloch) along the northern and southern boundaries (Fig. 1). In view of the fact that the gauge stations G1 and G3 are located at a fair distance from the western boundary of the ECDBM, the measured water levels at these stations were appropriately adjusted.

Comparisons of the main tidal constituents at several locations along the western boundaries of the Dithmarschen Bight Model (DBM) showed significant differences in amplitudes and phases between the central Dithmarschen Bight and the Elbe estuary (see points 3 and 4 in Fig. 3). As there are no gauge stations along the western boundary of the DBM, it was only possible to adopt the approach based on simulations using a larger model covering the adjacent sea area.

In this study the north-west European Continental Shelf Model (CSM) was used for this purpose (VERBOOM et al., 1992). This model has a grid spacing of about 9 km and implements two-dimensional depth-integrated flow approximations based on the DELFT3D modelling system developed by Delft Hydraulics in the Netherlands (ROELVINK and VAN BANNING, 1994). The 10 main harmonic tidal constituents (M2, S2, N2, K2, O1, K1, Q1, P1, NU2, and L2) were prescribed along the open sea boundaries of the CSM. In order to improve the descriptions of water levels along the coast a Large-Scale Model Nesting (LSMN) procedure was adopted (Fig. 4). The CSM was nested with the German Bight Model (GBM), which has a grid spacing ranging from 0.5 km to 1.9 km (HARTSUIKER, 1997). The water levels and current velocities along the open sea boundaries of the coastal models were obtained in successive steps. Simulations were first performed for the entire investigation period using the CSM. The information obtained along the open sea boundaries of the GBM were then used to drive this model, which in turn yielded the required boundary conditions along the open sea boundaries of the coastal models (CDBM, ECDBM and DBM).

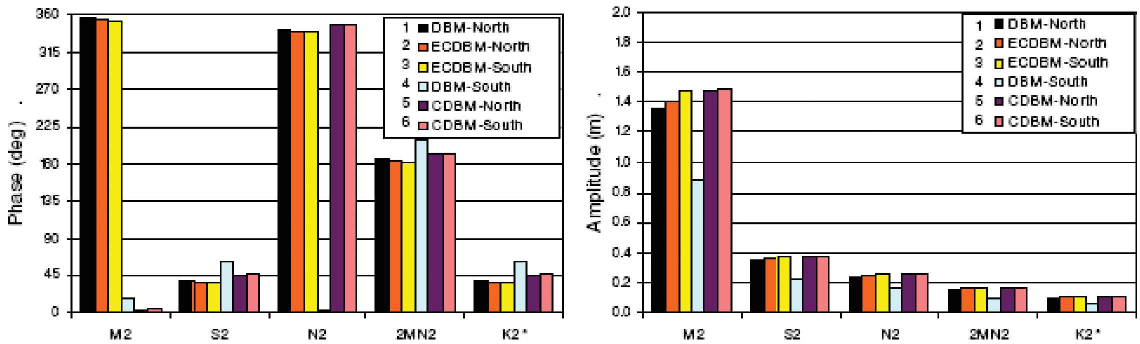

Fig. 3: Comparison of the main tidal components at the northern and southern corners of the open sea boundaries of the coastal models

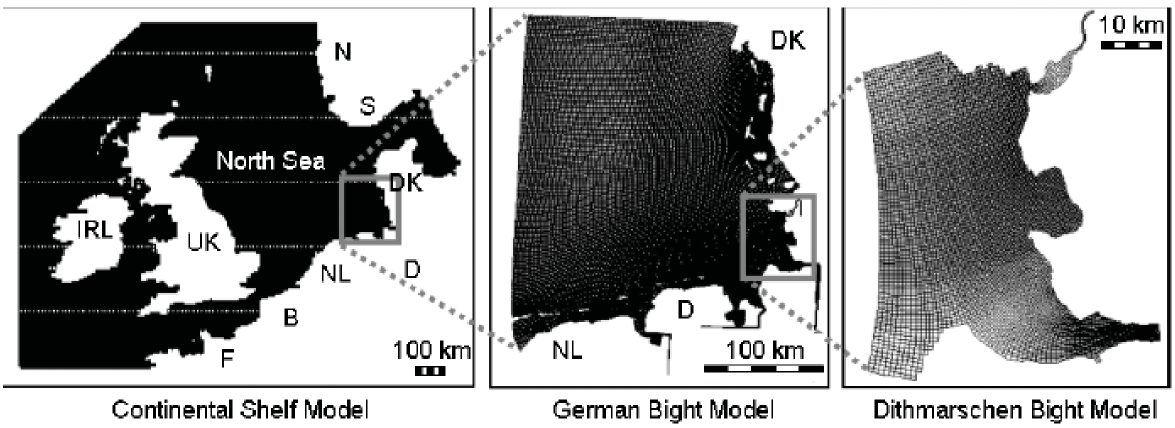

Fig. 4: Nesting sequence for the generation of open sea boundary conditions

In order to improve the descriptions of water levels along the open sea boundaries of the coastal models the results of simulations using the LSMN were subsequently adjusted. This was achieved by comparing measured and computed water levels at one of the gauge stations located at the entrance to the central Dithmarschen Bight. The discrepancies in amplitudes and phases at the Tertius gauge station (G2) were used to correct water levels along the open sea boundaries of the DBM. Owing to a lack of data at the Tertius station during storm periods, the Blauort gauge station (G1) was used instead to cover such periods.

Wind data was obtained using the PRISMA interpolation model developed by the Max Planck Institute of Meteorology in Hamburg (LUTHARDT, 1987). This model generates synoptic wind fields from a large set of measurements at locations along the coastline as well as from offshore data covering the entire North Sea. The PRISMA wind data is generated every three hours with an area resolution of 42 km. A comparison of computed wind data with wind measurements made by the Research and Technology Centre Westcoast (FTZ) of the University of Kiel over a period of 8 years confirms the high quality of the PRISMA model results (WILKENS, 2004).

3.2 Assessment of Modelling Approaches

The various approaches for determining environmental forcing in terms of prescribed water levels along the open sea boundaries were assessed by comparing measured and computed water levels at several locations (G1 to G5 in Fig. 1) over a wide range of conditions. Attention was focused on the effectiveness of the approaches for computing flows in the central parts of the Dithmarschen Bight.

Table 1 summarizes the periods considered in the assessment. These include periods lasting up to 65 days with relatively calm weather conditions (Periods P_{N1} to P_{N6}) as well as stormy periods (Periods P_{S1} to P_{S3}) with water level set-ups of up to about 4.6 m and wind velocities of up to about 30 m/s. Discrepancies between the computed and measured phases and amplitudes at high and low water were evaluated. For periods during which meteorological effects were not significant, comparisons were also made between the tidal constituents of measured and computed water levels.

3.2.1 Approach Based on Measured Water Levels (MWL)

An assessment of the approach based on measured water levels was tested for the CDBM and the ECDBM. In the case of the CDBM, measured water levels at either the Blauort gauge station (G1) or the Trischen gauge station (G3) were specified directly along the western boundary of the model. Along the northern and southern boundaries linear interpolation was applied between the water levels measured at the gauge stations G1 or G3 and G5. For periods during which meteorological effects were negligible (Periods P_{N1} to P_{N6} in Table 1) hindcasted water levels from tide tables were also used (TORO et al., 2005). As the western open sea boundary of the ECDBM is some distance from the Blauort and Trischen gauge stations, it was first necessary to apply corrections to the gauge data in order obtain representative water levels along this boundary. Optimum values were obtained by adjusting the measured phases and amplitudes by about 15 min and 5 %, respectively. Water levels along the northern and southern boundaries were obtained by applying linear interpolation between the corrected water levels on the western boundary and measurements at the Steertloch gauge station (G5) located nearer to the coast.

Simulations were carried out for the conditions listed in Table 1. Comparisons between the measured and computed water levels at gauge stations G2 and G5 are shown in Figs. 5 and 6, respectively. For the sake of compactness, only the results obtained for the period July 7 to July 22, 1990 (first two weeks of Period P_{N4} in Table 1) are shown. It should be noted that the high overlapping obtained between computed and measured water levels at gauge station G2 is due to the fact that the measured water levels at one of the gauge stations in the proximity of the open sea boundary were used to drive the CDBM. The predictive capability of the approach for simulating water levels under more adverse conditions is shown for gauge stations G1 and G4 in Figs. 7 and 8, respectively. Comparisons of the amplitudes and phases of the six main tidal constituents at gauge stations G1, G3, G4 and G5 are shown in Fig. 9 for

Table 1: Periods selected for testing the effectiveness of the various environmental forcing approaches

Period			Duration (days)	Characteristics
Relatively calm weather conditions	P_{N1}	May 31 to June 26, 1989	27	Wind velocities throughout the entire period lower than 8 m/s
	P_{N2}	May 31 to July 12, 1989	43	Incorporates 2 small storms with wind velocities of about 9 m/s and 11 m/s.
	P_{N3}	April 27 to June 30, 1990	65	Incorporates 4 small storms of short duration with wind velocities ≤ 10 m/s
	P_{N4}	July 7 to August 18, 1990	43	Incorporates 4 storms lasting longer than 1 day with wind velocities ≤ 10 m/s
	P_{N5}	August 15 to Sept. 15, 2000	32	Incorporates 5 storms lasting longer than 1 day with wind velocities ≤ 13 m/s.
	P_{N6}	Sept. 22 to Oct. 22, 2000	31	Incorporates 6 small storms of short duration with wind velocities ≤ 11 m/s, also a storm lasting longer than 1 day with wind velocities ≤ 18 m/s.
Storms	P_{S1}	Jan 25 to Jan 31, 1990	6	Wind velocity up to 30 m/s Water level set-up up to 4 m
	P_{S2}	Feb 25 to March 1, 1990	8	Wind velocity up to 25 m/s Water level set-up up to 4.5 m
	P_{S3}	Nov 26 to Dec 5, 1999	9	Wind velocity up to 33 m/s Water level set-up up to 4.4 m

periods during which meteorological effects were negligible. Details of the tidal analysis are summarised in TORO et al. (in this volume). Since the methods based on MWL and TT rely on water levels measured close to the western boundaries, the effectiveness of these methods was only assessed at locations nearer to the coast. It is seen that the results given by all approaches for the amplitudes and phases of the main tidal constituents are in good agreement with observations. Considering the six main constituents, and taking into account MWL and TT, the ratios between the computed and measured tidal constituents were less than 20 % and 25 % for the Buesum (G4) and Steertloch (G5) gauge stations, respectively. The approaches based on MWL and TT yielded phase lags of up to 11 min and 14 min, respectively.

Comparisons of the Mean Absolute Errors (MAE) and Mean Errors (ME) and their Standard Deviations (StDev) are shown in Figs. 10 and 11. Values are given for the gauge stations G1, G2, G4 and G5. The results obtained using MWL along the open sea boundaries of the CDBM and ECDBM are comparable. Better agreement between amplitude values was obtained at high water levels. The average MAE values are generally less than 5 cm and 10 cm (about 1.5 % and 3 % of the mean tidal range) at high and low water level, respectively. The MAE values of the phase lags at high water levels and low water levels were on average less than about 3 % (about 25 min) and 5 % (about 35 min) of the tidal period, respectively. Based on average ME values there is a tendency towards an underestimation of tidal elevations, particularly at low water levels. Moreover, the high and low water levels are attained in advance of the observed values at the stations nearer to the coast. The highest MAE is obtained for the approach in which water levels hindcasted from tidal constituents

(TT) are specified on the open sea boundaries. At high and low water levels the approach based on TT resulted in average MAE values at the station nearer to the coast of less than about 20 cm and 35 cm, respectively. The corresponding MAE values for the phase lags were about 30 min and 33 min. The discrepancies in amplitudes and phases are comparable to those obtained by comparing the hindcasts using TT and measured water levels (see TORO et al., in this volume).

3.2.2 Approach Based on Simulations using Large-Scale Model Nesting (LSMN)

The water levels along the open sea boundaries of the coastal models may also be obtained from simulations using a model covering the adjacent sea area. In this study the north-west European Continental Shelf Model (CSM) was used for this purpose. A nesting sequence was developed to improve the predictive capability of the models in shallow water areas. Details of these models are summarised in the foregoing. In order to improve predictions along the open sea boundaries water level corrections were applied by comparing measured and computed water levels at a gauge station located at the entrance to the tidal channels. The Tertius gauge station (G2) was used for this purpose in the present study. The amplitudes and phases of the values obtained along the open sea boundaries were adjusted on the basis of the discrepancies between measured and computed values. The effectiveness of this approach was verified for the ECDBM and DBM. Simulations were performed for the conditions listed in Table 1.

Comparisons between measured and computed water levels from July 7 to August 18, 1990 (Period P_{N4} in Table 1) at gauge stations G2 and G5 are shown in Figs. 5 and 6, respectively. It is seen that modelled water levels are slightly better at station G2 than at G5, which may be explained by the closer proximity of station G2 to the western boundary. It is also found that larger discrepancies between modelled and measured water levels occur when astronomical constituents are used for hydrodynamic forcing. The predictive capability of this approach for simulating water levels under more adverse weather conditions is shown for gauges G1 and G4 in Figs. 7 and 8, respectively. Fig. 9 shows comparisons of the main tidal constituents at gauge stations G1, G3, G4 and G5 (see Fig. 1). Comparisons of the MAE, ME and StDev are shown in Figs. 10 and 11 for gauge stations G1, G2, G4 and G5 during Period PN4 listed in Table 1.

The MAE values obtained using the ECDBM and DBM are comparable and less than about 10 cm and 20 cm on average (about 3 % and 6 % of the mean tidal range) at high and low water levels, respectively. The corresponding MAE values of the phase lags are about 25 min and 20 min (about 3 % of the tidal period) at high and low water levels, respectively. Similar to the approach based on MWL there is a tendency towards underestimation of low water levels and the occurrence of high and low water levels in advance of those observed.

Investigations to verify the effect of the quantity specified (water levels or current velocities) along the open sea boundaries of the DBM on the momentum balance were also carried out. The DBM was driven along the open sea boundaries using water levels and current velocities obtained from simulations performed using the model nesting sequence shown in Fig. 4. Comparisons of the resulting water levels and current velocities at several locations within the model domain showed only minor discrepancies.

3.3 Discussion

It was found that the simulated conditions along the open sea boundaries given by the approaches based on MWL and LSMN all are in good agreement with observations. Slightly better agreement between observed and computed water levels was obtained for the smaller model, which was driven directly by measured water levels on the open sea boundary. The highest MAE values result from the approach in which astronomical constituents are imposed on the open sea boundaries. The discrepancies are comparable to those obtained from the hindcasted values using astronomical constituents. This approach thus offers an alternative method for prescribing water levels along the open sea boundaries for conditions in which meteorological effects are negligible and measured water levels or larger models are not available. The approach based on simulations using the larger model also proved to be quite effective in all model domains. A correction of the conditions along the open sea boundaries obtained from simulations using measured water levels is essential for ensuring high predictive capability. As measurements covering long periods are seldom available, this approach may be used for generating long-term time series of open sea boundary conditions provided wind fields are available over the surrounding sea area.

The effectiveness of the approaches adopted for prescribing water levels as open sea boundary forcing conditions proved to be quite satisfactory (see PALACIO et al., in this volume). The mean absolute errors between computed and observed depth-averaged velocities at several cross-sections in the tidal channels were generally found to lie below 0.2 m/s, which represents less than 20 % of the tidally-averaged value. In terms of the quality standards usually adopted (VAN RIJN et al., 2002), the performance of the model with regard to current velocity predictions was found to lie between good and excellent.

Comparisons were also made between the results obtained using 2DH and 3D flow model approximations. The suitability of the approaches for prescribing water levels along the open sea boundaries was investigated. The reference grid of the 2DH model was extended to include 10 layers in the vertical direction. The vertical grid spacing of the 3D model was chosen to follow a logarithmic distribution in order to reproduce the vertical flow profile more accurately. Comparisons between the flow model computations were made for water levels at several locations and current velocities at a number of cross-sections. In general, it was found that the results given by the two flow models are fairly similar during most of the tidal cycle, except during slack water periods when current reversal occurs (see PALACIO et al., in this volume).

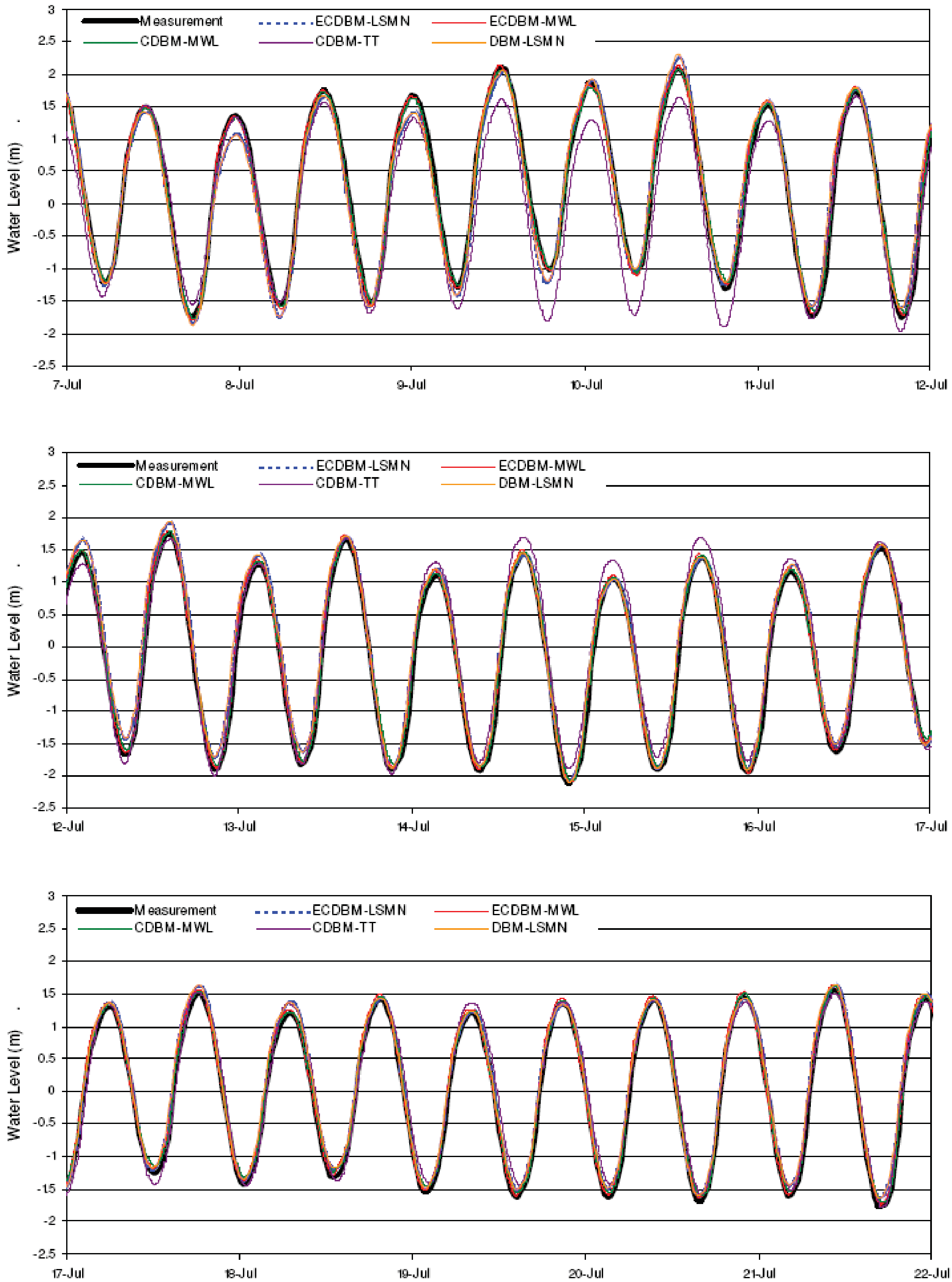

Fig. 5: Measured versus computed water levels at the Tertius gauge station (G2) during Period P_{N4}

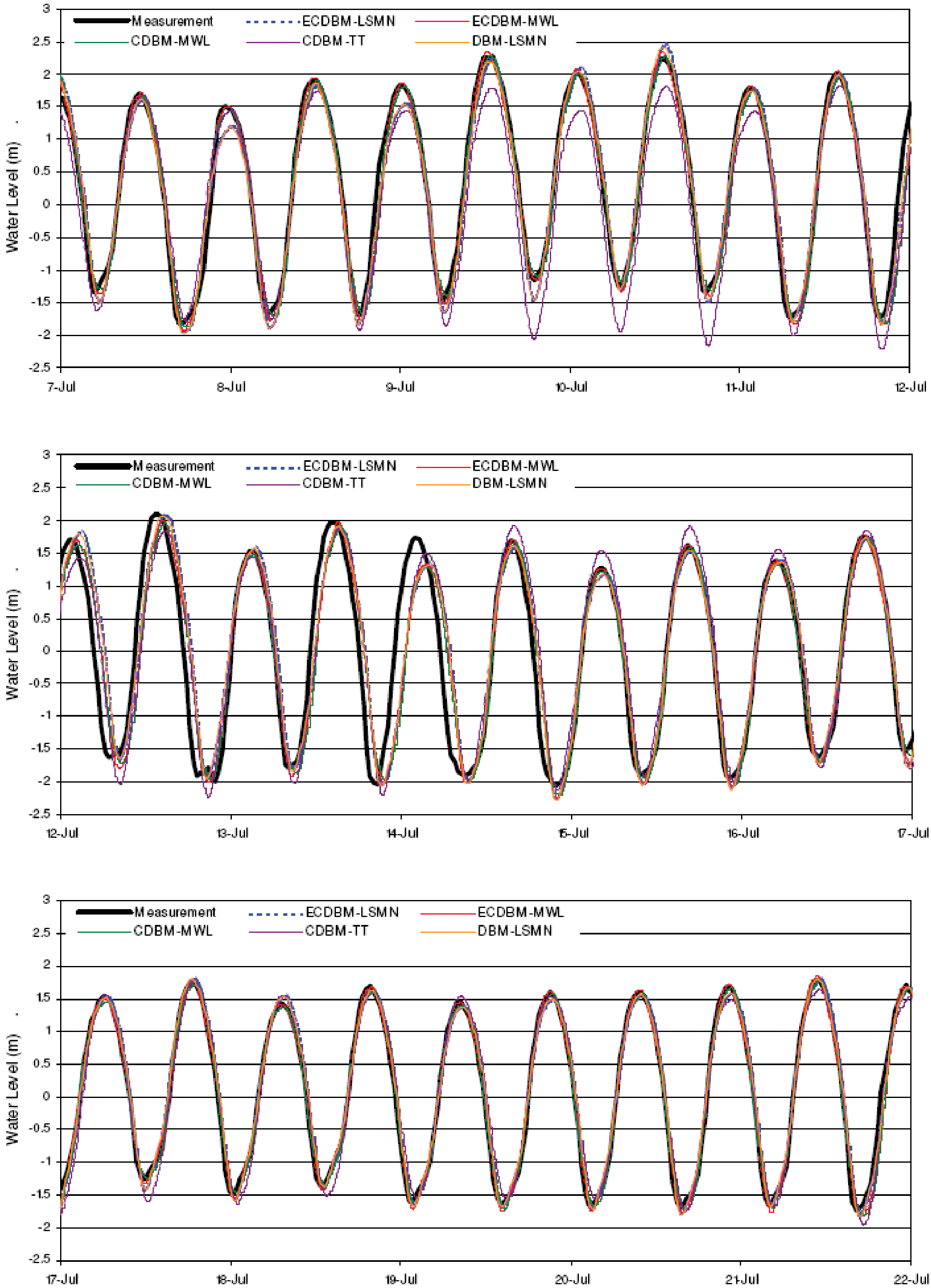

Fig. 6: Measured versus computed water levels at the Steertloch gauge station (G5) during Period P_{N4}

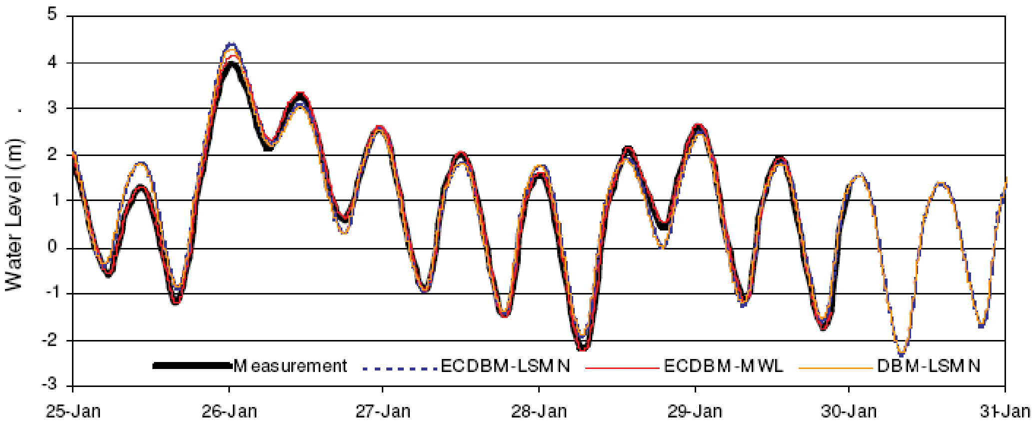

a) Period S1: Jan 25 to 31 of 1990

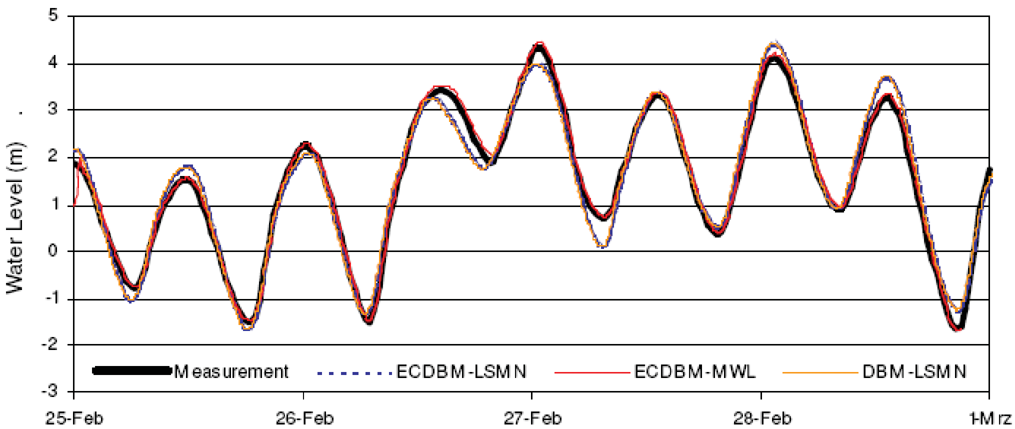

b) Period S2: Feb 25 to March 1 of 1990

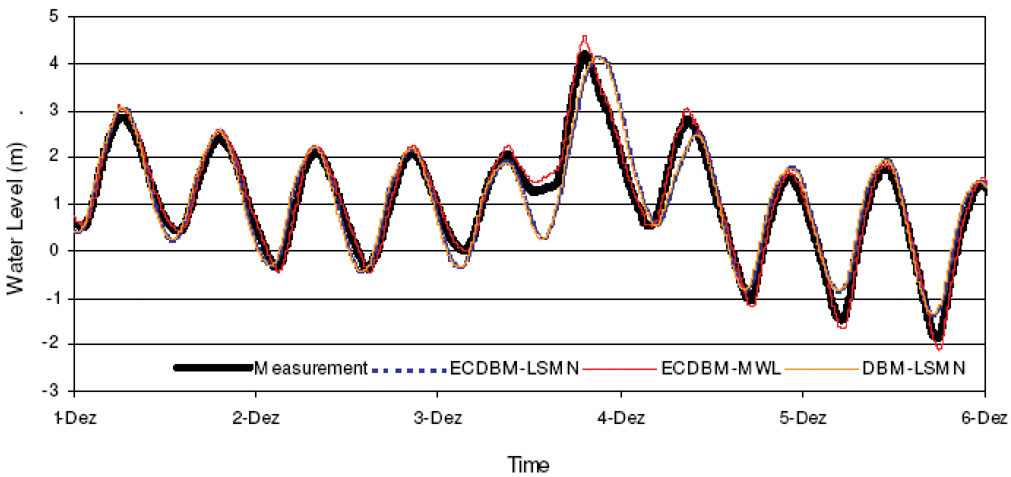

c) Period S3: Nov 26 to Dec 05 of 1999

Fig. 7: Measured versus computed water levels at the Blauort gauge station (G1) during stormy periods

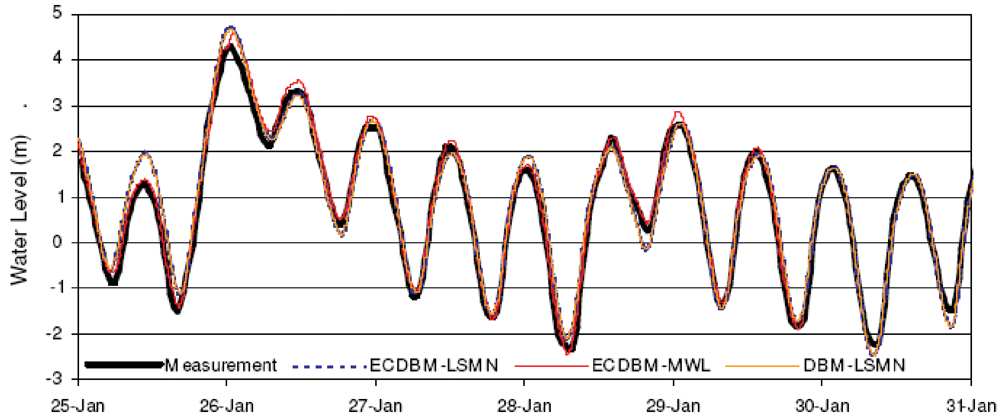

a) Period P_{S1}: Jan 25 to 31 of 1990

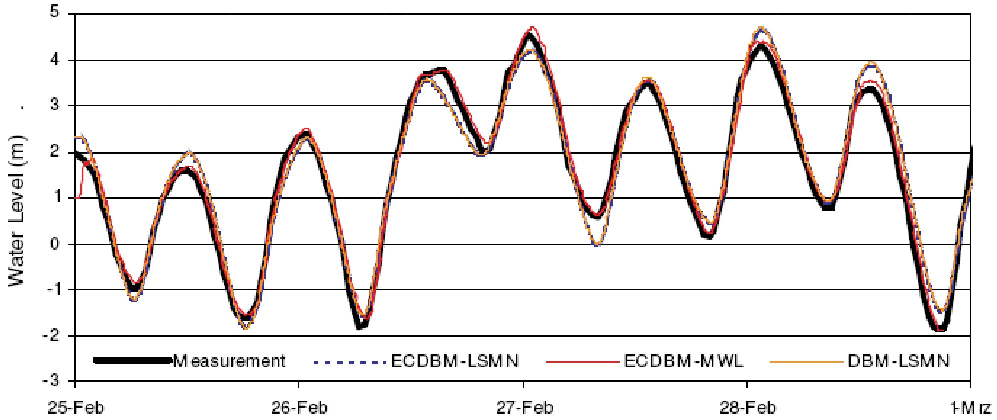

b) Period P_{S2}: Feb 25 to March 1 of 1990

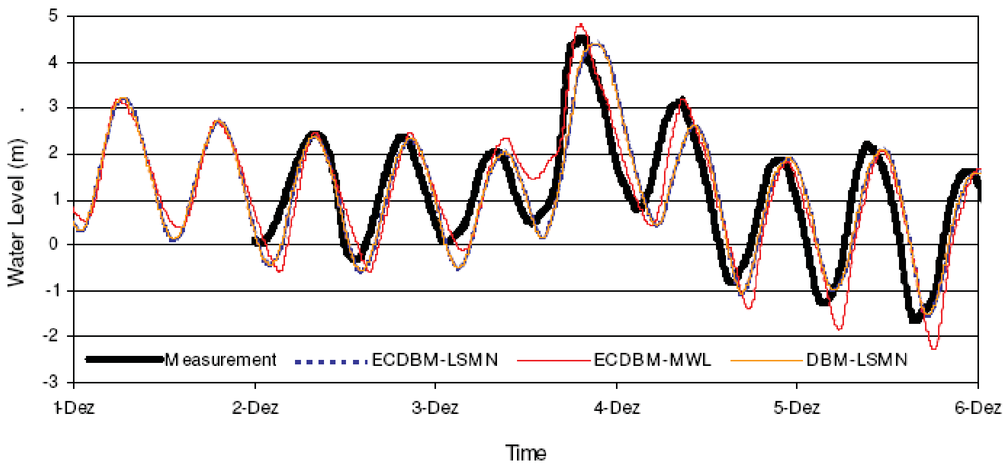

c) Period P_{S3}: Nov 26 to Dec 05 of 1999

Fig. 8: Measured versus computed water levels at the Buesum gauge station (G4) during stormy periods

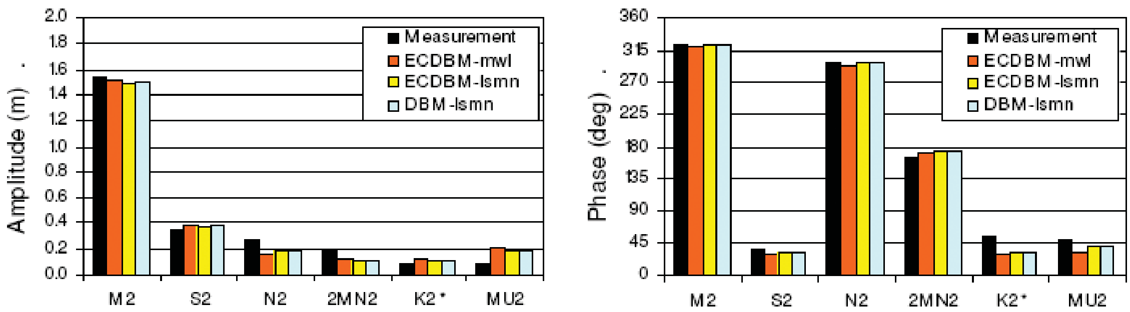

a) Tidal constituents at Trischen (G3)

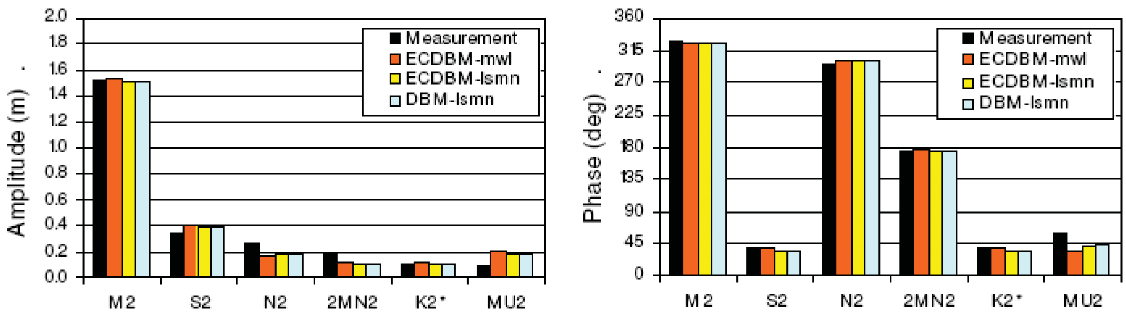

b) Tidal constituents at Blauort (G1)

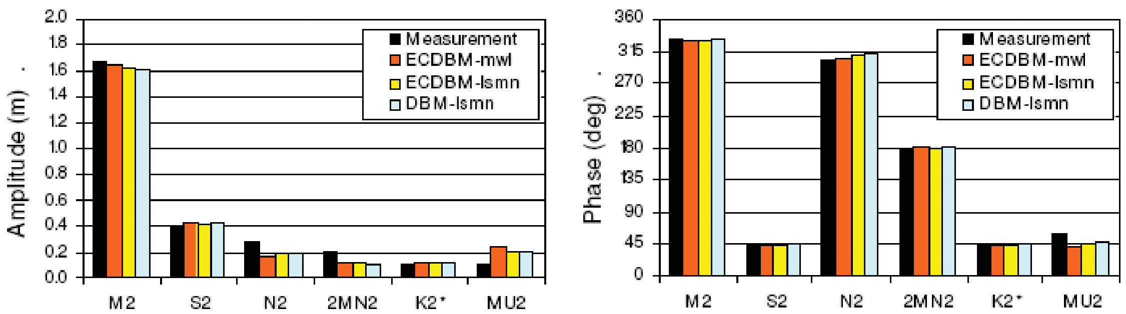

c) Tidal constituents at Buesum (G4)

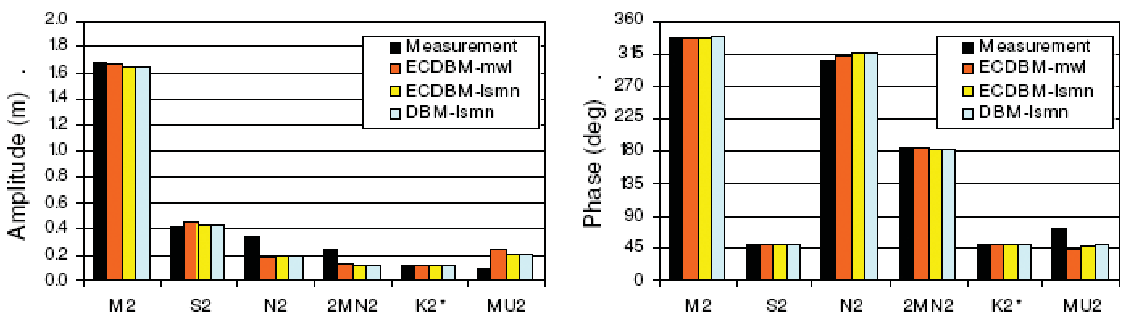

d) Tidal constituents at Steertloch (G5)

Fig. 9: Comparisons of measured and computed tidal constituents at gauge stations G1, G3, G4 and G5 during Period PN4

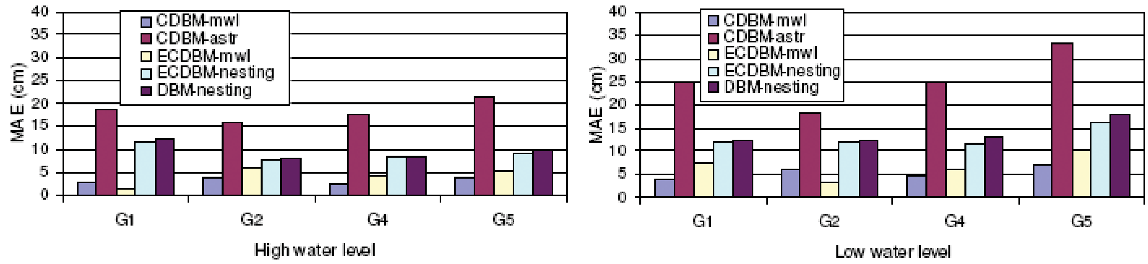

a) Amplitude

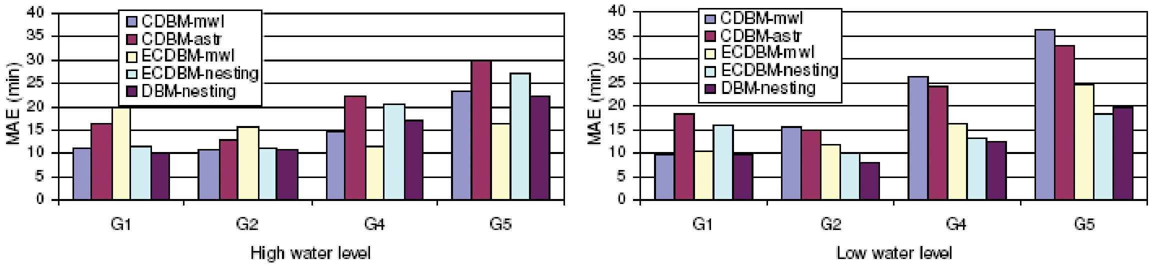

b) Phase

Fig. 10: MAE of computed water levels at several gauges during Period P_{N4}

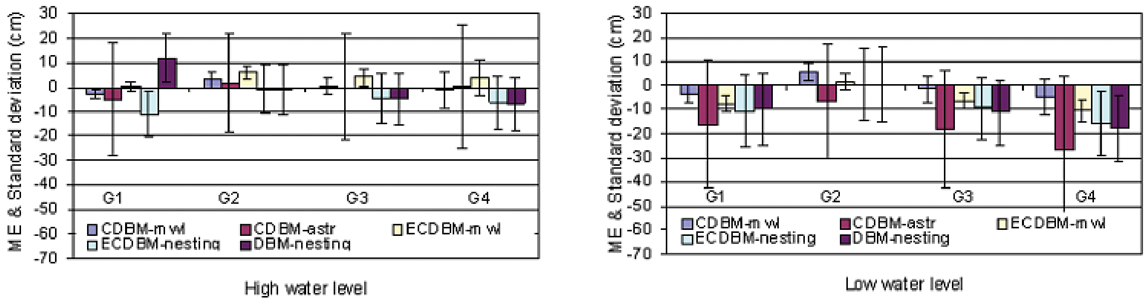

a) Amplitude

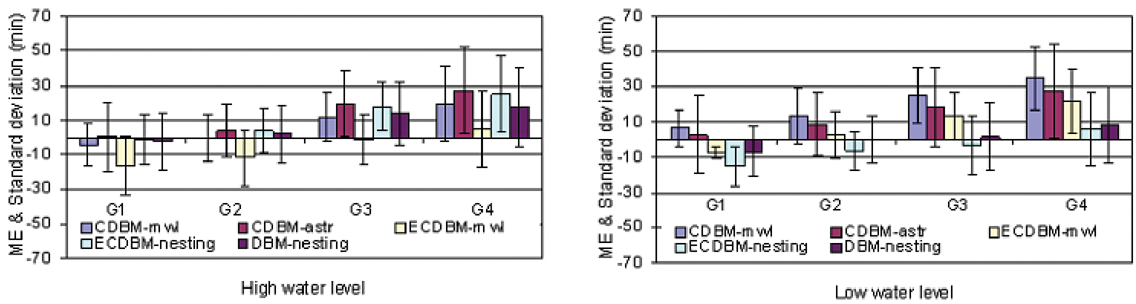

b) Phase

Fig. 11: ME and StDev of computed water levels at several gauges during Period P_{N4}

4. Wave Models

Several approaches are available for modelling waves in coastal areas. Wave models may either be stationary or instationary, and phase-averaged or phase-resolving. Instationary models are applied in situations where the time taken for wave energy to travel through the model domain is significantly longer than the period during which wind and wave boundary conditions are constant. In such models, previous states of wave energy distribution are taken into account when computing the wave energy distribution at a certain point in time. In stationary models, on the other hand, a final state based on the imposed wind and wave boundary conditions is assumed. Phase-resolving models are used when the hydrodynamic variations during a wave period are of significance. This is the case, e.g. in studies of wave impact on coastal structures or for investigating the wave transformation in harbours. Due to the fact that the computational costs of instationary models and phase-resolving models are much higher than for stationary and phase-averaged approaches, the latter approaches are preferably used if permitted by the objectives of the study. As the model considered here was set-up to determine the general wave conditions for morphodynamic modelling in a coastal area of limited size, the latter approach was adopted in this study.

Conditions along the open sea boundary of a wave model may be specified parametrically by means of a pre-defined spectral shape, e.g. a JONSWAP-spectrum, or by imposing a user-defined spectrum. The conditions specified along the open sea boundaries may either be spatially varying or constant. Data records of boundary conditions may either stem from wave measurements at locations near the open sea boundaries, from the results of a larger wave model (model nesting), or may be estimated using relationships between wind conditions and fetch lengths. The latter approach is generally limited to water bodies subject to small spatial variations in meteorological conditions. Unless this is the case, this method would become too complex and too inaccurate for practical application.

4.1 Model Domain and Modelling Approaches

The wave model developed for the Dithmarschen Bight is based on the SWAN wave model (BOOIJ et al., 1999; RIS et al., 1999). This model was coupled to a flow model in order to include the effects of ambient currents and water levels on the computed wave characteristics. Calibration and validation of the wave model yielded good results regarding a visual comparison of the computed and observed time series as well as a statistical evaluation based on the Relative Mean Absolute Error (RMAE), as proposed by VAN RIJN et al. (2002). The set-up, evaluation and application of this model is described in detail by WILKENS et al. (in this volume). The computational grid and bathymetry of the wave model are shown in Fig. 2. Based on the results of a sensitivity analysis, only the western boundary was defined as an open sea boundary through which wave energy can enter the domain. The shallow tidal flats in the proximity of the southern and northern boundaries prevent the intrusion of a significant amount of wave energy at these locations. The main purpose of the wave model was to compute the general wave characteristics throughout the study area for medium-scale morphodynamic simulations. For this reason the wave model focuses on characteristic wave parameters rather than actual wave energy spectra. Wave conditions along the open sea boundary are thus imposed parametrically, i.e. by defining the significant wave height, peak period and mean wave direction. The following two approaches were adopted for defining the open sea boundary conditions.

In the first approach, records of wave parameters deduced from wave measurements at a buoy located close to the middle of the open sea boundary (Position 2 in Fig. 12) were subsequently specified as boundary conditions. Owing to the relatively small variations between the observed wave characteristics at Positions 1 and 2 and the inaccuracies introduced by interpolating between the values at these locations, it was decided to impose uniform conditions along the open sea boundary. The wave data recorded during September and October 1996 were kindly provided by the Coastal Research Station of the Lower Saxony Board of Ecology on Norderney, who carried out measurements within the framework of the KFKI project 'Bemessung auf Seegang' (Grant No. KFKI 45) funded by the German Ministry of Education and Research (BMBF) under Grant No. MTK 0561 (NIEMEYER, 1997).

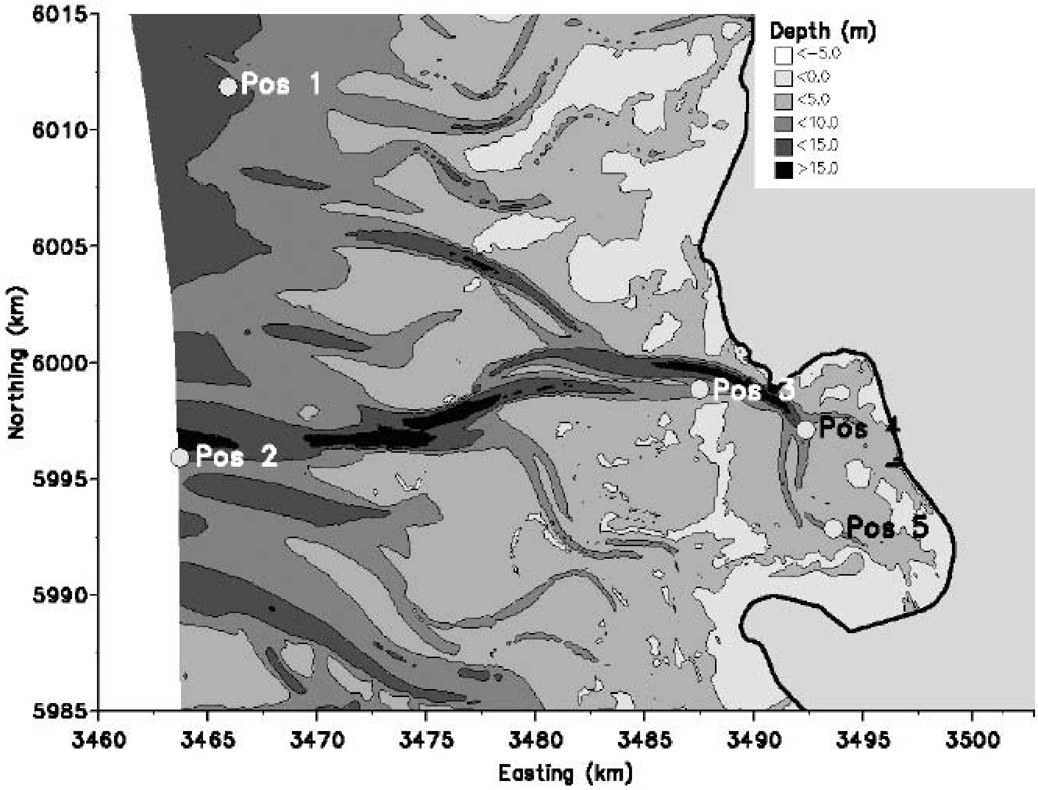

Fig. 12: Wave measurement locations during September and October 1996

In the second approach, the Dithmarschen Bight Model (DBM) was nested in the larger German Bight Model (GBM) (see Fig. 4). This nesting sequence was applied for flow simulations, commencing with the even larger Continental Shelf Model (CSM). The GBM was forced by wind only, neglecting any incoming wave energy through the open sea boundaries. From a sensitivity study it was concluded that the extra computational costs of nesting the GBM in the CSM were not justified due to only slight differences in wave parameters along the boundary of the DBM. The stationary version of the GBM was thus implemented for wave computations. Although the data generated in this way are subject to inaccuracies inherent to model results, this approach permits the definition of acceptable boundary conditions outside the observation periods.

4.2 Assessment of Modelling Approaches

The results of the validated wave model have shown that incoming swell energy does not penetrate the entire tidal flat area during moderate weather conditions (WILKENS et al., in this volume). Although the limit of swell energy is generally close to the 10 m isobath, swell may penetrate slightly further into the domain via the tidal channels. Although wave penetration through the tidal channels is possible due to their greater depths, it may be hindered by channel geometry.

Eastwards of the 10 m isobath, waves are mainly generated by local winds. Under average conditions an improvement of the open sea boundary conditions is thus only relevant over the outer tidal flats. It thus only possible to assess the quality of the imposed boundary conditions on the basis of measurements carried out near the open sea boundary. Furthermore, the quality of the model results at locations within the model domain depends partly on the imposed boundary conditions and partly on the performance of the model itself. A proper assessment of the quality of the boundary conditions should thus be made at locations in the vicinity of the open sea boundary. The method of imposing values measured in the direct proximity of the open sea boundaries clearly yields the most accurate results. Considering the wave characteristics at Position 2, the results of the second approach were therefore compared with the results of the first approach for the observation period September/October 1996. Comparisons between observed and computed significant wave heights, peak periods and mean directions at Position 2 during the period September/October 1996 are shown in Figs. 13, 14 and 15, respectively. Although only minor tuning of the model parameters was carried out in this study, fair agreement is obtained between observations and computed results. A possible reason for the differences between the GBM results and observations could be the inaccurate representation of bathymetry due to a fairly coarse grid resolution. Another reason might be the stationary nature of the applied model, whereby changes in meteorological conditions are directly transferred to the resulting wave fields without consideration of previously generated waves. Apart from minor differences between observed and computed wave heights in some instances, the model results reflect the major trends fairly well.

Besides a visual and somewhat subjective comparison of the time series of the aforementioned parameters, they are also compared in scatter plots in Figs. 16 and 17. In order to obtain a more objective evaluation of the quality of the model results the data pairs of the scatter plots were used to compute the following relative mean absolute error (RMAE, see Eq. 1), as defined by VAN RIJN et al. (2002).

$$\mathrm{RMAE} = \frac{\overline{\max\{|P_c - P_m| - \Delta P_m, 0\}}}{\overline{P}_m}$$

in which:

P_m = measured parameter (either wave height or period);

P_c = computed parameter; and

ΔP_m = inaccuracy of the measured parameter (values of 0.1 m and 0.3 s were assumed for wave height and period, respectively).

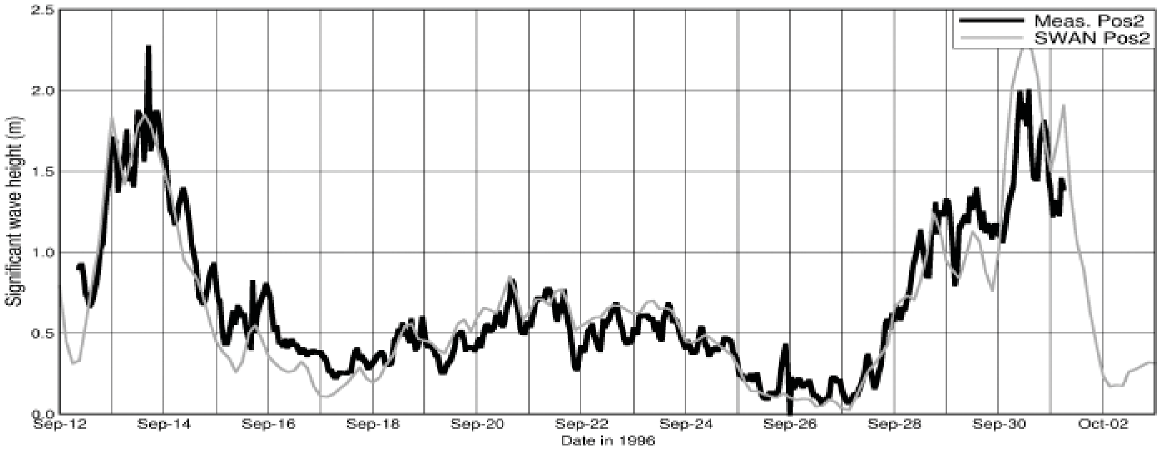

Fig. 13: Comparison between observed and computed significant wave heights at Position 2

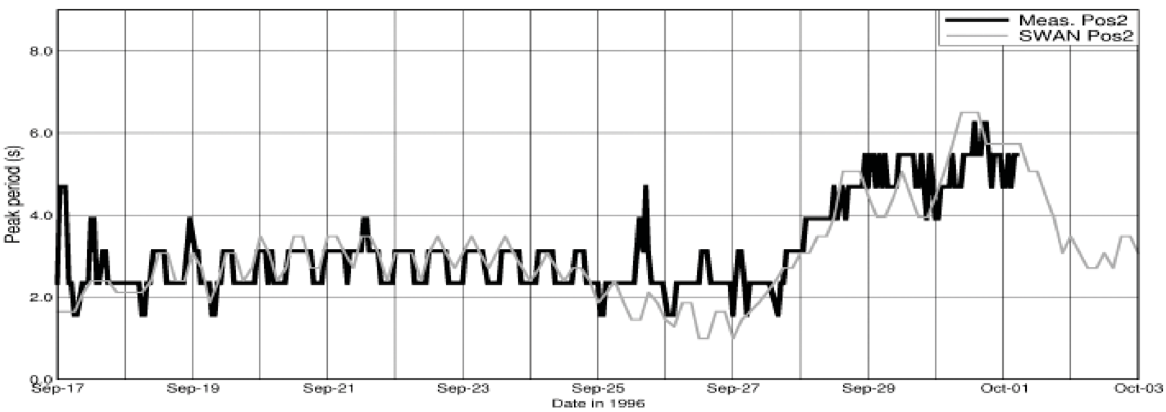

Fig. 14: Comparison between observed and computed peak periods at Position 2

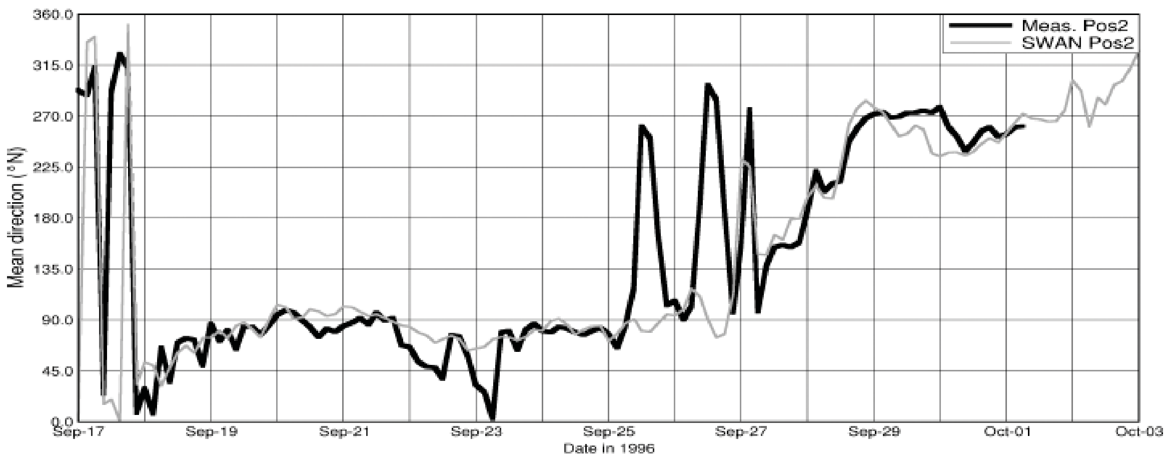

Fig. 15: Comparison between observed and computed mean wave directions at Position 2

The numerator and denominator of Eq. 1 are averaged over the evaluation period. The quality of a model in terms of simulated significant wave heights is rated on the basis of the RMAE value according to the classification of VAN RIJN et al. (2002) shown in Table 2. No such rating scheme is available at present for wave periods. In view of the definition of the RMAE, it is not possible to apply this rating scheme to wave directions.

Table 2: Quality of simulated wave heights based on RMAE values (VAN RIJN et al., 2002)

Rating	RMAE value
Excellent	< 0.05
Good	0.05–0.10
Reasonable / fair	0.10–0.20
Poor	0.20–0.30
Bad	> 0.30

As is evident from the scatter plots of Figs. 16 and 17, fairly good correlations are obtained between observed and simulated values for the three parameters considered. Considering the RMAE value of 0.08 obtained for significant wave heights, the model results may be rated as 'good' according to the classification of VAN RIJN et al. (2002). Applying the same classification scheme to peak periods with an RMAE value of 0.17, a rating of 'reasonable/fair' is obtained.

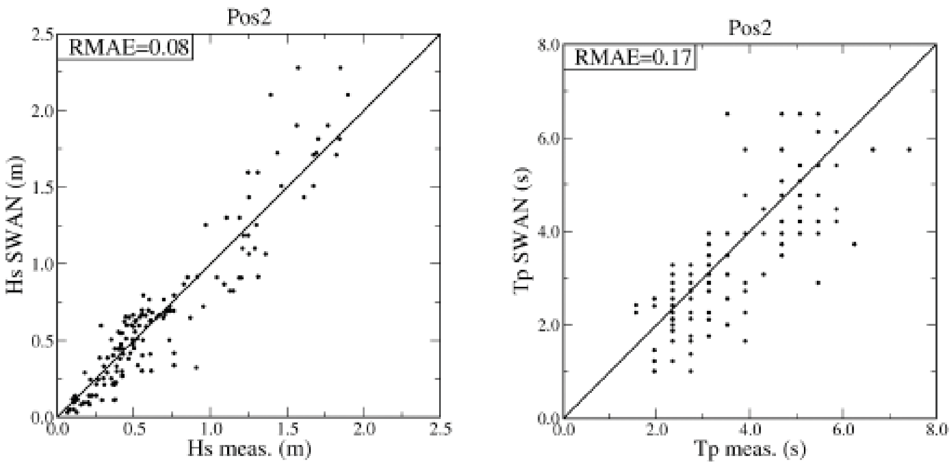

Fig. 16: Scatter plots and RMAE values for significant wave heights and peak periods at Position 2

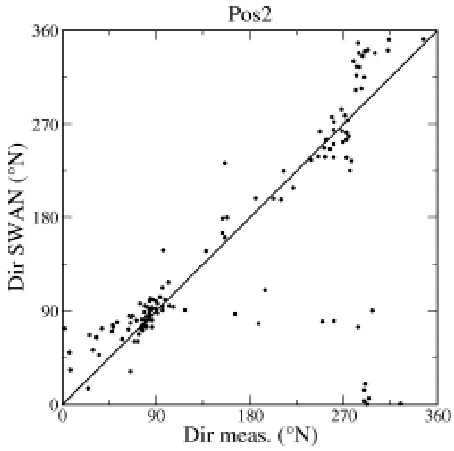

Fig. 17: Scatter plot of mean wave direction at Position 2

4.3 Discussion

On the basis of the foregoing it is seen that the results obtained from the stationary version of the GBM are in fair agreement with observations. Imposing these model results along the open sea boundary of the DBM, the slight deviations from observed values are likely to have some effect on the results of the DBM. If direct observations close to the open sea boundary of the DBM are available for the modelling period in question, however, it is clearly preferable to use such data rather than the results of GBM simulations. Observations are generally not available over large time spans, however. In view of this, the model nesting approach offers a valuable alternative for defining open sea boundary conditions. Although the application of the instationary version of the GBM might lead to further improvements, these should however be weighed against additional computational costs.

Imposing measured wave characteristics directly on the open sea boundary is obviously the most accurate approach, provided measurements are made in the proximity of the open sea boundary concerned. In the case of wave measurements further away, however, additional errors may be introduced due to changes in prevailing conditions, e.g. changes in water depths and current velocities. Moreover, this method is only applicable for periods during which measurements are available. It was shown in the foregoing that the application of model nesting yields fairly good results even when a stationary wave model is used. If wind data are available for the model domains in the nesting sequence, this approach serves as a valuable alternative to direct measurements.

5. Conclusions

In this paper the relevance of hydrodynamic forcing on the predictive capability of process-based flow and wave models has been demonstrated for a coastal area model on the German North Sea coast. Two-dimensional depth-averaged (2DH) flow models based on the DELFT3D modelling system developed by Delft Hydraulics in the Netherlands (ROELVINK and VAN BANNING, 1994) as well as the phase-averaged spectral wave model SWAN (BOOIJ et al., 1999; RIS et al., 1999) were implemented in the study.

The selection of the model limits for the coastal area using the results of preliminary model runs covering a larger area proved to be quite effective. The orientation of the western open sea boundary was chosen be orthogonal to the direction of propagation of the tidal wave and swell entering the coastal area. It was found that the flow conditions in the study area are mainly determined by the conditions specified along this boundary.

Several approaches usually adopted for determining open sea boundary conditions for driving flow and wave models were compared for a coastal area on the German North Sea coast. Approaches based on water level measurements and the results of simulations using a model covering the entire North Sea were investigated. It was shown that both approaches are capable of providing water levels along the open sea boundaries for driving the 2DH flow models. In the majority of the tests carried out in this study better agreement with observations was obtained at locations in deeper water and closer to the open sea boundaries where the effects of bathymetry and bottom roughness are less pronounced.

In the case of the flow model it was found that the best agreement with observations was obtained using direct measurements along the open sea boundaries. This approach, however, is usually restricted to smaller domains in which gauge stations are located in the proximity of the open sea boundaries. Under normal conditions the mean absolute errors (MAEs) in amplitudes were found to be less than 5 cm (1.5 % of the mean tidal range) and about 10 cm (3 % of the mean tidal range) at high and low water levels, respectively. The MAE of phase lags was found to be less than about 35 min (about 5 % of the tidal period), whereas during storm conditions, the MAE for water levels was found to be less than 35 cm. The use of simulation results from a larger model covering the adjacent sea area also proved to be quite effective. The robustness of the method for correcting water levels along the open sea boundaries based on comparisons between measured and computed water levels has been demonstrated. The application of the approach to three model domains yielded comparable results. The mean absolute errors in amplitudes and phases during periods with calm winds were found to be less than 3 % (about 10 cm) and 6 % (about 18 cm) of the tidal range and 4 % (about 27 min) and 3 % (about 20 min) of the tidal period at high and low water levels, respectively, whereas the MAE of water levels during storm conditions was found to be less than about 26 cm. Compared with the approaches based on measured water levels or large-scale model nesting (LSMN), the approach based on astronomical constituents gave the poorest agreement with observations. The resulting discrepancies were found to be of the same order as those obtained by comparing hindcasts using tide tables and measured values. This approach offers an alternative means of determining water levels along the open sea boundaries in cases where measured water levels or larger models covering the adjacent sea area are not available. It should be pointed out, however, that the latter approach is limited to periods with moderate winds.

The effectiveness of specifying water levels along the open sea boundaries in relation to the preservation of momentum balance was also verified. Comparisons between the model results obtained at several locations in the study area from simulations with a)water levels and b)current velocities specified on the western open sea boundary showed fair agreement. Moreover, the various approaches adopted in this study were found to reproduce current velocities over several cross-sections in close agreement with observations. The results of model validation using measured current velocities are summarised in PALACIO et al. (in this volume).

In order to confirm the suitability of the approaches adopted for prescribing water levels along the open sea boundaries for a 3D model approximation, a comparison was made between the results obtained from 2DH and 3D flow model simulations. In general, it was found that the results given by the two flow models are fairly similar during most of the tidal cycle, except during slack water periods when current reversal occurs (see PALACIO et al., in this volume).

An evaluation of the generation of open sea boundary conditions for the wave model by model nesting showed that this approach yields acceptable results. The general trends in wave characteristics are reproduced fairly well, with good correlation between computed and measured values. A statistical evaluation based on the RMAE yielded the rating 'good' for wave heights and 'reasonable / fair' for wave periods. As is generally known, the latter parameter is difficult to model accurately. As indicated by the scatter plot of Fig. 17, good results were also obtained for mean wave directions. Generally speaking, it may be concluded that the model nesting approach is a reliable alternative for estimating wave conditions along the open sea boundary of wave models. An advantage of this approach, of course, is that it may be applied during periods when direct measurements are not available.

6. Acknowledgements

The results presented in this paper form a contribution to the research project "Predictions of Medium-Scale Morphodynamics – PROMORPH" funded by the German Ministry of Education and Research from 2000 to 2002 (fonding number 03 F 0262 A). The authors wish to thank the Office for Rural Development (ALR) in Husum for providing extensive water level measurements as well as the Coastal Research Station of the Lower Saxony Board for Ecology on Norderney for providing the wave data and making available the German Bight Model developed by Delft Hydraulics (The Netherlands) within the German-Dutch project WADE (Wadden Sea Morphodynamical Development), also funded by the German Ministry of Education and Research. The splendid cooperation with the staff of the participating institutes is also gratefully acknowledged. The authors are also indebted to Dr. Ian Westwood for his meticulous corrections and final proofreading of the English manuscript. Finally, we wish to thank Dr.-Ing. V. Barthel as well as the anonymous reviewers for their constructive remarks.

7. References

ANNAN, J. D.: Hindcasting Coastal Sea Levels in Morecambe Bay. Estuarine, Coastal and Shelf Science, Nr. 53, pp. 459–466, 2001.

ASPELIEN, T. and WEISSE, R.: Assimilation of Sea Level Observations for Multi-Decadal Regional Ocean Model Simulations for the North Sea. GKSS-Forschungszentrum Geesthacht GmbH, ISSN 0344-9629, 2005.

BOOIJ, N.; RIS, R. C. and HOLTHUIJSEN, L. H.: A Third-Generation Wave Model for Coastal Regions, Part I, Model Description and Validation. Journal of Geophysical Research, Vol. 104, C4, 1999.

BRUMMELHUIS, P. G. J TEN; GERRITSEN, H. and KAAIJ, T.: Sensitivity Analysis and Calibration of the Hydrodynamic PROMISE Model Using Adjoint Modelling Techniques. WL|Delft Hydraulics, Report Z2025, 1997.

DICK, S.; KLEINE, E. S.; MÜLLER-NAVARRA, H.; KLEIN, H. and KOMO, H.: The Operational Circulation Model of BSH (BSHcmod)-Model Description and Validation. Berichte des Bundesamtes für Seeschifffahrt und Hydrographie, Nr. 29, 2001.

ELIAS, E. P. L.; WALSTRA, D. J. R.; ROELVINK, J. A.; STIVE, M. J. F. and KLEIN, M. D.: Hydrodynamic Validation of Delft3D with Field Measurements at Egmond. Proc. 27th Int. Conf. on Coastal Engineering. ASCE, New York, pp. 2714–2727, 2000.

HARTSUIKER, G.: Deutsche Bucht and Dithmarschen Bucht, Set-up and Calibration of Tidal Flow Models. Delft, Delft Hydraulics, Report H1821, 1997.

HOLTHUIJSEN, L.; BOOIJ, H. and HERBERS, T. H. C.: A Prediction Model for Stationary, Short-Crested Waves in Shallow Water with Ambient Currents. Coastal Engineering, Vol. 13, 1989.

JUNGE, I.; WILKENS, J.; HOYME, H. H. and MAYERLE, R.: Modelling of Medium-Scale Morphodynamics in a Tidal Flat Area in the South-Eastern German Bight, Die Küste, Heft 69, 2005.

LUTHARDT, H.: Analyse der Wassernahen Druck- und Windfelder über der Nordsee aus Routine-Beobachtungen. Hamburger Geophysikalische Einzelschriften, Fachbereich Geowissenschaften, Universität Hamburg, Germany, Reihe A83, in German, 1987.

MEWIS, P.; ZANKE, U. and DE JONGE, J.: Numerical Study of the Morphology Around the East Frisian Islands. Proceedings of the 3rd ICHE, Cottbus, Germany, 1998.

MILBRADT, P. and PLÜSS, A.: Numerical Modelling of Wave Current Interaction in an Estuary. COPEDEC VI, Colombo, Sri Lanka, 2003.

NIEMEYER, H. D.: Bemessung auf Seegang. Entwicklung abgesicherter Verfahren zur Ermittlung der Bemessung des Wellenauflaufs. KFKI-project No. 45, in German, 1997.

PALACIO, C.; WINTER, C. and MAYERLE, R.: Set-Up of a Hydrodynamic Model for the Meldorf Bight. Proceedings of the ASCE/EWRI World Water and Environmental Resources Congress 2001, Orlando, USA, 2001.

PALACIO, C.; MAYERLE, R.; TORO, M. and JIMÉNEZ, N.: Modelling of Flow in a Tidal Flat Area in the South-Eastern German Bight, Die Küste, Heft 69, 2005.

RIS, R. C.; BOOIJ, N. and HOLTHUIJSEN, L. H.: A Third Generation Wave Model for Coastal Regions, Part II, Verification, Journal of Geophysical Research, Vol. 104, C4, 1999.

ROELVINK, J. A. and VAN BANNING, G.K.F.M.: Design and Development of DELFT3D and Application to Coastal Morphodynamics, Proc. Hydroinformatics 1994 (Delft, the Netherlands), H.H. Balkema Publishers, Rotterdam, the Netherlands, 1994.

SIEGLE, E.; HUNTLEY, D. A. and DAVIDSON, M. A.: Modelling Water Surface Topography at a Complex Inlet System – Teignmouth, UK. UK J. Coastal Res. SI 36: pp. 675–685, 2002.

TORO, F.; MAYERLE, R.; POERBANDONO and WILKENS, J.: Patterns of Hydrodynamics in a Tide-Dominated Coastal Area in the South-Eastern German Bight, Die Küste, Heft 69, 2005.

VAN RIJN, L. C.; WALSTRA, D. J. R.; GRASMEIJER, B.; SUTHERLAND, J.; PAN, S. and SIERRA, J. P.: Simulation of Nearshore Hydrodynamics and Morphodynamics on the Time Scale of Storms and Seasons Using Process-Based Profile Models. In: Van Rijn, L. C., B. G. Ruessink and J. P. M. Mulder (ed.), The Behaviour of a Straight Sandy Coast on the Time Scale of Storms and Seasons: Process Knowledge and Guidelines for Coastal Management: End Document March 2002. EC MAST Project, MAS3- CT97-0086 COAST3D – EGMOND, 2002.

VERBOOM, G. K.; DE RONDE, J. G. and VAN DIJK, R. P.: A Fine Grid Tidal Flow and Storm Surge Model of the North Sea, Continental Shelf Research, Vol. 12, No. 2/3, pp. 213–233, 1992.

WILKENS, J.; ASP NETO, N. E.; RICKLEFS, K. and MAYERLE, R.: Medium-Scale Morphodynamic Modelling in the Meldorf Bight, Proceedings of the EWRI/ASCE World Water and Environmental Resources Congress, Orlando, USA, 2001.

WILKENS, J.: Medium Scale Morphodynamics of the Central Dithmarschen Bight, Ph.D. thesis, University of Kiel, Germany, (available under http://e-diss.uni-kiel.de/diss_1369/d1369.pdf), 2004.

WILKENS, J. and MAYERLE, R.: Modelling of Medium-scale Morphodynamics in a Tidal Flat Area in the German Wadden Sea, Proceedings of the 29th ASCE International Conference on Coastal Engineering (ICCE 2004), Lisbon, Portugal, 2004.

WILKENS, J.; JUNGE, I. and HOYME, H.: Modelling of Waves in a Tidal Flat Area in the South-Eastern German Bight, Die Küste, Heft 69, 2005.

WINTER, C.; POERBANDONO; HOYME, H. and MAYERLE, R.: Modelling of Suspended Sediment Dynamics in Tidal Channels of the German Bight, Die Küste, Heft 69, 2005.

Die Küste, 69 PROMORPH (2005), 1-420

Dimension and Roughness Distribution of Bed Forms in Tidal Channels in the German Bight

By ROBERTO MAYERLE, GATOT PRAMONO and CARLOS ESCOBAR

Summary

The results of investigations of the spatial and temporal variations of the dimensions of bed-form features and associated bed roughness are presented in this paper. The study was carried out in the main tidal channels of the central Dithmarschen Bight on the German North Sea coast. Measurements of the dimensions of bed forms were carried out at several locations using side scan sonar and echo sounders. Current velocities were also measured using acoustic profilers in the near-bed region. The spatial variation of the dimensions of bed-form features was found to be quite significant and highly dependent on the layer thickness of potentially mobile sediments, the characteristics of surficial seabed sediments and local flow conditions. The temporal variation of bed-form dimensions during a tidal cycle was found to be appreciable, especially with regard to length. A verification of existing empirical equations proposed for predicting bed-form dimensions showed poor agreement with observed values. Fair agreement was obtained, however, with regard to bed-form roughness values. A numerical procedure for predicting bed-form dimensions and associated bed roughness values is suggested. The identification of bed-form types and the estimation of bed-form dimensions and equivalent roughness sizes were obtained using the results of flow model simulations. Maps of bed-form dimensions and roughness in the tidal channels were derived from the latter. The importance of bed roughness is highlighted in relation to simulated current velocities and suspended sediment concentrations. The results clearly indicate the relevance of bed roughness, particularly with regard to sediment transport predictions. It was found that the accuracy of simulated sediment transport rates is highly dependent on the formulation used to predict the bed roughness. Different bed roughness sizes were found to influence both the magnitude and phase of suspended material concentrations.

Zusammenfassung

In diesem Beitrag sind die Ergebnisse räumlicher und zeitlicher Variationen der Dimensionen von Bodenformen am Seegrund und der damit in Zusammenhang stehenden Rauigkeit zusammengefasst. Die Untersuchungen erfolgten in den Hauptgezeitenströmen der Zentralen Dithmarscher Bucht an der Deutschen Nordseeküste. Die Messungen zur Dimensionierung von Bodenformen wurden an mehreren Lokalitäten unter Anwendung von Seitensicht-Sonar und Echolot durchgeführt. Auch Messungen der Strömungsgeschwindigkeiten erfolgten mit Akustik-Profilern nahe der Seegrundoberfläche. Die räumliche Variation der Dimensionen der Bodenform-Ausprägungen waren signifikant und hochgradig abhängig von der Schichtdicke potentiell mobiler Sande, den Charakteristiken oberflächennaher Sedimente und den örtlichen Strömungsbedingungen. Die zeitlichen Variationen der Bodenform Dimensionen im Verlauf eines Tidezyklus waren in Bezug auf deren Längen beträchtlich. Die Ergebnisse der Verifizierungen bestehender empirischer Gleichungen, die zur Vorhersage von Bodenform-Dimensionen und -Rauigkeiten vorgeschlagen sind, zeigten nur geringe Übereinstimmungen mit den beobachteten Werten. Eine mäßige Übereinstimmung wurde jedoch zu den Bodenform-Rauigkeiten erzielt. Es wird eine Prozedur zur Vorhersage von Bodenform-Dimensionen und damit in Zusammenhang stehenden Bodenrauigkeitswerten vorgeschlagen. Die Identifikation von Bodenform-Typen und die Abschätzung der Bodenform-Dimensionen und äquivalenten Rauigkeitsgrößen wurden aus den Ergebnissen von Strömungsmodell-Simulationen erzielt. Aus diesen wurden Karten von Bodenform-Dimensionen und -Rauigkeiten in den Gezeitenrinnen abgeleitet. Die Bedeutung *der Bodenrauigkeit wird in ihrer Beziehung zur simulierten Strömungsgeschwindigkeit und den Konzentrationen suspendierten Sediments beleuchtet. Die Ergebnisse weisen deutlich auf die Relevanz der Rauigkeit insbesondere in Bezug auf Vorhersagen des Sediment Transports hin. Die Genauigkeit der simulierten Sediment-Transportraten erwiesen sich als hochgradig abhängig von den Formulierungen, die zur Vorhersage des Bodenrauigkeit verwendet wurden. Es ergab sich ferner, dass unterschiedliche Bodenrauigkeiten sowohl Größe als auch die Phase der suspendierten Sedimentkonzentrationen beeinflussen.*

Keywords

Bed Forms, Bed Roughness, Spatial Bed-Form Distribution, Temporal Bed-Form Variation, Field Measurements, Modelling, Dithmarschen Bight, Tidal Flats, Tidal Channels, North Sea, DELFT3D, SWAN, PROMORPH

Contents

1. Introduction

The seabed exhibits a variety of morphological patterns as a result of sediment motion due to current and/or wave action. These features, known as bed forms, interact with the flow by introducing resistance. The fact that information on bed-form dimensions and roughness sizes in the field is normally not available continues to represent one of the greatest obstacles to the accurate prediction of sediment transport rates. The bed roughness, which is difficult to measure or estimate in engineering practice, is a sensitive parameter in the computation of current velocities and sediment transport rates. Investigations carried out by van Rijn et al. (2001) and Winter and Mayerle (2003) have shown that relatively small changes in the prescribed bed roughness can have a major effect on sediment transport rates. A proper understanding and estimation of the variation of bed-form dimensions and associated roughness sizes is thus essential for satisfactory predictions of flow and sediment transport rates.

The type and dimensions of bed-form features depend primarily on the magnitude and nature of the flow, wave-induced motion, geological features and sediment characteristics. In the case of movable beds consisting of non-cohesive sediments the effective bed roughness is mainly comprised of grain roughness due to skin friction and form roughness generated by pressure forces acting on the bed forms. Although various equations for estimating bed-form dimensions and roughness sizes have been proposed, most of these rely on experiments carried out in the laboratory. Due to a lack of field measurements very little information is available on the effectiveness of the equations under field conditions, particularly in tidal channels. The flow conditions in tidal channels are subject to continuous change and the behaviour of bed forms under the action of shear stress is not clearly understood.

This paper presents the results of field investigations of the spatial and temporal variation of the dimensions of bed-form features and associated bed roughness. The investigations were carried out in the main tidal channels of the central Dithmarschen Bight on the German North Sea coast. Measurements of bed-form lengths were made in the main tidal channels. Simultaneous measurements of bed-form dimensions and current velocities were also carried out at one location in each of the tidal channels in order to obtain information on the temporal variation of bed-form dimensions and associated roughness values. Equivalent roughness values were estimated from a best-fit line of measured velocity profiles in the bottom boundary layer. The characteristics of the surficial seabed sediments as well as the geological features of the channels were also taken into consideration in the analysis. The dimensions of bed forms and equivalent roughness values were used to verify existing empirical equations for predicting bed-form dimensions and form roughness, most of which are based on laboratory experiments. A numerical procedure is also outlined for predicting bed-form dimensions and roughness values in the tidal channels of the study area based on a two-dimensional depth-integrated (2DH) flow model implementing existing empirical equations. The relative effects of seabed geological features, bed-form dimensions and roughness, and varying roughness sizes on flow velocities and sediment transport are also demonstrated by way of numerical simulations.

2. Description of the Investigated Coastal Area

Investigations were carried out in a tidal flat area on the German North Sea coast. The area is located between the Eider and Elbe estuaries. The morphology of the study area is dominated by tidal flats, tidal channels and sandbanks over the outer region. This study focuses on flow and morphological conditions along the intertidal channels, i.e. the Norderpiep located in the northwest part of the domain and the Suederpiep in the southwest. These two channels converge within the study area to form the Piep tidal channel (Fig. 1). Maximum water depths in the channels are of the order of 23 m, and approximately 50 % of the study area is intertidal. The hydrodynamics and sediment dynamics of the study area are driven by the combined effects of tides, waves and wind-induced currents. Under average conditions the tidal influence is predominant. The semi-diurnal tide has a mean range of 3.2 m, varying between 2.4 m at neap tides and 4.2 m at spring tides. Westerly winds (SW-W) prevail in the study area. Wave heights in the outer region may attain 3.5 m, with wave-breaking occurring along the outer margins of the area of interest. Maximum current velocities in the tidal channels are of the order of 2 m/s. The temporal and spatial variations of the currents are strongly influenced by the complex bathymetry. Storm surges can result in water level set-ups of up to 5 m, favouring wave propagation into normally shallow regions. The surficial seabed sediment in the tidal channels and on the tidal flats consists mainly of sands with varying proportions of silt and clay. The grain sizes of material in suspension are up to 5 times smaller than those of mobile sediments on the sea bed (POERBANDONO and MAYERLE, in this volume).

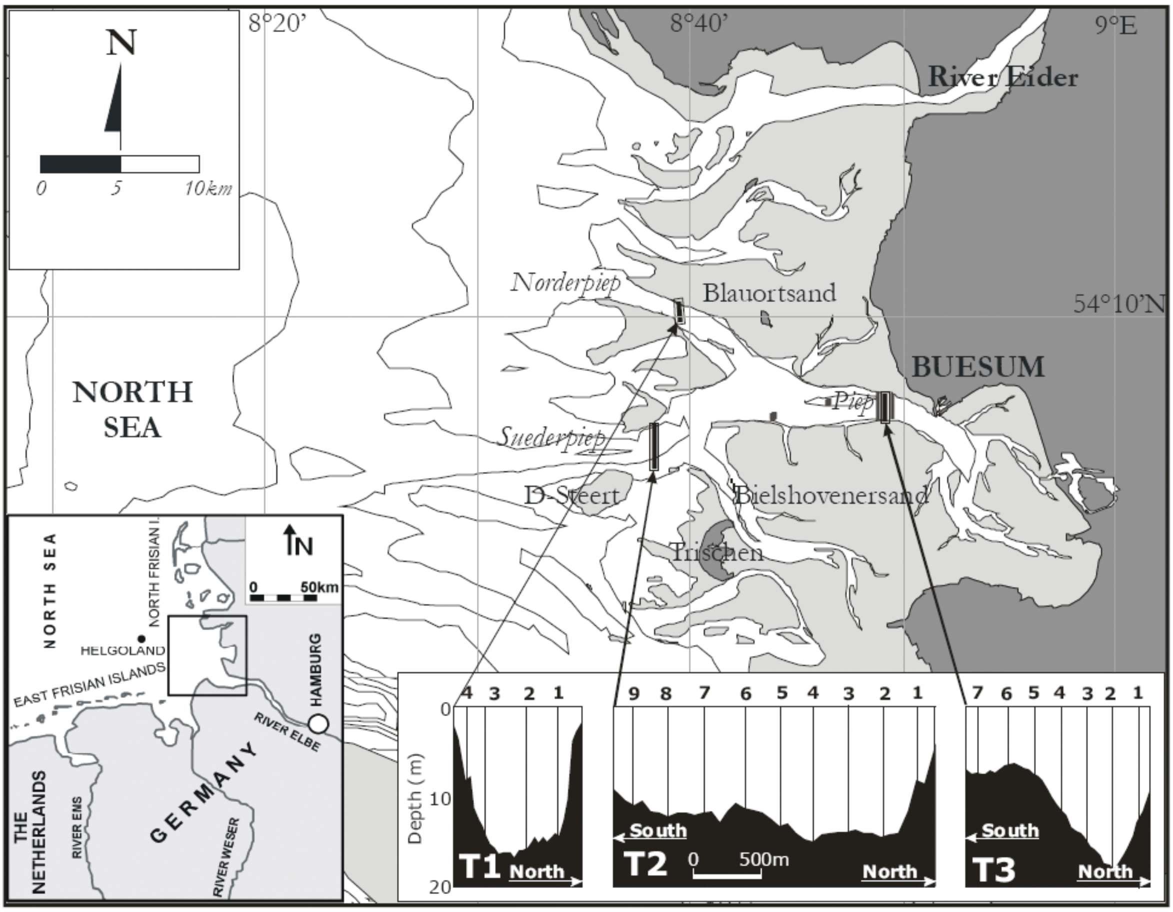

Fig. 1: Investigation area

3. Recent Sediment Deposits and Surficial Seabed Sediments

The composition of the sediment deposits in the study area largely corresponds with recent tidal flat sediments. As shown in Fig. 2, the layer thickness of the intertidal sediment deposits in the study area is about 20 m (ASP NETO et al., 2001; ASP NETO, 2004). The early Holocene layer (EHL) consists of consolidated cohesive sediments and forms a type of natural base that hinders erosion in the tidal channels. In the central parts of the channels, where shear stresses are high, entire removal of the non-cohesive deposits has resulted in exposure of the EHL. The thickness of the potentially mobile sediment layer increases towards the northern and southern banks of the main tidal channels.

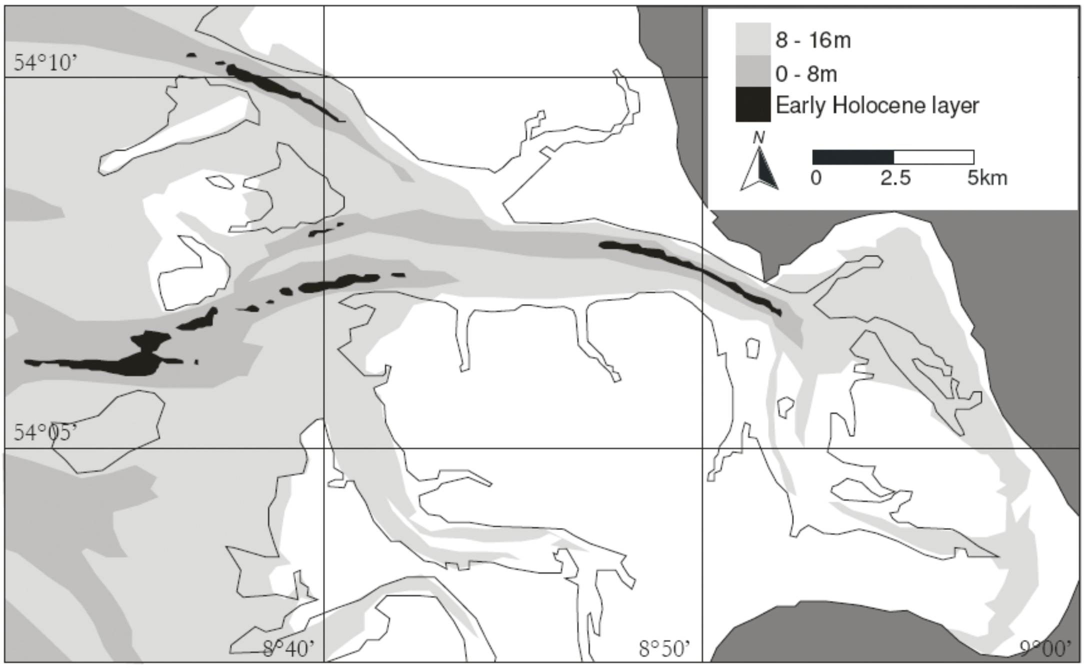

Fig. 2: Thickness of the potentially mobile sediment layer above the EHL (modified after ASP, 2004)

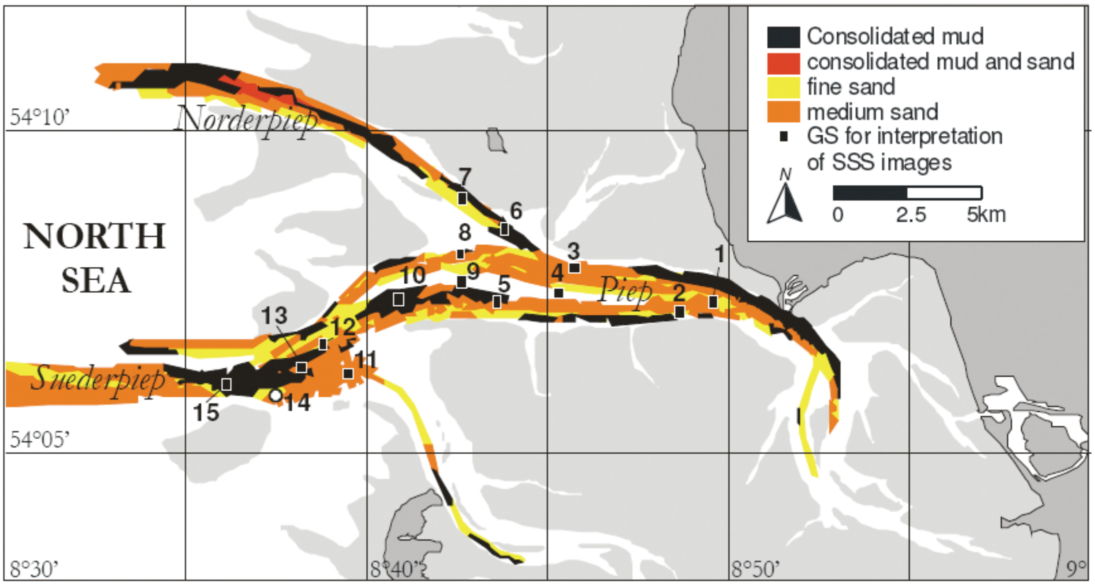

Fig. 3: Surficial seabed sediment distribution in the main tidal channels
(modified after VELA-DIEZ, 2001)

Fig. 3 shows sediment types in the tidal channels derived from side-scan sonar images (SSS) calibrated with grab samples (VELA-DIEZ, 2001). The spatial distribution of the surficial seabed sediments is quite variable. Areas were identified with essentially sandy sediments and mud, and often with consolidated deposits. The sands are mainly very fine to fine with some isolated patches of medium sands. The d_{50} of the surficial seabed sediments of the grab samples taken for interpretation of the SSS images varies between 80 µm and 230 µm, corresponding to very fine to fine sands. The majority of these sands was found to be well-sorted.

Consolidated fine sediments are found at a number of deeper locations in the tidal channels. An analysis of the mud content (% of fines) in the less-exposed tidal channels confirmed the presence of mud in all grab samples. A sediment analysis indicated that the silt and clay content of the sediment samples is generally greater than 5 %, attaining maximum values of 75 %–80 %. Moreover, values exceeding 10 % were found in about 50 % of all samples (POERBANDONO and MAYERLE, in this volume).

4. Spatial Variation of the Dimensions of Bed Forms

Spatial variations of the lengths and heights of bed forms in the tidal channels were derived from SSS images and echo soundings, respectively. Fig. 4 shows the scope of the measurements in the main tidal channels covering an area of about 30 km^2. Details of these measurements are given in VELA-DIEZ (2001) and POERBANDONO and MAYERLE (in this volume). Fig. 5 shows typical SSS images obtained at several locations in the tidal channels at different stages of the tidal cycle. In order to obtain adequate information on the lengths of the bed forms the SSS images were arranged rectilinearly to avoid distortions in the along-track and across-track directions.

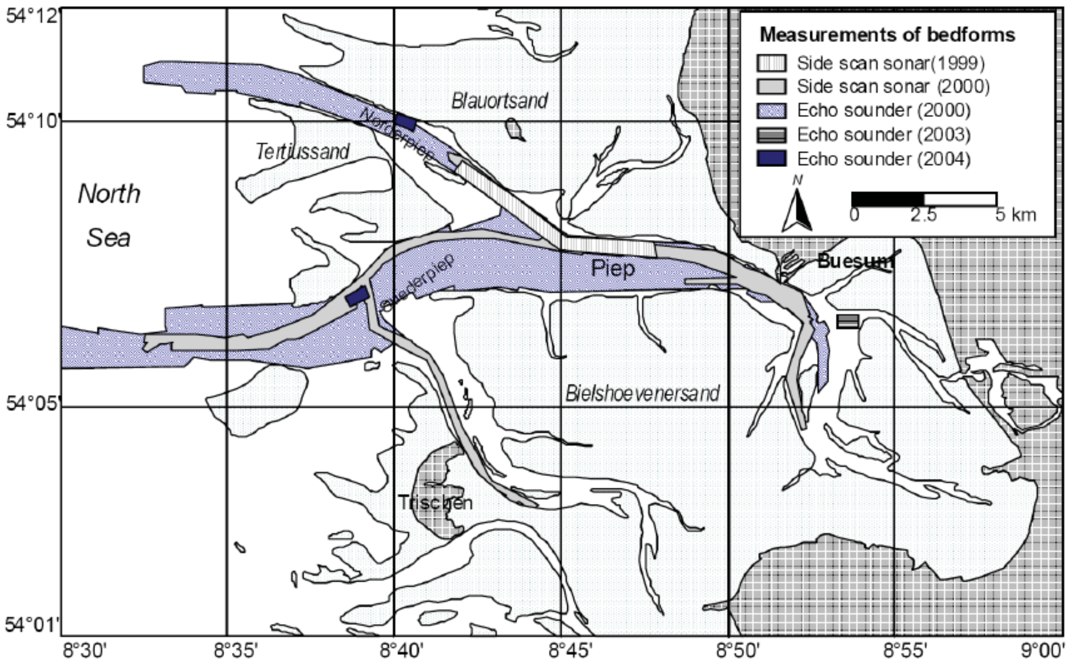

Fig. 4: Coverage of field measurements of bed forms in the tidal channels

Fig. 6 shows the bed-form types and lengths obtained from SSS surveys. It is noted that although the measurements achieved full spatial coverage, the hydroacoustic detection of bed-form features, particularly smaller ripples, was not always clear. Moreover, the fact that the measurements were carried out during different tidal cycles and phases explains the variations in the dimensions of bed-form lengths at the same locations. Mainly megaripples and dunes were detected during the surveys. These surveys revealed that bed forms develop primarily in the most exposed areas of the Suederpiep, at the intersection of the Suederpiep and the Bielshoevener Loch, and along the sides of the channels, especially in the Norderpiep and Piep. Megaripples with lengths varying from about 3 m to 22 m were mainly observed. The average bed-form lengths varied between 7 m and 10 m in the Suederpiep and Piep tidal channels and between about 3 m and 6 m along the Norderpiep channel. The largest bed forms were observed at the intersection of the Suederpiep tidal channel and the Bielshoevener Loch. Sand dunes with lengths of up to 22 m were recorded. Measurements of bed-form heights using echo sounders, which were limited to only a few locations (see Fig. 4), gave values of up to about 0.7 m. In general, the crests of sand dunes and ripples, which are not very steep, are perpendicular to the flow direction, i.e. parallel to the sonar track (Fig. 5).

Fig. 7 shows regions in the tidal channels with potentially mobile sediment deposits and locations where bed forms were observed. As may be seen in the figure, these regions overlap. The majority of the bed forms were observed at locations with mobile sediment deposits characterized by relatively low percentages of mud content. The mud content of sediments may significantly increase the critical shear stress above that required for non-cohesive sediments. Bed forms were not detected in the deeper parts of the tidal channels due to the exposed EHL.

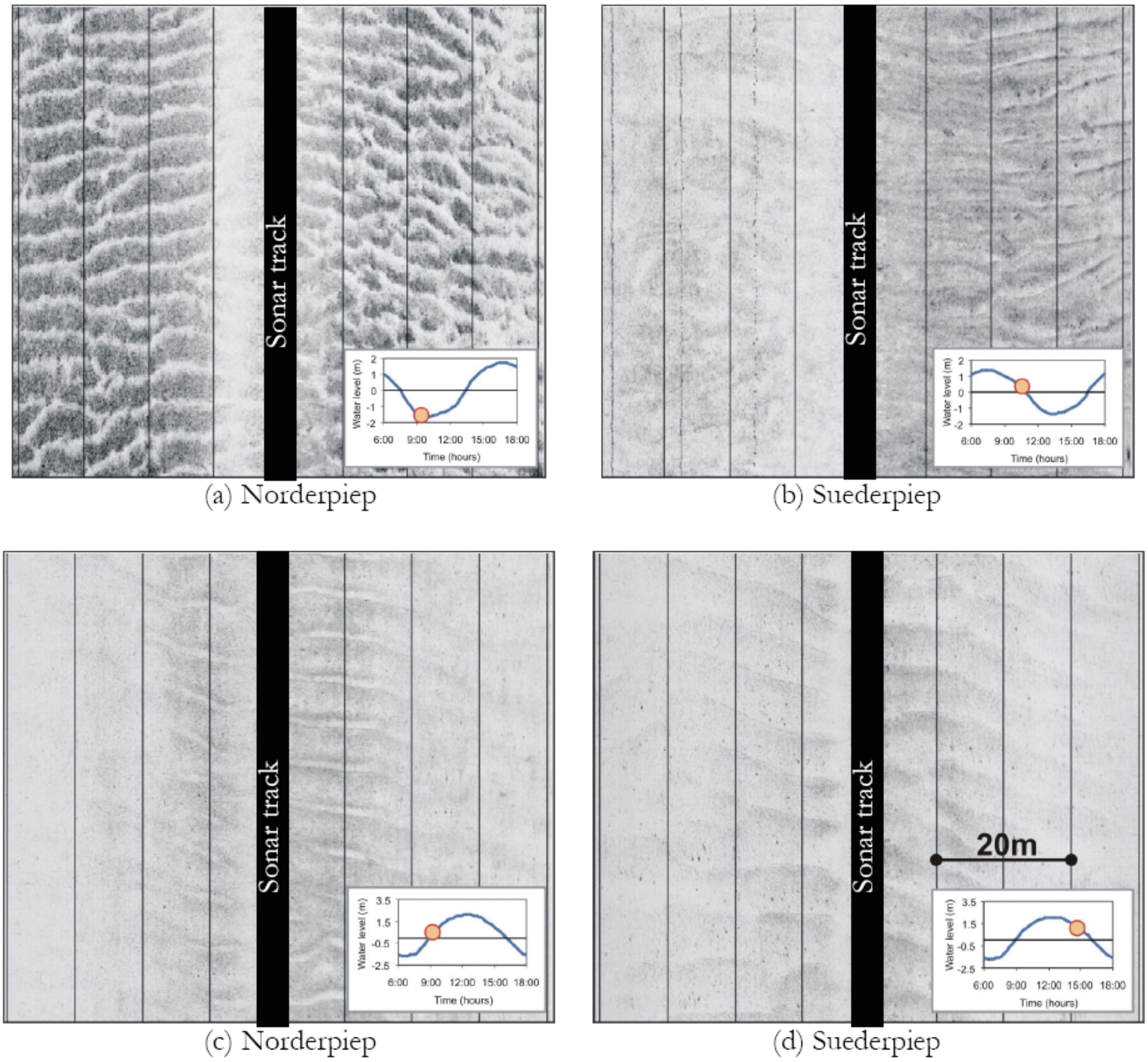

(a) Norderpiep (b) Suederpiep

(c) Norderpiep (d) Suederpiep

Fig. 5: Typical SSS images

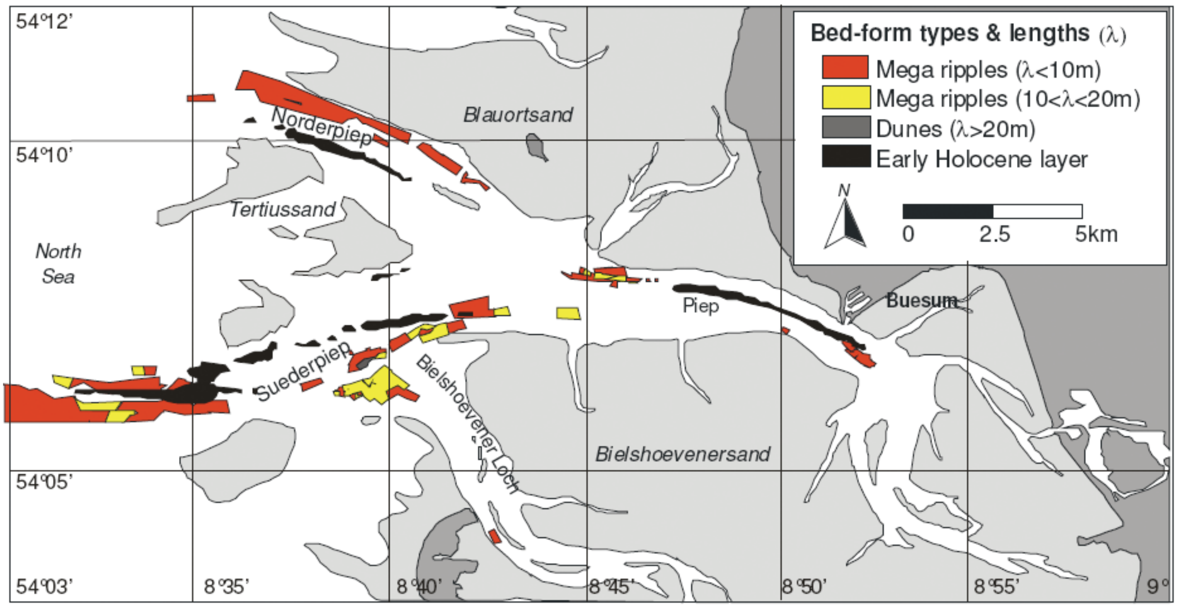

Fig. 6: Spatial variation of bed forms (MAYERLE et al., 2002)

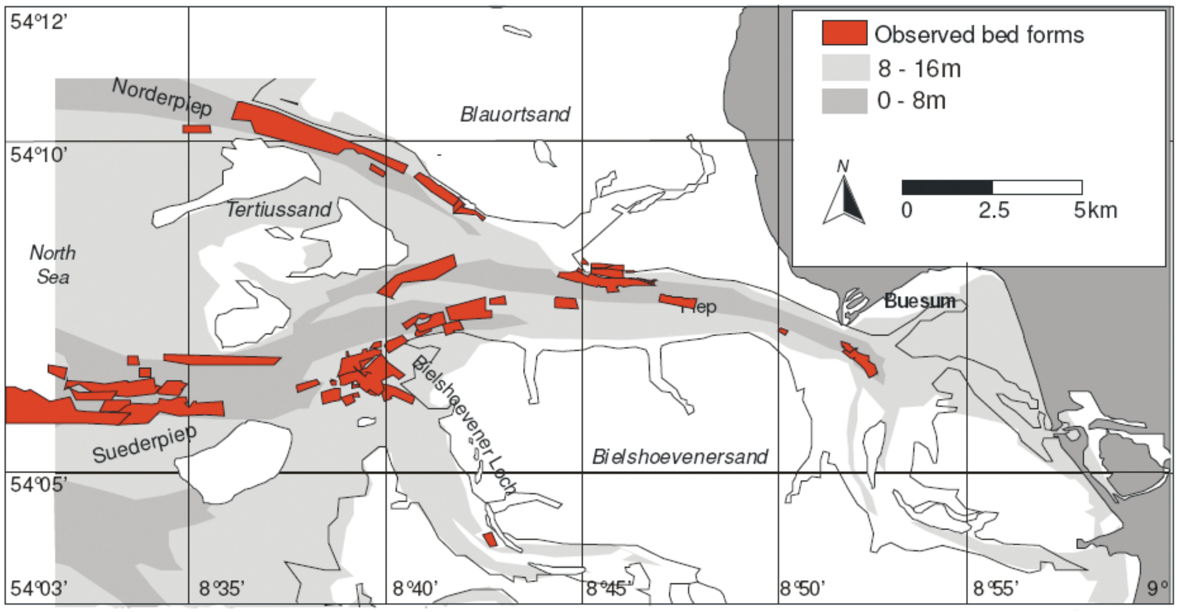

Fig. 7: Regions where bed forms were observed, also indicating the thickness of the potentially mobile sediment layer above the EHL

5. Temporal Variation of the Dimensions of Bed Forms

In order to study the temporal variation of bed-form heights (Δ) and lengths (λ), measurements of bed-form dimensions were carried out using an echo sounder in conjunction with measurements of current velocity profiles by means of an acoustic profiler. The location of measurements in the inner Piep tidal channel is shown in Fig. 4 (see echo sounder measurements made in 2003). Altogether, 32 profiles of 200 m in length were surveyed from a moving vessel at regular time intervals on a track perpendicular to the crest of the sand dunes. The measurements were made using an echo sounder operating at a frequency of 200 kHz. The seabed at this location consists of very fine and loosely deposited sandy sediments with a mean particle size of about 100 µm. Measurements were carried out over 9 hours during the tidal period of a spring tide with a tidal range of 3.9 m. The water depths during measurements varied between 2.5 m and 6.4 m.

Calm weather conditions prevailed during the survey, which commenced at low water slack and covered the entire flood phase and part of the ebb phase. The maximum depth-integrated velocities during the flood and ebb phases were about 0.8 m/s and 0.5 m/s, respectively. Typical measured bed profiles with exaggeration of the vertical scale are shown in Fig. 8. Bed forms were detected during the entire observation period. The small steepness of the bed features and smoothness of the seabed profile are clearly evident in Fig. 9, which shows a typical bed form without scale distortion.

Fig. 10 shows the temporal variation of a bed-form height (upper figure) and length (lower figure) with varying water depth and depth-averaged current velocity. The mean values of the heights and lengths of bed forms were determined by averaging the measured values along each 200 m transect. The differences in bed-form dimensions observed during the same back-and-forth survey are due to the different paths followed by the survey vessel. The mean bed-form heights ranged between 0.22 m and 0.36 m, with standard deviations ranging between 0.05 m and 0.11 m. Despite the difficulty of following the same path in the back and forth directions, no significant temporal variation of the mean bed-form heights was detected during the observation period. VAN RIJN (1993) reported an increase in the bed-form heights with increasing bed shear stresses for unidirectional flow conditions in rivers and flumes. Although a similar behaviour was not observed in the present study, care should be taken in the interpretation of the results, bearing in mind the relatively small heights of the observed bed-form features and the averaging procedure adopted for estimating their dimensions.

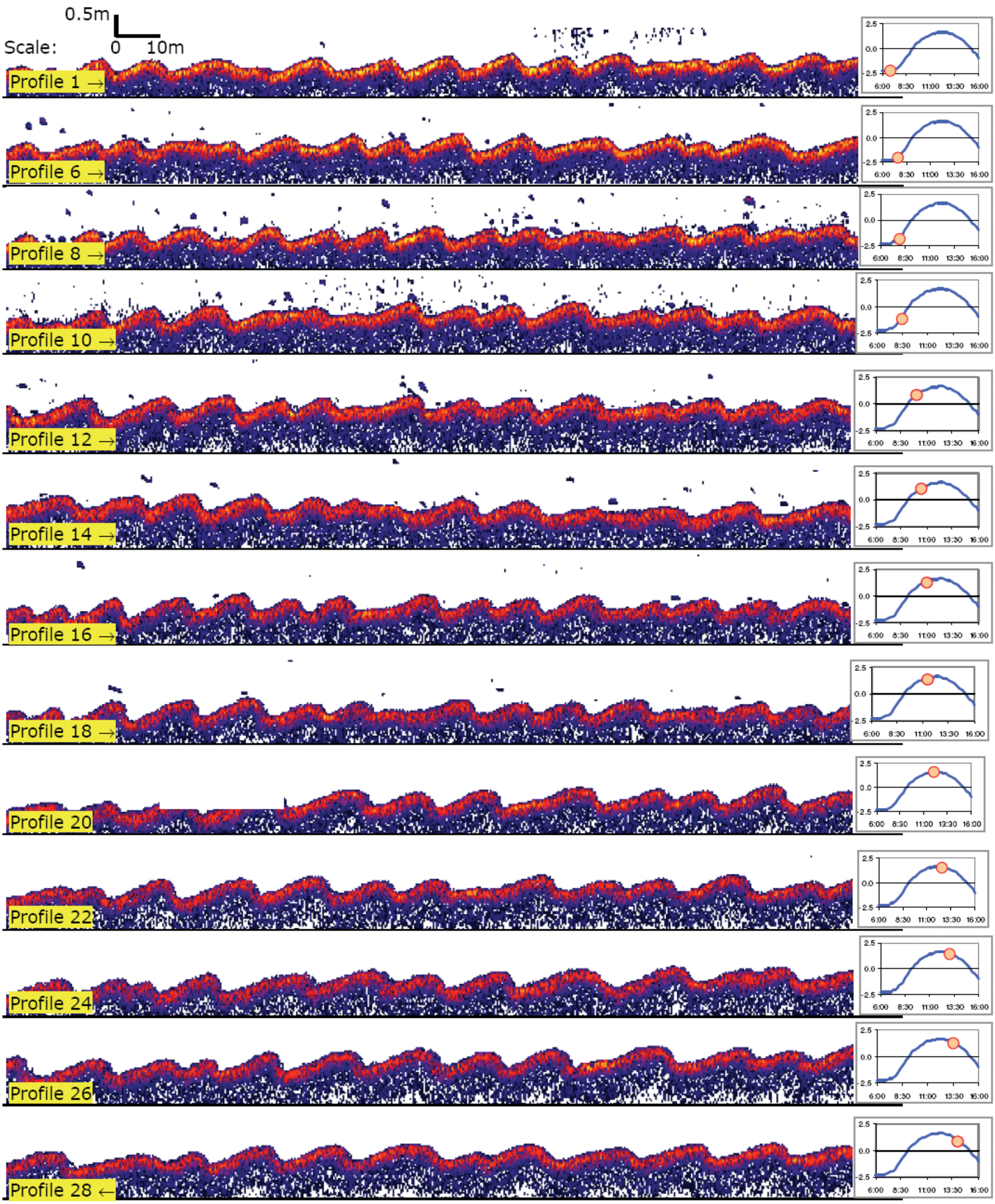

Fig. 8: Measured bed profiles with exaggeration of the vertical scale in the inner Piep tidal channel

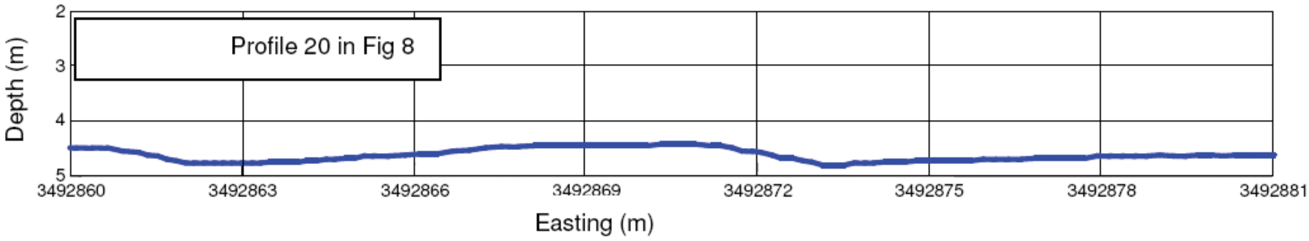

Fig. 9: Typical bed-form feature without scale distortion in the inner Piep tidal channel

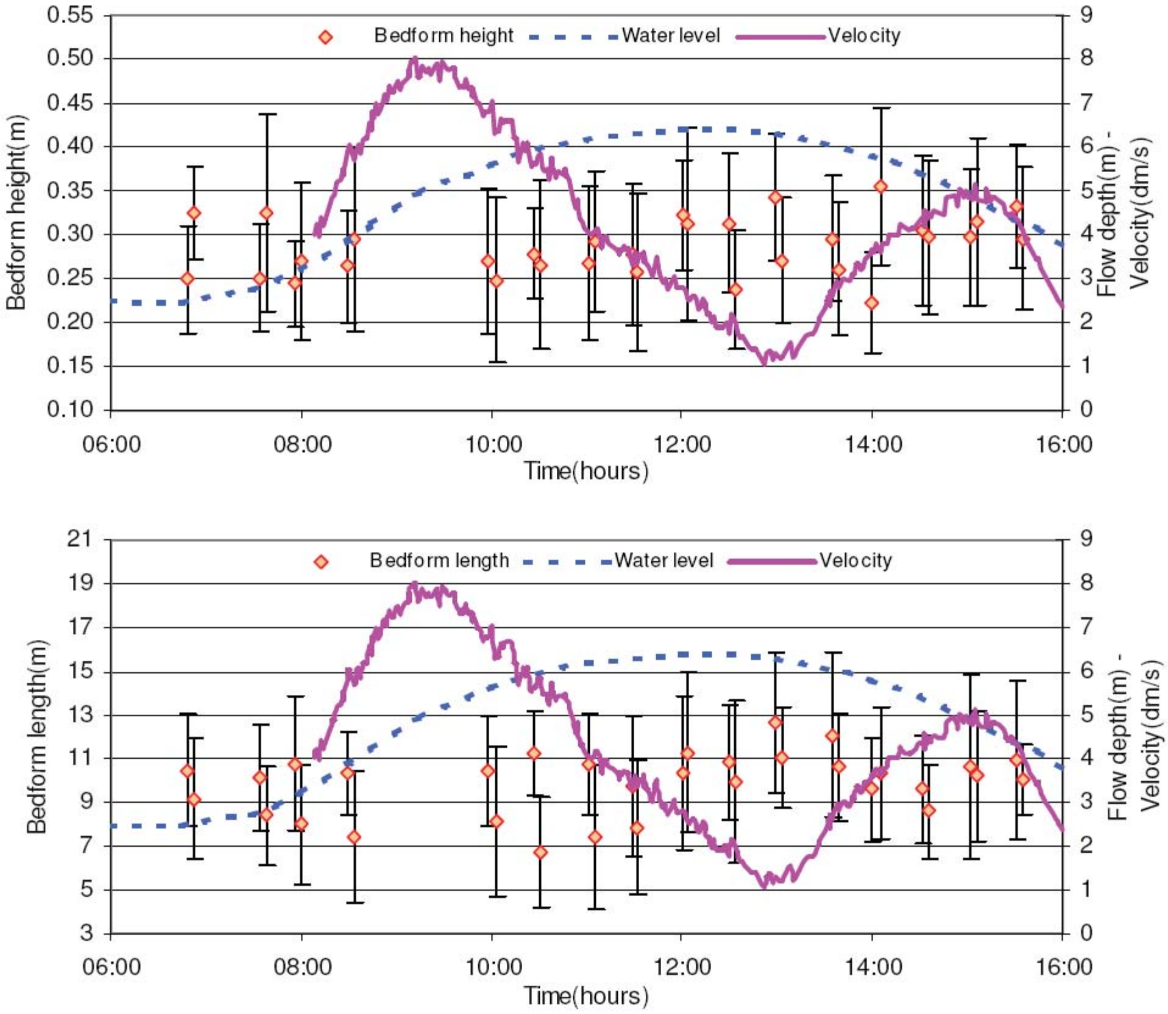

Fig. 10: Temporal variation of bed-form dimensions in the inner Piep tidal channel; upper: bed-form heights; lower: bed-form lengths

The mean lengths of the observed bed forms ranged from about 6.7 m to 12.7 m during the flood phase and just after high water, respectively. An increase in bed-form length was observed with increasing flow depth (h = German reference datum ± water level). Larger lengths were observed during the phase of smaller flow velocities around high water. The observed bed-form lengths at the measuring location in the inner Piep tidal channel (Fig. 4) were of the order of four times and two times the measured flow depth ($\lambda = 4$ h and $\lambda = 2$ h) at low and high water, respectively. The standard deviations of the bed-form lengths in each profile varied between 1.6 m and 4.2 m.

Migration of the bed forms during the measurement period was subsequently analysed. Echo soundings of the bed profiles measured along approximately the same vessel path from about mean water level during the flood phase to mean water level during the ebb phase are plotted in Fig. 11. The times at which the bed profiles were recorded are also indicated in Fig. 8. The bed forms were found to migrate in the shoreward direction (strongest currents) at a rate about 1 m/h.

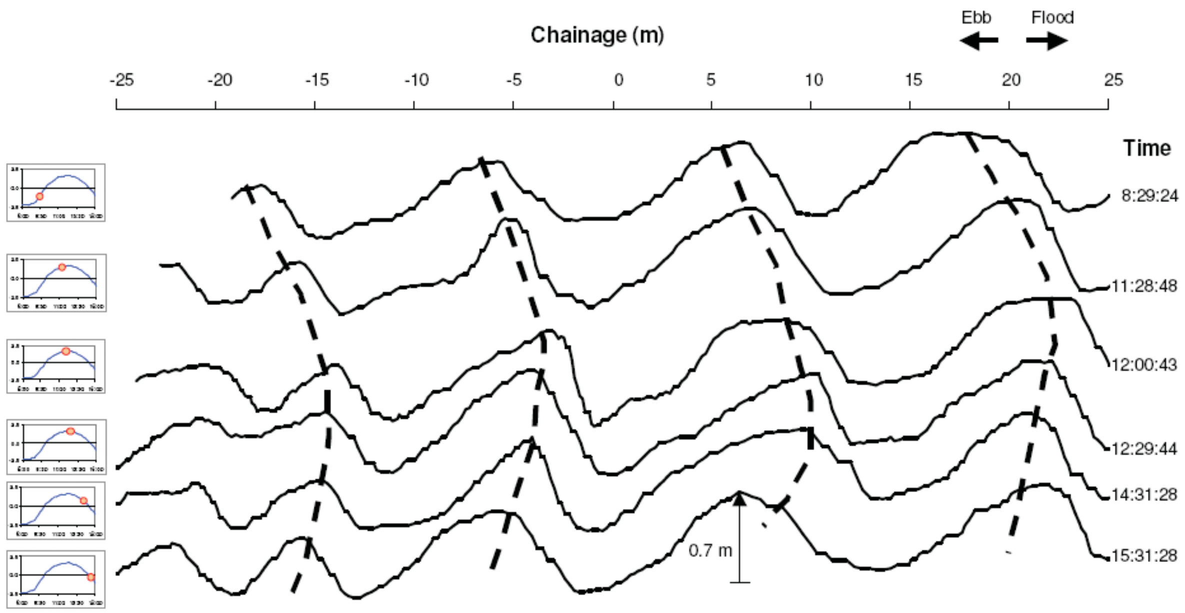

Fig. 11: Migration of bed forms during a tidal period

6. Roughness Values Associated with Different Bed Forms

The bed roughness values associated with the various bed forms observed in the field were analysed. Roughness values (*ks*) were estimated from continuous velocity profiles obtained using a 1200 MHz Acoustic Doppler Current Profiler (ADCP) manufactured by RD Instruments. The ADCP, which was set to record a 0.15 m bin size at a time interval per sub-ping of 0.04 s, was deployed pointing downwards from a stationary rubber dinghy for the continuous measurement of current velocity profiles (Fig. 12). Estimates of the bed shear stress and effective roughness were derived from the measured profiles averaged over a period of 300 s.

Only mean velocity profiles with depth-integrated velocities exceeding 0.3 m/s and small standard deviations of the velocity directions were considered. This procedure guarantees a logarithmic distribution over the vertical. Shear stresses and roughness values were obtained by fitting a logarithmic profile to the velocity data in the lower 20 % of the flow depth from the bed. About five point measurements were obtained in the wall region. Only

Fig. 12: Deployment of the acoustic profiler

those profiles with log-law fit correlation coefficients exceeding 0.90 were included in the analysis. Bearing in mind the limited number of point measurements in the wall region, the selected bin size, which does not reflect point measurements, and uncertainties in defining the reference datum of the measured velocity profiles, the interpretation of the results showed be treated with caution. The resulting roughness values were found to range between 0.03 m and 0.17 m with an average equivalent roughness of 0.1 m. Due to the limited number of velocity profiles selected for determining the roughness sizes, it was not possible to investigate the variation of bed-form roughness during the tidal period.

7. Empirical Equations for Predicting the Dimensions and Roughness of Bed Forms

Several methods for identifying bed-form types, including equations for determining bed-form dimensions and associated bed roughness coefficients, have been proposed (YALIN, 1972; RAUDKIVI, 1988; SOULSBY, 1997; VAN RIJN, 1993). The underlying experiments cover a wide range of flow conditions and sediment characteristics. The large majority of these empirical formulae, however, are based on the results of laboratory experiments with well-controlled, unidirectional steady flows mainly under equilibrium conditions, and with loosely packed non-cohesive sediments.

For such conditions the analysis is usually carried out in three stages. Firstly, the type of bed form is defined. Secondly, the bed-form dimensions are estimated for the given conditions and sediment characteristics. Finally, the associated roughness values are determined on the basis of the bed-form dimensions and flow conditions. The roughness values are usually determined by combining grain and form roughness. Grain roughness (*ks'*) is related to the largest particles of the uppermost seabed sediment layer, whereas form roughness (*ks''*) depends on the height (Δ), length (λ) and steepness (Δ/λ) of the bed form. Under tidal conditions, in which current velocities are subject to continuous change, bed forms are unable to fully adapt to varying flow conditions. For this reason the validity of the equations may be questionable.

VAN RIJN (1993) proposed a classification diagram for identifying bed-form types based on the particle-size parameter (D_*) as follows:

$$D_* = d_{50} \left[(\rho_s/\rho - 1)g/\nu^2\right]^{1/3} \tag{1}$$

with d_{50} = medium particle diameter of bed material in m
ρ_s = sediment density in kg/m^3
ρ = fluid density in kg/m^3
ν = kinematic viscosity coefficient in m^2/s
g = gravitational acceleration in m/s^2.

and the bed shear stress parameter (T):

$$T = (\tau'_b - \tau_{b,er})/\tau_{b,er} \tag{2}$$

with τ'_b = grain-related bed shear stress in N/m^2
$\tau_{b,er}$ = critical shear stress after Shields in N/m^2.

Table 1 summarizes the proposed equations for predicting bed-form dimensions and associated roughness values based on flume and river measurements. The bed-form heights are determined on the basis of the transport stage parameter (T), the water depth (h) and the particle size. In the case of non-cohesive sediments the lengths of bed forms are usually related to the water depth only. The variation of form roughness, on the other hand, depends on the steepness and shape factor (γ) of the bed form.

Comparisons between the results given by the equations of VAN RIJN (1993) and the corresponding relative bed-form heights and associated bed roughness values determined in the present study are shown in Figs. 13 and 14, respectively. According to the morphological bed-form classification of VAN RIJN (1993), megaripples are expected to develop at the measurement location. Reasonable agreement exists between the results given by the proposed equations and the results obtained in the present study, despite the fact that the empirical equations were derived from experiments under unidirectional flow conditions. The scatter of the experimental results is comparable to the scatter observed in other measurements carried out in the laboratory and in rivers. The relative bed-form heights were found to be as much as 8 times greater than the values predicted by the empirical equations (Fig. 13).

More significant discrepancies were identified in the length of the bed forms. The observed lengths (λ = 2 h to 4 h) were found to lie between the values predicted by the empirical equations for megaripples (λ = h/2) and dunes (λ = 7.3 h). The fact that the flow conditions during a tidal period are subject to continuous change may explain why the bed-form features are unable to fully develop. As illustrated by Fig. 14, on the other hand, the estimated bed-form roughness values are in reasonable agreement with those predicted by VAN RIJN'S equations (Table 1). As already pointed out, form roughness is highly dependent on the dimensions and steepness of bed forms. The fact that the larger heights of the bed forms at the measurement location are counterbalanced by longer lengths explains why the effective roughness values based on measurements are comparable to those predicted.

Table 1: Equations proposed by VAN RIJN (1993)

	Bed-form type	Equations	
Bed-form dimensions	Megaripples	$\frac{\Delta_r}{h} = 0.02\,(1 - e^{-0.1T})\,(10 - T)$	(3.a)
		$\lambda_{mr} = 0.5\,h$	(3.b)
	Dunes	$\frac{\Delta_r}{h} = 0.11\left(\frac{d_{50}}{h}\right)^{0.3}(1 - e^{-0.5T})\,(25 - T)$	(4.a)
		$\lambda_d = 7.3\,h$	(4.b)
Form roughness	Megaripples	$k''_{s,r} = 20\,\gamma\Delta_r\,\frac{\Delta_r}{\gamma_r}$	(5)
	Dunes	$k''_{s,r} = 1.1\,\gamma\Delta_d\,(1 - e^{-25\Delta_d/\lambda_d})$	(6)

Note: Subscripts r and d denote megaripples and dunes, respectively

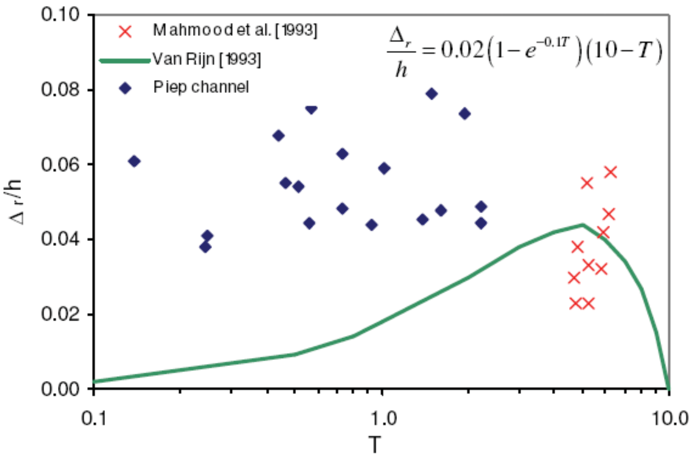

Fig. 13: Relative bed-form heights of megaripples after VAN RIJN (1993)

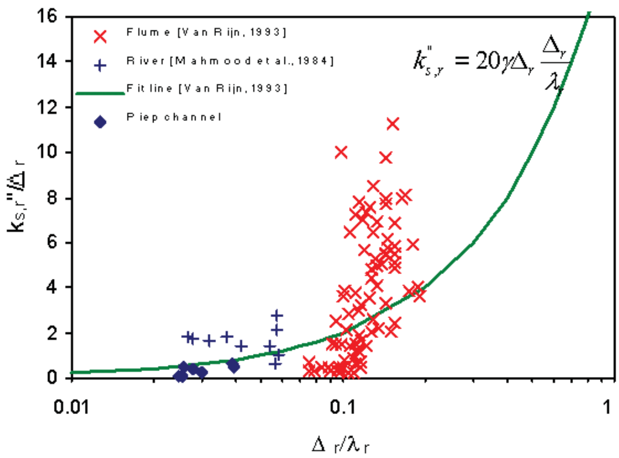

Fig. 14: Relative form roughness of megaripples after VAN RIJN (1993)

8. Numerical Procedure for Predicting the Dimensions and Roughness of Bed Forms

After analysing the spatial and temporal variations of bed-form features in the tidal channels, a numerical procedure was developed for predicting the dimensions of bed forms and hence the associated bed roughness. The identification of bed-form types and the estimation of bed-form dimensions and equivalent roughness sizes were derived from the results of flow model computations.

The methods proposed by VAN RIJN (1993) for identifying bed-form types and formulating bed-form dimensions and equivalent roughness sizes were implemented in a numerical model. The roughness values (k_s) were determined for given sediment characteristics and flow conditions as follows. Firstly, the type of bed form is identified. Secondly, the bed-form dimensions are estimated for the corresponding shear stress values. Shear stress values at maximum current velocities were considered in the present study, i.e. the temporal variations of bed-form dimensions were disregarded. Finally, the characteristics of the surficial seabed sediment and the dimensions of the bed forms were used to estimate the grain roughness (k_s') and form roughness (k_s"), respectively, hence yielding the effective bed roughness value. The k_s values were obtained by iteration. Constant Chezy coefficients were assumed throughout the domain initially. Updates were then determined iteratively until the computed *ks* values approximately matched the assumed values.

This procedure was applied to the tidal channels of the Dithmarschen Bight using a two-dimensional depth-integrated flow model covering the entire Dithmarschen Bight area. A curvilinear grid with a grid spacing ranging from 60 m to 180 m was employed. Details of the flow model are presented in PALACIO et al. (in this volume).

The layer thickness of the potentially mobile sediment deposits and the sediment characteristics in the tidal channels shown in Figs. 2 and 3 were taken into consideration in the simulations. The simulations were carried out for a spring tide with a tidal range of about 4 m.

Maps of the predicted heights and lengths of bed forms in the tidal channels are shown in Figs. 15 and 16, respectively. Regions with mud content and EHL sediment deposits are indicated. A considerable variation in the size of the predicted bed forms is evident, with bed-form heights attaining as much as 1 m. Larger heights are predicted in the central parts of the main tidal channels and in the most exposed areas of the Suederpiep tidal channel at locations where the shear stresses are larger. The predicted bed-form lengths are as much as about 40 m.

Fig. 17 shows the predicted roughness values in the tidal channels using the procedure outlined above. Higher values were obtained in the central parts of the main tidal channels (Suederpiep and Piep) and in the most exposed areas of the Suederpiep tidal channel. In regions with non-cohesive tidal deposits the predicted roughness values were as much as about 1 m. At locations where the EHL has already been reached the roughness sizes were set to 0.06 m (SOULSBY, 1997).

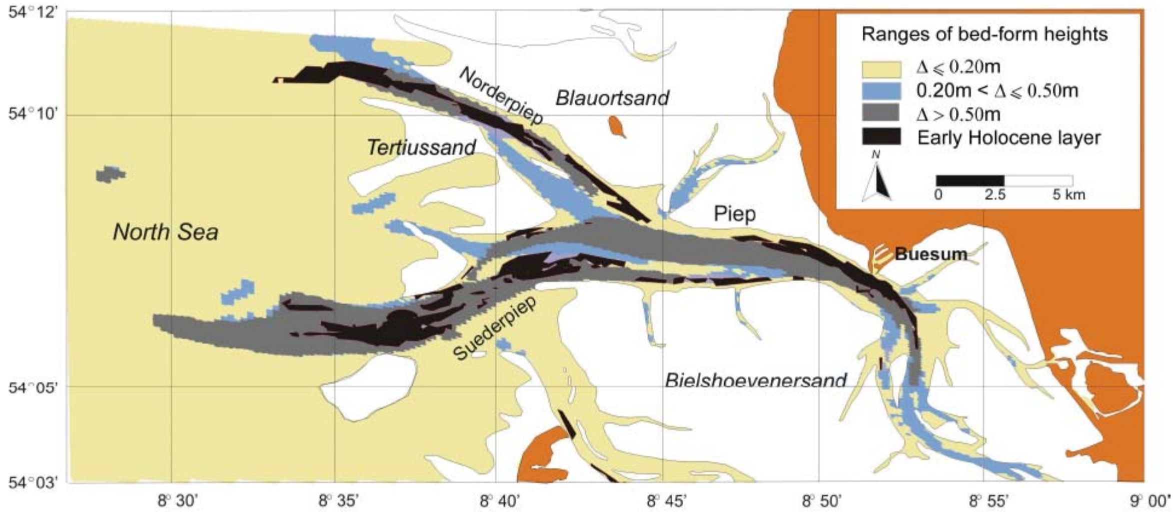

Fig. 15: Predicted heights of bed forms in the tidal channels for a spring tide

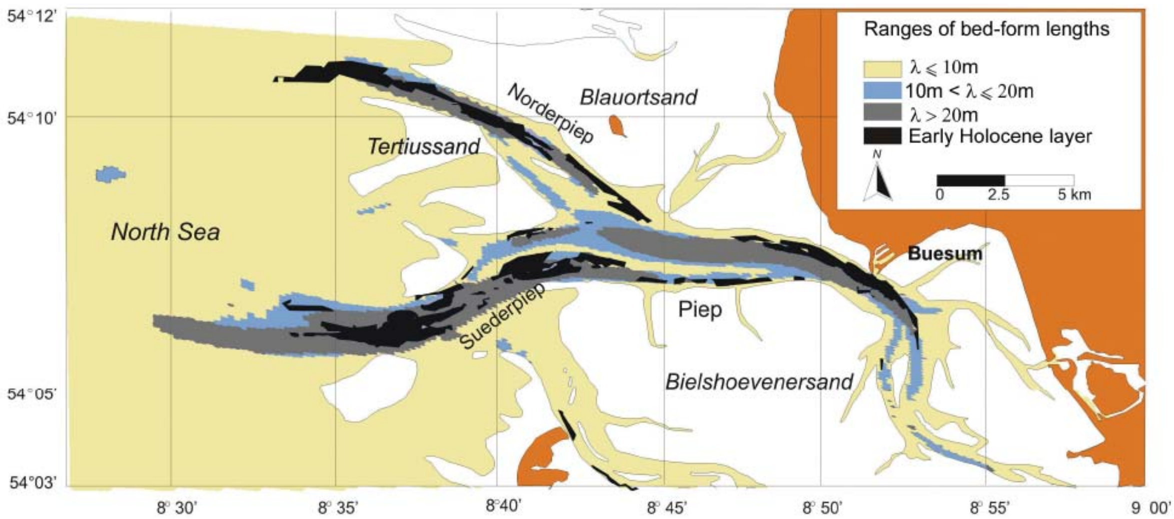

Fig. 16: Predicted lengths of bed-form features in the tidal channels for a spring tide

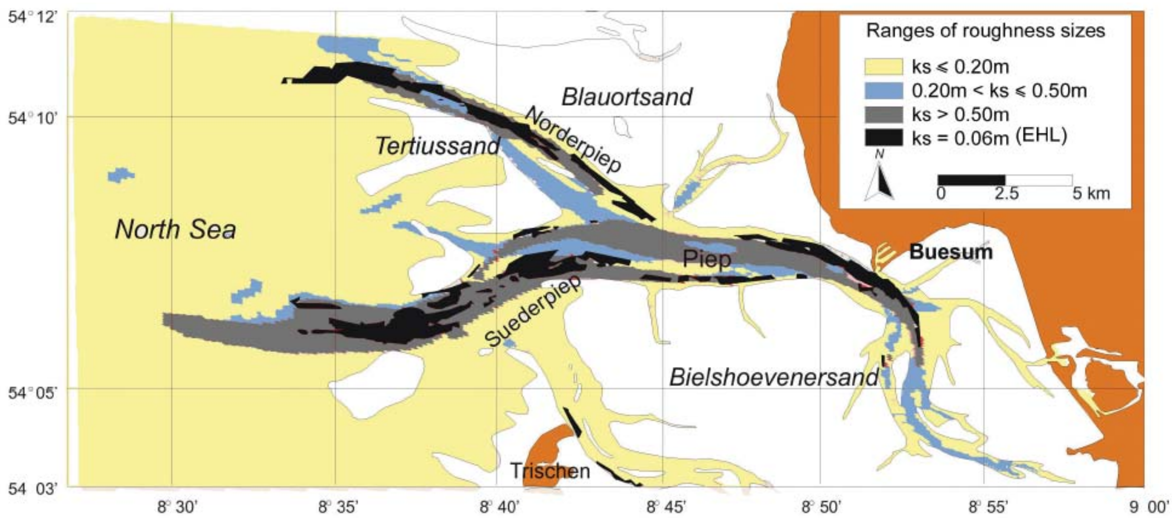

Fig. 17: Roughness values computed using empirical equations

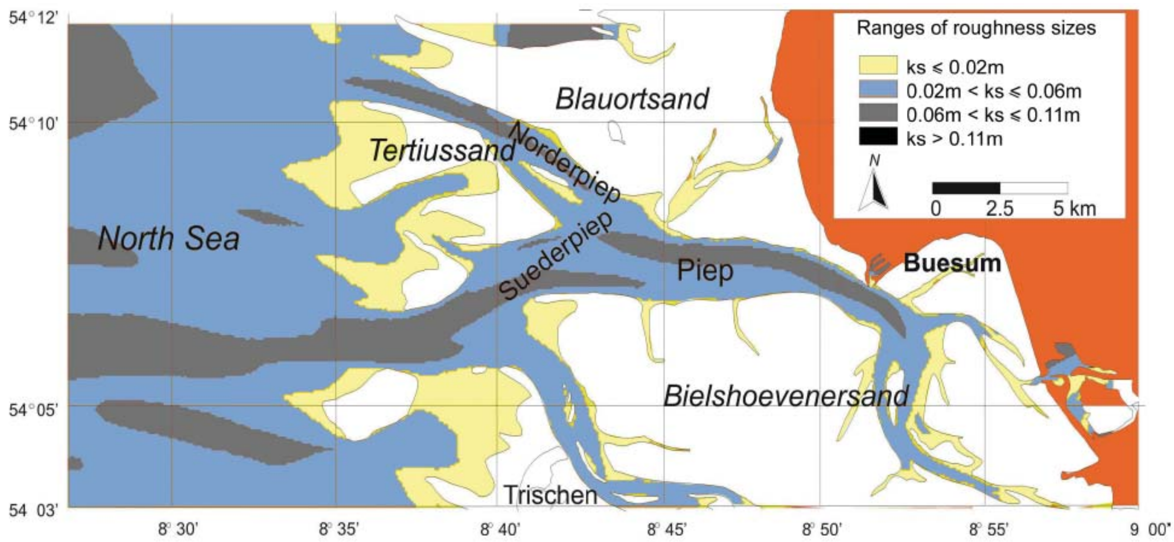

Fig. 18: Roughness values based upon a constant Chezy coefficient of 60 $m^{1/2}/s$

9. Effect of Bed Roughness on Current Velocity and Sediment Concentration

In order to illustrate the sensitivity of current velocity and suspended sediment concentration to the choice of bed roughness (k_s), simulations were carried out using a two-dimensional depth-integrated process-based flow and sediment transport model (PALACIO et al., in this volume; WINTER et al., in this volume). Bed load and suspended load were treated separately in the sediment transport model. Whereas bed-load transport was calculated using algebraic formulations, suspended material concentration and transport were computed by solving the advection-diffusion equation with appropriate bed boundary conditions. The pick-up function proposed by VAN RIJN (1984) was implemented with the same model settings as those adopted in the calibration and validation of the sediment transport model (WINTER et al., in this volume).

In order to demonstrate the effect of different bed roughness values on simulated current velocities and suspended sediment concentrations two prescribed bed roughness conditions were considered in the tidal channels of the Dithmarschen Bight: a) bed roughness obtained by applying the procedure outlined above (see Fig. 17) and b) bed roughness based on a constant Chezy coefficient of 60 $m^{1/2}/s$ (see Fig. 18). A uniform grain size of 100 m was assumed in the simulations, which were carried out for a spring tide with a tidal range of about 3.7 m.

Comparisons of the simulated depth-averaged current velocities and suspended sediment concentrations obtained using the two maps of bed roughness (Figs. 17 and 18) are shown in Figs. 19 and 20, respectively. The resulting variation of current velocities and suspended sediment concentrations over a tidal period are shown at three cross-sections of the main tidal channels, i.e. T1 and T2, representing Norderpiep and Suederpiep at the entrance to the tidal area, respectively, and T3 across the Piep tidal channel in the inner part of the study area (Fig. 1). T1, located in the Norderpiep tidal channel in the northeast part of the study area, is about 775 m wide with water depths varying from 2.8 m to 16.1 m. T2, located in the Suederpiep tidal channel in the southeast part of the study area, is about 2040 m wide with water depths varying from 7.3 m to 15.6 m, and T3, located in the Piep tidal channel near the coast, is about 1200 m wide with water depths varying from 6.2 m to 17.9 m.

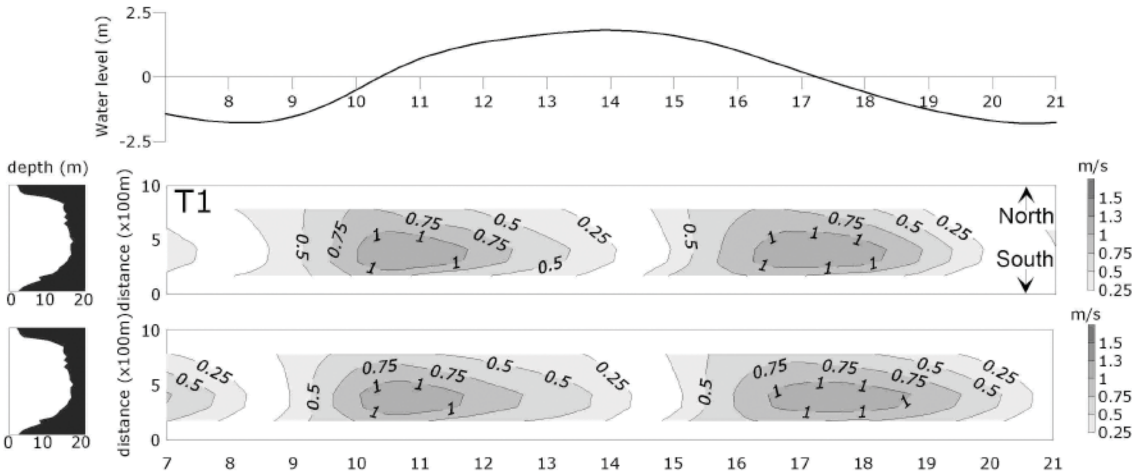

(a) Cross-section T1

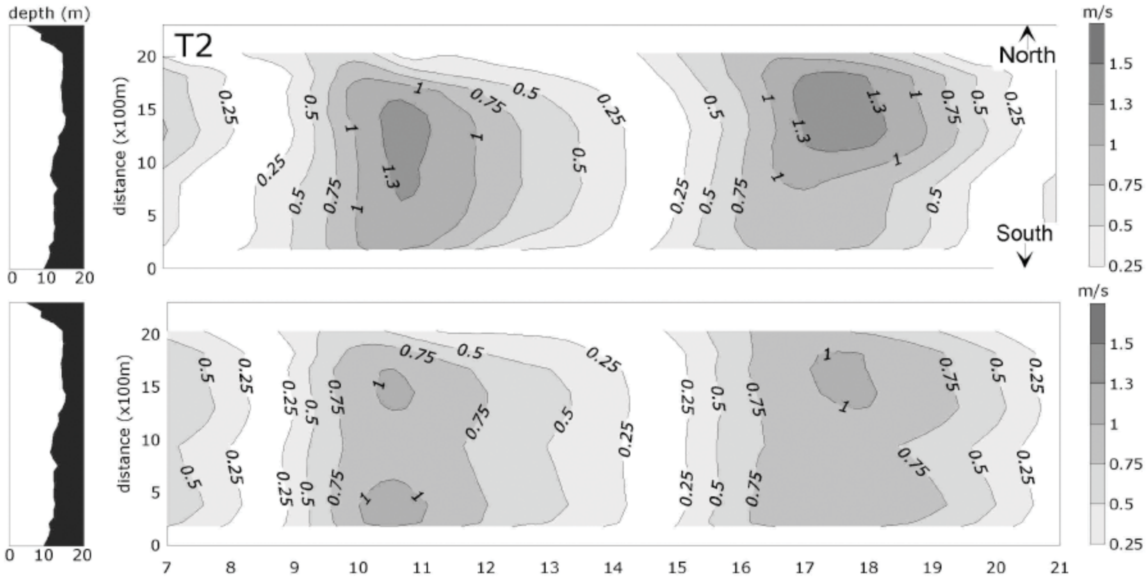

(b) Cross-section T2

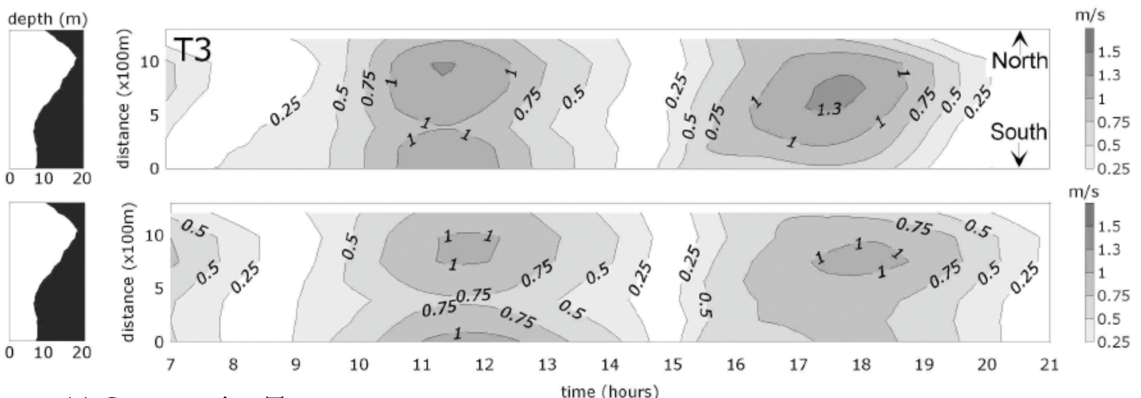

(c) Cross-section T3

Fig. 19: Influence of bed roughness on the computed variation of depth-averaged velocity for a spring tide at cross-sections T1, T2 and T3. Upper plot: constant Chezy coefficient; lower plot: predicted bed roughness

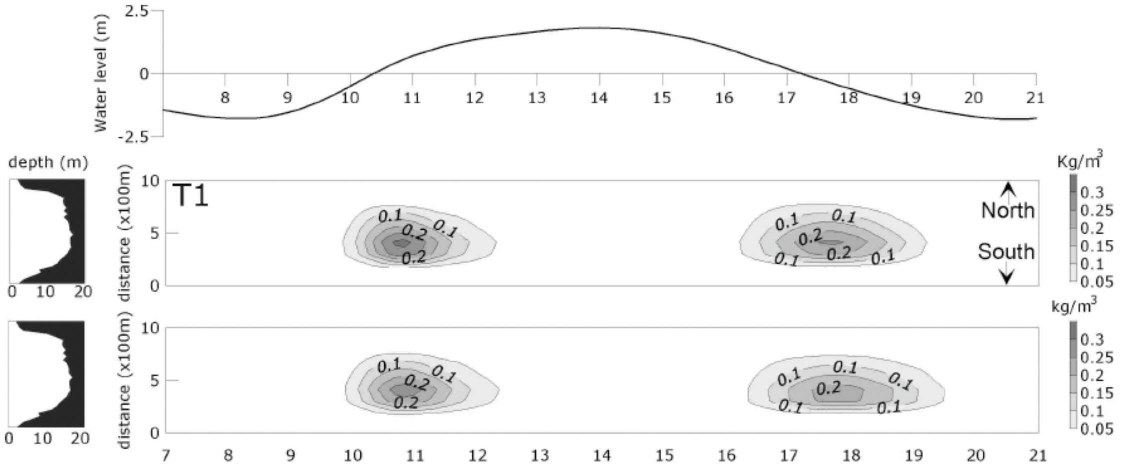

(a) Cross-section T1

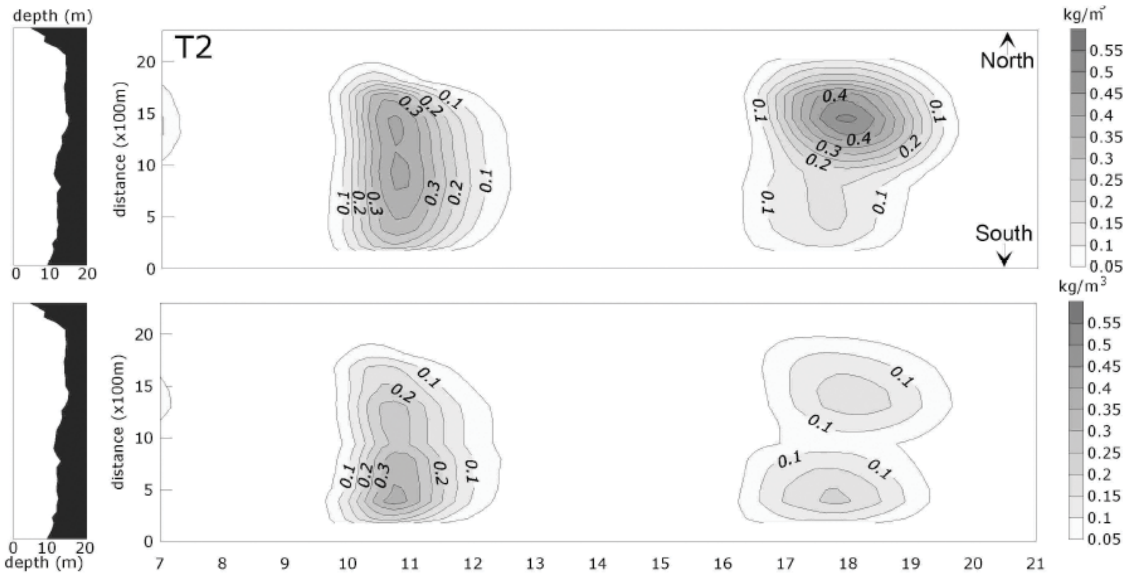

(b) Cross-section T2

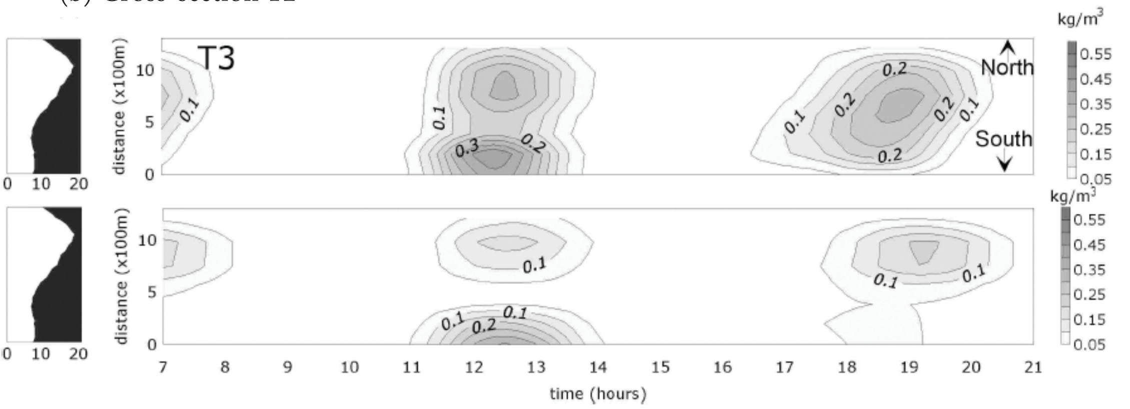

(c) Cross-section T3

Fig. 20: Influence of bed roughness on the computed variation of depth-averaged suspended sediment concentration for a spring tide at cross-sections T1, T2 and T3. Upper plot: constant Chezy coefficient; lower plot: predicted bed roughness

The effect of bed roughness on flow velocities and suspended sediment concentrations is clearly evident. A slight reduction in the magnitudes and changes in the patterns of depth-averaged current velocities due to a higher bed roughness are observed particularly at cross-sections T2 and T3. At cross-section T1 in the northwest part of the study area the differences are only marginal. A similar behaviour is observed regarding the effect of bed roughness on the simulated depth-averaged suspended sediment concentrations. More significant differences were observed at cross-sections T2 and T3. Besides a change in the patterns of concentration distribution over the cross-sections, an approximately twofold reduction in the magnitude of depth-integrated concentrations resulted at cross-section T2 due to the larger bed roughness values at this location. These findings are in accordance with the results of previous studies by VAN RIJN et al. (2001) and WINTER and MAYERLE (2003). It is interesting to note that higher roughness values tend to delay the times of occurrence of peak velocities.

10. Conclusions

A realistic characterization of surficial seabed sediments and geological features based on field measurements has proved to be of major importance for correctly describing flow and sediment transport conditions in the study area. The spatial variation of the dimensions of bed-form features in the tidal channels of the Dithmarschen Bight was found to be highly dependent on the thickness of the potentially mobile sediment layer as well as the characteristics of surficial seabed sediments and flow conditions. An analysis of field measurements has shown that bed-form features develop primarily in the most exposed areas of the Suederpiep, at the intersection of this tidal channel with the Bielshoevener Loch and along the channels banks, especially in the Norderpiep and Piep. In regions with mobile sediment deposits, megaripples and dunes with lengths of up to 20 m were mainly observed. The maximum height of bed forms measured at only a few locations was found to be of the order of 0.7 m. Bed forms were not found in regions of the tidal channels where the surficial seabed sediments are mainly comprised of mud or at locations with consolidated deposits. At locations where the EHL is exposed, consolidated sediment bed forms cannot develop.

Investigations of the temporal variation of the dimension of bed forms at a single location showed that the heights of observed bed forms remain approximately unchanged during a tidal period, whereas their lengths may double in size. The small steepness of the observed bed forms gives the impression of a fairly smooth seabed. The largest values of measured roughness sizes correspond to about half of the observed bed-form heights. This is in accordance with the initial estimate of form roughness suggested by VAN RIJN (1993).

The effectiveness of empirical equations for predicting the dimensions and roughness of bed-form features was tested on the basis of observations in the tidal channels. A comparison between predicted and observed bed-form dimensions showed significant differences, with observed relative bed-form heights of up to 8 times higher and observed lengths of about 4 to 8 times longer than those predicted by the empirical equations. Fairly good agreement was obtained, however, between the bed-form roughness values estimated from measurements and those predicted by the empirical equations.

The numerical procedure outlined for predicting the dimensions of bed forms, and hence bed roughness, in the tidal channels proved to be quite effective. Bed-form dimensions and equivalent roughness values were estimated from the results of two-dimensional depth-integrated flow model computations, taking into account sediment characteristics and the thickness of the potentially mobile sediment layer. The sensitivity of flow and suspended sediment concentration to the choice of bed roughness was demonstrated. Numerical model simulations using a 2DH flow and sediment transport model were also carried out. These simulations indicated that bed roughness has a significant effect on sediment concentrations. Increased bed roughness was found to result in an approximately twofold reduction in the maximum depth-averaged suspended sediment concentration. This underlines the importance of accurately estimating the dimensions of bed forms and associated roughness values. The results of the simulations also showed that an increase in roughness values additionally leads to changes in the patterns of distribution of depth-averaged suspended sediment concentration over a tidal period. This effect is more pronounced in the main tidal channels, i.e. in the Suederpiep and Piep, at cross-sections T2 and T3, respectively.

Field measurements of bed-form dimensions and associated roughness values proved to be extremely valuable for adjusting the empirical equations so as to obtain a better representation of conditions in the tidal channels and hence improve the predictive capability of numerical models. Additional measurements at different locations and for a wider range of surficial seabed sediment characteristics and flow conditions are recommended to improve our understanding of the spatial and temporal variation of the dimensions of bed forms and associated roughness values. Simultaneous measurements of current profiles and suspended sediment concentrations in the near-wall region with higher vertical resolution are also recommended to permit a more precise determination of equivalent roughness values, which is an essential prerequisite for future investigations of the effects of roughness on sediment concentration and transport.

11. Acknowledgements

This investigation was carried out within the framework of the project PROMORPH. We would like to thank the German Ministry of Education and Research (BMBF) for funding the project (Funding number 03 F 0262A). Funding provided by the German Academic Exchange Service (DAAD) to support the doctorate studies of Dr. Gatot Pramono is also highly appreciated. We also wish to thank the staff of the Research and Technology Centre Westcoast of the University of Kiel for conducting the field surveys. The Office for Rural Areas (ALR) in Husum is also gratefully acknowledged for providing the water level data and bathymetric data for the tidal flats, as well as the Federal Maritime and Hydrographic Agency (BSH) in Hamburg for providing the bathymetric data for the tidal channels. We are also indebted to Dr. Ian Westwood for his meticulous corrections and final proofreading of the English manuscript. The constructive comments by Dr.-Ing. V. Barthel and an anonymous reviewer are also gratefully acknowledged.

12. References

Asp Neto, N. E.: Long- to Short-term Morphodynamic Evolution of the Tidal Channels and Flats of the Dithmarschen Bight, German North Sea, Ph.D. thesis, University of Kiel, Germany, 2004.

Asp Neto, N. E.; Wilkens, J.; Ricklefs, K. and Mayerle, R.: Geology and Morphodynamics of a Tidal Flat Area of the German North Sea Coast and its Support to a Medium-scale Morphodynamic Modelling. In Procedings of VIII Congresso da ABEQUA, Mariluz/ Imbe, Brazil, 14–20 October, 2001.

MAYERLE, R.; RAZAKAFONIAINA, T.; PALACIO, C. and PRAMONO, G.: Bed Forms and Equivalent Roughness Sizes in Tidal Channels. Proceedings of the International Conference on Fluvial Hydraulics (River Flow 2002), IAHR, Louvain-la-Neuve, Belgium, 2002.

MAHMOOD, K.; MERHDAD, M. H. and HAQUE, M. I.: Bed-Form Data in ACOP-Canals 1979–1980. Civil Mechanical and Environmental Engineering Department, George Washington University, Washington DC, USA, 1993.

POERBANDONO and MAYERLE, R.: Composition and Dynamics of Sediments in Tidal Channels of the German North Sea Coast, Die Küste, Heft 69, 2005.

PALACIO, C.; MAYERLE, R.; TORO, M. and JIMÉNEZ, N.: Modelling of Flow in a Tidal Flat Area in the South-Eastern German Bight, Die Küste, Heft 69, 2005.

RAUDKIVI, A. J.: The Roughness Height Under Waves. Journal of Hydraulic Research, 26(5): 569–584, 1988.

SOULSBY, R. L.: Dynamics of Marine Sands. Pub. Thomas Telford, ISBN 072772584X, London, 1997.

VAN RIJN, L. C.: Sediment Transport, Part I: Bed Load Transport, and Part II: Suspended Load Transport. Journal of Hydraulic Engineering, ASCE , vol. 110, 1431–1641, 1984.

VAN RIJN, L. C.: Principles of Sediment Transport in Rivers, Estuaries and Coastal Seas. Aqua Publications, Amsterdam, The Netherlands, 1993.

VAN RIJN, L. C.; Davies, A. G.; VAN DE GRAAF, J. and RIBBERINK, J. S.: Sediment Transport Modelling in Marine Coastal Environments, Aqua Publications, ISBN 90-800356-4-5-, Amsterdam, The Netherlands, 2001.

VELA-DIEZ, S.: Sediment Mapping of the Tidal Flat Channels off Buesum. Master Thesis. Coastal Research Laboratory, University of Kiel, Germany, 2001.

WINTER, C. and MAYERLE, R.: Calibration and Validation of a Sediment Transport Model with Extensive Data-sets for a Tidal Channel System in the German Wadden Sea. Coastal Sediments Conference, 2003.

WINTER, C., POERBANDONO, HOYME, H. and MAYERLE, R.: Modelling of Suspended Sediment Dynamics in Tidal Channels of the German Bight, Die Küste, Heft 69, 2005.

YALIN, M. S.: Mechanics of Sediment Transport. Pergamon Press Ltd., Braunschweig, Germany, 1972.

Die Küste, 69 PROMORPH (2005), 1-420

Modelling of Suspended Sediment Dynamics in Tidal Channels of the German Bight

By CHRISTIAN WINTER, POERBANDONO, HELGE HOYME and ROBERTO MAYERLE

Summary

The performance of two-dimensional depth averaged numerical sediment transport models has been evaluated based on extensive field data within the framework of the BMBF founded research project "Predictions of Medium Scale Morphodynamics (PROMORPH)". A validated two-dimensional depth integrated hydrodynamic coastal area model has been complemented by a transport module. The dynamics of suspended sediment concentration are computed from an advection diffusion equation. The bed load and equilibrium transport is determined based on commonly accepted algebraic formulations (VAN RIJN, 1984; BIJKER, 1971). Sensitivity studies show the dependency of the model results on input parameters, mainly the bottom roughness. Acceptable results therefore necessarily require a thorough model calibration. This has been carried out by comparison to measured suspended sediment concentrations at three cross-sections of the Dithmarschen Bight to find the most suitable set of input parameters. A quantitative assessment of the model performance has been based on parameters as the discrepancy ratio and the relative mean absolute error. Similar accuracy was achieved for both the calibration data and independent validation data-sets. It is concluded that after calibration the model can be expected to produce reasonable results. However significant deviations from field data in terms of absolute (quantitative) values might occur locally.

Zusammenfassung

Im Rahmen des vom BMBF geförderten Forschungsprojekts „Prognose mittelfristiger Morphologieänderung (PROMOPRH)“ wurden umfangreiche Naturmessdaten für die Kalibrierung und Validierung von numerischen Sedimenttransportmodellen verwendet. Ein validiertes zweidimensional-tiefenintegriertes hydrodynamisch-numerisches Flächenmodell wurde um ein Sedimenttransportmodul erweitert. Die Dynamik suspendierten Sediments wird durch die numerische Lösung einer Advektions-Diffusionsgleichung beschrieben. Der Geschiebetransport wird durch bekannte algebraische Formulierungen (BIJKER, 1971, VAN RIJN, 1984) ausgedrückt. Sensitivitätsstudien zeigen die Abhängigkeit des Modells von Eingabeparametern, insbesondere der Bodenrauhigkeit. Es wird deutlich, dass auch bei der Verwendung allgemein akzeptierter und weit verbreiteter Transportformeln eine Kalibrierung der Modelle an Naturmessdaten notwendig ist. Diese wurde anhand gemessener Sedimentkonzentrationen an drei Rinnenquerschnitten der Dithmarscher Bucht durchgeführt. Zur quantitativen Beurteilung der Modellgüte wurden statistische Kenngrößen verwendet. Eine Validierung des Sedimenttransportmodells anhand unabhängiger Datensätze zeigt gleiche Qualität. Es wird gezeigt, dass das Modell die Schwebstoffdynamik im Untersuchungsgebiet weitgehend nachbildet. Allerdings muss lokal mit zum Teil erheblichen quantitativen Abweichungen gerechnet werden.

Keywords

Suspended Sediment Transport, Coastal Area Model, Calibration, Validation, Promorph, Meldorfer Bucht, Dithmarscher Bucht, Nordsee, North Sea

Contents

1. Introduction

Coastal dynamics are mainly affected by hydrodynamic and climatic forcing, local sedimentology and morphology. Sediment continuously is eroded, transported and deposited leading to an ongoing evolution of the bed in all spatial and temporal scales. The investigation and understanding of the governing dynamic processes is crucial for the prediction of future coastal development e.g. the impact assessment of coastal structures. Comprehensive studies of sediment- and morphodynamics combine field measurements and modelling approaches of different structure and complexity. Two main model concepts can be distinguished: Empirical models on the one hand, which are based on empirical relationships between the geometry of the coastal environment and physical parameters. Dynamic models, on the other hand, which base their predictions on mathematical formulations of the relevant physical processes. These process based models involve different concepts such as coastline models, for the large scale description of longshore behaviour; coastal profile models, which simulate the cross-shore morphological evolution and coastal area models, in which both horizontal dimensions are taken into account. Here the focus is set on the latter process-based coastal area models which typically are developed for and applied in engineering time and length scales (days to months, tens to hundreds of kilometres). A number of these, following different physical and numerical approaches and strategies have been developed in the past decades (NICHOLSON et al., 1997). A majority are based on the quasi steady assumption, that the bed may be considered immobile in hydrodynamic timescale. This leads to a decoupling of computational modules, i.e. a separate, successive calculation of currents, waves, sediment transport and bed evolution.

Adapted field data has to be available to set-up, calibrate, validate and drive numerical models. Vice versa the validated model can be applied for the spatial and temporal inter- and extrapolation of measured data (hindcast), and predictive (forecast) studies. Within the framework of the BMBF funded research project 'Prognosis of Meso-scale Morphodynamics (PROMORPH)' (ZIELKE et al., 2000) a large set of field data has been obtained from measurement campaigns designed for the development of numerical models. This paper describes the set-up, calibration and validation of a numerical model for the simulation of sediment dynamics in the tidal channels of the Dithmarschen Bight of the German Wadden Sea.

Generally, model validation with field measurements is based on discrete series of measured and computed data. To overcome a purely descriptive and qualitative evaluation values are often presented as anomalies (differences) or correlations. Recent comparative studies tend to present model quality in terms of the discrepancy ratio, i.e. the percentage of computed versus observed concentrations that range within a certain distance from parity (e.g. DAMGAARD et al., 2001). VAN RIJN et al. (2002) proposed a quantitative measure to evaluate the performance of numerical wave and current models based on a relative mean absolute error, adjusted for the accuracy of the measuring device. As this measure is less sensitive to outliers than e.g. the mean error, it was chosen to serve as a quality criterion in this study.

In the following chapter a brief overview is given about the study area and the field measurements which have been carried out throughout the research project PROMORPH. The third chapter describes the numerical modelling system and the set-up of a model of the Dithmarschen Bight. Also the parameters used for model evaluation are introduced. The calibration of the sediment transport model using field data is presented in the fourth chapter. The validation of the model and a quantitative evaluation is given in the fifth chapter. Results then are discussed and final conclusions are drawn in chapter 6.

2. Study Area

The study area covers the tidal flats and channels of the Dithmarschen Bight in the South-Western North Sea (Fig.1). Focus is set on the main tidal channel system comprising the Norderpiep, Suederpiep and Piep tidal channels which connect the open North Sea with the Meldorf Bight. Tides are semi-diurnal with a mean tidal range of about 3.2 m. The tidal prism of this channel system is in the order of $500 \cdot 10^6$ m³.

The composition of the well sorted bed sediments is of mainly very fine to fine sands with median grain sizes (D_{50}) varying from 80 to 170 µm (D_{90} are about 1.2 to 2 times D_{50}). Bed sediments with larger mud content are found in some of the deeper parts of the main channels, where a consolidated, rigid mud layer crops out. The sediments transported in suspension are finer: Sampled mean grain sizes here range from 6 to 86 µm. In general, fairly uniform vertical distributions of suspended sediment concentration were found.

Within the framework of the project extensive field measurements of current velocities and suspended sediment concentrations in the tidal channels were carried out (TORO et al., in this volume; POERBANDONO and MAYERLE, in the volume). The campaigns mainly cover climatically mild conditions due to technical restrictions of ship based surveys. Three cross-sections, i.e. T1 on the Norderpiep tidal channel on the Northwest of the domain, T2 on the Suederpiep tidal channel on the centre of the domain and T3 on the Piep tidal channel closer to the coast have been monitored. Current velocities were measured from moving vessels using acoustic profilers covering the entire cross-sections. Measurements of suspended sediment concentration over the vertical at defined locations of the cross-sections were made simultaneously with the current velocity measurements. Optical transmissometers that have been calibrated using direct water samples were employed. The depth-integrated suspended sediment concentrations in the tidal channels vary from a background concentration about 0.05 kg/m³ at slack water to 0.4–0.5 kg/m³ after maximum flood and ebb currents. Table 1 summarizes the surveys conducted at the three cross-sections the data sets of which have been used here for the calibration and validation of the hydrodynamic and sediment dynamic models.

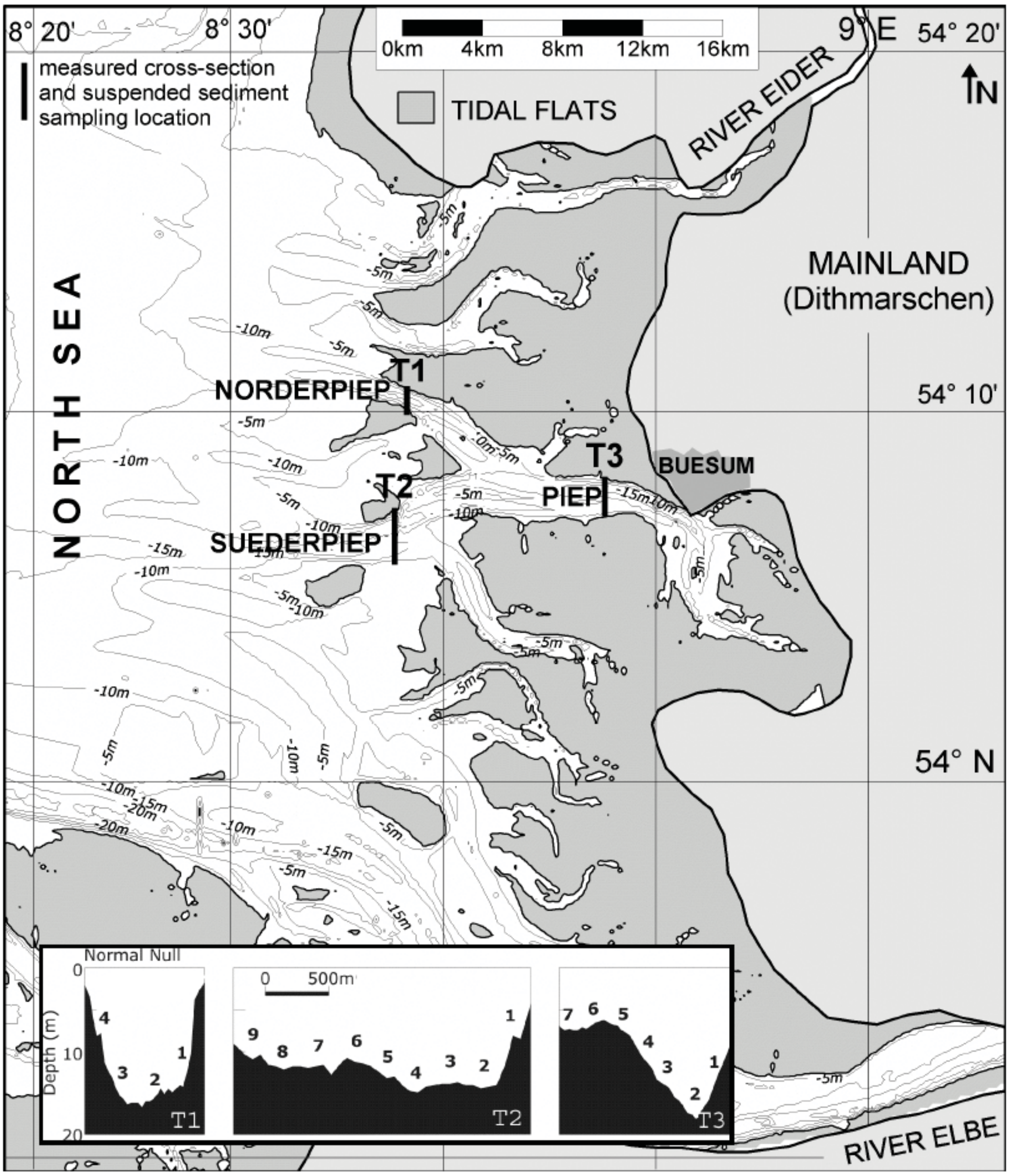

Fig. 1: Study area Dithmarschen Bight in the South Eastern North Sea and monitored cross-sections T1, T2, T3 with numbered measuring positions

Fig. 2 exemplarily shows the variation of measured depth-integrated velocity and suspended sediment concentration at the cross-sections T1, T2 and T3. Measurements were carried out on March 21 to 23, 2000 over full tidal cycles around spring tide. This period was characterised by calm weather conditions with westerly winds below 5 m/s.

Current velocities in the 0.8 km wide, 15 m deep, u-shaped northern channel Norderpiep (T1) may reach up to 1.25 m/s and are centred in the middle of the cross-section during flood. During ebb the depth averaged velocities are slightly higher (<1.25 m/s) and their maximum is found to be shifted towards the North. Depth-averaged sediment concentrations range between 0.08 and 0.14 kg/m³ during flood and up to 0.19 kg/m³ during ebb in the southern part of the cross-section. The peak in concentration lags the maximum ebb velocities by about 90 minutes.

Table 1: Field data on suspended sediment dynamics used for calibration and validation of the models

Data Set	Measuring Campaign	Date	Tidal Range [m]	Cross Section	Measuring Stations	Duration [h]	Remarks
1	March, 2000	22	4.0	T1	4	12:00	
		21	4.1	T2	9	11:55	Calibration
		23	4.2	T3	7	13:04	
2	June, 2000	5	3.7	T1	4	06:36	
		5	3.7	T2	12	08:26	Validation
		6	3.9	T3	7	08:12	
3	September,	5	3.1	T1	4	10:28	
	2000	5	3.1	T2	12	09:54	Validation
		6	2.9	T3	7	10:47	
4	September,	12	3.3	T1	4	11:38	
	2000	12	3.3	T2	10	10:59	Validation
		13	3.5	T3	7	04:34	
5	December,	5	2.3	T1	4	05:33	
	2000	5	2.3	T2	10	10:50	Validation
		6	2.5	T3	6	12:06	

Depth averaged flood currents in the Suederpiep tidal channel reach 1.5 m/s in the southern part of the 2 km wide cross-section T2. Maximum ebb currents go up to 1.2 m/s mainly at the northern part of the cross-section. Depth averaged sediment transport concentrations range from 0.1 to 0.2 kg/m³ in the northern part, and up to 0.5 kg/m³ in the southern part of the cross-section. The time lag between maximum flood currents and maximum concentrations is about 2 hours. Maximum concentrations lag the maximum ebb currents for about one hour.

The 1.2 km wide cross-section T3 is located east of the confluence of the main Piep tidal channel and a smaller, shallower tributary channel. This channel has been found to have a unique local bed morphology and sediment characteristics: In the northern part of the channel the bed sediment mainly consists of consolidated mud. Bedforms rarely exist. In the southern part of the channel the bed sediment consists of mainly fine sand with a mud content of less than 5%. Maximum flood currents occur in two maxima in the northern and southern part of the cross-section with depth averaged velocities up to 1.1 m/s. The ebb current is centred in the northern part of the cross-section with maximum depth averaged velocities of 1.4 m/s. The local sedimentology influences the transport behaviour: Depth averaged sediment transport concentrations range from 0.1 to 0.2 kg/m³ in the northern part and up to 0.3 kg/m³ (flood) and 0.4 kg/m³ (ebb) in the southern part of the cross-section. Depth averaged concentrations lag maximum flood currents by about one hour and ebb currents by about 30 min.

The calculated flow discharge and suspended transport load at the three cross-sections is plotted in Fig. 3. The main mass flux into and out of the Meldorf Bight is exchanged through the Suederpiep tidal channel, with a maximum flow discharge in the order of 30×10^6 m³/s and maximum suspended sediment loads of 10 t/s. The contribution through cross-section T1 is considerably smaller: Maximum flow discharge ranges in the order of 10×10^6 m³/s and maximum suspended sediment loads reach around 2 t/s. Due to the restrictions to only a few surveyed tidal cycles and limited cross-sections no final conclusions on budgets and ebb or flood domination of channels are drawn from the measurements.

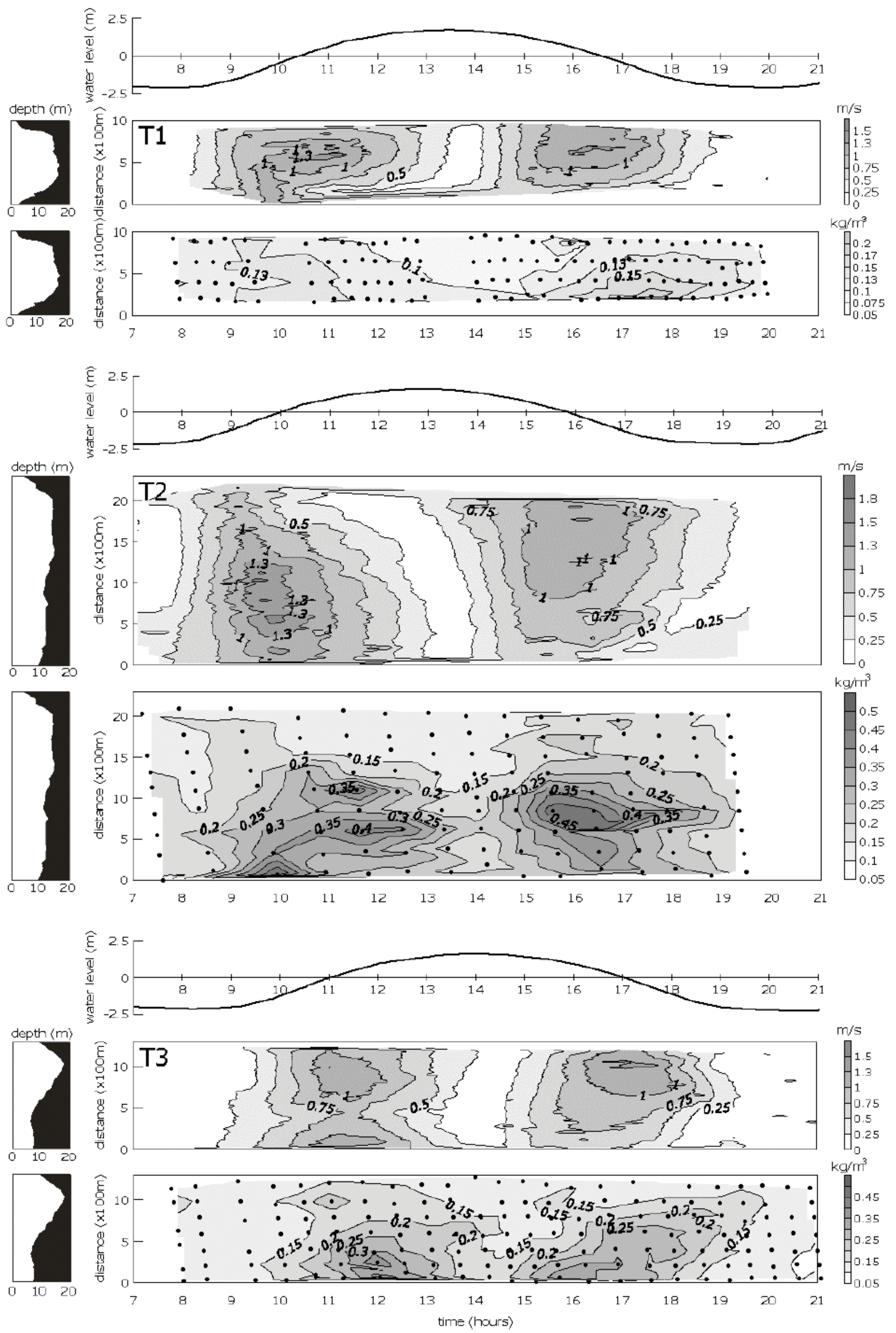

Fig. 2: Depth-integrated velocity and suspended sediment concentration over tidal cycles at the cross-sections T1, T2 and T3. Dots represent the stations of vertical optical transmission profiles

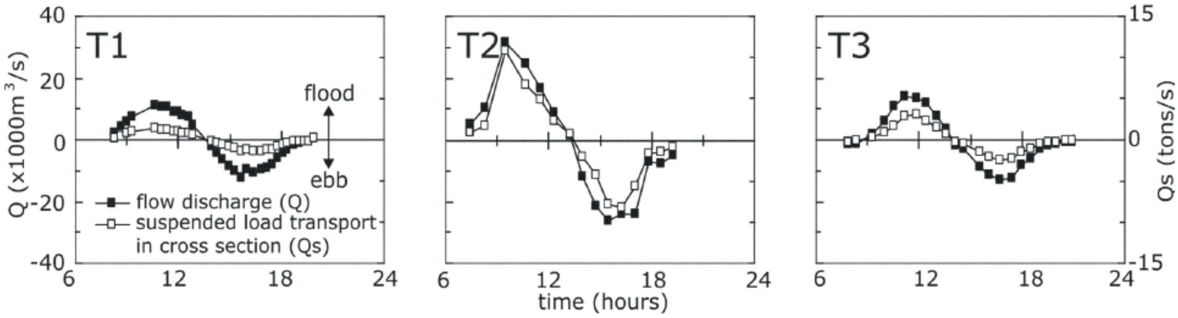

Fig. 3: Measured flow discharge and suspended transport load at the cross-sections T1, T2 and T3 on March 21 to 23, 2000

3. Numerical Model

For a further analysis and understanding of the suspended sediment dynamics and spatial and temporal extrapolation of measured data, numerical models for the simulation of hydrodynamics, sediment dynamics and morphodynamics have been set up. The set of field data, obtained from measurement campaigns within the research project, was used for an extensive calibration and validation of the models. The process-based coastal area model solves the mathematical equations describing the relevant physical processes on a computational grid. Driven by specified conditions at the open model boundaries (e.g. wind on the surface, waterlevels and sediment concentration at the lateral boundaries) the advective and diffusive processes within the model domain are simulated.

3.1 Modelling System

The process-based Delft3D modelling system has been applied. It comprises computational modules for the simulation of currents, waves, sediment transport and morphological evolution. These modules can be interlinked for the simulation of wave-induced currents, sediment transport and resulting morphological changes (ROELVINK et al., 1994). Here a quasi-stationary coupling of the computational modules is performed, where the bed is assumed immobile throughout the hydrodynamic and sedimentdynamic computations and the influence of the sediment concentration on the flow is neglected. This allows a successive simulation of the hydrodynamics, the sediment transport and the bed evolution in separate modules.

The set-up, calibration and validation of the hydrodynamic models are described in detail in PALACIO et al. (in this volume), PALACIO (2002) and PALACIO et al. (2001). All computations have been performed using two dimensional depth integrated (2DH) models. A curvilinear computational grid with quadrangular elements, covering the Meldorf Bight and the adjacent tidal channels has been used. About 43000 elements, with grid spacing ranging from 60 to 200 m were considered to discretise the domain with acceptable accuracy. Bathymetric data from recent echo soundings was interpolated on the grid using linear triangulation.

Water levels specified along the western open sea boundaries of the model have been derived from larger models covering the German Bight (WL|DELFT HYDRAULICS, 1997) and the European Continental Shelf (VERBOOM et al., 1992) using a nesting scheme (MAYERLE et al., in this volume, and WINTER, 2003). PALACIO (2002) gives long-term RMS-errors around

0.15 m/s in the Piep and Norderpiep and circa 0.25 m/s in the Suederpiep for the depth-integrated current velocities. The RMS-error of the water levels was between 0.02 and 0.04 m for high tide and between 0.05 and 0.12 m during low tide, based on the maximum and minimum water levels of a two-month period.

For the periods considered here, the differences between measured and computed water levels at the position Norderpiep are below 0.1 m at high-water and about 0.3 m at low water which corresponds to approximately 3 % and 8 %, respectively, of the maximum tidal range (3.6 m). At the gauge Büsum differences in water level remain below 0.15 m at high water and 0.4 m at low water giving about 4 % and 10 %, respectively, of the maximum tidal range (3.9 m). Although covering climatically mild periods only, a wave model (HISWA) was used to compute the wave field. At the open sea model boundaries, constant wave heights of 0.4 m and mean periods of 2 s were used. This model computes on a rectilinear grid with element sizes of 200 x 400 m covering the domain of interest. Model results indicate that the effect of small waves on the current velocities is moderate on the tidal flats and negligible in the tidal channels.

3.2 Sediment Transport Model

The transport module computes the sediment dynamics for a 2D horizontal area taking into account the flow and optionally wave parameters derived by the hydrodynamic models. As shown above, high velocity gradients and small grain sizes of the sediments transported in suspension cause considerable lag effects between local current velocities and the suspended sediment concentration. Thus the advection and diffusion of suspended sediment dynamics are computed by the numerical solution of an advection-diffusion equation. The bedload transport is separately derived from algebraic formulations. In this study two algebraic total load formulas, which distinguish between bed load and equilibrium suspended load, have been applied, being the BIJKER (1971) and the VAN RIJN (1984) formulation.

The BIJKER (1971) total load formula $S = S_b + S_{se}$ separately accounts for bed load (S_b) and the instantaneous equilibrium suspended load (S_{se}). The bed load relation is a modified version of the bed load formula by FRIJLINK (1952), for which a wave term was added. This formula has been initially verified with wave basin data with fine sand (D_{50} = 220 µm). It is commonly used in comparative and applied studies (e.g. DAVIES et al., 2002; BAYRAM et al., 2001; CAMENEN and LARROUNDÉ, 2003). It reads:

$$S_{bBIJKER} = b_1\, D_{50} \frac{u}{C} \sqrt{g}\ (1-p) \exp\left(\frac{-0.27(s-1)\, D_{50}\, \rho g}{\mu \tau_{b,wc}} \right) \tag{3.1}$$

With:
b_1 = empirical coefficient
C = Chezy coefficient, based on D_{50}
D_{50} = median particle diameter
u = current velocity
g = acceleration of gravity
p = porosity
s = $(\rho_s - \rho)$ relative sediment density

μ = $(C/C_{90})^{1.5}$ ripple factor
C_{90} = Chezy coefficient, based on D_{90}
$\tau_{b,wc}$ = shear stress at the bed

The original reference assigns $b_1 = 5$. However the formula has been found to overestimate measured transport rates (BAYRAM et al., 2001). Thus in practice it is considered to range between 1 and 5 depending on local conditions. The distribution of the suspended load is based upon the EINSTEIN (1950) approach:

$$S_{seBIJKER} = 1.83 S_{bBIJKER} \left(I_1 \ln\left(\frac{33.0\,h}{r_c}\right) + I_2 \right) \tag{3.2}$$

With: I_1, I_2 = Einstein integrals (Einstein, 1950)
h = water depth
r_c = bottom roughness

The Van Rijn (1984) total load equation is a widely used formulation for situations without waves. This total load formulation $S = S_b + S_{se}$ also separately defines bed load (S_b) and suspended load (S_{se}). The formula for the bed load transport reads:

$$S_{bVANRIJN} = \begin{cases} 0.053\sqrt{s\,g\,D_{50}^3}\; D_*^{-0.3} T^{2.1} & \text{for } T < 3.0 \\ 0.1\sqrt{s\,g\,D_{50}^3}\; D_*^{-0.3} T^{1.5} & \text{for } T \geq 3.0 \end{cases} \tag{3.3}$$

With: T = $(\mu_c\ \tau_{b,c} - \tau_{bcr})/\tau_{bcr}$, dimensionless shear stress parameter
τ_{bcr} = critical bed shear stress according to Shields
τ_{bc} = the effective shear stress
D_* = dimensionless particle diameter

The suspended sediment load is given as:

$$S_{seVANRIJN} = 0.015\, f_{cs}\, u\, h\, b_2 \frac{D_{50} T^{1.5}}{r_c D_*^{0.3}} \tag{3.4}$$

With: f_{cs} = $((r_c/h)/(1 - r_c)/h)^{1.2} \cdot \ln(r_c/h)$ shape factor
b_2 = empirical coefficient (O(1))

The expressions for the instantaneous equilibrium suspended load S_{se} as given above may be directly used for the calculation of suspended sediment concentrations if lag effects between hydrodynamics and sediment dynamics are small. However, if the adaption length of the suspended sediment is larger than the computational grid size, the entrainment, deposition, advection and diffusion of the suspended sediment must be determined by an advection-diffusion equation:

$$\frac{\partial hc_s}{\partial t}+\frac{\partial huc_s}{\partial x}+\frac{\partial hvc_s}{\partial y}-\frac{\partial}{\partial x}\left(\varepsilon h\frac{\partial c_s}{\partial x}\right)-\frac{\partial}{\partial y}\left(\varepsilon h\frac{\partial c_s}{\partial y}\right)=\frac{w_s\left(c_{se}-c_s\right)}{T_{sd}} \quad (3.5)$$

With:
- u,v = current velocities along the horizontal directions x and y
- ϵ = horizontal dispersion coefficient
- w_s = settling velocity
- T_{sd} = dimensionless adaptation time for the vertical concentration profile (GALAPPATTI and VREUGDENHILL, 1985)
- c_{se} = S_{se}/uh local equilibrium concentration
- S_{Se} = equilibrium suspended sediment transport rate

This equation is solved for the depth-integrated suspended sediment concentration c_s where the source/sink term is proportioned to the instantaneous equilibrium concentration c_{se}, derived from one of the algebraic sediment transport formulas. The suspended sediment components in x and y directions then are calculated:

$$S_{sx}=q_x c_s-h\varepsilon\frac{\partial c_s}{\partial x} \qquad S_{sy}=q_y c_s-h\varepsilon\frac{\partial c_s}{\partial y} \quad (3.6)$$

With: q_x, q_y = local discharge in x,y direction.

3.3 Model Set-Up and Sensitivity Analysis

The set-up of a numerical model comprises the spatial discretisation of physical parameters which characterise the domain of interest. This includes a large amount of data reduction and generalisation, as input data is averaged over grid-cells or even considered uniform over the whole computational domain. Also some processes which certainly are of an instationary nature are treated as constant in time. As shown above, some empirical parameters in the transport formulas also have to be specified. Finally, there are also physical input parameters that only can be estimated by the modeller, as field data may be not sufficient or not available at all. All this brings about the necessity of a thorough analysis of the model sensitivity to input parameters when setting up the numerical model.

The transport module uses the same curvi-linear grid and bathymetric information as the flow module. Hydrodynamic quantities such as the wave-forces, depth averaged current velocities and water levels are read in from previous simulations. The numerical algorithm requires the definition of initial conditions describing the suspended sediment concentration at start-up time and suspended sediment concentration information at the open model boundaries throughout the simulation period. In order to avoid discontinuities in the initial conditions, every computation is started with a full tidal cycle spin-up, which is not taken into account for further analysis. For inflow conditions at the open model boundaries (e.g. flood current at the western boundaries) local equilibrium concentrations or specified time-series of concentrations are to be prescribed. For outflow conditions (e.g. ebb current at the western boundaries) the upstream computational cell concentration is imposed by setting the derivative of the suspended sediment concentration in stream-wise direction to zero. The influence of the prescribed boundary conditions on the computed suspended sediment dynamics was found to be limited to a region, not farther than five kilometres from the open model boundaries (RIZZO, 2003).

The observed suspended sediment dynamics show pronounced lag effects. In that respect the direct application of the instantaneous equilibrium suspended sediment concentration derived from algebraic formulations would produce unrealistic results. Instead the advection and diffusion of suspended sediment concentration has been simulated by the numerical solution of equation 3.5.

As shown above the suspended sediment concentration derived from the solution of the advection diffusion equation is highly dependent on the algebraic formulations which describe the equilibrium suspended sediment transport. Thus a sensitivity analysis has been performed to critically ascertain the response of the computed concentrations to variations in grain sizes and settling velocities, empirical coefficients and the bottom roughness. Based on these studies, preliminary settings to be considered in the later calibration as well as their ranges are defined.

Simulations considering the Bijker formula, which accounts for the effect of waves, showed that the effect of local waves on the suspended sediment concentrations in the tidal channels is negligible for significant wave heights less than 0.3 m. Computed sediment concentrations with and without waves differed less than 0.01 kg/m^3, which is less than the measured background concentration. Certainly the importance of waves is expected to be more pronounced in storm situations.

Simulations were carried out considering uniform bed grain sizes with D_{50} varying from 40 to 160 µm. These computations should clarify if the transport formulae produce reasonable results for particle sizes outside the ranges of derivation of these equations. For the range of particle sizes considered here, computed sediment concentrations differ within a factor 2.

A range of settling velocities from 0.1 mm/s to 4 mm/s (considering suspended sediment particle sizes from 10 to 80 µm) was also considered. The effect on the sediment concentration is mainly pronounced during slack water. As expected, computed concentrations are lower with higher settling velocities in periods with smaller current velocities. Maximum concentrations differ within 30 %.

The variation of the calibration parameters b_1 in the Bijker formula and b_2 in the Van Rijn formula proportionally affects the computed concentration. Thus this coefficient may be considered as a linear tuning factor for computed depth averaged suspended sediment concentrations.

The bottom roughness term r_c is delicate in the sense that it influences the computed suspended transport magnitude profoundly and at the same time it is difficult to measure or estimate in engineering practice. MAYERLE et al. (2002) found that bed forms in the domain vary significantly during a tidal cycle ranging from less than one millimetre (flat bed) to several decimeters (rippled bed). Computations were carried out covering the range of r_c from one millimetre to 0.5 m. Fig. 4 exemplarily shows the resulting sediment concentrations which range within three orders of magnitude. Bed roughness values of a few centimetres to decimetres provide sediment concentrations within the range of the measured values.

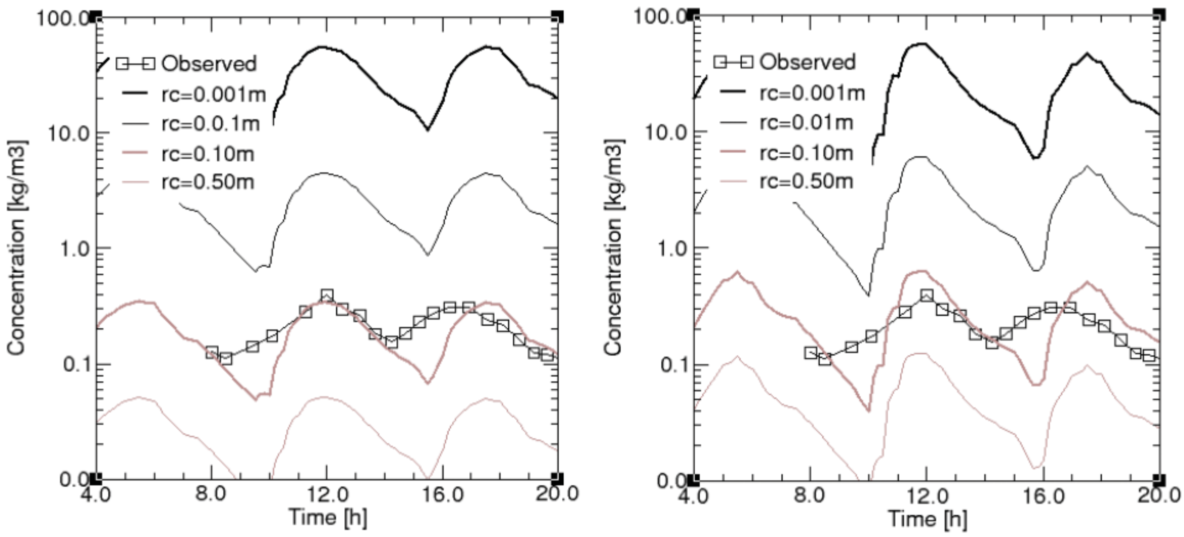

Fig. 4: Computed suspended sediment concentrations at Position 4 of cross-section T2. Modified bottom roughness r_c using the BIJKER (1971) (left) and VAN RIJN (1984) (right) equation

Initial computations with an estimated bottom roughness r_c = 0.1 m, grain sizes of D_{50} = 100 µm and D_{90} = 150 µm, and the empirical coefficients b_1 = 5 for the BIJKER formula and b_2 = 1 for the VAN RIJN formula result in differences between the two approaches up to factor 3, depending on the location. In this case the VAN RIJN formula leads to an underestimation of the suspended sediment concentration, whereas the BIJKER formula overestimates the measured values (Fig. 5).

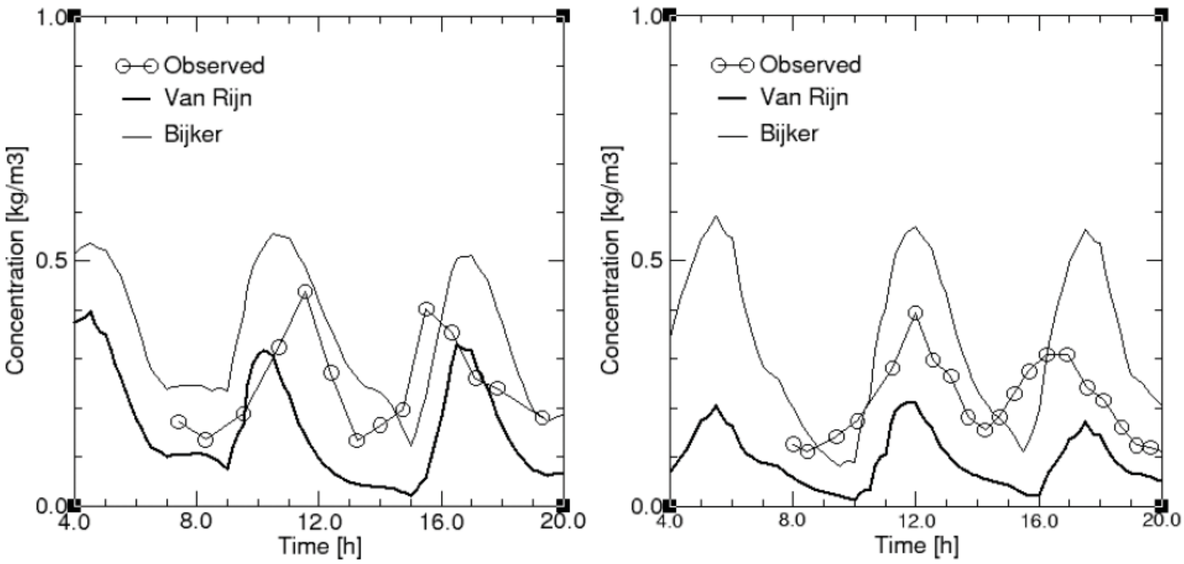

Fig. 5: Computed suspended sediment concentrations for initial settings at position 4 of cross-section T2 (left) and position 4 of cross-section T3 (right)

3.4 Evaluation Parameters

The calibration and validation of models are based on comparisons between field measurements and model simulations. To overcome purely descriptive and qualitative evaluations, statistical parameters are used to quantify the model quality. Yet, model evaluation still lacks universal and commonly accepted methods for an objective assessment of the model quality. However certain types of presentation seem to have formed a habit:

Generally the evaluation with field measurements is based on discrete data series of measured (c_m) and computed (c_c) values. Recent publications on intercomparisons of sediment transport models (e.g. DAMGAARD et al., 2001) tend to assess the model performance on the basis of the discrepancy ratio, i.e. the percentage of computed versus observed values that range within a certain distance from parity ($c_m/c_c = 1$). The distances typically are taken as factor 2 ($0.5< c_m/c_c<2$) or factor 5 ($0.2< c_m/c_c<5$).

VAN RIJN et al. (2002) proposed a quantitative measure to evaluate the performance of numerical wave and current models based on the Adjusted Relative Mean Absolute Error (ARMAE). This procedure has been adopted for the sediment transport simulations described here. The ARMAE is preferred above the Mean Square Error (MSE) as it is more robust against outliers and takes into account the accuracy of the measuring device. The formula reads:

$$ARMAE = \frac{< |c_c - c_m| - \Delta c_m >}{<| c_m |>} \tag{3.7}$$

With: c_c = computed value
c_m = measured value
Δc_m = device accuracy
|..| = absolute value
<..> = average over time

The expression $<|c_c-c_m|-\Delta c_m>$ is set zero for negative values, as it indicates that the difference between measured and computed values is smaller than the device accuracy. An appraisal by results for suspended sediment concentrations is not provided; however, the qualifications given in VAN RIJN et al. (2002) for wave heights and current velocities are cited in Table 2.

Table 2: Qualification of error ranges of the process parameters according to VAN RIJN et al. (2002)

Qualification	Waves : ARMAE [m]	Velocity : ARMAE [m/s]
Excellent	<0.05	<0.1
Good	0.05–0.1	0.1–0.3
Reasonable	0.1–0.2	0.3–0.5
Poor	0.2–0.3	0.5–0.7
Bad	>0.3	>0.7

4. Model Calibration

The survey of March 2003 provides a comprehensive set of suspended sediment concentration data at twenty positions on three cross-sections. Although the data and the calibration of the optical device cannot be completely free of errors because of the nature of the measurements carried out, they still offer a unique possibility of calibrating the model in space and time. Measured values and model results were compared at twenty cross-sectional positions during three tidal cycles (WINTER and MAYERLE, 2003).

A uniform and constant bed composition of fine sand with D_{50} and D_{90} values equal to 100 µm and 150 µm, respectively, was assumed. The calibration focused primarily on the bed roughness r_c and coefficients b_1 and b_2 in the algebraic equations. Uniform values of bed roughness ranging from 0.08 to 0.5 m, and coefficients in the algebraic equations varying from 1 to 5 were considered.

Comparisons of measured and computed values for the ranges of bed roughness are shown in Fig. 6. Three stations (station 4 on cross-section T1, station 4 on cross-section T2 and station 4 on cross-section T3) were selected to exemplify the change in model performance. It can be seen that uniform bed roughness values ranging from 0.1 to 0.3 m give results in the order of magnitude of the measured ones. Also the empirical coefficients b_1 and b_2 were adapted to correct for the under-estimation of the VAN-RIJN and the over-estimation of the BIJKER formula.

The magnitude of calculated suspended sediment concentrations can be adjusted to the measured values at single positions. However, the low background concentration around slack water mostly is under-predicted. Since the target of the project is the simulation of coastal morphodynamics which are governed by high loads, no further correction for this underestimation has been performed. Best parameter settings differ according to location and time. In order to select uniform and constant parameters that lead to the best possible agreement with measurements throughout the entire domain and at all times, approaches which enable a quantitative assessment of the model performance were considered. First, the discrepancy ratio, i.e. the percentage of computed versus observed concentrations that range within a factor of 2 and 5 has been chosen as a skill score. A number of different model runs with different settings has been evaluated based on dataset 1 (March 21 to 23, 2000):

Fig. 7 shows the discrepancy ratios of simulations after calibration: Best results using the BIJKER formula in the transport model set-up, with constant and uniform settings throughout the whole model domain, respectively resulted in 74 %, 74 % and 75 % for the cross-sections T1, T2 and T3 (all: 75.1 %) of the computed concentration values at the three cross-sections within a factor 2 compared to the measured. At the cross-sections T1 and T3 100 % and at cross-section T2 97 % (all: 98 %) are within a factor of 5. It shall be pointed out that outliers mostly belong to positions at the channel banks such as position 4 in cross-section T1, positions 1, 8 and 9 in cross-section T2, and position 7 in cross-section T3.

Best results applying the Van Rijn formula in the transport model set-up result in 61 %, 51 % and 58 % for the cross-sections T1, T2 and T3, respectively (total: 57 %) of the computed concentrations within a factor 2 compared to the measured. At the cross-sections T1, T2 and T3 94 %, 95 % and 91 %, respectively (all: 93 %) are within a factor of 5. Again outliers, underpredicting the observed concentrations mostly belong to positions near the channel banks such as position 4 in cross-section T1, positions 1, 8 and 9 in cross-section T2, and position 7 in cross-section T3. The ascertained settings are specified in Tab. 3.

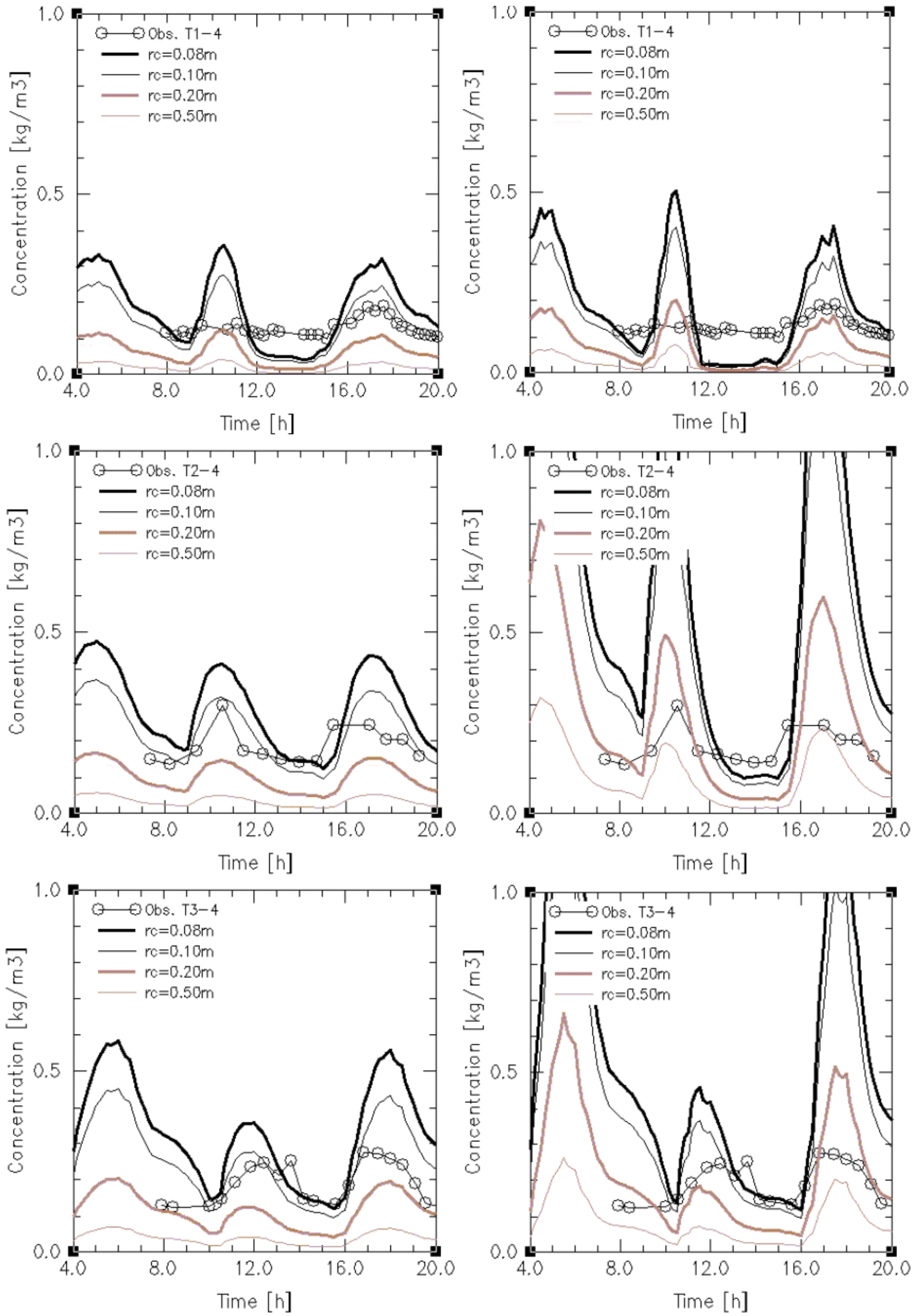

Fig. 6: Calibration with respect to bottom roughness r_c (Dataset 1). Measured (o-o) vs. computed (---) depth averaged suspended sediment concentrations at position 4 of transect T1 (upper), at position 4 of transect T2 (middle), at position 4 of transect T3 (lower). Results from simulations using the BIJKER (left) and the VAN RIJN (right) approach

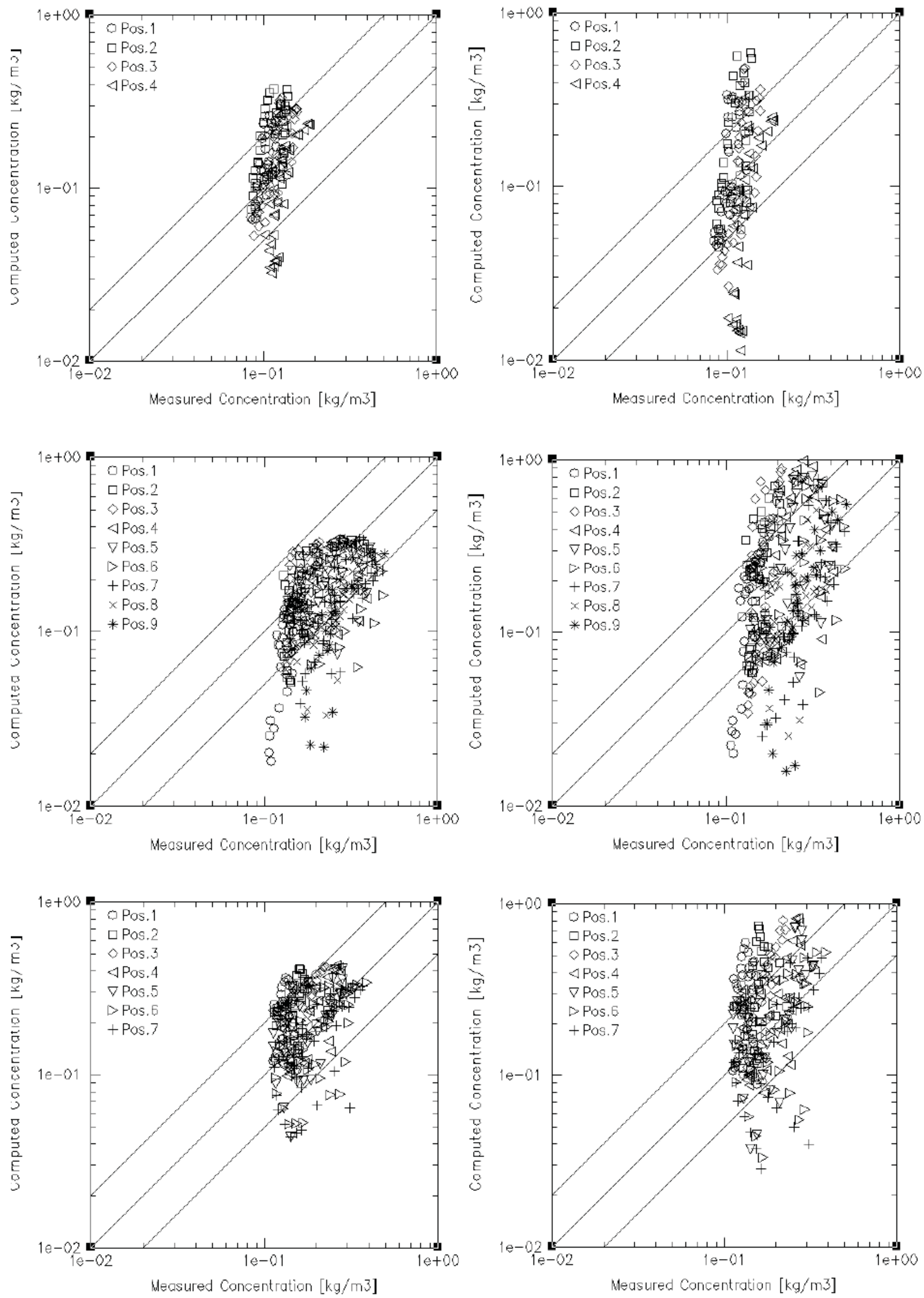

Fig. 7: Computed versus measured concentrations at cross-sections T1 (upper), T2 (middle), T3 (lower) using BIJKER (left) and VAN RIJN (right) formula. Solid lines indicate the range of factor 2

Table 3: Model settings after calibration

	$D50$ [µm]	$D90$ [µm]	b [–]	r_c [m]	w_s [mm/s]
BIJKER	100	150	3	0.2	0.1
VAN RIJN	100	150	2	0.2	0.1

To provide a quantitative measure of the model quality after calibration, which takes into account the accuracy of the measuring device, the mean ARMAE value for the twenty stations along the three-cross-sections were obtained with the same model settings used above. Assuming 30 % accuracy, the mean ARMAE for all twenty stations resulted to 0.17 kg/m³ for the Bijker formula and 0.28 kg/m³ for the VAN RIJN formula.

The computed variations of the depth-integrated velocity and concentration over the tidal cycle at the three cross-sections are shown in Fig. 8 for comparison with Fig. 2. Simulations were carried out using the BIJKER formula and the model settings given in Table 3. Apart from the concentrations computed for the flood phase in cross-section T1 which show far too high values, the observed characteristics could be reproduced reasonably well. Maximum concentrations can be computed at the right times and locations. The model is also capable of determining phase lag between maximum currents and concentration.

5. Model Validation

5.1 Validation of suspended sediment concentration

A meaningful evaluation of the model quality must be performed with independent datasets, which have not been used for calibration. Thus field data of suspended sediment concentrations from sets 2 to 4 (see Tab. 1) were used here. Data set 2 measured on June 5 and 6 (spring tidal range of 3.9 m) and dataset 3 measured on September 5 and 6, 2000 (average tidal range of 3.1 m) are chosen. Model validation was performed for computed suspended sediment concentrations and cross-sectional loads which are shown in the following sections. No additional tuning of model parameters was done.

The model quality in terms of depth averaged suspended sediment concentration is exemplarily shown for single positions at the three cross-sections in Fig. 9. In contrast to the results that were obtained for the calibration period the model overpredicts the marginally fluctuating concentration values at cross-section T1 for both periods (Fig. 10). Simulation results applying the BIJKER formulation are within the ranges of accuracy of the measuring device at the cross-sections T2 and T3. The VAN RIJN approach tends to over-estimate the maxima and under-estimate slack-water low values. Statistical parameters for these simulations are given in Table 4.

Table 4: Validation of simulated suspended sediment concentrations for datasets 2 and 3

	Mean ARMAE	Mean Absolute Error	Mean Relative Error	Data within Factor 2
BIJKER	0.12	0.05 kg/m³	41 %	75 %
VAN RIJN	0.40	0.08 kg/m³	73 %	52 %

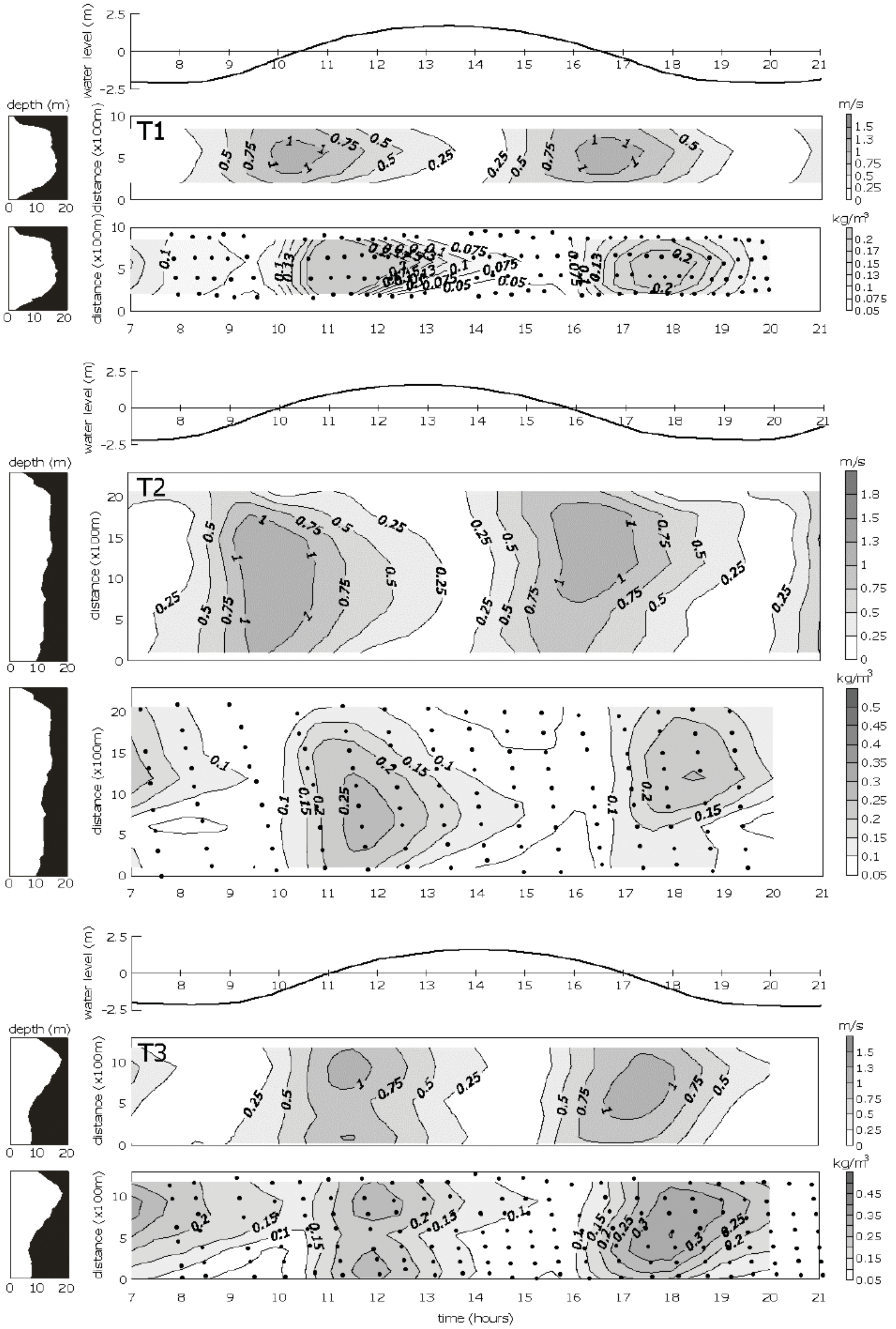

Fig. 8: Computed water levels, depth-integrated velocity and suspended sediment concentration hindcasting dataset 1 (March 2000) at the cross-sections T1, T2 and T3. For comparison see Fig. 2

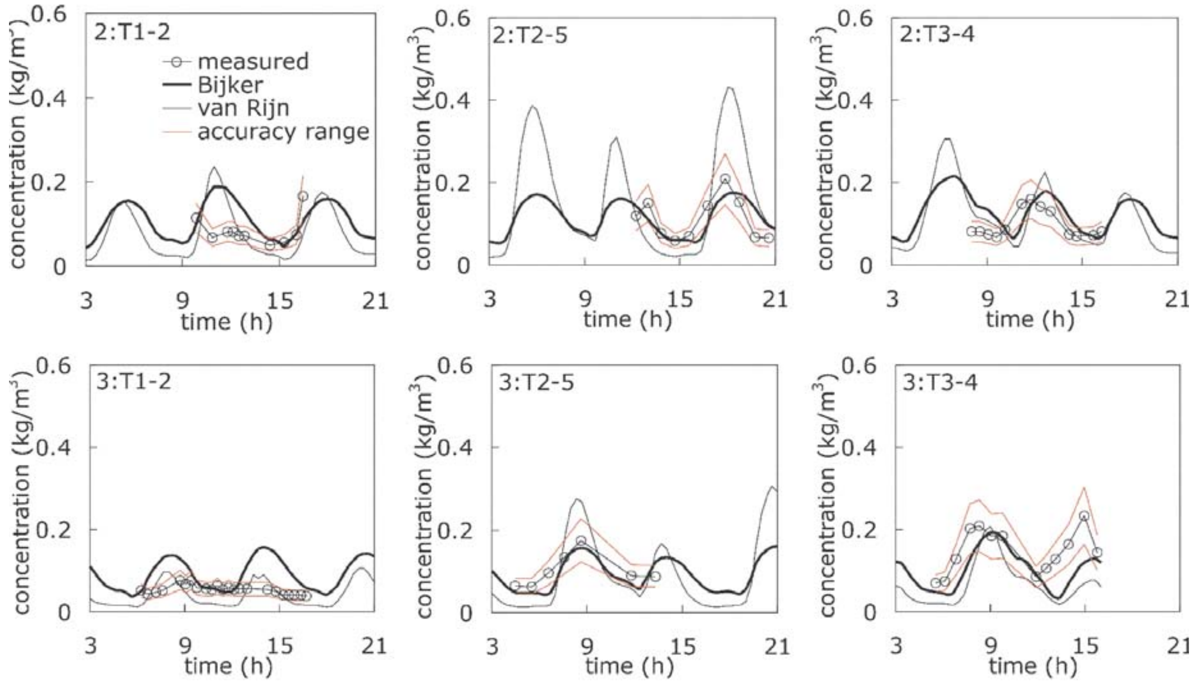

Fig. 9: Comparison of measured and predicted depth integrated concentration for datasets 2 (upper) and 3 (lower). Results for selected stations at cross-sections T1 (left), T2 (middle), and T3 (right)

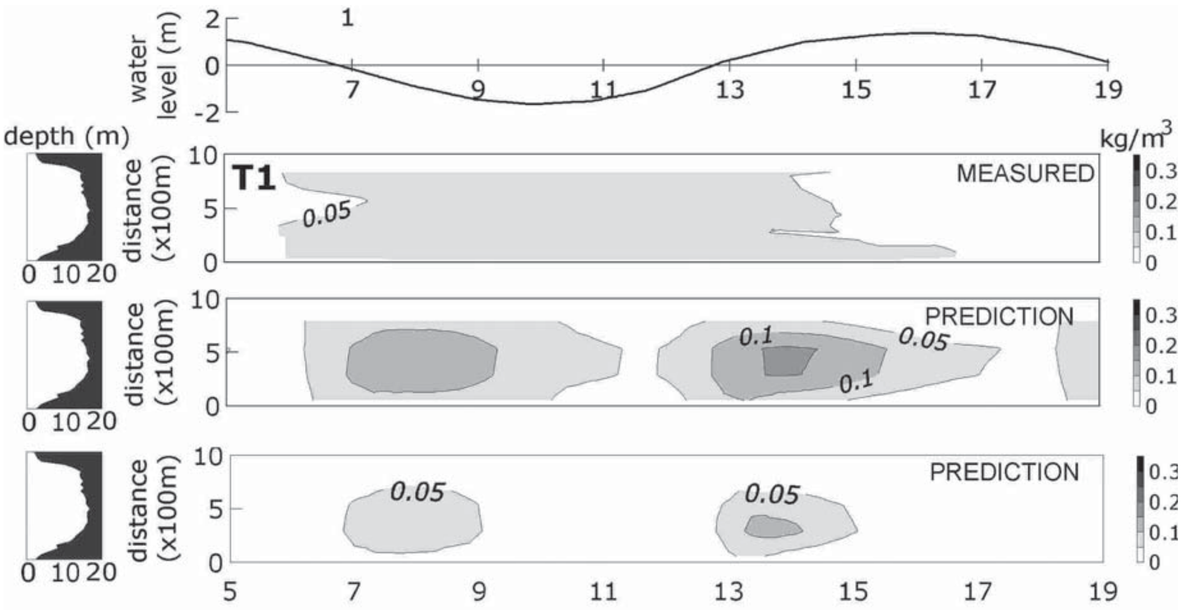

Fig. 10: Measured (upper) vs. computed (BIJKER: middle, VAN RIJN: lower) variation in suspended sediment concentration at cross-section T1 (Norderpiep) for dataset 3 (September 5, 2000)

The Suederpiep channel (cross-section T2) has been found to have the largest variation in depth-integrated concentration. In this cross-section, a clear response to the increasing tidal range can be observed. During this campaign the depth-integrated concentration varied between 0.06 to 0.33 kg/m³. Unfortunately, due to technical reasons measurements could not cover the entire flood phase. The prediction results generally follow the dynamic pattern of the depth-integrated concentration magnitudes (Fig. 11). The time of occurrence of maximum concentrations is captured well by both model approaches. However, the absolute values are under-estimated. The corresponding deviation is up to a factor of 2. Using the Van Rijn formula leads to a closer fit to the measured data.

The Piep (T3) channel's bed morphology and sediment characteristics influence the transport behaviour in a sense that the ebb currents mobilise material mainly in the shallow and sandy southern part (Fig. 12). Two hours later than in the southern region a weaker concentration peak of sediment – brought into suspension in the tidal flats upstream – is also observed in the northern part, which features a rigid bed of consolidated cohesives in the vicinity of the cross-section. The suspended sediment concentration during flood shows a twofold maximum from the southern and slightly later from the northern channel. The model is able to reproduce significant features of depth-integrated concentration dynamics in this cross-section: These are the twofold concentration maxima during flood and the lagged response of the northern channel. However the prediction of the absolute magnitudes generally tends to be underestimated by both model approaches.

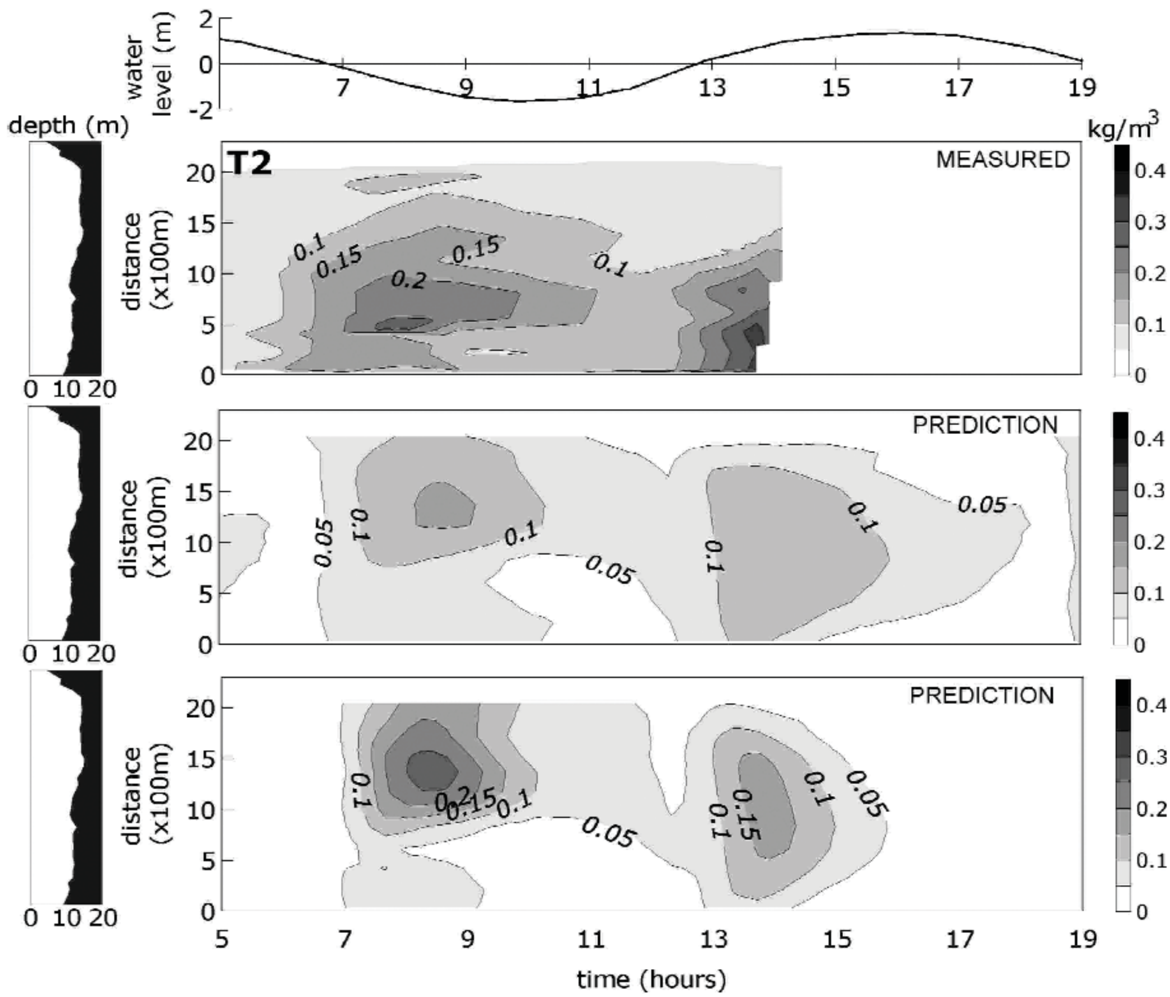

Fig. 11: Measured (upper) vs. computed (BIJKER: middle, VAN RIJN: lower) variation in suspended sediment concentration at cross-section T2 (Suedererpiep) dataset 3 (September 5, 2000)

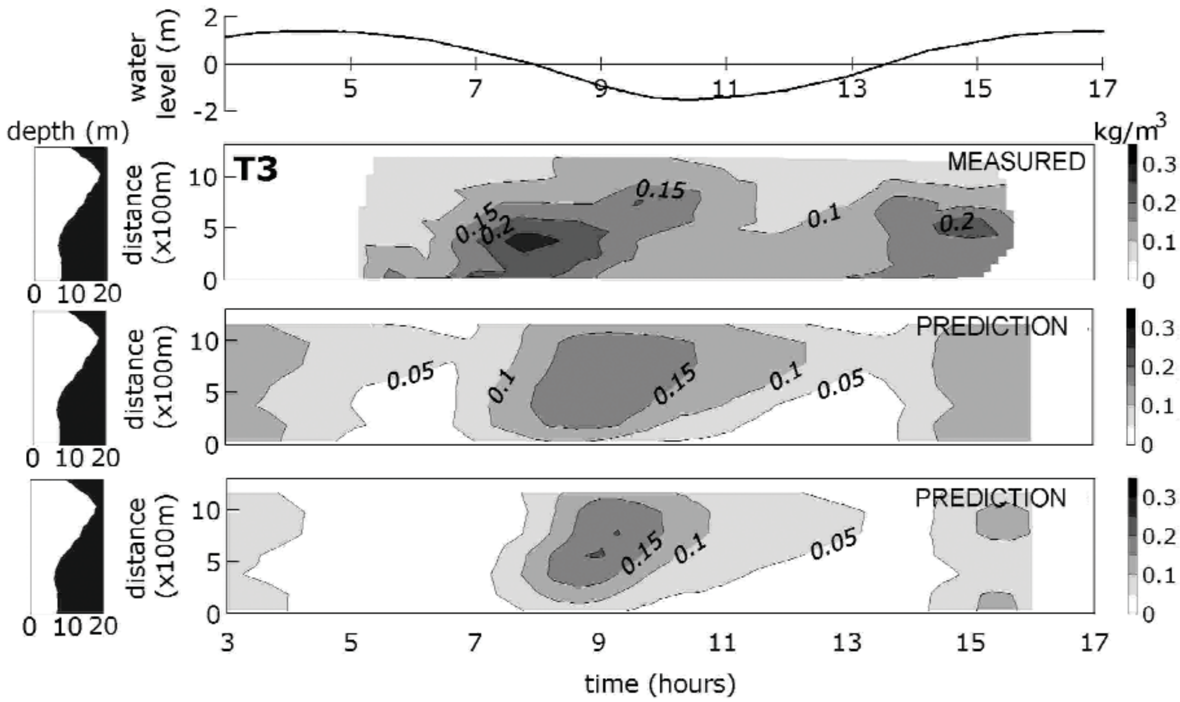

Fig 12: Measured (upper) vs. computed (BIJKER: middle, VAN RIJN: lower) variation in suspended sediment concentration at cross-section T3 (Piep) for dataset 3 (September 5, 2000)

5.2 Validation of cross-sectional transport load

As shown above the calibrated model is able to hindcast prominent characteristics of suspended sediment concentration during a tidal cycle. However considerable disagreement is observed in terms of local concentration magnitudes. In order to further assess the model quality with respect to the overall aim of the research project, being the simulation of morphodynamics, the prediction of total load transport at cross sections is investigated hereafter. By comparison with measured values an evaluation of the models ability to simulate the right amount of material transported over time is possible. The total load transport at a cross-section was integrated over time from the product of current velocity and suspended sediment concentration at all measuring stations. Data sets 1 (spring tide), 4 (mean tide) and 5 (neap tide) are chosen to represent different tidal conditions. The computed values generally are within the order of magnitude of the measured ones. The pattern of total load transport over a tidal cycle and the dependency of the amount of material transported on the tidal range is also captured (Fig. 13).

Acceptable agreement is generally achieved in cross section T1 (Norderpiep) for all tidal cycles. Here the average deviation of the predicted values with respect to those measured in the field is about 0.3 ton/s. About 50 % of data ranges within a factor 2. The model approach using the Bijker formula generally performs slightly better. At cross section T2 (Suederpiep) all simulations underestimate the measured values. Here major disagreement occurs for maximum tidal range; here the corresponding deviation is up to a factor of 4. The average deviation of the predicted values is about 1.5 ton/s. The average percentage of data within a factor of 2 is about 30 %. Simulated cross-sectional transport loads at cross section T3 show again a higher degree of conformity with measured values. The spring tide event is captured with a slight underestimation, whereas the values for the mean and neap tide are overestimated. The average deviation of the predicted values is less than 1 ton/s. The average percentage of data within a factor 2 is of about 35 %.

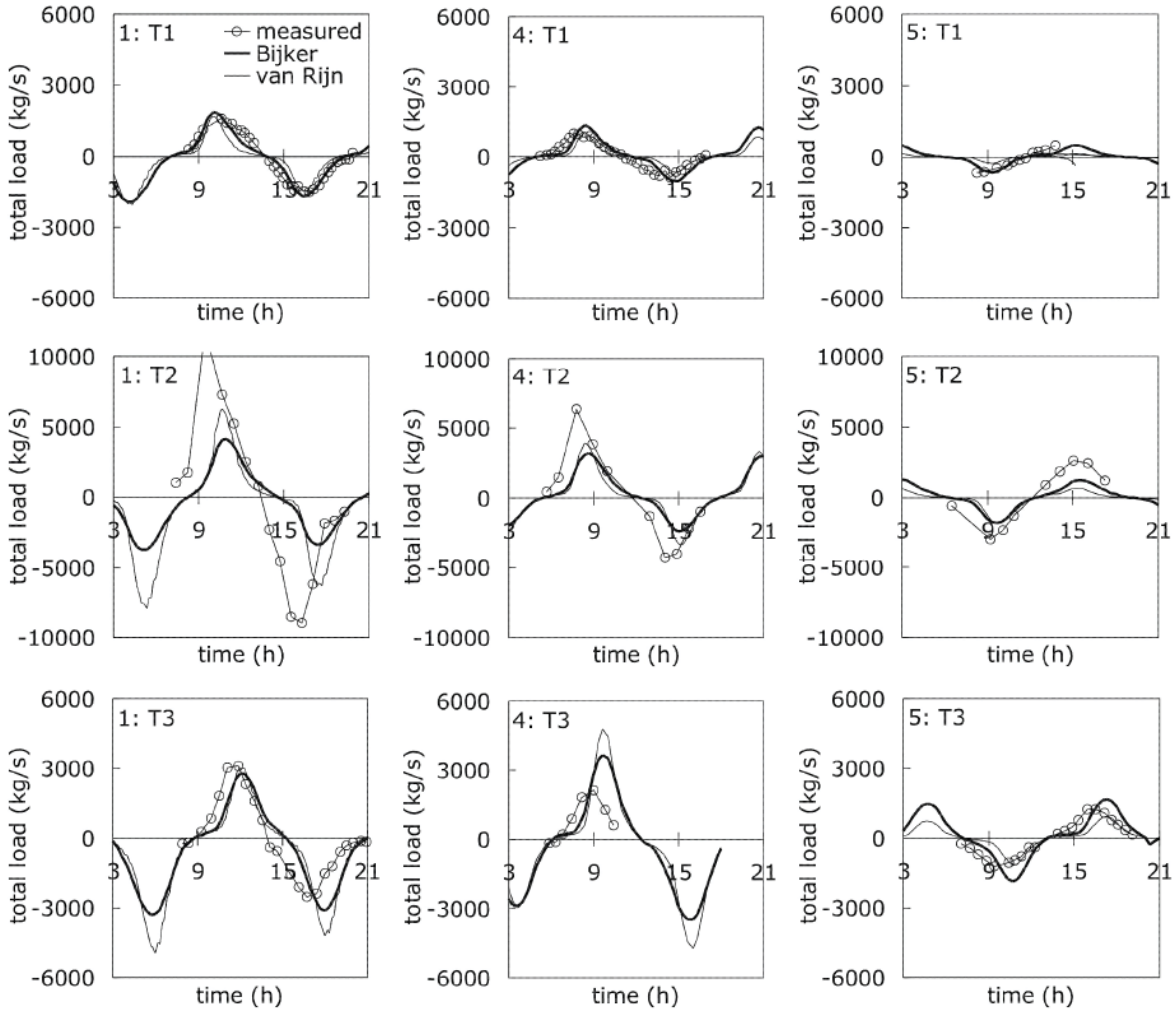

Fig 13: Validation of cross-sectional flux at the three cross-sections T1 (upper), T2 (middle) and T3 (lower row) for tidal cycles of dataset 1 (left), 4 (middle) and 5 (right column)

6. Conclusions

The set-up, calibration and validation of a numerical model for the simulation of sediment transport in the tidal channels of Dithmarschen Bight on the German Wadden Sea are described. In order to capture the complex suspended sediment dynamics the numerical solution of an advection diffusion equation has been applied, where the sink/source term is proportioned to the equilibrium suspended sediment concentration derived from algebraic formulations by BIJKER (1971) and VAN RIJN (1984). Sensitivity studies show the effect of input parameters on the calculated suspended sediment concentrations: The variation of the bed mean particle size within the range of samples from tidal channels resulted in differences in computed sediment concentrations within a factor 2. A clear effect of modified settling velocities from 0.1 mm/s to 4 mm/s was limited to periods around slack water. The empirical coefficients in the algebraic formulations may be considered as linear tuning factors as they proportionally influence the computed suspended sediment concentration. The bottom roughness term profoundly influences the computed suspended transport magnitude and is considered as a calibration parameter within its physical range. Bed roughness values of a few decimetres provide sediment concentrations within the range of the measured values.

It became clear that a pointwise model calibration to single position data could result in a high similarity between simulation and measurements at that specific location. However an over-calibration of models to single positions and periods might involve significant deviations for different conditions. In this case also the quality of underlying hydrodynamics has to be taken into account. As expected the model quality is reduced when uniform and constant parameters are applied throughout the domain. Generally the low background concentration around slack water is under-predicted and the maximum concentrations may be over-estimated by the model. A physical explanation can be given based on the analysis of instationary bed forms and bottom roughness of the domain (MAYERLE et al., 2002). They report that bed form dimensions vary throughout the tidal cycle from a smooth bed after slack water to bed forms of several decimetres after maximum tidal currents. As the numerical model used here applies a constant bottom roughness, it under-predicts the suspended concentrations at slack water and may over-estimate concentrations at times of high current velocities. However, the definition of spatially varying roughness requires rather extensive and costly surveys of the whole domain of interest and does not necessarily lead to better results (SUTHERLAND et al., 2004). Also the implementation of bed roughness predictors into transport models has not led to satisfactory results yet (DAVIES and VILLARET, 2003). It was therefore decided to apply uniform settings that produce best mean results at all measuring stations: A uniform bed roughness of 0.2 m was derived. Further improvement was achieved by the adaption of empirical coefficients in the algebraic formulations. The coefficient in the BIJKER formula, originally set to 5 to account for wave conditions was reduced here to a value of 3. The VAN RIJN formula, initially derived from flume experiments with coarser material (D_{50} > 200 µm) was adapted to the physical setting by increasing the relevant coefficient to a value of 2.

To overcome purely descriptive and qualitative evaluations, the model performance is assessed on the basis of the discrepancy ratio as proposed by recent publications: BAYRAM et al. (2001) give results of transport rates of six formulas at two locations of which 62 % to 84 % of the results are inside a factor of 5. Also CAMENEN and LARROUNDÉ (2003) compare calculated transport rates of five formulas to field data. In current-only situations they range from 60 % to 84 % inside factor 2. In situations with waves and currents only 18 % to 48 % yield this score. DAVIES et al. (2002) evaluated four non-calibrated sand transport models: Suspended sediment concentrations were hindcasted within a factor of 2 in 22 % to 66 % of the measured values, depending on the model formulation used. The model presented here resulted in 75 % of suspended sediment concentration data at all stations within factor 2 if using the Bijker formulation for datasets 1 to 3. This is more accurate than using the Van Rijn formulation, for which 57 % of data are within factor 2 for dataset 1 and 52 % of data are within factor 2 for dataset 2 and 3. Similar accuracy was achieved for the calibration data and independent data-sets used for validation. Thus the derived model set-up ranges well within published model quality. It should be noted that a large part of the deviations from parity is due to the under-prediction of the background concentration. This is of no relevance considering the application to morphodynamic simulations.

Also the Adjusted Relative Mean Absolute Error (ARMAE) of model results has been calculated to allow for future comparative studies. The mean ARMAE value for the twenty stations along the three-cross-sections, assuming 30 % accuracy, resulted to 0.17 kg/m³ for the Bijker formula and 0.28 kg/m³ for the Van Rijn formula.

It has to be pointed out, that all times and all sampling stations have been taken into account without weighting for the calculation of discrepancy ratios and errors: Highest discrepancies appear during slack-water times because of the under-estimation of the background concentration and generally at the channel banks.

In order to further assess the model quality the prediction of total load has been evaluated for different tidal conditions. The models ability to simulate the right amount of material transported over time leads to acceptable agreement in cross section T1 (Norderpiep) for all tidal cycles. The average percentage of data within a factor of 2 is about 50 %. At cross-section T2 (Suederpiep) all simulations underestimate the measured values. The average percentage of data within a factor of 2 is reduced to only about 30 %. Simulated cross-sectional transport loads at cross section T3 again show a higher degree of conformity with measured values. The average percentage of data within a factor of 2 is of about 35 %.

As profiling ship based measurements of hydro- and sediment dynamics are only practical in fair weather conditions, this study had to be restricted to those. It is understood that suspended sediment characteristics differ during higher energy conditions.

However, despite the somewhat basic model set up in terms of two-dimensional, depth averaged formulations and uniform and constant grain size and bottom roughness distributions, the model proved to be able to reproduce the main characteristics of suspended sediment transport across tidal channels of the Dithmarschen Bight using both BIJKER and VAN RIJN approaches.

7. Acknowledgements

The research project was funded by the German Federal Ministry of Education and Research (BMBF). The authors would also like to thank the following authorities for their support: Water level data could be obtained by the German Office for Rural Areas (ALR-Husum). Bathymetric data was provided by the Federal Maritime and Hydrographic Agency of Germany (BSH). A numerical model of the German Bight was obtained from the Coastal Research Station of the Lower Saxony State Agency for Ecology in Norderney. We appreciate the cooperation with all our colleagues within the project PROMORPH (funding number 03 F 0262 A): The staff of the Research and Technology Center, Westcoast in Büsum (Kiel University), the Institute for Fluid Dynamics and the Institute for Meteorology (Hannover University) and GKSS Research Center in Geesthacht. The constructive comments from Dr.-Ing. V. Barthel and an anonymous reviewer are gratefully acknowledged.

8. References

BAYRAM, A.; LARSON, M.; MILLER, H. C. and KRAUS, N. C.: Cross-shore Distribution of Longshore Sediment Transport: Comparison Between Predictive Formulae and Field Measurements. Coastal Engineering, 44, 79–99, 2001.

BIJKER, E. W.: Longshore Transport Computations: Journal of the Waterways, Harbours and Coastal and Engineering Division, 97, 687–701, 1971.

CAMENEN, B. and LARROUDE, P.: Comparison of Sediment Transport Formulae for the Coastal Environment.: Coastal Engineering, 48, 111–132, 2003.

DAMGAARD, J. V. R., L. C.; HALL, L. J.; SOULSBY, R. L.; L. C. D.; VAN RIJN, A. G.; VAN DE GRAAFF, J. and RIBBERINK, J. S.: Intercomparison Of Engineering Methods For Sand Transport. SEDMOC – Sediment transport modelling in marine coastal environments, Aqua Publications, Amsterdam, CJ1–CJ12, 2001.

DAVIES, A. G.; VAN RIJN, L. C.; DAMGAARD, J. S.; VAN DE GRAAFF, J. and RIBBERINK, J. S.: Intercomparison of Research and Practical Sand Transport models. Coastal Engineering, 46, 1–23, 2002.

DAVIES, A. G. and VILLARET, C.: Sediment Transport Modelling for Coastal Morphodynamics. Coastal Sediments '03 (Clearwater, Florida), 2003.

EINSTEIN, H. A.: The Bed-load Function for Sediment Transport in Open Channel Flow, U.S. Department of Agriculture, Washington, D.C., 1950.

FRIJLINK, H. C.: Discussion des Formules de Debit Solide de Kalinske, Einstein et Meyer – Peter et Mueller Compte Tenue des Mesures Recentes de Transport dans les Rivieres Nederlandaises. 2me Journal Hydraulique Societe Hydraulique de France, Grenoble, 1952.

GALAPPATTI, G. and VREUGDENHIL, C. B.: A Depth Integrated Model for Suspended Sediment Transport. Journal of Hydraulic Research, vol. 29, no. 6, 727–739, 23, 1985.

MAYERLE, R.; RAZAKAFONIAINA, T. and PRAMONO, G.: Bed Forms and Equivalent Roughness Sizes in Tidal Channels. River Flow 2002, IAHR, Louvain-la-Neuve, Belgium, 2002.

MAYERLE, R.; WILKENS, J.; ESCOBAR, C. and WINDUPRANATA, W.: Hydrodynamic Forcing Along Open Sea Boundaries of Small-Scale Coastal Models, Die Küste, Heft, 69, 2005.

NICHOLSON, J.; BROKER, I.; ROELVINK, J. A.; PRICE, D.; TANGUY, J. M. and MORENO, L.: Intercomparison of Coastal Area Morphodynamic Models. Coastal Engineering, 31, 97–123, 1997.

PALACIO, C.: Metodologia para la Validacion de Modelos Hidrodinamicos Utilizando Amplia Informacion de Campo: Aplicacion a la Bahıa Meldorf en la costa del Mar del Norte Aleman, Ph.D. thesis, National University of Colombia, Medellin, In Spanish., 2002.

PALACIO, C.; WINTER, C. and MAYERLE, R.: Set-up of a Hydrodynamic Model for the Meldorf Bight, Proceedings of the World Water and Environmental Resources Congress, 2001.

PALACIO, C.; MAYERLE, R.; TORO, M. and JIMENEZ, N.: Modelling of Flow in a Tidal Flat Area in the South-Eastern German Bight, Die Küste, Heft 69, 2005.

POERBANDONO: Sediment Transport Measurements and Modelling in the Meldorf Bight Tidal Channels, German North Sea Coast. Coastal Research Laboratory, Kiel University, 2003.

POERBANDONO; WINTER, C. and MAYERLE, R.: Field Measurements of Sediment Transport Dynamics in Tidal Channels: Preliminary Results. Coastal Sediments '03 (Clearwater, Florida), 2003.

POERBANDONO and MAYERLE, R.: Composition and Dynamics of Sediments in Tidal Channels of the German North Sea Coast, Die Küste, Heft 69, 2005.

ROELVINK, J. A. and VAN BANNING, G. K. F. M.: Design and Development of DELFT3D and Application to Coastal Morphodynamics. Hydroinformatics '94 (Verwey), Balkema, Rotterdam, 1994.

RIZZO, R.: Open Boundary Conditions for Sediment Transport in Near Coastal Areas. Coastal Research Laboratory, Kiel University, 2003.

ROELVINK, J. A. and VAN BANNING, G. K. F. M.: Design and Development of DELFT3D and Application to Coastal Morphodynamics. Hydroinformatics '94, Verwey, Minns, Babovic & Maksimovic (eds); 1994 Balkema, Rotterdam, 451–456, 1994.

SUTHERLAND, J.; WALSTRA, D. J. R.; CHESHER, T. J.; VAN RIJN, L. C. and SOUTHGATE, H. N.: Evaluation of Coastal Area Modelling Systems at an Estuary Mouth. Coastal Engineering, 51, 119–142, 2004.

TORO, F.; MAYERLE, R.; POERBANDONO and WILKENS, J.: Patterns of Hydrodynamics in a Tide-Dominated Coastal Area in the South-Eastern German Bight, Die Küste, Heft, 69, 2005.

VAN RIJN, L. C.: Sediment Transport, Part I: Bed Load Transport, and Part II: Suspended Load Transport. Journal Hydraulic Engineering, 1431–1641, 1984.

VAN RIJN, L. C. W.; D. J. R.; GRASMEIJER, B.; SUTHERLAND, J.; PAN, S. SIERRA, J. P.; L. C.; VAN RIJN, B. G. RUESSINK and MULDER, J. P.: Simulation of Nearshore Hydrodynamics and Morphodynamics on the Time Scale of Storms and Seasons using Process-based Profile Models. COAST3d-EGMOND, The behaviour of a straight sandy coast on the time scale of stoms and seasons. End Document, Aqua Publications, Amsterdam, S1–S33, 2002.

VERBOOM, G. K.; DE RONDE, J. G. and VAN DIJK, R. P.: A Fine Grid Tidal Flow and Storm Surge Model of the North Sea, Continental Shelf Research, 12, 213–233, 1992.

WINTER, C.: Validation of the CSM-GBM Nesting, Determination of Open Sea Boundary Conditions for Small Scale Coastal Models, Coastal Research Laboratory, University of Kiel, Germany, Report no. 04-03. 2003.

WINTER, C. and MAYERLE, R.: Calibration and Validation of a Sediment Transport Model with Extensive Data-sets for a Tidal Channel System in the German Wadden Sea, Proceedings of Coastal Sediments, Clearwater Beach, 2003.

WL|DELFT HYDRAULICS: Deutsche Bucht and Dithmarschen Bucht: Set-Up and Calibration of Tidal Flow Models, Report H1821, 1997.

ZIELKE, W.; GROSS, G.; HOYME, H.; MAYERLE, R.; RICKLEFS, K.; WINTER, C.; EPPEL, D. and WITTE, G.: Predictions of Medium-Scale Morphodynamics – PROMORPH – In: Proceedings of the 27th Conference on Coastal Engineering, Sydney, 2000.

Modelling of Medium-Scale Morphodynamics in a Tidal Flat Area in the South-Eastern German Bight

By Ingo Junge, Jort Wilkens, Helge Hoyme and Roberto Mayerle

Summary

On the basis of extensively calibrated and validated models for the simulation of tides, waves and sediment transport morphodynamic models have been developed, employing two existing modelling systems. For both systems, approaches are defined for input and process filtering, for the purpose of medium scale morphodynamic simulations, i.e. a temporal scale up to a decade combined with a spatial scale in the order of several kilometres. At this scale, the present investigation focuses on morphological features such as sand banks, tidal flats and channels. The models were calibrated and validated on the basis of sedimentation and erosion patterns as well as on a volumetric analysis for several sub-domains in the central Dithmarschen Bight. The volumetric analysis yielded objective and quantitative comparisons between computed and observed morphological changes. It was concluded that the models produce good results and are able to correctly reproduce the significant morphodynamic trends. After calibration and validation these models were applied to predict morphological changes in the study area between 1999 until 2009. A number of significant changes were computed, related mainly to a predicted splitting of the tidal flat Tertiussand between the two major tidal channels Norderpiep and Suederpiep.

Zusammenfassung

Die mesoskalige Simulation von morphodynamischen Entwicklungen im Küstenvorfeld wird durch den Aufbau und die Anwendung zweier Modellsysteme vorgestellt. Mesoskalig kennzeichnet hier Zeiträume von einem Jahrzehnt und eine räumliche Ausdehnung von mehreren Kilometern. Die morphologisch relevanten Prozesse wie Tideströmung, Seegang und Sedimenttransport werden durch unabhängige Einzelmodelle erfasst und separat kalibriert und validiert. Die Kopplung dieser Prozesse führt zu rechenintensiven Gesamtmodellen, so dass Methoden zur Prozessfilterung und zur Reduzierung von Eingabedaten erforderlich sind. Das Untersuchungsgebiet umfasst das Pieprinnensystem der Dithmarscher Bucht an der schleswig-holsteinischen Nordseeküste. Für die Kalibrierung und Validierung der Gesamtmodelle werden Erosions- und Depositionsmuster analysiert und Volumenbilanzen für einzelne Wattflächen und Rinnenabschnitte ausgewertet. Ein Vergleich mit Messungen zeigt, dass die Modelle die morphologischen Änderungen und Trends qualitativ wie auch quantitativ gut reproduzieren. Abschließend werden die Modelle für eine morphologische Prognoserechnung für den Zeitraum 1999 bis 2009 eingesetzt. Das Ergebnis zeigt einige deutliche Bathymetrieänderungen, wie zum Beispiel die Zerteilung der Wattfläche Tertiussand zwischen Norder- und Süderpiep.

Keywords

Morphodynamic Modelling, Morphology, Dithmarschen Bight, Promorph, Calibration, Validation, Medium Scale, DELFT3D, TELEMAC

Contents

1. Introduction

The major objective of this investigation is to set-up, optimise and apply several process-based numerical models to investigate and predict medium scale morphodynamic behaviour in the central Dithmarschen Bight, situated in the south eastern part of the North Sea. Medium scale morphodynamics are defined here as changes occurring on the spatial scale of tidal channels, tidal flats and sand banks. The corresponding time scale is in the order of several years. The existing morphodynamic models include the calibrated and validated individual process models for the same area, as described in PALACIO et al. (in this volume), WILKENS et al. (in this volume), and WINTER et al. (in this volume) for tidal flow, coupled flow and waves, and coupled flow, waves and sediment transport, respectively. The good results obtained from an evaluation of the individual models form a sound basis for the overall morphodynamic models and increase their reliability for analysing the significance of designated processes and conditions governing the morphodynamic behaviour of the study area.

The model is driven by means of a limited number of imposed conditions determined with the aid of input reduction methods for tidal, swell and wind conditions. Tidal conditions were obtained from a model-nesting sequence whereas swell and wind conditions were defined on the basis of long-term data sets derived from measurements at nearby locations.

The morphodynamic models were optimised and evaluated on the basis of bathymetric data covering the period 1977 to 1999. Calibration and validation of the models were carried out for the periods 1977 to 1987 and 1990 to 1999, respectively. Evaluation of the models is based on a volumetric analysis of selected tidal channel sections and a tidal flat.

The measured data used in the investigation are described in Section 2. The applied morphodynamic modelling systems and the set-up models are presented in Section 3. The input reduction methods are discussed in Section 4, followed by a description of the calibration and validation procedures in Section 5. The results of a 10-year model prediction study are presented in Section 6, followed by the conclusions in Section 7.

2. Measurement Data

Bathymetric data for the central Dithmarschen Bight (Fig. 1) were available from two sources. The Federal Maritime and Hydrographic Agency (BSH) in Hamburg provided data from yearly bathymetric surveys. These surveys cover the tidal channels and lower tidal flats in the study area. A combination of approximately three years of data yielded full coverage of the deeper areas. A bathymetric data set with full area coverage based on data collected around 1990 was provided by the Office of Rural Development (ALR) in Husum. This data set also covers the higher tidal flats and was therefore very useful for supplementing the data provided by the BSH. Since no other sets of bathymetric data are available for the shallow areas, these were also used to generate model bathymetries for years other than 1990.

Additional data required in the investigation were long-term swell and wind data. Since long-term swell data were not available for the study area, wave statistics from observations near Sylt were used to provide a data base (BMFT, 1994). The fact that this location is somewhat more exposed to the open sea means that the measured wave climate is likely to be more severe than in the study area. These wave statistics, however, provide an insight into

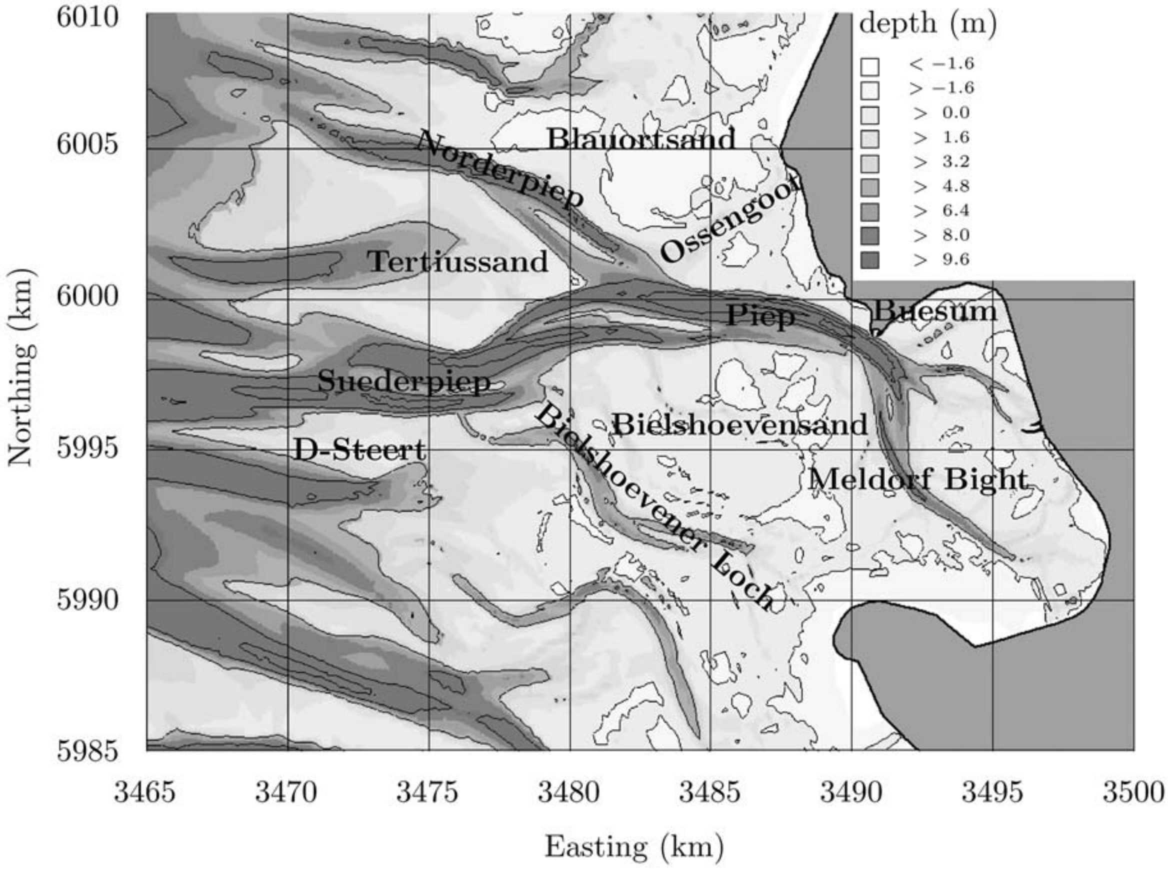

Fig. 1: The study area of the central Dithmarschen Bight (WILKENS, 2004)

the approximate wave conditions in the Dithmarschen Bight. The wind data applied in the investigation were provided by the PRISMA interpolation model, a synoptic meteorological model with a 42 km resolution (LUTHARDT, 1987). The results from this model were used in preference to data from measurement stations since they give a spatially consistent overview of dominant wind conditions. The wind data were verified on the basis of observations made at the measurement station of the Research and Technology Centre Westcoast in Buesum (FTZ). This verification showed good agreement between wind speed as well as wind direction (WILKENS, 2004).

3. Description of the Applied Morphodynamic Models

Two modelling systems were applied within the scope of this study; the DELFT3D package, developed by Delft Hydraulics in the Netherlands (ROELVINK and VAN BANNING, 1994) and the TELEMAC modelling system, developed by the Laboratoire National d'Hydraulique of the Electricité de France (HERVOUET, 2000; GALAND et al., 1991).

The DELFT3D model is based on a curvilinear grid that covers the entire Dithmarschen Bight including the Elbe and Eider estuaries. The TELEMAC model covers the centre of the Dithmarschen Bight with a higher resolution. The computational grids and bathymetries of these models are shown in Figs. 2 and 3. The DELFT3D model incorporates the SWAN wave model (BOOIJ et al., 1999; RIS et al., 1999) whereas the TELEMAC model implements the TOMAWAC wave model. The depth-integrated approach is adopted in both hydrodynamic models.

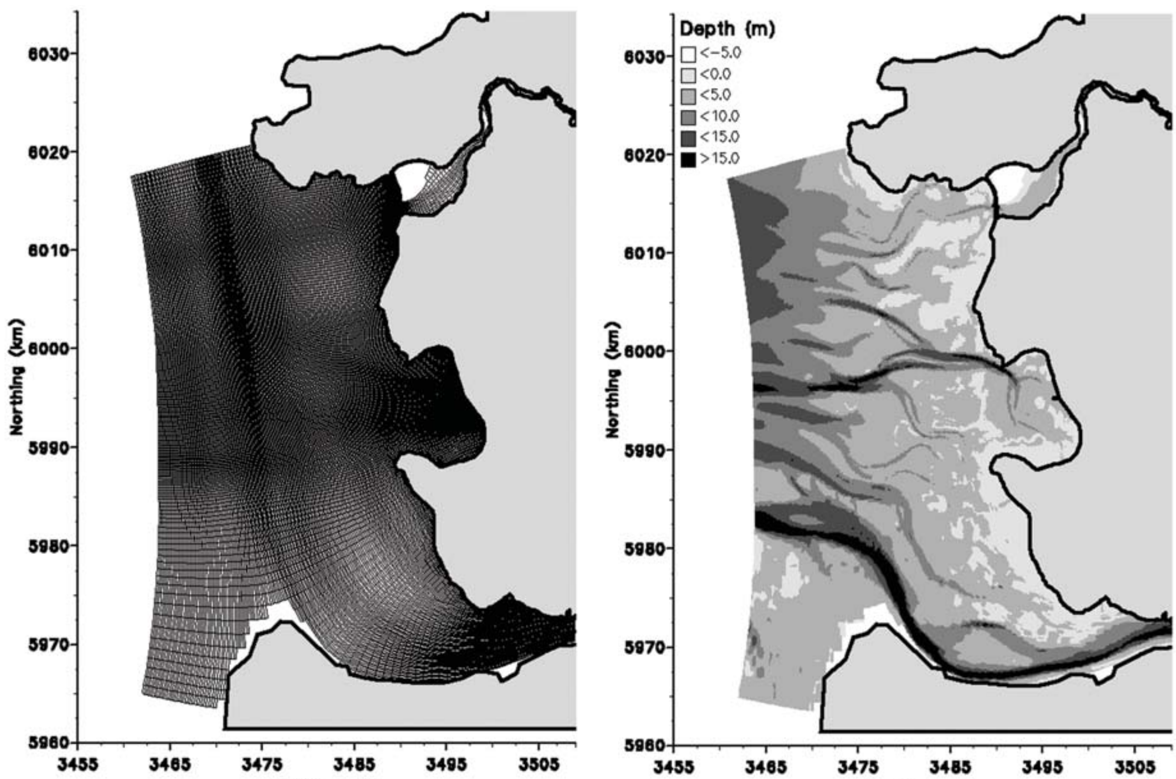

Fig. 2: Model grid and bathymetry of the DELFT3D morphodynamic model (WILKENS, 2004)

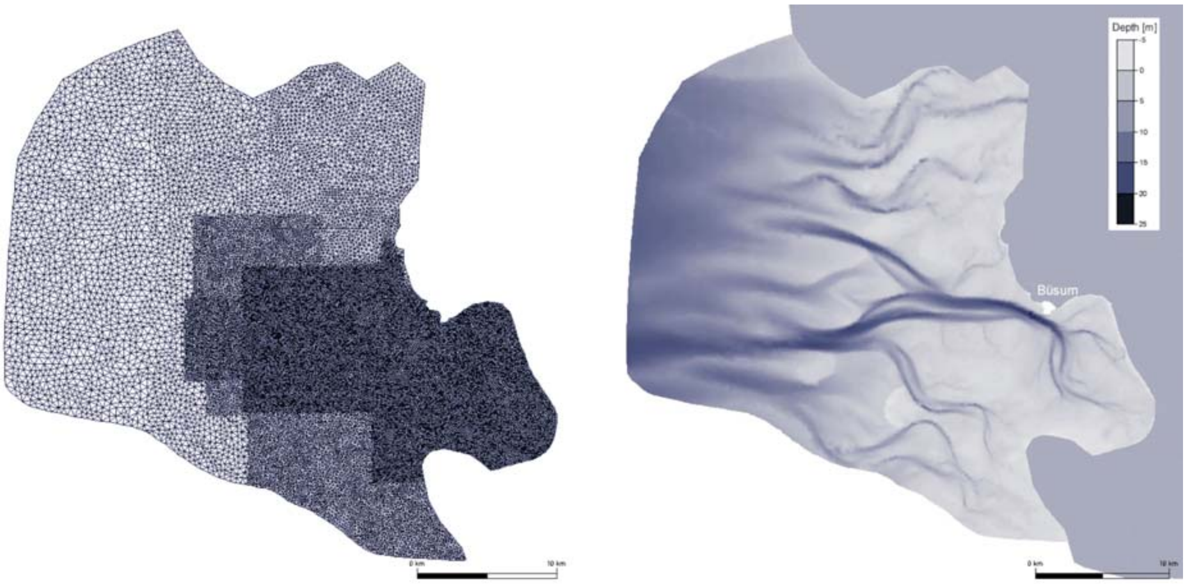

Fig. 3: Model grid and bathymetry of the TELEMAC morphodynamic model

An overview of the general model characteristics is given in Table 1.

Table 1: General settings of the applied morphodynamic models

Model	**DELFT3D**	**TELEMAC**
Grid type	Finite difference, curvilinear	Finite elements
element size	80 – 600 m	30 – 80 m
Flow model	DELFT3D-FLOW	TELEMAC2D
model type	2Dh	2Dh
Wave model	SWAN	TOMAWAC
model type	Stationary	Instationary
Sediment transport model	DELFT3D-TRSSUS	SISYPHE
transport formula	BIJKER, 1971	BIJKER, 1971/ENGELUND-HANSEN, 1967
Morphodynamic model	DELFT3D-MOR	TELEMAC

The DELFT3D and TELEMAC models are constructed from calibrated and validated individual process models. Details about these models may be found in PALACIO et al. (in this volume), WILKENS et al. (in this volume) and WINTER et al. (in this volume) for tidal flow, coupled flow and waves, and coupled flow, waves and sediment transport, respectively. The fact that the calibration and validation of these underlying models yielded good results implies that the individual processes are correctly modelled in both qualitative and quantitative terms. This guarantees the reliability of the models for predicting morphological evolution in the study area.

In stationary wave models, the assumption is made that the imposed conditions with respect to local wind as well as to the imposed swell along the open boundaries are relatively constant for the period of time needed for waves to travel through the model domain. Since the imposed conditions are strongly reduced through statistical methods, a stationary approach is generally acceptable for medium scale morphodynamic modelling.

The sediment transport formula by BIJKER (1971) is defined as:

$$S_{tot} = S_{bed} + S_{susp}$$

$$S_{bed} = bD_{50}\frac{u}{C}\sqrt{g}\,(1-p)\exp\left(\frac{-0.27(s-1)D_{50}\rho g}{\mu\tau_{b,wc}}\right)$$

$$S_{susp} = 1.83 S_{bed}\left(I_1 \ln\left(\frac{33.0h}{r_c}\right) + I_2\right)$$

With:

S_{tot}	Total load transport
S_{bed}	Bed load transport
S_{susp}	Suspended load transport
b	Empirical constant
D_{50}	Median grain size
u	Current velocity
C	Chézy coefficient
g	Gravity constant
p	Porosity
s	Relative sediment density
μ	Ripple factor
$\tau_{b,cw}$	Shear stress at the bed due to currents and waves
I_1,I_2	Einstein integrals (EINSTEIN, 1950)
h	Water depth
r_c	Bottom roughness

The transport formula by ENGELUND and HANSEN (1967) reads:

$$q_b = 0.05\left(\frac{1}{1-p}\right)\sqrt{(s-1)\frac{d_{50}^3}{g}C^2 T_2^{5/2}}$$

With:

q_b	Sediment transport
p	Porosity
s	Relative sediment density
d_{50}	Median grain size
G	Gravity constant
C	Chézy coefficient
T_2	Transport capacity, related to current related shear stress

4. Computation Reduction Methods

The hydrodynamic components (flow and wave models) of morphodynamic models are by far the most expensive in terms of computational costs. Two methods are generally applied to reduce computation time without a significant loss in accuracy. The first method concerns the modelling scheme of the morphodynamic simulations. The second method concerns the number of hydrodynamic conditions that are modelled within a morphodynamic simulation.

Due to the differing characteristics of the DELFT3D and TELEMAC modelling systems, these approaches are applied in different manners for each system. These approaches are discussed separately in the following.

4.1 DELFT3D Modelling Scheme

The DELFT3D model consists of separate modules for currents, waves, bed load and suspended load sediment transport, and bottom evolution. These are coupled as shown in Fig. 4. The hydrodynamic computation over a double tidal cycle is followed by a calculation of sediment transport. Morphological updating is carried out on the basis of the average sediment transport over the second tidal cycle. This approach eliminates possible initialisation effects. The update is performed over a dynamic time step determined by the magnitude of the computed sediment transport and the grid size, taking into account the Courant number limitation for explicit numerical schemes. The old bathymetry is then replaced by the newly-computed bathymetry at the beginning of the loop, and the computations are repeated until the end of the defined simulation period has been reached.

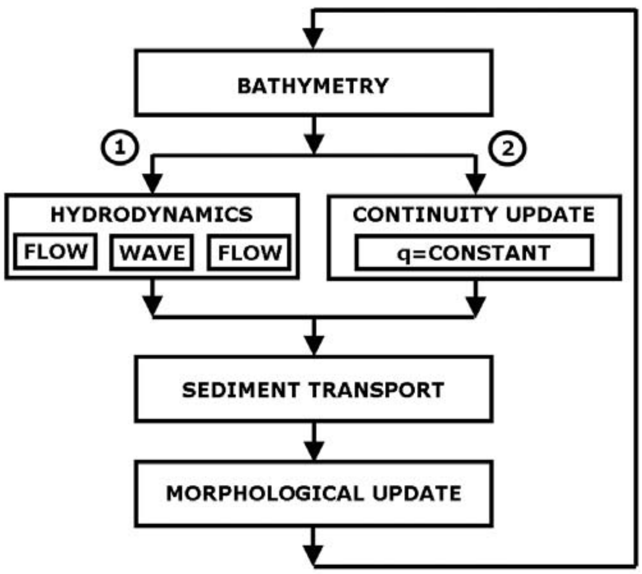

Fig. 4: Morphodynamic model scheme of the DELFT3D Dithmarschen Bight model

Generally speaking, small morphological changes do not significantly influence horizontal flow patterns. Considering this fact, a continuity update may be carried out instead of a full hydrodynamic computation (indicated by ①). In this continuity update, indicated by ②, the discharge at a location is assumed to be constant and the velocity is corrected for the changed water depth. After a number of such updates a new hydrodynamic computation is necessary, as the underlying assumption of constant horizontal flow patterns no longer holds. For the underlying model a maximum of five continuity updates was found to be the optimum on the basis of a sensitivity analysis. This approach greatly reduces the required computation time without a significant loss of accuracy in the morphodynamic results.

4.2 DELFT3D Input Reduction

In order to limit the computational requirements of the medium scale morphodynamic simulations, input reduction was applied for the tidal, swell and local wind boundary conditions. A single representative tidal cycle was defined under consideration of the approaches by STEIJN (1992) and LATTEUX (1995). The computed sediment transport values at a number of locations in the study area were averaged over a full spring-neap tidal cycle. These average transport values were compared to the average transport values over each single tidal cycle. Subsequently, the tidal cycle with average transport values closest to those of the entire spring-neap tidal cycle for the majority of the locations was defined as being representative.

A number of representative conditions were defined for swell and local wind behaviour. These conditions were deduced from long-term measurements. On the basis of a statistical reduction the observed conditions were grouped into a limited number of representative conditions with corresponding probabilities, which together make up the representative swell and wind climates. These representative climates form the starting point for a sensitivity analysis in which the morphological response of the model over a 10-year period is investigated. The climates were optimised to yield an overall response in agreement with the observed morphological changes.

Each year of the morphodynamic simulation is subdivided into a number of sub-simulations with varying representative conditions for swell and local wind behaviour. This is shown schematically in Fig. 5. The length of these sub-simulations corresponds to the probabilities of the imposed conditions. These swell and local wind conditions are combined with a representative tidal cycle. A definition of the representative conditions is described in the following sub-section. In applying this technique the same conditions are repeated for consecutive years. Although a sensitivity analysis showed a limited effect on the computed results of the order of the imposed conditions, the conditions were mixed with regard to their severity, i.e. wind speed, wave height and wave period.

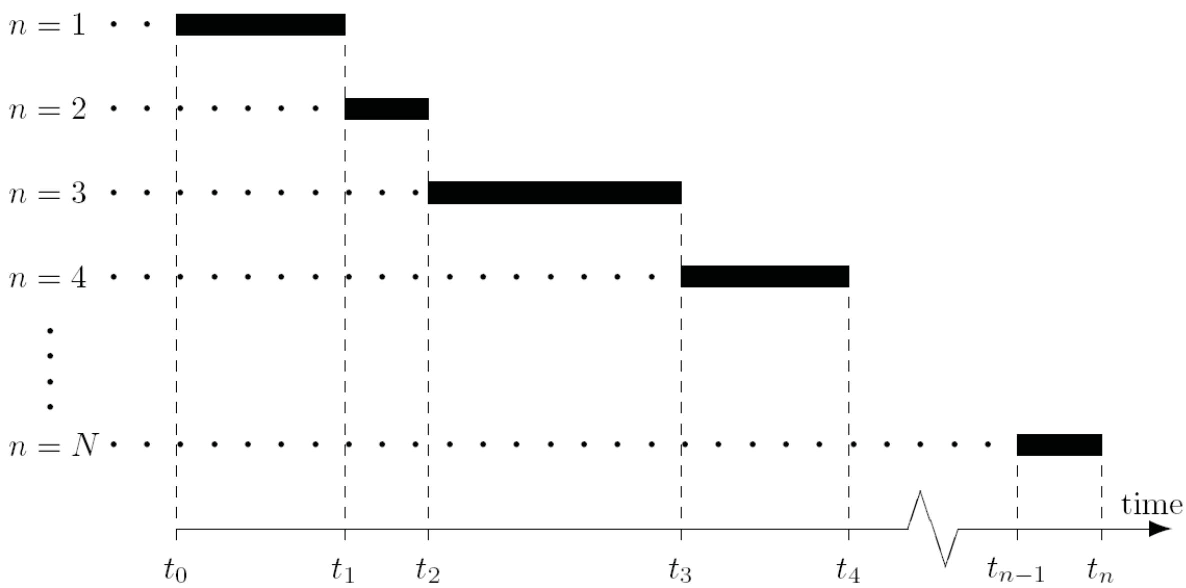

Fig. 5: Scheme for dividing the simulation into N sub-simulations with varying conditions and simulation periods. For each sub-simulation n the scheme of Fig. 4 is implemented (WILKENS, 2004)

4.2.1 Representative Tidal Conditions

A total of 31 locations (17 in the tidal channels and 14 on the tidal flats) were defined as representative for deducing the morphologically representative tide (see also WILKENS, 2004). These locations are shown in Fig. 6. A simulation with the coupled flow-sediment transport model was performed over a full tidal cycle. Both models were thoroughly calibrated and validated as described in PALACIO et al. (in this volume) and WINTER et al. (in this volume). The computed sediment transport values in both horizontal directions were averaged over the simulation period for each of these locations. These average transport values were to be reproduced as accurately as possible by the single representative tide. In order to determine this optimum tide the computed sediment transport values were temporally averaged for each tidal cycle within the simulation period. Factors $\lambda_{x,i}$ and $\lambda_{y,i}$ define the quality of representation and were determined for tide i in the x and y directions, respectively, as being the ratio of the tide average to the spring-neap average. A value of $\lambda = 1$ thus indicates a perfect match.

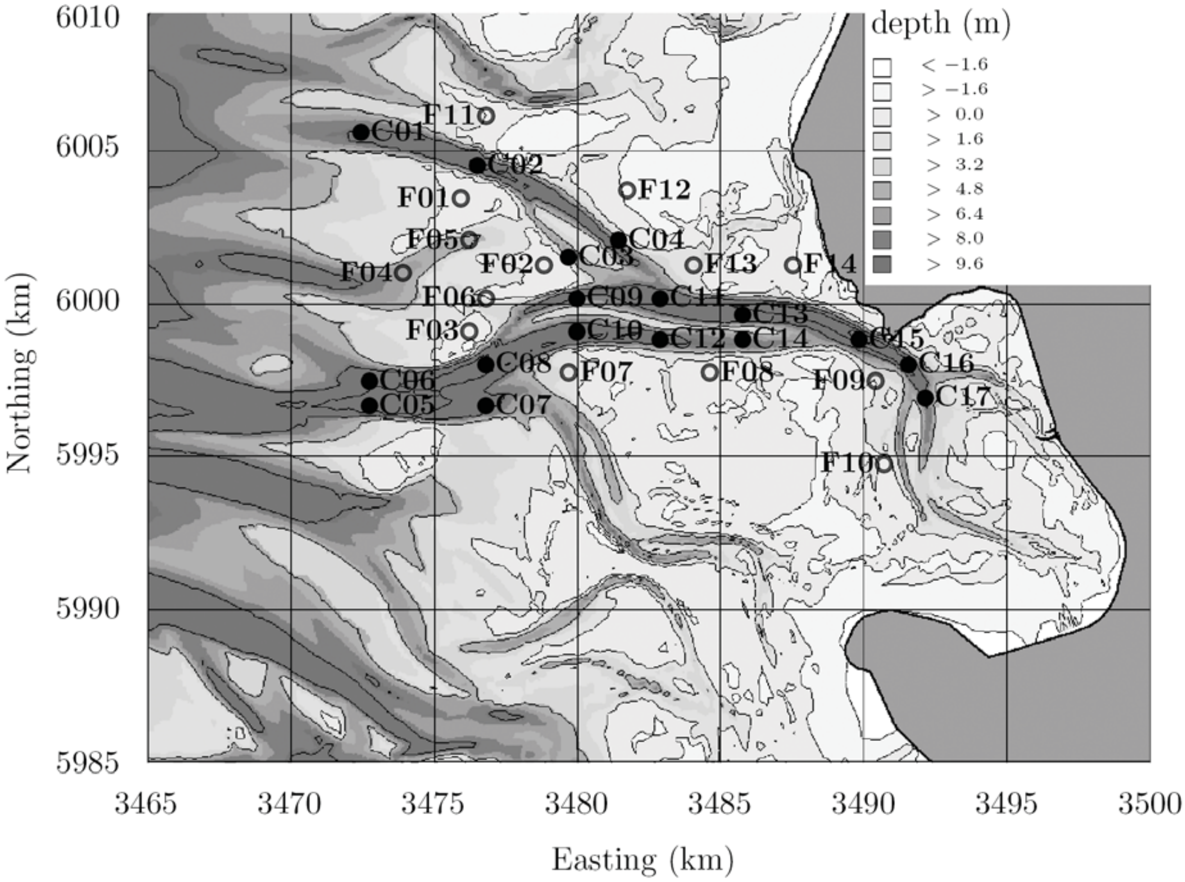

Fig. 6: Location of the defined points in the channels (dots) and on the tidal flats (circles) for the selection of the representative tidal cycle (WILKENS, 2004)

An evaluation of this procedure showed that a tidal cycle with an average tidal range of about 3.5 m yields the optimum representation for the area under consideration. The minimum and maximum values of λ were found to be 0.7 and 1.3, respectively, with values ranging between 0.95 and 1.05 for about 80 percent of the selected locations. It is thus concluded that representation of the considered spring-neap tidal cycle by an average tide is justified.

Compared to the results of the previously-mentioned studies by STEIJN and LATTEUX, the tidal range of this representative tide is found to be lower. The authors suggest representative tidal cycles with a tidal range of 10 percent higher, respectively 7 to 20 percent higher than the average tidal range. These differences may well be related to differing characteristics of the coastal areas investigated, such as the dominant acting forces and sediment characteristics.

Comparisons of the computed morphological effects over a one-month period were made in order to assess the applicability of the defined representative tide (WILKENS, 2004). In the first case, only tidal forcing was considered in the computations. In the second case tidal forcing was combined with representative wind and swell climates; definitions of the latter are given in the following sub-sections. For both cases a simulation was performed for both the full spring-neap tidal cycle and the representative tide. The resulting deposition and erosion patterns are shown in Figs. 7 and 8. It should be noted that the results were obtained from the validated morphodynamic model.

These results indicate that the computed morphological changes for the full spring-neap tidal cycle and the representative tide are very similar. It is thus concluded that the selected representative tide is acceptable for correctly simulating medium scale morphodynamics.

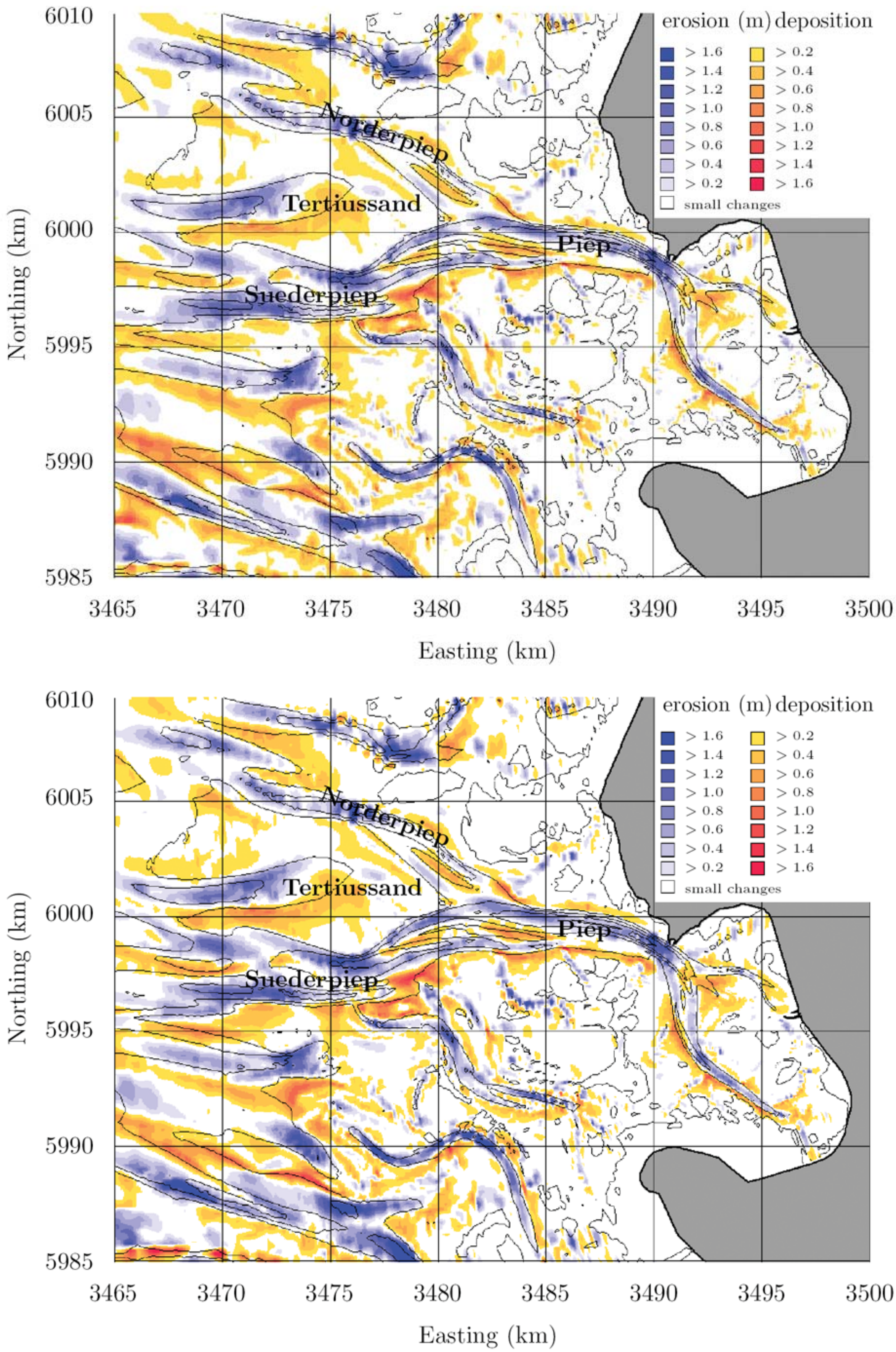

Fig. 7: Computed deposition and erosion over a one-year period using a representative tide (upper) and full spring-neap tidal cycle (lower). Simulations without wind and swell (WILKENS, 2004)

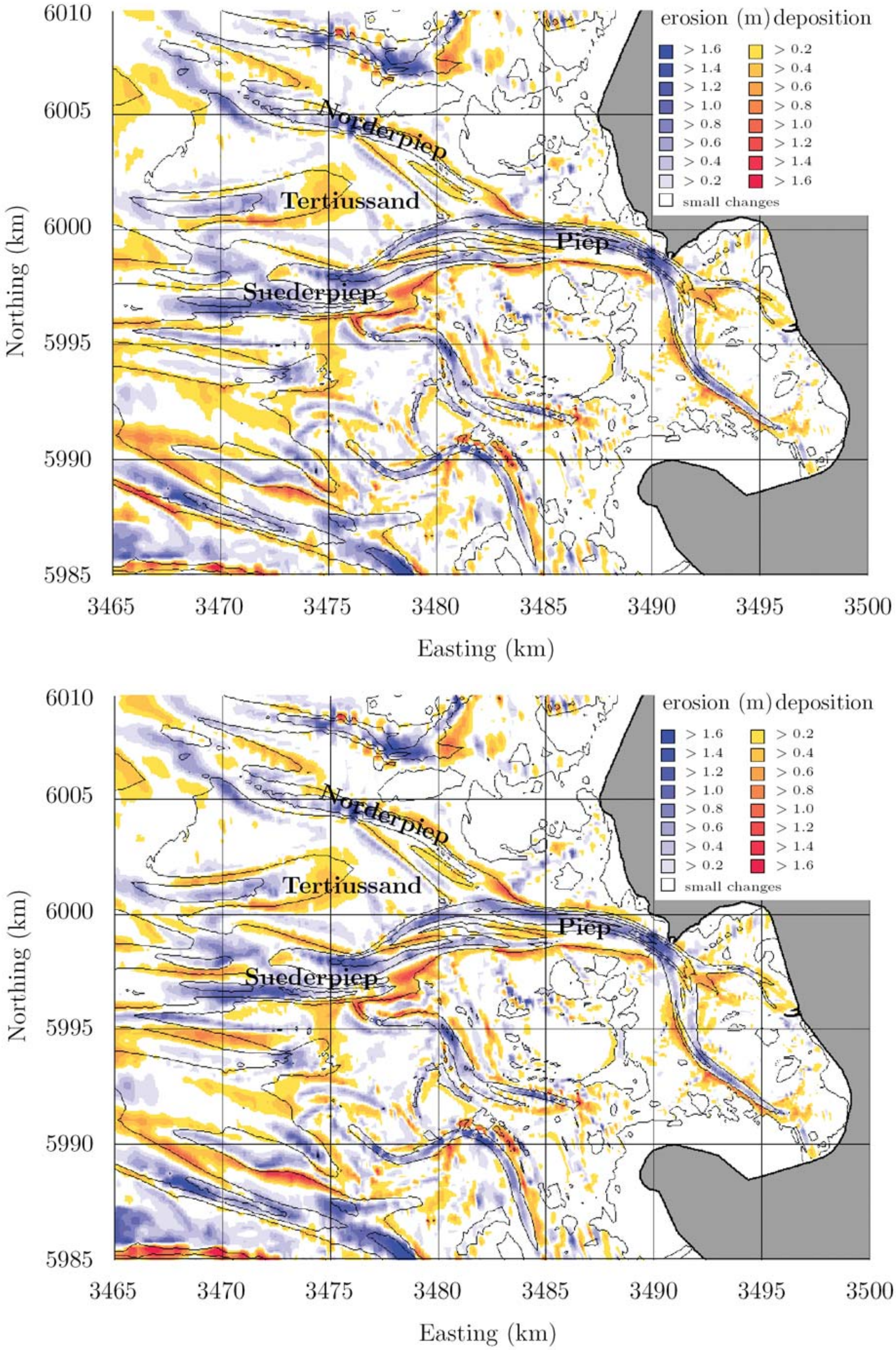

Fig. 8: Computed deposition and erosion over one year using a representative tide (upper) and a full spring-neap cycle (lower). Simulations include representative wind and swell climates (WILKENS, 2004)

4.2.2 Representative Swell Conditions

A limited number of representative swell conditions were determined. The swell data used in the analysis are based on long-term wave climate statistics derived from a study carried out in the coastal zone of the Island of Sylt (BMFT, 1994). Statistical values include the probability of occurrence of wave heights for wave height intervals of 0.25 m and directional sectors of 30 degrees, combined with related wave periods. Although these observations were made some distance from the Dithmarschen Bight and in an area somewhat more exposed to incoming swell from the North Sea, they provide a good measure of swell and its characteristics along the western boundary of the model and are shown in the form of a wave rose in Fig. 9.

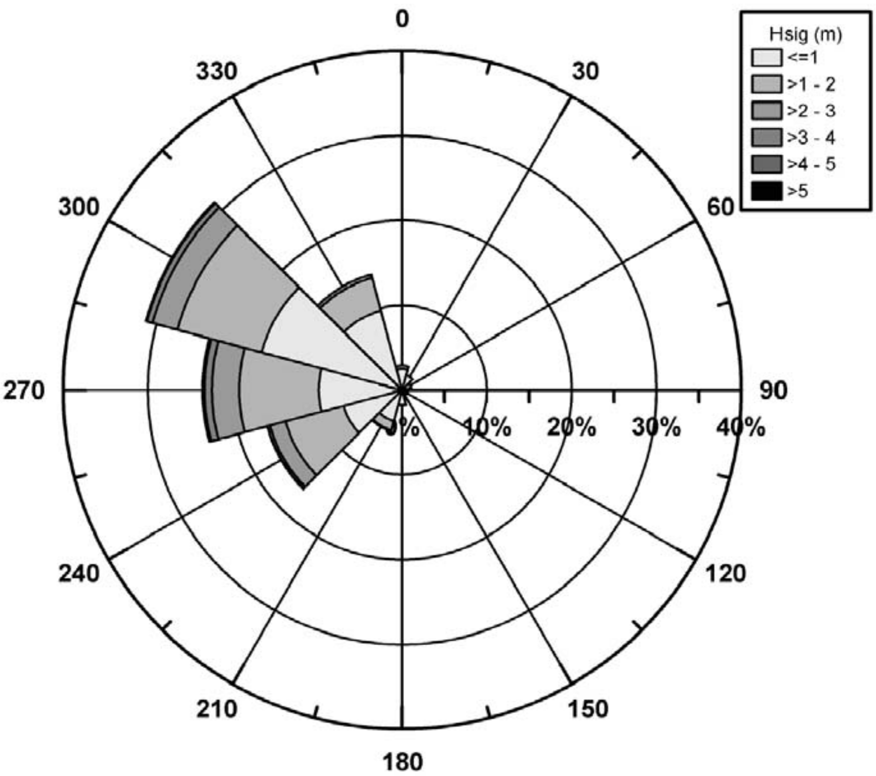

Fig. 9: Wave rose for the Island of Sylt, based on wave climate statistics as presented in BMFT (1994). The directions are in nautical convention; the percentages on the radial axis denote the probability of occurrence per wave height interval (WILKENS, 2004)

The present study follows the approach by STEIJN (1992), in which the effect of waves on the morphology is subdivided into the effects of wave-induced currents and stirring effects. Wave-induced currents are proportional to $H_s^{2.5}$, whereas the stirring effect is proportional to H_s. By applying these relationships the large number of swell conditions (combinations of wave height and direction) are subdivided into three categories, as shown in Table 2. The large reduction of the number of swell conditions is acceptable since the swell is limited to the small directional sector between 240 and 330 °N (see Fig. 9). It is acknowledged that swell from the southwest is probably less significant for the area under investigation than for the Island of Sylt. A sensitivity analysis showed that subdivision of the swell climate into as many as ten categories did not influence the computed morphodynamics to such an extent that justifies the additional computational effort otherwise required.

Table 2: Representative swell conditions

Condition	H_s (m)	T_p (s)	Θ (°N)	Probability (%)
Low	0.2	2.0	300	16
Moderate	1.0	4.0	300	73
High	2.0	7.0	270	11

The representative swell conditions defined in this way formed the starting point for the calibration. A qualitative calibration of these boundary conditions was found necessary in order to approximately simulate the correct morphological response of the outer tidal flats. This aspect is described in more detail in Section 5.

4.2.3 Representative Local Wind Conditions

Local wind conditions were defined so as to account for local wave generation. As will be shown in Section 6, local wind conditions have an effect on morphodynamic evolution in parts of the study area. A sensitivity analysis showed that wind-induced currents are not so important at the medium scale considered in the present investigation.

The definition of representative local wind conditions is based on a twelve-year data set derived from the synoptic PRISMA model (LUTHARDT, 1987). On the basis of observations along the coastline and at other locations such as oil platforms, this meteorological model computes wind velocities and air pressure fields for the North Sea by the application of interpolation techniques. A comparison of the PRISMA data with direct meteorological observations at the Research and Technology Centre Westcoast in Buesum showed good agreement between both data sets. The resulting wind rose is shown in Fig. 10.

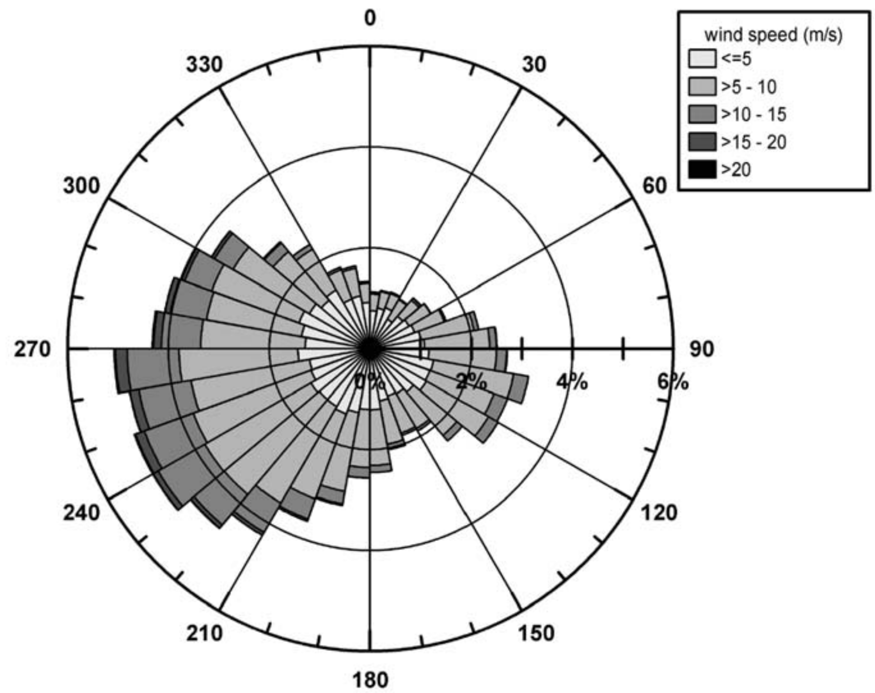

Fig. 10: Wind rose for the study area, based on data extracted from the synoptic PRISMA meteorological model (LUTHARDT, 1987). Nautical convention for the direction; the radial axis shows the probability of occurrence per wind speed interval (WILKENS, 2004)

A statistical reduction of the number of wind conditions (combinations of wind speed and direction) leads to the five representative wind conditions listed in Table 3. The directional sectors (of 30 degrees) with the highest probability per wind speed were defined as being representative for the respective wind speed interval (of 5 m/s). The related probabilities were set equal to the total probability for the considered wind speed interval. The consequence of this approach is that the less probable easterly directions are neglected. The main influence of local wind on morphodynamics is related to locally-generated waves. The method adopted is acceptable since easterly wind directions have a very limited fetch in the study area.

Table 3: Representative wind conditions

Condition	U_w (m/s)	Θ_w (°N)	Probability (%)
1	2.5	180	27.7
2	7.5	240	49.8
3	12.5	255	19.3
4	17.5	270	3.0
5	22.5	300	0.3

4.2.4 Sediment Transport and Morphological Conditions

At the open boundaries, conditions also have to be specified for the sediment transport and morphology. Long-term information about the bed load and suspended load sediment transport at locations near the open boundaries is not available, however. Thus, statistically representative conditions could not be determined. An alternative is available, however, in which simplified conditions are imposed. These simplified conditions are given either as a constant value or as a function of the local hydrodynamic quantities.

In this study, the simplified conditions have been imposed by defining the bed level at the open boundaries to remain at its initial value, together with conditions for the suspended load sediment transport. The latter are divided into an inflow-condition and an outflow-conditions. In the case of inflow, during the flood phase, the equilibrium concentration and subsequently the suspended load sediment transport are determined with the sediment transport formula considering the local flow conditions. For outflow, the up-stream concentration is applied to the open boundary, effectively setting the sediment concentration gradient to zero.

Due to the remote location of the open boundaries, the effect of these conditions is rather limited. This is true also for medium term simulations over periods of up to ten years, as a sensitivity analysis has shown. The somewhat unrealistic morphodynamic behaviour near the open boundaries does not affect the model results in the area of interest.

4.2.5 Summary

The selected representative conditions for tide, swell and wind were combined to yield a representative annual climate. Mild and severe conditions were arbitrarily mixed in order to avoid a prolonged sequence of storm or mild conditions. With regard to driving the morphodynamic model, such a sequence could well result in irreversible morphological changes that would not otherwise occur under thoroughly mixed conditions (see for example SOUTHGATE, 1995).

The results are listed in Table 4. Due to the low probability of occurrence of a 22.5 m/s wind speed condition, this condition is only represented in combination with the medium swell condition. These conditions were imposed in the initial morphodynamic model prior to calibration. Although a number of severe wind and wave conditions are included, specific storm conditions are not represented. In order to simulate storm events realistically it is necessary to include highly deformed water level signals, intruding swell and high locally-generated waves. This requires high temporal resolution of the imposed conditions and computed morphological changes and hence, a rather different model set-up. WILKENS (2004) and WILKENS and MAYERLE (in this volume) describe such simulations for the central Dithmarschen Bight and compare computed morphological changes to average yearly morphological changes. From these studies it was concluded that the inclusion of one or two storms in a one-year morphodynamic simulation has a very limited effect on the resulting morphodynamics at the medium scale of the applied model. Storm conditions were thus considered to be represented by the imposed swell and wind climate.

Table 4: Combined representative climate for swell and wind

Condition	H_s (m)	Θ (°N)	U_w (m/s)	Θ_w (°N)	Probability (%)
1	0.2	300	2.5	180	4.43
2	0.2	300	7.5	240	7.97
3	0.2	300	12.5	255	3.09
4	0.2	300	17.5	270	0.48
5	1.0	300	2.5	180	20.22
6	1.0	300	7.5	240	36.35
7	1.0	300	12.5	255	14.09
8	1.0	300	17.5	270	2.19
9	1.0	300	22.5	300	0.22
10	2.0	270	2.5	180	3.05
11	2.0	270	7.5	240	5.48
12	2.0	270	12.5	255	2.12
13	2.0	270	17.5	270	0.33

4.3 TELEMAC Modelling Scheme

The modelling strategy adopted in the TELEMAC model essentially corresponds to the previously-described procedure implemented in the DELFT3D model (see Fig. 11). In the first step a hydrodynamic simulation is performed over a period of 24 hours. If waves are taken into consideration, water levels, currents and wind data over a time interval of 15 minutes are transferred to the instationary wave model TOMAWAC. The subsequent one-day sea-state simulation also generates wave parameters at 15 minute intervals for the investigation area. Thereafter, the hydrodynamic simulation may be repeated with the inclusion of wave-induced flow forces. The updated flow field then enters the morphology module together with the wave parameters. This module computes sediment transport rates over a period of 24 hours and solves the bottom evolution equation. By subsequently repeating the morphodynamic computation seven times, the bottom evolution is calculated for a period of one week. Similar to the procedure adopted in the DELFT3D model, the currents are modified by means of the continuity equation. Following each week of bottom evolution the flow field is updated by performing a new hydrodynamic computation. The simulated one-day flow field may be generated on the basis of a representative double tidal cycle or a sequence of several days, e.g. a neap-spring cycle.

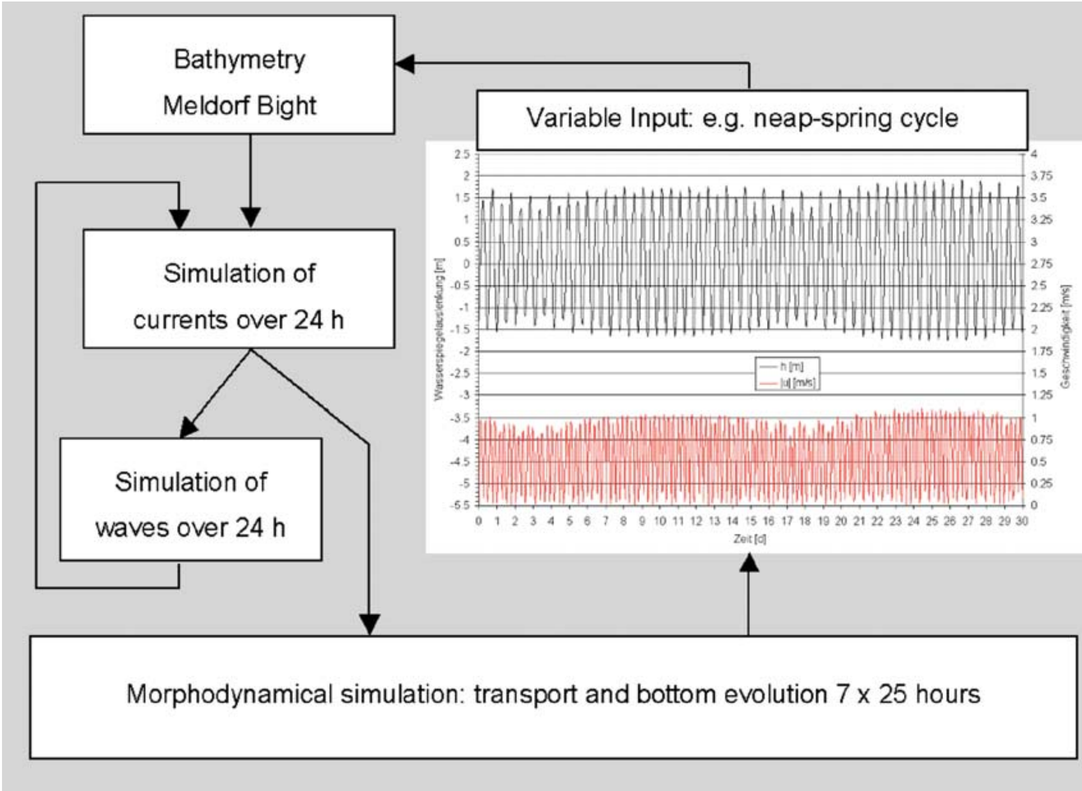

Fig. 11: Morphodynamic simulation scheme

4.4 TELEMAC Input Reduction

The application of the TELEMAC program system for long-term morphodynamic simulations requires the extraction and reduction of boundary conditions similar to the method described in the preceding section for the DELFT3D model. A reduction in computational effort is particularly important in the case of the TELEMAC model due to the fact that the hydrodynamic computations are performed for instationary wave characteristics using the finite element method.

4.4.1 Representative Tidal Conditions

A sequence of different tidal inputs was tested to determine feasible boundary conditions for the hydrodynamic simulation. Considering the modelling scheme shown in Fig. 11, the flow dynamics of the month September 1990 and a neap-spring cycle were specified along the open boundary over a 30-day simulation period. The resulting deviations of the morphodynamic development are comparatively small (ZIELKE, 2001). In this context long-term simulations were also performed using a representative tide, which is described in detail in

ZIELKE (2001). This tide could be implemented in the simulation scheme after doubling to a 25 hour period. Comparatively long-term simulations showed that the use of only one representative tide is an acceptable approach. Fig. 12 presents the simulated bathymetric changes under the boundary conditions stipulated for September 1990 with varying wind as well as for a representative tide with constant wind. September 1990 was chosen as the simulation period because it includes a moderate storm event. The simulations were performed using the ENGELUND-HANSEN formula (1967) with an average grain size of 300 µm. A comparison of the results of the two simulations (see Fig. 12) shows that the patterns of morphological changes are almost identical, with a slightly higher intensity of bottom evolution for the case of a representative tide. These results indicate that both boundary inputs are suitable for long-term simulations. This is also confirmed by a further simulation using real boundary conditions for the period 1990 to 1995 without a sevenfold morphological time step (ZIELKE, 2003). In this case the boundary conditions were determined for each day from PRISMA data (LUTHARDT, 1987). The results of the so-called 1 to 1 simulation are found to only differ slightly from the results presented in Fig. 12. It may thus be concluded that the modelling strategies adopted in the present investigation do not significantly impair the quality of results.

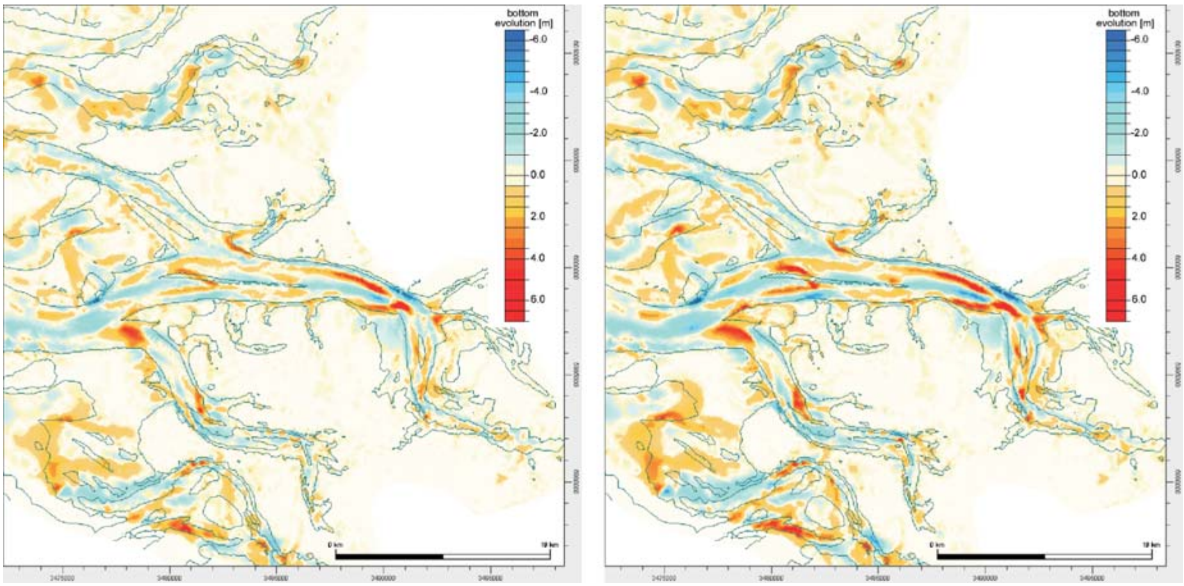

Fig. 12: Five-year simulation under prototype (monthly) conditions with varying wind (left) and for a representative tide with constant wind (right); red: accretion, blue: erosion

4.4.2 Representative Local Wind and Sea State Conditions

Compared to the specification of hydrodynamic boundary conditions, far more effort is generally required for specifying a variable sea state on the model boundary due to the additional statistical analysis of the input data, particularly if the amount of available data is insufficient. It is thus helpful if the wave model is able to deduce wave information from wind data without an explicit presetting of wave parameters along the open boundary. The instationary wave model TOMAWAC (WILKENS et al., in this volume), which belongs to the TELEMAC program system (BENOIT et al., 1996), generates wave parameters along the open

Die Küste, 69 PROMORPH (2005), 1-420

model boundary under consideration of wind data, an imposed wind fetch and the predefinition of a JONSWAP wave spectrum.

Table 5: Wind statistics for the Dithmarschen Bight study area

U_w (m/s)	Θ_w (°N)	Probability (%)	Probability within 14 tides [tide]
2.5	180	27.7	4
7.5	240	49.8	7
12.5	255	19.3	3 (13.3 m/s, 257.5°N)
17.5	270	3.0	
22.5	300	0.3	

Table 5 shows the statistically analysed wind situation for the Dithmarschen Bight study area (WILKENS, 2004). If the probability of occurrence is distributed over a period of 14 tides, the wind conditions may be expressed over a cycle of one week with only two one-day wind sequences (see Fig. 13). The first wind field of weak to moderate intensity is combined with a fetch of 20 km and a duration of four days. During the remaining three days the stronger wind field is combined with a fetch of 50 km. In order to ensure harmonic transitions when changes in the wind field occur, the transitions are undertaken during slack water when the wave influence is low in the investigation area. For the same reason the two wind fields start and end with a moderate wind phase.

For the hydrodynamic calculation a constant wind with an intensity of 8.75 m/s from the southwest direction was imposed. This presetting is the result of a detailed statistical

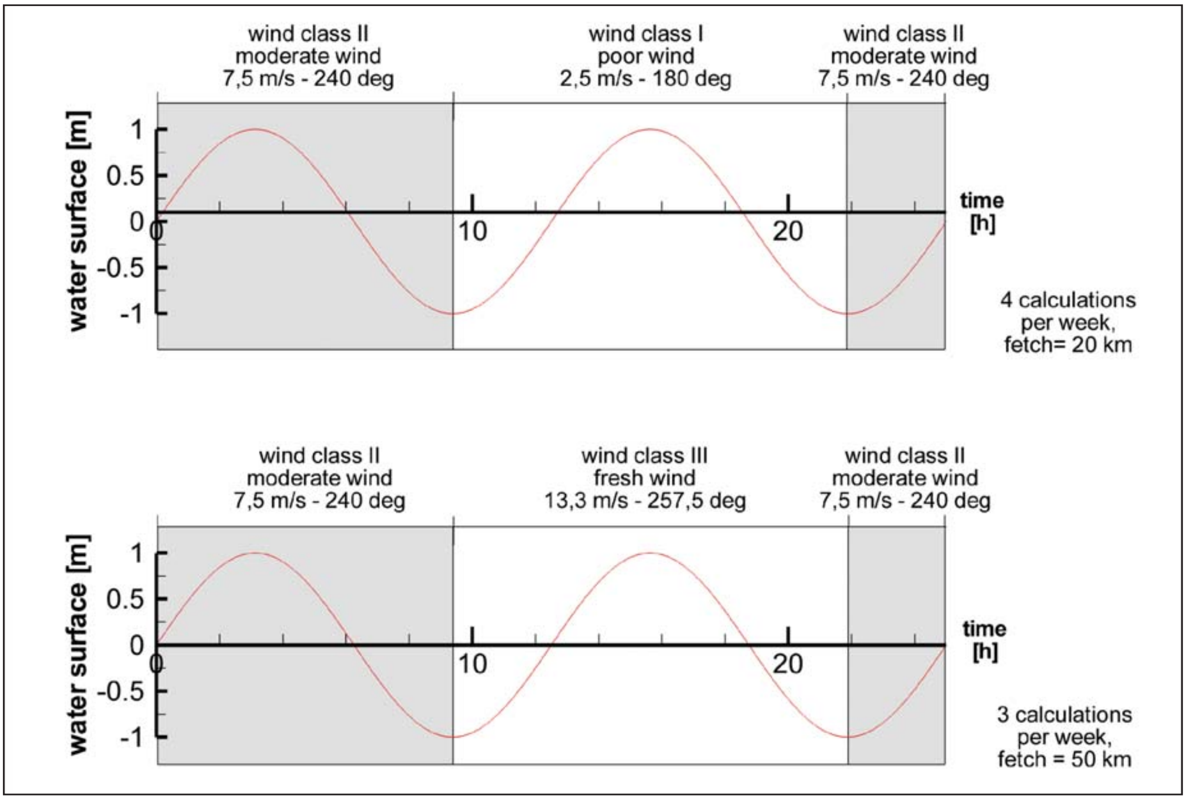

Fig. 13: Representative wind fields for wave modelling

analysis (ZIELKE, 2003) and serves as a representative average value for the investigation area. Comparative calculations with a selected measured wind sequence over 30 days showed no significant improvement in the results.

5. Calibration and Validation of the Morphodynamic Models

The morphodynamic model was calibrated and validated for medium scale periods of about ten years. The evaluation was based on bathymetric measurements from surveys carried out by the BSH. Due to the varying extent of coverage of these surveys, full coverage of the main channels Norderpiep, Suederpiep, Piep and the tidal flat Tertiussand (see Fig. 1) was available every three years. Calibration and validation of the DELFT3D model were carried out for the periods 1977 to 1987 and 1990 to 1999, respectively. Only the period 1990 to 1999 was considered for calibrating the two versions of the TELEMAC model.

In conjunction with a qualitative comparison between computed and observed deposition and erosion patterns and depth contours a quantitative evaluation was made using the two versions of the TELEMAC model under consideration of the volumetric changes in several sub-domains (see Fig. 14). Due to the limited availability and questionable quality of bathymetric data in areas above mean sea level (MSL; German Normal Null – NN), only

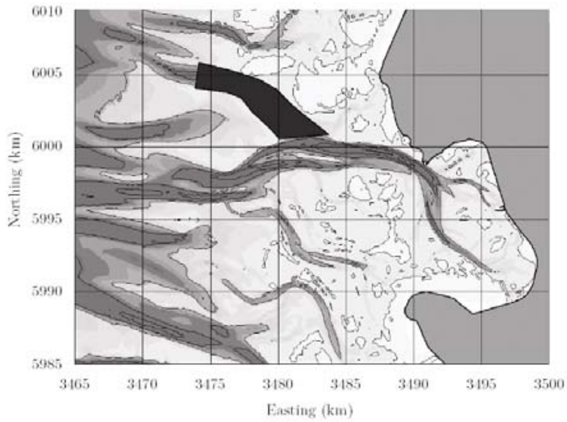

(a) Sub-domain Norderpiep

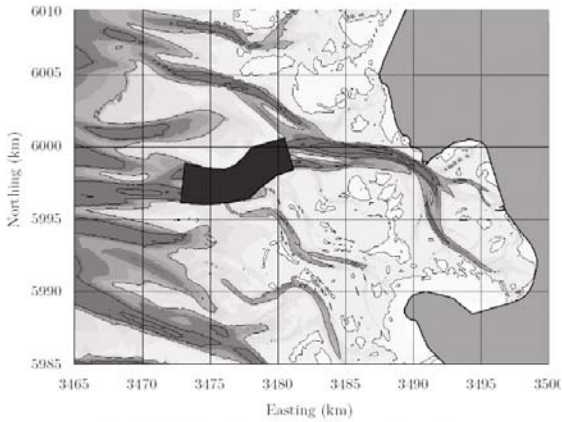

(b) Sub-domain Suederpiep

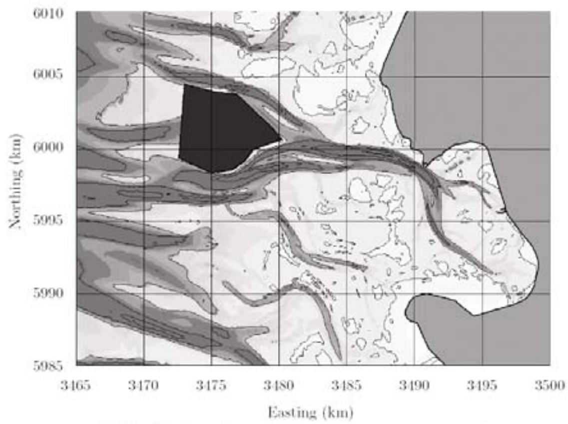

(c) Sub-domain Tertiussand

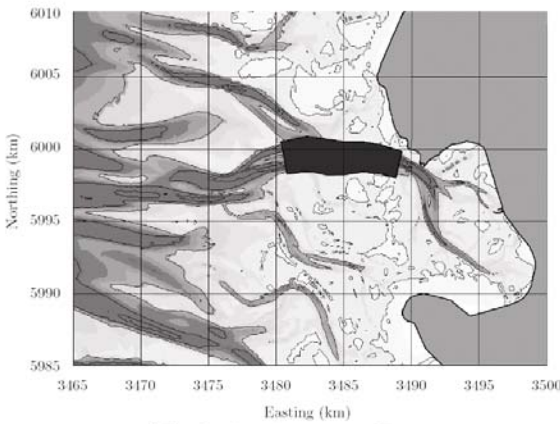

(d) Sub-domain Piep

Fig. 14: Location of the sub-domains considered in the volumetric analysis (WILKENS, 2004)

wet volumes below this level were considered. Furthermore, the available data for the eastern Meldorf Bight did not permit an acceptable volumetric analysis. The volumes considered in the analysis are related to the volumes for the year 1977 as follows:

$$V_{rel,i} = \frac{V_i}{V_{1977}} * 100\%$$

with:

Vrel,i	relative wet volume below MSL of a sub-domain in year ***i***
V_{1977}	wet volume below MSL of a sub-domain in 1977
V_i	wet volume below MSL of a sub-domain in year ***i***

5.1 Calibration and Validation of the DELFT3D Model

Calibration of the DELFT3D model was carried out in two stages. An in-depth description may be found in WILKENS (2004). The first stage concerns an *external calibration*, in which the imposed conditions were optimised starting from the defined representative conditions (see Section 4). In this calibration the imposed wind and swell climates were adapted to realise an overall correct response of the computed morphological changes. This mainly affected the westerly tidal flats and channels, whose morphological behaviour is highly dependent on the imposed swell climate. A reduction of 50 % of the imposed wave heights yielded the best results. Improvements could also be achieved by a reduction of the local wind climate. In this case also, a reduction of 50 % proved to optimal.

The reductions of the imposed wind and swell conditions are quite large. It is noted that the computed morphological changes depend on the one hand on the imposed conditions and on the other hand on the sediment transports induced by these conditions. The magnitude of these sediment transports depends on the applied formula; in this study being the formula by BIJKER (1971) as described in Section 3. The use of another formula or different parameter settings in the current one could lead to different magnitudes of reduction of the imposed conditions. The 50 %-reduction is thus the result of a balance between the imposed conditions and the applied formula.

Furthermore, it is noted that the considered wave data stem from measurements off the coast of Sylt. This location protrudes further into the North Sea and it is therefore likely that the amount of wave energy is higher here than along the open boundaries of the Dithmarschen Bight Model. The necessity of reducing the statistically determined wave climate on the basis of these data thus appears logical, to the purpose of approaching the actual conditions along the model boundaries in a better way.

The second stage is an *internal calibration*. In this case the time management set-up and several parameters in the sediment transport model were adapted to improve the results. In the time management set-up the number of wave calculations per tidal cycle and different types of interaction between the modules was evaluated. In this respect the set-up described in Subsection 4.1 was found to be optimal. Since the sediment transport model has already been calibrated and validated (see WINTER et al., in this volume) further changes to the model were not deemed to be necessary. Since the evaluation of the sediment transport model was based on calm weather situations without significant wave action, however, further calibration was found to be necessary. The calibration parameter that yielded the largest improvements is related to the balance and intensity of sediment transport due either to tidal currents or to wave action. This parameter is referred to as the constant b in BIJKER's transport formula (BIJKER, 1971).

In the validated sediment transport model chosen, this parameter is defined uniformly with a constant value of 3. As a result of further calibration a varying value ranging from 1 to 5 proved to be optimal. A value of 1 is applied for deep-water wave conditions whereas for shallow-water wave conditions a value of 5 is adopted; interpolation between these values is carried out for intermediate conditions. The influence of waves on the total sediment transport is thus enhanced relative to the influence of tidal currents.

The results of the volumetric analysis for a simulation using the calibrated model over the period 1977 to 1987 are shown in Figs. 15 to 18 for the four investigated sub-domains. This includes the period 1990 to 1999. As may be seen in the figures, the observed values are not perfectly consistent in time. This may be due to shorter-term fluctuations as well as to inaccuracies in the bathymetric measurements (including interpolation errors). It is also evident that the observed medium-term trends are reproduced fairly well by the model during both the calibration and the validation period. Although some differences are noticeable, the quality of the model results is sufficient to justify the application of the model as a useful tool for predicting morphodynamic evolution as well as for analysing the underlying physical processes.

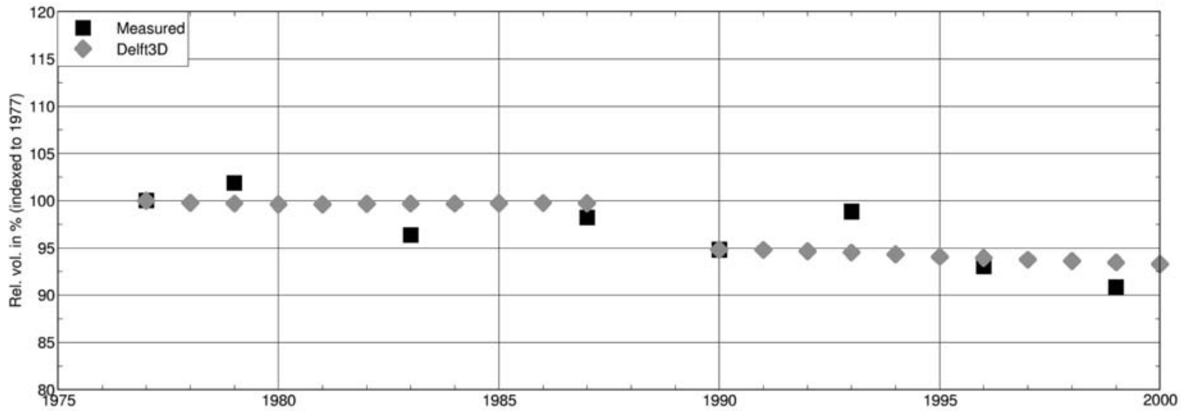

Fig. 15: Relative wet volume changes below MSL for sub-domain Norderpiep

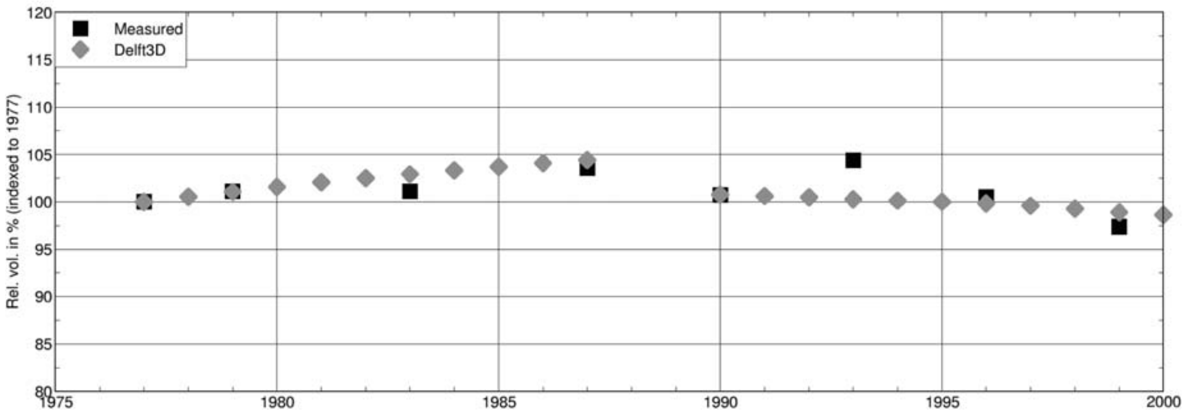

Fig. 16: Relative wet volume changes below MSL for sub-domain Suederpiep

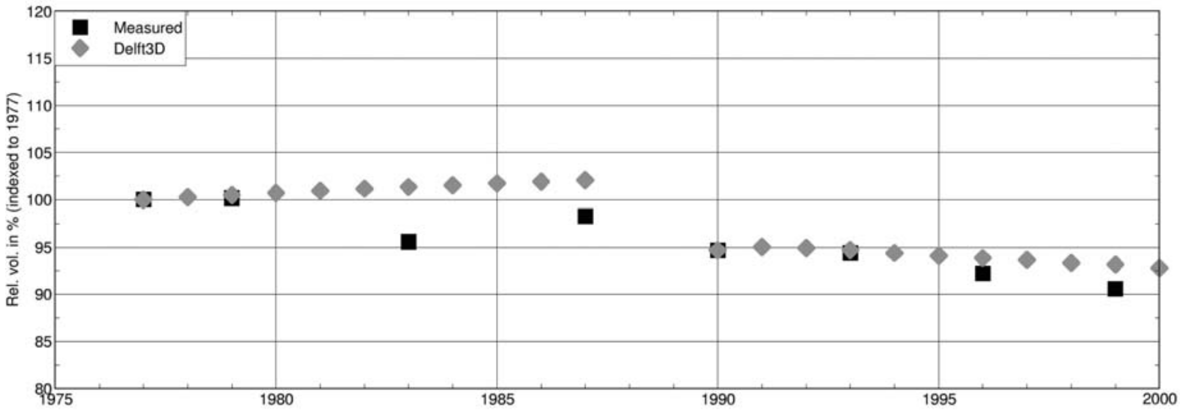

Fig. 17: Relative wet volume changes below MSL for sub-domain Piep

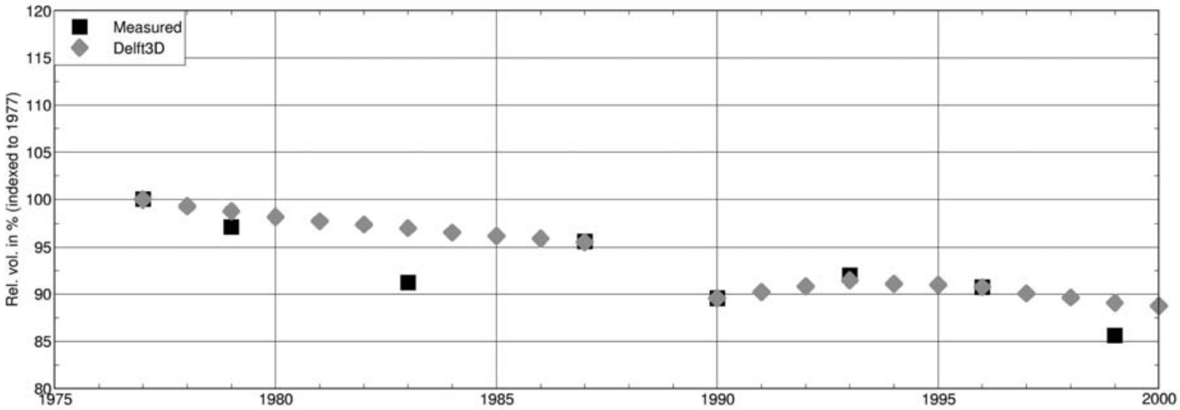

Fig. 18: Relative wet volume changes below MSL for sub-domain Tertiussand

5.2 Calibration and Validation of the TELEMAC Model

Although the calibration and validation process for the TELEMAC model is similar to the strategy for the DELFT3D model, the simulated periods are shorter. The simulations mainly relate to the period from 1990 to 2000, for which extensive field measurements are available.

A reliable method of verifying the results of morphodynamic models is to examine the extent to which the changed sediment volume in specific areas agrees with measurements. Especially in tidal flat areas, this procedure provides a good indication of the quality of the simulated results. As shown in Fig. 19 (left), three tidal flat areas in the Dithmarschen Bight were specified for a volumetric analysis according to the method already outlined in the preceding subsection. The yearly bathymetric measurements provided by the BSH were interpolated onto the model grid and the "wet" volume, i.e. the volume of water below MSL, was calculated. A comparison between measured and simulated wet volumes, expressed as a percentage of the reference value in 1977, is shown in Fig. 21. The trends indicate that the wet volume decreases in Polygon P1, whereas in P3, it increases. This result implies overall erosion in P3 and an overall accretion of sediment in P1. The same trends are followed by the simulated results. In Polygon 2 the simulation yields a slight erosion trend which cannot be clearly confirmed by measurements. The yearly measurements should be treated with caution, however, as they do not cover the complete study area in all cases.

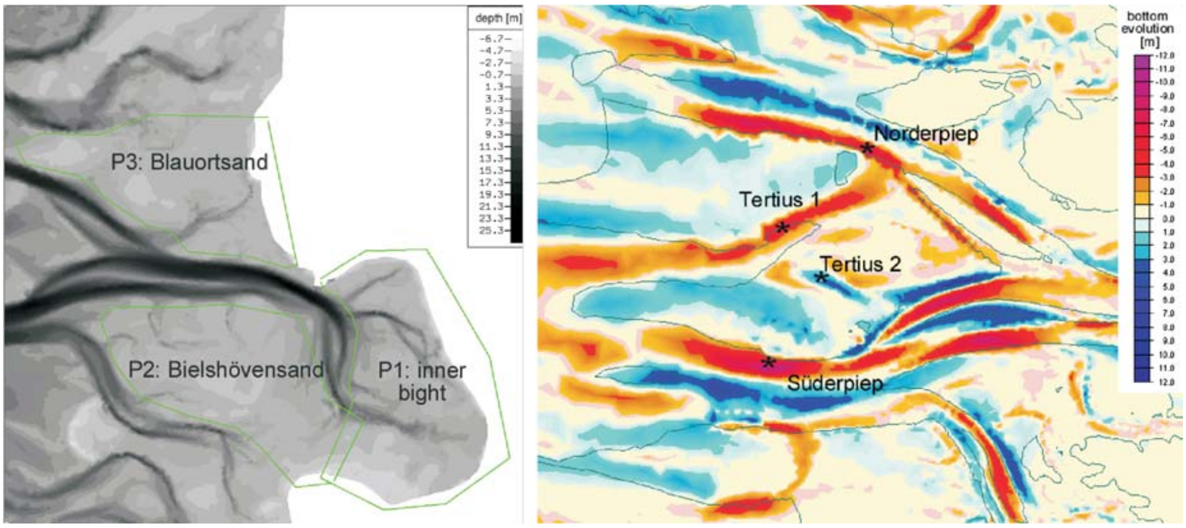

Fig. 19: Location of the polygons for a mass balance on the tidal flats (left); bathymetric changes based on measurements (1990 to 2000) in the vicinity of Tertiussand, indicating positions of observation points (right)

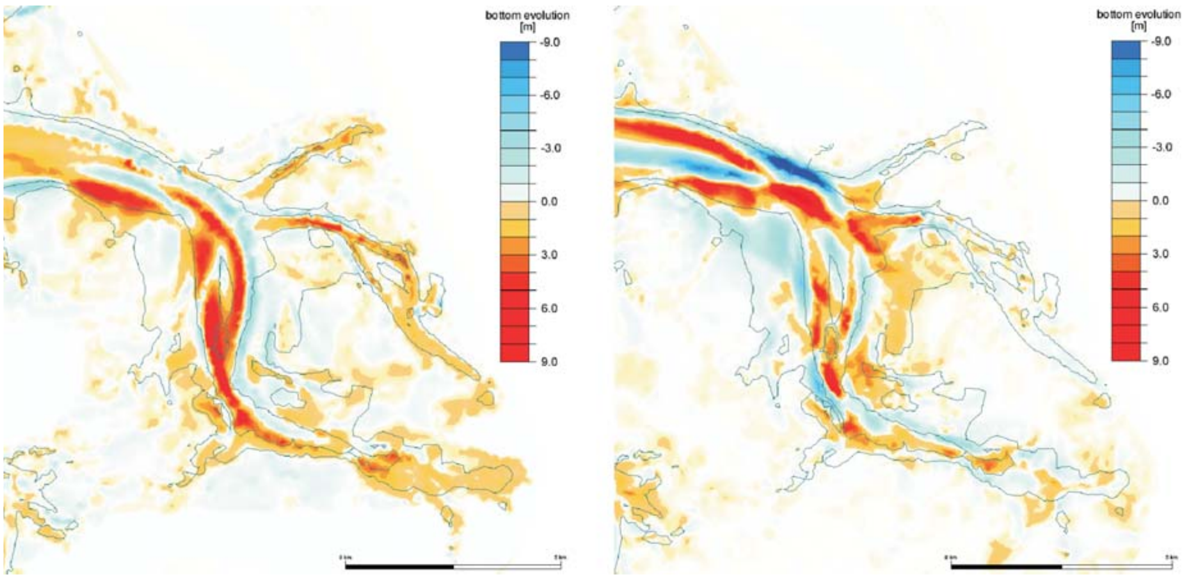

Fig. 20: Measured (left) and simulated bottom evolution (1990-1999) in the Meldorf bight: red = deposition, blue = erosion

The measured and computed bathymetric changes within the Piep and the Meldorf bight area are shown in Fig. 20. Many morphologic developments are well reproduced by the model, even though some changes are somewhat exaggerated. The significant erosion and sedimentations patterns near Buesum, the long narrow erosion band along the northern and eastern banks of the Piep channel and the strong accretion of the sand bank in the Piep southerly of Buesum are reproduced rather well. The computed erosion trend on the Biels-hoevensand cannot be clearly confirmed by measurements. Possibly additional influx of sediment due to wave action over the Bielshoevensand causes this effect as was suggested by HIRSCHHAEUSER (2004).

The results presented in Figs. 20 and 21 were computed using the transport formula of ENGELUND and HANSEN (1967) with a representative tide at the seaward boundary. This means that the influence of waves is not taken into account. Although this is acceptable in the region of the Meldorf Bight and the eastern Piep channel (see WILKENS, 2004), wave influence cannot be neglected in the outer regions, i.e. Tertiussand, Norderpiep and Suederpiep. Against this background a further simulation was performed under consideration of sea state using the transport formula of BIJKER (1971). The wave parameters were generated by the instationary wave model TOMAWAC (WILKENS et al., in this volume) under consideration of representative wind conditions likewise introduced in Subsection 4.4.2. In order to investigate the influence of waves a morphodynamic simulation was performed for a 10-year period using both transport formulae. The measured bottom evolution for the region bordering Tertiussand is plotted on the right in Fig. 19. Fig. 22 shows the morphological evolution at four observation points placed at the centres of regions in which significant bottom changes occur. It may be seen in the Figure that the results obtained using the transport formula of BIJKER (1971) (under consideration of waves) are in close agreement with the observed trends. The computation using the formula of ENGELUND and HANSEN (1967), which yields good results in the middle and eastern part of the study area, is unable to correctly reproduce the trends over the exposed tidal flats in the west. This impression is confirmed by the results of a volumetric analysis, as shown in Fig. 23. The polygons used are the same as those already introduced in Fig. 14. The morphological trends calculated according to ENGELUND and HANSEN (1967) agree well with measurements in the Piep and Tertiussand polygon. The results of the BIJKER (1971) simulation fit the trends more appropriately, even though the calculated changes seem to be somewhat excessive. The predicted erosion trend for the Tertiussand is caused by strong sediment movement to the border regions which are not completely covered by the analysed sub-domain.

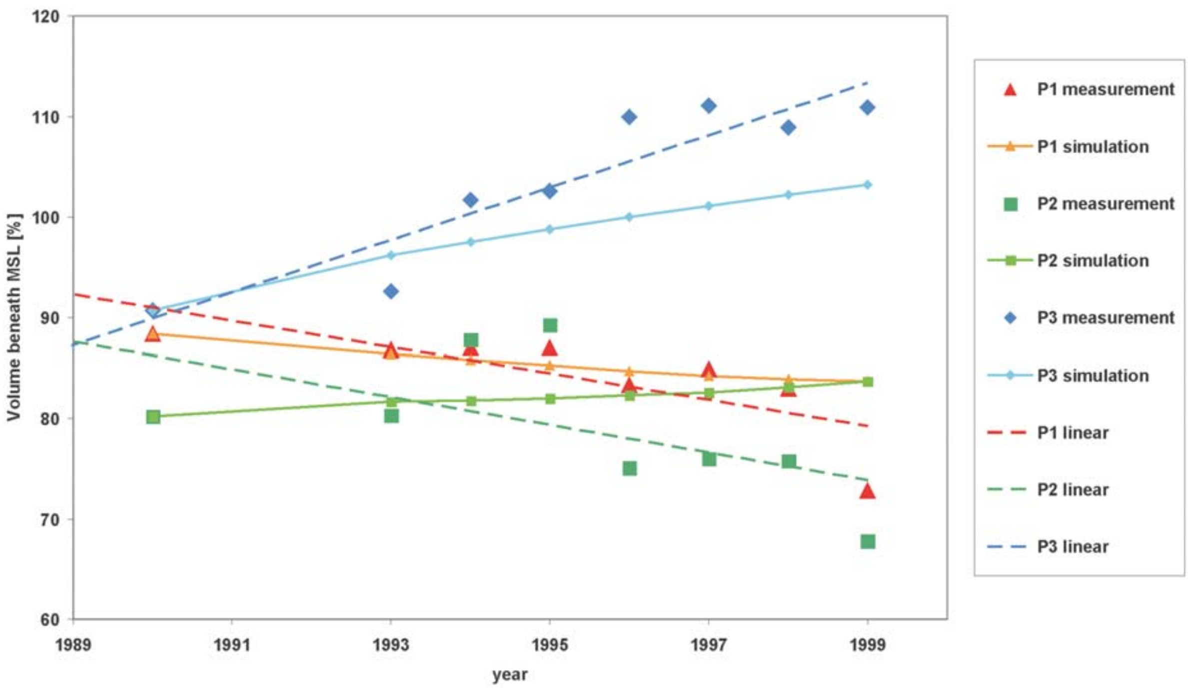

Fig. 21: Comparison of measured and computed (numerical simulation) water volumes below MSL

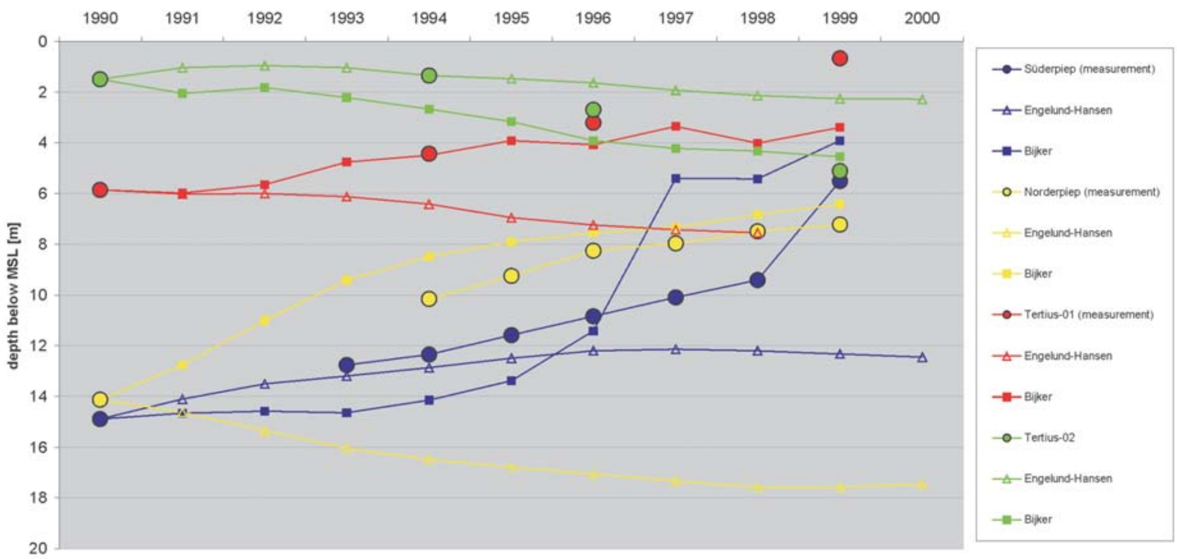

Fig. 22: Bottom evolution at different observation points in the region of Tertiussand (1990–2000)

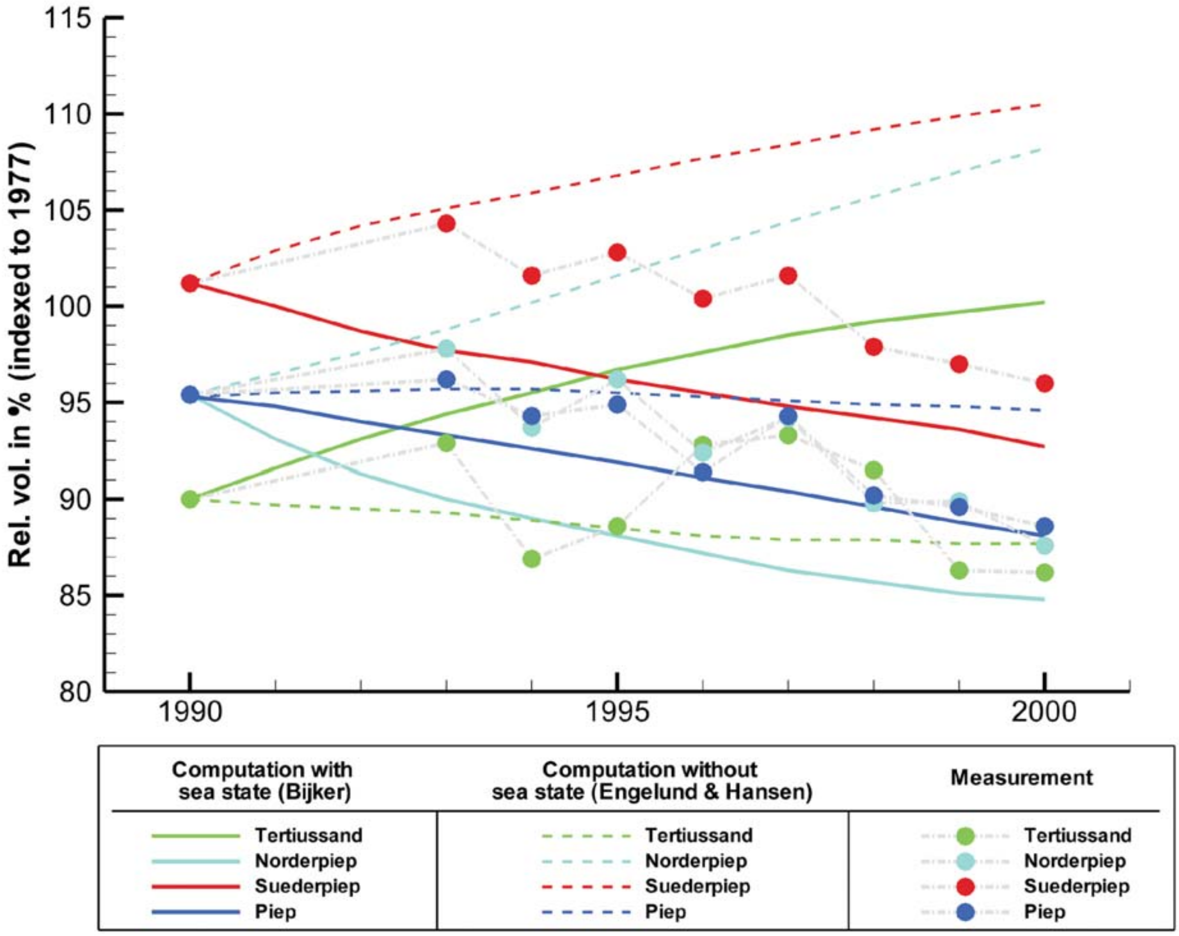

Fig. 23: Relative wet volume changes below MSL for different sub-domains

6. Model Predictions over a Ten-Year Period

The calibrated and validated models were applied to predict morphological evolution in the study area during the period 1999 to 2009. The results of the DELFT3D model prediction for the tidal channel system of the central Dithmarschen Bight, covering the afore-mentioned sub-domains, are presented in the following. Furthermore, the results of the TELEMAC model are presented for the easterly Meldorf Bight.

6.1 Model Prediction for the Central Dithmarschen Bight with the DELFT3D Model

Applying the optimised settings for the imposed boundary conditions and model parameters, as defined in the calibration phase of the model, a simulation was performed to estimate the morphological evolution of the tidal channel system. The initial bathymetry for this simulation is shown in Fig. 24 while the final bathymetry predicted for 2009 is shown in Fig. 25. The morphological changes are shown in Fig. 26.

As may be seen in the figures, a number of significant changes are predicted, especially in the region of Tertiussand. The small channel branching from the Suederpiep is seen to gradually break through the tidal flat, thereby forming a connection to the open sea. The cut-off part of Tertiussand to the south is seen to migrate further southward towards the Suederpiep. Due to the fact that the southern channel bank is retained by the presence of the D-Steert shoal, this migration results in a narrowing of the Suederpiep. A progression towards the northeast is discernable on the north-eastern side of Tertiussand, as also confirmed by measurements over the past twenty years (WILKENS, 2004). The south-western sub-channel of the Norderpiep is seen to gradually fill with sediment, creating a connection between the tidal flat and the submerged bar in this channel. On the southeastern side the Suederpiep channel is seen to erode the edge of Tertiussand. This process is enhanced by the presence of the newly-created channel through the tidal flat. Further deepening of the Piep is also predicted towards the east. The submerged bar in this channel shows signs of erosion, which is contrary to the observed and computed accretion between 1977 and 1999. This change of behaviour may also be related to the initiation of the channel over Tertiussand due to a re-orientation of the main current patterns.

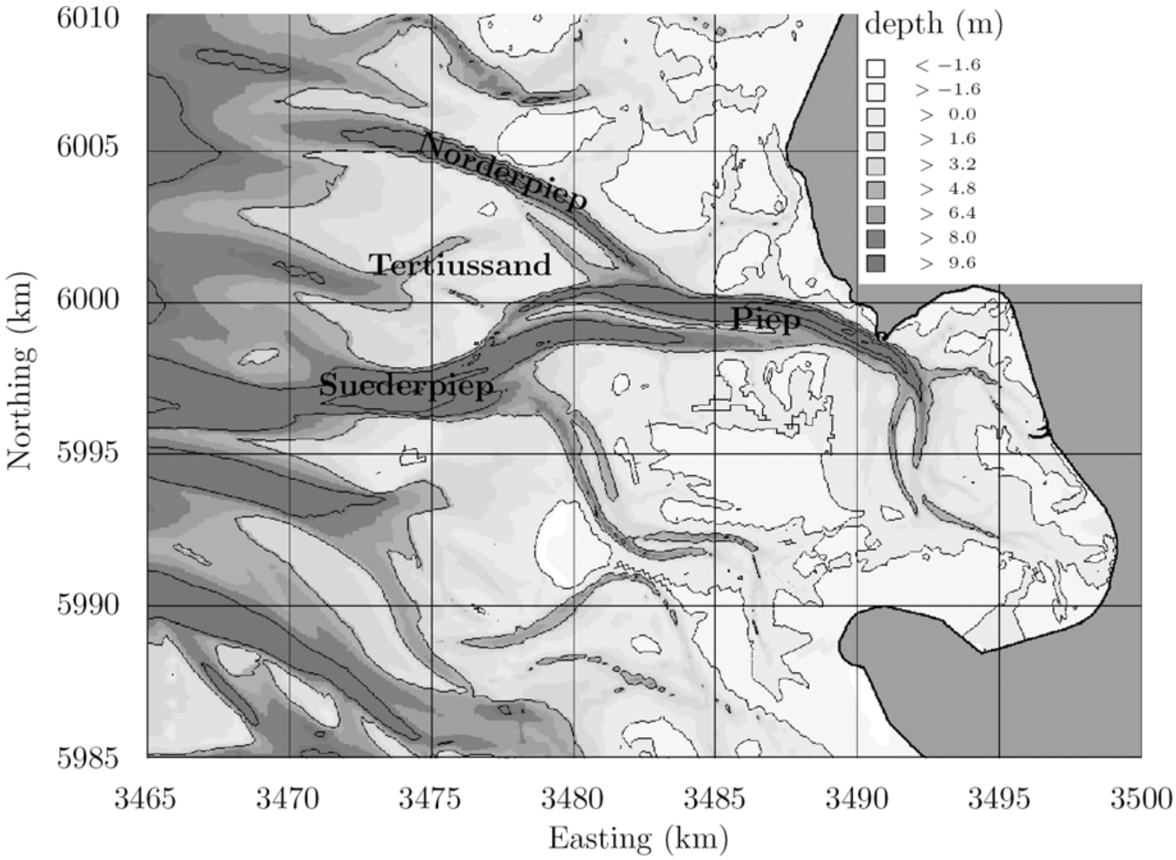

Fig. 24: Initial bathymetry (1999) for the DELFT3D model simulation (WILKENS, 2004)

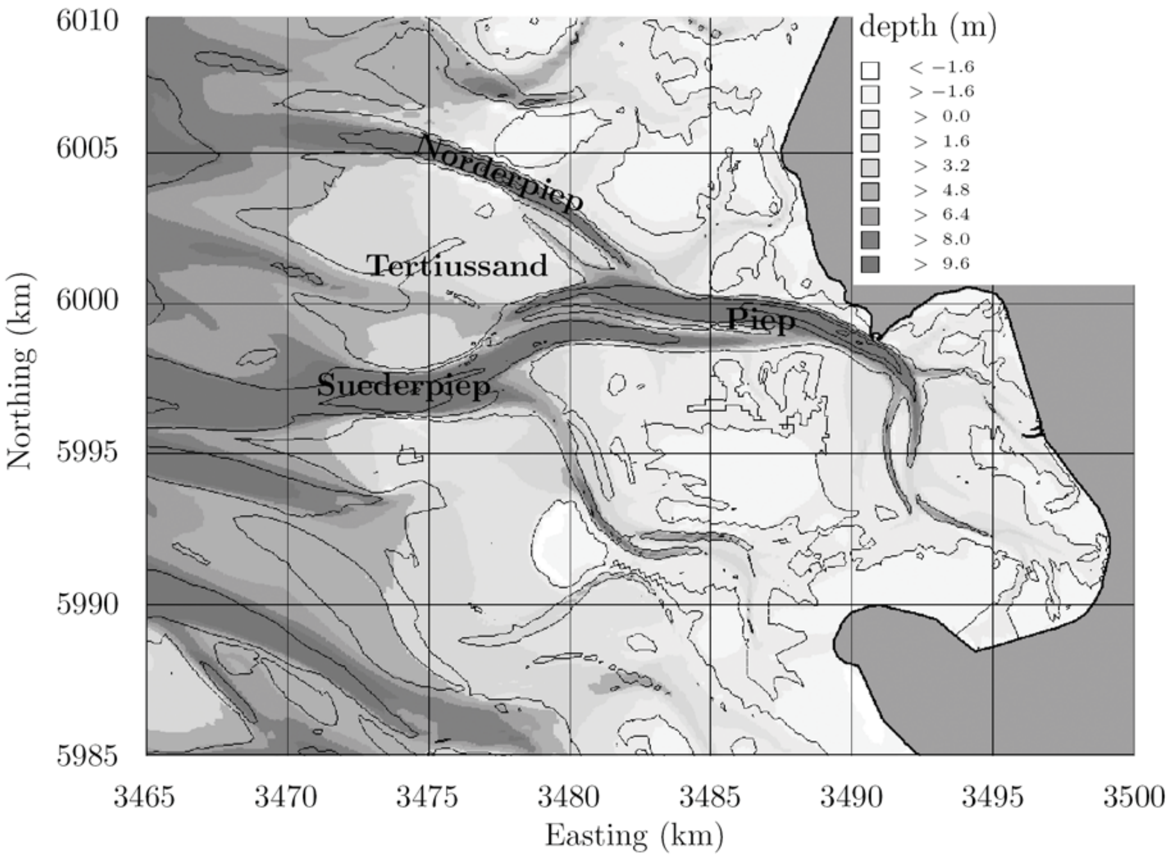

Fig. 25: Bathymetry predicted by the DELFT3D model for 2009. Iso-lines from 1999 (WILKENS, 2004)

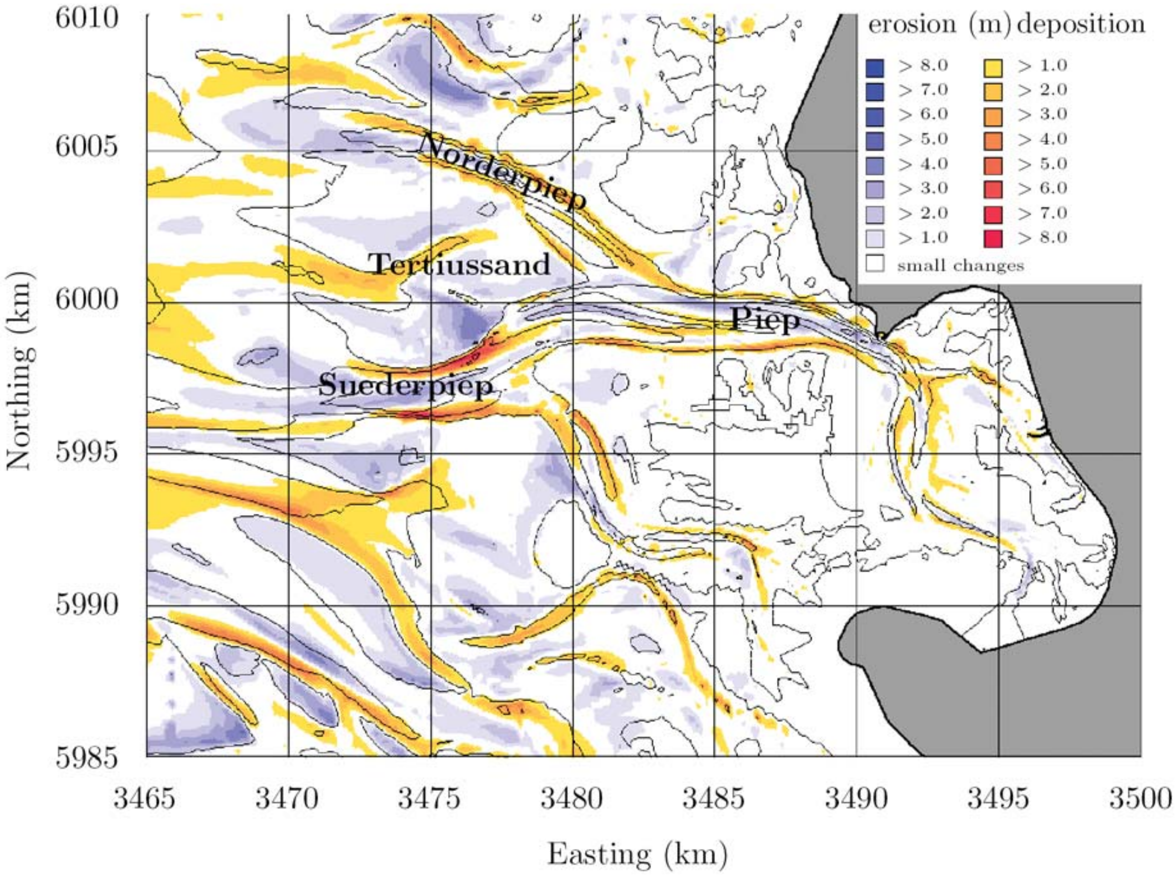

Fig. 26: Morphological changes predicted by the DELFT3D model from 1999–2009 (WILKENS, 2004)

6.2 Model Prediction for the Meldorf Bight with the TELEMAC Model

A simulation over a period of ten years was performed for the Meldorf Bight in order to test whether the model is capable of simulating morphodynamic evolution over a longer period in this study area. The various bathymetries relating to this simulation are shown in Fig. 27. The images in the top part of the Figure represent the measured bathymetries of 1990 and 1999. The bathymetry of 1999 is also used as the initial bathymetry for the 10-year simulation. The boundary conditions for the simulation are based on observations for the month September 1990, as shown in Fig. 11. Sediment transport was calculated using the transport formula of ENGELUND and HANSEN (1967) with a grain size of 300 µm.

It was found that many tendencies in the observed morphological behaviour are also predicted by the simulation, e.g. shifting of the Ossengoot channel (location 1) to the southeast and deepening and shifting of the interstitial channel at location 2. The deepening of the Suederpiep (location 3) and the narrowing of the Marner Plate (location 4) as well as the shifting of the Piep in the vicinity of Buesum (location 5) to the northeast proceed rapidly. It will be interesting to verify whether the deepening and creation of a new interstitial channel at location 5 will in fact occur during the coming years. This trend seems to be indicated in the 1990 to 1999 measurements. Another area of massive sediment movement is around the sandbank in the Piep channel south of Buesum. The sandbank is seen to grow rapidly

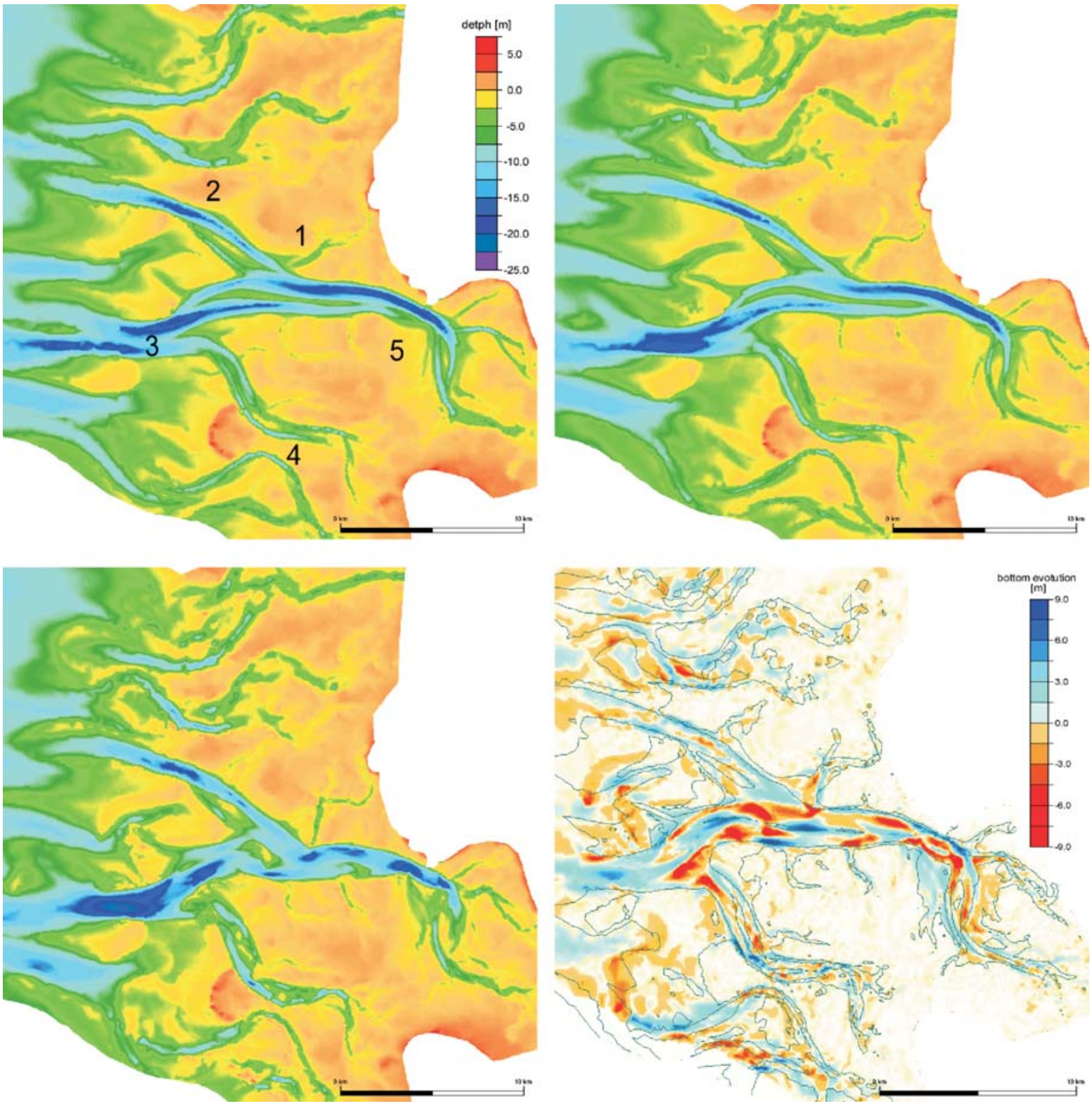

Fig. 27: Results of a 10-year morphological simulation: bathymetry surveyed in 1990 (top left), initial bathymetry of 1999 for the model simulation (top right), predicted bathymetry after 10 years (bottom left) and bed evolution: red = deposition, blue = erosion (bottom right)

in the southern direction, dividing the Piep channel into two tidal creeks. This trend is also observed in the simulation results. Due to the creation of a new interstitial channel at location 5 the southern Meldorf Bight now mainly drains via the western channel, which is different to the observed situation in 1999. The simulated bottom changes between 1999 and 2009 are presented in the lower right part of Fig. 27. Especially for the region of the Meldorf Bight, the bathymetric development is found to agree well with the morphological behaviour observed between 1990 and 1999 (see HIRSCHHAEUSER, 2004). In summing up, it may be stated that the model yields plausible results in most areas for a 10-year simulation period.

7. Conclusions

The combination of thoroughly calibrated and validated individual models for the simulation of tides, waves and sediment transport forms a sound basis for the construction of morphodynamic models for simulating bathymetric changes. Since a new model is formed when these individual models are combined, recalibration and revalidation of the combined model system are necessary. By implementing input and process filtering techniques it was possible to extend the applicability of the models to morphodynamic modelling on the medium scale. The resulting calibrated and validated models proved to be suitable for making morphodynamic predictions. The use of an objective, quantitative approach for model evaluation based on a volumetric analysis places higher confidence in the models than would be expected from the single application of a subjective evaluation of sedimentation and erosion patterns. Based on the promising evaluation results obtained during the model calibration and validation phases the models were subsequently applied to predict morphological changes in the study region over the period 1999 to 2009. Although some significant changes are predicted, these are not deemed to be unrealistic, considering the solid basis underlying the validated process models. Using both modelling systems it was possible to perform realistic simulations of morphodynamic evolution.

8. Acknowledgements

This investigation was carried out within the framework of the project PROMORPH, funded by the German Ministry of Education and Research (BMBF) under number 03 F 0262A. We thank the Federal Maritime and Hydrographic Agency (BSH, Hamburg) and the Office of Rural Development (ALR, Husum) for providing the bathymetric data. We are grateful to the Max-Planck Institute of Meteorology (MPI-M) of the University of Hamburg for providing the PRISMA wind data. The cooperation with the staff of the participating institutes is gratefully acknowledged.

9. References

BENOIT, M.; MARCOS, F. and BECQ, F.: Development of a Third Generation Shallow-Water Wave Model with Unstructured Spatial Meshing. Proc. 25th Int. Conf. on Coastal Eng. (Orlando, USA), 1996.

BIJKER, E. W.: Longshore Transport Computations, Journal of the Waterways, Harbors and Coastal Engineering Division, Vol. 97 (WW4), 1971.

BMFT: Optimierung des Küstenschutzes auf Sylt – Phase II, Bundesministerium für Forschung und Technologie, Amt für Ländliche Räume Husum, in German, 1994.

BOOIJ, N.; RIS, R. C. and HOLTHUIJSEN, L. H.: A Third-Generation Wave Model for Coastal Regions, Part I, Model Description and Validation. Journal of Geophysical Research, Vol. 104, C4, 1999.

EINSTEIN, H. A.: The bed-load function for sediment transport in open channel flow, U.S. Department of Agriculture, Washington, D.C., 1950.

ENGELUND, F. and HANSEN, E.: A Monograph on Sediment Transport in Alluvial Streams, Teknisk Vorlag, Copenhagen, Denmark, 1967.

GALLAND, J.-C.; GOUTAL, N. and HERVOUET, J.-M.: TELEMAC A New Numerical Model for Solving Shallow Water Equations, Adv. Water Resources, 14 (3), 1991.

HERVOUET, J.-M.: TELEMAC Modelling System: an overview. In: Hervouet, J.-M. and P. Bates. Special Issue: The TELEMAC Modelling System. Hydrological Processes, 14 (13), 2209–2210, 2000.

HIRSCHHAEUSER, T.: Langfristige Sedimentdynamik des Systems Tidebecken-Ebbdelta unter besonderer Berücksichtigung von Verändertem Seegang und Wasserständen, Die Küste, Heft 68, 2004.

HOYME, H. H.: Mesoskalige morphodynamische Modellierungen am Beispiel der Meldorfer Bucht, Ph.D. thesis, University of Hanover, Germany, in German, 2002.

LATTEUX, B.: Techniques for Long-Term Morphological Simulation under Tidal Action, Marine Geology, Vol. 126, 1995.

LUTHARDT, H.: Analyse der Wassernahen Druck- und Windfelder über der Nordsee aus Routinebeobachtungen, Hamburger Geophysikalische Einzelzeitschriften, A 83, in German, 1987.

PALACIO, C. A.; MAYERLE, R.; TORO, M. and JIMÉNEZ, N.: Modelling of Flow in a Tidal Flat Area in the South-Eastern German Bight, Die Küste, Heft 69, 2005.

RIS, R. C.; BOOIJ, N. and HOLTHUIJSEN, L. H.: A Third Generation Wave Model for Coastal Regions, Part II, Verification, Journal of Geophysical Research, Vol. 104, C4, 1999.

ROELVINK, J. A. and VAN BANNING, G. K. F. M.: Design and Development of DELFT3D and Application to Coastal Morphodynamics, Proc. Hydroinformatics 1994 (Delft, the Netherlands), H.H. Balkema Publishers, Rotterdam, the Netherlands, 1994.

SOUTHGATE, H. N.: The Effects of Wave Chronology on Medium and Long Term Coastal Morphology, Coastal Engineering, Vol. 26, pp. 251–270, 1995.

STEIJN, R. C.: Input Filtering Techniques for Complex Morphological Models, Delft Hydraulics Report, H 824.53, 1992.

WILKENS, J.: Medium Scale Morphodynamics of the Central Dithmarschen Bight, Ph.D. thesis, University of Kiel, Germany (available under http://e-diss.uni-kiel.de/diss_1369/d1369.pdf), 2004.

WILKENS, J.; JUNGE, I. and HOYME, H. H.: Modelling of Waves in a Tidal Flat Area in the South-Eastern German Bight, Die Küste, Heft 69, 2005 (a).

WILKENS, J. and MAYERLE, R.: Morphodynamic Response to Natural and Anthropogenic Influences in the Dithmarschen Bight, Die Küste, Heft 69, 2005 (b).

WINTER, C.; POERBANDONO; HOYME, H. and MAYERLE, R.: Modelling of Suspended Sediment Dynamics in Tidal Channels of the German Bight, Die Küste, Heft 69, 2005.

ZIELKE, W.: PROMORPH – Prognose mittelfristiger Küstenmorphologieänderungen (Prognosis of Medium-Term Coastal Morphology, Jahresbericht 2000, BMBF 03F0262A/B, 2001.

ZIELKE, W.: PROMORPH – Prognose mittelfristiger Küstenmorphologieänderungen (Prognosis of Medium-Term Coastal Morphology, Schlussbericht, BMBF 03F0262A/B, 2003.

Morphodynamic Response to Natural and Anthropogenic Influences in the Dithmarschen Bight

By JORT WILKENS and ROBERTO MAYERLE

Summary

In this paper a validated process-based model for the simulation of medium-scale morphodynamics (WILKENS, 2004; WILKENS and MAYERLE, 2004; JUNGE et al., in this volume) is applied to investigate the significance of both natural and anthropogenic influences in the central Dithmarschen Bight on the German Wadden Sea coast. Medium-scale morphodynamics are here defined as changes on the scale of tidal channels, tidal flats and sand banks.

Simulations involving the activation of one or more natural driving forces due to e.g. tidal action, swell waves, wind and locally-generated wind waves were carried out covering a two-year period. A definition of the strength and character of these forces, i.e. associated with tidal range, wave heights and directions, wind velocity and direction, was based on the conditions that were found to be representative for medium-scale morphodynamics (WILKENS, 2004). By comparing the resulting morphological changes it was possible to determine a distribution of the significance of each of the investigated forces. It could be shown that tidal action plays an important role over the entire study area whereas swell influences only the western-most part, and the effects of locally-generated waves are significant mainly in the centre. Typical behaviour of medium-scale morphological features could be related to one or more of these forces.

The influence of storm events on the morphodynamic model results was investigated on the basis of a ‘real time’ hindcast of a well-documented severe storm in the south easterly part of the German Bight. The boundary conditions were determined with the aid of a sequence of nested and coupled models for flow, waves and sediment transport, starting from a model for the entire North Sea. This approach yielded hydrodynamic results that were in good agreement with available water level and wave measurements. The computed medium-scale morphological changes due to the storm event were found to be rather limited with respect to the average yearly changes.

The computed morphological changes under medium-scale representative conditions were found to be clearly different in character from average medium-scale changes and less than 10 % of computed yearly changes in terms of magnitude. The influence of two land reclamations in 1972 and 1978, respectively, was assessed by evaluating the model results of three consecutive morphodynamic simulations each covering a period of approximately ten years. An analysis of volumetric changes in the inner Meldorf Bight, from which land was reclaimed, showed a tendency towards the development of a new dynamic equilibrium of its medium-scale morphodynamics.

Zusammenfassung

In diesem Beitrag wird ein validiertes, prozess-orientiertes Modell für die Simulation mittelskaliger Morphodynamik (WILKENS, 2004; WILKENS and MAYERLE, 2004; JUNGE et al., diese Ausgabe) beschrieben, mit dem die Signifikanz der natürlichen und anthropogenen Einflüsse in der zentralen Dithmarscher Bucht im Deutschen Wattenmeer untersucht werden soll. Mittelskalige Morphodynamik ist hier definiert als Änderungen in der Größenordnung von Prielen, Watten und Sandbanken.

Simulationen deckten einen Zeitraum von 2 Jahren ab, unter Berücksichtigung einer oder mehrerer natürlicher Antriebskräfte, d.h. Tiden, Wellen und Wind. Durch Vergleiche der morphologischen Änderunge konnte bestimmt werden, in welchen Gebieten welche Antriebskräfte am bedeutendsten waren. Es wurde gezeigt, dass die Tide im gesamten Gebiet einen signifikanten Einfluss auf die Morphodynamik hat; Dünung ist jedoch nur im äußersten Westen von Bedeutung und örtliche Windsee spielt in der Mitte des Gebietes eine Rolle. Die typische Dynamik der mittelskaligen morphologischen Einheiten konnte mit einer oder mehreren Antriebkräften in Beziehung gesetzt werden.

Die Bedeutung von Sturmereignissen wurde auf der Basis einer ‚Echtzeit'-Simulation eines ausführlich dokumentierten Sturmes in der südöstlichen Deutschen Bucht untersucht. Die Randbedingungen wurden bestimmt mit einer Kette von gekoppelten Modellen für Strömung, Wellen und Sedimenttransport, wobei mit einem Modell für die ganze Nordsee angefangen wurde. Dieser Ansatz lieferte hydrodynamische Ergebnisse welche eine gute Übereinstimmung mit verfügbaren Wasserstands- und Seegangsdaten zeigten. Die berechneten mittelskaligen morphologischen Änderungen waren relativ klein im Vergleich zu den mittleren jährlichen Änderungen.

Die berechneten morphologischen Änderungen zeigten ein unterschiedliches Verhalten im Vergleich zum durchschnittlichen mittelskaligen Verhalten, wobei die Änderungen im Umfang weniger als 10 % der jährlichen Änderungen mit mittelskaligen repräsentativen Randbedingungen betrugen. Der Einfluss von zwei Landgewinnungsmaßnahmen wurde mittels einer Volumen-Analyse der Modell-Ergebnisse dreier aufeinander folgender morphodynamischer Simulationen für Zeiträume von je etwa zehn Jahren untersucht. Es wurde eine Tendenz zu einem dynamischen Gleichgewicht der mittelskaligen Morphodynamik in der Meldorfer Bucht festgestellt.

Keywords

Morphology, Medium-Scale, Morphodynamics, Modelling, Dithmarschen Bight, Meldorf Bight, Tidal Flats, Tidal Channels, Storm Event, Land Reclamation, PROMORPH, DELFT3D

Contents

1. Introduction

The present paper describes an investigation of the forces responsible for driving morphological evolution in the central Dithmarschen Bight, a tidally-dominated bight located in the southeast part of the German Bight. A calibrated and validated medium-scale morphodynamic model (WILKENS, 2004; WILKENS and MAYERLE, 2004; JUNGE et al., in this volume) was applied in the investigation. Medium-scale morphodynamics are here defined as changes on the scale of tidal channels, tidal flats and sand banks.

Various medium-scale conditions were defined for forcing the model over a simulation period of two years. By subsequent intercomparison of the model results it was possible to identify several areas with different dominating forces. The observed morphological changes from 1977 to 1999 are correlated to these dominant forces. The complex interactions between individual morphological features, such as e.g. tidal channels, tidal flats and shoals, were analysed considering the dominance of either tidal action, wave action or a combination of both. In addition, morphological development was interpreted in the context of land reclamation undertaken at the beginning of the investigation period, i.e. in 1972 and 1978. Considering the good performance of the applied morphodynamic model as well as the underlying individual process modules for flow (PALACIO et al., in this volume), coupled flow and waves (WILKENS et al., in this volume), and sediment transport (WINTER et al., in this volume), this study provides a good insight into the distribution of the governing processes in the investigated tidal flat area.

2. The Central Dithmarschen Bight

The Dithmarschen Bight, located between the Eider and Elbe estuaries in the southeast part of the North Sea, contains of a number of tidal channels and tidal flats. The bathymetry of the Dithmarschen Bight is shown in Fig. 1. The two major channels Norderpiep and Suederpiep join in the middle of the bight and continue as the Piep channel towards the east, which subsequently spreads over the shallow Meldorf Bight. Maximum water depths in the channels are of the order of 20 m, and up to 15 m near the western edge of the outer tidal flats, e.g. at Tertiussand.

The mean grain sizes of bed material mainly lie in the range of 80 µm to 200 µm whereas the grain diameters of much finer suspended sediment lie between 10 µm and 90 µm. The hydrodynamics of the area are characterised by a tidal range varying between 3.0 m and 3.5 m and maximum wave heights of up to 3.5 m along the western edge of the bight and 0.5 m in

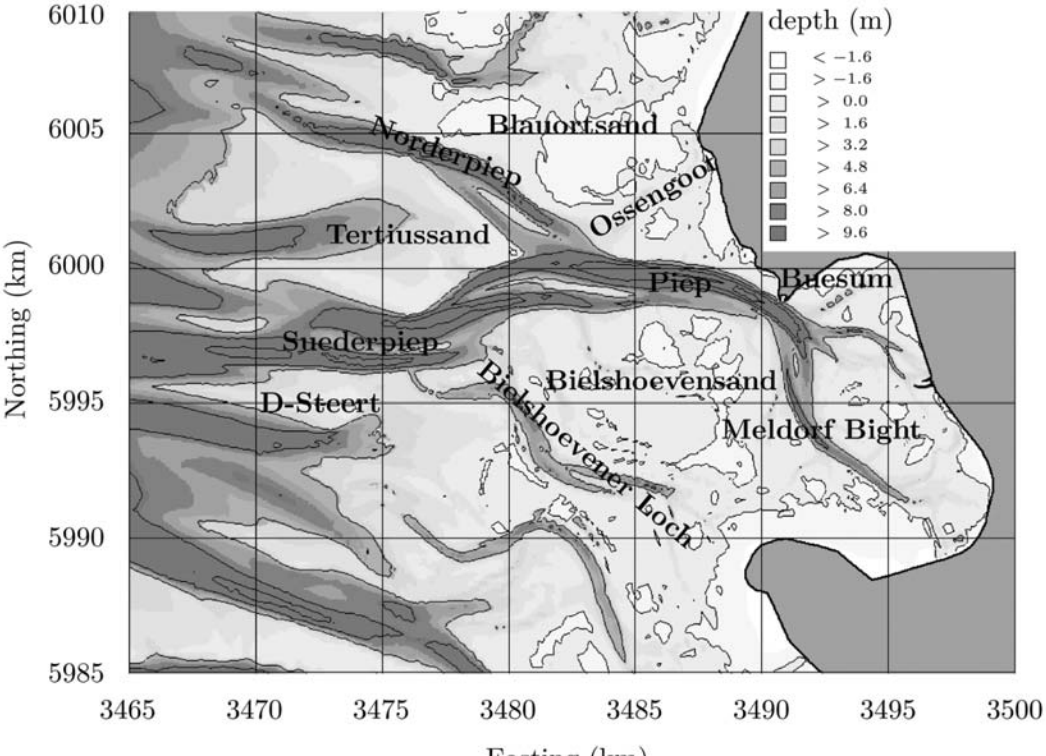

Fig. 1: Bathymetry of the central Dithmarschen Bight in 1977, indicating the main morphological features (WILKENS, 2004)

the eastern part. About 50 % of the study area is exposed during normal low tide. Applying the classification by HAYES (1979), the outer western part falls within the 'slightly tidally-dominated' and the more sheltered eastern part within the 'highly tidally-dominated' classifications, considering mean values of tidal range and wave heights, as indicated in Fig. 2.

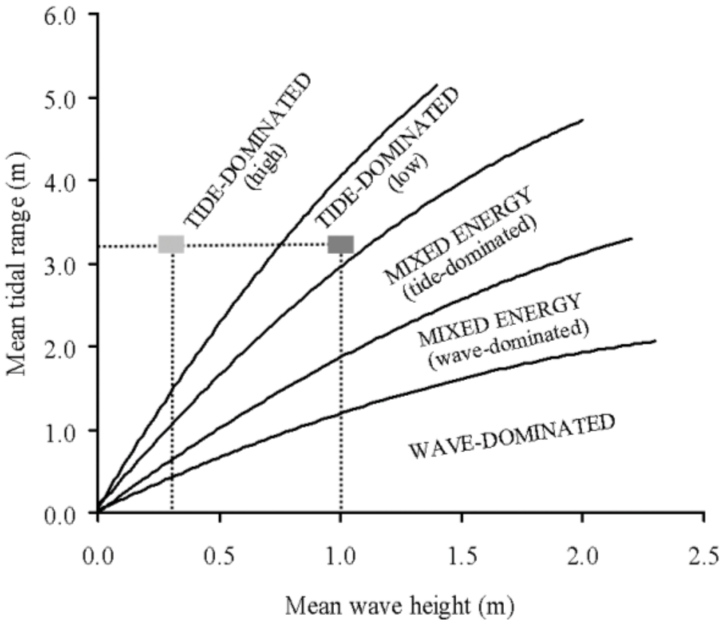

Fig. 2: Classification of tidal areas according to HAYES (1979) for mean tidal range and wave height conditions. The dark and light grey boxes indicate the western and eastern parts of the Dithmarschen Bight, respectively (WILKENS, 2004)

As shown in Fig. 3, two dikes were constructed in 1972 and 1978, respectively, along the eastern boundary of the Meldorf Bight for the purpose of land reclamation. As a result of land reclamation (11.5 km^2 in 1972 and a further 22.5 km^2 in 1978) the area of the Meldorf Bight was reduced by approximately 40 %, thereby decreasing the drainage area of the Piep tidal channel.

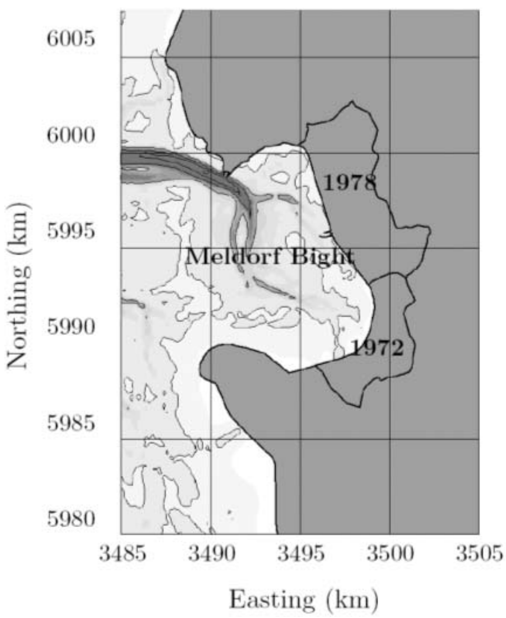

Fig. 3: Dike constructions in the Meldorf Bight in 1972 and 1978 (WILKENS, 2004)

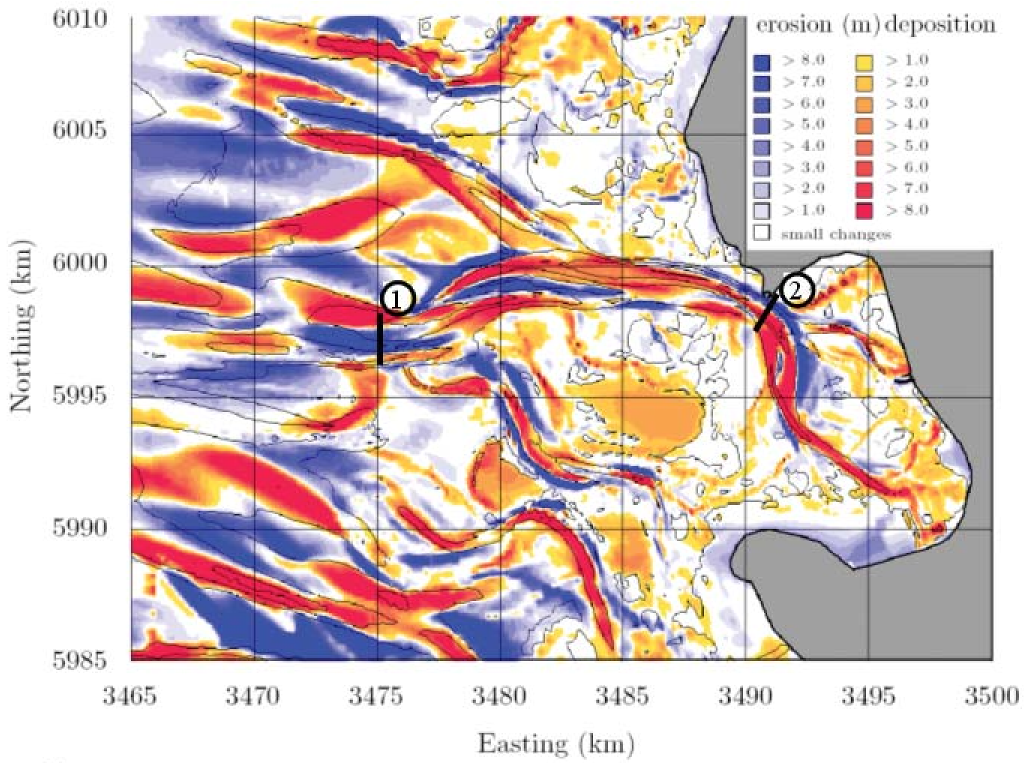

Fig. 4: Sedimentation and erosion in the Dithmarschen Bight between 1977 and 1999. Isolines shown for 1977 bathymetry (WILKENS, 2004). Transects of Figs. 5 and 6 are indicated (1 and 2 respectively)

Fig. 4 shows the observed morphological changes from 1977 to 1999 based on bathymetric measurements carried out by the Federal Maritime and Hydrographic Agency (BSH) in Hamburg and the Office of Rural Developments (ALR) in Husum. The changes on the eastern tidal flats should be interpreted with caution, however, as the density of bathymetric measurements in these areas is sparse. As clearly evident in the figure, the morphology is fairly dynamic. This may be related to the high tidal range and strong wave action along the edge of the outer tidal flats. The observed changes in depth of up to 8 m are mainly due to the migration of channels, flats and shoals. The western edge of the Tertiussand tidal flat is seen to retreat, with transportation of (part of) the eroded material towards the east. The expansion of this tidal flat towards the south and northeast is seen to cause further changes to the Norderpiep and Suederpiep channels. The Norderpiep migrates towards the northeast, as evidenced by parallel stretches of sedimentation and erosion.

Near the 3475 km Easting line the Suederpiep (transect 1 in Fig. 4) shows accretion along its northern bank combined with erosion in the middle of the channel. As may be seen in Fig. 5, this erosion is mainly characterised by a reduction in the size of the submerged bar in the middle of the channel. Erosion of the two sub-channels on either side of the bar is limited due to the presence of a layer of consolidated, fine-grained material ('Dithmarscher Klei', see ASP NETO, 2004; RICKLEFS and ASP NETO, in this volume). The presence of the 'D-Steert' shoal just south of the Suederpiep channel prevents this channel from migrating southwards. This shoal also shows a landward migration, indicated by erosion on its western side and sedimentation on its eastern side. Increased meandering is evident at the S-shaped bend in the Suederpiep east of the 3475 km Easting line while erosion is observed along the northern bank bordering Tertiussand.

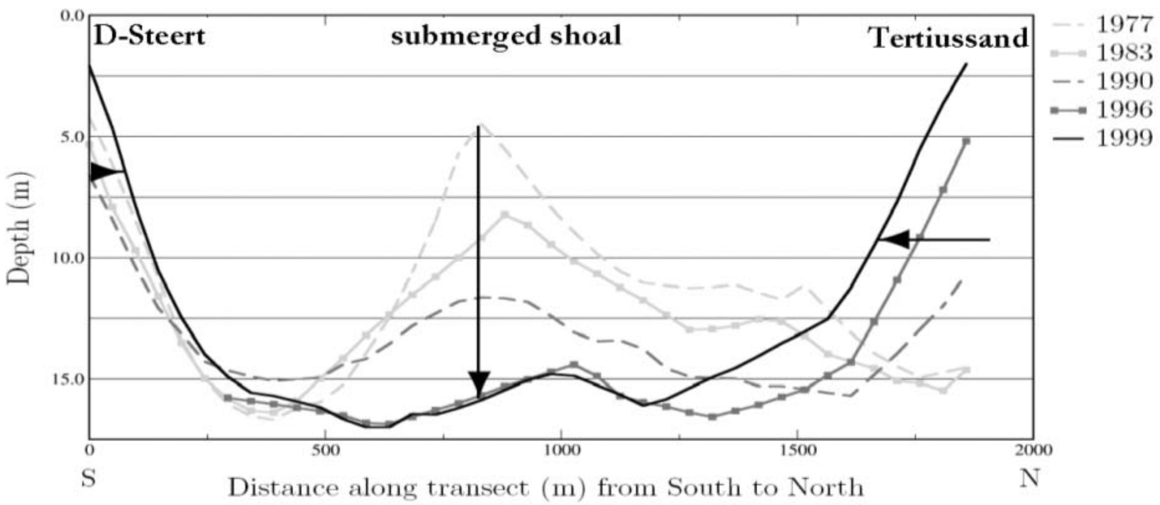

Fig. 5: Changes in the Suederpiep channel profile near 3475 km Easting

The parallel stretches of sedimentation and erosion in the Suederpiep indicate the northward migration of the submerged shoal in this channel. This is accompanied by accretion along the southern channel bank. Eastward of the merging of the Norderpiep and Suederpiep a general decrease in the channel depth is observed. This may be related to the reduced discharge owing to the decreased size of the drainage area resulting from land reclamation in the Meldorf Bight. Near Buesum, where the Piep bends towards the south, meandering of the channel occurs due to sedimentation along the inner bank and erosion on the north-eastern side of the channel. The harbour protection structures at Buesum are seen to limit the north-eastward migration of the channel bank on this side. As the 'Dithmarscher Klei' layer outcrops in the middle of the channel (ASP NETO, 2004; RICKLEFS and ASP NETO, in this volume) the channel cross-section can only be maintained by a steepening of the north-eastern bank, as shown in Fig. 6 (transect 2 in Fig. 4). An eastward migration of the Piep channel is observed south of Buesum. This is accompanied by an overall sanding-up of the minor channels in the Meldorf Bight with general accretion on the tidal flats in this area. It is likely that both effects are a result of the reduced drainage area caused by land reclamation.

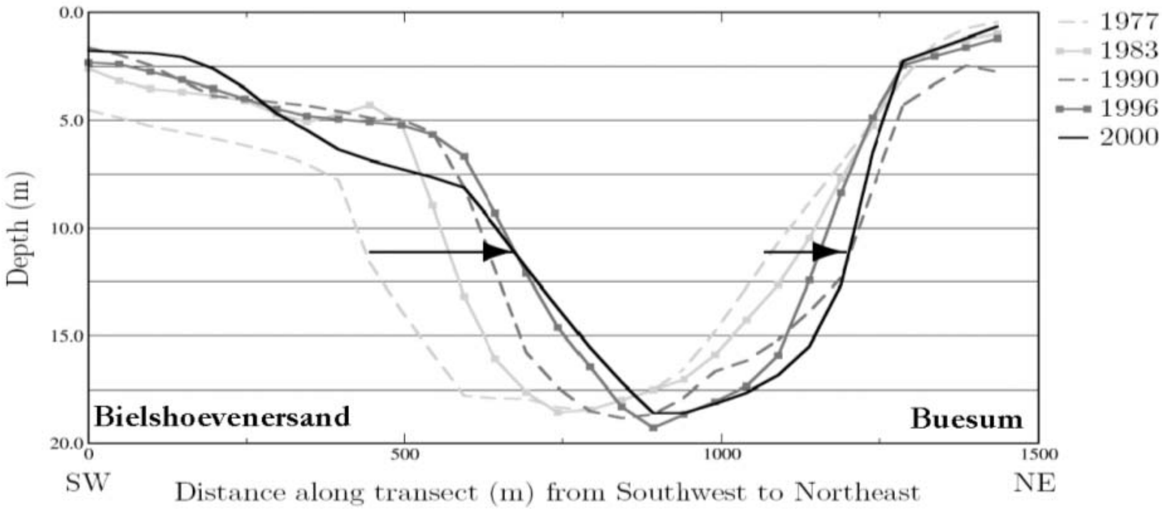

Fig. 6: Changes in the Norderpiep channel profile near Buesum

3. The Morphodynamic Model

The morphodynamic model applied in this investigation was calibrated and validated on the basis of over 20 years of bathymetric measurements. The morphological evolution during medium-scale periods of up to ten years was simulated to evaluate and improve model performance. A comparison between model results and measurements was made on the basis of a visual comparison of sedimentation and erosion patterns as well as a volumetric analysis of several sub-domains. This is described in detail in WILKENS (2004) and JUNGE et al. (in this volume). The model was set-up using the Delft3D modelling system developed by Delft Hydraulics in the Netherlands (ROELVINK and VAN BANNING, 1994).

Following coupling of the process modules for flow, waves and sediment transport, the morphodynamic 'shell' was defined. Input filtering and model reduction is performed in the morphodynamic shell. Forcing of the model with respect to representative tidal, wave and wind climates conditions is determined in the input filtering procedure. These conditions are imposed on the open boundaries of the process modules, i.e. the free surface and the lateral boundaries towards the open sea. Model reduction is achieved by morphodynamic time-stepping, i.e. the results of a single tidal cycle are extrapolated over a varying time step based on model stability criteria. These approaches significantly speed up morphodynamic simulations while conserving realistic model results of good quality. For details the reader is referred to WILKENS (2004) and JUNGE et al. (in this volume).

4. Dominant Medium-Scale Processes

The dynamics of the central Dithmarschen Bight are not directly influenced by the discharges of the rivers Elbe and Eider as extensive tidal flats separate these systems from the study area. Even under storm conditions there is no evidence that an interaction takes place over these shallow areas. The possible driving forces for morphological evolution are thus restricted to tidal action, wave action and the effects of wind. Wave action may be present due to incoming swell from remote areas or as a result of local wave generation. Wind effects may include the afore-mentioned wind-induced wave generation as well as the forcing of wind-driven currents. The enhanced wave action and currents may initiate additional sediment transport and change the patterns of sediment dynamics.

Model sensitivity studies have shown that although wind-driven currents may develop on the shallow tidal flats, the effect of wind-driven currents on medium-scale morphodynamics is rather limited. Attention was thus focussed on the morphodynamic significance of tidal action, swell and locally-generated waves in the present study.

These forces and their effects may interact. For example, sediment brought into suspension by wave action may be transported by tidal currents. This interaction may result in significant morphological changes which would not otherwise have occurred through wave action or tidal currents alone. It was thus important in the model investigations to carefully consider which processes should be included in or excluded from the simulations in order to properly assess the significance of each of the processes under examination.

5. Model Investigations and Results

Several morphodynamic simulations were carried out covering a period of two years. This period was determined to be sufficiently long to make initialisation effects negligible relative to the changes induced by the imposed forcing on a medium scale. Moreover, the computation time required for a two-year simulation was found to still lie within practical limits. The initial bathymetry for these simulations was based on bathymetric measurements made in 1977. This bathymetry also formed the initial bathymetry for calibrating the morphodynamic model, thus enabling the results of a variety of sensitivity and calibration simulations to be confidently used for a more conclusive interpretation of the results of the simulations discussed in the following.

A comparison of computed sedimentation and erosion patterns served as a means of assessing the model performance. In the first instance a reference simulation was performed in which representative conditions determined from model calibration and validation simulations were imposed. The sedimentation and erosion patterns resulting from this reference simulation are shown in Fig. 7.

In the western part of the domain relocation of sediment can be seen both in the channels and on the tidal flats. The largest changes are generally along channel banks, indicating a change of slope or a migration of these banks. Towards the east, a gradual limitation of morphological changes to the channels is evident. In the Meldorf Bight east of Buesum (see Fig. 1) only slight sedimentation near the channels is seen, accompanied by erosion in the Piep channel.

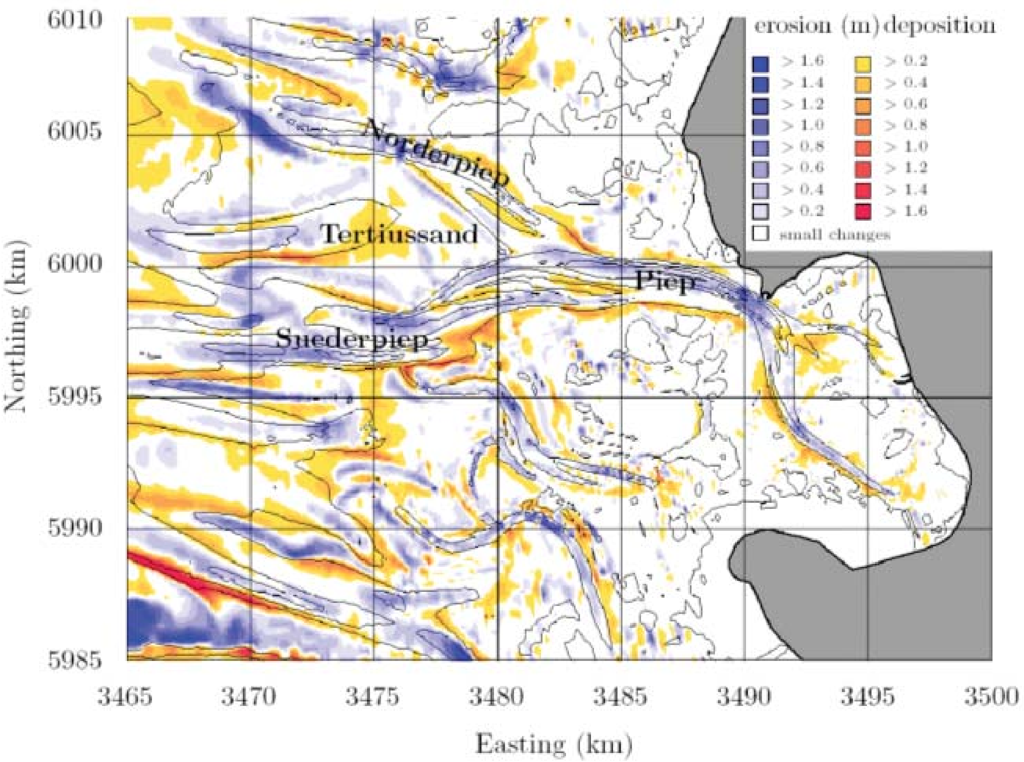

Fig. 7: Computed morphological changes from 1977 to 1979 based on morphologically representative tidal, swell and wind conditions (WILKENS, 2004). Isolines shown for 1977 bathymetry

5.1 Significance of Tidal Effects on Morphodynamics

With swell and wind forcing excluded from the boundary conditions in the morphodynamic simulation, the morphological changes shown in Fig. 8 result. These are caused by the tide alone and are characterised by high erosion in significant parts of the tidal channels and deposition of sediment on the tidal flats. The most prominent differences are indicated by the letters A to D in Fig. 8.

In order to compare the results of both simulations the positive and negative differences between the final bathymetries were represented using a graded colour scale, as shown in Fig. 9. Blue areas indicate that the computed sea bed is lower for the simulation without wind and swell than for the reference simulation (negative differences). It should be noted that the colour scale of Fig. 9 differs from that of the sedimentation and erosion plots of Fig. 8.

At location A the stretch of high erosion is replaced by accretion. The channel running through the Tertiussand tidal flat (see Fig. 1) shows enhanced erosion compared with the reference simulation results. At location B to the south of this channel overall accretion is observed, which is contrary to the erosion computed in the reference simulation. The southward expansion of Tertiussand near location B is no longer evident. At location C near the eastern edge of Tertiussand a progression of this tidal flat towards the northeast no longer occurs in the simulation without swell and wind action. The stretch of erosion given by the reference simulation is now replaced by sedimentation. An extension of Tertiussand towards the west also occurs due to increased deposition. In the neighbouring channels Norderpiep and Suederpiep a slight increase in erosion can be seen. Sedimentation at location D is found to decrease when wind and swell effects are excluded. This indicates that when swell and wind are absent as driving forces, the channels are larger than in the reference case.

From Fig. 9 it is clearly seen that the differences between the results of the two simulations are more pronounced in the western part of the study area. This result is in keeping with the fact that this area is closest to the seaward boundary and is thus mostly affected by wave action. In contrast to the latter, only small differences are found in the sheltered part of the investigation area to the east of the 3485 km Easting line. A general deepening of the tidal channels is observed throughout the study area whereas the submerged bars in the larger channels show accretion. The development or extension of a number of secondary channels is found to occur at various locations on the adjacent tidal flats.

Summarising the results, it is concluded that pure tidal forcing tends to enhance the development of channels as well as bars and tidal flats. The tidal currents are concentrated in the channels, where they encounter the least resistance due to bottom friction. This means that relatively high shear stresses develop in the channels, thus causing them to deepen. In contrast to this, accretion tends to occur in the remaining shallow areas where shear stresses are far lower. Moreover, the absence of wave attack along the western tidal flats enables them to extend in the seaward direction. Owing to the virtual absence of differences between the simulation results in the most easterly part of the study area it is concluded that this part is tidally-dominated.

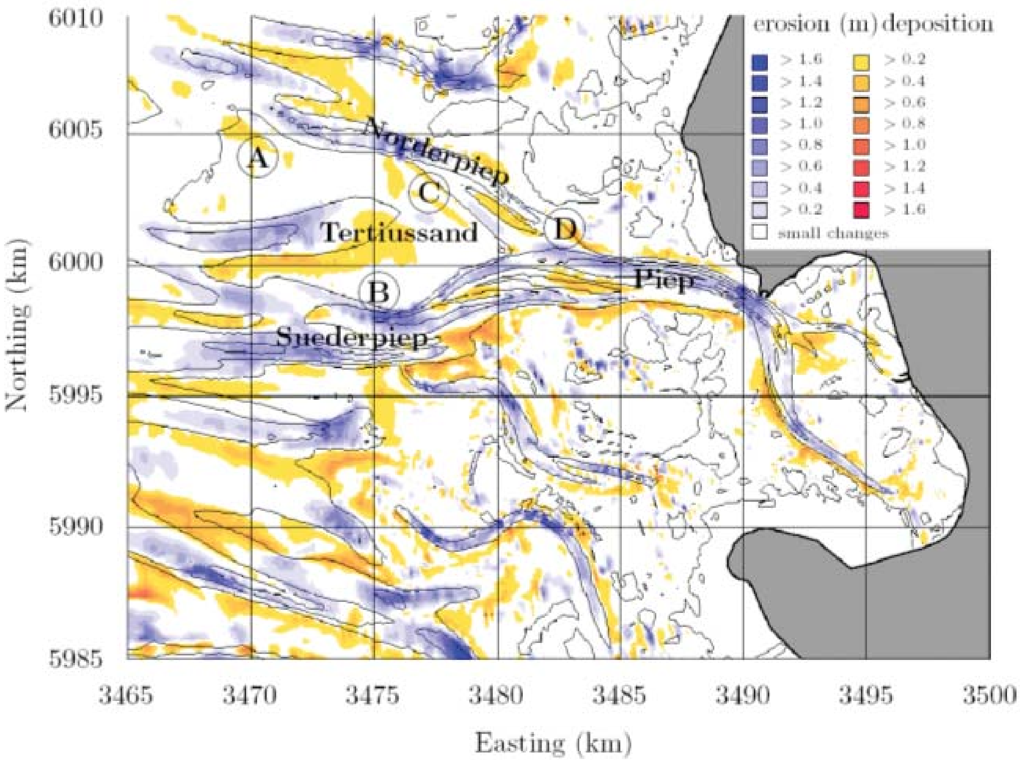

Fig. 8: Computed morphological changes from 1977 to 1979 – tides only. Isolines shown for 1977 bathymetry

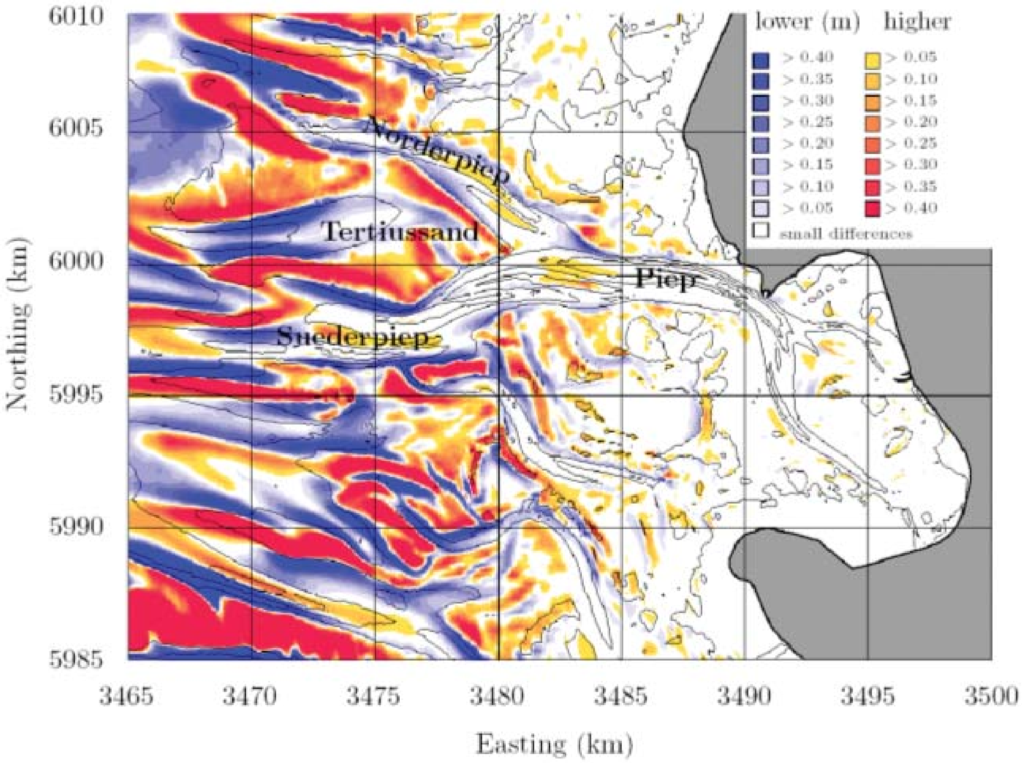

Fig. 9: Differences between the final bathymetries of the reference simulation and the simulation without imposed swell and wind conditions. Negative differences between the latter and former are indicated in blue. Isolines shown for 1977 bathymetry

5.2 Significance of Swell Effects on Morphodynamics

In order to evaluate the significance of imposed swell conditions the results of the simulation without swell (i.e. with tidal and local wind forcing only) were compared with the results of the reference simulation. Similar to the previous investigation, the resulting sedimentation and erosion patterns were compared. These are shown for the simulation without swell in Fig. 10. Adopting the same graded colour scale representation as in the previous subsection, the differences in the final bathymetries are shown in Fig. 11.

As may be seen in Fig. 10, the erosion near location A is now replaced by accretion. Near location B on the north-western side of Tertiussand a similar effect is observed; compared to the reference simulation, in which erosion was computed at this location, a large patch of sedimentation is now evident. The narrow stretch of erosion along the Norderpiep channel computed in the reference simulation is now reduced in size. In the Norderpiep itself far more erosion is computed in the simulation without swell. The progression of the edge of Tertiussand in the north-eastern direction is not distinguishable in Fig. 10. Less erosion is seen directly east of location C while the erosion computed in the reference simulation west of location C has completely disappeared. The southward migration along the southern edge of Tertiussand obtained under reference conditions is no longer present in the results of the simulation without swell.

Differences between the final bathymetries (Fig. 11) are only found in the western part of the study area. It is also noted that the part of the study area in which differences now occur (approximately along the 3480 km Easting line) is shifted further westward compared to the simulation results with tidal forcing only (cf. Fig. 9).

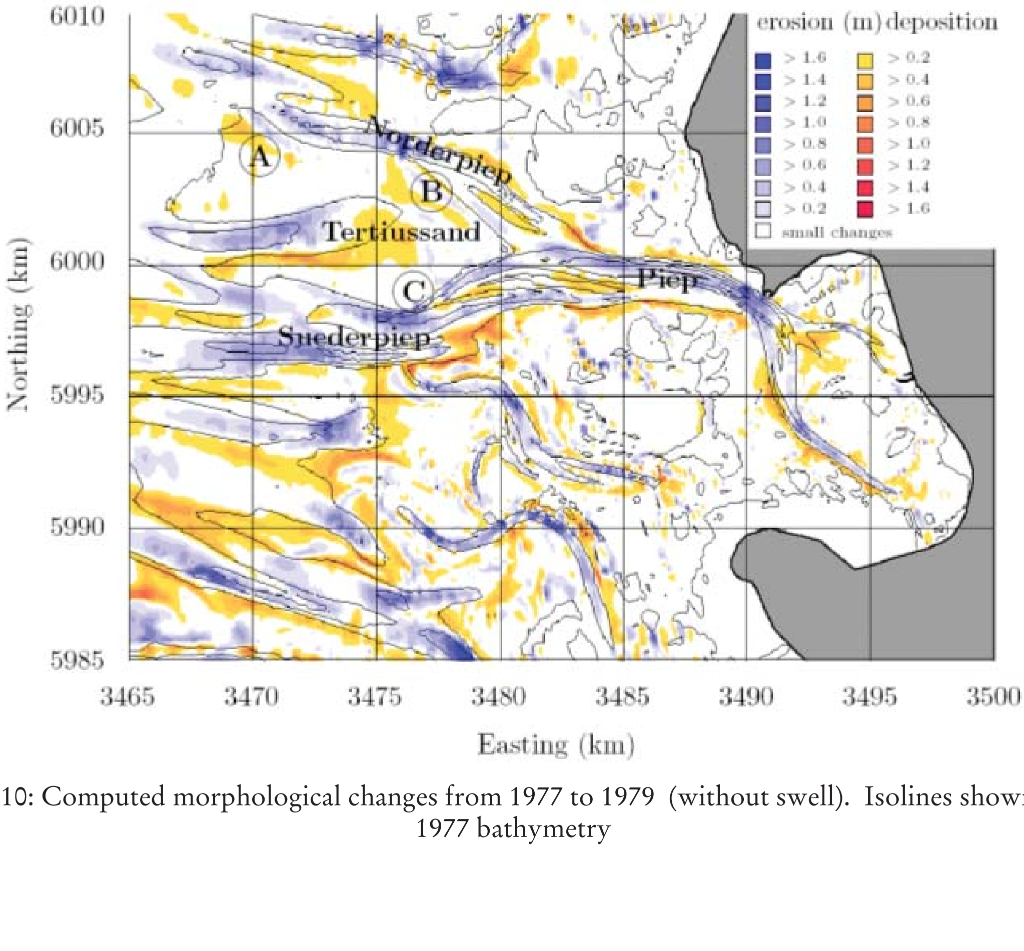

Fig. 10: Computed morphological changes from 1977 to 1979 (without swell). Isolines shown for 1977 bathymetry

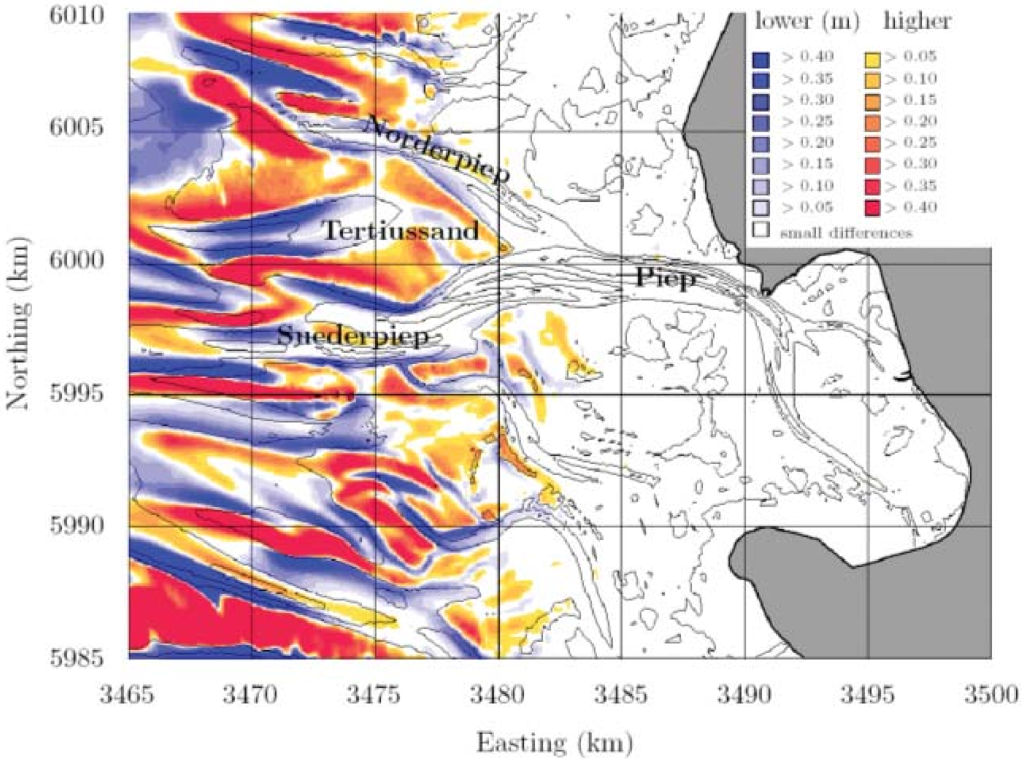

Fig. 11: Differences between the final bathymetries of the reference simulation and the simulation without imposed swell. Negative differences between the latter and former are indicated in blue. Isolines show for 1977 bathymetry

Summarising the results, it may be concluded that swell mainly influences the morphodynamics of the western part of the investigation area, particularly in the region of Tertiussand and its adjacent channels. This result is not surprising, as it is known from observations that most swell waves break on the outer tidal flats. The effects of swell are mainly evidenced by a reduction in height of the shallower areas combined with a reduction in depth of the neighbouring deeper areas. It would appear that sediment is stirred up by swell mainly in the wave-breaking zones where depths decrease rapidly, and then transported to deeper areas by tidal and wave-induced currents.

5.3 Significance of Local Wind Effects on Morphodynamics

In order to investigate the significance of local wind on the morphodynamics of the study area a simulation was carried out in which the local wind was greatly reduced compared to the representative conditions imposed in the reference simulation. It was necessary to impose a very mild wind climate for stability reasons, especially regarding swell wakes behind dry shoals or tidal flats. As local wind conditions are imposed in both the flow and wave modules, the reduced wind climate affects wind-induced currents as well as local wave generation. Further effects may be expected due to influencing of the incoming swell waves. The resulting sedimentation and erosion patterns over the two-year simulation period are shown in Fig. 12. Fig. 13 shows the differences between the final bathymetries of the reference simulation and the simulation without local wind. As before, the areas coloured in blue indicate negative differences in seabed levels between the simulation without local wind and the reference simulation.

The main differences on Tertiussand are the slightly lower depositions near locations A and B, and the reduced erosion along its north-western and south-eastern edges. Several less pronounced differences are found along the main channels. The Norderpiep shows less sedimentation along its north-eastern bank while the Suederpiep exhibits less sedimentation along its southern bank. A comparison of the final bathymetries shown in Fig. 13 reveals that the differences are mainly confined to the middle of the investigation area. Furthermore, these differences are much smaller than those observed in the difference plots of the previous Sections (cf. Fig. 9 and Fig. 11).

Summarising the results, it is concluded that local wind has a relatively limited effect on the morphodynamics of the study area, being mainly restricted to the middle of the domain between the 3475 and 3485 km Easting lines. The fact that the model results on the eastern tidal flats bordering the Piep channel are not appreciably different indicates that the fetch in these areas is too small to produce significant wind-induced currents or local wave generation. Although this is true for the imposed representative tidal cycle, it is noted that this may not be true for significant water level set-up during storm surges. In the middle of the study area, however, where water depths are greater and fetches are longer, the above-mentioned wind-induced currents and waves do become important with regard to morphological evolution. Further towards the west, the influence of the local wind is again very limited. It would appear that the dominance of swell in this area is so large that the presence or absence of local wind does not significantly affect the model results.

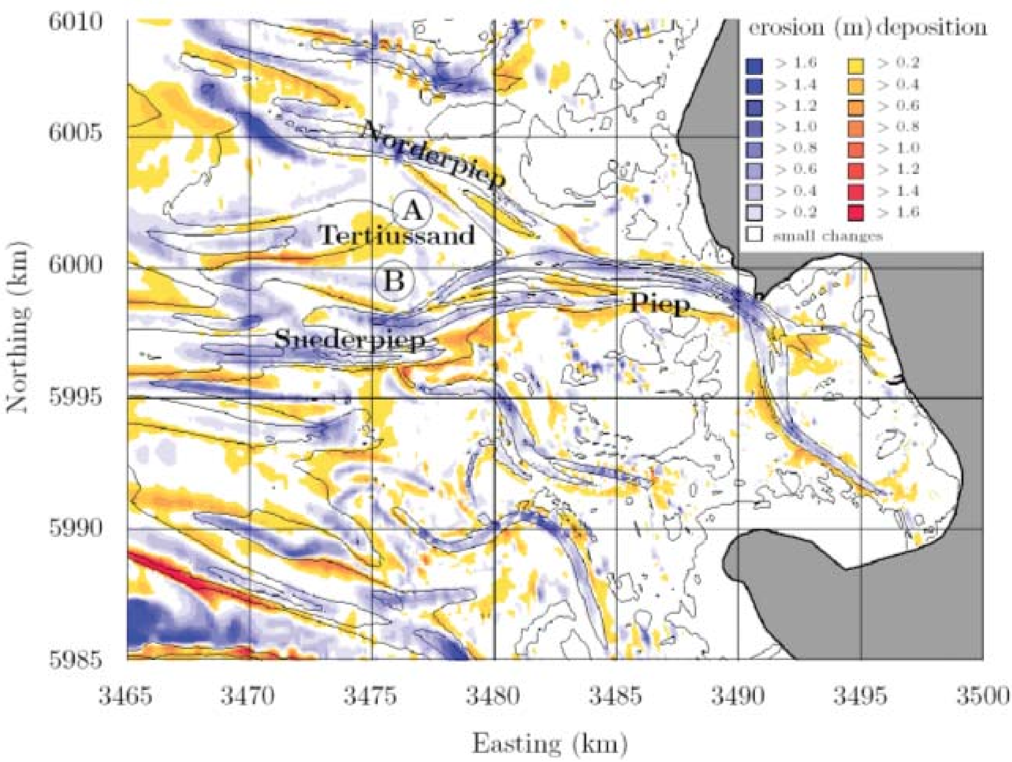

Fig. 12: Computed morphological changes from 1977 to 1979 (without wind). Isolines shown for 1977 bathymetry

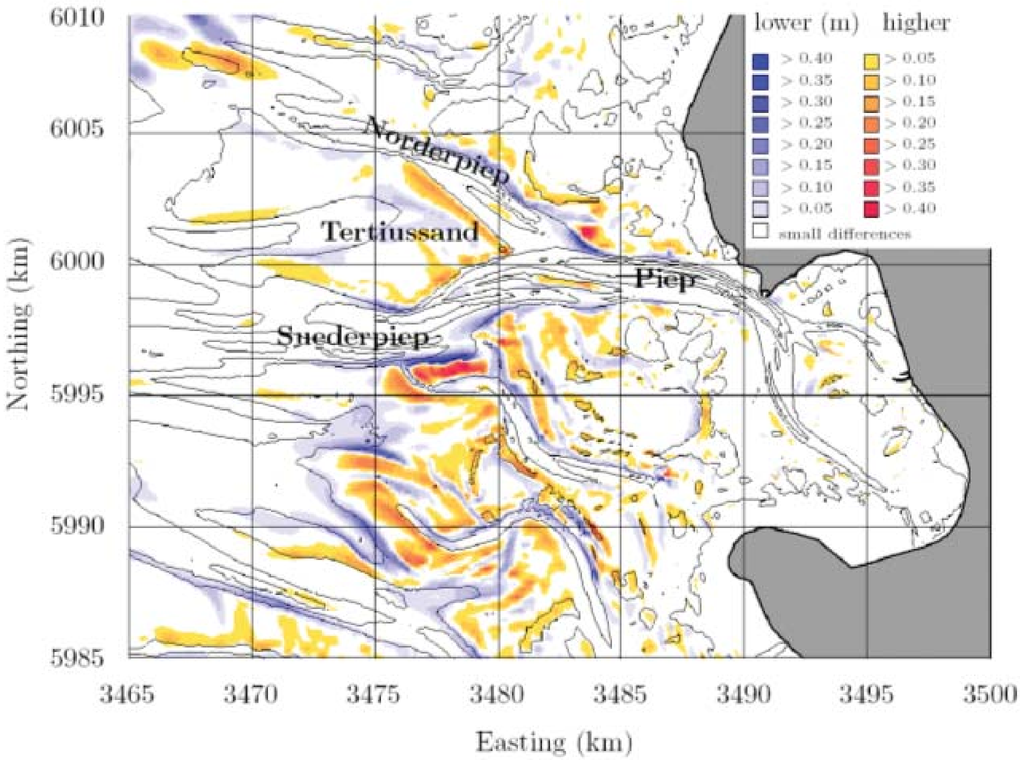

Fig. 13: Differences between the final bathymetries of the reference simulation and the simulation without imposed wind. Negative differences between the latter and former are indicated in blue. Isolines shown for 1977 bathymetry

5.4 Significance of Storm Events on Morphodynamics

In order to evaluate the significance of storms on the morphodynamics, an approach somewhat different from the afore-described approach has been used. To represent the hydrodynamic conditions during a storm the wind conditions over the entire North Sea have been taken into account. The nesting sequence of Fig. 14 was applied to generate open boundary conditions for the Dithmarschen Bight Model, where these wind conditions were imposed in each of the models.

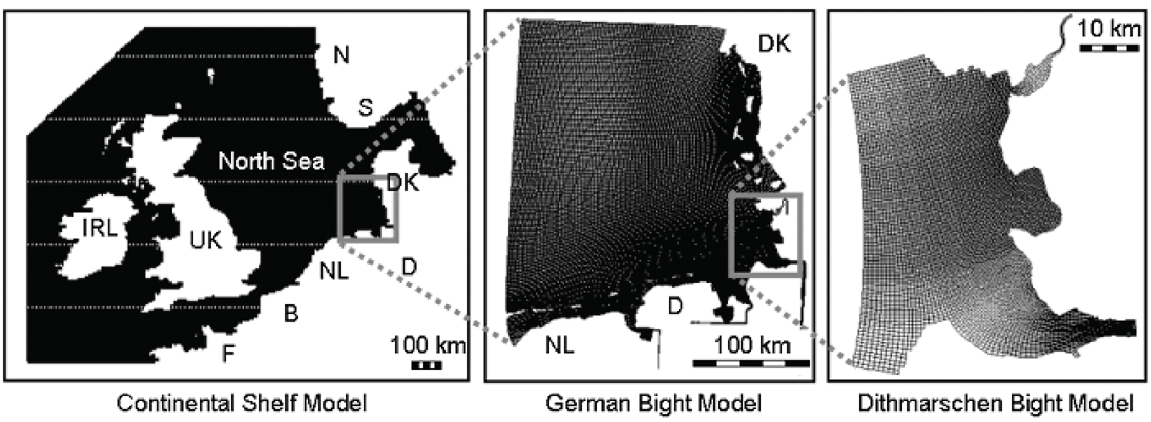

Fig. 14: Nesting sequence from the Continental Shelf Model towards the Dithmarschen Bight Model

Die Küste, 69 PROMORPH (2005), 1-420

The wind data have been taken from the synoptic PRISMA model (LUTHARDT, 1987). Starting from the German Bight Model, the flow models have been coupled to modules for waves and sediment transport. Nesting was applied for both modules to provide open boundary conditions for the Dithmarschen Bight Model. Morphodynamic updating has been limited to the latter model, leading to model results concerning the morphological changes induced during the considered storm period.

The morphological impact of the storm event has been compared to computed morphological changes over an entire year on the basis of morphologically representative boundary conditions (WILKENS, 2004; JUNGE et al., in this volume).

5.4.1 The Storm Event Anatol

The storm event selected for the evaluation was the relatively well-documented storm "Anatol" in the beginning of December 1999 that formed one of the most severe storms of the last decade (DWD, 2000). Anatol was a typical low pressure area that moved from west to east across the central North Sea and caused strong onshore winds combined with a storm surge of approximately 2.7 m above MHW at Buesum (refer to Fig. 1). The wind fields in Fig. 15 show the path and intensity of the storm across the North Sea. It shows increasing wind speeds after December 3rd, 09.00 UTC, with a gradual shift in direction from west-southwest to west. When the low pressure centre passes the wind velocities reach their maximum value of approximately 30 m/s (11 Beaufort) and the wind direction is west-northwest. Once the low pressure area has passed the wind velocities decrease and the direction changes back to west.

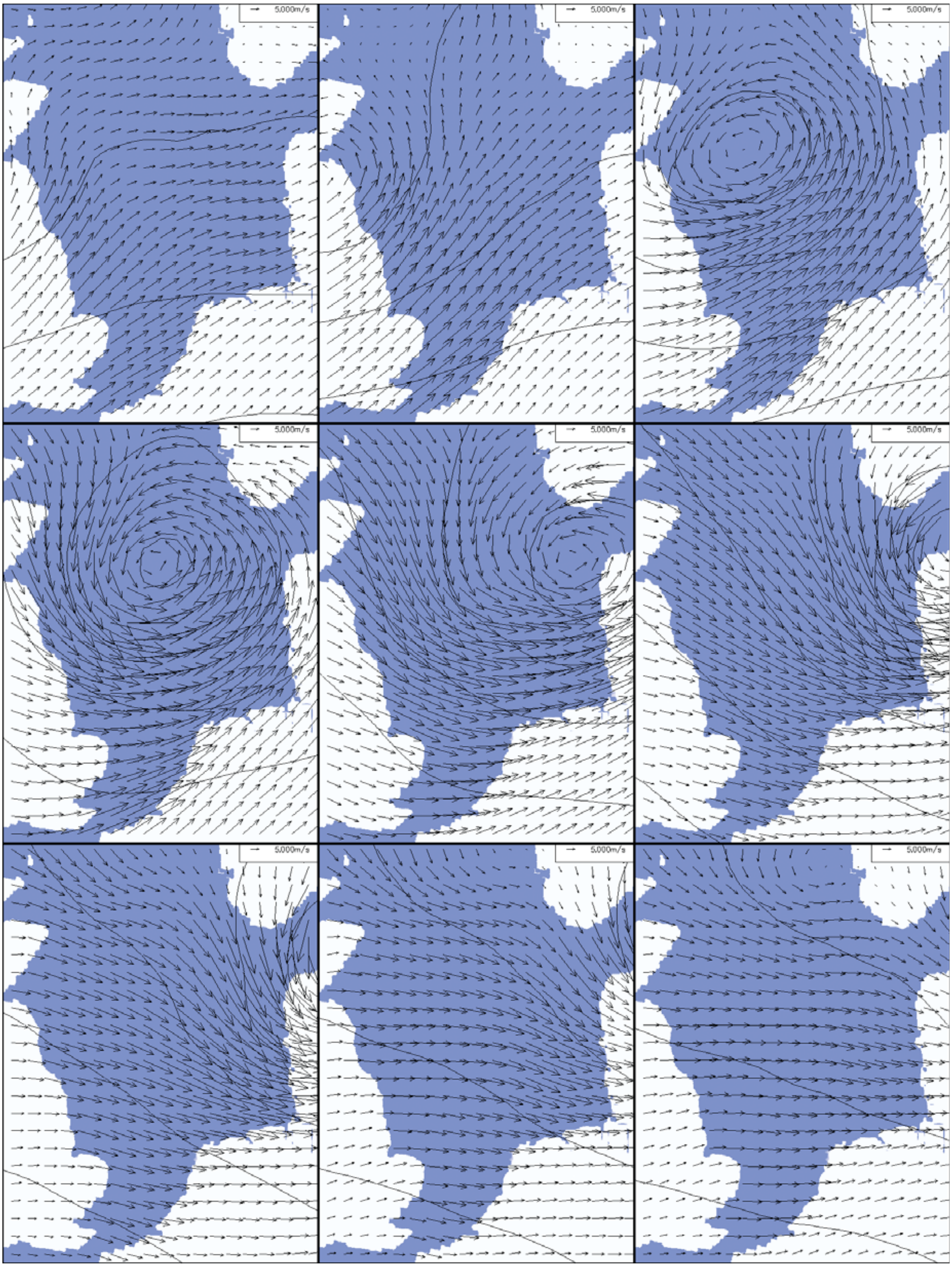

Fig. 15: Wind velocity fields over the North Sea during the storm Anatol in 3-hour intervals from 3 December, 03.00 until 4 December, 03.00 UTC (WILKENS, 2004). Based on synoptic data from the PRISMA model (LUTHARDT, 1987)

5.4.2 Hydrodynamics

Several records of wave heights and water levels were available during Anatol for the locations shown Fig. 16 (wave data from the Federal Maritime and Hydrographic Agency (BSH) in Hamburg and water level data from the Office of Rural Development (ALR) in Husum). The wave measurements were made outside the model domain of the Dithmarschen Bight model and have therefore only been compared to the results of the German Bight wave model. The observed and modelled wave heights are shown in Fig. 17. An under-prediction between 0.5 and 1.0 m can be seen around the peak wave heights; in general the wave heights are reproduced rather well, however. It should be noted that a stationary wave model has been used in this study, inherently leading to discrepancies as for a model domain with the extension of the German Bight an instationary model would generally be preferred. However, the results were deemed to be suitable for the purpose of this study.

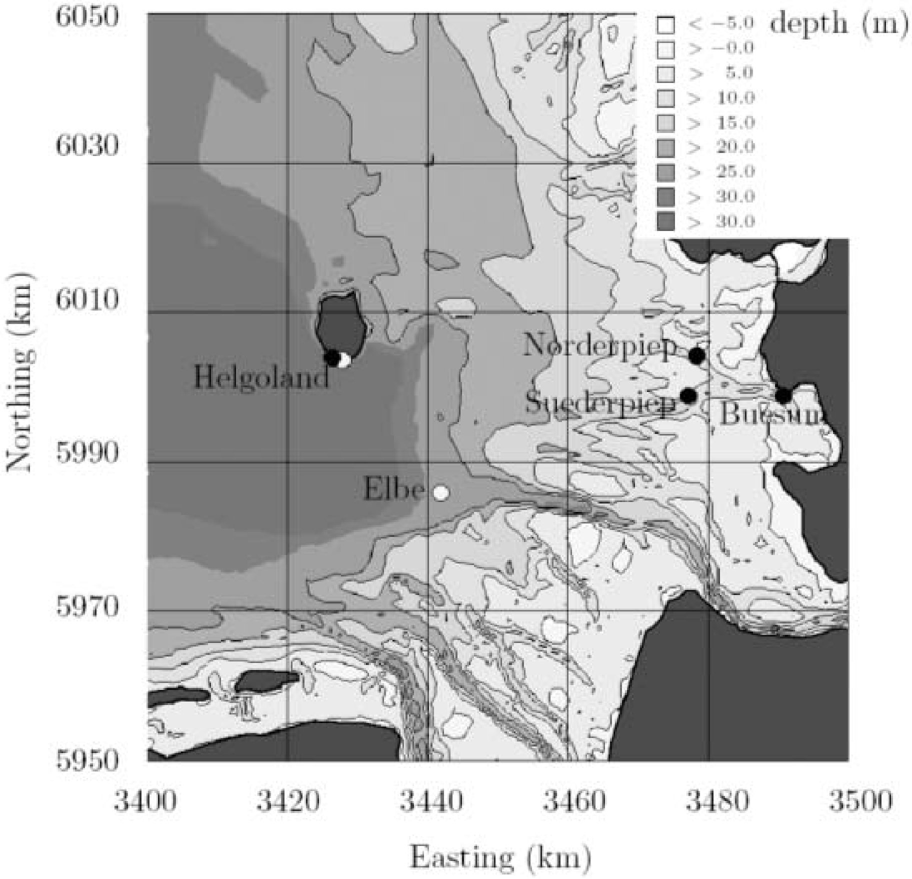

Fig. 16: Location of the wave buoys (white) and water level gauges (black)

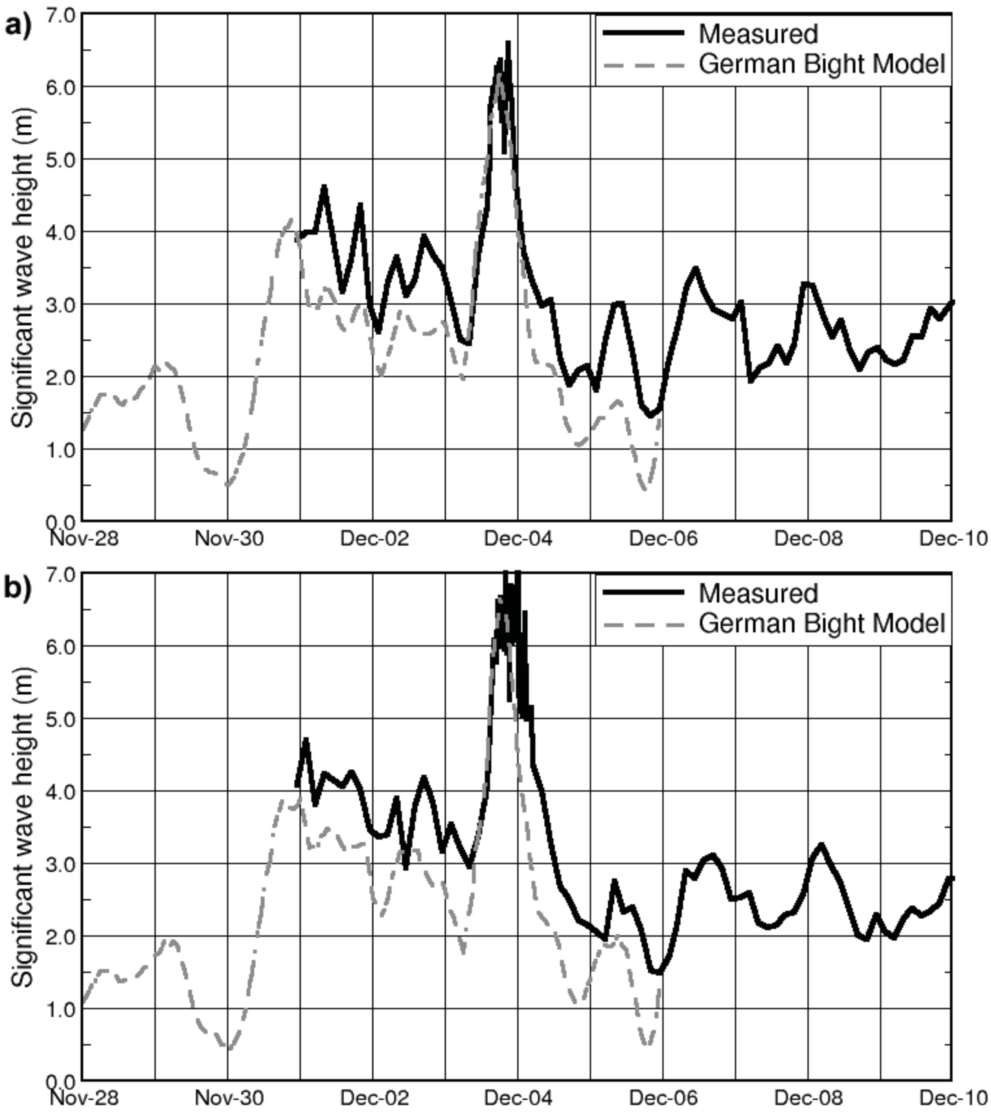

Fig. 17: Observed and computed wave heights at the a) Helgoland and b) Elbe buoys, using the German Bight model

Comparisons of the observed and computed water levels are shown in Fig. 18. It is seen that the storm surge is reproduced very well. Differences can be seen mainly for some of the troughs in the water level records and in some phase lags. The largest phase lag can be noted for the Suederpiep (Fig 18c). As one may see, the measured water level signal at this location is clearly ahead of those near Buesum and in the Norderpiep. Such a phase lag is especially unlikely between the Norderpiep and Suederpiep, both gauges being located at a similar distance from the edges of the tidal flats. The authors therefore suspect that an error occurred in the data processing for the Suederpiep data. The peak values of approximately 4.5 m are captured rather accurately, thus yielding the right volumes that enter and leave the study area apart from the normal tidal prisms.

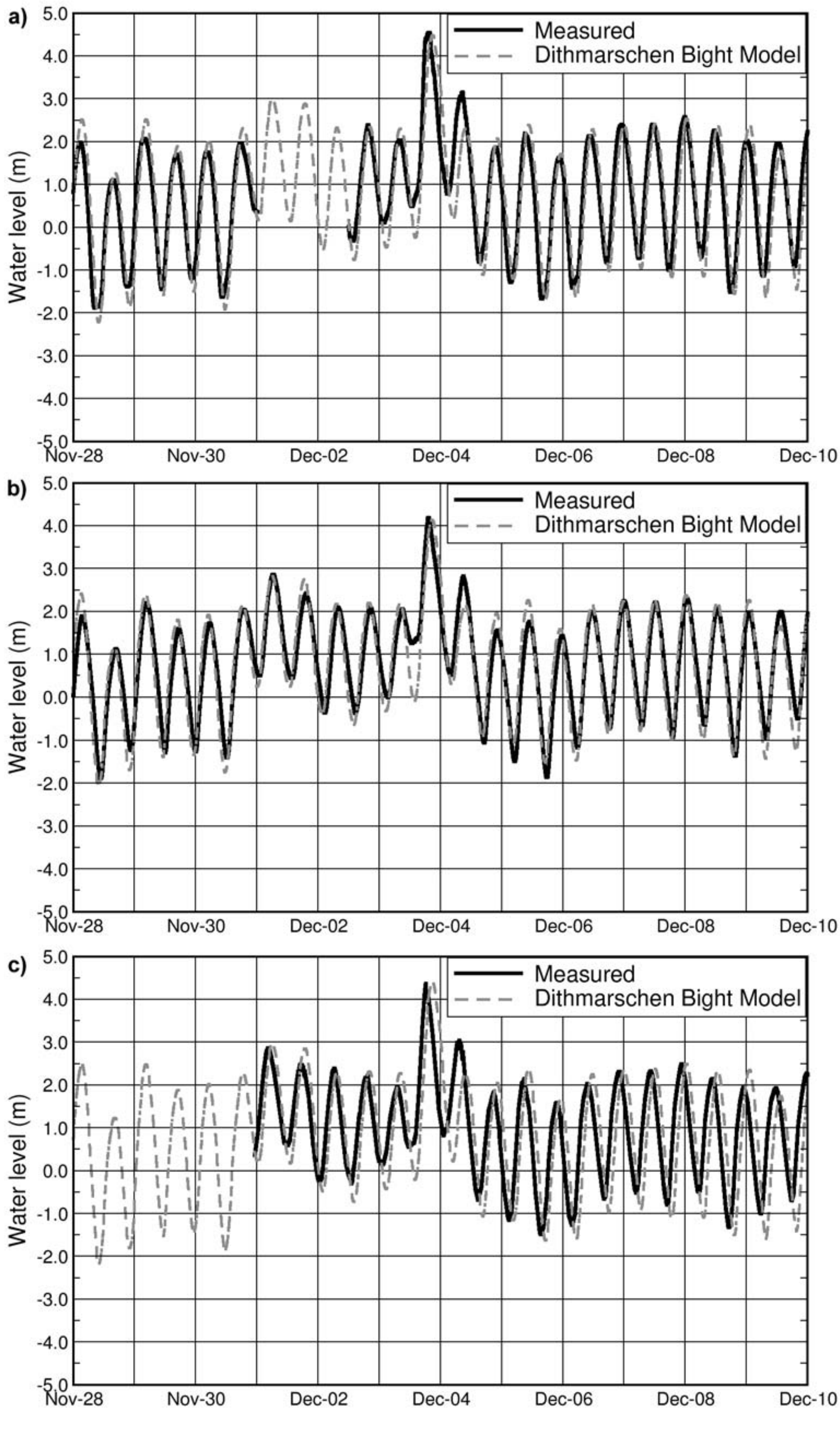

Fig. 18: Observed and computed water levels at gauge stations a) near Buesum, in the b) Norderpiep and c) Suederpiep, using the Dithmarschen Bight model

5.4.3 Morphodynamics

The bed load and suspended load transports were computed on the basis of the above presented hydrodynamic model results. The model settings were taken from the validated medium-scale morphodynamic model (WILKENS, 2004; JUNGE et al., in this volume). The total simulation of the storm event was built up of a sequence of sub-simulations of one hour. In each sub-simulation the sequence of hydrodynamic, sediment transport and morphodynamic models has been executed, where the final results of each were used as initial conditions for the subsequent one. This led to a smooth morphodynamic simulation over the period from 30 November 0.00 UTC until 6 December 0.00 UTC. A warming-up period of five days was considered, preceding this simulation. The resulting patterns of sedimentation and erosion are shown in Fig. 19.

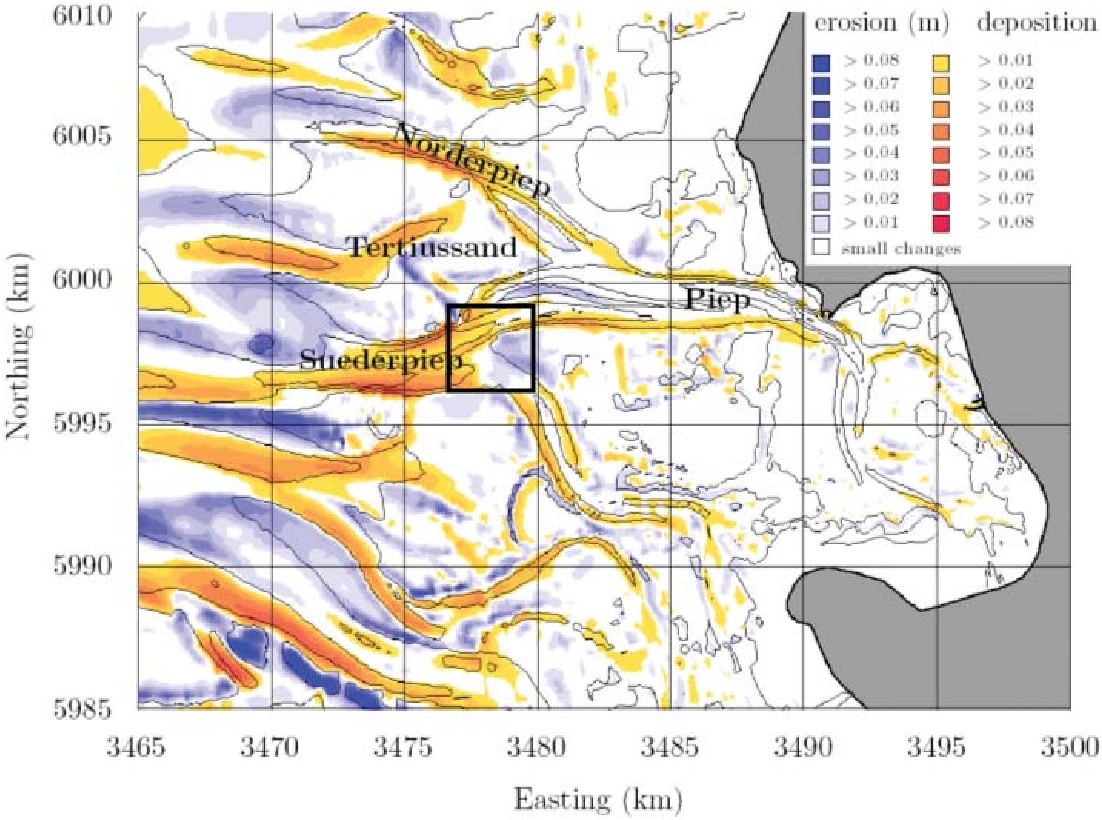

Fig. 19: Computed sedimentation and erosion during the storm period of six days (WILKENS, 2004). The square indicates the area investigated by WINTER et al. (2005)

The computed maximum morphological changes in the study area are within a range of approximately 40 mm over the six day-period, being notibly lower than expected for such a storm. Relatively strong sedimentation occurs in the channels Norderpiep and Suederpiep, as well as in the sub-channel on the western side of the tidal flat Tertiussand. Erosion is seen at the western side of the tidal flats and shoals, caused by the incoming swell waves. The sediment that eroded from these shallow areas was deposited in the neighbouring channels. In the channel Piep stretches of sedimentation can be seen along its banks. Interestingly, the storm event has little to no impact on the eastern part of the domain even though a storm surge of approximately 2.7 m above MHW occurred, which caused stronger currents and higher waves even in the shallower parts of the domain.

To assess the impact of the storm, the resulting morphological changes have been compared to those computed for an entire year with morphologically representative boundary conditions. These representative conditions were found to be optimal for computing the medium-scale morphodynamics in the calibration of the morphodynamic model, considering periods of ten years. The results of the simulation of the one-year period are shown in Fig. 20. It should be noted that the scaling of the graded colours differs by a factor of ten.

In general, a deepening of the tidal channels is seen, accompanied by stretches of accretion along the channel banks and on the majority of the submerged shoals in the channels Norderpiep, Suederpiep and Piep. The centre of Tertiussand shows sedimentation and the surrounding areas of this tidal flat show slight erosion. At the western edges of the tidal flats extended patches of sedimentation can be found. The mediocre imposed wave climate is thus too mild to cause a retreat of these tidal flats. The eastern part of the Piep and the Meldorf Bight show significant changes, with deepening of the channels and accretion in the shallower areas.

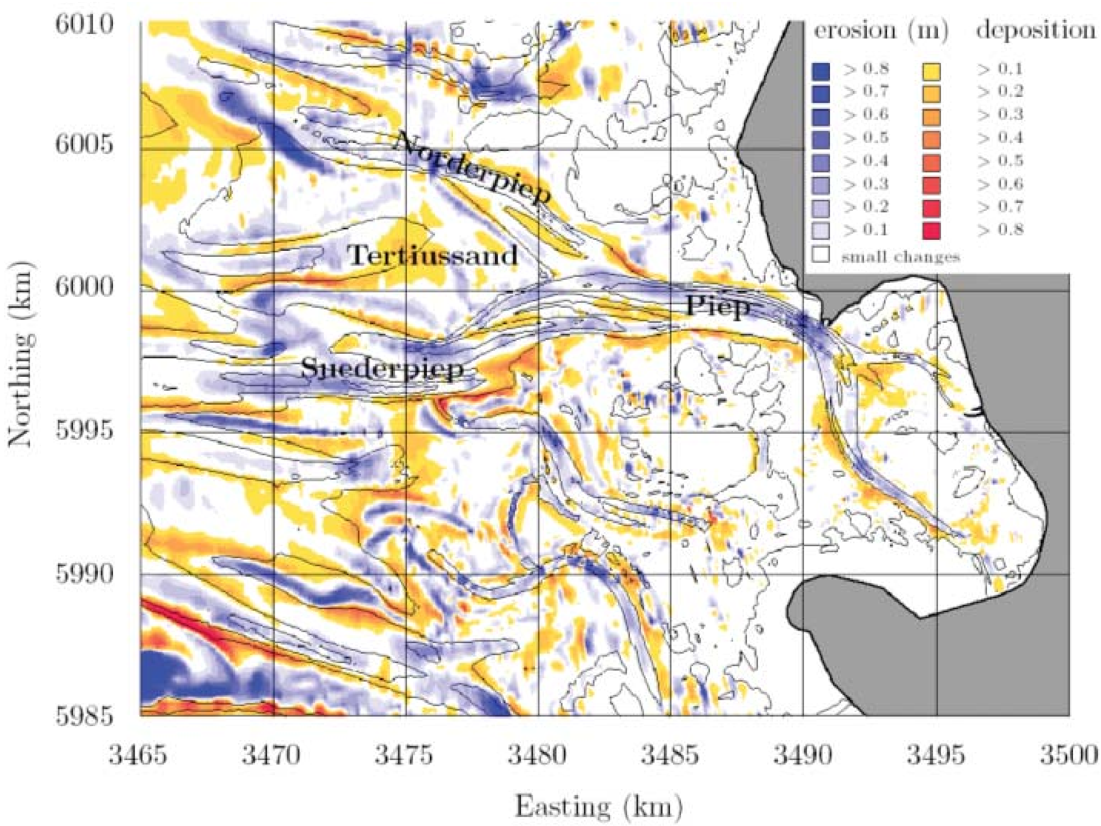

Fig. 20: Computed sedimentation and erosion for a one- year period with representative conditions (WILKENS, 2004)

Comparison of Fig. 19 and Fig. 20 shows that the magnitude of the computed morphological changes over an entire year is a factor ten larger than those computed for the storm event. The horizontal distribution of the areas of sedimentation and erosion is rather different, however. The severity of the imposed waves, their intrusion into the study area due to the storm surge and the current velocities induced by the increased water level changes at the beginning and end of the surge are the causes for these differences. Evidently, the simulated storm has a rather different impact on the area than the averaged, representative conditions. Elevated areas are eroded and deeper areas are filled up. The computed impact of the storm event is limited, however, with maximum changes generally below 0.05 m.

WINTER et al. (2005) presented an evaluation of the storm Anatol for a small scale area (4 km^2) at the southern bank of the Suederpiep on the basis of high resolution multi-beam echo sounder data. Three cross-sectional profiles, measured approximately one month before and two and a half months after the storm, respectively, were compared. This revealed local sedimentation in the channel up to 0.3 m and erosion of the tip of the tidal flat in the Southeast up to 0.25 m over a period of three months including the storm Anatol. For large parts of the investigated profiles the changes were below 0.10 m and therefore within the mentioned measurement accuracy. However, their results do evidence that locally larger morphological changes can occur than those seen in the model results presented here. With the limited spatial resolution of the medium-scale model it was not possible to reproduce these local changes. A model grid and bathymetric data with a higher resolution and perhaps a three-dimensional approach would be necessary for modelling such small-scale morphological changes.

6. Synthesis of the Results

Considering the findings of the previous section in combination it may be concluded that both the tide and swell have a large influence on the medium-scale morphodynamics of the study area. It has been shown that the tide is mainly responsible for initiating, maintaining, extending and migrating tidal channels, shoals, bars and flats. Without the influence of waves and, less significantly, local wind, these morphological features tend to become more pronounced. Along the mutual borders of these features, restrictions on their further extension naturally become established. When swell is introduced into the morphodynamic simulation, an equalising of these morphological features takes place. High-lying areas tend to erode whereas tidal channels tend to become partly filled with sediment. Furthermore, swell is found to be the main driving force responsible for the expansion of Tertiussand in the north-easterly and southerly directions as well as for erosion along its western extremity. Although local wind and wind-generated waves are shown to have a less pronounced influence on medium-scale morphological evolution, their influence cannot be ignored altogether.

The simulation of the storm event showed that even severe swell and wind conditions in combination with a storm surge do not significantly affect the eastern part of the domain. The exposed tidal flats and neighbouring channels in the west are indeed altered by such events. In contrast to general medium-scale trends in the morphodynamics, shallow areas are eroded and channels show sedimentation. However, the model results suggest that the extent to which the medium-scale morphology is changed by a single storm is generally less than 10 % of yearly bathymetrical changes. On a much smaller morphological scale larger changes may occur.

The afore-mentioned findings do not fully comply with the dominance of hydrodynamic forces on morphodynamic evolution, as would be expected according to the classification of HAYES (1979) given in Fig. 2. Instead of being only slightly tidally-dominated, the western part of the study area should rather be defined as a mixed-energy zone, as swell plays an important role in the development of the investigated Tertiussand tidal flat as well as (indirectly) its adjacent channels. As the deep channels Norderpiep and Suederpiep are also maintained in the reference simulation, a tidally-dominated mixed-energy description appears to be more appropriate. It has already been shown that swell and local wind effects have no appreciable influence on the results of the morphodynamic simulations presented for this part of the area of investigation. It is thus concluded that a classification of the eastern part of the study area as highly tidally-dominated (see also Fig. 2) agrees well with model results.

In overall terms it may be stated that the application of a validated morphodynamic model provides a valuable insight into the underlying morphodynamic driving forces and serves as a powerful tool in this respect for verifying and improving initial estimates based on empirical assumptions.

7. Morphological Response to Land Reclamations

The morphological changes calculated from field surveys in the Meldorf Bight presented in Section 2 indicate a general filling-up of the tidal (sub-)channels and an accretion of the tidal flats. Although the results for the tidal flats must be interpreted with caution due to the relatively poor data availability, a net import of sediment into the Bight is evident. This is most likely directly related to the land reclamations of 1972 and 1978 which led to reduced drainage area of the main Piep channel. Bearing in mind that the Meldorf Bight is highly tidally-dominated, as concluded in Section 6, the average import of sediment in the medium-term is relatively independent of the wind and wave climates. It should be noted that this is not necessarily true for storm conditions, which were not included in the analysis discussed in the previous section as only more moderate, representative conditions were considered.

The morphological response to land reclamation in the Meldorf Bight was investigated by performing simulations with the presented morphodynamic model. The medium-scale character of this model does not allow for a proper representation and analysis of the small-scale channels and gullies in detail. However, the model may be used to evaluate the behaviour of the Meldorf Bight as a whole. The study was thus limited to an evaluation of the relative changes of the wet volume below mean sea level (approximately German Normal Null). Any changes in the morphology above mean sea level were thus ignored, which is justified by the poor data coverage of especially the higher tidal flats.

These relative volumes are defined as:

$$V_{rel,i} = \frac{V_i}{V_{1977}} \times 100\ \%$$

with:

$V_{rel,i}$ relative wet volume of the Meldorf Bight below MSL in year *i*
V_{1977} wet volume of the Meldorf Bight below MSL in 1977
V_i wet volume of the Meldorf Bight in below MSL year *i*

Based on the simulation results of the validated morphodynamic model the relative volumes were determined for the periods 1977–1987, 1990–1999 and 1999–2009. These three periods were investigated for calibration, validation and model prediction, respectively, as discussed in WILKENS (2004), WILKENS and MAYERLE (2004) and JUNGE et al. (in this volume). For each period the model bathymetry at the beginning of the simulation was updated to comply with bathymetric measurements of the respective starting year in order to prevent excessive deviations from actual morphological developments (WILKENS, 2004). The relative volume was computed each year for the area shown in Fig. 21.

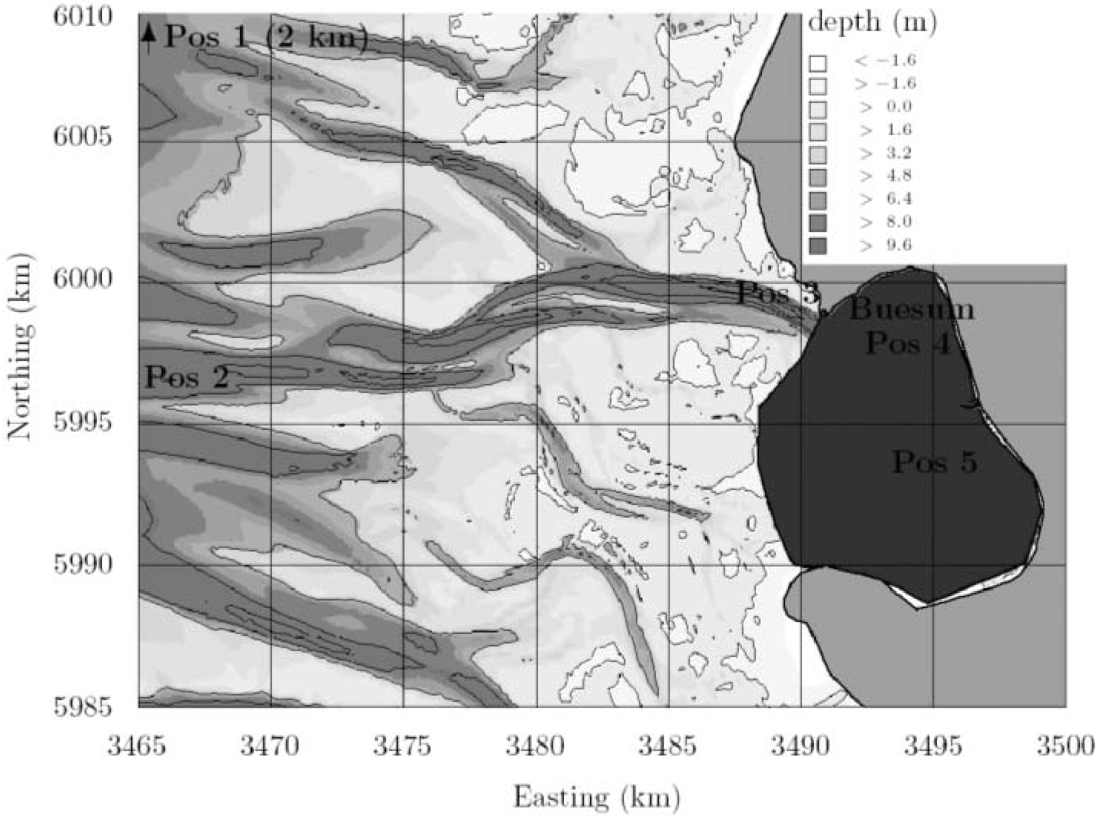

Fig. 21: The Meldorf Bight, as considered in the volumetric analysis

The results of the volumetric analysis are shown in Fig. 22. The values based on measurements indicate a gradual decrease in the wet volume of approximately 30 % between 1977 and 1999. The first 20 % of this reduction occurred between 1977 and 1990, followed by a clearly less-pronounced decrease during the subsequent decade. The decreasing rate of volume reduction during the latter period might indicate the approach to a state of (dynamic) equilibrium. However, the fluctuations over the investigation period do not permit any definite conclusions in this respect. The results of the three model simulations yield volume decreases of 7 %, 4 % and 0 % of the 1977 volume, respectively. An approach to actual bathymetric changes could only be achieved by updating the bathymetry at the beginning of each simulation according to corresponding observations. A perfect fit between the model results and the observed morphological evolution was not expected, however, since the morphodynamic model and its validation were based on the central tidal channel system rather than the inner Meldorf Bight. Nevertheless, the model results clearly predict a decrease in the wet volume and, more interestingly, a reduction in the rate of volume changes with time. The results of the model simulation from 1999 to 2009 predict a fairly stable wet volume in the Meldorf Bight, indicating that a state of equilibrium has been reached.

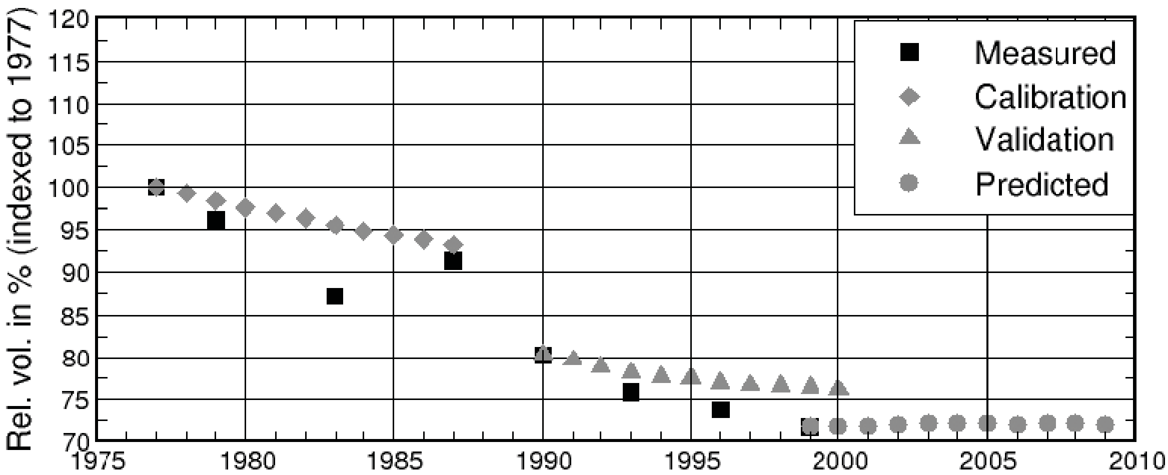

Fig. 22: Relative wet volume of the Meldorf Bight (WILKENS and MAYERLE, 2004)

Once the morphodynamics in the Meldorf Bight have attained a new equilibrium state, the import of sediment due to land reclamation will have come to an end. This new equilibrium state may well have an impact on the future development of the seaward tidal flats and channels, as they will no longer need to supply sediment to the Meldorf Bight in this respect. Independent of the latter, other processes may of course still lead to sediment exchange between both areas, e.g. the import of sediment to adapt to a rising mean sea level. As such, a state of dynamic equilibrium in the Meldorf Bight would appear to be a more realistic description.

Since the rates of volumetric changes were not reproduced too well in quantitative terms, the model in its current form cannot be used to draw conclusions about the adaptation time of the Meldorf Bight to land reclamations. However, the decrease in the observed wet volume reduction and the fairly stable volume predicted by the model for the simulation period 1999 to 2009 do indicate that the Bight is reaching, or has already reached, a new state of dynamic equilibrium.

8. Conclusions

The present study has shown that the validated morphodynamic model is a useful tool for investigating the driving processes responsible for morphological evolution in the study area. The fact that the individual process-based modules for tides, waves and sediment transport as well as the overall morphodynamic model were calibrated and validated increases the trustworthiness of the model results and the conclusions drawn from them. When applying the model for such studies, however, it is important to bear in mind the temporal and spatial scale for which the model has been validated.

On the basis of the model studies carried out in the present investigation it was concluded that the outer tidal flats are only slightly tidally-dominated whereas swell has a relatively high influence along the seaward boundary of the study area. This deviates from the well-known classification by HAYES (1979), according to which a highly tidally-dominated characterisation would follow. In the central part of the study area close to the junction of the Norderpiep and Suederpiep channels into the Piep channel the morphology was shown to be sensitive to locally-generated waves and tidal action. Further eastward, the morphodynamics are purely dominated by the tides and thus comply well with HAYES' classification.

The significance of storm conditions was shown to be rather limited in the morphodynamic model results on the medium-scale. The rather different character of the effects does make storm events a significant force that should be represented either individually or as part of the morphologically representative conditions in medium-scale morphodynamic modelling. Since storms generally cause morphological changes differing from the medium-scale trends, the representative conditions should induce morphodynamics that represent the combined effects of long periods with mediocre conditions and short periods with quite different severe conditions, without resolving these individually.

The land reclamations in the Meldorf Bight were found to cause an imbalance between local hydrodynamics and morphology, which is compensated for by a net import of sediment. The latter thus represents an additional forcing mechanism in the study area. Due to the limited database and the medium-scale character of the applied model it was only possible to draw weak conclusions regarding the response of the morphology to dike constructions. Both measurements and model results showed a clear tendency towards a reduction in the wet volume at a diminishing rate with respect to time. Although the model results indicate relatively stable conditions after 1999, the trend in observations suggests a further slight decrease. Considering the model results in combination with observations, it is anticipated that the morphology is reaching, or has already reached, a new state of dynamic equilibrium commensurate with the current dimensions of the drainage area.

9. Acknowledgements

This investigation was carried out within the framework of the project PROMORPH, funded by the German Ministry of Education and Research (BMBF) under number 03 F 0262A. We thank the Federal Maritime and Hydrographic Agency (BSH, Hamburg) and the Office of Rural Development (ALR, Husum) for providing the bathymetric data, water level and wave data. We further thank the Max Planck Institute for Meteorology in Hamburg for providing the PRISMA model. The cooperation with the staff of the participating institutes is gratefully acknowledged. The Coastal Research Station at Norderney are thanked for providing the German Bight Model, which has been developed by Delft Hydraulics (the Netherlands) within the German-Dutch project WADE (Wadden Sea Morphodynamical Development of Wadden Sea Areas), funded by the German Ministry of Education and Research. Dr. Ian Westwood is greatly acknowledged for his English corrections and proofreading. Finally, we thank Dr.-Ing. V. Barthel as well as an anonymous reviewer for their constructive remarks.

10. References

ASP NETO, N. E.: Long- to Short-term Morphodynamic Evolution of the Tidal Channels and Flats of the Dithmarschen Bight, German North Sea, Ph.D. thesis, University of Kiel, Germany, 2004.

DWD, Orkantief Anatol vom 3./4. Dezember 1999, Homepage of the German Meteorological Service (Deutsche Wetter Dienst), 2000, in German.

HAYES, M. O.: Barrier Island Morphology as a Function of Tidal and Wave Regime. In: Leatherman, S. P. (eds.) Barrier Islands from the Gulf of St. Lawrence to the Gulf of Mexico, 1979.

JUNGE, I.; WILKENS, J.; HOYME, H. H. and MAYERLE, R.: Modelling of Medium-Scale Morphodynamics in a Tidal Flat Area in the South-Eastern German Bight, Die Küste, Heft 69, 2005.

LUTHARDT, H.: Analyse der wassernahen Druck- und Windfelder über der Nordsee aus Routinebeobachtungen, Hamburger Geophysikalische Einzelschriften, Reihe A 83, 1987, in German.

PALACIO, C. A.; MAYERLE, R.; TORO, M. and JIMÉNEZ, N.: Modelling of Flow in a Tidal Flat Area in the South-Eastern German Bight, Die Küste, Heft 69, 2005.

RICKLEFS, K. and ASP NETO, N. E.: Geology and Morphodynamics of a Tidal Flat Area Along the German North Sea Coast, Die Küste, Heft 69, 2005.

ROELVINK, J. A. and VAN BANNING, G. K. F. M.: Design and Development of DELFT3D and Application to Coastal Morphodynamics, Proc. Hydroinformatics 1994 (Delft, the Netherlands), H. H. Balkema Publishers, Rotterdam, the Netherlands, 1994.

WINTER, C.; POERBANDONO; HOYME, H. H. and MAYERLE, R.: Modelling of Suspended Sediment Dynamics in Tidal Channels of the German Bight, Die Küste, Heft 69, 2005 (a).

WINTER, C.; RIETHMUELLER, R.; HEINEKE, M.; ERNSTSEN, V. B. and NOORMETS, R.: Observed Storm Surge Morphodynamics and Implications to Numerical Modelling Schemes, Proceedings of the 5th International Conference on Coastal Dynamics (CD 2005), Barcelona, Spain, 2005 (b).

WILKENS, J.: Medium-scale Morphodynamics of the Central Dithmarschen Bight, Ph.D. thesis, University of Kiel, Germany, (available under http://e-diss.uni-kiel.de/diss_1369/d1369.pdf), 2004.

WILKENS, J. and MAYERLE, R.: Modelling of Medium-scale Morphodynamics in a Tidal Flat Area in the German Wadden Sea, Proceedings of the 29th ASCE International Conference on Coastal Engineering (ICCE 2004), Lisbon, Portugal, 2004.

WILKENS, J.; JUNGE, I. and HOYME, H. H.: Modelling of Waves in a Tidal Flat Area in the South-Eastern German Bight, Die Küste, Heft 69, 2005.

Die Küste, 69 PROMORPH (2005), 1-420

Exchange and Archiving of Measurement Data within the Research Project PROMORPH

By INGO JUNGE and BJÖRN SCHUBERT

Summary

Coastal engineering research projects produce increasing amounts of data during field campaigns. In many cases data are collected and stored at different places. In the context of the research project PROMORPH – PROgnosis of medium-term coastal MORPHology, two different internet based data management systems were developed and tested at the Institute for Fluid Mechanics and Computer Applications in Civil Engineering of Hannover University. Both systems provide efficient data administration and sustainable archiving. In addition, a simple information and data exchange should be warranted between all project participants working at different places. Further functionalities such as searching and visualization tools were implemented to promote the general acceptance by users.

Zusammenfassung

Wasserbauliche Forschungsprojekte werden zunehmend durch umfangreiche Naturmessprogramme begleitet, deren Messdaten häufig an unterschiedlichen Orten gesammelt und vorgehalten werden. Im Rahmen des Forschungsprojekts PROMORPH – PROgnose mittelfristiger MORPHologieänderungen – wurden zu diesem Zweck am Institut für Strömungsmechanik und Elektronisches Rechnen im Bauwesen der Universität Hannover zwei internetbasierte Datenmanagementsysteme entwickelt und getestet. Neben einer effizienten Datenverwaltung und -archivierung wurde im Besonderen Wert auf einen reibungslosen Informations- und Datenaustausch zwischen den Projektteilnehmen gelegt. Darüber hinaus sollen weitere Funktionalitäten, wie z.B. Such- und Visualisierungsmethoden die allgemeine Akzeptanz der beiden Datenhaltungssysteme erhöhen.

Keywords

Data Base, Data Management, MetaView, Promorph

Contents

1. Introduction

Today's coastal research projects tend to handle continuously growing amounts of data, which require efficient data administration and archiving. At the same time, simple and reliable data exchange plays a substantial role for suppliers and/or data users who frequently work at distributed places. Against this background storage of project data with an access via the internet offers a practical solution for data management, availability to all project participants and for sustainable archiving.

With the design of a decentralized data management questions concerning the requirements and the function range generally arise: Is the system primarily intended for data exchange, or should further options be made available to the user, e.g. for data search or visualization of data or merely to display meta-information? In case of visualization one has to consider that input data probably require reformatting or preprocessing. This additional effort usually has to be carried out by the data supplier and would greatly reduce the acceptance of a system. It may even lead to a certain hesitance to update the data bank frequently. Therefore, a system has to be designed, which requires minimum effort for data input.

Information systems, which access externally stored data of associated data suppliers have great advantages. The recently established North Sea and Baltic Sea Coastal Information System NOKIS (LEHFELDT and HEIDMANN, 2003) connects independent meta-data bases generated and maintained at various institutions in the German coastal zone. Data can be accessed via the internet through a web portal http://nokis.baw.de. The data suppliers use efficient data bases locally for the administration of mass data, which prevents data duplication and improves acceptance. However, it remains difficult to design a balanced system, which offers both simple and fast data input to the data supplier and, at the same time, convenient methods of a high performance information system. A good example of the convenient range of functions offered by a data base for hydraulic engineering is the information system developed within the KFKI-project MORWIN (LEHFELDT and BARTHEL, 2001).

In the PROMORPH research project (ZIELKE, 2002), two separate internet based data management systems (DMS) were developed and tested at the Institute for Fluid Mechanics and Computer Applications in Civil Engineering of Hannover University, Germany. The project, funded by the German Federal Ministery of Education and Research (BMBF) started in 2000 and was successfully concluded in 2002. Because of the multitude of data collected within the project in extensive field campaigns and from other sources (ALR Husum, BSH), an efficient system for data administration and sustainable archiving had to be developed. In addition, a simple data exchange was to be ensured between all project participants working at different locations. A voluminous data pool forms the basis for numerical modelling of hydrodynamic and morphodynamic processes in the investigation area and the exchange of project data via internet is a basic feature. Therefore, a secure and limited access to the data pool has to be guaranteed by the data base system. The proposed system differs from other information systems (e.g. KLIWA project – Arbeitskreis KLIWA, 2001, Umweltdatenkatalog – Nouhuys, 1998), which only support users in searching for data but offer no download options The PROMORPH data base is predominantly designed for data exchange and archiving within a small project group consisting of a manageable number of participants from different locations. During the PROMORPH project about 15 scientists worked at 5 locations. Considering the fact that all data suppliers are well known, quality assurance of data base content plays a minor role.

In the first phase, a concept is introduced which is based on a hierarchical administration of HTML pages guiding the user through the data description (meta-information) and offering access to the externally stored field data. A basic version of this concept was successfully implemented in the research project COSINUS (MARKOFSKY, 2000).

During the PROMORPH project further development of this system confirmed simple handling and a high flexibility concerning the meta-data input. However, flexibility of the input also leads to a non-uniform structure of meta-data, which causes increasing efforts related to data searching, also impaired by a lack of search functions. For this reason, a second DMS called MetaView (www.metaview.de) was developed. Here, the meta-information is stored in a relational data base (MYSQL) whereby convenient search functions can be implemented and offered to the user. MetaView is a long term application, where meta-information about collected and archived project data is made accessible to the general public via this data base. In addition, further data collections from other scientific projects can be stored and administered separately by the system.

In the following section 2, we discuss set-up and functionalities of the first data management system. Section 3 presents the MetaView data base system. The paper finishes in section 4 with notes on the current state of both system solutions.

2. Concepts of the PROMORPH Data Base System

It is important to distinguish between data and meta-data. Data are the values/numbers that were actually measured or calculated. Meta-data are the descriptions, in this instance stored in HTML text (Hyper Text Markup Language) and made accessible via the internet (see Figure 1). For the creation of these HTML documents, the data management system provides an editor as input tool to the data supplier, so that knowledge of HTML programming is not necessary.

For the structuring of meta-data the user has the option of organizing the text in hierarchically ramified levels. This opens up the opportunity of constructing a ramified description which helps to supply explanations relevant to a data group of a higher level and to supply special information for individual data sets of a lower level. In this way an extensive data description can be clearly structured into a report. At the end of a (sub-)chapter a link leads the user to the desired data stored on the (external) server of the respective data owner.

The decentralized concept of web-based data management was chosen for the PROMORPH project for the following reasons:

- The data are stored locally at their source which enhances the acceptance of such a system by the data owner as compared to a centralized solution. This also facilitates maintenance and up-dating of the data base.
- The visualization of research results and exchange via the internet are state-of-the-art methods and indispensable tools for scientists.
- Already existing HTML pages can be integrated into the data description by setting respective links. Thus, the data description can easily be extended.
- Before an authorized user can access data he is always led through the data description.
- Each PROMORPH project partner can read all the meta-data but can only change his own data.

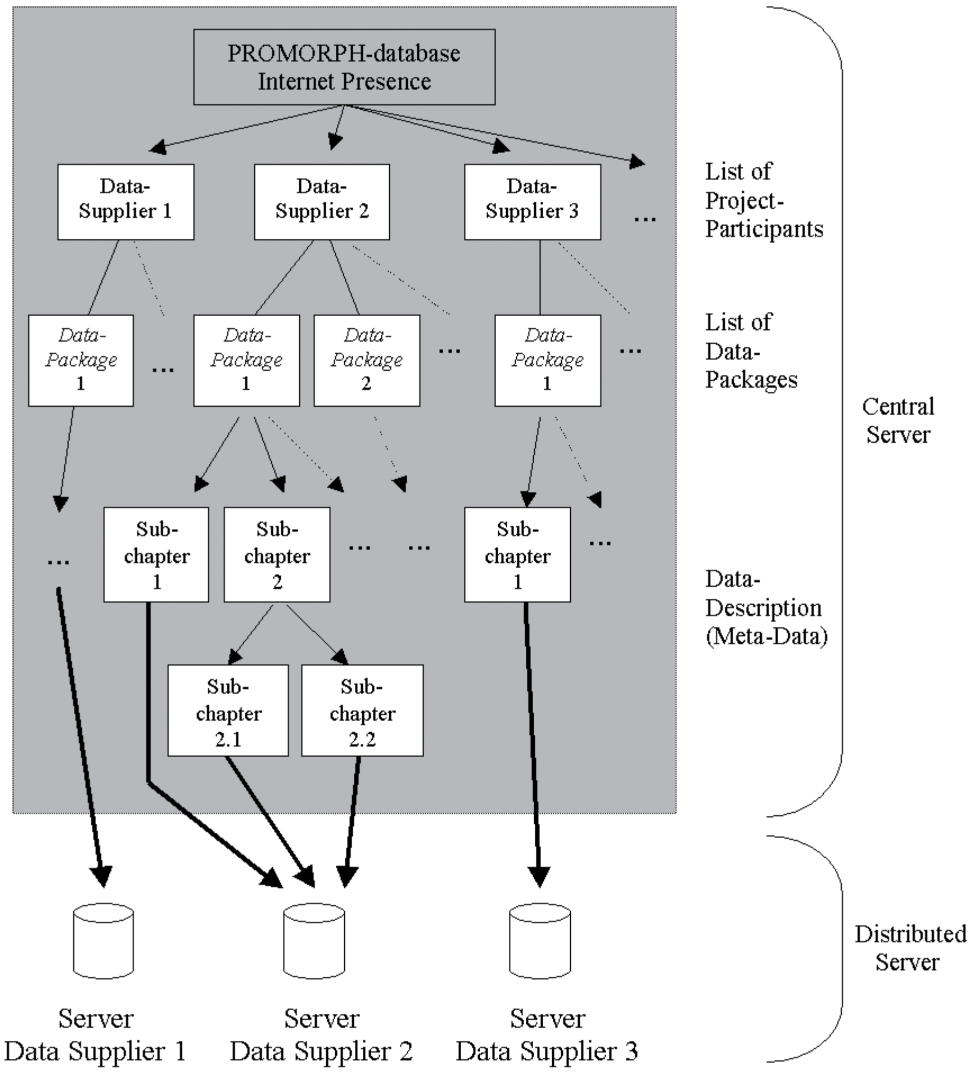

Fig. 1: PROMORPH Data Base Concept

2.1 Description of the Decentralized Data Management in PROMORPH

The data in the PROMORPH data base are organized in data packages. Each package consists of one or more hierarchically structured HTML pages which supply information (meta-data) on the current data.

All institutions involved in the project are listed in a table on the data base start page. After selecting a participant, a list of data packages supplied by the partner opens. Behind each package, the name of the person who created the package appears in parentheses.

Selecting a data package first leads to the data description (see Fig. 3). If the meta-data were subdivided into different sub-chapters, one can find the link to the sub-chapters at the bottom of the page and the link to the previous page at the top.

The sub-chapters are structured identically. At the end of a data description the user will find a link to the desired data. Usually a password query takes place. Before setting the data link, the user has the possibility of summarizing essential meta-data (e.g. measurement location, time, instrumentation etc.) in a header table. It is not necessary to fill in such a table. It only clarifies and simplifies access to keywords with an optional implementation of search algorithms.

2.2 The DataBase Input Tool

The input of meta-data is supported by the input tool, a simple Java applet editor, which is available through the data base internet page. In the first step, an access window opens and checks the access authorization of the user by a password query. This procedure assures that a data base user can only edit his own packages (meta-data and links to the current data). When the login is successful, an input window appears in which the user can enter and modify his meta-data (see Fig. 2). The input tool offers options to:

- create a new package
- create a new sub-chapter
- delete a chapter (with all sub-chapters)
- edit text into a chapter
- connect an external data file to a string in this chapter
- connect a reference to a string in this chapter
- rename chapters
- generate the status last stored (undo function)
- create a header-table
- select meta-information from data files.

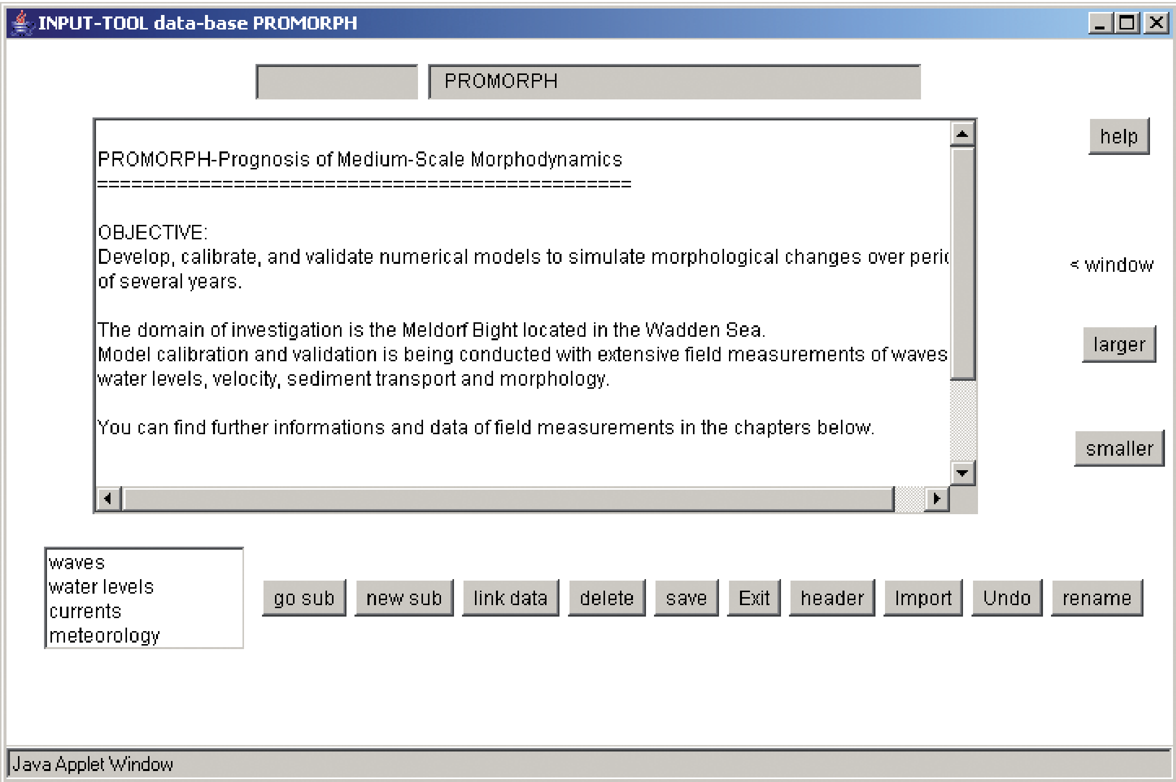

Fig. 2: Entry of Meta-Data via the Input Tool

The header table outlined above is useful to summarize the essential meta-data in a compact table. The input tool offers a mask with 24 possible entries to be filled in by the user.

Another helpful function of the input tool is the possibility to extract meta-information from a set of data files, which show a uniform format. In many cases, data files contain introductory information referring to the measurements (time, place, instrumentation, data-owner etc.). This information can be selected by using a function called import tool. This tool searches in pre-selected data-files for previously defined keywords. When a keyword is detected, the associated line with meta-information is transferred into the input window. It is also possible to extract a predefined number of lines from each data file.

When all meta-data and required links to the data proper are entered, the input must be saved. The input tool then converts the chapter into a HTML document, which is shown after each storage behind the input window in a second frame (see Fig. 3). This allows the user to verify the completed HTML-page and modify the result if necessary.

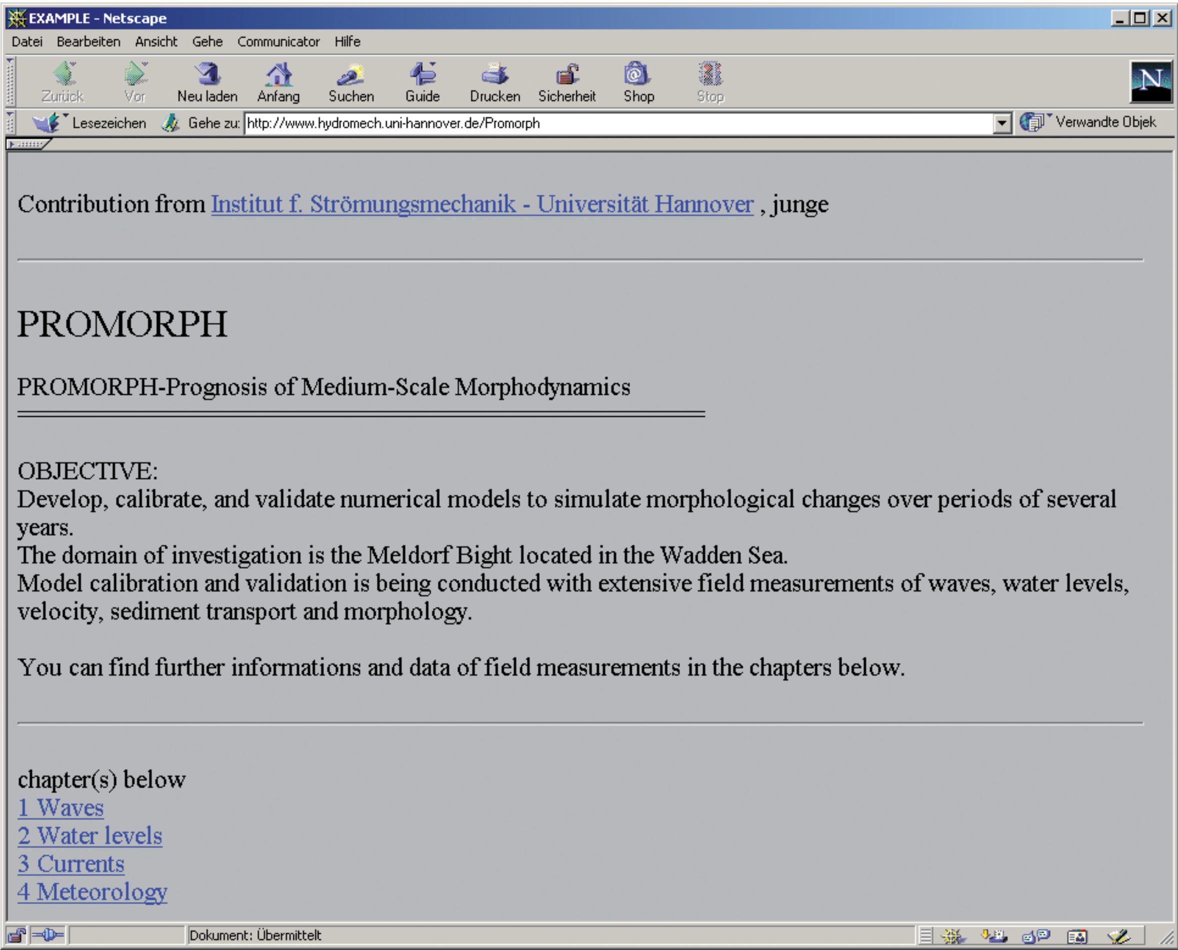

Fig. 3: Meta-Information in the PROMORPH Data Base

3. The DataBase MetaView

The data management system introduced in the previous section has many advantages. The simple and unformatted input of meta-data permits a fast but non-standard adapted input of meta-information. However, this flexible input leads to a non-uniform structure of meta-data which implies an increasing orientation effort for the data search, impaired by the non-existence of search functions. Due to the present amount of available data, this aspect is not significant for the PROMORPH project participants. In consideration of the fact that project data will be made accessible to the general public, it is vital to ensure an easy navigation within the data description, also to non-project members. For this reason a second internet-based information system named MetaView was implemented (see Fig. 5). It has access to the same external data pool but provides the user with improved and more extensive functionalities.

3.1 Concepts of MetaView

The MetaView system only contains meta-information about measurement data stored inside a relational data base system. The original measurement data sets remain on the data servers of the participating institutions. Thus, necessary hardware resources have been distributed between several institutions. The structure of the system is illustrated in Fig. 4. It largely resembles the described PROMORPH data base. The significant difference is storage of meta-information in a MYSQL data base instead of using unstructured hierarchically linked HTML pages.

In order to generate the meta-information from measurement data sets, the MetaView system offers an integrated import module, which converts any measurement data file into a uniform format. As an important prerequisite of the system a file format called VA format was developed at the Institute for Fluid Mechanics and Computer Applications in Civil Engineering of Hannover University. A detailed description of the VA data format is given by ZIELKE (2001) and the online system information at www.metaview.de. By converting all data sets registered in the MetaView system into one common format, the user is able to access data sets from different institutions in the same format. In addition to the download facility, the MetaView system offers a graphic tool for quick visualization of selected data sets.

3.2 The Input of Data Sets

When adding new data sets to the MetaView system, a data supplier has first to generate a new group of data sets and attach meta-information concerning the measurement, i.e. time, location, data type and range. If the system already contains files of similar format, the data supplier can select an existing import mask, otherwise the design of a new mask is necessary. Finally, the user must specify the URL address to the external data server and the password if the access is restricted. If the data directory of an external server contains further files in addition to the desired ones (e.g. protocol files), the usage of so-called regular expressions allows access to a specific selection of data files. In this case, the MetaView system considers only those file names, which contain e.g. a given sequence of characters.

A further helpful parameter is the so-called scan cycle which can be defined for each

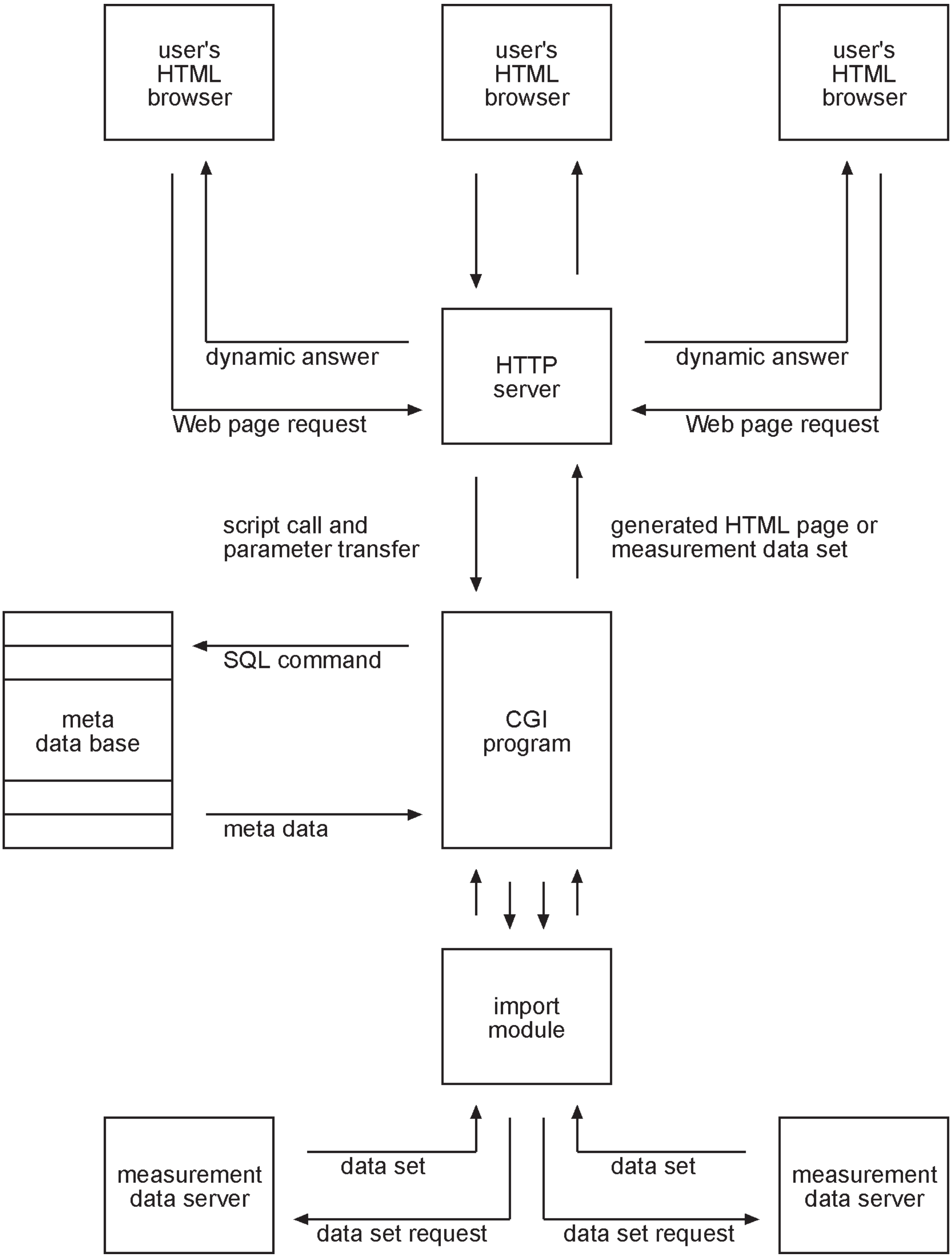

Fig. 4: Structure of the MetaView system

group of data sets. It schedules the dates when the system has to search through the directories of external data servers for new measurement data sets. The MetaView system is able to automatically read the new data records with the help of an appropriate import mask. This method should help to minimize the input effort for further measured data. Continuously recorded data (e.g. weather station) are added to the appropriate directory on the data server. MetaView checks these directories in given time intervals and reads new entries independ-

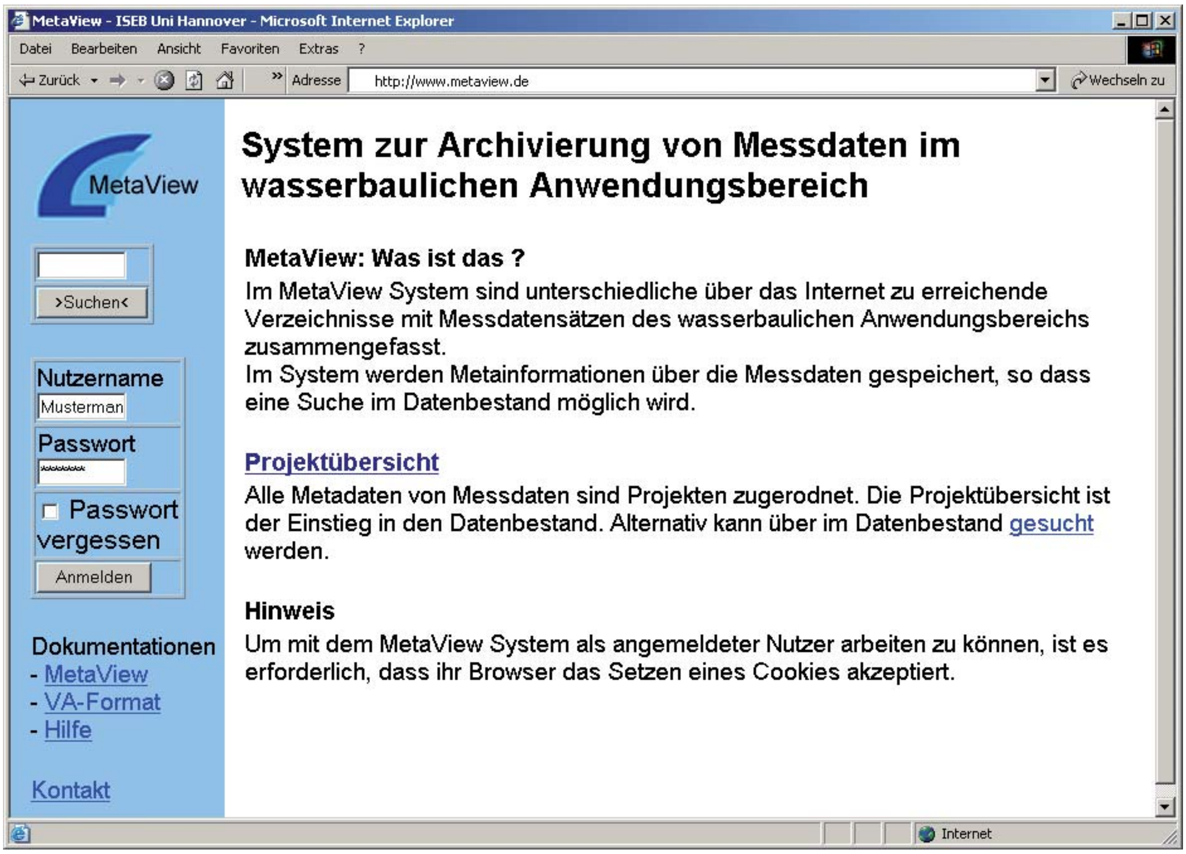

Fig. 5: Initial MetaView window

ently, if desired. If the data files contain special information concerning the measurement (e.g. time, location, etc.), the system can extract and process this meta-information with the help of the known import mask. Thus, the content of MetaView growes automatically.

Access to measured data can be restricted by an integrated user administration and access control system in order to make measurement data available to selected groups of users. The user administration allows to define single users and also groups. Thus, only little effort is required to define access to data sets for different users. During the project period, access to this data collection is restricted to the project participants. Later on, access can be granted to the general public by a simple adaptation of the access rights.

3.3 Data Search and Download

All measurement data to be extracted via the MetaView system are assigned to individual projects. Therefore, it is possible to collect further hydraulic data within the scope of similar research projects or other suitable measuring campaigns and to administer them by the MetaView system independently from the PROMORPH data pool. Each entry in the project list contains a description of the project and a list of groups of data sets already mentioned above. A group of data sets consists of a number of data sets, which represent the currently available measurement data files (see Fig. 6). In practice, several uniform data files pertaining to a measuring campaign (ADCP measurements, water level, sea state, etc.) are

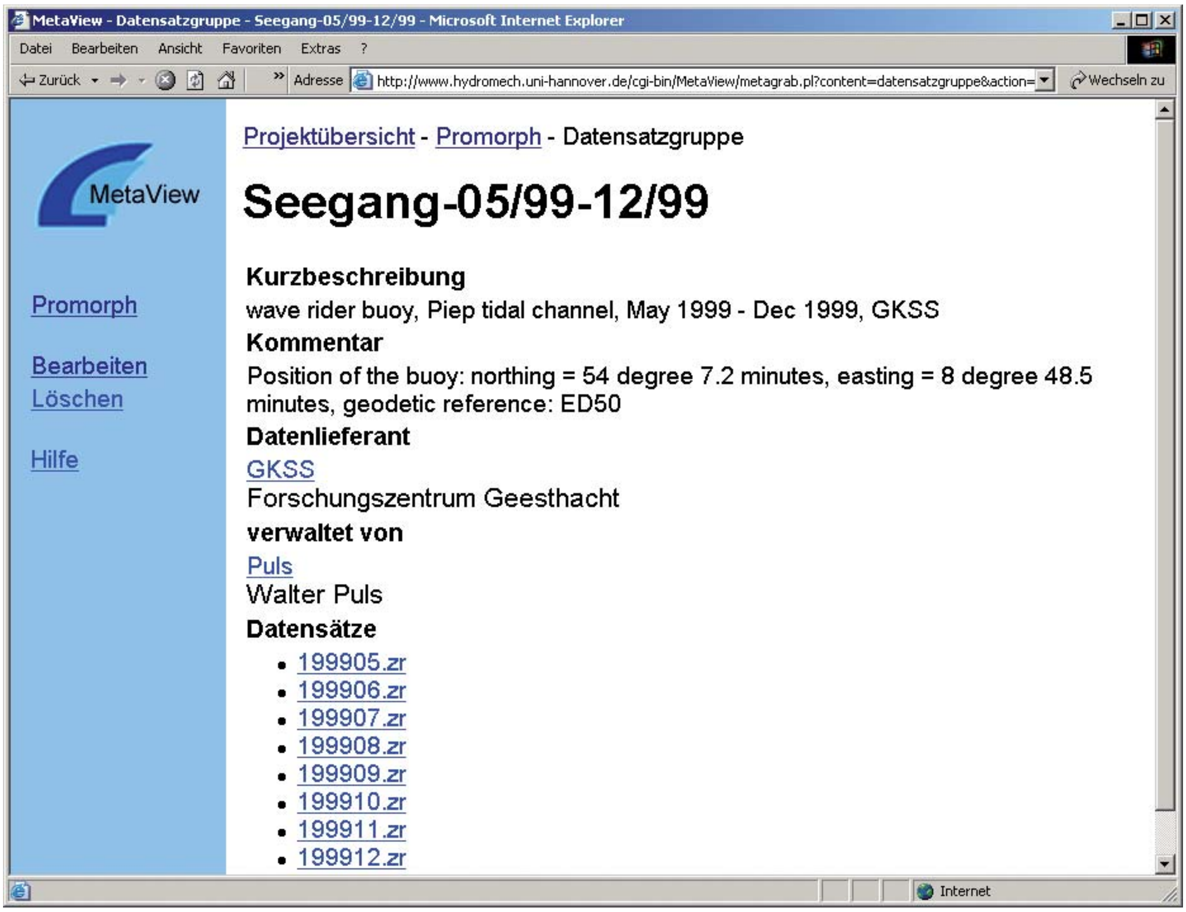

Fig. 6: Group of data sets containing sea state measurements over eight months

generally stored in a separate server directory. In the MetaView system, a group of data sets corresponds to such a directory, where each data set represents one individual measurement data file.

For an efficient data search, a user only needs to examine the project list and the list of available groups of data sets. This flat hierarchical structure allows fast access to measurement data. Alternatively, the user can utilise a convenient search function, which allows a full text search or a restricted search for projects, group of data sets, data sets, or also data suppliers. The user receives data files in the original data format or in a converted VA format. Each download is logged by the system in order to ensure an overview of the use of the measurement data sets. For this purpose, the user and the selected data format (VA or original) are stored together with the current time.

3.4 Visualisation of Data

The internal conversion of all data files into the uniform VA format facilitates visualisation of data. For this purpose, the MetaView system offers a special Java applet. In the simplest two-dimensional case, this tool selects the converted measured data suited for graphical presentation and lists all different measurement categories in two equal tables. The user can select a measurement category from each table, which defines the two axes of a simple xy-diagram (see Fig. 7), in the presented case a time series of wind velocities. In addition, the choice of more than one variable in the second table is also possible and permits plotting of several curves in one diagram. By a repeated selection of other measured variables in the table beneath the plot, a quick and convenient visualisation of further measurement categories is possible.

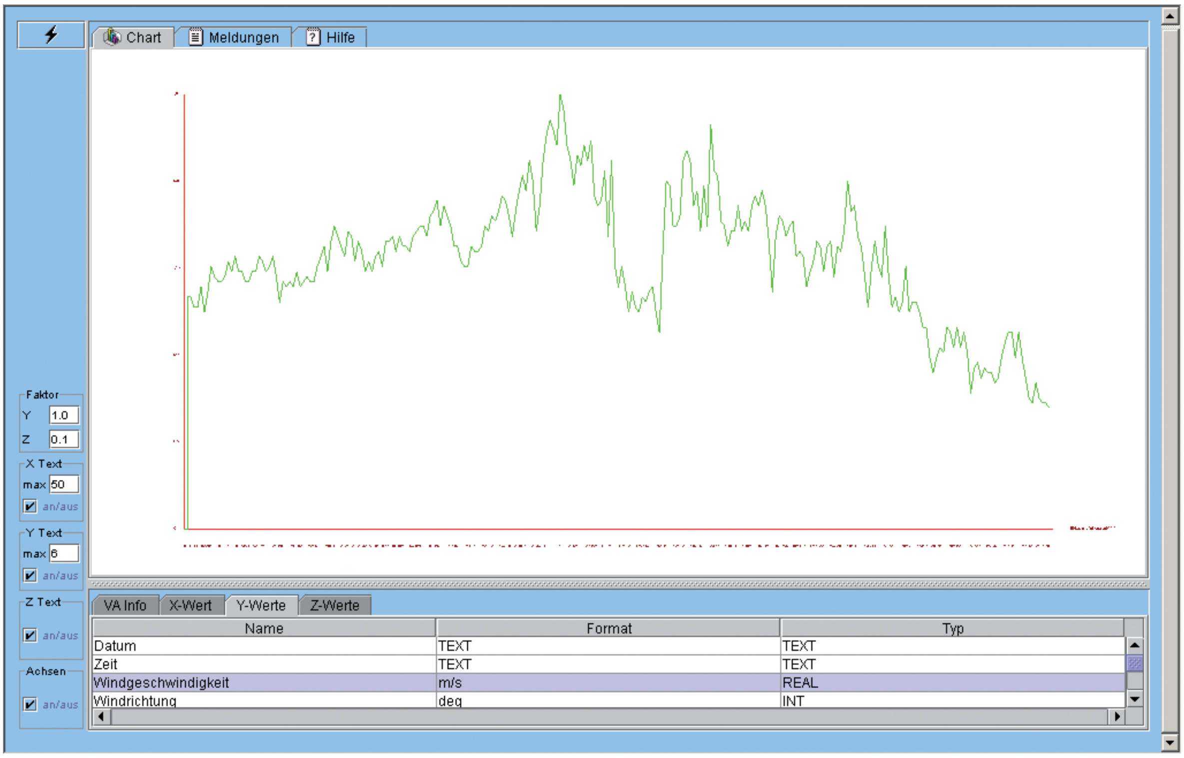

Fig. 7: Presentation of a simple xy-plot in the MetaView system.
This example is a 24-hour distribution of wind velocity at station Büsum

Three-dimensional data can also be visualised under certain conditions. Many measurement data files may consist of a sequence of several data blocks. In this case, a data block generally contains the results of measurements at one location with each subsequent block valid for a different time window or a different location. The graphic tool permits representation of two measured variables of one data block as an xy-plot. A third variable distinguishes the individual data blocks (e.g. time or local specification) and is then selected for defining a third axis. As an example, Fig. 8 shows continuous vertical velocity profiles in a cross-section of the Norderpiep as a result of an ADCP measurement. Each individually measured vertical profile corresponds to an individual data block. The user can vary the number of displayed verticals by selecting a respective number of data blocks from the table below. A display of individual data blocks is also possible. Conveniently, the plot can be rotated, shifted, and scaled by mouse control.

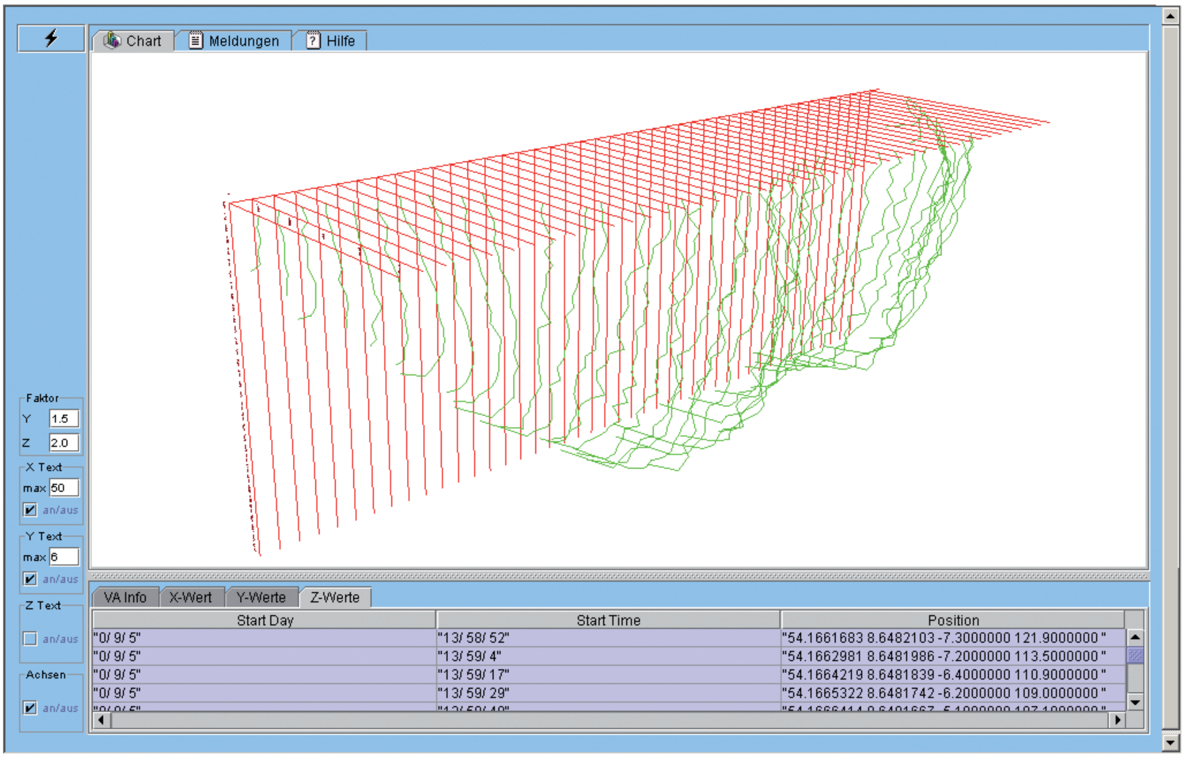

Fig. 8: Velocity distribution in a cross section of the Norderpiep in the Meldorf Bight.
The visualisation tool for vertical velocity profiles provides an efficient data quality check

4. Conclusion

The current data volume of both data management systems includes ADCP measurements, waves, meteorological conditions, bathymetric surveys and results from CTD measurements. More than 5400 data files can be accessed by the participants of the PROMORPH project. The measurement data can partly be viewed (only MetaView) and, if desired, downloaded by the user. The MetaView system provides access to the same measurement data pool as the first PROMORPH data base introduced in section 2. Project data are externally stored on servers at participating institutions. A redundancy of measuring data due to the two different data management systems does not appear.

It can be expected that the content of the MetaView system will increase continuously due to future measurement campaigns and the possible listing of other research projects. Presently, the concept of the MetaView system is used to set up a data base to support a wind energy research project also funded by the German Federal Ministery of Education and Research (BMBF).

5. References

ARBEITSKREIS KLIWA: Meta-Informationssystem für KLIWA-Daten, Forschungsvorhaben KLIWA-Klimaveränderung und Konsequenzen für die Wasserwirtschaft, Bereich C, Projekt C4, Statusbericht 2001; http://www.kliwa.de/de/.

LEHFELDT, R. and BARTHEL, V.: MORWIN – Morphodynamische Modellierung von Windwatten – Netzgestützte Projektbearbeitung im Küsteningenieurwesen. Abschlussbericht 1997–2000, 2001.

LEHFELDT, R. and HEIDMANN, C.: NOKIS – Erstellung eines Metadateninformationssystems für die Küstenforschung und das Küsteningenieurwesen. Zwischenbericht 2003, 2003.

MARKOFSKY, M.: The COSINUS Database for Cohesive Sediment Transport in Estuaries and Coastal Zones. 6th. Int. Conf. On Nearshore and Estuarine Cohesive Sediment Transport INTERCOH 2000, Delft, September 2000.

NOUHUYS, J. et al.: UMWELT-Datenkatalog des Bundes, FuE-Vorhaben 297 12 120/03; Endbericht, 1998.

SCHUBERT, B.: Entwicklung eines internetbasierten Metainformationssystems mit dezentraler Datenhaltung für den wasserbaulichen Anwendungsbereich. Master Thesis – Institute for Fluid Mechanics and Computer Applications in Civil Engineering, 2001.

ZIELKE, W. et al.: Datenmanagementsystem zur Sicherung der Erfassung, Verfügbarkeit und Vergleichbarkeit von Messungen in kontaminierten Grundwasserleitern. VEGAS-Abschlußbericht 1999, Institut für Strömungsmechanik, Universität Hannover, 1999.

ZIELKE, W. et al.: PROMORPH – Prognosis of Medium-Term Coastal Morphology. Final Report, Institute for Fluid Mechanics and Computer Applications in Civil Engineering 2003.

Die Küste, 69 PROMORPH (2005), 1-420

Near Bed Suspended Sediment Dynamics in a Tidal Channel of the German Wadden Sea

By KERSTIN SCHROTTKE and FRIEDRICH ABEGG

Summary

Research has been undertaken focusing on the sediment transport processes in the water column of tidal channels, but often neglecting the last few decimetres above the seabed, due to limited application of conventional measuring devices within the near-bed zone. This paper introduces a new instrument, called NEBOSS, which has been designed for measuring and sampling sediment suspensions down to 10 cm above the seabed. In an attempt to overcome the spatial limitations of NEBOSS, the echo-sounder system DSLP® of General Acoustics GmbH was simultaneously deployed in the Dithmarschen tidal channel Piep at different tidal phases. It provides data of near-bed acoustic interfaces, defined as suspension layers in a high temporal and spatial resolution. Even complex, tide dependant near-bed sediment processes can be derived from the NEBOSS data with suspended sediment concentrations (SSC) > 1 g/l, a higher ratio of particles > 20 µm and clastic components during flood and ebb tides. Sand transport is not limited to the first decimetre, but also occurs 1 m above the seabed in highly variable amounts, due to turbulent mixing processes. In total, the amount of sand is less than expected, especially close to the seabed under tidal flows with mean velocities up to 57 cm/s. A near-bed suspension layer of an average thickness of 20 cm, as always detected with DSLP, is also reflected in the NEBOSS data, except at slack tides. A tidal signal is visualised with DSLP regarding an increased thickness of the suspension sub-layer closest to the seabed during slack tide.

Zusammenfassung

Sedimenttransportprozesse in Tiderinnen wurden bereits mehrfach untersucht, oft aber ohne die letzten Dezimeter über der Gewässersohle mit einzubeziehen. Grund hierfür ist die eingeschränkte Einsatzmöglichkeit kommerzieller Messgeräte im sohlnahen Bereich. In dieser Arbeit wird das neue Messsystem NEBOSS vorgestellt, das zur Erfassung und Beprobung von Sedimentsuspensionen bis 10 cm über Grund entwickelt worden ist. In einem Versuch, die räumlich limitierte Aussagekraft von NEBOSS zu erweitern, wurde das Echolotsystem DSLP® von General Acoustics GmbH zeitgleich in der Dithmarscher Tiderinne Piep zu unterschiedlichen Tidephasen eingesetzt. Es dient der akustisch basierten Erfassung sohlnaher Sedimentsuspensionen. Mit NEBOSS lassen sich selbst komplexe, tideabhängige Sedimenttransportprozesse 10 cm über Grund mit Suspensionskonzentrationen > 1 g/l, höheren Anteilen von Partikeln > 20 µm und vermehrt klastischen Bestandteilen zu den Flut- und Ebbphasen erkennen. Sand wird nicht nur innerhalb der untersten Dezimeter transportiert, sondern auch 1 m über der Gewässersohle in unterschiedlichen Mengen, was auf turbulente Durchmischungsprozesse zurückführbar ist. Insgesamt ist weniger Sand anzutreffen, als bei den vorherrschenden Tideströmungen mit mittleren Geschwindigkeiten bis zu 57 cm/s erwartet wird. Ein sohlnaher, durchschnittlich 20 cm mächtiger Suspensionshorizont, wie er ausnahmslos mit DSLP zu allen Tidephasen detektiert wird, lässt sich aus den NEBOSS-Daten außerhalb der Stauwasserphasen ebenfalls ableiten. Ein Tidesignal zeigt sich in den DSLP-Daten bezüglich einer Mächtigkeitszunahme des sohlnächsten Suspensionshorizontes zu Stauwasser.

Keywords

Near-Bed Sand Transport, Dithmarschen Bight, North Sea, Field Measurements, Measuring Techniques, SSC, SPM, OBS, NEBOSS, Echo-Sounder DSLP®

Contents

1. Introduction

The extensive tidal flats and channels of the German North Sea wadden coast underlie remarkable morphological changes on various time scales (WIELAND, 2000; ASP NETO, 2004). Intensive utilisation of this coastal zone emphasises the need of reliable forecasts of its morphological evolution in time frames of months, years and decades. This becomes even more important regarding potential changes induced by a rise of the global sea level or an increase in storm activity and intensity. To apply morphodynamic numerical models to achieve this task, a detailed knowledge of the processes, controlling the coastal morphology is strongly required.

Morphological changes of tidal flats and channels are mainly caused by sediment movement due to water motion. Dependent on the hydrodynamic energy input as well as on the particle size, type and shape, these sediments are transported in suspension or as bedload (REINECK and SINGH, 1980; ZANKE, 1982; VAN RIJN, 1993). In the field, it is less obvious where and under which transport mechanism especially sand is moved, particularly in turbid environments. In the literature, the term 'suspended particulate matter (SPM)' is often used as a synonym for all transported particles, disregarding their mode of transportation.

Fine-grained, highly concentrated near-bed suspensions (> 1 g/l, EISMA, 1993) are a well known phenomenon in many tidal estuaries (ROSS and METHA, 1989; SMITH and KIRBY, 1989; SHI et al., 1996; VELEGRAKIS et al., 1997). The dynamics of cohesive sediment suspensions are different from non-cohesive ones and cannot easily be transferred to those sediments found in the investigation area.

The Dithmarschen tidal flats are predominantly composed of sand (KÖSTER, 1998). Thus, sand must be transported in reasonable volumes. However, former field measurements of the suspended sediment concentration (SSC) and composition in the water column of the North Sea tidal flats and channels showed that the retrieved amount of sand was either non-existent or negligible (RICKLEFS, 1989, 1998; RICKLEFS and AUSTEN, 1994; POERBANDONO, 2003; JOERDEL et al., 2004). From these results it can be assumed that sand is predominantly transported close to the seabed, as also reported in a study focusing on the transport of sand suspensions and transport on the Middelkerke bank (Southern North Sea). It was shown that up to 73 % of the entire sediment volume in the water column was transported at heights of 0–30 cm above the seabed (VINCENT et al., 1998).

The purpose of this field study is the verification of a pronounced near-bed sediment transport in a tidal channel, combined with measurements of water depth and current velocity.

2. Methods

The development of measuring techniques for studying sediment transport in aquatic environments has made remarkable advances during the last decades. Different methods are available including water sampling systems (HICKEL, 1984; CHRISTIANSEN, 1985; PIERCE and NICHOLS, 1986; VAN RJIN, 1993; SHI et al., 1996; KERN and WESTRICH, 1999) and coring devices (ZAMPOL and WALDORF, 1989) for selective measurements of particle concentration and distribution in the water column. Instruments based on optical (OHM, 1985; STERNBERG, 1989; STERNBERG et al., 1989; GREEN and BOON, 1993; VAN DE KREEKE et al., 1997; FUGATE and FRIEDRICHS, 2002), acoustical (HAY, 1983; THORNE et al., 1991, 1993; VELEGRAKIS et al., 1997; VINCENT et al., 1998; GREEN et al., 1999, 2000; WEBB and VINCENT, 1999) and x-ray techniques (NIELSEN, 1984) are used for profiling measurements, providing indirect information on particle concentration and distribution.

To simultaneously measure SPM concentration and distribution as well as current velocity in a high temporal resolution even 10 cm above the seabed, a new NEar-Bed Observation and Sampling System, called NEBOSS has been developed (Fig. 1). The essential parts of NEBOSS are two streamlined, isokinetic water-sediment samplers of the type *US-P61 point integrating sediment sampler* (71.1 cm long; 18.6 cm wide) with a sample volume capacity of 0.5 l (VAN RIJN, 1993). The filling time of a sample bottle varies between seconds and minutes, dependant on the current velocity (in this study: 00:00:31 h – 00:10:30 h). Both samplers are mounted in a tripod frame, which is lowered to the seabed by a supporting vessel crane (Fig. 1). Once the frame is positioned, one sampler is lowered to the seabed with a small electronic underwater winch. The approach of the sampler to the seabed is controlled by a pressure sensor for depth measurements (pressure range 0–2.5 bar, accuracy 1 % of the total measuring range) and an electromechanic bottom detector. Current velocity near the nozzle of the movable sampler is simultaneously registered with a one-axial vane type current meter (sample rate 1Hz, accuracy ± 0.5 cm/s) which is 5 cm in diameter and 1 cm wide. The second sampler is permanently mounted in the frame for sampling 1 m above the seabed (Fig. 1).

Each sampler is equipped with a 12 cm × 2.5 cm large, optical backscatter sensor (OBS) by Seapoint for high temporal resolved (sample rate 1 Hz) turbidity measurements near the nozzle. A source wave length of 880 nm is used and the scattered light is detected from a small water volume within 5 cm of the sensor window. A sensor sensitivity of 10 mV / FTU (Formazine turbidity unit) with a range of 500 FTU was applied in this study. A linear correlation between SSC and OBS intensity is expected, despite sensor limitations of a particle size-dependant response (FUGATE and FRIEDRICHS, 2002; HOITINK and HOEKSTRA, 2005).

All sensors can be deployed both for measurements in discrete water depths and in a vertical profiling mode. The whole system is electronically controlled from the support vessel via cable.

The samples were vacuum filtered through pre-weighed Whatman GF/C glass microfibre filters, retaining particles > 1.2 µm for determining SSC. The amount of particulate organic carbon (POC) was calculated from weight loss after heating to 550 °C for 5 h. The

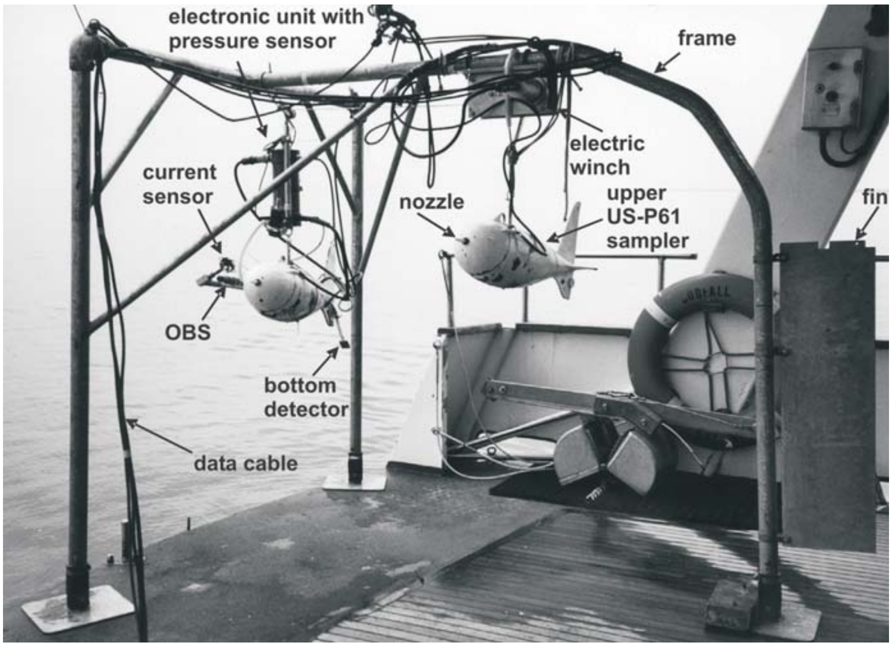

Fig. 1: Deployment of the new near-bed observation and sampling system (NEBOSS) from the RV Südfall

solids of tidal waters often occur in the shape of particle flocs, which are mostly aggregated clays and silts, combined with organic matter (EISMA, 1986, 1993; RICKLEFS, 1989; JOERDEL et al., 2004). To detect and quantify aggregated structures, all samples were analysed twice with a CIS laser particle analyser (REIMERS, 1999). Initially, the samples were analysed as collected in the field. Afterwards, ultrasound and H_2O_2 treatments were carried out to split the flocs and remove organic substances.

To overcome the spatial limitation of NEBOSS while deploying it at one location at a time, the echo-sounder system DSLP (Detection of Sediment Layers and Properties) by General Acoustics GmbH was simultaneously used (EDEN et al., 2005). This device has been developed for a high spatial and temporal resolved, precise detection of interfaces in a complex stratification of suspensions and sediments (EDEN et al., 1999, 2000, 2001). The resolution is in the range of millimetres, the system accuracy amounts ± 1.5 mm. The DSLP device was used stationary and in a profiling mode, applying frequencies of 12.5, 110 and 200 kHz. Geographical positioning was performed by a high presision DGPS with a land based reference station.

A 1200 kHz broadband Acoustic Doppler Current Profiler (ADCP) of RD Instruments© was deployed to measure current velocity and direction in a profiling mode with a depth cell size of 25 cm. Information on the amount of SPM is given by the strength of the retrieved backscatter signal (DEINES, 1999). Tidal data from the Büsum gauge was provided by the regional office of the Federal Administration for Waterways and Navigation.

3. Regional Setting

The data presented in this study are based on surveys carried out from October 2000 to November 2001 in the tidal channel Piep under different tidal phases (always between neap and spring tide), and wind speeds of about ≤ 4 m/s (Fig. 2). The Piep is located in the tidal flat area of the Dithmarschen Bight (Fig. 2). The channel system is the main pathway for the semidiurnal exchange of tidal water masses between the open sea and the Dithmarschen Bight with mean flow velocities of up to 2 m/s and a mean tidal range of 3.2 m. In the Piep, the cross-sectional averaged current velocities vary between highest mean values of 0.87 m/s (neap) and 1.03 m/s (spring) during flood tide and 0.91 m/s (neap) and 1.05 m/s (spring) during ebb tide (ASP NETO, 2004). Ebb-dominated flows prevail in summer and during neap tides, whereas flood currents dominate in winter and during spring tides. A lateral asymmetry of the tidal flow is controlled by the Coriolis force (ASP NETO, 2004).

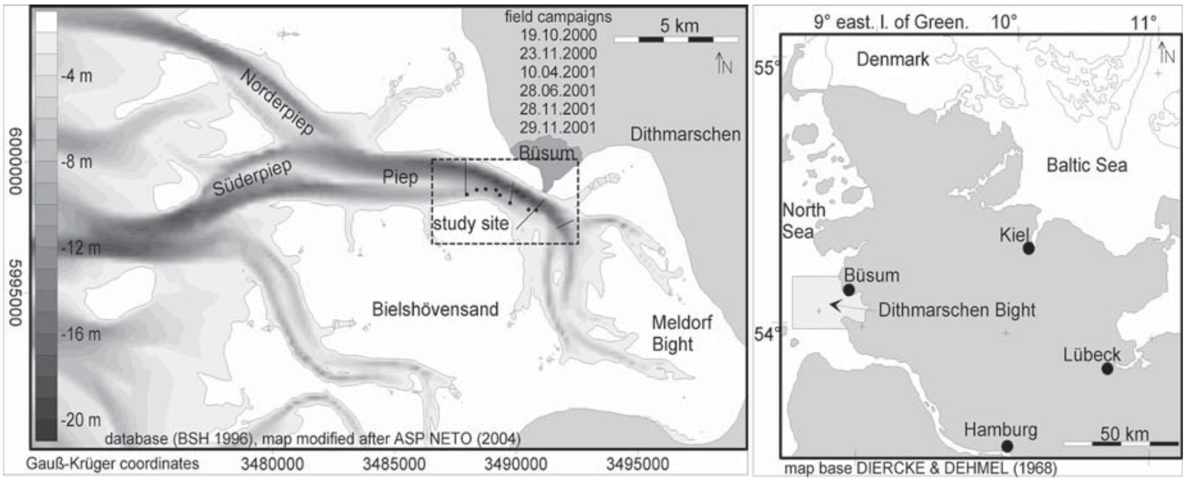

Fig. 2: Bathymetric map of the Dithmarschen Bight (North Sea, Germany), showing the study site (positions of stationary measurements are marked with dots; cross profiles with lines)

The average salinity in the water column is about 25 ppt, with tidal fluctuations of up to 2.5 ppt. The mean water temperature varies between 6 °C in winter and 18 °C in summer, with tidal variations of about 1°C. These values are based on measurements in summer (28 June 2001) and winter (28 November 2001). Fresh-water discharge can be expected on an irregular basis from sluices gates.

The tidal flats are intersected by the Piep channel, in parts reaching depths > 21 m below sea level, where consolidated clays of early Holocene origin occasionally outcrop (ASP NETO, 2004). These clays are present in the deepest section and at the steep northern slope of the Piep channel (Fig. 2). Often, its subsurface is dissected leaving a prominent pattern of ridges and grooves. The southern slope is only gently inclining toward the Bielshövensand and its rippled surface is composed of very fine to medium sand (POERBANDONO and MAYERLE, in this volume). The maximum depth-averaged SSC in the water column of the Piep down to 1 m above the seabed is about 0.5 g/l (POERBANDONO and MAYERLE, in this volume). The median size of suspended particles is in a range of 6 µm – 86 µm (untreated) and 4 µm –19 µm (aggregates dissolved), respectively (POERBANDONO, 2003).

4. Results

4.1 NEBOSS Measurements

The signal intensities of the OBS linearly correlate with SSC in the water column at the 95 % significance level (Fig. 3a–b). The correlation coefficients from the data sets 10 cm above the seabed increase up to $R^2 = 0.97$ ($\alpha = 0.05$; n = 6) when focusing on single surveys.

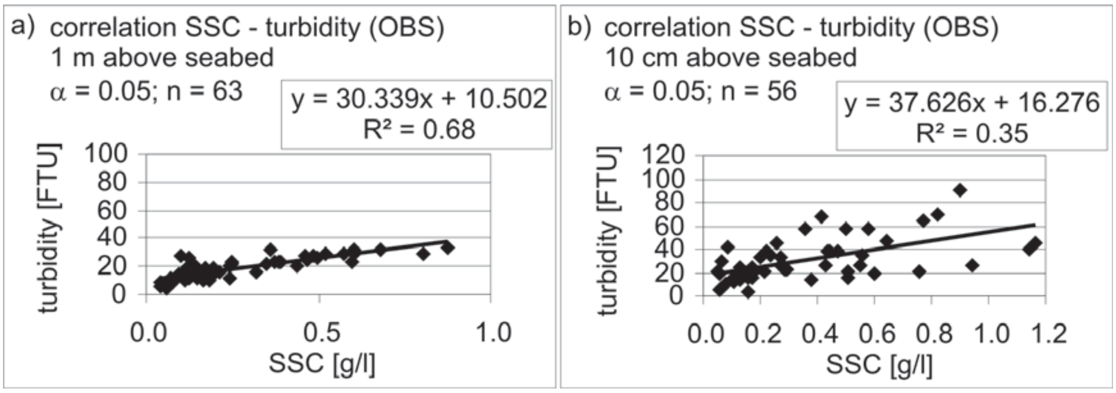

Fig. 3a–b: Linear regressions, relating (a) OBS turbidity to SSC at 1 m and (b) 10 cm above the seabed, based on data sets from all surveys

An increase of the OBS intensity und thus the SSC trough the water column towards the seabed was repeatedly registered at the study site, a good example being shown in figure 4. Highest values of 28 FTU (> 0.3 g/l) in this case occur close to the seabed. Simultaneously, the current velocity decreases from ~ 100 cm/s near the water surface to 40 cm/s near-bed (Fig. 4).

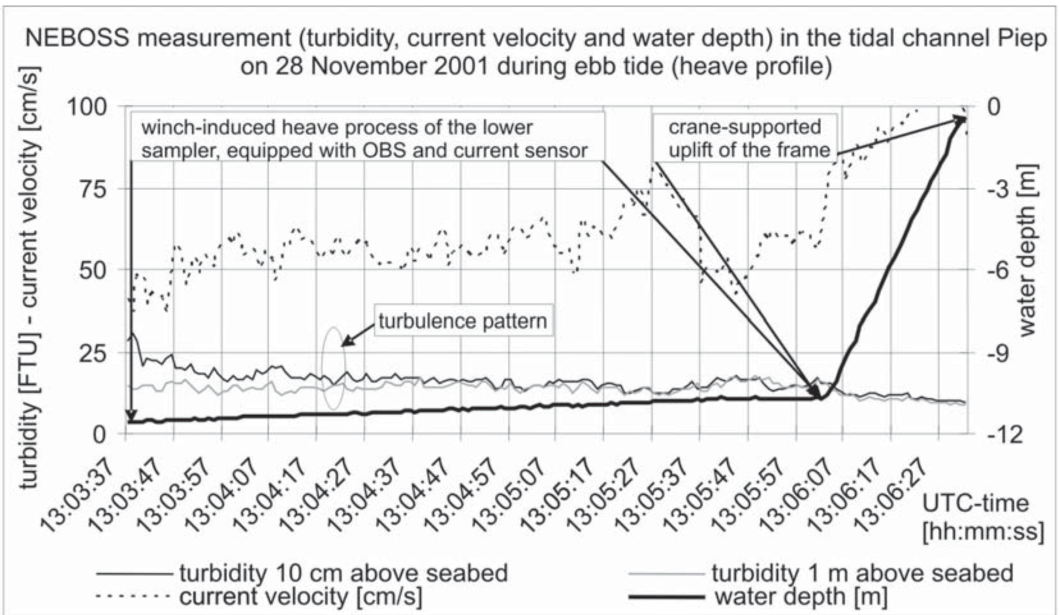

Fig. 4: Turbidity and current measurements in the tidal channel Piep on 28 November 2001 during ebb tide (heave profile)

During high-water slack tide, a slight downward increase of the OBS intensity is visible with highest values of 15 FTU, corresponding to 0.15 g/l (Fig. 5). Also, there is no distinct differentiation between the signal strength 10 cm and 1 m above the seabed. The near-bed current velocity is < 10 cm/s.

Regarding data from both OBS in further detail, there is a considerable variability of the signal intensity over short time intervals of only a few seconds visible (Fig. 4, 5). This is linked to small-scale variations of the current velocity, representing ongoing turbulent mixing processes. They are even more noticeable during ebb tide with higher hydrodynamic energy input (Fig. 4). Thus, SPM is turbulently moved up- and downwards the lower water column. As a result, the SSC at 10 cm and 1m above the seabed is occasionally similar for a few seconds (Fig. 4).

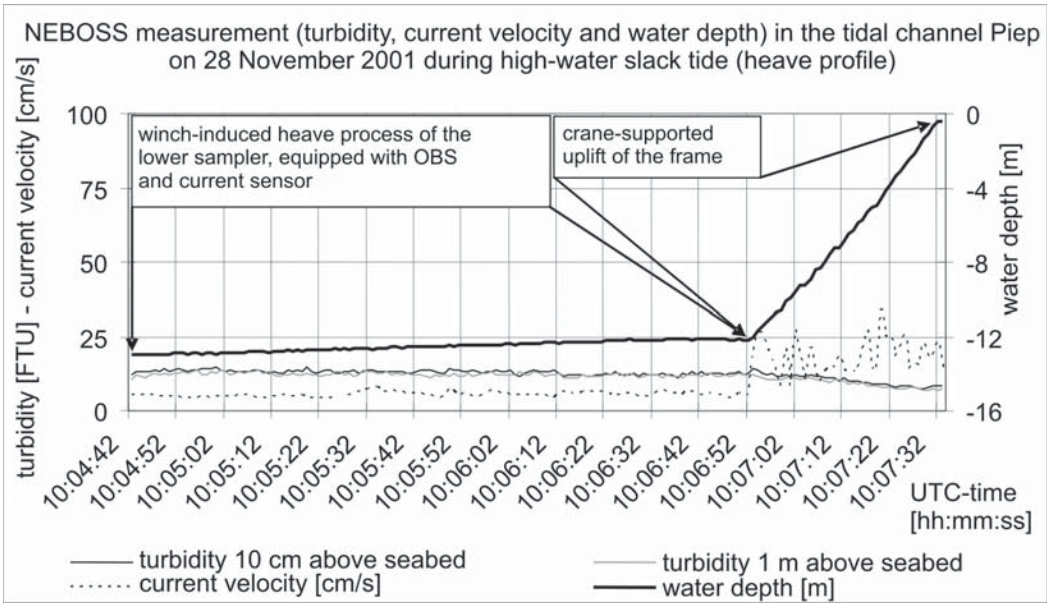

Fig. 5: Turbidity and current measurements in the tidal channel Piep on 28 November 2001 during high-water slack tide (heave profile)

Tide dependant variations of the near-bed SPM dynamics, even in a channel section with complex tidal current patterns, can be derived from the NEBOSS and selected ADCP data (Fig. 6a–e). The stationary measurements represent the near-bed current and sediment situation on 29 November 2001 (4 days before spring tide) eastwards of the Bielshövensand in 10 m water depth over a tidal cycle at 30 minutes time intervals. NEBOSS and ADCP current velocity and backscatter data linearly correlate at the 95 % significance level ($\alpha = 0.05$, $n = 24$; $R^2 = 0.82$). Similar results are given for the OBS intensity and ADCP backscatter ($\alpha = 0.05$, $n = 24$; $R^2 = 0.70$).

In the example shown here, the flood current decreases evenly towards slack water, whereas an irregular decrease of the ebb current velocity occurs with a second peak right after flow reversal (Fig. 6a–b). This reversal is not synchronous with low-water slack tide. Tide dependant changes of the hydrodynamics are also reflected by temporal variations of the SSC at 10 cm and 1 m above the seabed, with higher values occurring exclusively during flood and ebb tide (Fig. 6a–b). A time offset of about 30 minutes emerges between peak current velocity and SSC (6a–b). Highest SSC > 1 g/l appears only close to the seabed, although a considerable amount of SPM up to 0.6 g/l is also found at the higher elevation for a few times (Fig. 6b).

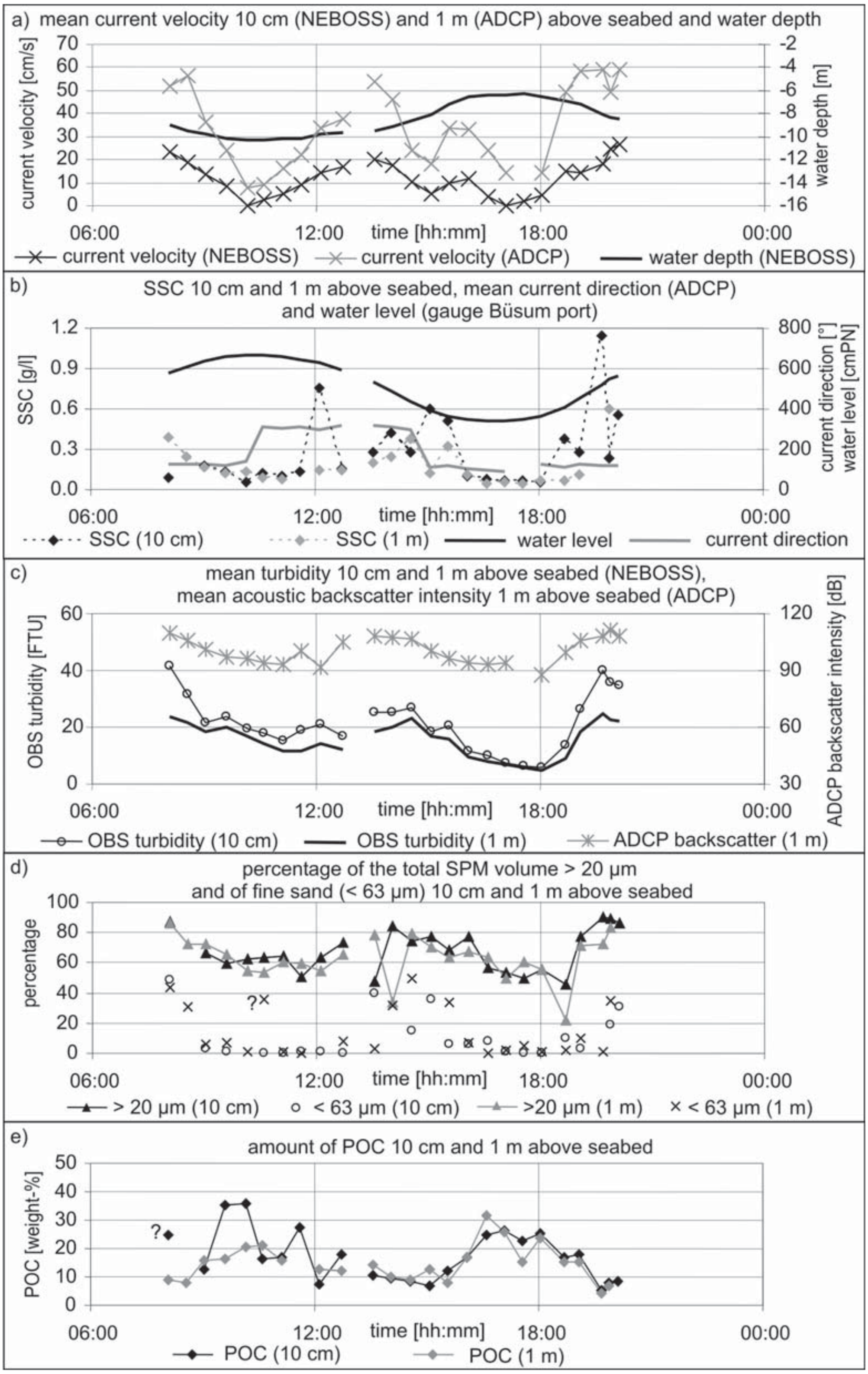

Fig. 6a–e: Stationary NEBOSS and ADCP measurements on 29 November 2001 over a tidal cycle

During slack water, the SSC decreases to ≤ 0.15 g/l at both depths, with slightly higher values during high-water slack tide (Fig. 6b). SSC exceeding values of 0.15 g/l are encountered in up to 50 % and 34 % of all measurements at 10 cm and 1 m above the seabed, respectively.

The mean OBS and ADCP backscatter signal intensities also show less SPM during slack water (Fig. 6a–c). Both sensors similarly reflect the SPM situation 1 m above the seabed, despite different measuring positions from the vessel. Comparing them with the time-variation curve of the lower OBS, higher values are restricted to the near-bed, in particular during maximum flood flow (Fig. 6c). However, there is not much difference visible between both depths during slack water, especially during low-water slack tide. The particle size and composition of the SPM change closely related to the tides (Fig. 6d–e). The percentage of particles > 20 µm is comparatively higher during flood and ebb flows as during slack water. A downward coarsening of suspended particles is not distinguishable in the shown case (Fig. 6d). On average, 25 % of the SPM volume appears flocculated. Suspended sand only turns up under higher flow conditions, but is not restricted to peak flows. Whereas the amount of sand up to 40 % is similarly high at both depths during flood tide, more fluctuations occur during ebb tide (Fig. 6d). A predominant sand transport close to the seabed cannot be derived from the data. Furthermore, the amount of sand, as in the example shown here, was not regularly found during all measuring campaigns, even under stronger currents.

Contrary to the time-variation curve of the clastic components found in suspension during flood and ebb currents, there is a higher ratio of POC during slack water (Fig. 6e). During high-water slack tide POC values > 25 % of the total SPM weight only occur close to the seabed, whereas during all other tidal phases the POC amount is similar at both depths.

4.2 DSLP Measurements

One result obtained from all DSLP measurements is the distinct increase of signal intensity a few decimetres above the seabed. The presence of a near-bed suspension layer of 20 cm on average is derived, based on the acoustic detection criteria for suspensions, which is defined as an abrupt change of the signal characteristics due to a significant or erratic increase of the particle density (Fig. 7).

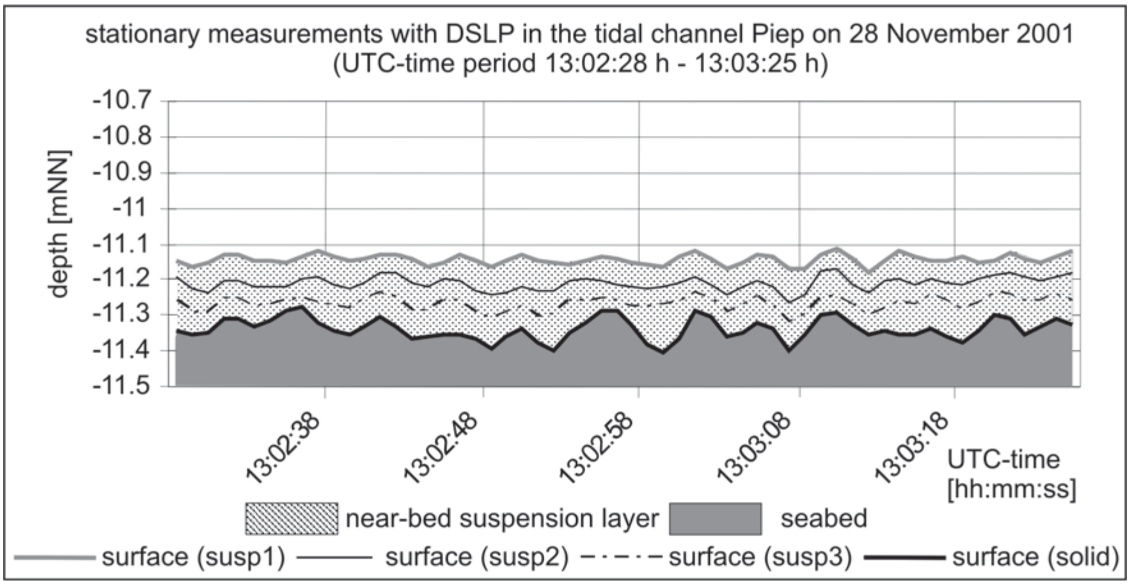

Fig. 7: Stationary measurements with DSLP on 28 November 2001, showing a roughly 20 cm thick, stratified near-bed suspension layer. The vertical sub-division is based on a downward increase of acoustic attenuation (susp1 – susp3)

The relatively low signal intensity (linear and weakly nonlinear acoustic signal characteristics) returning from the above water column is equated with SSC < 0.3 g/l (based on NEBOSS data). This near-bed suspension layer can be further vertically subdivided, based on a downward increase of the acoustic attenuation (Fig. 7). The layer boundaries are defined at 5 % (susp1 – susp2) and 50 % (susp2 – susp3) of the total acoustic attenuation of the near-bed suspension layer. These sub-layers were present at all measuring sites and during all tides. Short-term variations of the layer thickness indicate turbulent mixing processes, as also seen in the OBS data (Fig. 4–5). The mean layer thickness varied in a range of 1–3 cm during the stationary measurements (Fig. 8). A linear relationship between the mean near-bed current velocity and the thickness of lowermost layer susp3 ($\alpha = 0.05$; $n = 24$; $R^2 = 0.399$) exists in the example shown here, with a vertical increase of the layer thickness congruently with a decrease of the current velocity. The mean layer thickness of susp1 differs between both slack tides with higher values during high-water slack, as illustrated in figure 8. These findings are comparable to the mean OBS and ADCP data (Fig. 6c).

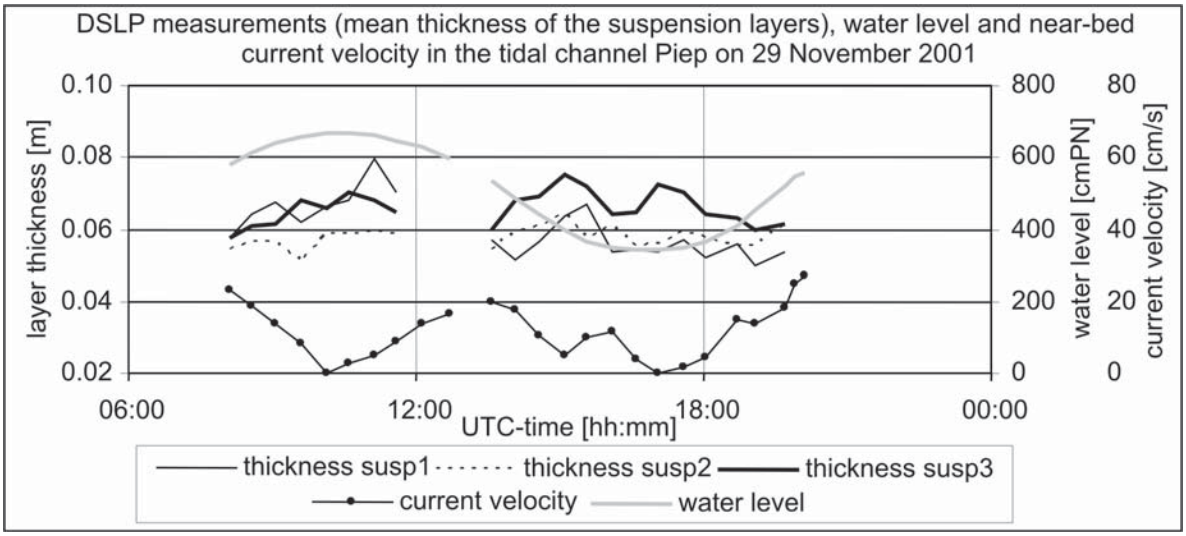

Fig. 8: Mean thickness of the near-bed suspension sub-layers (DSLP), and mean current velocity (NEBOSS) in the tidal channel Piep on 29 November 2001 during a tidal cycle

The differences in mean thickness of the detected near-bed suspension layer were small during stationary measurements, but remarkable variations repeatedly occurred, regarding profiles across the tidal channel Piep (Fig. 9). Furthermore, a thinner near-bed suspension layer was found at the sandy channel section near the Bielshövensand as in the deeper part of the channel or at its northern flank, where clays partly outcrop (chapter 3). This spatial distribution was not restricted to slack water. In addition, a stratified suspension layer was measured at each cross section.

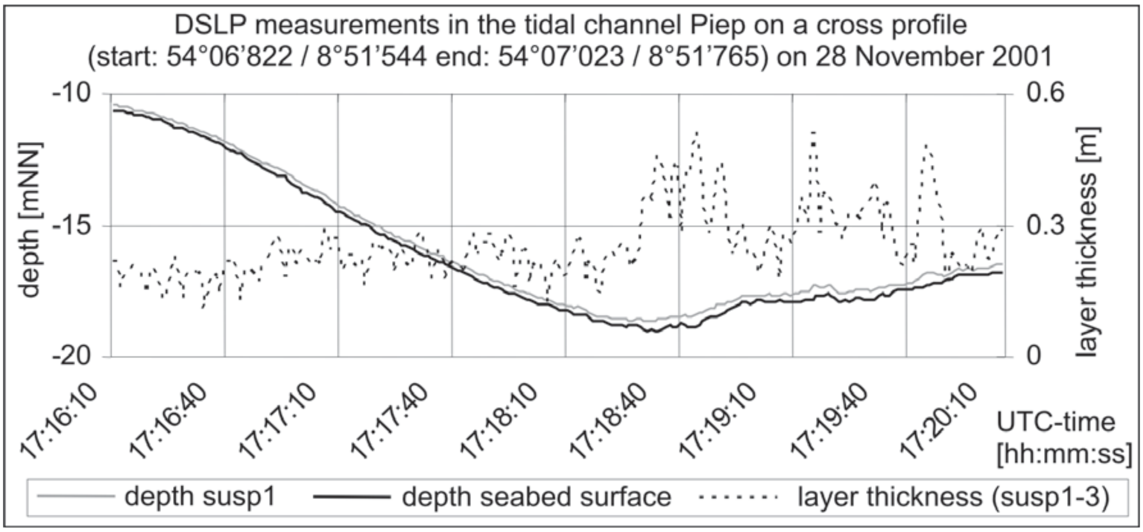

Fig. 9: Bathymetry and mean thickness of the near-bed suspension layer in the Piep on 28 November 2001 over a cross profile, based on DSLP measurements

5. Discussion

The near-bed sediment dynamics in the Piep is controlled by the semidiurnal tide, as demonstrated with the NEBOSS data. Influences by waves during the measurements can be excluded. It has been shown that the SSC increase at both considered depths corresponding to higher current velocities during flood and ebb tides (mid lunar cycle) with values > 1 g/l at 10 cm above the seabed. Isochronal, the composition of the SPM shifts towards coarser fractions and the amount of clastic components rises in relation to the organic matter. These findings reveal that the near-bed SSC is considerably higher as estimated from extrapolations of calibrated optical beam transmissometer profiles in the Piep with SSC values up to 0.25 g/l (POERBANDONO, 2003).

Considerable amounts of sand up to 69 % of the SPM volume were only found when mean near-bed current velocities exceeded > 10 cm/s. However, flow magnitude and amount of sand do not correlate at the 95 % significance level. At the same time, hardly any differences between sand trapped 10 cm and 1 m above the seabed were found. Turbulent mixing processes, as derived from the OBS data, lead to up- and downward directed transport of sand and thus prevent a downward particle coarsening. The time offset between maximum flow velocity and SSC can be ascribed to the processes of lag effects in resuspension and settling of SPM (DYER, 1986).

Overall, higher amounts of suspended sand were expected to appear close to the seabed congruently with higher SSC. The hypothesis, that the main pathway of sand is focused on the near-bed horizon has basically been proven to be true. Consequently, the amount of sand trapped in the lower sampler was expected to be constantly high during mean current velocities up to 57 cm/s above a sandy seabed, also according to the Shields criterion (SOULSBY, 1997). In a study on near-bed sand transport (0.26 m and 2.36 m above the seabed) in an inlet throat at the Dutch Frisian coast under low wave activity, a threshold velocity between 20 and 30 cm/s was detected (HIBMA and VAN DE KREEKE, 2001). Near-bed suspended sand concentrations of up to 0.2 g/l were obtained with an acoustic device. Despite different regional settings, the values were in the same range as in the Piep. Moreover, higher values were not restricted to the near-bed elevation (HIBMA and VAN DE KREEKE, 2001). Similar values were reported from a sandy tidal site in the outer Thames estuary (WHITEHOUSE, 1995). There, the amount of sand 5 cm above the seabed (based on pump samples) rose up to 0.27 g/l under currents velocities of 0.4 m/s, which were measured at 1 m elevation.

Investigations of SPM composition within the water column of the tidal channel Piep showed that there was hardly any sand in suspension (POERBANDONO and MAYERLE, 2005), matching the results of former investigations (RICKLEFS, 1989, 1998; RICKLEFS and AUSTEN, 1994). An uplift of sand into the water column by local eddies even to the surface as described by JACKSON (1976) can not be derived from the actual data sets of the Piep channel. These comparisons lead to the implication that sand is more likely to be mobilised during higher hydrodynamic input e.g. during simultaneous spring tide and storm conditions or that a larger amount of sand is transported as bedload even below the lowermost measuring depth of NEBOSS.

Slack tides in the Piep clearly illustrate reduced near-bed sediment transport as expected (EISMA, 1993). Then, the SSC drops down to 0.15 g/l at both depths which can be defined as background concentration and coincides with a size decrease of clastic particles and a higher ratio of organic matter. These values are similar (0.15 g/l – 0.22 g/l) to near-bed SPM values found in the Chesapeake Bay (USA) during slack water (FUGATE and FRIEDRICHS, 2002).

A near-bed suspension layer of 20 cm in thickness on average as present during flood and ebb tides was also detected with DSLP during slack water, but not with NEBOSS. A response to tidal variations can only be seen in the increased thickness of the lowermost suspension sub-layer during slack water. This can be explained with particle accumulation induced by settling processes. Similar results were reported from a tidal channel in New Zealand, where settling sand intermittently formed a 2 cm thick deposit during slack water (GREEN et al., 2000).

The evaluation of the DSLP results is more difficult, considering the presence of a few decimetres thick near-bed suspension layer, irrespective of the tide. Short-term fluctuation of the layer thickness can be ascribed to turbulent mixing processes, although with much smaller amplitudes as derived from NEBOSS. A sudden distinct volume expansion of the near-bed suspension layer (‘burst’) of up to 1 m above the seabed was not detected by the DSLP at any time. A remarkable change in layer thickness only occurred spatially with increasing values in the deeper part of the channel where clays outcrop, producing a prominent relief. This cause extra turbulence due to increased bed roughness. However, the spatial distribution and volume expansion of a near-bed suspension remained constant over the tidal cycle.

6. Conclusions

In this study, it has been shown that the new measuring device NEBOSS is capable of identifying tide dependant near-bed sediment transport processes, such as turbulent movement of SPM, particularly during flood and ebb tides. Even complex flow patterns and resulting complex near-bed sediment transport processes can be visualised with NEBOSS. The hypothesis, that sand is transported close to the seabed can be seen to be true. However, higher amounts of sand have been expected to be trapped at the lower elevation. In this case, further measurements are needed with samplings even closer to the seabed while surveys include periods of higher hydrodynamic energy input.

By means of NEBOSS and DSLP, a near-bed suspension layer of about 20 cm in thickness were detected during flood and ebb tides, which indicates a prominent near-bed sediment transport. However, differing results were found when it comes to the tide dependant decrease of this layer during slack water. Other discrepancies occurred, regarding the SSC > 0.3 g/l which was repeatedly registered 1 m above the seabed with NEBOSS. This does not match the thickness of the near-bed suspension layer detected with the DSLP.

Sediment transport processes a few centimetres above the seabed as indicated by DSLP can not be resolved with NEBOSS due to its limitation in the lowermost measuring depth. The results indicate, that tide dependant SSC is equal or lower than 10 cm above the seabed (0.15 g/l – 1.2 g/l) than closely above it (1–2 cm). However, the acoustic signal characteristics of DSLP within the lowermost centimetres above the seabed cannot be verified with SSC data or other particle characteristics such as particle size and composition in this study. Indications are that different near-bed sediment transport mechanisms occur at both depth ranges.

7. Acknowledgements

The work presented in this paper was part of an interdisciplinary project funded by the Federal Ministry of Education and Research (funding number 03 F 0262 B). The authors express their sincere thanks to Dr. K. Ricklefs, who initiated and coordinated the project. We would also like to thank our project partners of General Acoustics for their much appreciated cooperation throughout the project. The assistance of G. Bojens and B. Meier in the development and deployment of the NEBOSS device is also gratefully acknowledged. We would also like to thank the captain and crew of the RV SÜDFALL of the Research and Technology Centre Westcoast of Kiel University for their valuable assistance in the measuring campaigns.

8. References

ASP NETO, N. E.: Long- to Short-term Morphodynamic Evolution of the Tidal Channels and Flats of the Dithmarschen Bight, German North Sea. Berichte, Forschungs- und Technologiezentrum Westküste der Universität Kiel, 34: 166 p, 2004.

CHRISTIANSEN, H.: Erste Ergebnisse aus Schwebstoffmessungen mit dem CUX-Sampler in der Elbe. Die Küste, H. 42: 123–134, 1985.

DEINES, K. L.: Backscatter Estimation Using Broadband Acoustic Doppler Current Profilers, in Proceedings of the IEEE Sixth Working Conference on Current Measurements, San Diego, CA, March 11–13, 249–253, 1999.

DIERCKE, C. and DEHMEL, H. E.: Diercke Weltatlas, Georg Westermann 143: 218 p, 1968.

DYER, K. R.: Coastal and Estuarine Sediment Dynamics. John Wiley and Sons, Chichester: 342 p, 1986.

EDEN, H.; MÜLLER, V. and VORRATH, D.: DSLP-Method – A New Surveying Technology. In AUGATH, W. (ed.) Gewässervermessung und hydrographische Informationssysteme. DVW-Schriftenreihe 37: 106–115, 1999.

EDEN, H.; HENSSE, J. and MÜLLER, V.: Investigations on Transient Sediment Dynamics by DSLP-Method. Die Küste, H. 69, 2005.

EDEN, H.; MÜLLER, V. and VORRATH, D.: DSLP – An Innovative Echo Sounding Technology. HANSA International Maritime Journal 10: 36–39, 2000.

EDEN, H.; MÜLLER, V. and VORRATH, D.: Exact Detection of Suspension and Sediment Layers – a New Surveying Technology. Sea Technology, 42 (10): 31–36, 2001.

EISMA, D.: Flocculation and De-flocculation of Suspended Matter in Estuaries. Netherlands Journal of Sea Research, 20 (2/3): 183–199, 1986.

EISMA, D.: Suspended Matter in the Aquatic Environment: 315 p, 1993.

FUGATE, D. C. and FRIEDRICHS, C. T.: Determining Concentration and Fall Velocity of Estuarine Particle Populations Using ADV, OBS and LISST. Continental Shelf Research 22: 1867–1886, 2002.

GREEN, M. O. and BOON, J. D.: The Measurement of Constituent Concentrations in Non Homogeneous Sediment Suspensions Using Optical Backscatter Sensors. Marine Geology 110: 73–81, 1993.

GREEN, M. O.; BELL, R. G.; DOLPHIN, T. J. and SWALES, A.: Silt and Sand Transport in a Deep Tidal Channel of a Large Estuary (Manukau Harbour, New Zealand). Marine Geology 163: 217–240, 2000.

GREEN, M. O.; DOLPHIN, T. J.; SWALES, A. and VINCENT, C. E.: Transport of Mixed-size Sediments in a Tidal Channel. Specialty Conference, Coastal Sediments '99, A.S.C.E, New York: 644–658, 1999.

HAY, A. E.: On the Remote Acoustic Detection of Suspended Sediment at Long Wavelengths. Journal Geophysical Research, 88 (C12): 7525–7542, 1983.

HIBMA, A. and VAN DE KREEKE, J.: Tidal Variations in Sand Concentration in the Frisian Inlet. Proceedings of the Coastal Dynamics Conference, Lund, Sweden: 453–462, 2001.

HICKEL, W.: Seston in the Wadden Sea of Sylt (German Bight, North Sea). Netherlands Institute for Sea Research 10: 113–131, 1984.

HOITINK, A. J. F. and HOEKSTRA, P.: Observations of Suspended Sediment from ADCP and OBS Measurements in a Mud-dominated Environment. Coastal Engineering 52: 103–118, 2005.

JACKSON, R. G.: Sedimentological and Fluid-dynamic Implications of the Turbulent Bursting Phenomenon in Geophysical Flows. Journal Fluid Mechanics 77: 531–560, 1976.

JOERDEL, O.; FLEMMING, B. W. and BARTHOLOMÄ, A.: Flocculation, Floc Breakup and Grain-size Composition of Suspended Sediments in Tidal Waters of the Southern North Sea. In: FLEMMING, B. W., HARTMANN, D. and DELAFONTAINE, M. T. (eds), From Particle Size to Sediment Dynamics, Int. Workshop, Delmenhorst, Germany, Abstract Vol.: 86–89, 2004.

KERN, U. and WESTRICH, B.: Methoden zur Erkundung, Untersuchung und Bewertung von Sedimentablagerungen und Schwebstoffen in Gewässern. Arbeitskreis „Schweb- und Schadstoffe in Fließgewässern“ im DVWK-Fachausschuss „Sedimenttransport in Fließgewässern“ Deutscher Verband für Wasserwirtschaft und Kulturbau e.V. (ed.) 128: 430 p., 1999.

KÖSTER, R.: Wattsedimente. In: Landesamt f. d. Nationalpark Schleswig-Holsteinisches Wattenmeer [Hrsg.]: Umweltatlas Wattenmeer, Bd. I: Nordfriesisches und Dithmarscher Wattenmeer: 40–41, 1998.

KREEKE VAN DE, J.; DAY, C. M. and MULDER, H. P. J.: Tidal Variations in Suspended Sediment Concentration in the Ems Estuary: Origin and Resulting Sediment Flux. Journal of Sea Research 38: 1–16, 1997.

NIELSEN, P.: Field Measurements of Time-averaged Suspended Sediment Concentrations Under Waves. Coastal Engineering 10: 23–31, 1984.

OHM, K.: Optische Messungen zur Bestimmung von Schwebstofftransporten. Die Küste, H. 42: 227–236, 1985.

PIERCE, J. W. and NICHOLS, M. M.: Change of Particle Composition from Fluvial into an Estuarine Environment: Rappahannock River, Virginia. Journal of Coastal Research, 2 (4): 419–425, 1986.

POERBANDONO and MAYERLE, R.: Effectiveness of Acoustic Profiling for Estimating the Concentration of Suspended Material. Die Küste, Heft 69, 2005.

POERBANDONO: Sediment Transport Measurement and Modelling in the Meldorf Bight Tidal Channels, German North Sea Coast. Dissertation, Christian-Albrechts-Universität zu Kiel, 151 p, 2003.

REIMERS, H.-C.: Wirkungsweise von Buschlahnungen auf den Sedimenthaushalt von aufwachsenden Deichvorländern an der schleswig-holsteinischen Westküste. Berichte, Forschungs- und Technologiezentrum Westküste der Universität Kiel 17: 140 p, 1999.

REINECK, H. E. and SINGH, I. B.: Depositional Sedimentary Environments with Reference to Terrigenous Clastics: 551 p, 1980.

RICKLEFS, K.: Zur Sedimentologie und Hydrographie des Eider-Ästuars. Berichte-Reports, Institut für Geowissenschaften, Universität Kiel 35: 182 p, 1989.

RICKLEFS, K.: Die Verteilung von Schwebstoffen im Hörnum-Tief. Die Küste, H. 60: 142–160, 1998.

RICKLEFS, R. and AUSTEN, G.: Ergebnisse von Schwebstoff- und Strömungsmessungen in den Rückseitenwatten der Insel Sylt (Nordsee/Deutsche Bucht). Meyniana 46: 91–106, 1994.

RIJN VAN, L. C.: Principles of Sediment Transport in Rivers, Estuaries and Coastal Seas, 700 p., 1993.

ROSS, M. A. and METHA, A. J.: On the Mechanics of Lutoclines and Fluid Mud. Journal of Coastal Research 5: 51–61, 1989.

SHI, Z.; REN, L. F. and LIN, H. L.: Vertical Suspension Profile in the Changjing Estuary. Marine Geology 130: 29–37, 1996.

SMITH, T. J. and KIRBY, R.: Generation, Stabilisations and Dissipation of Layered Fine Sediment Suspensions. Journal of Coastal Research 5: 63–73, 1989.

STERNBERG, R. W.: Measuring Sediment Dynamics, Continuous Suspended Load Sampler. In SEYMOUR, R. J. (ed.) Near Shore Sediment Transport, Chapter 5c: 95–102, 1989.

STERNBERG, R. W.; SHI, N. C. and DOWNING, J. P.: Measuring Sediment Dynamics, Continuous Measurements of Suspended Sediment. In: SEYMOUR, R. J. (ed.) Near Shore Sediment Transport, Chapter 11c: 231–257, 1989.

SOULSBY, R.: Dynamics of Marine Sands. Thomas Telford, 249 p, 1997.

THORNE, P. D.; HARDCASTLE, P. J. and SOULSBY, R. L.: Analysis of Acoustic Measurement of Suspended Sediments. Journal of Geophysical Research 98 (C1): 899–910, 1993.

THORNE, P. D.; VINCENT, C. E.; HARDCASTLE, P. J.; REHMAN, S. and PEARSON, N.: Measuring Suspended Sediment Concentrations Using Acoustic Backscatter Devices. Marine Geology 98: 7–16, 1991.

VELEGRAKIS, A. F.; GAO, S.; LAFITE, R.; DUPONT, J. P.; HUAULT, M. F.; NASH, L. A. and COLLINS, M. B.: Resuspension and Advection Processes Affecting Suspended Particulate Matter Concentrations in the Central English Channel. Journal of Sea Research 38: 17–34, 1997.

VINCENT, C. E.; STOLK, A. and PORTER, C. F. C.: Sand Suspension and Transport on the Middelkerke Bank (southern North Sea) by Storms and Tidal Currents. Marine Geology 150: 113–129, 1998.

WEBB, M. P. and VINCENT, C. E.: Comparison of Time-averaged Acoustic Backscatter Concentration Profile Measurements with Existing Predictive Models. Marine Geology 162: 71–90, 1999.

WHITEHOUSE, R.: Observation of the Boundary Layer Characteristics and the Suspension of Sand at a Tidal Site. Continental Shelf Research 15 (13): 1549–1567, 1995.

WIELAND, P.: Trischen – die Geschichte einer alluvialen Insel im Dithmarscher Wattenmeer. Die Küste 62: 101–140, 2000.

ZAMPOL, J. A. and WALDORF, B. W.: Measuring Surf Zone Dynamics, Discrete Sampling of Bedload and Suspended. In: SEYMOUR, R. J. (ed.) Near Shore Sediment Transport, Chapter 5a: 81–89, 1989.

ZANKE, U.: Grundlagen der Sedimentbewegung: 402 p, 1982.

Die Küste, 69 PROMORPH (2005), 1-420

Investigations of Transient Sediment Dynamics by the DSLP®-Method

By HENDRIK EDEN, JENS HENSSE and VOLKER MÜLLER

Summary

Within the framework of the PROMORPH project, measurements of highly-dynamic sediment processes were performed with the aid of DSLP('Detection of Sediment Layers and Properties')-technology in the benthic boundary layer of the PROMORPH investigation area. The aim of these measurements was to obtain in-situ data for assessing the applicability of various models for simulating near-bottom sediment transport. DSLP - technology has proven its ability to resolve near-bottom sediment transport phenomena convincingly. Exemplary results are presented to illustrate the practical application of the DSLP-method.

Zusammenfassung

Im Rahmen des PROMORPH-Projektes wurden mittels der DSLP-Technologie ('Detection of Sediment Layers and Properties') Messungen zu den hochdynamischen sedimentologischen Prozessen in der benthischen Grenzschicht innerhalb des Untersuchungsgebietes durchgeführt. Ziel dieser Messungen war es, in-situ Messdaten zu bekommen, um die Anwendbarkeit verschiedener Modelle zum bodennahen Sedimenttransport bewerten zu können. Die DSLP-Technologie hat ihre Fähigkeit, bodennahe Sedimenttransportvorgänge aufzulösen, überzeugend nachgewiesen. Beispielhafte Ergebnisse werden hier dargestellt.

Keywords

DSLP-technology; echo-sounder; acoustic classification; fluid-solid interface; near-bottom sediment transport; suspension concentration; bathymetric changes; PROMORPH

Contents

1. Introduction

Investigations concerned with the dynamics of sedimentological processes are characterized by a large variety of requirements. In particular, information on the dynamics of sedimentological processes is of great importance for effective dredging management, port maintenance and development, waterways management, and coastal and flood protection systems. Information on the origins, whereabouts and quantities of transported sediment as well as the temporal variation of these processes is essential in this context. This places high demands on the temporal resolving power of the methods used to acquire this information. By means of the DSLP-method it is now possible to fulfil these high requirements. The implementation of DSLP-technology in different measuring techniques, combined where necessary with concomitant flow measurements, leads to hitherto unattainable high-quality remote sensing data on the dynamics of sedimentological processes.

These special features of the DSLP-method were required for the purpose of data acquisition within the framework of the PROMORPH project. This paper describes the DSLP-measuring technology and also presents exemplary results which demonstrate the application of the method for investigating highly instationary sediment dynamics. A detailed analysis of the scientific results of the measurement campaigns using the DSLP-method is presented by SCHROTTKE and ABEGG (in this volume).

2. Measurements based on DSLP-Technology

2.1 DSLP-Technology for Investigating Sediment Dynamics

The DSLP-method ('Detection of Sediment Layers and Properties') developed by General Acoustics GmbH (EDEN et al. 2000, 2001; SEEFELDT et al. 1999) is an innovative hydro-acoustic method for measuring the properties of suspended and near-bed sediment layers. The underlying technology of the DSLP-method is essentially different to that implemented in commonly-used echo sounders such as single or multi-frequency two or three-dimensional echo sounders or sediment echo sounders. The fundamental difference between this method and other echo sounding systems is that the DSLP-system operates independently of the utilized acoustic frequencies, thereby permitting an unambiguous and definite high-resolution physical analysis of the acoustical interaction between sound waves and targets (e.g. suspended matter and sediment types). This permits the detection of suspensions with a wide range of concentrations (e.g. fluid mud, suspended sediments, sand suspensions, etc.) and a wide range of thicknesses (3 cm up to several metres). The physically-proven accuracy of detecting interfaces such as e.g. the fluid-solid interface between suspensions and consolidated sediments is of the order of 3 cm. An estimation of the depth of these interfaces is always independent of the results of other measurements and/or calibrations. In contrast to conventional echo sounding systems, which operate with a measurement accuracy of no less than a decimetre, the DSLP-method thus permits high-accuracy detection of near-bottom sediment suspensions as well as high-precision determination of layer thicknesses and concentration-related parameters. This capability of the DSLP-method adds to the importance of remote sensing of near-bottom sediment and suspension dynamics.

Two main features of the DSLP-method are utilised in particular. The first feature is the ability to detect the fluid-solid interface with high definition owing to the first significant appearance of acoustic reflection over the full applied wave band. Technically, this could be achieved by high-resolution complex signal analysis of the received acoustic waves. The transmitted acoustic pulses are affected by scattering, reflection and damping (frequency-dependent and frequency-nondependent processes), thus providing an unambiguous representation of material structure and stratification. In the present case the adopted wave band ranges from 12.5 to 200 kHz and the signal analysis for detecting the fluid-solid interface is bounded by an aperture angle of 3 degrees. Bathymetric variations over the bottom area exposed to sonic waves are neglected. The resulting depth value is then set to its highest value within this area, which is an admission requirement for navigation echo sounders.

The second feature used is the ability to differentiate between various types of scattering. Often a correlation between backscatter strength and suspension concentration is applied, as determined from probe samples. It is well-known that (mostly linear) interpolation between discrete values is questionable due to the unknown basic acoustic scattering processes which govern the measured value of backscatter strength. The complex signal analysis of the multi-frequency acoustic signal in the DSLP-method results in a differentiation of the various type of scattering processes such as single and multiple scattering or diffusive scattering. These distinct processes are classified according to so-called "nonlinear damping parameters". In the DSLP-method a detected suspension or sediment layer is thus classified not only by the (depth-corrected) backscatter strength but also by a set of nonlinear damping parameters. The latter is referred to as acoustic classification. Temporal and/or local changes in the values of this parameter set (not essentially a change in backscatter strength) represent a structural change in sediment/suspension stratification. On account of this outstanding feature, combined with high depth-resolution, the DSLP-method is extremely suitable for measuring highly concentrated near-bottom suspension layers (MÜLLER et al., 2001).

2.2 Measurements

Having confirmed the capabilities of the DSLP-method (EDEN et al., 1998; LIEBETRUTH, 2004) for measuring highly instationary sediment dynamics, a measuring strategy aimed at gaining a deeper insight into local (point and cross-sectional) sediment dynamics over a tidal cycle was developed in cooperation with the Research and Technology Center Westcoast (FTZ) in Büsum (SCHROTTKE and ABEGG, in this volume). The high depth-resolving capability of the DSLP-method, combined with a sampling frequency of up to 10 Hz, permits high-resolution measurements of local sediment dynamics processes.

The DSLP-measurements were carried out within the framework of the measuring campaigns undertaken by the FTZ Büsum. The technical equipment of the complete DSLP-system was adapted to the available infrastructure on board the research vessel "Südfall". A high-precision DGPS with an outboard reference station was included in the DSLP-system to fulfil the requirements of accuracy (horizontal local resolution of 1 cm, height resolution of 1 cm with an accuracy of 2 cm). The accuracy of the DGPS-system was also sufficient to compensate for heave.

Two different measuring schemes were implemented. Firstly, high-frequency (5 Hz) point measurements were made to investigate high-frequency sediment dynamics at a local position. Secondly, continuous measurements in a cross-section were made over a tidal cycle in order to resolve the tidal dependence of near-bottom sediment dynamics. The request on the positioning accuracy at both measuring schemes is extremely different. DGPS together with a good seamanship were responsible for the fact that the measurements over a cross-section were almost perfect. But these prerequisites are not sufficient for performing point measurements. Although motion compensation methods were used, a sufficient local stability due to movements of the moored vessel (Fig. 1) could not be reached. Thus, the measured depth

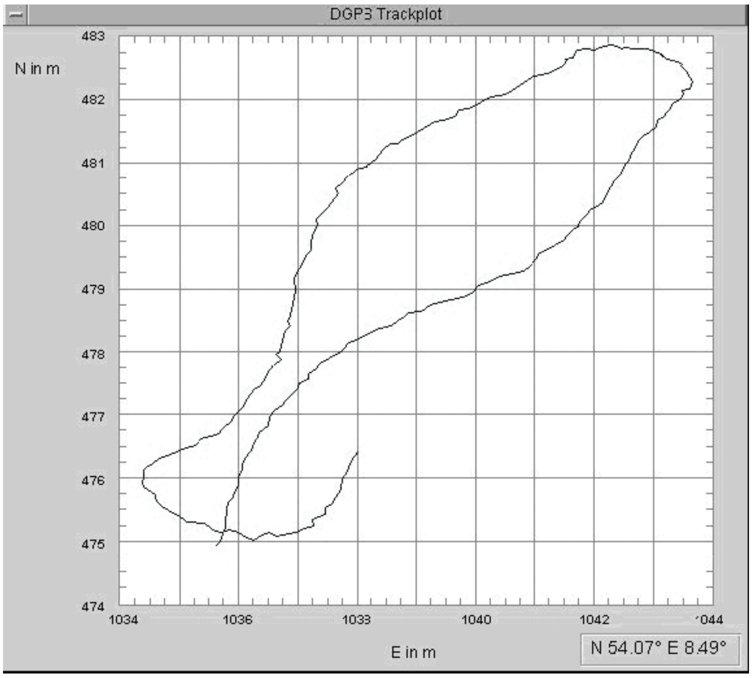

Fig. 1: Example of a local measurement; duration: 240 sec, mean flow velocity: 20 cm/s; local stability could only be attained over an area of 10 × 10 metres; the figure was obtained by running DSLP-software during measurements

levels of the various suspension layers are mostly found to be a non-resolvable combination of small bathymetric changes (cf. a depth accuracy of 3 cm) and instationary changes in the thickness of these suspension layers.

3. Results and Evaluation

3.1 Point Measurements

In all DSLP-measurements (during 6 measuring periods at run time and at all measurement locations) the same basic qualitative suspension/sediment characteristics were detected. Generally speaking, two distinct near-bottom suspension layers were identified. The overall thickness of these two high-concentration suspension layers was found to be small, i.e. mostly of the order of 10 centimetres (dynamic rise of up to 40 cm). Above these two layers, an additional suspension layer was detected. According to the afore-mentioned acoustic classification (linear scattering), it is deduced that the sediment concentration within this layer is extremely low. The fluid-solid interface borders the bottom suspension layer abruptly with increasing depth (Fig. 2). Although dynamic changes in the local depth of this interface were detected, it was not possible to draw a clear distinction between highly transient sediment/suspension dynamics and small bathymetric changes due to the inability to differentiate between the local instability of the research vessel and bathymetric variations within an area of 10 × 10 metres. A necessary prerequisite for such investigations, i.e. high depth-resolution and accuracy, is given by the DSLP-system. These investigations thus underline the need for a fixed mounting to differentiate between the latter two effects.

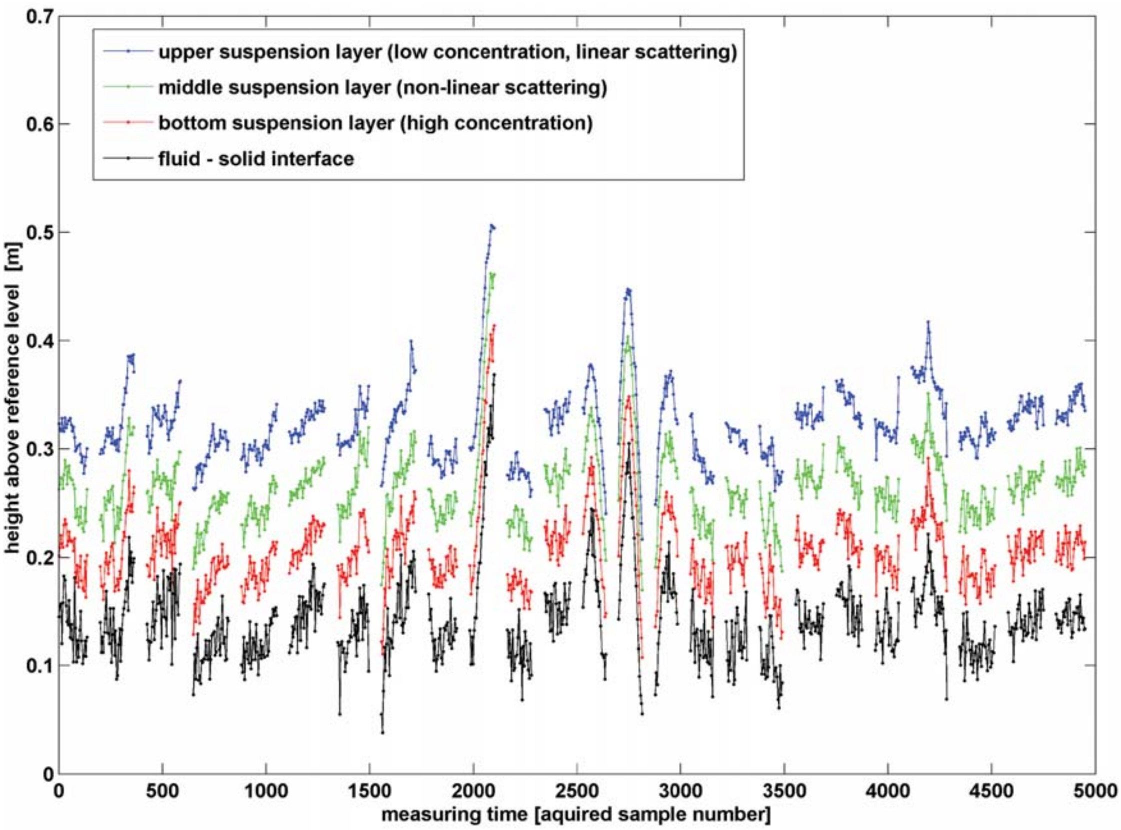

Fig. 2: Typical results of local DSLP-measurements; 1-second mean values of 5 Hz measurements, 25 measuring cycles (30 s) uniformly distributed over a full tidal cycle at a single location; the reference depth is taken to be the lowest single value of the fluid-solid interface ever measured at this location

The overall thickness of both high-concentration suspension layers is small, mostly in the range of 10 centimetres (dynamic rise of up to 40 cm). Acoustically, these suspension layers are classified by a set of nonlinear damping parameters. These are numerical parameters that describe typical signal characteristics dependent on the different (nonlinear) sound-matter interactions found in the complex multi-frequency acoustic signal. In the present case an individual characteristic acoustic parameter of this type was found for every suspension layer. A variation of the value of this parameter is typical for a change in the layer concentration (increasing nonlinear damping implies increasing concentration). The significance of the presence of a parameter of this subset is typical for a special inner structure of this layer. Due to the mainly simple inner structure of the detected suspension layers in this case, they are described by only one parameter. A correlation between the significance of parameters derived from the subset and their assigned values to an inner structure of matter or a specific concentration can only be realised by an accompanying analysis of probe samples taken at the same location and time.

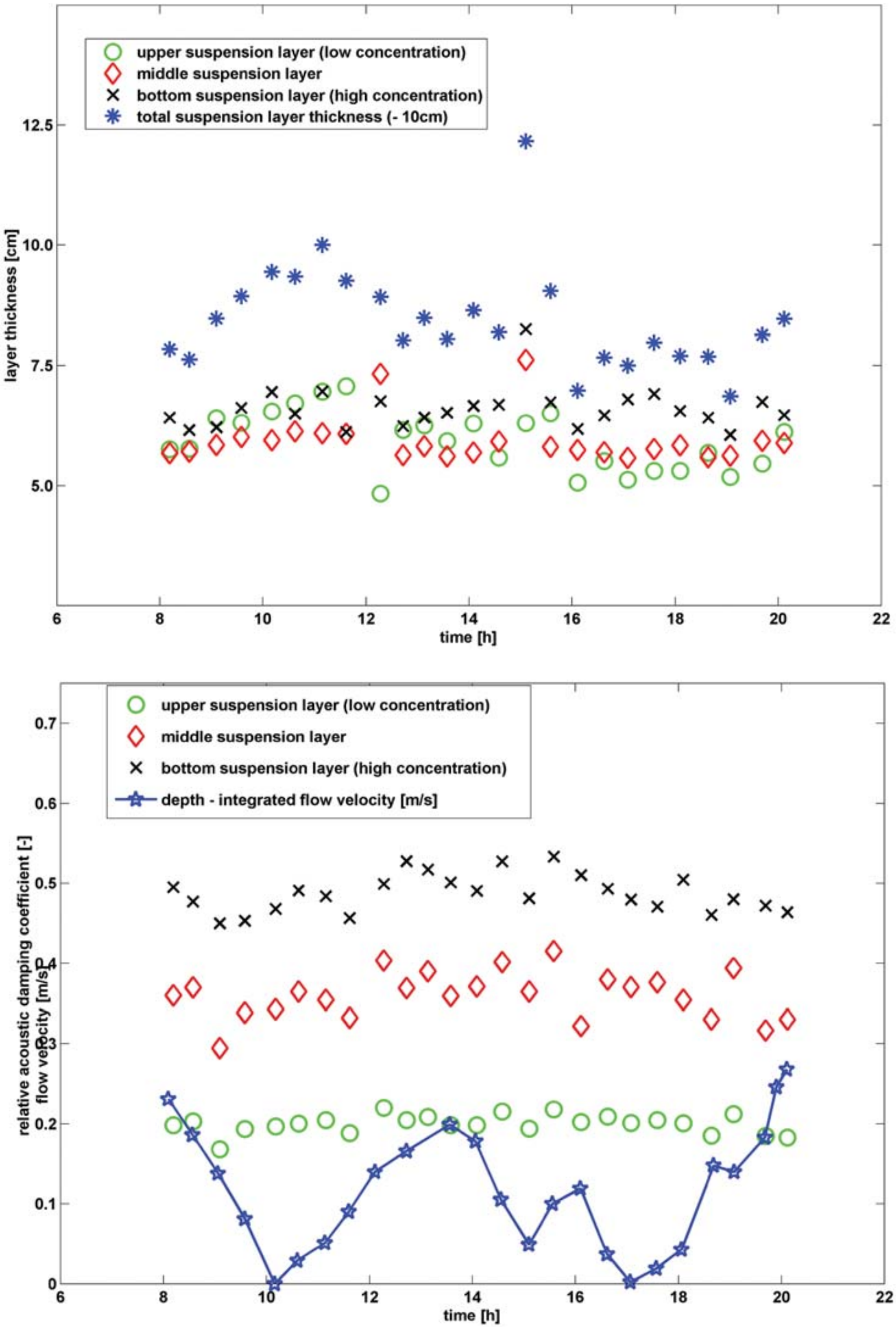

Fig. 3: Thickness of the detected suspension layers (upper figure) and values of the layer-specific acoustic parameter (lower figure) in relation to the time dependence of the mean flow velocity; the values of each single acoustic parameter describe the concentration variations within the represented layer. However, the relationship between values in different layers on a specific date cannot be linearly transferred to obtain a relationship between suspension concentrations

At all measuring locations the suspension layers are described by the value of the layer-significant acoustic parameter and the thickness of this layer. An interface between the suspension layers may either be characterised by an abrupt change in concentration (density jump) or an abrupt change in the inner structure, which is not necessarily accompanied by a density change. The interfaces between layers are always recognised in this case as interfaces between slightly different inner structures. Variations in the specific layer-significant parameter over the measured tide as well as variations in the thickness of the detected layers are small (Fig. 3), but not negligible. The qualitative layer dynamics are comparable to the results of other surveys (EDEN et al., 1998). An estimate of the concentration profile within a layer is not possible. This is due to the depth accuracy of 3 cm associated with the DSLP-system and a mean thickness of 6–7 centimetres for each identified layer. Owing to the fact that a systematic collection of probe samples with a depth resolution of 3–6 centimetres within the near-bottom suspension layers could not be performed by means of the sampling technique available, it was not possible to correlate the DSLP-results with probe samples.

3.2 Measurements in a Cross-Section

In contrast to the above-mentioned investigations of short-term sediment dynamics processes (Section 3.1), emphasis is now placed on the high-resolution measurement of suspension/sediment dynamics in a cross-section over a full tidal cycle (Fig. 4). By means of the DSLP-method it is not only possible to determine the depth positions of the individual suspension interfaces, but also to resolve the concentration classes of the suspension layers. Thus, it is also possible to determine a balance between the suspension and bed load.

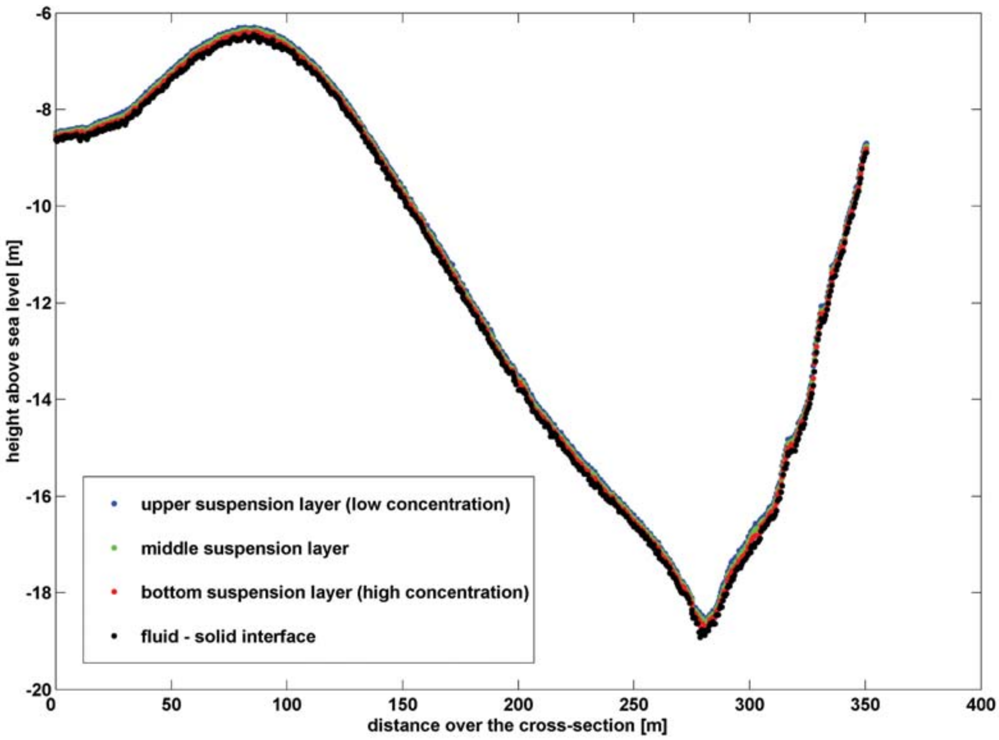

Fig. 4: Typical results of cross-sectional DSLP-measurements which resolve a) the interface between "clear" water and a low-concentration upper suspension layer, b) the interface between this upper layer and the first high-concentration suspension layer, c) the interface between the two high-concentration suspension layers and d) the fluid-solid interface (interface between the bottom suspension layer and the first layer of consolidated sediment exhibiting the property of solid matter)

The temporal development of the layer thickness of the characteristic suspension layers detected in a 350m-wide cross-section (Fig. 4) over a period of 12 hours is presented in Fig. 5. In combination with concomitant level and/or flow measurements, it seems possible to assign the layer dynamics to e.g. fluid dynamic events. Regions as well as periods of higher layer dynamics are easily recognisable. During the measuring period only weak sediment and suspension dynamics was observed. The overall thickness of the near-bottom high-concentrated suspension layers is smaller than 3 dm. Temporal variations of the layer thicknesses are distinct at the deepest part of the cross-section and especially for the bottom suspension layer. The results give not an indication of a significant vertical (turbulent) transport at the depth range up to 3 dm above bottom, which would lead to a significant change of thickness of these layers. If there exist any near bottom transport and which amount of suspension at the depth range up to 3 dm above bottom will be transported can not be concluded directly from these measurements. Therefore a combination with flow measurements and/or simulation results as well as with measurements of local suspension concentration with a desired depth resolution better than 1 dm are necessary.

Combination of the DSLP-results, which were ordered by the Research and Technology Center Westcoast (FTZ), with other results as well as further discussion is presented by SCHROTTKE and ABEGG (in this volume).

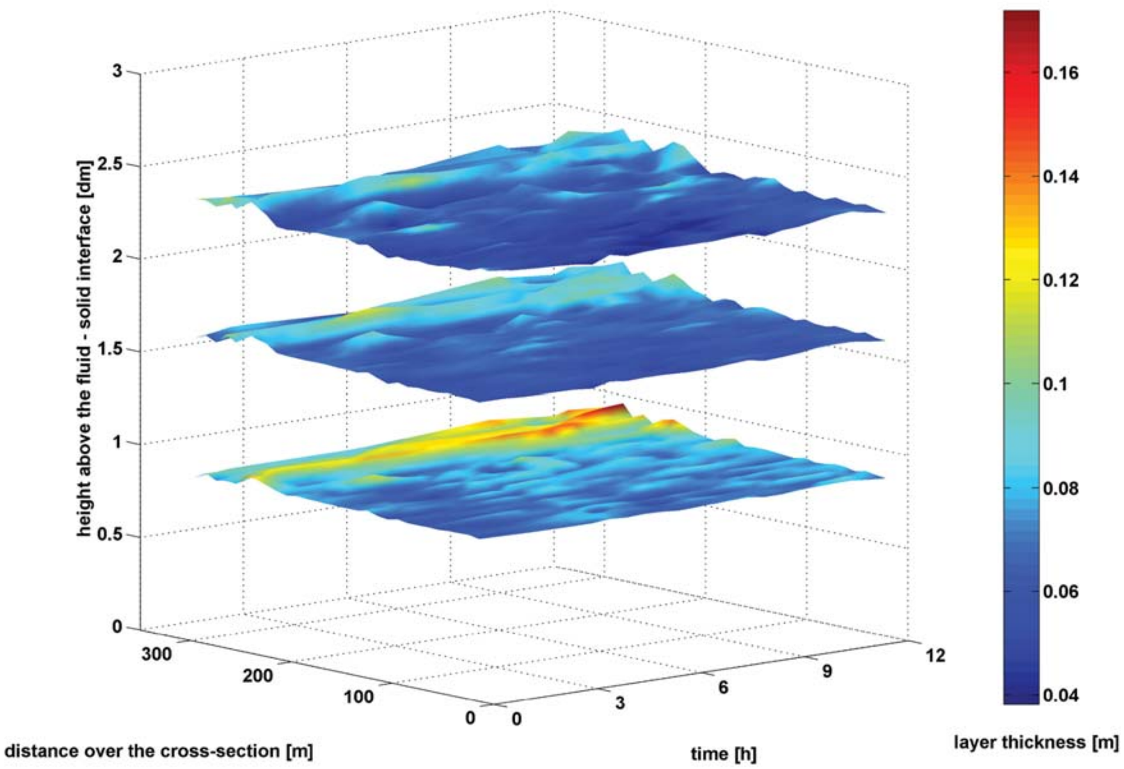

Fig. 5: Results of DSLP-measurements in the 350 m wide cross-section of Fig. 4; three different suspension layers were detected which could be distinguished by their acoustic behaviour; the mean concentration of the distinct layers is almost constant; here the selected representation of the results is an extension of the representation of local results like presented at Fig. 3 to the 3rd dimension – the distance over the cross-section

4. Conclusions

The DSLP-method is the first "echo sounder" method that permits the measurement of sediment dynamics processes over time intervals varying from seconds to days, and from weeks to months. This capability is based on the high depth-accuracy performance of the DSLP-method combined with the ability to differentiate between and uniquely classify physically classifiable sediment and suspension layers acoustically. On account of the implemented measurement technology and application characteristics of the DSLP-method it is possible to resolve sediment dynamics processes according to requirements. The information content of DSLP-measurements may be enhanced by the inclusion of accompanying measurements such as e.g. flow measurements. As confirmed by the present investigation, the DSLP-method offers new possibilities for measuring the dynamics of sedimentological processes.

5. References

EDEN, H.; VORRATH, D. and MÜLLER, V.: Erfassung von Sedimenten geringer Dichte. Final Report of the KFKI project 616-84020-MTK-0607, Kiel, 1998.

EDEN, H.; MÜLLER, V. and VORRATH, D.: DSLP® – an innovative echo sounding technology. Hansa, 137 (2000) 10, pp. 36–39, 2000.

EDEN, H.; MÜLLER, V. and VORRATH, D.: Exact Detection of Suspension, Sediment Layers: New Technology. Sea Technology, 42 (2001) 10, pp. 31–36, 2001.

EDEN, H. and MÜLLER, V.: High Resolution Detection of near Bottom Sediment Dynamics – a Challenge to acoustic remote sensing Techniques. Proceedings in HYDRO 2002 "Sounding the Future", Deutsche Hydrographische Gesellschaft e.V. (Herausgeber), Kiel, 2002.

LIEBETRUTH, F.: Ermittlung der nautischen Sohle der Ems von km 47,3 bis km 48,1, Stellungnahme zu den geotechnischen, rheologischen und Echolot-Vergleichsuntersuchungen vom 8. bis 10. September 2003. Bundesanstalt für Wasserbau – Außenstelle Küste, Hamburg, 2004.

MÜLLER, V.; EDEN, H. and VORRATH, D.: Remote Sensing of Near-Bottom Sediment Dynamics by combined DSLP®- and LOG_aFlow®-Technology. XXIX IAHR Congress (Beijing), Beijing, 2001.

SCHROTTKE, K. and ABEGG, F.: Near bed suspended sediment dynamics in a tidal channel of the German Wadden Sea. Die Küste, Heft 69, 2005.

Die Küste, 69 PROMORPH (2005), 1-420

Morphological Changes in a Tidal Flat Area: A Comparison of Radar, Optical and In-Situ Data

By KLAUS RICKLEFS, SUSANNE LEHNER and JAN RAUSCH

Summary

For assessing the suitability of in-situ bathymetric measurements and remote sensing satellite data (ERS-1 and 2, Landsat-TM and MSS, IRS-1C PAN and LISS-III) to detect morphological changes in tidal flats and the information content obtained by both methods, two highly morphodynamic test areas have been chosen within the Dithmarschen Wadden Sea (German Bight): the shoals Tertius Sand and D-Steert. Both sand banks show a distinct shoreward drift, which is due to sediment motion driven by general sea level rise and hydrodynamic forces such as waves and currents. Morphological changes related to sedimentation, erosion and redeposition can be shown by analysing in-situ data. Moreover, the shift of water level contours due to topographical changes can be quite efficiently demonstrated by comparing the contours extracted from satellite images of different years.

Zusammenfassung

Um die Brauchbarkeit und den Informationsgehalt von „klassischen" Seevermessungsdaten sowie Satellitenfernerkundungsdaten (ERS-1 and 2, Landsat-TM and MSS, IRS-1C PAN and LISS-III) zur Quantifizierung morphologischer Veränderungen in Wattgebieten abschätzen zu können, wurden zwei Testgebiete ausgewählt, die eine ausgeprägte Morphodynamik zeigen. Es waren dies die im Dithmarscher Wattenmeer (Deutsche Bucht) gelegenen Sände Tertius Sand und D-Steert. Beide Sandbänke zeigen infolge intensiver Sedimentumlagerungen, die durch einen Anstieg des Meeresspiegels sowie durch Wellen und Tideströmungen bedingt sind, eine ausgeprägte landwärts gerichtete Verlagerung. Morphologische Veränderungen als Folge von Ablagerung, Abtrag und Umlagerung von Sedimenten können durch die Auswertung von Peildaten hinlänglich erfasst werden. Die sich aus den Umgestaltungsvorgängen ergebenden Verlagerungen der Wasserlinien können darüber hinaus effizient aus dem Vergleich von Konturlinien abgeleitet werden, die sich aus Satellitenbildern unterschiedlicher Jahre extrahieren lassen.

Keywords

Remote Sensing, Optical Data, Radar, German North Sea Coast, Tidal Flats, Water Level Contours.

Contents

1. Introduction

For updating information on bottom topography of tidal flat areas, ship-based bathymetric measurements but also satellite monitoring can be applied. Satellite imagery is often used as a tool for obtaining a synoptic overview of the area under investigation, whereas in-situ measurements offer higher resolution for detailed mapping. Depending on the task, data from both methods can be used for calibration and validation of numerical morphodynamic models (ROMANEESSEN, 1998; LEHNER, 1999). The suitability and limitations of each type of data for assessing the morphodynamics of a coastal area is the main objective of this paper. Study area is the Dithmarschen Wadden Sea. Three types of datasets are the basis of this investigation: bottom topography interpolated from bathymetric measurements taken between 1974 and 1997, synthetic-aperture radar (SAR, onboard of ERS-1 and 2 satellites) images from 1992 to 1999 and optical images (Landsat-TM & MSS and IRS-1C PAN & LISS-III) from 1973 to 1997.

2. Investigation Area

The Dithmarschen tidal flat area, located in the southeastern part of the German Bight is part of the Wadden Sea of the Federal State of Schleswig-Holstein. The two chosen test areas Tertius Sand and D-Steert are indicated in Figure 1. These two shoals are built up of mainly fine sand with minor medium sand components. The tidal regime in the area is semidiurnal with tidal ranges from 3 to 3.5m. Located at the seaward borderline of the Dithmarschen Wadden Sea and bordered by deeper tidal channels in the North and South both sand banks are highly exposed to the energy of the North Sea waves. In combination with tidal currents this leads to pronounced morphological changes. The strong environmental dynamics result in lateral migration in mainly easterly direction and in changes of elevation, which, especially in the case of D-Steert, lead to the temporary formation of a supratidal sand.

3. Methods

3.1 Ship-Based Bathymetric Survey Data

The topographic data are result of ship borne bathymetric measurements carried out by the Federal Maritime and Hydrographic Agency of Germany (BSH). The investigated datasets acquired in 1977, 1984, 1992 and 1997 were chosen to meet the same time frame as the satellite data. The grid interpolation was carried out within the coordinate boundaries of the test areas for each year. The datasets were interpolated on a 12.5 x 12.5 m grid (same size as the SAR pixels). Sediment budget changes were calculated by subtracting the measurements of two years for one area, such that positive values indicate sediment accumulation and negative values erosion. All depth values are referred to the German Ordnance Datum ("Normalnull" = NN).

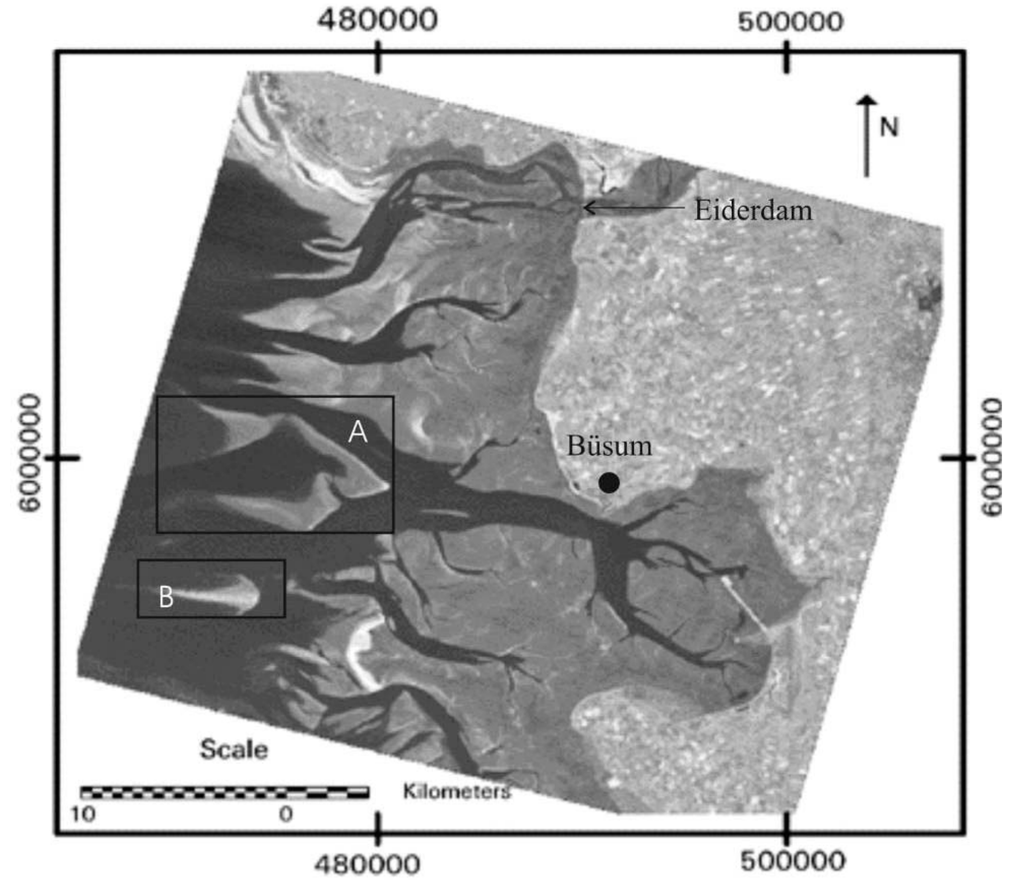

Fig. 1: The test areas within the Dithmarschen Wadden Sea. A = Tertius Sand, B = D-Steert (Image: Landsat-MSS, April 10th, 1976. Coordinates in UTM)

3.2 Remote Sensing

Data from both passive and active satellite borne sensors were used. Passive sensors are characterised by the ability to capture part of the radiation that is emitted and / or reflected from the earth's surface. The passive sensors applied in this study are mounted on Landsat and Indian Remote Sensing Satellite (IRS) satellite platforms (KRAMER, 1996). Landsat carries a multi spectral sensor (MSS) composed by four bands that simultaneously record reflected radiation in the green, red, and reflected infrared (2 bands) portions of the electromagnetic spectrum with a resolution of 70 m. Besides being able to map a larger variety of earth features due to its 7 bands, one of the advantages of Landsat Thematic Mapper (TM) sensors over MSS sensors lies within the Thematic Mapper's higher image resolution (30 m;

only band 6 has a resolution of 120 m). The second dataset used was taken from an IRS-1C platform. It carries three types of sensors on board, out of which two were used for this research: the LISS-III, with 23 m spatial resolution and a panchromatic sensor (PAN), with 5.8 m spatial resolution.

Radar is an active sensor, which emits its own source of energy and thus makes it independent from daylight and cloud cover. It directs the microwave radiation towards the targeted object in order to measure the returned energy of the backscattered signal. Launched by the European Space Agency (ESA) in 1991 and 1995, ERS-1 and ERS-2 were the first satellites collecting commercially available synthetic aperture radar (SAR) data during all weather conditions as well as during day and night (BAMLER and SCHÄTTLER, 1993). The SAR achieves its high-resolution by synthesising a long antenna, moving the antenna along the flight track and receiving the backscattered signals coherently. SAR processing transforms the received raw data to higher resolution (30 m) SAR images. Table 1 shows the investigated radar and optical images and their corresponding water levels.

Table 1: Investigated satellite datasets, with the corresponding water level at Büsum gauge (*German ordnance level Normal Null, NN)

Date	Time	Water level (m NN*)	Sensor
05.10.1973	09:57	–1.03	Landsat-MSS
10.04.1976	09:42	–2.10	Landsat-MSS
22.08.1984	09:56	–0.87	Landsat-TM
26.03.1992	10:24	–1.39	ERS-1
14.03.1996	10:25	–1.11	ERS-1
12.08.1997	10:45	–1.58	IRS-1C (Pan & LISS-III)
20.12.1997	10:22	–1.60	ERS-2
08.04.1999	10:25	–1.53	ERS-2

3.3 Water Level Contour Extraction

In this study, the main information extracted from the satellite data is the boundary between water and tidal flats or beaches (CHEN and SHYU, 1998; KOOPMANS and WANG, 1995; MASON and DAVENPORT, 1996; MASON, GURNEY and KENNETH, 2000; WANG and KOOPMANS, 1993). Tidal gauge water level recordings are correlated with shorelines extracted from the images. Main difficulties in this extraction process known as edge detection in SAR images are related to speckle noise. Due to the coherent nature of illumination, SAR images are speckled and therefore edges can only be extracted by means of a complex chain of algorithms. In a first step, a wavelet edge detection method suggested by MALLAT and HWANG (1992) is applied to detect all edges above a certain threshold. A block-tracing algorithm then determines the boundary area between land and water defining a coastal area. A refinement is achieved by local edge selection in this coastal area and propagation along the wavelet scales. In a final step, the refined edge segments are joined by an active contour algorithm. The method applied here is described in detail in NIEDERMEIER et al. (2000).

4. Results

4.1 Topography of D-Steert based upon Bathymetric Survey Data

The 1977 topography interpolated from in-situ bathymetric measurement data (Fig. 2) displays D-Steert as an elongated high sand body, stretching in east-west direction. The highest parts are between NN –1.0 and 0 m. The sand is flanked on its northern side by the tidal inlet Süderpiep extending from east to west. In the south it is bordered by a second channel which spreads into a wide shallow water area in easterly direction. The most obvious attribute of the D-Steert bank is its migration from west to east which is clearly depicted by the sequence of bathymetric data plots given in Figure 2. In 1977 the highest parts of the sand bank form a quasi symmetrical body with its main axis in the W-E direction. Increasing sediment accumulation on the southern part leads to an apparent effect of rotation of the main axis. In the 1997 image it is orientated in the WSW-ENE direction. The digital terrain model of this year also shows some quadratic patterns as far as heights above NN are concerned. Although these black patches represent areas which have not been surveyed it is obvious that, compared to the previous years, there was a significant accumulation of sediments that forced both a change in shape and an increase in volume.

The process of eastward migration described above is also clearly visible from the sediment balance maps (Fig. 2). Sediment accumulation is slightly higher on the southern part

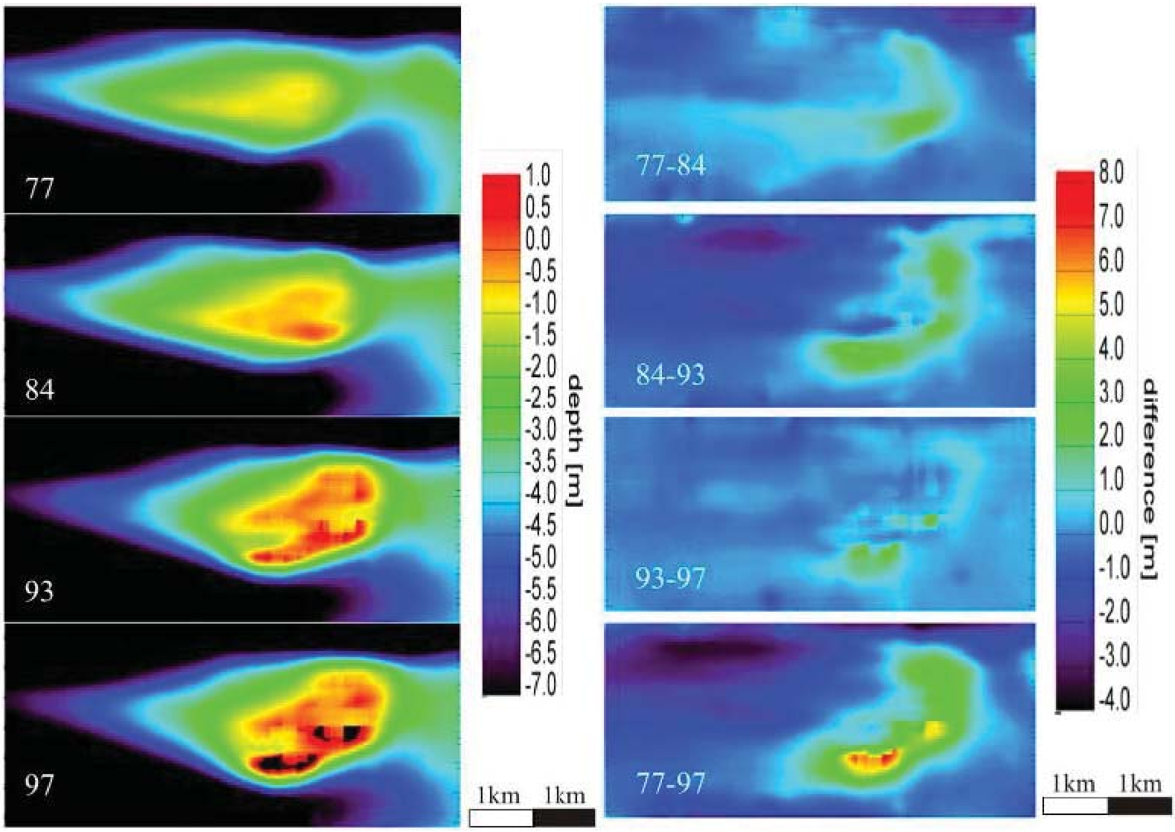

Fig. 2: Topography (left) based upon in-situ measurements of D-Steert in the years: 1977, 1984, 1993 and 1997 (top to bottom); and sediment balance (right) for sequences: 1977 to 1984, 1984 to 1993, 1993 to 1997 and 1977 to 1997 (top to bottom)

of the shoal. Erosion takes place on the western part, whereas towards east, accumulation increases. Between 1993 and 1997 erosion and accumulation are limited on D-Steert; only in the south-east 2 m of mainly sandy sediments were accumulated. During the twenty years between 1977 and 1997 the trend of erosion west of D-Steert and deposition east of it is confirmed by the volume analyses. Sediment deposition in the southern part reaches values of approximately seven metres. This redeposition results in a movement of D-Steert in a more south-easterly direction and characterises an eventual shift of the main axis from W-E to WSW-ENE.

4.2 Water Level Contours of D-Steert Extracted From Optical Data

Fig. 3 shows the evolution of D-Steert sand bank based on the extraction of water level contours from optical sensor data. These sensors permit long-term monitoring (24 years) of the evolution, an advantage over ERS-SAR data that have been available since 1992. The analysis of the images reveals that after a southward migration from 1973 to 1976 the D-Steert sand bank starts moving eastward in subsequent years. The initially elongated arrow-like shape changes rather drastically to an elliptic body oriented in the SW-NE direction in 1997. A similar shape can be also observed in the radar data.

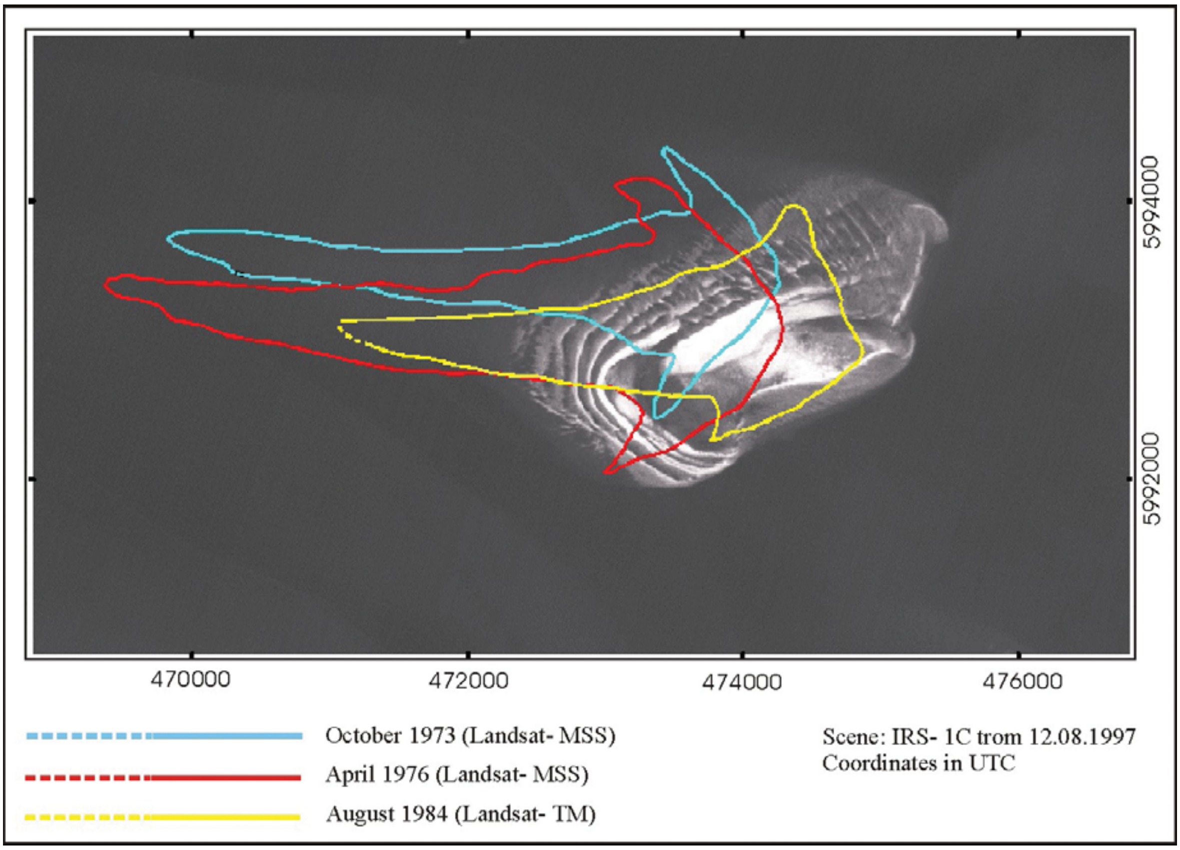

Fig. 3: Evolution of D-Steert's water level contours based upon optical data (over 1997 PAN image)

4.3 Water Level Contours of D-Steert Derived from SAR Data

Fig. 4 shows the results of the edge detection method extracting the water line around D-Steert from ERS SAR images for the years of 1992, 1996 and 1999. The northern boundary of D-Steert's eastern part clearly migrates towards east while water level contours move southward in the nsouthern part. Even more pronounced, the low water contour on the western bank also retreats in south-easterly direction. Overall, the erosional and depositional processes lead to a tendency of rotation of the longitudinal axis in a counterclockwise direction from W-E to SW-NE.

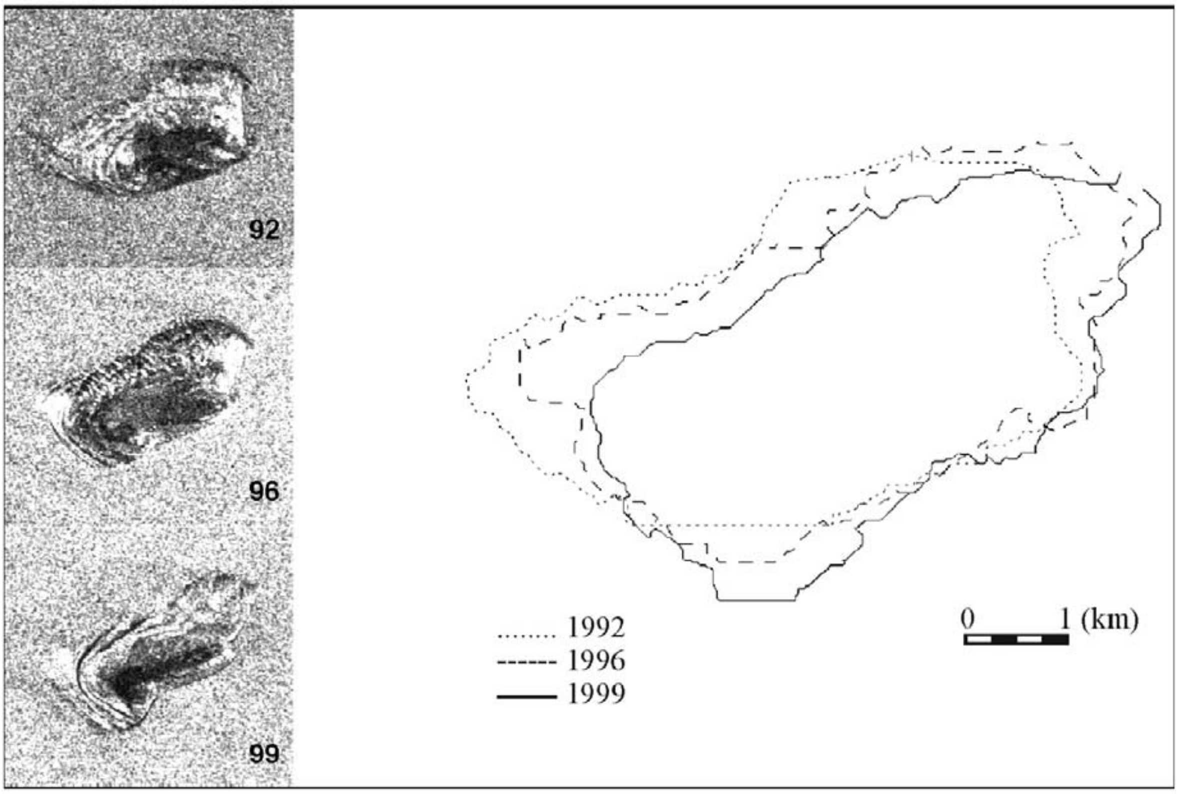

Fig. 4: Evolution of D-Steert's water level contours extracted from SAR

4.4 Summary of Topographic Changes of D-Steert

Changes of D-Steert's shape can be easily observed on satellite images. On the one hand, sediment accumulation occurs on the southern side. This is proven by sediment balance data but also clearly expressed by the advance of the water line derived from satellite images. On the other hand, a redeposition of sediments takes place from the western to the eastern side, also visible in the sediment balance data and as a migration of the remotely sensed water level contours. Besides the data from in situ measurements, the most reliable information on sand bank migration can be obtained from edge detection data extracted from the SAR. However, information derived from these data is limited to those areas which are dry during low water.

4.5 Topography of Tertius Sand based upon Bathymetric Survey Data

Tertius Sand is composed of three connected sand banks which will be named here for simplification (visible in Figs. 5, 6 and numbered in Fig. 7) as Island 1 for the northernmost one, Island 2 for the middle one and Island 3 for the southernmost one. In the north and in the south these three sands are bordered by the tidal channels of the Norderpiep and the Süderpiep, respectively.

The concave side of this group of sand banks is turned towards the open North Sea. As shown in Fig 5, the highest elevations (NN –1.0 m) are found on the southernmost part of the bank in 1977. From 1977 to 1997 its frontal crest clearly migrates landwards. Island 2 increases in height while Island 3 loses parts of its higher areas.

The most intensive accumulation takes place in the south eastern (landward) side of Island 1. Similarly, the side exposed to the open sea is subjected to erosion causing the intensive migration of this shoal. Accumulation also takes place north of Island 2 and south of Island 3. Strong sediment input can be perceived on the eastern border of Island 1 as well as in the south of Island 3. Erosion takes place mainly in the deeper parts of the Süderpiep channel and west of Island 1. The pattern of sediment changes is comparable for all four observed time windows indicating a strong movement of the northernmost Island of Tertius 1 towards the mainland as well as an accumulation that leads to a southward migration of Island 3.

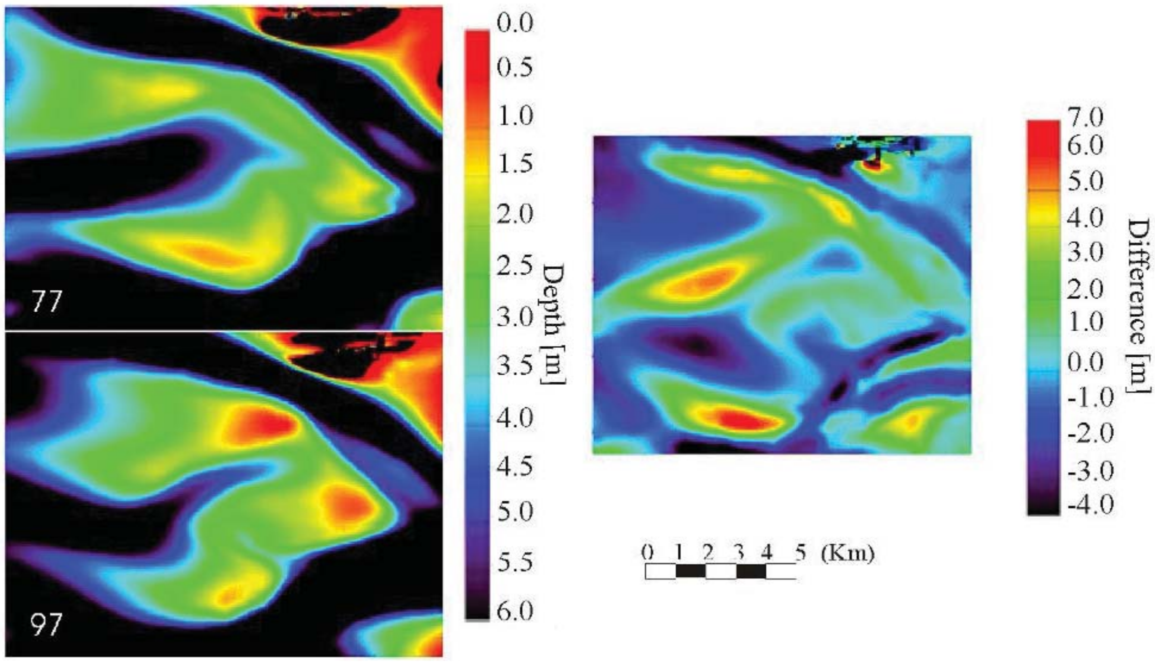

Fig. 5: Topography based upon in-situ measurements of Tertius Sand in 1977 (upper left) and 1997 (lower left) and sediment balance between 1977 and 97 (right)

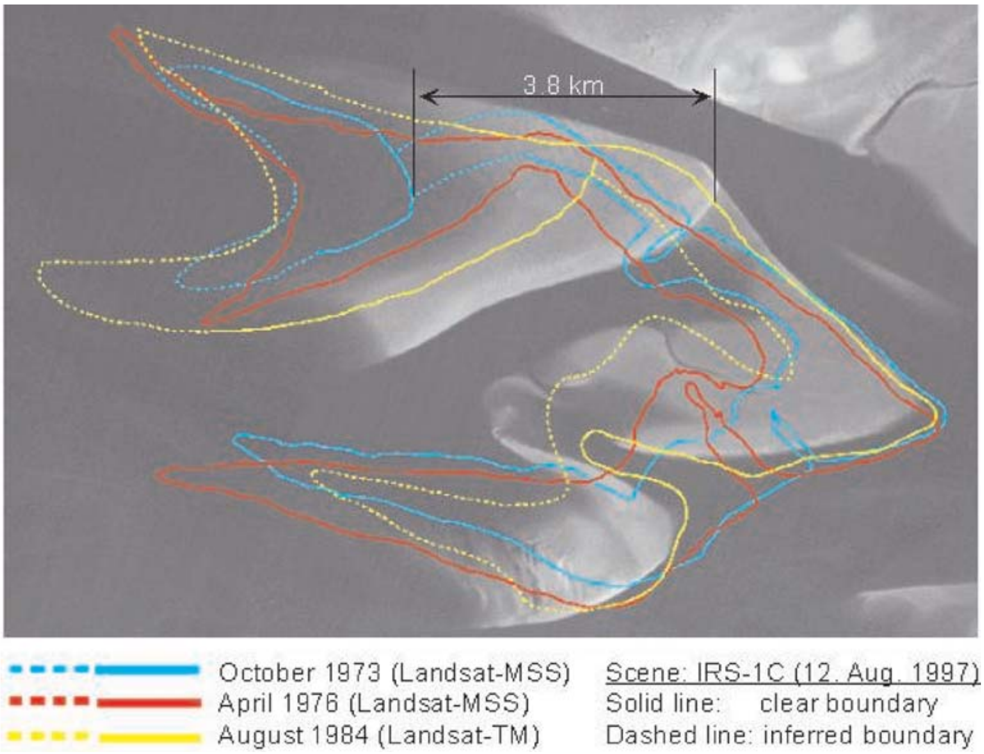

Fig. 6: Evolution of Tertius Sand's water level contours extracted from optical IRS-Pan data

4.6 Water Level Contours of Tertius Sand Extracted from Optical Data

The analysis of the waterlines derived from optical data (1973–1997) shows a reduction of the area of Island 3 combined with a tendency to migrate in a southwesterly direction (Fig. 6). The situation for Island 2 can be described by stability of the central part and a retreat of the southern boundary to the north. Contrary to Island 2, the marked water level contours of Island 1 exhibit a landward migration of the sand body of up to 3.8 km.

4.7 Water Level Contours of Tertius Sand Derived from SAR Data

In general, Tertius Sand can be identified very well on ERS-SAR images (Fig. 7, small image) and water level contours (Fig 7) can be precisely extracted from these data sets. Among other things, the morphological evolution of the area between 1992 and 1999 is characterised by strong changes of the seaside contours of the three islands, which form Tertius Sand. In contrast, those boundaries of the Island 2 and 3 that are facing towards the mainland remain stable or undergo very little changes. The same is true for the border line between Island 1 and the northern adjacent tidal channel of the Norderpiep. However, Island 1 as a whole (marked in the radar image, Fig. 7) slides along this line in the direction of the mainland. From 1992 to 1999 this migration is in the order of 700 m. That means that the entire Island 1 is in motion, unlike the other sand bodies, which are stable in their eastern and unstable in their western parts.

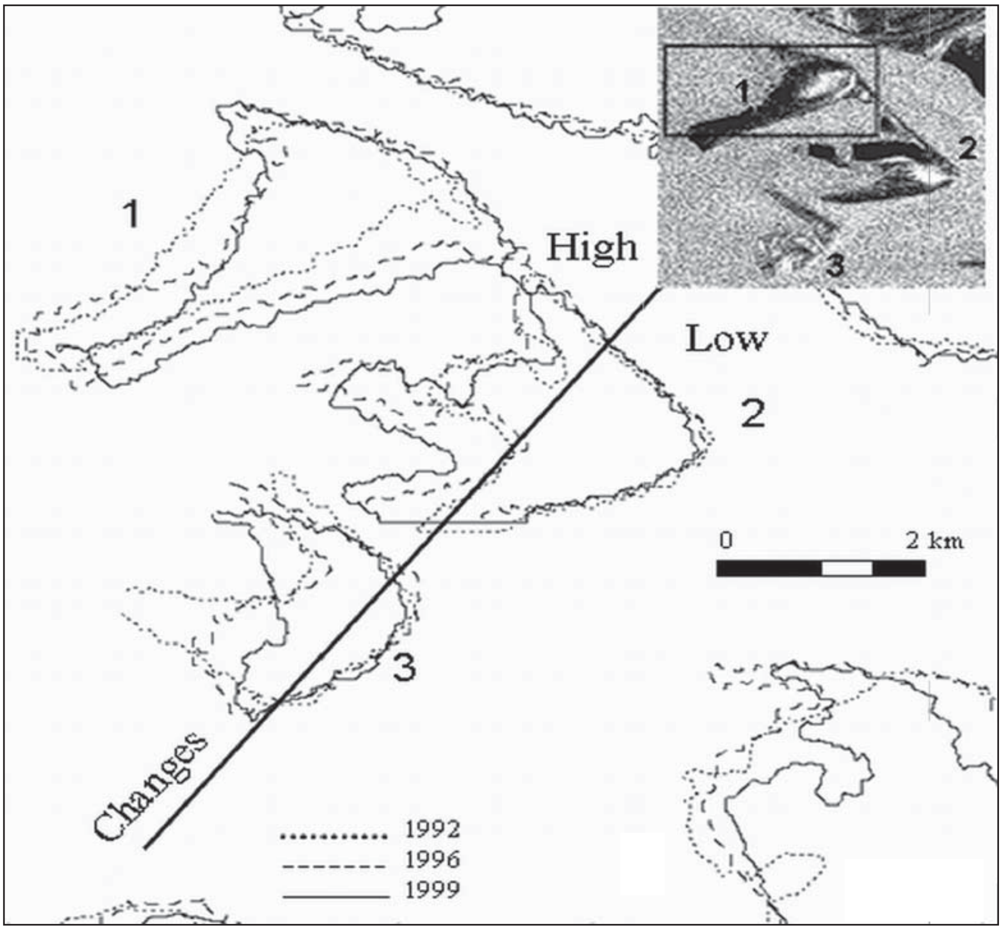

Fig. 7: Evolution of Tertius Sand's water level contours extracted from SAR

4.8 Summary of Topographic Changes of Tertius Sand

The sediment balance presented in Fig. 5 shows a tendency of accumulation in areas in the vicinity of the adjacent channels that already show a higher elevation. In contrast, there seems to be ongoing erosion in the westerly exposed lower lying areas. This evolution eventually leads to steeper seaward slopes of the shoals.

Results from bathymetric measurements (Fig. 5) and from optical remote sensing data clearly (Fig. 6) show a pronounced landward migration of the seaward parts of Tertius Sand. For the south-eastern part of Island 1 this tendency is also documented by the SAR data (Fig. 7). However, the landward migration is not very obvious for the SAR-data-derived water level contours in the north-western part of Island 1. This discrepancy displays a typical limitation of the used water level contour method in areas with relatively gentle slopes. Here small changes in the water level lead to an abrupt change in the area size and, therefore, to a pronounced advance or retreat of the water level contour.

5. Discussion

Fig. 8 shows a comparison between the water level contours resulting from bathymetric and radar data sets on an optical IRS-PAN base image of the entire Dithmarschen Wadden

Sea area of 1997. To take in to account water level slopes in the area, measured elevations were taken from two tidal gauges for the appropriate time window. For the outer parts we used data from Trischen Island gauge station (NN –1.3 m) and for the inner parts from Büsum gauge station (NN –1.6 m). In this way a better match between the topographic units visible in the base image and the water level contours can be achieved. The red lines in Figure 8 represent the NN –1.6 m (inner part) and the NN –1.3 m (outer part of the domain) isolines derived from a digital elevation model, which is based on in-situ bathymetric data. SAR data (Dec./20/1997) were acquired for a situation with the water level at NN –1.6 m at Büsum gauge station. The derived contour lines are given in yellow. In areas with distinct

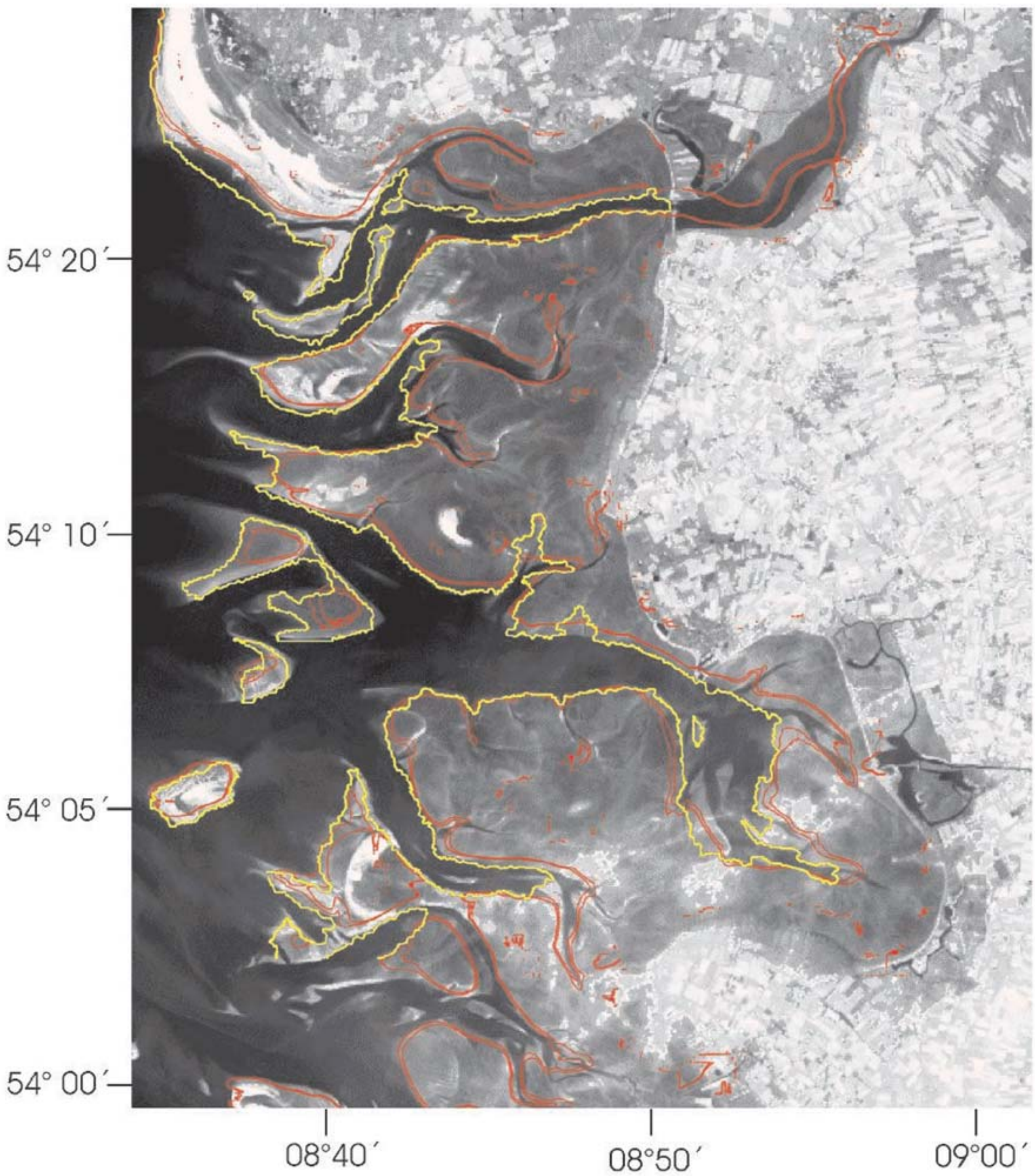

Fig 8: Water level contours for the year 1997 extracted from SAR data (yellow line) and from interpolated bathymetric data (red line)

"SAR-data-edges" tantamount to steep topographic gradients both isolines show a relatively good correlation and match well with the topographic units visible in the underlying optical image. Examples are the areas south of the Eider estuary and north of the Norderpiep. Isolines match less in areas which are characterised by gentle slopes. This applies to some parts of the Tertius Sand or the inner part of the Meldorf Bight.

The partly good correlation between the contour lines means that, although radar data are unavoidably contaminated by speckle noise, the used edge detection algorithm has proven to be efficient in tracing boundaries between intertidal areas and water. However, an important prerequisite for a good match is that both data sets are related to the same water level base. We are quite sure that this is not true for every case. Thus, unknown spatio-temporal variability of the tides or resulting water levels as well as the slope characteristics of the area account for some of the discrepancies. Due to the size of the area and the complexity of the factors, which may lead to local variability of water levels, an estimate of the error cannot be made.

6. Conclusions

The combination of data from SAR, IRS, Landsat and ship-based surveys has proven to be a useful tool for assessing topographical changes in the Wadden Sea. Remote sensing data basically yields information on the water level contours. Older, low resolution (MSS) optical sensors, can give information about the topographical evolution within a larger historic time span. High-resolution optical sensors (TM, PAN, LISS-III) are very suitable for extracting coastlines with simple algorithms at a high degree of accuracy. However, optical methods are dependent on daylight conditions and low cloud coverage.

For continuous coverage the extraction of tidal flat-water-boundaries from synthetic aperture radar data is a valuable method as it offers the advantage of data being available at all weather conditions on a weekly basis and, therefore, shows the potential of updating bottom topography between high and low tide in the Wadden Sea.

A main future challenge for further development of algorithms using radar remote sensing data is the extraction of water level contours at coastal areas with gentle slopes. In addition, interferometric methods making use of two or more images of the same area will be used to deduce topographic information in the Wadden Sea (SIEGMUND et al., 2004). With new high resolution radar satellites to be deployed in the TerraSAR-X mission which is to be launched in 2006 mapping of the Wadden Sea will be possible for a resolution higher than 5 m.

7. Acknowledgements

Part of the work was funded by the BMBF within the framework of the TIDE project. The topographic data has been kindly made available by the Federal Maritime and Hydrographic Agency (BSH).

8. References

BAMLER, R. and SCHÄTTLER, B.: SAR Data Acquisition and Image Formation. In: Schreier, G.: SAR Geocoding: Data and Systems, Wichmann, 1993.

CHEN, L. C. and SHYU, C. C.: Automated Extraction of Shorelines from Optical and SAR Images. Proceedings of the 19th Asian Conference on Remote Sensing, Manila, 1998.

EHLERS, J.: The Morphodynamics of the Wadden Sea. A. A. Balkema Publishers, 1988.

GÖHREN, H: Zur Dynamik und Morphologie der hohen Sandbänke im Wattenmeer zwischen Jade und Eider. Die Küste, Heft 27, 1975.

KOOPMANS, B. N. and WANG, Y.: Measurement of Land-Sea Transition from ERS-1 SAR at Different Phases of Tidal Water. Netherlands Remote Sensing Board Report 95–20, 1995.

KRAMER, H. J.: Observation of the Earth and its Environment- Survey of Missions and Sensors. Springer, 1996.

LEHNER, S. and ROMANEESSEN, E.: Satellitenradar: Morphodynmamik des Wattenmeeres. In: Petermanns Geographische Mitteilungen, Pilotheft 2000, 1999.

MALLAT, S. and HWANG, W. L.: Singularity Detection and Processing with Wavelets. IEEE Trans. Inform. Theory, 38, 1992.

MASON, D. C. and DAVENPORT, I. J.: Accurate and Efficient Determination of the Shorelines in ERS-1 SAR Images. IEEE Transactions of Geoscience and Remote Sensing, 34 (5), 1996.

MASON, D. C., GURNEY, C. and KENNETT, M.: Beach Topography Mapping – a Comparision of Techniques. Journal of Coastal Conversation, 6, 2000.

NIEDERMEIER, A.; ROMANEESSEN, E. and LEHNER, S.: Detection of Coastlines in SAR Images Using Wavelet Methods. IEEE Transactions on Geoscience and Remote Sensing, 38/5, 2000.

PETERSEN, M. and ROHDE, H.: Sturmflut. Die großen Fluten an den Küsten Schleswig-Holsteins und in der Elbe. Wachholz, 1991.

ROMANEESSEN E.: Improvement and Comparison of a Dynamic Tide Model in the Elbe Estuary with ERS-2 Satellite Data. Proceedings of OCEANS '98 Conference, Nice, 1998.

SIEGMUND, R.; BAO, M.; LEHNER, S. and MAYERLE, R.: First Demonstration of Surface Currents Imaged by Hybrid Along- and Cross-Track Interferometric SAR. IEEE, Trans. Inform. Theory, 42, 2004.

WANG, Y. and KOOPMANS, B. N.: The Topographic Mapping of the Tidal Flats Using Remote Sensing and GIS Techniques. A Case Study in the Wadden Sea Area, Netherlands. Proceedings of International Symposium of Operationalisation of Remote Sensing, Enschede, 1993.

Die Küste, 69 PROMORPH (2005), 1-420

Effectiveness of Acoustic Profiling for Estimating the Concentration of Suspended Material

By POERBANDONO and ROBERTO MAYERLE

Summary

In this paper the effectiveness of several empirical approaches for converting acoustic backscatter strength into suspended material concentration is investigated. The investigation is based on simultaneous measurements performed using an Acoustic Doppler Current Profiler, an Optical Beam Transmissometer and a Niskin bottle sampler in the main tidal channels of the Dithmarschen Bight on the German North Sea coast. A wide range of conditions regarding water depths and current velocities were covered. The approaches by DEINES (1999) and GARTNER (2002) were also taken into consideration. The effectiveness of the empirical approaches was evaluated by comparing the values estimated from acoustic and optical measurements. The results obtained from both approaches were found to differ by less than a factor of 2. In a range of tests the average relative error was found to be between 20 % and 30 %, with average absolute errors of ≤ 0.08 kg/m^3. The suspended material concentrations determined from acoustic backscatter measurements are presented for a cross-section surveyed at slack water as well as during conditions of maximum current velocity. In the surveyed cross-section it was found that the concentrations of suspended material estimated from acoustic and optical measurements were similar in terms of overall tendency and gradients. The results confirm the acceptability of the investigated empirical approaches for converting acoustic backscatter strength into suspended material concentrations for the conditions in question.

Zusammenfassung

In diesem Bericht wird die Effektivität von verschiedenen empirischen Ansätzen zur Konvertierung der Stärke der akustischen Rückstreuung in Schwebstoffkonzentration untersucht. Die Untersuchung basiert auf simultanen Messungen, die mit einem Acoustic Doppler Current Profiler, einem Optical Beam Transmissometer und einem Niskin Bottle Sampler in den Haupttiderinnen der Dithmarscher Bucht an der deutschen Nordseeküste durchgeführt wurden. Ein weiter Bereich von Bedingungen bezüglich Wassertiefen und Strömungsgeschwindigkeiten wurde abgedeckt. Die Ansätze von DEINES (1999) und GARTNER (2002) wurden ebenfalls berücksichtigt. Die Effektivität der empirischen Ansätze wurde ausgewertet, indem die abgeschätzten Werte der akustischen und optischen Messungen verglichen wurden. Die Ergebnisse aus den beiden Ansätzen unterscheiden sich um weniger als den Faktor 2. In einer Reihe von Tests wurde ein mittlerer relativer Fehler zwischen 20 % und 30 % bestimmt, mit mittleren absoluten Fehlern ≤ 0.08 kg/m^3. Die Schwebstoffkonzentrationen, die durch die Acoustic-Backscatter-Messungen bestimmt wurden, werden für einen Querschnitt zum Zeitpunkt des Stauwassers und der maximalen Strömungsgeschwindigkeiten gezeigt. Es zeigte sich, dass die aus den akustischen und optischen Messungen abgeschätzten Schwebstoffkonzentrationen in dem untersuchten Querschnitt ähnlich in Bezug auf generelle Tendenzen und Gradienten waren. Die Ergebnisse bestätigen die Eignung der untersuchten empirischen Ansätze zur Konvertierung der Stärke der akustischen Rückstreuung in Schwebstoffkonzentrationen.

Keywords

Suspended Material Concentration, Acoustic Doppler Current Profiler, Optical Beam Transmissometer, Tidal Channels, Wadden Sea, North Sea.

Contents

1. Introduction

Acoustic techniques, e.g. Acoustic Doppler Current Profilers (ADCPs), for estimating suspended material concentration have attracted increasing interest in recent years and now find wide application in practice. In this method the concentrations of solid material in a water column are related to the magnitudes of the acoustic echo intensity of the returned signal, i.e. backscatter. Acoustic devices such as ADCPs are less susceptible to biological fouling, non-intrusive and offer high spatial and temporal resolution. Several corrections are required, however, to account for sound attenuation due to the water body and scattering particles in the water column as well as acoustic energy loss. Due to the interdependency between acoustic propagation and water properties such as salinity and temperature, detailed data processing algorithms and reliable calibration methods are necessary.

The first attempts to obtain qualitative estimates of suspended material concentration using acoustic backscatter were made by SCHOTT and JOHNS (1987), FLAGG and SMITH (1989) and HEYWOOD et al. (1991). Reviews on backscatter theory are presented by LIBICKI et al. (1989) and THORNE and HARDCASTLE (1991). Methods based on a theoretical description of the backscatter from solid particles in suspension were introduced by THORNE et al. (1991). Empirical methods were introduced by YOUNG et al. (1982), VINCENT et al. (1986) and HANES et al. (1988). More recently, a number of empirical methods based on a simplified theoretical approach have been proposed by SONTEK (2002), DEINES (1999), PATINO and BYRNE (2002) and GARTNER (2002), and were tested with a certain degree of success.

In this paper the effectiveness of the empirical acoustic methods proposed by DEINES (1999) and GARTNER (2001) were verified on the basis of field measurements of suspended material concentration using an optical beam transmissometer. Simultaneous measurements of suspended material concentrations were performed using an ADCP, an optical beam transmissometer and a Niskin bottle sampler in several cross-sections under different conditions within the framework of the research project "Prediction of Medium-scale Coastal Morphodynamics" (PROMORPH). Comparisons of suspended material concentrations obtained by converting the backscatter of optical beam transmissometer measurements were carried out to verify the conversion methods. This paper compiles the results of preliminary investigations summarized in POERBANDONO and MAYERLE (2002, 2003) and further assesses the effectiveness of the empirical methods documented in POERBANDONO and MAYERLE (2004).

2. Field Surveys

2.1 Measuring Devices

The acoustic backscatter data were obtained using a 1200 kHz Broadband Direct Reading ADCP manufactured by RD Instruments, as shown in Fig. 1a. These data are corrected for loss of intensity due to beam spreading and attenuation, assuming a constant absorption coefficient of 0.618 dB/m. The backscatter value for each bin (measurement layer) is taken to be the average of the values measured by the four transmissometer beams. The instrument was set to record a 0.5 m bin size over a 12 seconds averaging ensemble.

The optical transmission data were measured by means of an optical beam transmissometer (Fig. 1b) mounted in Conductivity-Temperature-Depth (CTD) sensors and equipped with a Niskin bottle sampler (Fig. 1c). The device, which employs visible light with a wavelength of 660 ± 12 nm and a 2 cm travel distance, provides a relative measure of suspended material concentration in terms of the percentage of optical transmission. In order to convert the optical transmission data into suspended material concentrations the device was calibrated against the concentrations determined from direct samples.

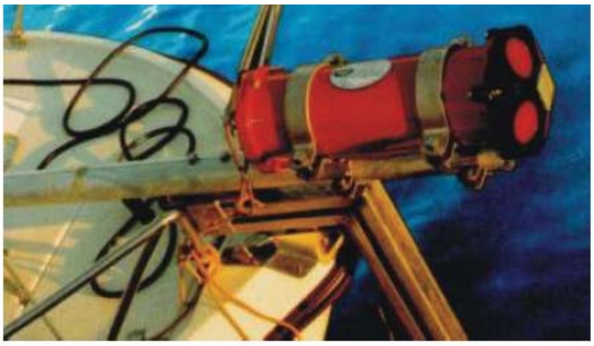

(a) Acoustic Doppler Current Profiler

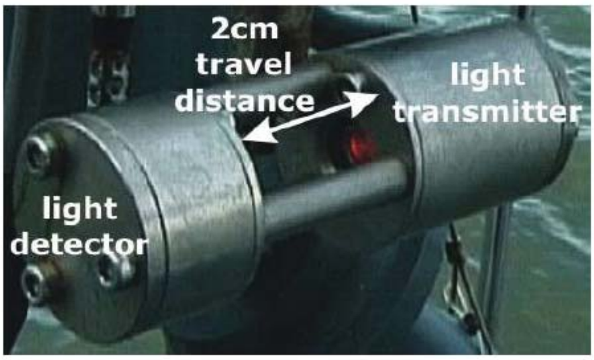

(b) Optical beam transmissometer

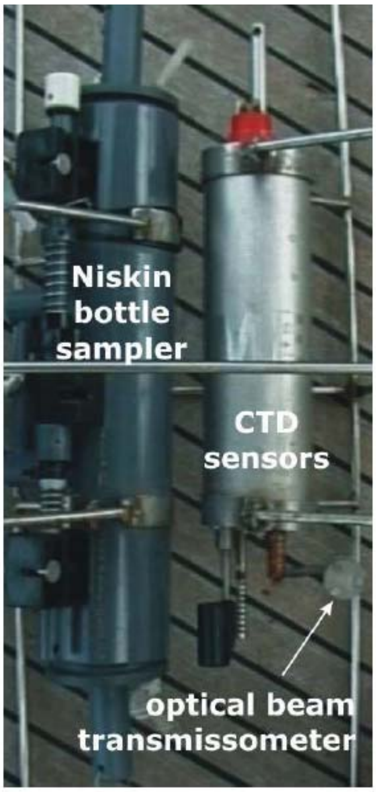

(c) Niskin bottle and CTD

Fig. 1: Measuring devices used in the study

The Niskin bottle sampler was used to collect water samples of approximately 2 litres of volume. The CTD probe was mainly used to provide information of depth where optical transmission measurements and sampling of water were executed. The suspended material concentration is determined by filtering the water sample and performing a gravimetric analysis following a standard protocol resumed by VAN DER LINDE (1998). A GF/F type filter was used for the filtration. The suspended material concentration of the sample is defined as the difference in the dry weight of the filter before and after filtration divided by the sample volume.

The optical transmission data were calibrated against the suspended material concentrations determined from 200 Niskin bottle samples according to the method described by OHM (1985) and RICKLEFS (1989). The concentrations were found to vary between 0.03 and 1.10 kg/m³. Fig. 2a shows the measured optical transmission (I) and the corresponding direct sample concentration (c). The following relationship was obtained between the suspended material concentration and optical attenuation:

$$c = (7A + 33)10^{-3} \tag{1}$$

with c = the suspended material concentration [kg/m³]
A = the attenuation coefficient $[-L^{-1}\ln(I)]$
L = the transmissometer path length [cm]
I = the optical transmission as a decimal fraction.

Linear correlation of the optical attenuation and suspended material concentration data resulted in the regression line (Eq. 1) shown in Fig. 2b. A correlation coefficient $r^2 = 0.9$ was obtained for this regression analysis. Further data sets (approx. 250 data pairs) with concentrations varying between 0.02 and 1.62 kg/m³ were used for validation purposes. In 80 % of all cases the difference between estimated and measured concentrations was less than twofold. The accuracy of optical measurements was estimated on the basis of agreement with concentrations determined from physical samples. It was found that the representative relative agreement between optical and direct sampling measurements is about 30 % POERBANDONO (2003). The optical estimation is limited to concentrations above approx. 0.03 kg/m³. This is due to an insufficient sensitivity of the optical beam transmissometer with a path length of only 2 cm for detecting low concentrations.

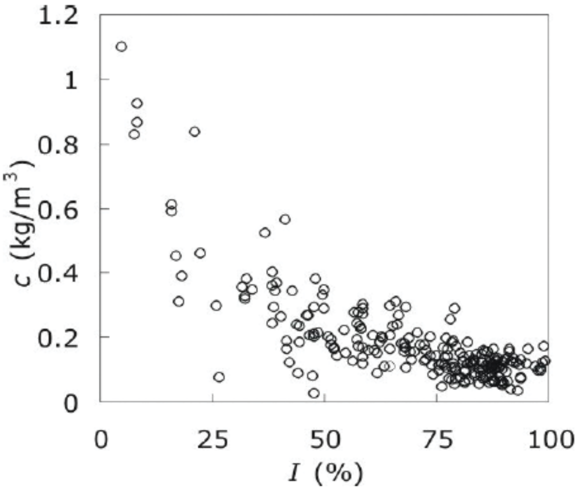

(a) Concentration (c) vs. transmissibility (I)

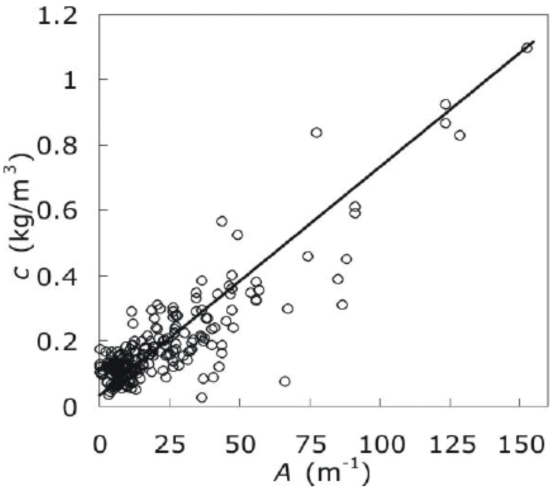

(b) Concentration (c) vs. optical attenuation (A)

Fig. 2: Calibration of optical concentration measurements

2.2 Field Measurements

Field measurements were carried out in the tidal channels of the Dithmarschen Bight. The locations of the measurement station S1 and cross-sections T1–T4 are shown in Fig. 3. In the study area the mobile bed sediments consist mainly of fine to very fine sands. Recent grab sampling surveys along the main channels indicate that the median grain size of bed sediments in the uppermost layer varies between 80 to 230 µm. The grain size of material transported in suspension is much smaller than that of bed material, with median values ranging between 10 and 90 µm. The distribution of suspended material concentration over the water column is fairly uniform (POERBANDONO et al., 2003).

Most of the field data used in this study were collected from moving vessels under calm weather conditions over the investigated cross-sections in different tidal channels. Measurements of acoustic backscatter and optical transmission profiles as well as the sampling of suspended material concentration were carried out along the cross-sections as shown in Fig. 4. The ADCP was directed downwards from the bow of the vessel and deployed for the continuous measurement of acoustic backscatter profiles over the cross-section. Measurements over the water column were made from about 1.6m below the free surface (due to the effects of transducer draught and blanking distance) down to the last 6 % of depth above the seabed (due to side lobe effects).

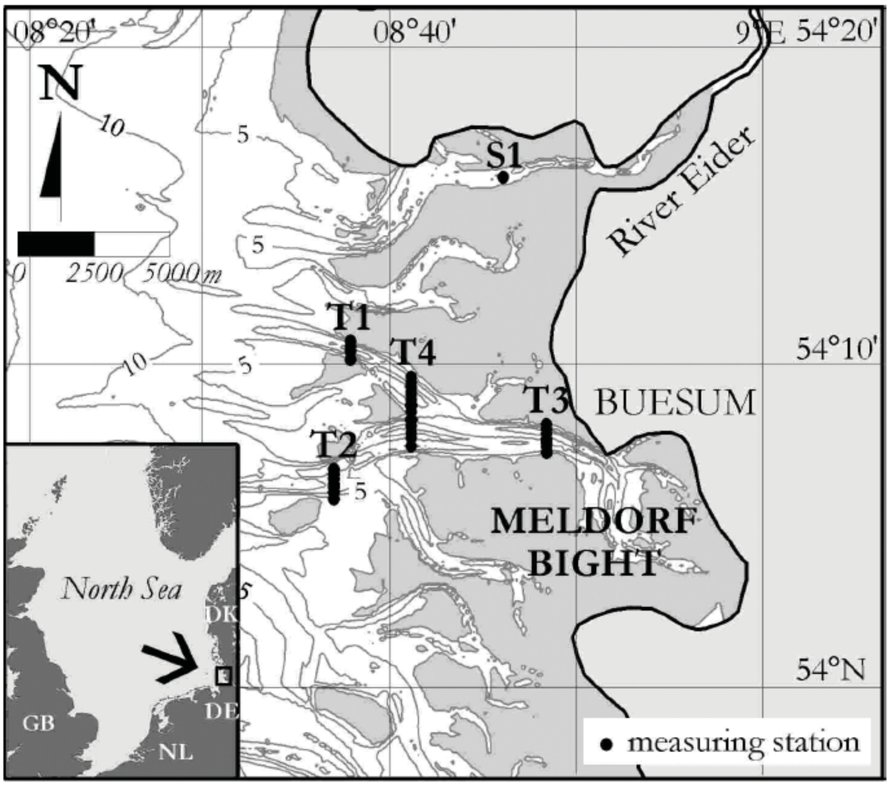

Fig. 3: Measurement locations in the study area

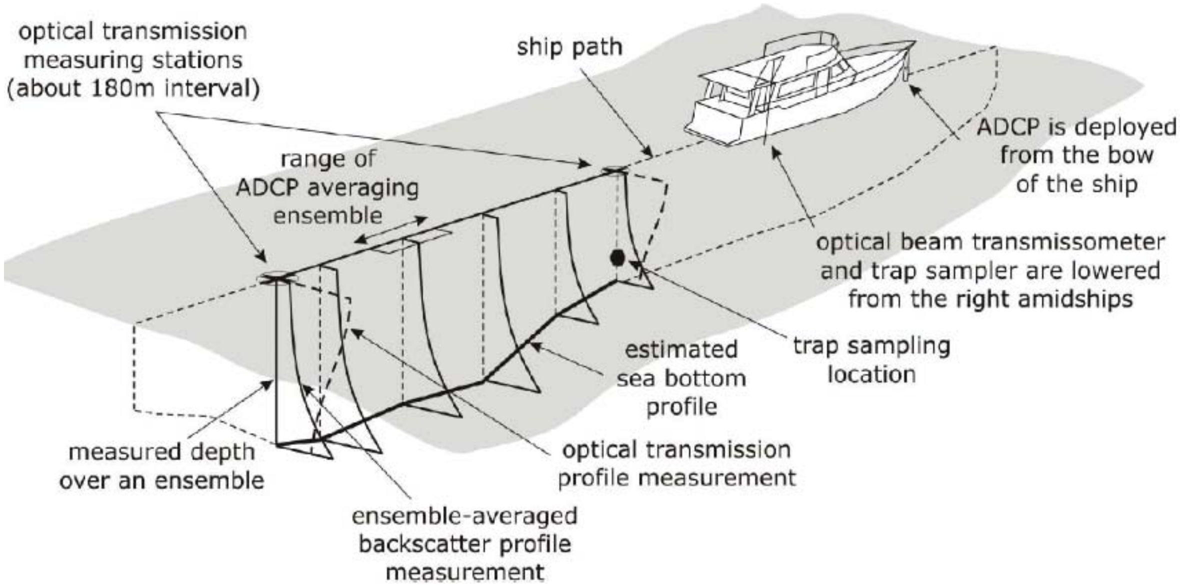

Fig. 4: Measurement procedure

Vertical optical transmission profiles at specified locations (measuring stations) at distances of about 180 m within the cross-section were measured simultaneously by lowering the optical beam transmissometer from starboard midships. The vertical resolution of the optical beam transmissometer was set to 0.2 m. The water depth and physical properties of the water column were also measured using CTD probe. Optical measurements over the water column were performed from close to the free surface down to about 0.25 m above the seabed. This restriction is due to the physical distance between the optical transmissometer and the protective frame mounted below the device. In addition, direct sampling of suspended material concentrations was also carried out deploying the Niskin bottle at a depth of approximately 1 m above the bottom. Suspended material concentrations determined from these samples varied between 0.02 to 1.15 kg/m^3.

3. Empirical Methods

A verification of the effectiveness of the two empirical methods for converting acoustic backscatter into suspended material concentration was carried out. Empirical methods are based on the assumption that the rate of acoustic attenuation is constant over the entire water column and that the grain size distribution of the sediments is uniform. In this study, two main categories were considered: a) methods based on the proportionality of the echo intensity increment between two depths in the water column and b) methods which directly relate the suspended material concentration to the echo intensity.

3.1 Methods based on the Proportionality between Echo Intensity Increments

The methods proposed by DEINES (1999) and SONTEK (2002) are based on the proportionality of the echo intensity increment ($\Delta EI = EI_z - EI_r$) between two depths in the water column. EI_z is the echo intensity value at a depth where the concentration is estimated from backscatter measurements (c_z) and EI_r is the echo intensity value at a depth where the sediment concentration is known. This level is also defined as the reference level. The suspended material concentration at the reference level (c_r) may be measured using any reliable device. The conversion equation is as follows:

$$10 \log_{10} (c_z/c_r) = K.\Delta EI \tag{2}$$

with K = proportionality constant

This method was simplified, assuming a constant acoustic attenuation coefficient, transmission power and pulse length. The best proportionality constant K was found to be 0.45 (POERBANDONO and MAYERLE, 2002). The concentration ratio between two measurement layers was thus assumed to be proportional to the echo intensity increment. The reference concentration c_r in Eq. 1 is obtained from the optically measured concentration. The reference echo intensity EI_r is the average of the backscatter values in the layer in which optical measurements are made. The choice of the reference level was found to influence the accuracy of suspended material concentrations. The effectiveness of the method improves with the number of reference levels over the vertical and proximity to the location of interest. At least one reference level is usually adopted for each vertical profile. The best agreement is achieved by setting the reference layer at mid-depth (POERBANDONO and MAYERLE, 2003).

3.2 Methods which relate Suspended Material Concentration to Echo Intensity

More simplified alternative methods relate suspended material concentration directly to echo intensity. An example of this is as follows:

$$10 \log_{10} (c_z) = a.EI_z + b \tag{3}$$

The coefficients of Eq. 3 are determined by a calibration based on simultaneous measurements of suspended material concentration using an acoustic and an alternative device. Optical devices or mechanical samplers may be used. The methods proposed by PATINO and BYRNE (2002) and GARTNER (2002) belong to this category. The advantage of this method is that the conversion does not require measurements at the reference level. The method proposed by GARTNER (2002) is evaluated. Fig. 5 shows the regression line relating backscatter data to the logarithm of concentration. 105 data sets were used in the calibration. The concentrations of physical samples collected from the Piep channel and the outer Eider Estuary were included in the analysis. These were found to vary between 0.03 and 0.7 kg/m^3. The resulting regression constants a and b in Eq. 2 obtained by calibration are 0.38 and 43.57, respectively. The conversion equation, with a corresponding correlation coefficient (r^2) of 0.81, was determined to be as follows:

$$c = 10^{(0.038EI - 4.357)} \tag{4}$$

with c = the suspended material concentration [kg/m^3]
EI = the acoustic backscatter [dB]

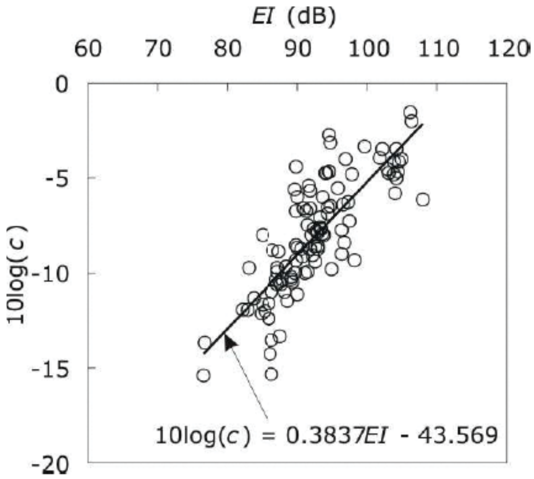

Fig. 5: Independent backscatter calibration based on direct sampling concentrations

4. Effectiveness of Empirical Methods

The effectiveness of the methods of DEINES (1999) and GARTNER (2002) for estimating suspended material concentrations is quantified on the basis of agreement with measurements obtained from the optical beam transmissometer. Table 1 shows the results of comparisons of the performance of the two methods, including a summary of the range of data used. Agreement between suspended material concentrations obtained from the conversion of acoustic backscatter and optical transmissibility is quantified on the basis of the average relative error (given in %), the average absolute error (given in kg/m^3) and the discrepancy factor (% of data with a scatter of less than a factor of 2 about the regression line). The performance of the two methods investigated here is comparable. The relative errors were found to be between 21 % and 29 %, and 28 % and 31 %, according to the methods of DEINES (1999) and GARTNER (2002), respectively. An average absolute error of ≤ 0.08 kg/m^3 is observed. Both methods show that the majority of the data is within a discrepancy factor of 2.

Fig. 6 shows plots of the suspended material concentrations obtained by conversion of the measured acoustic backscatter using the two methods described versus those obtained by conversion of optical beam transmissometer measurements. Lines indicating discrepancy factors of 2 are shown in the figure. It can be seen that the optical concentration is limited to a value of approximately 0.03 kg/m^3. In the case of DEINES' approach the discrepancies are fairly uniformly distributed over the entire range of concentration values. In the case of GARTNER's approach a steeper trend of increasing concentration is observed, leading to a wider range of estimated concentrations. GARTNER's approach, on the other hand, appears to be simpler as it may be applied on the basis of an independent calibration using direct sampling concentrations.

Table 1: Summary of test results

Test number	1	2	3	Average
Measurement locations	T1, T2 and T3	T3 and S1	T3 and T4	
Number of stations	201	205	345	
Number of data pairs	5174	2474	5325	
DEINES (1999):				
Relative error (%)	29	21	–	25
Absolute error (kg/m³)	0.06	0.07	–	0.07
Discrepancy factor of 2 (%)	97	97	–	97
GARTNER (2000):				
Relative error (%)	–	28	31	30
Absolute error (kg/m³)	–	0.08	0.03	0.06
Discrepancy factor of 2 (%)	–	94	93	94

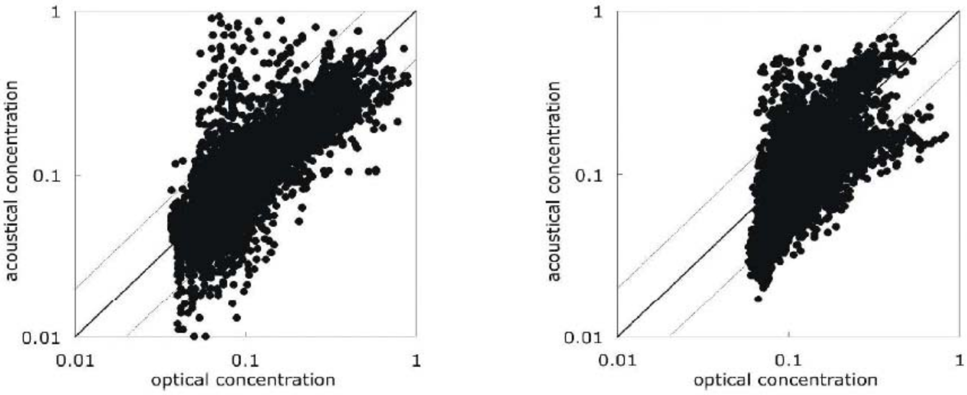

(a) DEINES (1999) approach (b) GARTNER (2002) approach

Fig. 6: Comparison of optical and acoustic concentration measurements in kg/m^3

Typical profiles of measured and converted sediment concentrations at two locations over cross-section T3 are shown in Figs. 7 and 8. An example of a non-uniform concentration profile is shown in Fig. 9.

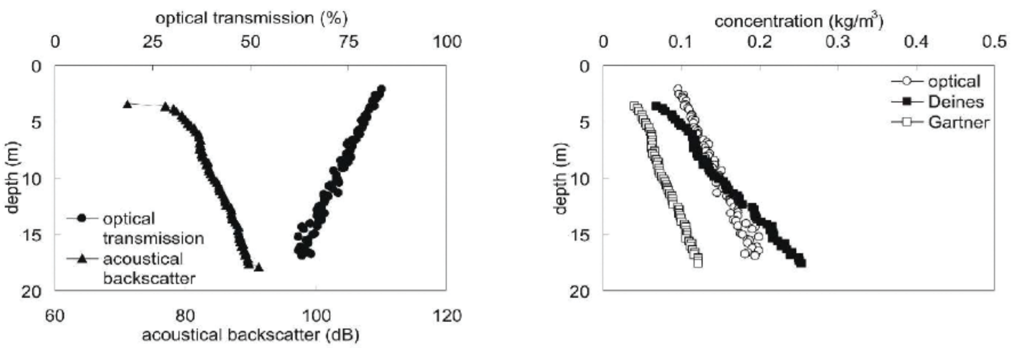

(a) Measured parameters (b) Estimated concentrations

Fig. 7: Profile measurement in cross-section T3 during slack water on 23 March 2000

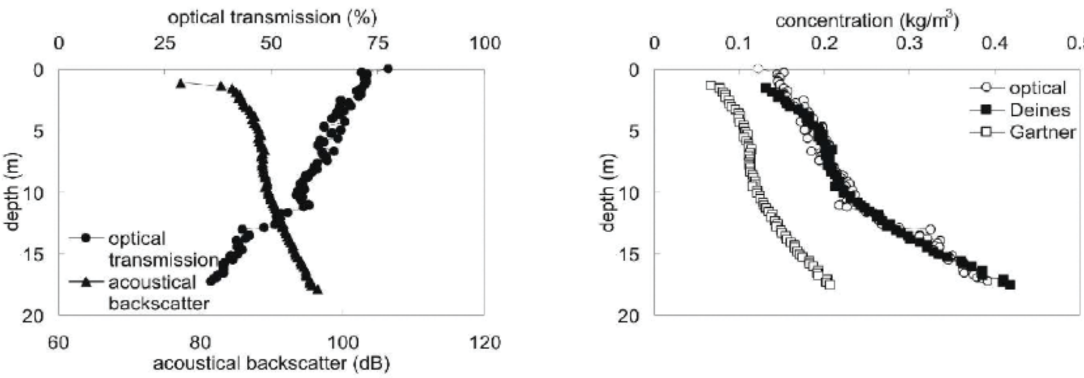

(a) Measured parameters (b) Estimated concentrations

Fig. 8: Profile measurement in cross-section T3 during maximum flood flow on 23 March 2000

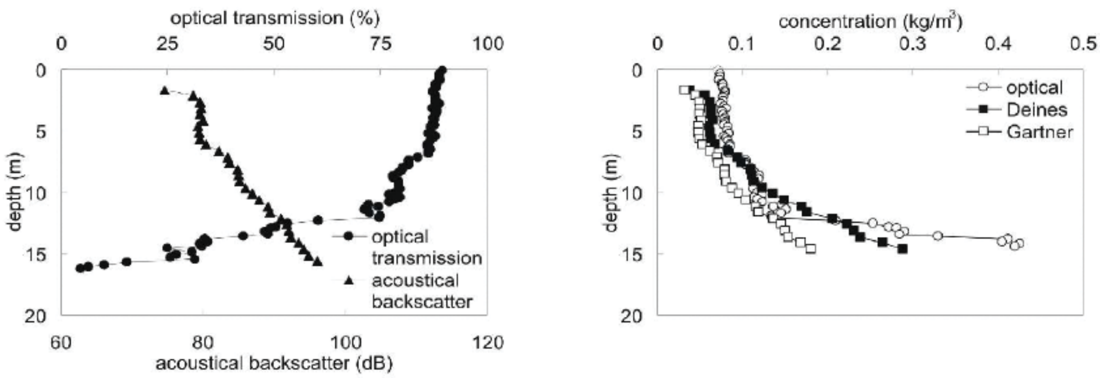

(a) Measured parameters (b) Estimated concentrations

Fig. 9: Profile measurement of high near-bed concentrations in cross-section T3 on 22 June 2001

The figures show the measured acoustic backscatter and optical transmissibility values as well as the suspended material concentrations obtained by conversion of the acoustic backscatter data using the two methods described as well as from optical transmissibility. The concentrations estimated from optical and acoustic measurements generally show a similar increase over the entire depth. The concentration profile obtained by DEINES' method exhibits gradient magnification due to the fact that this profile depends on the local reference concentration and the increment of backscatter values relative to the value at the reference level. The concentration profile obtained by Gartner's method tends to be underestimated.

Backscatter data recorded by the ADCP represent the scattering layer density of a water column. In the last bin (bin closest to the seabed) side lobe interference leads to a very high echo intensity value. In the bin closest to the transducers it is found that the backscatter data tend to be weaker. It is possible to identify such a tendency since the vertical profile of backscatter data usually exhibits extreme gradients in the second bin. This is due to the ADCP transient time required for transmitting and receiving a signal. A similar finding has also been reported by BIRCH et al. (1999) and LANE et al. (1999). For these reasons it is recommended to ignore the backscatter data from the first and last bins.

Figs. 10 and 11 show various measured quantities and suspended material concentrations obtained from conversions of optical and acoustic measurements over cross-section T3. Values are shown for slack water and maximum flood flow conditions for a spring tide on 23 March 2000. Acoustic backscatter measurements were performed over the entire cross-section whereas optical measurements were made at the point locations indicated in red in the figures.

According to the example shown in Fig. 10, the measured optical transmission during slack water is fairly evenly distributed over the cross-section, ranging between 70 % and 80 % (Fig. 10a). As may be seen in Fig. 10c, a similar tendency of uniform distribution in the measured acoustic backscatter was also obtained over the cross-section with values ranging between 80dB and 90dB. Higher turbidity was given by both optical and acoustic estimations in the deeper part of the channel. This is indicated by lower optical transmission and higher acoustic backscatter. The suspended material concentrations obtained from optical transmission and acoustic backscatter conversions are in very close agreement. The absolute suspended material concentrations given by DEINES' and GARTNER's methods differ from those obtained by optical transmission conversion by less than a factor of 2.

During maximum flow conditions, increased turbidity was observed with an increase in the magnitude and gradient of the measured optical transmission and acoustic backscatter profiles (Fig. 11). Optical transmission in the near-surface layer remains fairly constant at a value of about 80 % whereas close to seabed it decreases down to about 50 %. A similar tendency is also observed in the acoustic backscatter measurements. A slight increase in echo intensity is also observed in the upper layer. The measured acoustic backscatter is found to exceed 95 dB close to the seabed. Very close agreement is also obtained between the suspended material concentrations determined from optical transmission and acoustic backscatter conversions. Optical and acoustic measurements both indicate higher concentrations in the lower layer. In this case the acoustic concentration estimate based on Gartner's approach yields a very close value of approximately 0.3 kg/m^3, whereas acoustic estimation based on Deines' approach shows a slight deviation in the order of a factor of 1.5.

Investigations were also carried out to examine the possible dependency of discrepancies on various influencing factors such as spatial position, measurement location (different cross-sections and stations), water depth, velocity and levels of concentration (determined from optical measurements). A clear dependency of the discrepancies on location, water depth and magnitude of the current velocity was not identified.

5. Conclusions

The effectiveness of empirical methods for converting acoustic backscatter strength measured by an ADCP into suspended material concentration has been demonstrated. The performance of the methods was found to be comparable to estimations obtained from an optical beam transmissometer. The method of GARTNER (2002) appears to be advantageous for practical applications as it is simpler and offers comparable performance. In this case the conversion may be carried out directly without the need for measurements of suspended sediment concentrations using other devices. It is recommended, however, to apply this method only within the range of applicability of the equation derived for conversion. The application of DEINES' method (1999), on the other hand, requires measurements of suspended sediment concentrations.

The performance of the two methods was found to be comparable for conditions in

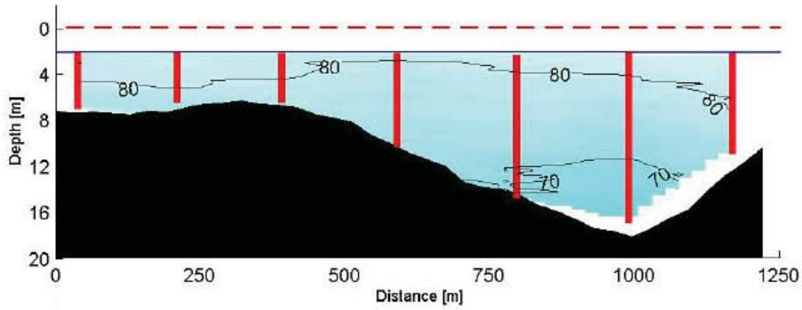

(a) Optical transmission in %

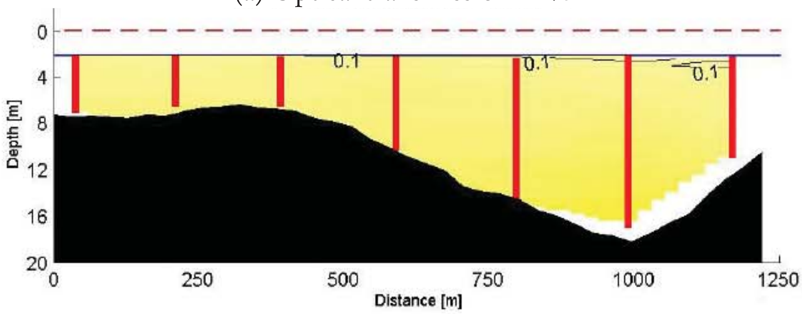

(b) Suspended material concentrations in kg/m^3 obtained from optical transmission conversion

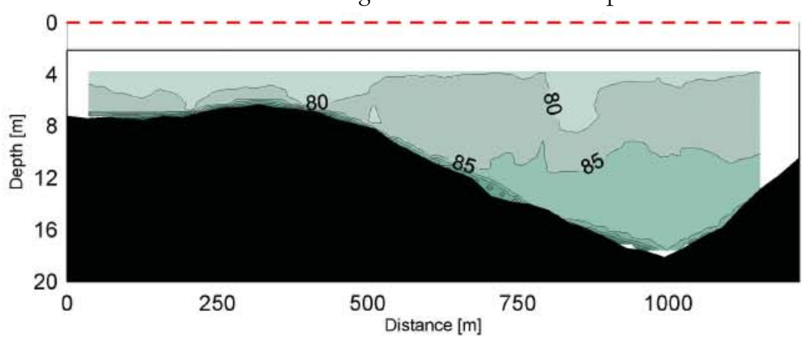

(c) Acoustic backscatter in dB

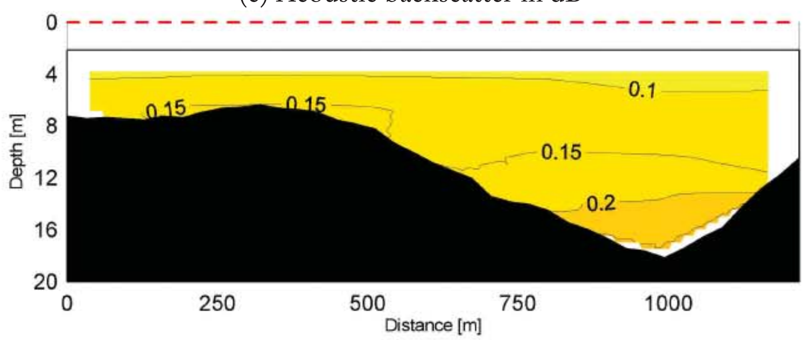

(d) Suspended material concentrations in kg/m^3 estimated using DEINES' approach

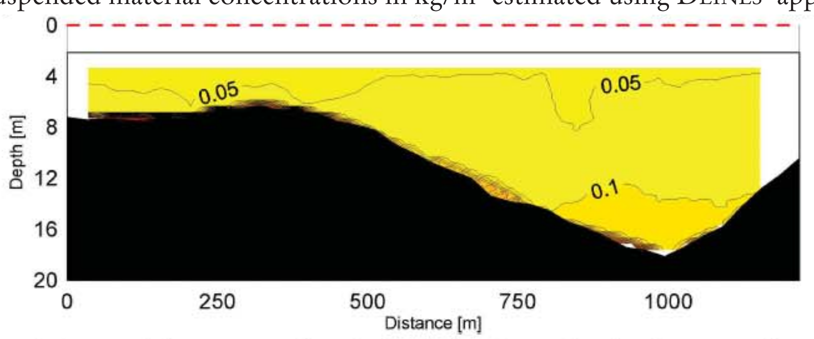

(e) Suspended material concentrations in kg/m^3 estimated using GARTNER's approach

Fig. 10: Measurements over cross-section T3 during slack water on 23 March 2000

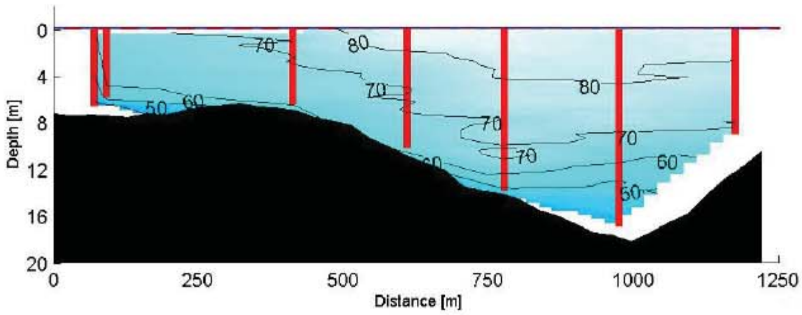

(a) Optical transmission in %

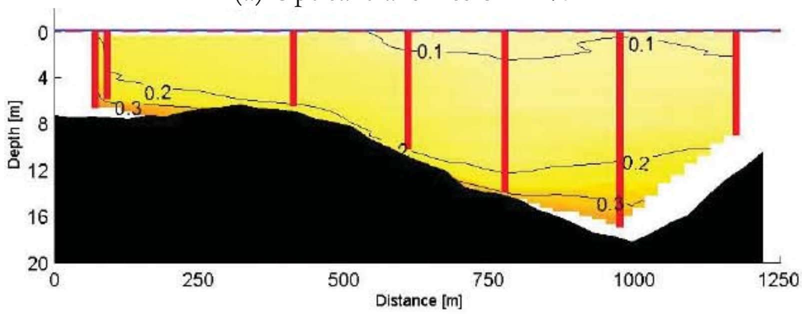

(b) Suspended material concentrations in kg/m³ obtained from optical transmission conversion

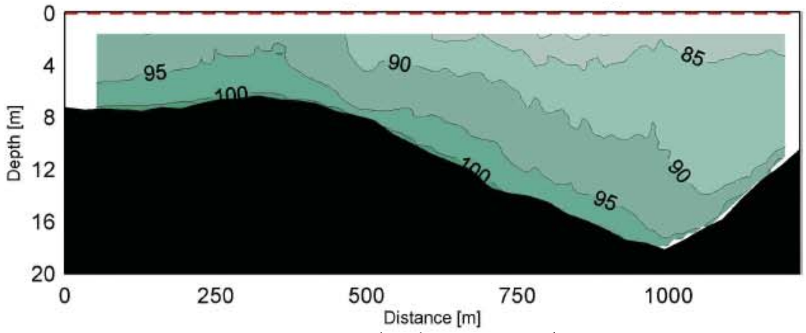

(c) Acoustic backscatter in dB

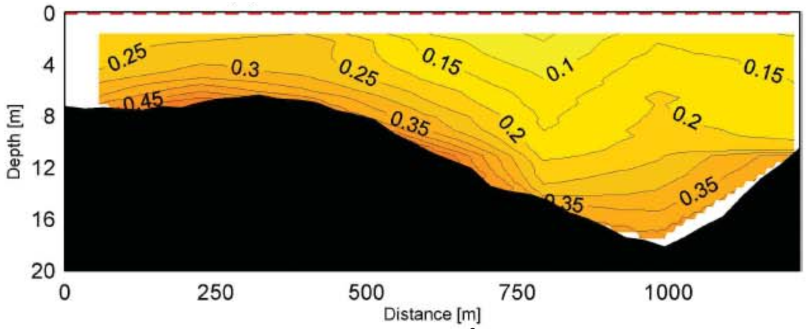

(d) Suspended material concentrations in kg/m³ estimated using DEINES' approach

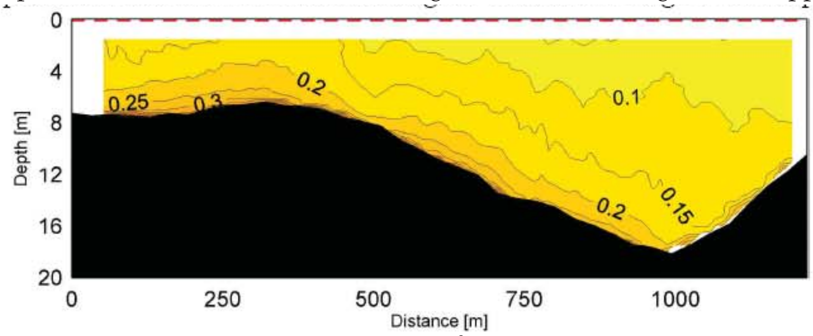

(e) Suspended material concentrations in kg/m³ estimated using GARTNER's approach

Fig. 11: Measurements over cross-section T3 during maximum flood flow conditions on 23 March 2000

the study area, with suspended sediment concentrations ranging between about 0.02 and 1.2 kg/m^3 . Estimates of suspended material concentration were found to be within a factor of 2 compared with measurements obtained using an optical beam transmissometer. The average relative error was found to be about 30 % whereas values the absolute error were found to be approximately equal to or better than 0.08 kg/m^3 on average. It was not possible to detect any effects of water depth, current velocity or location on the performance of the methods of conversion within the considered limit of a discrepancy factor of 2.

6. Acknowledgements

The authors wish to thank the German Ministry of Education and Research for funding the research project PROMORPH over a three-year period (2000 to 2002). We also appreciate the cooperation throughout the project with our colleagues from the Research and Technology Centre Westcoast (University of Kiel), the Institute of Fluid Mechanics and the Institute of Meteorology (University of Hannover), and the GKSS Research Centre (Geesthacht). The research would not have been possible without the financial support of Poerbandono by the German Academic Exchange Service (DAAD).

7. References

BIRCH, R.; GORDON, L.; LENTZ, S. and KOSRO, M.: Test of an Aquadopp Current Meter Near Sydney B.C., Nortek Technical Note No. 0010., 1999.

DEINES, K. L.: Backscatter Estimation Using Broadband Acoustic Doppler Current Profilers. In: ANDERSON et al. (Eds.), Proceedings of the IEEE 6th Working Conference on Current Measurement Technology, pages 249–253, 1999.

FLAGG, C. N. and SMITH, S. L.: On the Use of the Acoustic Doppler Current Profiler to Measure Zooplankton Abundance. Deep-Sea Research, 36(3): 455–474, 1989.

GARTNER, J. W.: Estimation of Suspended Solids Concentrations Based on Acoustic Backscatter Intensity: Theoretical Background. Turbidity and Other Sediment Surrogates Workshop. http://water.usgs.gov/osw/techniques/TSS/jgartner.pdf (31 January 2003), 2002.

HANES, D. M.; VINCENT, C. E.; HUNTLEY, D. A. and CLARKE, T. L.: Acoustic Measurements of Suspended Sand Concentration in the C2S2 Experiment at Stanhope Lane, Prince Edward Island. Marine Geology, (81): 185–196, 1988.

HEYWOOD, K. J.; SCROPE-HOWE, S. and BARTON, E. D.: Estimation of Zooplankton Abundance from Shipborne ADCP. Deep-Sea Research, 38(6): 677–691, 1991.

HOLDAWAY, G. P.; THORNE, P. D.; FLATT, D.; JONES, S. E. and PRANDLE, D.: Comparison between ADCP and Transmissometer Measurements of Suspended Sediment Concentration. Continental Shelf Research, (19): 421–441, 1999.

LANE, A.; KNIGHT, P. J. and PLAYER, R. J.: Current Measurement Technology for Nearshore Waters. Coastal Engineering, (37): 343–368, 1999.

LIBICKI, C.; BEDFORD, K. W. and LYNCH, J. F.: The Interpretation and Evaluation of a 3-MHz Acoustic Backscatter Device for Measuring Benthic Boundary Layer Sediment Dynamics. Journal of the Acoustic Society of America, (85), 1989.

OHM, K.: Optische Messungen zur Bestimmung von Schwebstofftransporten. Die Küste, Heft 42: 227–236, Heide/Holstein, 1985.

PATINO, E. and BYRNE, M. J.: Use of Acoustic Instruments for Estimating Total Suspended Solids Concentration in Streams – The South Florida Experience. Turbidity and Other Sediment Surrogates Workshop. http://water.usgs.gov/osw/techniques/TSS/Patino.pdf (31 January 2003), 2002.

POERBANDONO and MAYERLE, R.: Preliminary Result on the Estimation of Suspended Sediment Concentration from Acoustic Profilers. 10th ADCP User Workshop. Institute of Baltic Sea Research (IOW), Warnemünde, Germany, 2002.

POERBANDONO: Sediment Transport Measurement and Modelling in the Meldorf Bight Tidal Channels, German North Sea Coast. PhD Dissertation. Christian Albrechts Universität zu Kiel. Kiel, Germany, 2003.

POERBANDONO and MAYERLE, R.: Effectiveness of Acoustic Backscatter Measurements from Acoustic Profilers for Estimation of Suspended Sediment Concentration. In: RIZOLI (Ed.), Proc. of the IEEE 7th Working Conf. on Current Measurement Technology. San Diego, USA, 2003.

POERBANDONO and MAYERLE, R.: Assessment of Empirical Approaches for Converting Acoustic Echo Intensity into Suspended Sediment Concentration. In: Proc. of FIG 2004 Conf. Jakarta, Indonesia, 2004.

POERBANDONO; WINTER, C. and MAYERLE, R.: Field Measurements of Sediment Dynamics in Tidal Channels: Preliminary Results. In: Proc. of the 5th International Symposium on Coastal Engineering and Science of Coastal Sediment Process. Florida, USA, 2003.

RICKLEFS, C.: Zur Sedimentologie und Hydrographie des Eider-Ästuars. Berichte Nr. 35 – Geologisch-Paläontologisches Institut, Christian-Albrechts-Universität, Kiel, 1989.

SCHOTT, F. and JOHNS, W.: Half-year-long Measurements with a Buoy-mounted Acoustic Doppler Current Profiler in the Somali Current. Journal of Geophysical Research, 92 (C5): 5169–5176, 1987.

SONTEK, Inc.: ADP Versatility in San Felipe, Mexico Deployment. http:// www.sontek.com/ apps/ profiler/ adp-sf/ adp-sf.htm (27 May 2002), 2002.

THORNE, P. D. and HARDCASTLE, P. J.: Application of Acoustic Backscattering to Measuring Suspended Sediment Concentration. In: SOULSBY & BETTESS (Eds.), Euromech 262 – Sand Transport in Rivers, Estuaries and the Sea. Balkema, Rotterdam, The Netherlands, 1991.

THORNE, P. D.; VINCENT, C. E.; HARDCASTLE, P. J.; REHMAN, S. and PEARSON, N.: Measuring Suspended Sediment Concentrations using Acoustic Backscatter Devices. Marine Geology, (98): 7–16, 1991.

VAN DER LINDE, D. W.: Protocol for the Determination of Total Suspended material in Oceans and Coastal Zones. Space Applications Institute, Marine Environment. EC Joint Research Centre, Ispra, Italy. Technical Note No. I.98.182, 1998.

VINCENT, C. E.; HANES, D. M.; TAMURA, T. and CLARKE, T. L.: The Acoustic Measurement of Suspended Sand in the Surf-zone. In: Int. Conf. Measuring Techniques of Hydraulic Phenomena in Offshore, Coastal and Inland Waters, pp 443–451. Br. Hydraul. Res. Assoc., London, UK, 1986.

YOUNG, R. A.; MERRILL, J.; PRONI, J. R. and CLARKE, T. L.: Acoustic Profiling of Suspended Sediments in the Marine Boundary Layer. Geophysical Research Letter, 9(3): 175–178, 1982.

Die Küste, 69 PROMORPH (2005), 1-420

A Proposed Approach for the Determination of the Accuracy of Acoustic Profilers for Field Conditions

By SUSANA JIMÉNEZ GONZÁLEZ, ROBERTO MAYERLE and JUAN JOSÉ EGOZCUE

Summary

In this paper an innovative approach to estimate the accuracy of measuring devices for field measurements is proposed. The approach uses simultaneous measurements taken with identical devices close to each other. This method was successfully applied in the evaluation of the accuracy of a 1200kHz ADCP for cross-sectional measurements of current velocities in tidal channels. Measurements were carried out from measuring devices mounted on vessels moving close to each other on parallel tracks. Measurement campaigns covered tidal ranges of about 3.5 m and depth-averaged current velocities ranging from 0.30 to 1.05 m/s. Point estimates were defined by fitting a logarithmic velocity profile to the measured values. The variability of point measurements is estimated from the simultaneous measurements. The accuracy of the depth-averaged velocity values is obtained by computing several probability intervals on the basis of re-sampling techniques. The standard deviation for point measurements were found to be constant at 0.06 m/s and 0.14 m/s for distances above and below 1 m from the sea bottom, respectively. Results are in reasonable agreement with those reported by VAN RIJN et al. (2002a), despite the different instruments and experimental and environmental settings. The accuracy of an ADCP measuring the depth-averaged velocity values was approximately constant at ±0.015 m/s. Resulting accuracy values have been used in the calibration and validation of depth-averaged two-dimensional and three-dimensional flow models.

Zusammenfassung

In dieser Arbeit wird eine innovative Methode zur Abschätzung der Messgenauigkeit von Messgeräten unter Naturbedingungen vorgestellt. Der Ansatz impliziert zeitgleiche und eng benachbarte Messungen mit technisch identischen Geräten. Dieses Verfahren wurde erfolgreich zur Evaluation der Genauigkeit des 1200 kHz ADCP bei Querprofilmessungen der Strömungsgeschwindigkeit in Gezeitenrinnen angewendet. Die Messungen erfolgten mit Messgeräten, die auf Schiffen installiert waren. Diese fuhren denselben Kurs in unmittelbarer Nähe zueinander. Die Messkampagnen beziehen sich auf einen Tidehub von etwa 3,5 m und tiefenintegrierten Strömungsgeschwindigkeiten von 0,30 bis 1,05 m/s. Punktuelle Abschätzungen wurden durch Anpassung eines logarithmischen Geschwindigkeitsprofils an die Messwerte definiert. Die Variabilität der Punktmessungen wird aus den zeitgleichen Messungen geschätzt. Die Genauigkeit der tiefenintegrierten Geschwindigkeitswerte aus der Berechnung mehrerer Wahrscheinlichkeitsintervalle auf Grundlage von „Resampling“ Techniken erhalten. Die Standardabweichungen für Punktmessungen lagen konstant bei 0,06 m/s für Entfernungen von mehr als 1 m bzw. bei 0,14 m/s für Entfernungen von weniger als 1 m Bodenanstand. Trotz der Verwendung unterschiedlicher Geräte, Experiment- und Umwelt-Maßzahlen stimmten die Ergebnisse recht gut überein mit denen von VAN RIJN (2002a). Die Genauigkeit einer ADCP-Messung für tiefenintegrierte Geschwindigkeitsmessungen lag nahezu konstant bei ±0.015 m/s. Die ermittelten Messgenauigkeiten wurden bei der Kalibrierung und Validierung tiefenintegrierter zwei- und dreidimensionaler Strömungsmodelle eingesetzt.

Keywords

ADCP, Accuracy of Measuring Devices, Current Velocity, Bootstrap Method …

Contents

1. Introduction

In the framework of the German government funded research project entitled "Predictions of Medium Scale Morphodynamics- PROMORPH" selective measurements of current velocities using acoustic profiler were carried out at several tidal channels of a tidally-dominated area of the German Wadden Sea. The measurements aimed at calibrating and validating flow models for the area of investigation. A set of statistical parameters was used to assess the quality of the flow model results in relation to current velocities (PALACIO et al., in this volume). As measurements always include errors, a suggested approach to account for the influence of observational errors is to subtract these from the absolute error, thereby yielding an adjusted relative mean absolute error (WALSTRA et al., 2001; VAN RIJN et al., 2002b). While information on the accuracy of these devices is usually provided for laboratory conditions, very little is known about their performance in the field, particularly for depth-averaged velocity values.

In this paper an approach to estimate the accuracy of measuring devices for field conditions is proposed. The approach uses simultaneous measurements taken with identical devices mounted on vessels moving close to each other on parallel tracks. The proposed method was applied for field measurements of current velocities along cross-sections of tidal channels at the German North Sea coast. Results of the application of the approach to estimate the accuracy of a 1200 kHz Acoustic Doppler Current Profiler (ADCP) in the field are presented. The performance of the devices for point and depth-averaged velocity values is determined.

2. Acoustic Doppler Current Profilers (GORDON, 1996)

ADCPs use a principle that relies on the presence of particles (scatterers) in the water column to reflect back a transmitted acoustic signal. An acoustic short pulse of high frequency is transmitted to the water column with a fixed and known frequency through the transducer. Since the scattering particles move either closer or away from the device, the returned echoes experience a Doppler shift. Based on the measured shift, the speed of the scattering particle relative to the device can be determined and converted into current velocities. The principle of operation of ADCP relies on a number of assumptions, the most important of which in terms of data quality are homogeneity of the measurement layer, constant speed of sound over the measurement range and the average independent movement of scatterers to be zero.

Fig. 1 shows a typical output plot of a cross-section surveyed by an acoustic profiler, i.e. a path followed by a vessel during the measurements. Cross-sections are comprised of ensembles, i.e. columns of data along the vessel path. Ensembles are in turn divided into bins, i.e. measuring units with a thickness varying from about 10 cm to 1 m.

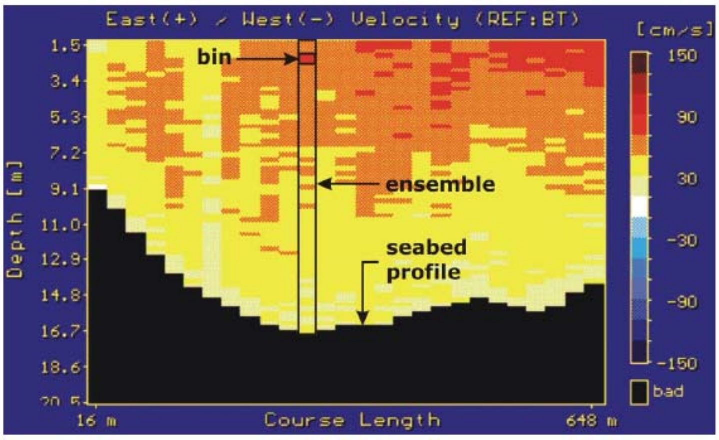

Fig. 1: Main elements of a transect obtained from a ship-mounted ADCP

The accuracy of ADCPs for point measurements under laboratory conditions is quite high in the order of a few mm/s. In the field, devices have been used mainly as bottom-mounted or as ship-mounted. Their performance is often strongly dependent on the environmental conditions. Moreover, the experimental settings, the characteristics and amount of suspended sediment matter and air bubbles in the water column, among others, can also affect their performance. VAN RIJN et al. (2002a) reported values of the accuracy of a 1500 kHz ADCP for field conditions. The accuracy of the bottom-mounted stand-alone device for point measurements is 1 % of the measured value and ± 0.5 cm/s at the maximum output rate. The downward looking ship-mounted ADCP shows an accuracy of ± 5.3 cm/s for 10 seconds averaging (1.0 m cells) and ± 5.1 cm/s for 30 seconds averaging (1.0 m cells).

3. Experimental Set-Up and Measured Data

The present investigation focuses on a tidal channel of the Central Dithmarschen Bight on the German North Sea coast (see Fig. 2). The study area is located about 100 km north of Hamburg between the Eider and Elbe estuaries. The morphodynamics of the study area is dominated by tidal flats and a tidal system composed of three channels: the Norderpiep in the northwest, the Suederpiep in the southwest, and the Piep tidal channels, which is formed at the intersection of the Norderpiep and Suederpiep. The flow conditions in the area are dominated by a combination of tidal, wave-induced and wind driven currents. Under normal conditions the tidal effect prevails. The area is characterized by a mean tidal range of 3.2 m.

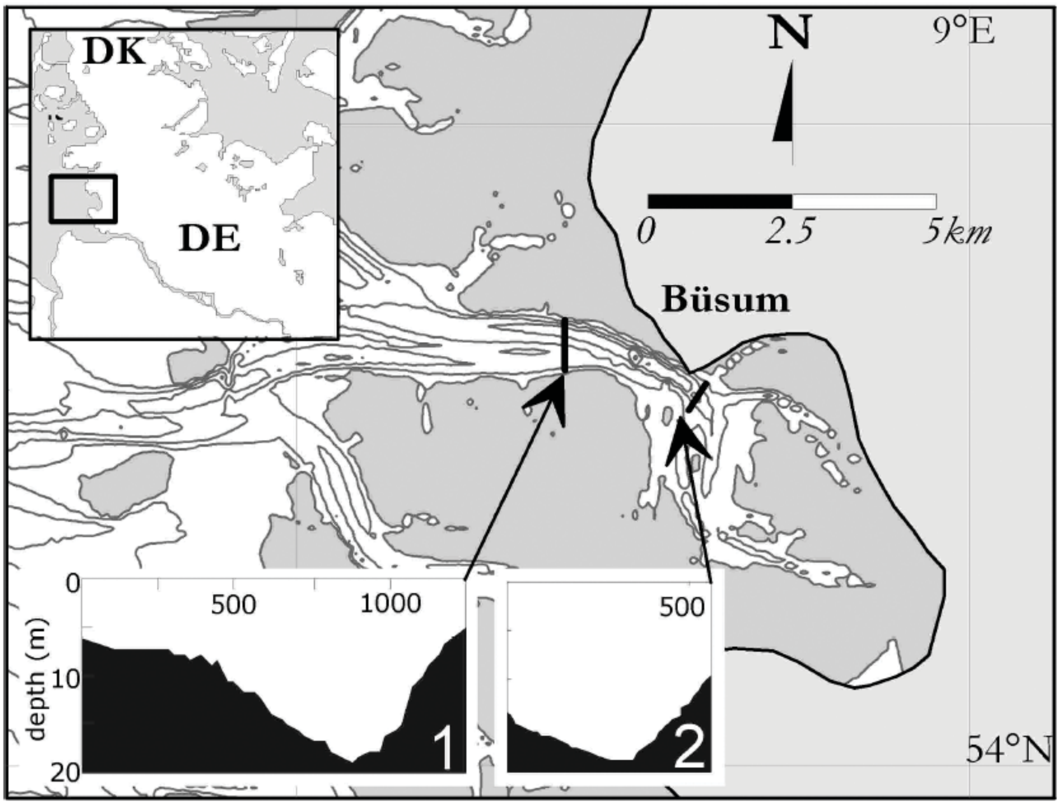

Fig. 2: Area of investigation

The water depths in the channels are up to about 20 m. The temporal and spatial variations of the current velocities are strongly influenced by the complex bathymetry. The current velocities in the tidal channels attain maximum values of about 2.8 m/s (TORO et al., in this volume).

The investigations were carried out at two cross-sections of the Piep tidal channel as indicated in Fig. 2. The mean water depth at the cross-sections varies from about 5–8 m to 18–20 m. The mean transect length is approximately 1000 m and 570 m at cross-sections 1 and 2, respectively. The cross-sections are about 3 km apart. Measurement campaigns in these two cross-sections were carried out on October 9, 2000 and February 1, 2001 at a tidal range of 3.5 m. The weather conditions during the measurements were essentially calm. Fig. 4 shows the time series of water levels during the measurement campaign indicating the times at which the cross-sectional measurements were taken. Measurements covered the ebb and flood phase during the 1st and 2nd measuring campaign, respectively. Details of the experimental settings are summarised in Table 1.

The data required for estimating the accuracy of an ADCP used for field measurements were obtained from identical instruments deployed on two vessels moving close to each other on a parallel course (Fig. 3). The two ADCPs, i.e. a 1200 kHz Workhorse Sentinel and a Direct Reading Broad Band, had been manufactured by RD Instruments. Their accuracy for point measurements under laboratory conditions is given as ± 0.25 % of the measured value ± 0.0025 m/s by the manufacturer. The instruments were mounted at the bow of the vessels pointing downward. Measurements covered the water column from about 1.6 m below the free surface (transducer draught and blanking distance) down to the seabed. The bin sizes during the measurements were set to 0.5 m.

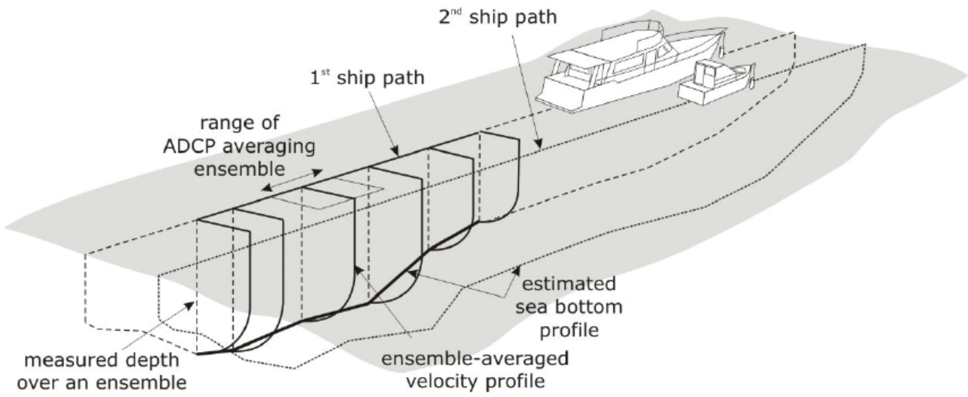

Fig. 3: Main elements of transect from ship-mounted ADCP

Several measurement runs within the tidal cycle were carried out. Altogether 21 runs, i.e. 5 from the 1st and 16 from the 2nd measuring campaign were considered for analysis. From these, a total of 686 current velocity profiles (207 from the 1st and 429 from the 2nd measuring campaign) were derived. To assure that the variation of the velocity over the depth follows a logarithmic distribution, the analysis focused on velocity profiles with a maximum point velocity exceeding 0.3 m/s. The depth-averaged velocity values used in the analysis range from 0.28 to 1.06 m/s.

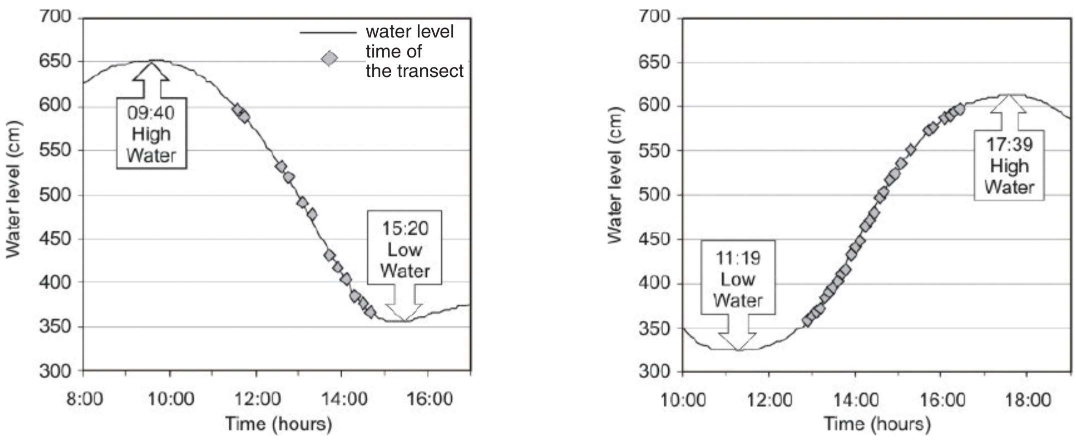

(a) 1st measurement campaign
Cross-Section 1

(b) 2nd measurement campaign
Cross-Section 2

Fig. 4: Time series of water levels and cross-sectional measurements

Table 1: Details of the measurement campaigns

	1st measurement campaign	2nd measurement campaign
Cross-Section	1	2
Date	October 9, 2000	February 1, 2001
Start and termination	11:34 till 14:40 hrs.	12:55 till 16:26 hrs.
Tidal cycle analysed	Ebb	Flood
Tidal range	3.5 m	3.5 m
Range of depth-averaged velocities	0.30–1.05 m/s	0.28–1.06 m/s
Number of parallel transects	5	16
Mean transect length	1000 m	570 m
Distance between vessels (mean)	2 to 24 m (6.5 m)	4 to 48 m (15 m)

Die Küste, 69 PROMORPH (2005), 1-420

4. Data Analysis and Discussions

4.1 Model for the Velocity Distribution Over the Vertical

The distribution of the velocity profile over the water column in steady uniform flows is known to follow a logarithmic distribution that can be mathematically expressed as follows:

$$\frac{u_z}{u} = \frac{1}{\ } \cdot \ln\left(\frac{z}{z_0}\right) \qquad (1)$$

with u_z = velocity magnitude in m/s at a distance z in m from the bottom
u = shear velocity in m/s
= von Karman coefficient assumed equal to 0.4
z_0 = zero-velocity crossing in m, which in case of rough regimes is a function of the roughness size only.

Flow in tidal channels is unsteady and non-uniform. Therefore, although the velocity profiles follow approximately a logarithmic distribution, the shear velocity and zero-crossing values are bound to vary in time. In this study the proposed model for describing the velocity distribution over the water column is written as:

$$u_z = a + b \ln(z) \qquad (2)$$

Equation 2 is linear in the form $u_z = a + bx(z)$. The values of the coefficients a and b that best adjust to the measured velocity values over the water column can be obtained by simple regression techniques. Measured sets of current velocity profiles in the water column, i.e. ADCP ensembles $\{(z_i, u_i), i = 1, \ldots, k\}$ were considered. z_i denotes the distance to the seabed; u_i is the velocity magnitude and k the number of bins, i.e. measured units (point measurements) over the vertical. Point estimators for the depth-averaged velocities at each vertical profile were obtained by analytical integration of the fitted profiles divided by the corresponding water depth.

4.2 Variability of Point Measurements

The simultaneous measurements carried out side-by-side from the two vessels lead to two vertical velocity distributions at approximately the same location. Although good agreement between the profiles is expected, this was not always the case. Fig. 5 shows typical measured vertical profiles; one showing good agreement (Fig. 5a) and the other one with discrepancies (Fig. 5b).

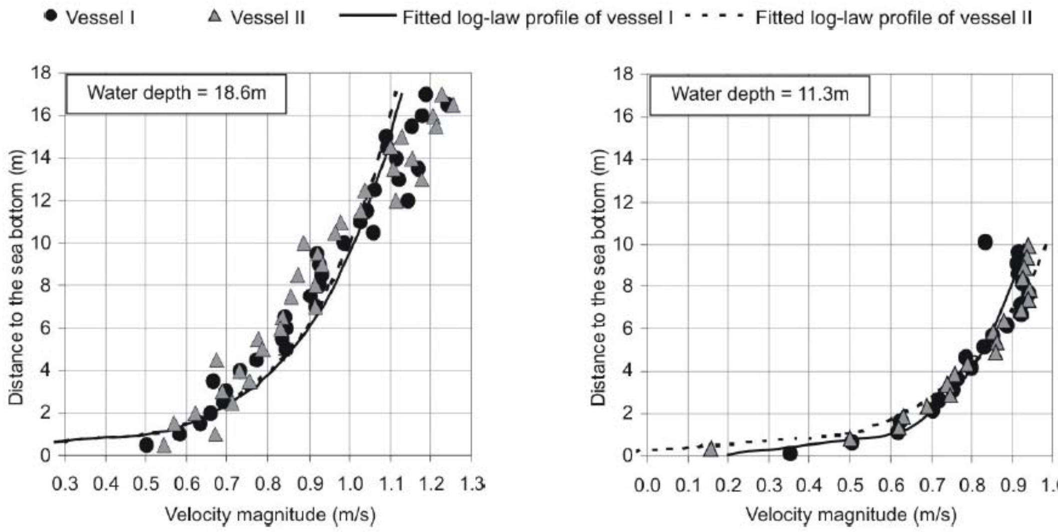

(a) Good agreement (b) Non-satisfactory agreement

Fig. 5: Comparison between simultaneous data sets

To check the agreement between the simultaneous data sets at the same location a multiple linear regression analysis was carried out. Several significance tests based on the t-distribution for the multiple regression coefficients were performed. A significance level of 5 % was considered to differentiate between a good and non-satisfactory agreement. In 43 % of the cases bad agreement resulted. Since the field data were collected using identical devices deployed simultaneously and very close to each other, the resulting discrepancies could be considered to correspond to the variability of point measurements in the field. In order to evaluate this variability, the differences between point velocity magnitudes belonging to simultaneous data sets were computed.

The accuracy of ADCP is known to decrease closer to the seabed due to decreasing intensity and side lobe interference. To account for this decrease, the variability was analysed with respect to the location of the point measurements within the water column. Weighting the percentage of acceptable values obtained by the ADCP was considered. Several F-tests were performed to figure out the optimal division of layers within the water column, so that the variability within each layer would remain approximately constant with significance levels of 10 %, 5 % and 1 %. The Kolmogorov-Smirnov goodness of fit test was applied to check the hypothesis of normality of the groups. Satisfactory results were obtained in all cases as summarised in Table 2. Two layers within the water column with approximately constant variabilities could be identified: a) bottom layer up to about 1m above the seabed and b) remaining water column up to about 1.6 m below the free surface. The standard deviation of the group sample in the lower layer turned out to be more than twice the value of the upper one. Considering the differences in instrumentation and environmental conditions, it should be noted that the results obtained in the upper layer are in good agreement with the ones reported by VAN RIJN et al. (2002a).

Table 2. Variability of point measurements over the vertical

Layer distribution	Standard deviation of the group sample (variability) in m/s
Bottom layer : up to 1m from seabed	0.143
Upper layer : from 1 m above the seabed up to 1.6 m below free surface	0.065

4.3 Variability of Depth-Averaged Velocity Values

The variability of the depth-averaged velocity values was obtained by applying re-sampling techniques. In this study the *bootstrap* method by EFRON and TIBSHIRANI (1993) was used. A brief description follows.

For each measured vertical current velocity profile, i.e. each ADCP ensemble, a data set $\{(z_i, u_i, g_i), i = 1, \ldots, k\}$ was considered. z_i denotes the distance to the seabed, u_i is the velocity magnitude, g_i the percentage of acceptable values given by the ADCP and k the number of points measured over the vertical (bins).

For each set of data, 10^4 *bootstrap samples* were computed. *Bootstrap samples* are random samples drawn with replacement from the original population. They consist of members of the original data set, some being absent, others appearing one or more times. For each *bootstrap sample* the coefficients a^* and b^* in Equation 2 were estimated by fitting the log-law distribution. The log-law profile defined by the simulated coefficients (a^* and b^*) represents an ideal state that never occurs in real measurements. Two sources of errors were accounted for: a) the variability of point measurements listed in Table 2 and b) the regression residuals defined by the differences between the measured values and the values predicted by the log-law fit.

The approach adopted to account for the probability intervals of the depth-averaged velocity is illustrated in Fig. 6. First, each of the fitted log-law profiles was discretised over the vertical with a 1 cm resolution. Then, for each discretised point a value corresponding to the residual values was simulated and added, following a normal distribution with zero mean and variance equal to the sum of the variance of the regression residuals and the one introduced by the variability of point measurements over the vertical. Finally, for each of the 10^4 *bootstrap samples*, the depth-averaged velocity values were computed. This was done by dividing the numerical integration of the discretised point velocity values by the corresponding water depth. The resulting sets of simulated values of the depth-averaged velocity in a vertical distribution over the water column allow the computation of percentiles which in turn enables the estimation of probability intervals. In the figure, the original field data and a bootstrap sample are shown in conjunction with their corresponding log-law fits. The points obtained by adding the simulated normally distributed residuals to the discretisation of the logarithmic profile fitted to the bootstrap sample are also indicated.

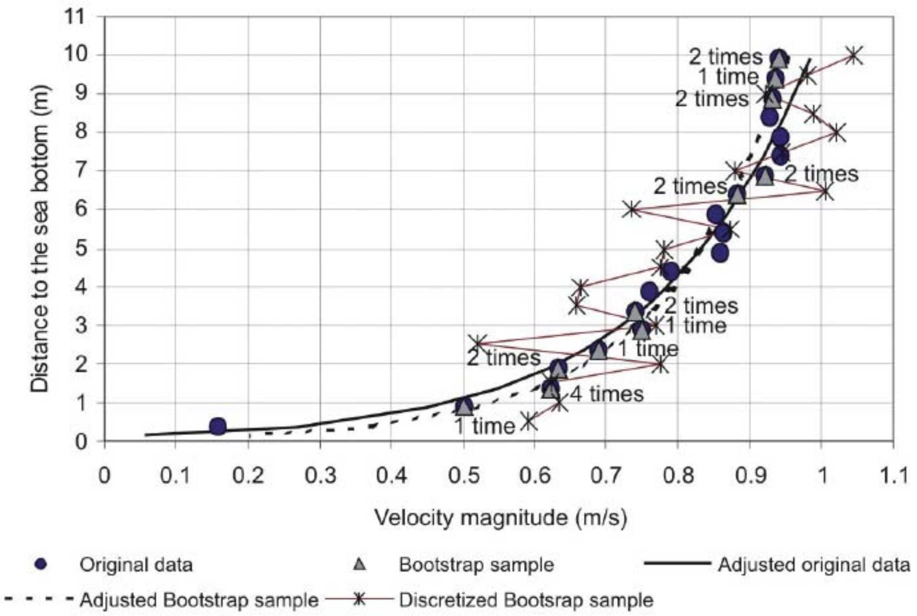

Fig. 6: Bootstrap procedure for a given vertical profile

4.4 Probability Intervals of Depth-Averaged Velocity Values

The accuracy of an ADCP in measuring depth-averaged velocity values for field conditions was estimated by computing six probability intervals corresponding to confidence levels of 98 %, 90 %, 80 %, 70 %, 60 % and 50 % on the basis of simulated depth-averaged velocity values.

Comparisons between the point estimators obtained by analytical integration of the measured values that were fitted to the original set of data divided by the corresponding water depth, and the mean and median values corresponding to the *bootstrap samples* led to a quite satisfactory agreement. The simulated data obtained by re-sampling techniques were homogeneously distributed without important asymmetries. Fig. 7 shows the distribution of the depth-averaged velocity values corresponding to the *bootstrap samples* for the two vertical profiles shown in Fig. 5. It can be seen that the point estimator of the values depth-averaged is well centered.

To create a better comparison, cross-sectional averages of the interval lengths of the depth-averaged velocity were calculated. These values were obtained by averaging the entire set of interval lengths corresponding to each ensemble. The cross-sectional averages of the probability interval lengths and their variances behave in a quite constant and regular way. Therefore, in general, they are found to be independent of the water level or the depth-averaged velocity.

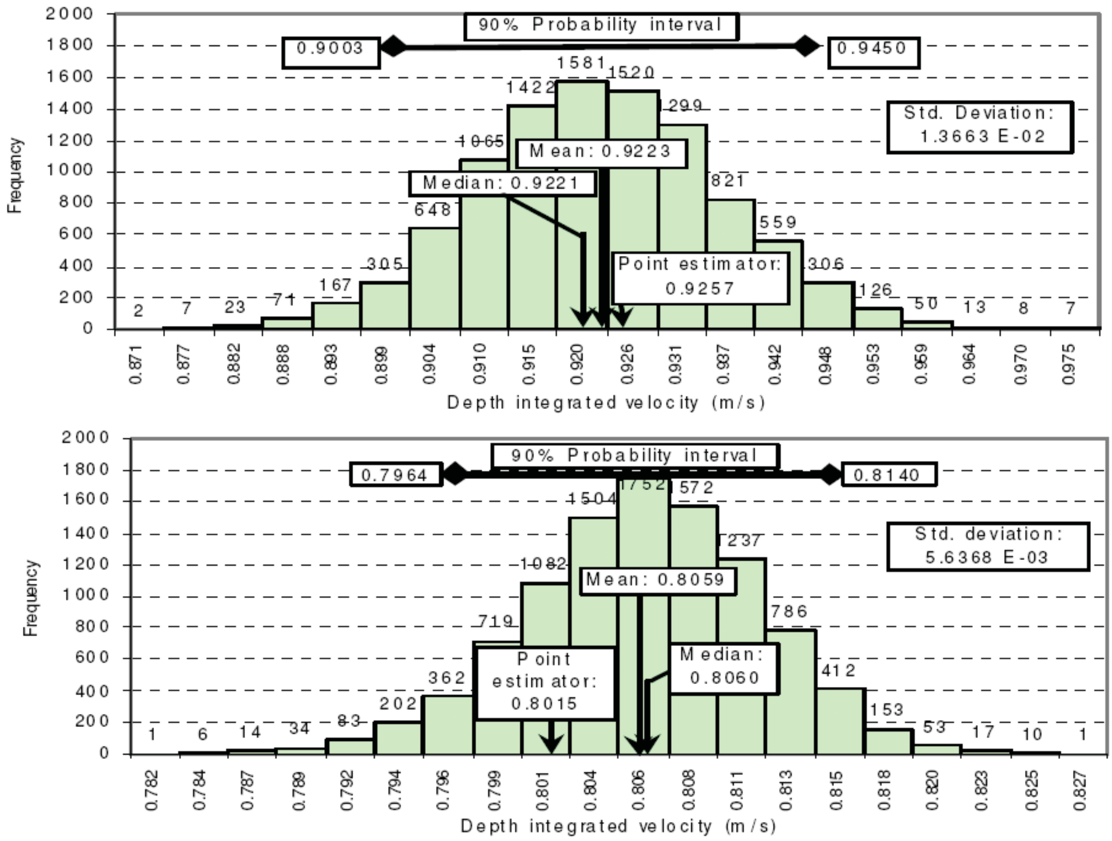

Fig. 7: Distribution of the bootstrap results for two given velocity profiles

Table 3 summarises the mean values of the resulting cross-sectionally averaged velocities for the various significance levels obtained by analysing the measured data from both measurement campaigns. The accuracy values were defined by assuming homogeneity and symmetry of the simulated sets of data obtained using *bootstrap techniques*. Moreover, it was assumed that the point estimator of the depth-averaged velocity is well centred in the *bootstrap sample*.

Table 3. Interval lengths and accuracy values of the depth-averaged velocity values

Confidence level	1st Measurement Campaign			2nd Measurement Campaign		
	Length[1] (m/s)	Accuracy (m/s)	Accuracy[2] (%)	Length[1] (m/s)	Accuracy (m/s)	Accuracy[2] (%)
98 %	0.037	± 0.018	2.07–2.85	0.048	± 0.024	2.73–3.75
90 %	0.026	± 0.013	1.45–1.99	0.034	± 0.017	1.90–2.62
80 %	0.020	± 0.010	1.14–1.56	0.026	± 0.013	1.48–2.03
70 %	0.016	± 0.008	0.91–1.25	0.021	± 0.012	1.19–1.64
60 %	0.013	± 0.007	0.74–1.02	0.017	± 0.009	0.97–1.33
50 %	0.011	± 0.006	0.60–0.82	0.014	± 0.007	0.80–1.09

[1] Length of the probability interval.
[2] Accuracy value given as percentage of the cross-sectional depth-averaged velocities.

It can be seen that the length of the confidence intervals is slightly larger for the 2nd measuring campaign. This can be attributed to the spatial dependence, different tidal phases, i.e. ebb and flood phase respectively during the 1st and 2nd measuring campaign and variation in distances between the vessel tracks. The fact that the two campaigns were carried out in the same tidal channel along two cross-sections not faraway makes the consideration of the spatial dependence doubtful. Bearing in mind that the length of the probability intervals was independent of water level and current velocity values, further rejects the hypothesis that the differences may be caused due to the different tidal phases. Therefore, the main reason of slightly larger values during the 2nd measuring campaign was attributed to the larger distances between the vessel tracks.

Taking into account the symmetry and homogeneity of the resulting sets of simulated data, a constant accuracy value of ± 0.015 m/s, based on the 90 % confidence levels from the two measuring campaigns, resulted for the depth-averaged velocity values.

5. Conclusions

In this paper an approach for estimating the variability and accuracy of measuring devices for field conditions is proposed. The method was applied successfully to the estimation of the accuracy of a 1200 kHz ADCP for field measurements of current velocities along cross-sections of tidal channels. The analysis focused on velocity profiles with maximum point velocity values exceeding 0.3 m/s giving depth-averaged velocity values from 0.28 to 1.06 m/s. The results indicate that the standard deviation of an ADCP for point measurements in the tidal channels of the central Dithmarschen Bight is constant at 0.14 and 0.06 m/s for vertical distances below and above 1m from the seabed, respectively. Results are in reasonable agreement with those reported by VAN RIJN et al. (2002a), despite the different instruments and experimental and environmental settings. The length of the probability intervals for the depth-averaged velocity is approximately constant and independent of water levels and the magnitude of depth-averaged velocities. A constant accuracy of about ± 0.015 m/s (at a 90 % confidence level) was obtained.

The approach offers an alternative and innovative way of estimating accuracies of measurement devices for field conditions. It attempts to account for the main factors that affect the variability of field measurements. Despite the fact that the experimental settings on the two parallel tracks are quite similar, other factors not directly taken into consideration, such as the variations of the suspended sediment during the measurements, insufficient suspended matter in the water column leading to insufficient signal detection as well as a complex and mobile bathymetry may also influence the accuracy.

6. Acknowledgements

The results presented here form a contribution to the research project "Predictions of Medium-Scale Morphodynamics – PROMORPH" funded by the German Ministry of Education and Research (BMBF) from year 2000 to 2002. The authors gratefully acknowledge the German Ministry of Education and Research for funding the project. We also wish to thank the staff of the Research and Technology Centre Westcoast of the University of Kiel for the planning and execution of the field measuring campaigns and for supporting in the interpretation of the results. Dr. Ian Westwood is greatly acknowledged for his English corrections and proofreading. The authors furthermore thank Dr.-Ing. V. Barthel as well an anonymous reviewer for their constructive remarks.

7. References

EFRON, B. and TIBSHIRANI, R. J.: An Introduction to the Bootstrap, Chapman & Hall, New York, 1993.

GORDON, R. L.: Acoustic Doppler Current Profiler. Principles of Operation. A Practical Primer. RD Instruments, San Diego, 1996.

PALACIO, C.; MAYERLE, R.; TORO, M. and JIMÉNEZ, N.: Modelling of Flow in a Tidal Flat Area in the South-Eastern German Bight, Die Küste, Heft 69, 2005.

TORO, F.; MAYERLE, R.; POERBANDONO and WILKENS, J.: Patterns of Hydrodynamics in a Tide-Dominated Coastal Area in the South-Eastern German Bight, Die Küste, Heft 69, 2005.

VAN RIJN, L. C.; GRASMEIJER, B. T. and RUESSINK, B. G.: Accuracy of Measurement Instruments. In: VAN RIJN et al., The Behaviour of a Straight Sandy Coast on the Time Scale of Storms and Seasons. Aqua Publications, Amsterdam, The Netherlands, 2002a.

VAN RIJN, L. C.; WALSTRA, D. J. R.; GRASMEIJER, B.; SUTHERLAND, J.; PAN, S. and SIERRA, J. P.: Simulation of Nearshore Hydrodynamics and Morphodynamics on the Time Scale of Storms and Seasons using Process-based Profile Models. In: VAN RIJN et al., The Behaviour of a Straight Sandy Coast on the Time Scale of Storms and Seasons: Process Knowledge and Guidelines for Coastal Management. Aqua Publications, Amsterdam, The Netherlands, 2002b.

WALSTRA, D. J. R.; VAN RIJN, L.; BLOGG, H. and VAN ORMONDT, M.: Evaluation of a hydrodynamic area model based on the COAST3D data at Teignmouth 1999. Paper D4 of: COAST3D Final Volume of Summary Papers. Report TR121, HR Wallingford, UK, pp D4.1 – D4.4, 2001.